Positronium and Muonium Chemistry

Hans J. Ache, EDITOR
Virginia Polytechnic Institute and State University

Based on a symposium sponsored by the Division of Physical Chemistry of the Chemical Institute of Canada at the Second Joint CIC/ACS Conference, Montreal, Canada, May 31–June 2, 1977.

ADVANCES IN CHEMISTRY SERIES 175

AMERICAN CHEMICAL SOCIETY
WASHINGTON, D. C. 1979

Publication Date: June 1, 1979 | doi: 10.1021/ba-1979-0175.fw001

Publication Date: June 1, 1979 | doi: 10.1021/ba-1979-0175.fw001

Library of Congress CIP Data

Positronium and muonium chemistry.
(Advances in chemistry series; 175 ISSN 0065–2393)

Includes bibliographies and index.

1. Positronium—Congresses. 2. Positron annnihilation—Congresses. 3. Muonium—Congresses.
I. Ache, Hans J. II. Chemical Institute of Canada. Physical Chemistry Division. III. American Chemical Society. IV. Series.

QD1.A355 No. 175 [QD461] 540'.8s [541'.38]
ISBN 0-8412-0417-9 ADCSAJ 175 1–376 1979
79–11709

PRINTED IN THE UNITED STATES OF AMERICA

Publication Date: June 1, 1979 | doi: 10.1021/ba-1979-0175.fw001

Advances in Chemistry Series

Robert F. Gould, *Editor*

In Positronium and Muonium Chemistry; Ache, H.;
Advances in Chemistry; American Chemical Society: Washington, DC, 1979.

Publication Date: June 1, 1979 | doi: 10.1021/ba-1979-0175.fw001

FOREWORD

ADVANCES IN CHEMISTRY SERIES was founded in 1949 by the American Chemical Society as an outlet for symposia and collections of data in special areas of topical interest that could not be accommodated in the Society's journals. It provides a medium for symposia that would otherwise be fragmented, their papers distributed among several journals or not published at all. Papers are reviewed critically according to ACS editorial standards and receive the careful attention and processing characteristic of ACS publications. Volumes in the ADVANCES IN CHEMISTRY SERIES maintain the integrity of the symposia on which they are based; however, verbatim reproductions of previously published papers are not accepted. Papers may include reports of research as well as reviews since symposia may embrace both types of presentation.

PREFACE

The symposium, "Positronium and Muonium Chemistry," was held at the Second Joint Conference of The Chemical Institute of Canada and the American Chemical Society, May 29–June 2, 1977. The objective of this symposium was to assess the role of positronium, which is the short-lived bound state of an electron and its antiparticle, the positron, and of muonium, which is the combination of an electron with a positive muon, as nuclear probes to the solution of chemical problems. Thus participants were requested specifically to aim for comprehensive state-of-the-art reviews and to emphasize the application of positronium or muonium atoms to chemical problems in their respective areas of interest. As a result of this a wide variety of topics ranging from the interactions of these "exotic atoms" in simple rare gases to the use of positronium in structure studies of complex biochemical compounds were discussed.

This symposium showed that these nuclear techniques offer great promise for the study of phase transitions (conformational and other structural changes) in the microenvironment in inorganic and organic materials, metals, polymers, and micellar and biomacromolecular systems. Here they can complement other conventional methods by providing information not accessible by these latter techniques. They also have been found to sensitively probe the properties and intermolecular interactions of molecules, cluster formation, etc. in gases at various densities. The most dramatic effects can be seen when positronium atoms (Ps), formed by the combination of an electron with a positron, are allowed to react with photon-excited molecules. The extremely large cross section observed for the interaction between positronium and these species makes this technique applicable to pollution research related to photochemical reactions in air.

The mechanism of positronium and muonium formation in the condensed phase involves a variety of radiation chemical phenomena. Thus, the investigation of these processes via positronium and muonium chemistry provides valuable information on the (very fast) reactions, mechnisms, and kinetics of radiolytically formed species in radiation spurs. The availability of low-energy positrons will be especially fruitful for these latter studies.

Because of the relative simplicity of the positronium or muonium atoms, theoretical calculations of the reactions of these species with other molecules and the structures of the intermediates involved in these reac-

In Positronium and Muonium Chemistry; Ache, H.;
Advances in Chemistry; American Chemical Society: Washington, DC, 1979.

tions always have been attractive to theoreticians and some of their results were discussed at this meeting.

In order to provide the reader with a comprehensive treatment of positronium and muonium chemistry, the editor also invited several authors who were not able to attend the Montreal symposium but who had participated in the symposium on "Chemical and Physical Applications of Positron and Muon Spectroscopy" at the ACS National Meeting in New Orleans, March 20–25, 1977, organized by the Division of Nuclear Chemistry and Technology, to contribute to this volume.

The editor is very grateful to his colleagues whose efforts made this volume possible. He also would like to thank the session chairmen: B. G. Hogg, The University of Winnipeg; S. J. Tao, The New England Institute; and especially G. R. Freeman, The University of Alberta, who initially suggested this symposium and also acted as co-organizer.

Virginia Polytechnic Institute
and State University
Blacksburg, Virginia 24061
March 20, 1979

HANS J. ACHE

Publication Date: June 1, 1979 | doi: 10.1021/ba-1979-0175.pr001

1

Positronium Chemistry: Present and Future Directions

HANS J. ACHE

Department of Chemistry, Virginia Polytechnic Institute and State University, Blacksburg, VA 24061

Publication Date: June 1, 1979 | doi: 10.1021/ba-1979-0175.ch001

In this review an attempt has been made to critically assess the present status of positronium chemistry and positron annihilation techniques as a chemical probe in general. Specifically, the concept that the interactions between positronium atoms and substrate occur primarily via positronium complex formation and that the rate of this reaction is therefore dependent on the nature of the environment in which they occur, has been developed to a method of determining the position of probe molecules in micelles and to evaluate formation constants for inclusion and acceptor–donor complexes of biological interest. Furthermore the positronium formation process was very sensitive to microphase transitions and was used for the assessment of critical micelle concentrations in aqueous and reverse micellar systems.

Among the various combinations of elementary particles and their antiparticles, which have become known during the recent years as exotic atoms, the positronium (Ps), which is the bound state of an electron and positron (e^+e^-), is undoubtedly the most thoroughly investigated species. This is probably owing to the fact that Ps atoms can be produced easily following the β^+ decay of certain radioactive nuclides, such as ^{22}Na. The properties of this species have been discussed in previous reviews (*1–7*).

Positrons emitted as a result of such a radioactive decay lose most of their (initially several hundred KeV) kinetic energy in inelastic and elastic collision until they reach nearly thermal energies at which point they can combine with electrons to form the Ps atom, whose binding

0-8412-0417-9/79/33-175-001$11.25/1

In Positronium and Muonium Chemistry; Ache, H.;
Advances in Chemistry; American Chemical Society: Washington, DC, 1979.

energy is 6.8 eV. The positronium formation probability depends on the nature of the environment: in water about 36% of all positrons form Ps, whereas in benzene the corresponding number is 57%.

Ps can be visualized as an analog of the hydrogen atom, in which the proton is substituted by a positron, and thus can be considered as the lightest isotope of the hydrogen (Figure 1). However, in contrast to the hydrogen atom which is a one-center system, the equal masses of the electron and positron make the positronium a two-center system, which leads to drastic differences not only in the physics but also in the chemistry of these two species.

Ps exists in two ground states, the singlet (para) Ps with antiparallel spin orientation ($\uparrow\downarrow$) (its self-annihilation lifetime is in free space 1.25×10^{-10} sec and it decays by two-photon emission), and the triplet (ortho) Ps with parallel spin orientation ($\uparrow\uparrow$) with a considerably longer intrinsic lifetime of 1.4×10^{-7} sec (Figure 2). Its self-annihilation occurs via three-photon emission. Ortho and para Ps are formed normally in the ratio of 3:1.

Despite this short lifetime, which rules out conventional product analysis as e.g. used in the reactions of tritium, the Ps is an excellent labelled hydrogen atom for the investigation of the properties and the chemical and physical processes in matter; this is because its lifetime and the mechanism of its annihilation process are determined by the chemical and physical states of the environment.

The potential of the positron annihilation and the Ps atom to the solution of physical problems has been recognized rather early by physicists, and here especially, in the area of solid-state physics, where this method is now well advanced and has become a standard technique e.g. for defect studies and for Fermi surface determinations in metals (*8*). On the other hand, the development of the positron annihilation

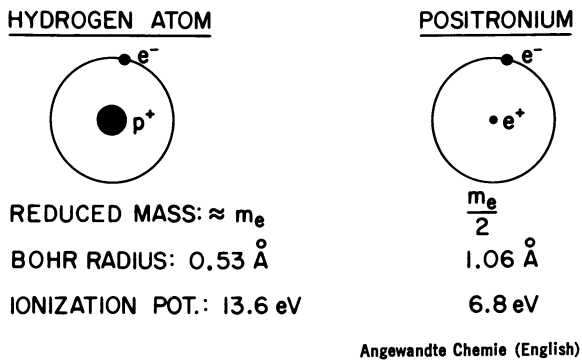

Figure 1. Characteristics of hydrogen and Ps atoms (5)

Publication Date: June 1, 1979 | doi: 10.1021/ba-1979-0175.ch001

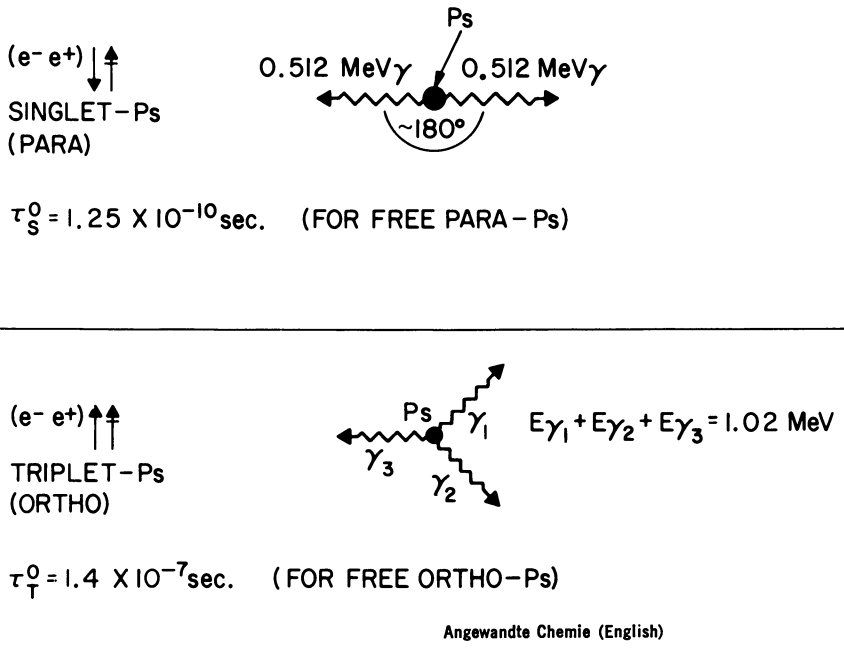

Figure 2. Ps annihilation characteristics (5)

method as a probe for chemical properties, i.e. the Ps chemistry, has proceeded rather slowly since the discovery of Ps by Martin Deutsch in 1951 (*9*).

It is interesting to note that in the early stages a major contribution in the area of Ps chemistry was and still is made by scientists trained by physicists.

However, despite all the pioneering efforts by these groups, chemists remained rather indifferent to this new atom and it was only during the past five to seven years that chemists of all persuasions have become more and more involved in the chemistry of this exotic atom, and have provided the diversity and expertise to develop this technique to a new general tool for the solution of chemical problems.

Thus I believe it is rather appropriate at this point in time to assess what has been accomplished so far in Ps chemistry, what we know about the reaction of the Ps, and where we are going from here.

As in the case of any new technique one can distinguish two stages. The first stage can be considered as the study of the basic features of this particular effect, or, as in this case, as the study of the underlying features, chemical or physical processes, which alter the fate of the Ps atom. The second stage of research carries more significance for the chemist and is concerned with the question of how we can in turn utilize

Publication Date: June 1, 1979 | doi: 10.1021/ba-1979-0175.ch001

the knowledge gained in the first stage to develop this new technique, or the reactions of the new atom to obtain new chemical information, over and above that of what can be assessed by other conventional techniques.

It is my contention that we have successfully finished the first stage and that we have to direct our attention now to the second stage, a task for which we need the cooperation of chemists in all areas of chemistry reaching from nuclear and radiation chemistry to bio- and enzyme chemistry. However, before I venture into a discussion of where or into which areas I see a special advantage in applying this nuclear technique, I would like to sumamrize briefly some of the essential features of Ps chemistry.

Basically the chemical information about the environment in which positron or Ps is formed comes from the observation of two processes: the Ps formation and the reactions of the Ps atom.

Let me explain the second process first and let us concentrate on the question of which reactions the ortho Ps (*o*-Ps) can undergo. (Because of the extremely short lifetime of the para species, the following discussion is restricted to the reaction of the *o*-Ps).

Publication Date: June 1, 1979 | doi: 10.1021/ba-1979-0175.ch001

Basic Features of Positronium Interactions with Matter

Quantum mechanics predicts that the annihilation lifetime of the positron is determined basically by the degree of overlapping of positron and electron wave functions, which leads e.g. to the intrinsic lifetime of *o*-Ps of 1.4×10^{-7} sec.

The laws of conservation of energy and momentum also require that the self-annihilation of the *o*-Ps occurs via three-quantum annihilation.

In the past, several reaction mechanisms were discussed, such as pick-off annihilation, oxidation, and spin conversion. All these processes result in a definite shortening of the positron lifetime and in a drastic increase of the two-photon annihilation rate (Figure 3). (Previous reviews can be found in References *1–7*).

Unfortunately, some of the concepts such as pick-off annihilation and the bubble model are foreign to the vocabulary of the organic or biochemist. Thus in order to describe the various reaction types between Ps atoms and molecules we more recently have discussed these reactions in a scheme which is based on simple gas kinetic principles familiar to every chemist (*10*).

As shown in Figure 4 the basic assumption is that in a collision between *o*-Ps and another molecule a more or less long-lived collision complex is formed, in which the electron density at the positron of the positron is increased drastically. The average time that the Ps spends in this complex will depend on the stability of this complex. If only weak (van der Waals) forces are operative in holding this complex together,

Publication Date: June 1, 1979 | doi: 10.1021/ba-1979-0175.ch001

REACTION	MECHANISM	AVERAGE LIFETIME OF PRODUCT (sec)	PHOTONS EMITTED	AVERAGE LIFETIME OF o-Ps APPEARS TO BE
PICKOFF	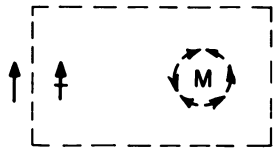	—	$2\gamma/3\gamma = 372/1$	SHORTER
CONVERSION		1.25×10^{-10} (p-Ps)	2γ	SHORTER
OXIDATION	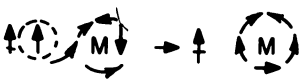	$\sim 0.5 \times 10^{-10}$ (IN COND. PHASE) (FREE POSITRON)	$2\gamma/3\gamma = 372/1$	SHORTER
COMPOUND FORMATION		est. $\sim 0.5 \times 10^{-10}$ (COMPLEX)	$2\gamma/3\gamma = 372/1$	SHORTER

Angewandte Chemie (English)

Figure 3. Quenching reactions of o-Ps (The ratio $2\gamma/3\gamma$ represents the ratio of annihilation events occurring via 2-photon and 3-photon emission). (Intrinsic lifetime $\tau_T^\circ = 1.4 \times 10^{-7}$ sec (5).)

In Positronium and Muonium Chemistry; Ache, H.; Advances in Chemistry; American Chemical Society: Washington, DC, 1979.

Publication Date: June 1, 1979 | doi: 10.1021/ba-1979-0175.ch001

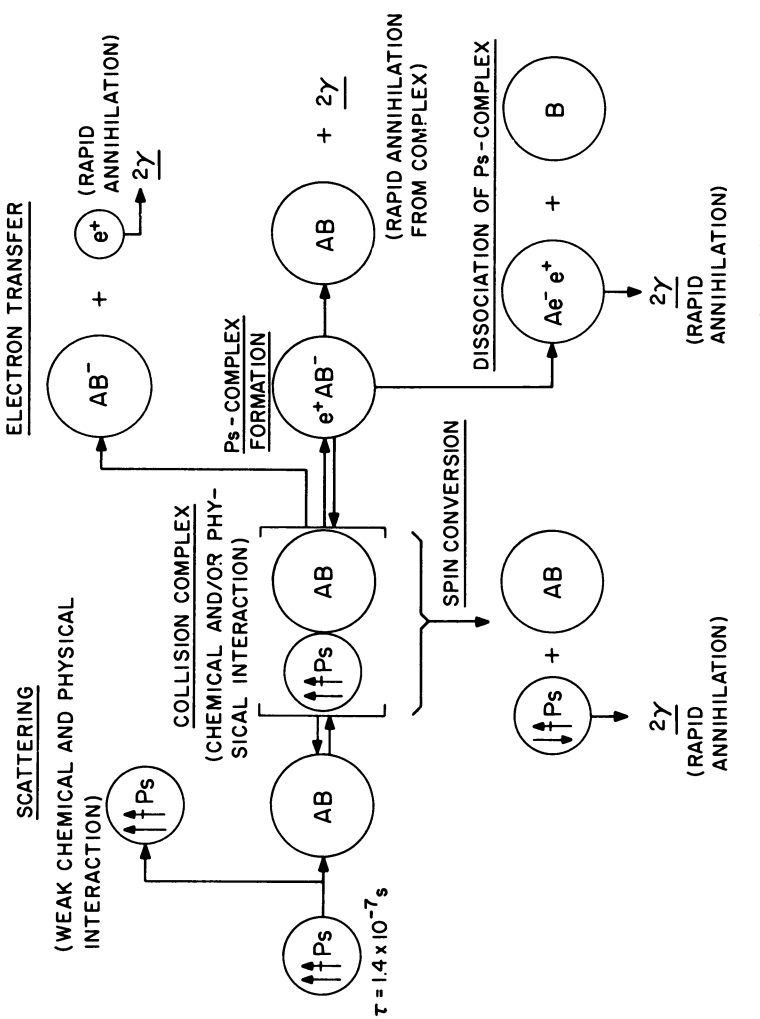

Figure 4. Schematic of possible o-Ps interactions with matter via Ps-M collision complex (10)

the Ps will spend only very little time in this environment, and the positron experiences the effect of the increased electron density only for a short time. Thus the average lifetime of the Ps appears only slightly shorter as compared with the intrinsic lifetime of the *o*-Ps. On the other hand, if this Ps collision complex undergoes stabilization involving genuine chemical forces, e.g. bond formation, then the positron will find itself in an environment of high electron density for a prolonged period and its lifetime will be reduced substantially. In other cases this complex may be just a transition state leading to electron transfer from Ps to substrate, i.e. oxidation of Ps. The product of this latter process is a free positron, whose lifetime in condensed matter is considerably shorter (0.1–0.5 nsec) than that of the *o*-Ps. If the substrate is paramagnetic the collision can result in a spin conversion from *o*- to *p*-Ps, whose intrinsic lifetime is only 1.25×10^{-10} sec. (Because of the extremely short intrinsic lifetime of the *p*-Ps, reactions of this species can be neglected). Thus, one generally can state that all interactions of the *o*-Ps with matter lead to a shortening of its apparent lifetime.

For an accurate determination of the reactivity of thermal Ps toward various substrates these qualitative predictions had to be developed to a quantitative method which allows the calculation of the chemical rate constants for the reactions between Ps and substrate (*10*).

This can be accomplished by setting up appropriate kinetic equations and subsequent integration of the resulting differential equations from which the population of the various states in which the positrons exist as *o*-Ps and PsM can be found as a function of time. From these values and the positron annihilation constants for these states, an equation for the time-dependent, two-photon annihilation rate can be obtained. This in turn allows the determination of the chemical reaction rate constants by utilizing sophisticated nuclear chemical lifetime measurement techniques as described in the following section.

Publication Date: June 1, 1979 | doi: 10.1021/ba-1979-0175.ch001

Experimental Measurements of Positronium Reactions and Formation

In order to observe changes in Ps reaction rates and in the Ps formation probability two different methods are most frequently used. (A complete discussion of the details of the various methods can be found in References *1–7*.)

Positron Lifetime Measurements. The first step for a quantitative evaluation of the experimentally accessible positron lifetime data and in terms of the kinetic parameters and rate constants for the chemical reaction between Ps and substrate molecules is to set up a reaction scheme which considers the various interactions between the reactants.

This can be demonstrated by using the reaction scheme on Figure 4 as an example. To simplify the issue we want to assume that the substrate AB or M is diamagnetic, which excludes spin conversion, and that the reaction between *o*-Ps and molecules M is solely caused by *o*-Ps–molecule-complex formation PsM, from which annihilation takes place. If oxidation occurs, the reaction proceeds via the *o*-PsM complex as the rate-determining step.

Thus the process can be described by the following reaction scheme:

$$2\gamma \xleftarrow[\lambda_p]{\text{annihilation in solvent}} o\text{-Ps} + \text{M} \underset{K_2}{\overset{K_1}{\rightleftharpoons}} o\text{-PsM} \xrightarrow[\text{annihilation in complex}]{\lambda_c} 2\gamma.$$

According to this scheme the following reactions have been considered: reactions of Ps with substrate M to form a Ps complex, PsM (rate constant K_1); decomposition of PsM (rate constant K_2); position annihilation in complex (decay constant λ_c); and annihilation of Ps in bulk solvent with annihilation constant λ_p.

Since the concentration of M remains essentially constant throughout the experiment, the mechanism can be simplified to:

$$K_1' = K_1[\text{M}]$$

$$2\gamma \xleftarrow{\lambda_p} o\text{-Ps} \underset{K_2}{\overset{K_1'}{\rightleftharpoons}} o\text{-PsM} \xrightarrow{\lambda_c} 2\gamma$$

Appropriate kinetic equations can be set up for the population of the various states N in which the positron can reside if no oxidation or spin conversion occurs and if reactions of the *p*-Ps are neglected because of its large self-annihilation constant, λ_s. N_F, N_T, N_S, and N_C denote the free positron state, the *o*-Ps, *p*-Ps, and the PsM complex (λ_F is the annihilation constant for free positrons; the self-annihilation of *o*-Ps can be neglected).

$$\frac{dN_F}{dt} = -\lambda_F[N_F]$$

$$\frac{dN_S}{dt} = -\lambda_S[N_S]$$

$$\frac{dN_T}{dt} = -(K_1' + \lambda_p)[N_T] + [K_2][N_C]$$

$$\frac{dN_C}{dt} = K_1'[N_T] - (K_2 + \lambda_c)[N_C]$$

Publication Date: June 1, 1979 | doi: 10.1021/ba-1979-0175.ch001

Since the time-dependent, two-photon annihilation rate, $R_{2\gamma}$, which is measured by the delayed coincidence counting as discussed below, is the result of the annihilation of free positrons, *p*-Ps, and the positron bound in the Ps complex, one has to know the time-dependent population of each of these states.

This is accomplished by the integration of the differential equations using the proper initial condition for $N_c = 0$ at time 0:

$$N_F = N_F{}^{\circ}{}^{\exp}[-\lambda_F t]$$

$$N_S = N_S{}^{\circ}{}^{\exp}[-\lambda_S t]$$

and for N_c: if $(K_2 + \lambda_C) >> K\,[M]$, ([M] is the substrate concentration), and one can approximate:

$$N_C = C(\exp[-(\lambda_c + K_2)t] + \exp\left[-\left(\lambda_p + \frac{K_1\lambda_c}{K_2 + \lambda_c}[M]t\right)\right]$$

since

$$R_{2(t)} = \lambda_F N_F + \lambda_S N_S + \lambda_C N_C$$

$$R_{2\gamma(t)} = A\exp[-\lambda_F t] + B\exp[-\lambda_s t] + C\exp[-(\lambda_c + K_2)t] + C\exp\left[-\left(\lambda_p + \frac{K_1\lambda_c}{K_2 + \lambda_c}[M]\right)t\right].$$

In condensed matter it is assumed that the annihilation constants for free positron, *p*-Ps, and annihilation positrons in the complex are approximately the same:

$$\lambda_1 = \lambda_F \simeq \lambda_s \simeq \lambda_c >> \left(\lambda_p + \frac{K_1\lambda_c}{K_2 + \lambda_c}[M]\right).$$

The following two-exponential equation for $R_{2\gamma(t)}$ can be derived from the above equation:

$$R_{2\gamma(t)} = D\exp[-\lambda_1 t] + C\exp[-\lambda_2 t]$$

where:

$$\lambda_2 = \lambda_p + \underbrace{\frac{K_1\lambda_c}{K_2 + \lambda_c}}_{K_{obs}}[M].$$

Publication Date: June 1, 1979 | doi: 10.1021/ba-1979-0175.ch001

By determining λ_p, which is identical (in dilute solutions) with λ_2 measured in the pure solvent, and knowing the solute concentration, [M], the apparent constant for Ps reaction is given by:

$$K_{obs} = \frac{\lambda_2 - \lambda_p}{[M]}.$$

In order to obtain rate constants for the reaction of Ps (or positrons) with substrate molecules or to follow changes in the reactivity of a certain medium towards Ps, the time-dependent, two-photon annihilation rate (*see* above) has to be determined. This is accomplished by positron lifetime measurements utilizing conventional fast–slow, γ–γ coincidence methods.

The positron emitter used is ^{22}Na, which decays under emission of a positron to the excited state of ^{22}Ne, which in turn undergoes de-excitation under emission of a 1.28-MeV photon. The lifetime of the excited ^{22}Ne is only 3 psec, so that for all practical purposes the emission of the positron and 1.28-MeV photon is considered to occur simultaneously (Figure 5).

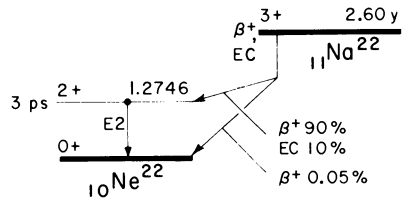

Angewandte Chemie (English)

Figure 5. Decay scheme for ^{22}Na (5).

Thus the positron lifetime distribution can be determined by observing the time elapsed between the generation of the 1.28-MeV photon and the appearance of the 0.51-MeV photons resulting from the annihilation of the positron. These time measurements can be carried out by conventional fast–slow coincidence techniques (Figure 6).

The 1.28-MeV photon is observed with a plastic detector, e.g. Naton 136. The output signal from the anode of the attached photomultiplier serves as the starting signal for the time–pulse height converter (TPHC). A second, similar type of detector observes one of the two annihilation photons (0.51 MeV). The signal from this detector serves as the stop signal for the TPHC. The amplitude of the output signal of the TPHC is thus proportional to the time difference between the arrival of the start signal and that of the stop signal in the TPHC. The time calibration of the system is effected by a built-in delay unit. The signal from the TPHC passes into a multichannel pulse height analyzer, and is recorded on one of the channels according to its pulse height, provided that the instrument has been activated by a signal from the slow coincidence unit (*see* below).

Publication Date: June 1, 1979 | doi: 10.1021/ba-1979-0175.ch001

Publication Date: June 1, 1979 | doi: 10.1021/ba-1979-0175.ch001

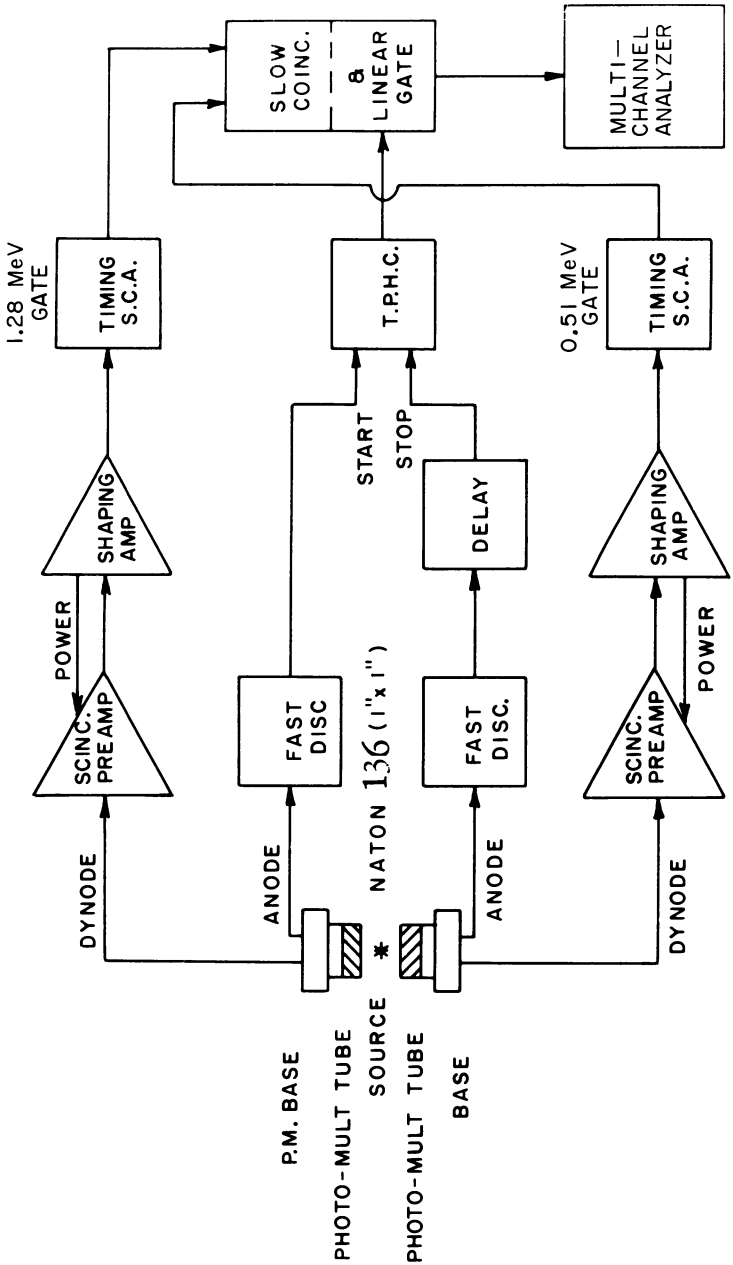

Figure 6. Typical experimental arrangement using the principle of delayed coincidence (simple fast–slow timing system)

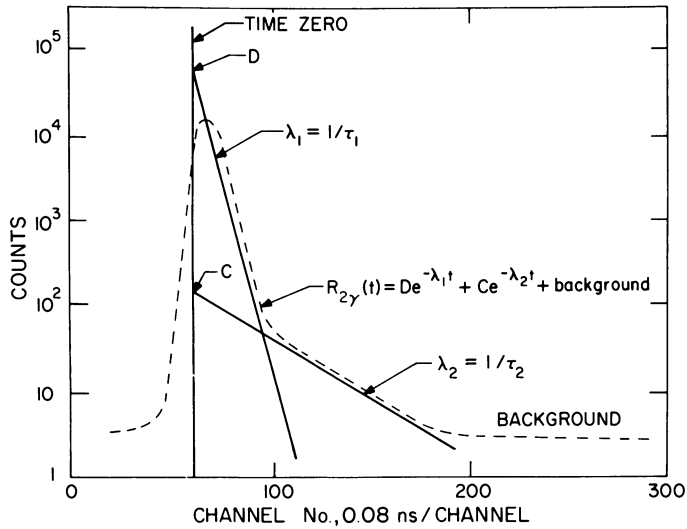

Figure 7. Typical positron lifetime distribution curve as acquired by fast–slow coincidence technique

To reduce the number of random coincidences and to improve the time resolution of the measuring equipment, a second slow coincidence circuit should be incorporated. For this purpose, a signal from the dynode of the photomultiplier, after passage through a preamplifier and a main amplifier, is led into single-channel pulse height analyzers, one of which passes only signals corresponding to a photon energy of 1.28 MeV, while the other passes only signals corresponding to a photon energy of 0.51 MeV. If two signals filtered in this way by the two single-channel pulse height analyzers enter the slow coincidence unit within a specified period (usually 1 μsec), they activate the multichannel pulse height analyzer (*see* above) for a short time and allow the signals arriving from the TPHC during this time to be recorded. (A more detailed description of the various components used in these lifetime measurements and further references can be found in Reference *4*.)

A positron lifetime spectrum, Figure 7 recorded in this way should represent the two-photon annihilation rate and correspond to the two-exponential equation as discussed above. It can be dissolved into two components. Several computer programs, such as POSITRONFIT (*11*), POSITRONFIT EXTENDED (*12*), PAL (*13*), and others (*15*) are available for this purpose.

Consistent with the rate equation for the two-photon annihilation, the short-lived component with an associated lifetime τ_1 or decay constant and intensity I_1 can be attributed to the annihilation of the free positron, the annihilation of the products formed in the reaction of hot *o*-Ps, and

Publication Date: June 1, 1979 | doi: 10.1021/ba-1979-0175.ch001

the self-annihilation of *p*-Ps. The long-lived component displaying a lifetime τ_2, decay constant, and intensity I_2 is attributed to the annihilation of thermalized *o*-Ps.

If other processes such as oxidation or spin conversion are involved the reaction scheme will have to be altered and other kinetic equations generated. Examples for these procedures can be found in several review articles (*1–7*).

Determination of Positronium Yields and Positron and Positronium Reaction Measurements in Two-Quantum Annihilation (*1–7*). In two-quantum annihilation the deviation of the angle between the emission directions of the two-quantum annihilation of the two 0.51-MeV photons from 180° corresponds to

$$\Delta\Theta \sim 2\,v/c$$

where c is the velocity of light and v is the velocity of the center of mass of the electron and the positron in the system in question. The deviation, which is only a few milliradians in all practical cases, can be measured with the aid of the system outlined in Figure 8. The 0.51-MeV photons produced in the same act of annihilation are recorded in this system as a function of $\Delta\Theta$. The form of such angular distribution curves provides a basis for conclusions regarding both the various annihilation mechanisms and the reactions of *o*-Ps and its formation.

Free positrons usually annihilate with electrons located in outer shells of the atom, which have a certain momentum; the angle between the two annihilation quanta therefore differs considerably from 180°, and leads to

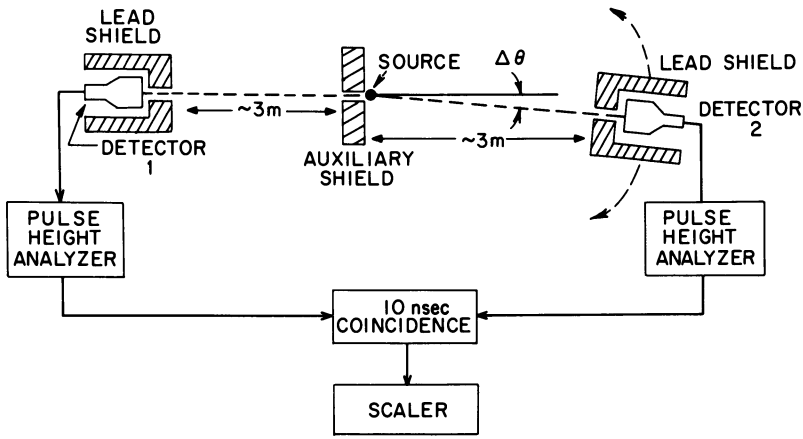

Angewandte Chemie (English)

Figure 8. Typical experimental arrangement for determining the angular distribution (ΔΘ = deviation from 180°) (5)

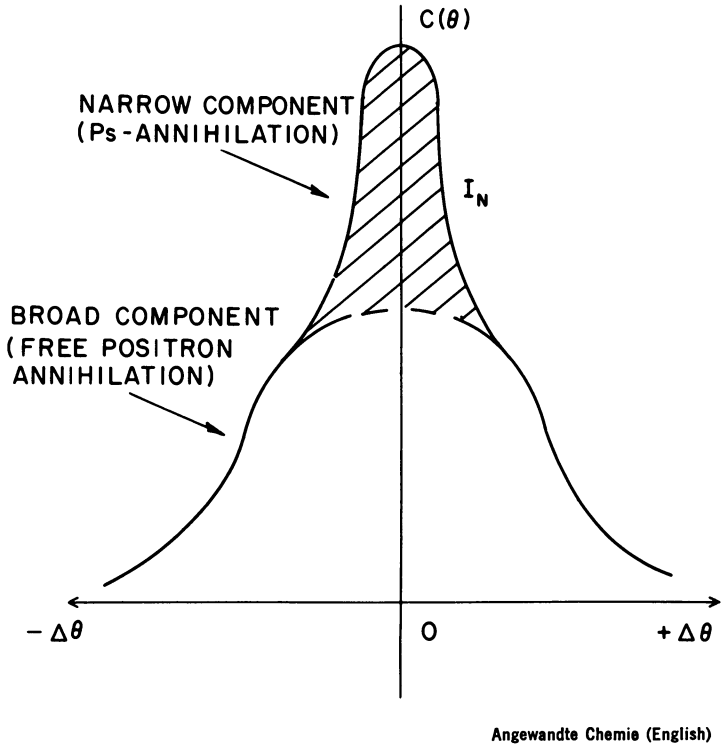

Figure 9. Angular distribution in two-quantum annihilation: frequency of 2γ coincidences (C(Θ)) as a function of ΔΘ. The narrow component (I_N) is shaded (5).

the broad component in the angular distribution curves (Figure 9). The heavier *p*-Ps, on the other hand, loses most of its kinetic energy very rapidly after its formation and has very little momentum left at the instant of annihilation; the photons emitted in this case deviate only slightly from 180° and are responsible for the occurrence of the narrow component in the angular distribution curves. The formation of *p*-Ps can be very readily recognized from the presence of the narrow component (Figure 9), and a change in the *p*-Ps formation yield can be observed by a relative increase or decrease of the area under the narrow component. However, this method is not confined to the detection of Ps. It also can be used to follow its various reactions. Increased ortho–para conversion, for example, causes more positrons to be annihilated in the form of *p*-Ps. This causes increased two-quantum annihilation with a relatively wide angular distribution; the intensity of the broad component increases, while that of the narrow component does not change. However, if *p*-Ps also is involved in the chemical reaction or in the pick-off (this is generally possible only if

Publication Date: June 1, 1979 | doi: 10.1021/ba-1979-0175.ch001

these reactions are much faster than the self-annihilation of *p*-Ps), the result is an absolute weakening of the narrow component instead of a relative weakening. Computational methods for the analysis of these angular correlation data such as the PAACFIT program (*16*) are available.

Positronium Reaction via Positronium Molecule Complex Formation

The experimental results show pronounced differences in the capabilities of the various chemical substances to annihilate Ps atoms more or less effectively. The compounds investigated generally can be divided into two categories (Table I) (*11–37*). The first one which shows only weak interaction with Ps ($K_{obs} < 10^8\ M^{-1}\ sec^{-1}$), is composed of hydrocarbons, halogenated hydrocarbons, aliphatic nitro compounds, and diamagnetic inorganic ions whose standard redox potentials in aqueous solution are more negative than −0.9 eV. The second group encompasses nitroaromatics, quinones, halogens, conjugated anhydrides, tetracyanoethylene, organic ions, and inorganic ions with a standard redox potential of greater than −0.9 eV and displays a strong reactivity towards Ps ($K_{obs} > 10^8\ M^{-1}\ sec^{-1}$).

On the basis of the above reaction scheme (Figure 4) the rather small reactivity of e.g. the alkanes toward Ps can be explained by assuming that in these cases only relatively weak attraction (in the collision complex) exists between Ps and molecules, which is mainly caused by the weak Van der Waals forces. Since Van der Waals interaction is a function of the polarizability of the molecule, the stability of the Ps–M complex and thus the positron lifetime (and the reaction constant for the Ps molecule reaction) should also be a function of the polarizabilities, a relationship which has indeed been observed (*17*) (Figure 10).

Table I. Examples of Chemical Compounds Showing Strong/Weak Interactions with Thermal Positronium Atoms (*10*)

Strong Interaction $K_{obs} > 10^8\ M^{-1}\ s^{-1}$	*Weak Interaction* $K_{obs} < 10^8\ M^{-1}\ s^{-1}$
Nitroaromatics	simple aliphatic or aromatic hydrocarbons:
Quinones	alkanes, benzene, anthracene, etc.
Maleic anhydride	aniline, phenol, haloalkanes
Tetracyanoethylene	
Halogens	halobenzenes, aliphatic nitro compounds
Inorganic ions in solution ($E_o > -0.9$ eV)	phthalic anhydride, benzonitrile
Organic ions in solution	(diamagnetic) inorganic ions in solution ($E_o < -0.9$ eV)

Publication Date: June 1, 1979 | doi: 10.1021/ba-1979-0175.ch001

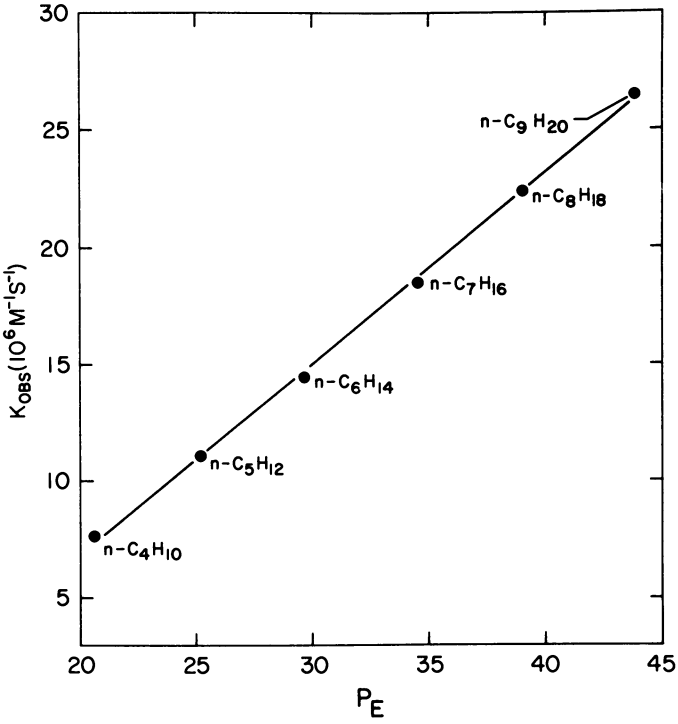

Figure 10. Electronic polarizabilities P_E of simple hydrocarbons plotted against rate constants K_{obs} for reactions with thermal o-Ps

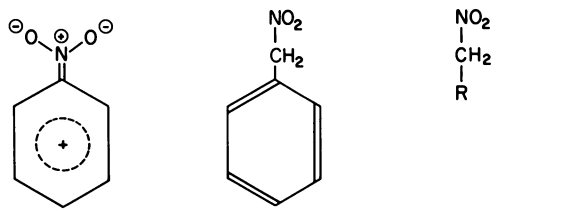

2.7 x 10^{10} 1.46 x 10^8

R:	
-H	3.47 x 10^7
$-CH_3$	4.55 x 10^7
$-CH_2CH_3$	5.17 x 10^7

Journal of the American Chemical Society

Figure 11. Demonstration of the steric effect on the Ps rate constants (K_{obs}) by introducing methyl groups in ortho position at the nitro group. (K_{obs} measured in dilute benzene solutions at 20°). (Isolating the nitro group from the π system lowers the rate constants (M^{-1} sec^{-1}).) (10)

In the case of the strongly reactive (diamagnetic) neutral organic substances shown in Table 1 one has to realize that these compounds are highly conjugated and contain strongly electronegative elements such as oxygen and nitrogen. All of them are strong electron acceptors and form stable molecular complexes with conventional compounds. We therefore suggested that their reactions with Ps can be considered as Ps–M complex formation (*10*). The reaction mechanism in solution then can be formulated as follows:

$$\mathrm{Ps} + \mathrm{M} \underset{K_2}{\overset{K_1}{\rightleftharpoons}} \mathrm{PsM}$$

annihilation with solvent ↓ 2γ annihilation in complex ↓ 2γ

This analogy is further supported by the fact that the same parameters that enhance the stability of conventional molecule complexes as reported in References *38*, *39*, and *41* also increase the stability of the Ps–M complexes, as indicated by the observed complex formation enthalpies ΔH. In the series of the nitrobenzene derivatives the ΔH is clearly a function of the nature of the derivative and is in the case of the *p*-dinitrobenzene–Ps complex about −8 Kcal/mol, whereas the less stable *p*-nitroaniline–Ps complex exhibits a ΔH of only −1 Kcal/mol.

The effect of the electron density distribution in the molecule on the capability of the molecule to form the Ps–molecule complexes also is clearly demonstrated in the ortho effect: while the complex formation

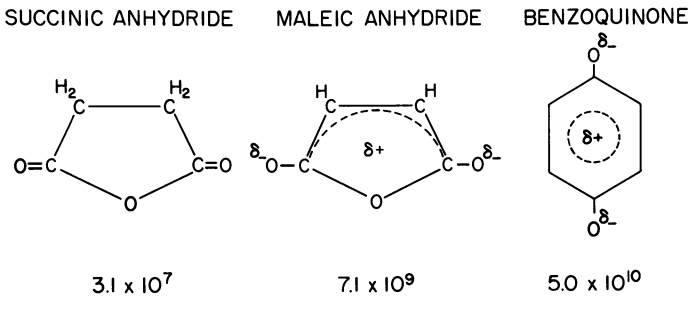

Journal of the American Chemical Society

Figure 12. Demonstration of the effect of conjugation on the Ps rate constants K_{obs} in cyclic anhydrides (K_{obs} measured in dilute benzene solutions at 20°) (10)

Publication Date: June 1, 1979 | doi: 10.1021/ba-1979-0175.ch001

enthalpy ΔH for *p*- and *m*-nitrotoluene is about −4.3 Kcal/mol, the corresponding values for *o*-nitrotoluene or 2,6-dimethylnitrotoluene are only −3.8 and −2.0 Kcal/mol, respectively (*23, 24*). The explanation for this behavior can be seen in the fact that in the latter cases the ortho substituent prevents the nitro group from being in the plane of the acceptor ring, i.e. the coplanarity and conjugation will be reduced (Figure 11). The importance of the degree of conjugation available in the acceptor also becomes clearly visible by comparing the rate constants for the highly reactive) fully conjugated maleic anhydride on one hand and succinic anhydride, where no conjugation exists, on the other hand (Figure 12). It is also apparent in the case of the (non-conjugated) α-nitrotoluene and the aliphatic nitro compound, where the reactivity toward Ps is reduced drastically (*10*) (Figure 13).

While similar complexes can be postulated for the interaction of the halogens with Ps the results observed in aqueous solutions of simple inorganic ions may be understood as electron transfer reactions possibly proceeding via the postulated collision complex (Figure 4):

$$A_{aq}^{n+} + Ps \rightarrow A_{aq}^{(n-1)+} + e_{aq}^{+}$$

$$\downarrow$$

$$2\gamma$$

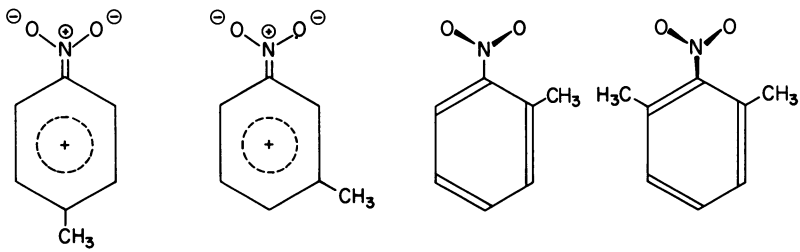

2.2 x 10^{10} 2.1 x 10^{10} 0.85 x 10^{10} 0.039 x 10^{10}

Journal of the American Chemical Society

Figure 13. Demonstration of the effect of conjugation on Ps rate constants (K_{obs}) in various nitro compounds (K_{obs} measured in dilute benzene solutions at 20°). (The steric interaction of the methyl group forces the nitro group out of the plane of the ring. Loss of configuration results in a reduction of the rate constants (M^{-1} sec^{-1}).) (10)

Publication Date: June 1, 1979 | doi: 10.1021/ba-1979-0175.ch001

Publication Date: June 1, 1979 | doi: 10.1021/ba-1979-0175.ch001

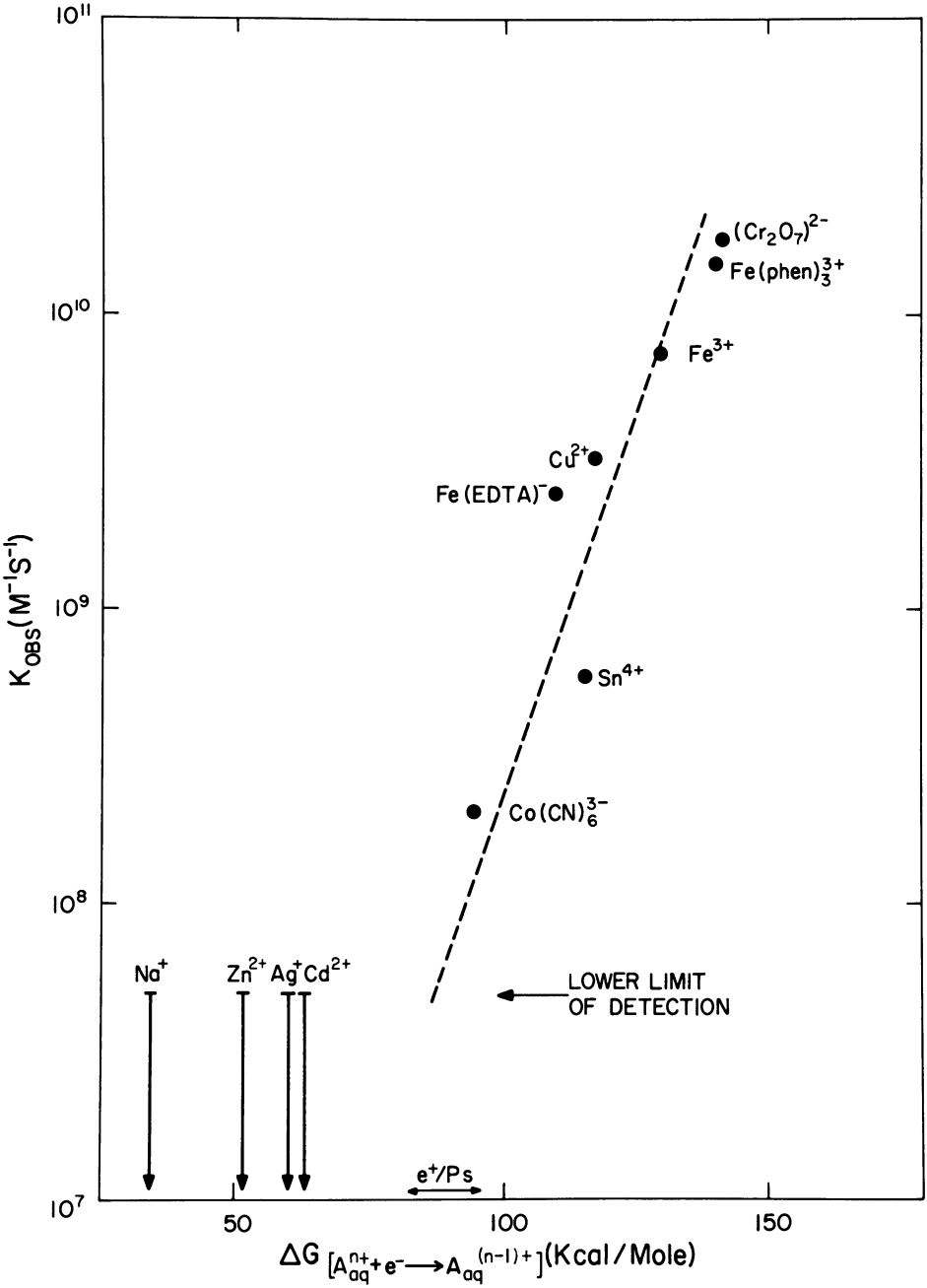

Figure 14. Rate constants of Ps atom reactions with various inorganic ions in aqueous solutions as a function of ΔG for one-electron transfer (at room temperature)

Table II. Calculated Positron and Positronium

	Positron Affinity[a] *eV*	*Positronium Affinity*[a] *eV*
C_6H_6	−.06	−7.62 ± .60
$C_6H_5CH_3$	.46	−2.32 ± .19
C_6H_5F	.17	−2.68 ± .36
$C_6H_5NO_2$	−.16	1.11 ± .81
C_6H_5CN	.24	−1.84 ± .08
C_6H_5CHO	.44	−0.09 ± .47
p-$C_6H_4O_2$	−.35	−1.88 ± .03

[a] Ref. *43*.
[b] Ref. *47*.
[c] Uncertainties are caused by an incompletely determined parameter, $k^{(+)}$, in their method.

Publication Date: June 1, 1979 | doi: 10.1021/ba-1979-0175.ch001

This reaction can take place when it is energetically possible. A systematic investigation of these oxidation reactions suggests a correlation between the standard redox potentials and the observed rate constants. A more refined treatment would have to take into account rearrangement entropies, etc. (*32*) from which a hypothetical standard redox potential of −0.9– −1.1 V can be obtained (Figure 14).

Ps also can be formed with excess kinetic energies as discussed below in which case additional reaction channels become available, e.g. the reduction of inorganic ions such as Mg_{aq}^{2+}, Zn_{aq}^{2+}, with a standard redox potential more negative than −0.9 V (*28, 33*).

Positronium Reactions as a Probe for Intermolecular Interations

How can a study of Ps interactions contribute to our understanding of chemical reactions in general? From the above discussion of the correlation between the reactivity of the Ps and characteristic properties of the substrate molecule it is quite obvious that the Ps atom used as a chemical probe is quite sensitive to molecular properties and in turn can be used to solve fundamental problems in physical chemistry, e.g. determination of electron density distribution in molecules, intermolecular interactions, and the assessment of the role of kinetic and diffusion-controlled processes in solution.

Fundamentally the studies on Ps–molecule complex formation (*10*) as described above can be considered as the first step of a more in-depth study of the factors governing the intermolecular interaction between molecules in general by using the Ps as a chemical probe. If it can be demonstrated conclusively, (and the experiments with Ps in solution seem to indicate it so far) that the energy of interaction between Ps and substrate is indeed controlled by the same parameters as in the con-

In Positronium and Muonium Chemistry; Ache, H.;
Advances in Chemistry; American Chemical Society: Washington, DC, 1979.

Affinities of Benzene and Related Compounds

Positronium Affinity[b, c] *eV*	ΔH_{eq} *(Kcal/mol) Obeserved for Ps Complex Formation*[d]	K_{obs}[e] *for Reactions with Compound* M^{-1} s^{-1}[d]
-2.18 ± 3.80	< 0.1	3.8×10^7
-2.20 ± 3.85	< 0.1	3.9×10^7
1.05 ± 3.25	< 0.1	3.2×10^7
0.31 ± 4.42	-8.0	2.7×10^{10}
-0.21 ± 4.49	< 0.1	5.2×10^7
3.44 ± 3.45	< 0.1	4.9×10^7
3.50 ± 4.13	-8.0	5.0×10^{10}

[d] Ref. *10*.
[e] Determined at room temperature.

Publication Date: June 1, 1979 | doi: 10.1021/ba-1979-0175.ch001

ventional molecular complexes, i.e. by electrostatic and resonance terms, then it is feasible to use the Ps atom as a powerful probe for the study of the kinetics and mechanisms of molecule complex formation. Since the simple nature of the Ps particle lends itself both to reasonably straightforward theoretical calculation (*42–47*) and to relatively easy experimental tests of theoretical models of intermolecular interaction, this method appears to be uniquely suitable for such an investigation. A comparison of the results obtained in some tentative quantum mechanical calculation (*43, 47*) of the Ps affinity with experimental results (*10*) is made in Table II.

Furthermore, the stability of the Ps–M complex is a function of the nature of the solvent (*10, 48, 49*); thus this method also may be used to study the solvation capabilities of a series of solvents. It is very important that Ps reactions, because of the extremely small mass of the Ps, should occur via tunneling even at room temperature. This would allow a convenient study of this quantum mechanical phenomenon.

Positronium Reactions as a Nuclear Probe in Biological Systems

A practical application of the Ps interactions which we investigated recently in our laboratory was the determination of the molecular association constants of various molecules of biological interest (*50, 51*). This opens up an interesting new field for utilizing this new technique in the study of biological reactions.

This method is based on the fact that the reactivity of an acceptor molecule toward Ps is altered drastically if it has formed a molecular complex with a conventional donor (Table III) (*50, 51, 52, 53*).

Instead of a two-compound system, in which the Ps reacts either with the substrate molecule or the solvent, one has now to consider a sys-

Table III. Complex Formation Constants, K_c, and Apparent Rate Nitrobenzene

Compound	$K_{obsd} \times 10^{-10}\ M^{-1}\ s^{-1}$
TCNE	3.9 ± 0.2
TCNE–HMB	1.8 ± 0.2
TCNE–mesitylene	0.24 ± 0.02
NB	2.7 ± 0.2
NB–HMB	1.2 ± 0.2
NB–mesitylene	0.35 ± 0.02

[a] Determined by positron annihilation techniques.
[b] Also included are their molecule complexes with hexamethylbenzene and mesitylene in benzene solutions at room temperature.

Publication Date: June 1, 1979 | doi: 10.1021/ba-1979-0175.ch001

tem consisting of three components: the substrate in its uncomplexed form (A), in its complexed form (B), and the solvent (S). This equilibrium can be described schematically as follows:

$$2\gamma \xleftarrow{\lambda_c} \mathrm{PsB} \underset{K_B}{\overset{K_B'}{\rightleftharpoons}} \mathrm{Ps} + \mathrm{A} + \mathrm{B} + \mathrm{S} \underset{K_A}{\overset{K_A'}{\rightleftharpoons}} \mathrm{PsA} \xrightarrow{\lambda_c} 2\gamma$$

$$K_S \uparrow\downarrow K_S'$$

$$\mathrm{PsS}$$

$$\downarrow \lambda_c$$

$$2\gamma$$

By setting up the appropriate kinetic equations it is possible to correlate the experimentally observed two-photon annihilation rate with the complex formation constant or molecular association constant. Some of these examples are shown in Tables III and IV.

This method might prove to be most useful in cases where the uncomplexed donor or acceptor absorb at similar wavelengths as the molecule complex or where the solvent absorption interferes with the spectrophotometric determination of the complex formation constant.

For example, we were able to measure the complex formation constant for a series of molecular complexes of vitamin K_1 and α-tocopherolquinone with donors such as mono-, di-, and tri-*n*-butylamines, indol, and vitamin D_2 in solutions (*51*). To the best of our knowledge this is the first time that these constants have been determined.

The molecular association constants of the systems (K_c) studied in this investigation are generally very small, indicating that only very weak complexes are formed. The K_c observed for the vitamin K_1 complexes with mono-, di-, and tributylamine decreases in this order. The amines and indole were chosen because these groups are essential components of

Constants K_{obsd} for the Reactions of Tetracyanoethylene (TCNE) and (NB)[b] (50)

K_c, M^{-1}	K_c *spectrophotometric* M^{-1}
9.0 ± 1.0	12.95 ± 0.05
0.094 ± 0.01	
1.1 ± 0.3	
0.058 ± 0.01	

proteins which are known to act as donors in molecular complex formation in biological reactions with vitamin K_1 which, e.g. are responsible for the maintenance of the normal blood coagulation.

Since it is believed that the charge transfer in the complexes is accomplished by the unpaired electron of the nitrogen to the quinone group of the vitamin K_1 (or α-tocopherolquinone), this effect should be enhanced by the presence of additional *n*-butyl groups. The fact that the opposite was observed, namely that K_c decreases with the number of *n*-butyl groups present, is therefore not the result of an inductive effect, but could be explained in terms of a steric hindrance which makes the formation of the molecular complexes with the higher *n*-butyl-substituted donors more difficult.

Table IV. Complex Formation Constants, K_c, and the Apparent Rate Constants, K_{obs}, for the Acceptors Vitamin K_1, and α-Tocopherolquinone[a] (51)

Compound	$K_{obs} \times 10^{10}\ M^{-1}\ s^{-1}$	$K_c\ M^{-1}$
Vitamin K_1 in benzene	2.45	
Vitamin K_1–indole in benzene	1.51	0.50
Vitamin K_1 in cyclohexane	1.96	
Vitamin K_1–*n*-butylamine in cyclohexane	not detectable[b]	0.72
Vitamin K_1–dibutylamine in cyclohexane	not detectable[b]	0.54
Vitamin K_1–tributylamine in cyclohexane	not detectable[b]	0.24
Vitamin K_1–vitamin D_3 in cyclohexane	not detectable[b]	0.83
α-Tocopherolquinone in benzene	2.15	
α-Tocopherolquinone–indole in benzene	0.85	0.29

[a] Also included are their various molecular complexes determined by the positron annihilation technique.

[b] The reactivity of the molecular complex toward Ps is below the detectable limit ($K_{QD(obs)} < 0.2 \times 10^{10}\ M^{-1}\ s^{-1}$) inherent to the method of evaluation.

Vitamin D_3 has been known as a good electron donor in biological molecular complex formation. The results of the present study where the formation constants K_c for vitamin K_1–vitamin D_3 complexes have been assessed in cyclohexane solution confirm this observation and suggest very similar donor capabilities for vitamin D_3 and mono-*n*-butylamine.

The strong reactivity displayed by α-tocopherolquinone, which is believed to be one of the major products in the oxidation process of vitamin E, toward Ps may open up an interesting possibility of studying the oxidation process of vitamin E.

While α-tocopherolquinone reacts very rapidly with Ps, the rate constant is 2.5×10^{10} M^{-1} sec^{-1} in benzene, and is even relatively reactive in its complex with indole ($K_{obs} = 0.85 \times 10^{10}$ M^{-1} sec^{-1}), the nonoxidized vitamin E shows (in benzene solution) hardly any reactivity toward Ps. Thus this drastic difference in the behavior of the oxidation product of vitamin E and vitamin E itself could be utilized for further studies of the biologically interesting autoxidation of the unsaturated fatty acids.

In summary, these initial investigations of molecular associations in biological systems by positron annihilation techniques seem to support the feasibility of this new technique in the study of biological reactions.

Positronium Reactions as a Nuclear Probe for the Properties of Inclusion Compounds

This type of work can be extended to another group of compounds—the so-called inclusion compounds. The most prominent compounds in this respect are the cycloamyloses and their most interesting characteristic is their ability to complex a variety of guest molecules in a cavity of about 4.5 Å diameter which they form and thus catalyze or inhibit certain reactions. The rates of this complex formation has been studied in the past

Table V. Inclusion Complex Formation Constants, K_c, and Apparent Rate Constants, K_{obs}, for *p*-Nitrophenol, Nitrobenzene, and *p*-Benzoquinone[a] (54)

Compound	K_{obs} (10^{10} M^{-1} sec^{-1})	K_c (M^{-1})	K_c *Spectroscopic* (M^{-1})
p-Nitrophenol	.88	—	—
p-Nitrophenol–CD	.11	341	385[b]
Nitrobenzene	1.38	—	—
Nitrobenzene–CD	.09	48.6	—
Quinone	1.37	—	—
Quinone–CD	not determined	6.8	—

[a] Also included are their inclusion compounds with cyclohexaamylose (α-cyclodextrin, CD) at $p = 3.5$, $I = .5$ in water solution.
[b] Ref. 55.

mostly with temperature jump techniques and UV spectroscopy. We have used the different reactivity which compounds like nitrobenzene, *p*-nitrophenol, and *p*-benzoquinone show toward Ps in their uncomplexed form and after incorporation into inclusion compounds, such as α-cyclodextrin (*60*), to study the molecular association constants (*54*).

In the initial study we measured the molecular association constants by using the positron annihilation techniques and compared, e.g., the constant for the nitrophenol–CD complex with the previously reported constant, (Table V) and found it in agreement with the result of the spectroscopic measurement (*55*).

Positronium Reactions as a Nuclear Probe in Micellar Systems

This technique also can be used for the study of micellar systems. Surface-active compounds are used frequently to solubilize molecules which otherwise would not be soluble in water. The mechanism of this solubilization involves the formation of aggregates of surfactant mole-

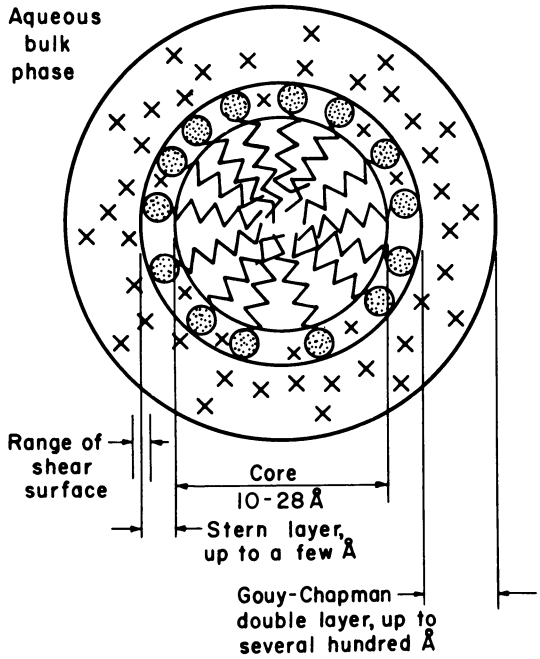

Figure 15. A two-dimensional representation of the regions of a spherical ionic micelle. The counterions (×), the head group (⊛), and the hydrocarbon chains (⁓) are indicated schematically to denote their relative locations but not their numbers, distribution, or configuration (57).

Publication Date: June 1, 1979 | doi: 10.1021/ba-1979-0175.ch001

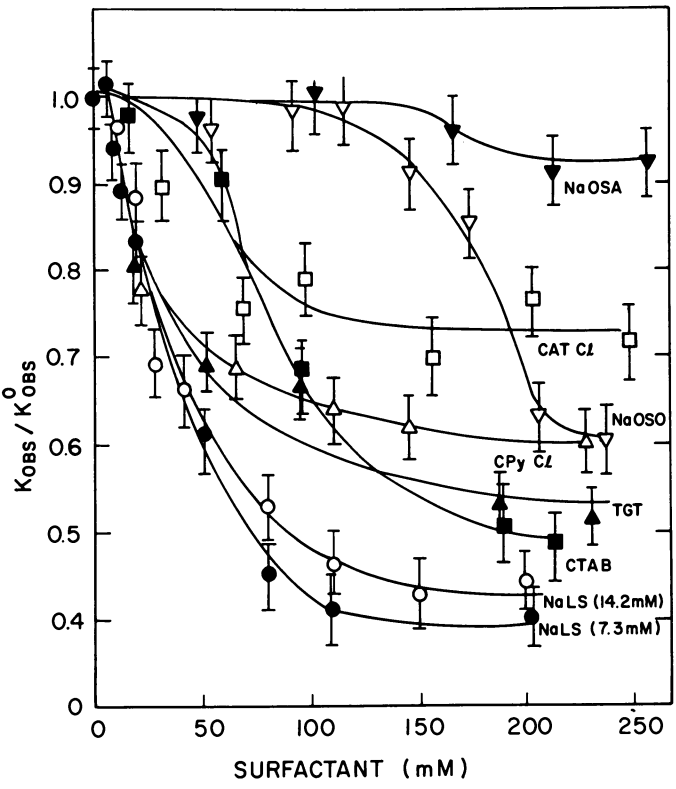

Journal of the American Chemical Society

Figure 16. Relative reaction rate constants $K_{obs}/K°_{obs}$ vs. surfactant concentration in aqueous nitrobenzene solutions (room temperature) ($K°_{obs}$ rate constant observed without surfactant) (62)

Publication Date: June 1, 1979 | doi: 10.1021/ba-1979-0175.ch001

cules which are called micelles and in which the solubilizate is contained (Figure 15). Because of the great practical importance of the micellar chemistry in detergency processes, tertiary oil recovery, and energy conversion as well as its relationship to the natural aggregation of hydrophobic moieties which form biomembranes, this area of chemistry has been under active investigation in the recent past. Several reviews describing micelles and micellar phenomena have been published and can be found in References *56–61*.

While the structure of a micelle is fairly well understood in terms of an entity with a viscous hydrocarbon-like core and a polar exterior containing the charged head groups of the surfactant molecule, still more detailed information is needed about the location of the solubilizate in the micelle as well as about the dynamics of the solubilization process.

Several techniques such as NMR and fluorescence techniques have been used to define the location of the solubilizate in the micelle. By comparing the spectral characteristics of probe molecules observed in the presence of micellar systems with those which the probe molecules display in a homogeneous aqueous solution or in an alkane, which would resemble the hydrocarbon-like core of the micelle, conclusions have been reached as to the positron of the probe molecules in the micelle.

Since micellar systems catalyze many reactions, extensive studies were made to evaluate the influence of the micelle on the course of the reaction by comparing reactions in micellar and homogeneous solutions. Among other things these studies involved the external quenching of the fluorescence of probe molecules and the reactions of hydrated electrons. In the latter case a clear dependence of the reaction rates on the micellar charge was observed.

In the following section the results of a study shall be reported in which the reactions of Ps with probe molecules in micellar systems were investigated as a potential new tool for the determination of the location of a probe molecule in the micelle and the effect of micelles on the chemical reaction process (*62*).

In previous studies we were able to show that Ps–molecule complexes were stabilized to various degrees in different solvents—a fact which is reflected in different overall reaction rate constants, depending on the

Table VI. Rate Constants for Positronium–Nitrobenzene Interactions in Various Solvents (*62*)

$$[\mathrm{Ps} + \mathrm{NB}]_{\mathrm{solv}} \underset{k_2}{\rightleftarrows} [\mathrm{PsNB}]_{\mathrm{solv}} \xrightarrow{\lambda_c} 2\gamma$$

$$k_{obs} = \frac{k_1 \lambda_c}{k_2 + \lambda_c}$$

Solvent	K_{obs} [10^{10} M^{-1} s^{-1}] (at 22°C)
Benzene	2.55
Toluene	2.58
H_2O	1.05
Propanol	1.00
n-Pentanol	0.86
n-Hexane	0.30
n-Heptane	0.34
n-Octane	0.69
n-Decane	1.19
n-Dodecane	1.28
n-Hexadecane	1.15

Publication Date: June 1, 1979 | doi: 10.1021/ba-1979-0175.ch001

In Positronium and Muonium Chemistry; Ache, H.;
Advances in Chemistry; American Chemical Society: Washington, DC, 1979.

nature of the solvent (Table VI) (*10, 48*). Thus the comparison of the rate constants obtained for Ps interaction with probe molecules in micellar systems with those observed in the aqueous solution or in an appropriate alkane should provide information about the location of the probe molecule in the micelle, since Ps reactions are fast in relation to the time to transfer the probe molecule from a micellar to an aqueous environment. Ps is a neutral species that should not be repelled by the charges on the micelle surface; and it should be able to effectively penetrate into the micelle.

Thus, the Ps reaction rate constants with nitrobenzene and $CuCl_2$ were determined in micellar solutions of seven surfactants (Figure 16 and Table VII) at various surfactant concentrations (*62*). While the reac-

Publication Date: June 1, 1979 | doi: 10.1021/ba-1979-0175.ch001

Table VII. Rate Constants for Positronium–Nitrobenzene[a] Interactions in Aqueous Micellar Systems (K_{mic}) in the (Pure) Liquid Surfactant (K_{surf}) and in the Corresponding *n*-Alkane (K_{alk}) (*62*)

Surfactant	K_{mic} 10^{10} M^{-1} s^{-1}	K_{surf} 10^{10} M^{-1} s^{-1}	K_{alk} 10^{10} M^{-1} s^{-1}
Anionic			
NaLS (sodium dodecylsulfate)	0.41	—	1.28 (C_{12})
NaOSA (sodiumoctylsulfate)	0.90	0.47	0.69 (C_8)
NaOSO (sodiumoctylsulfonate)	0.60	—	0.69 (C_8)
Cationic			
CTAB (hexadecyltrimethylammonium bromide)	0.48	—	1.15 (C_{16})
CTACl (hexadecyltrimethylammonium bromide)	0.73	0.39	1.15 (C_{16})
CPyCl (hexadecyl pyrydiniumchloride)	0.60	—	1.15 (C_{16})
Nonionic			
TGT (tergitol–NPX)	0.53	0.13	—

[a] $K°_{obs}$ in aqueous nitrobenzene 1.05×10^{10} s^{-1}.

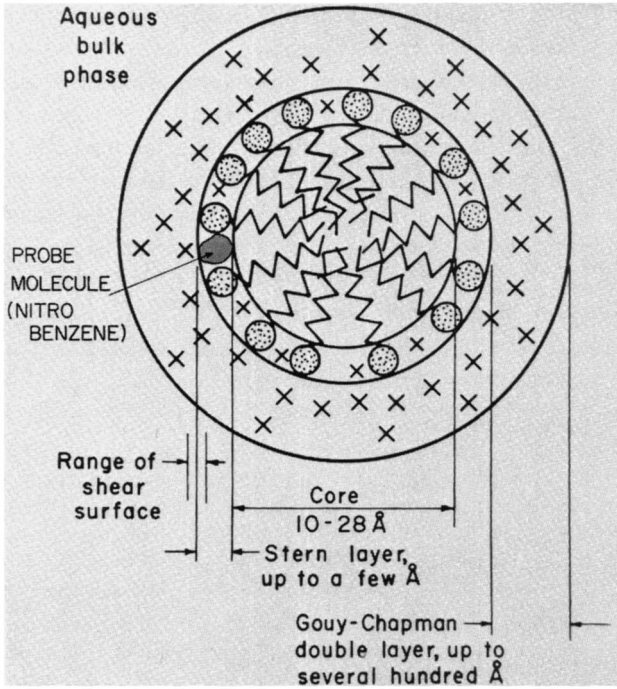

Figure 17. Schematic of location of probe molecule in micelle

tivity of the nitrobenzene toward Ps is reduced in each of the micellar systems with respect to its reactivity in water or the corresponding alkane, neutral and cationic micelles have relatively little or no effect on the Ps reactivity towards Cu^{++}. The results can be discussed by assuming that nitrobenzene molecules are preferentially located in the Stern layer (Figure 17) where they form (complexed) species which show a lower reactivity toward Ps, and that Cu^{++} ions are absorbed on the surface of the micelle where their reactivity toward Ps is reduced substantially.

A continuation of this work was the application of the positron annihilation technique to the investigation of the physical and structural changes which micelles undergo upon addition of solvents (*64*), in as much as they might affect the physical and chemical properties of solubilized species, such as the location of the probe molecules in the micelle and the permeability of the micelle.

For this purpose a series of experiments was carried out. The rate constants for the reactions between Ps and nitrobenzene or Cu^{++} ions in various micellar systems such as sodium dodecylsulfate (NaLS), hexadecylpyridinium chloride (CPyCl), hexadecyltrimethylammonium bro-

Publication Date: June 1, 1979 | doi: 10.1021/ba-1979-0175.ch001

mide (CTAB), sodium octylsulfonate (NaOCO), and Tergitol–NPX (TGT) were determined in the presence of several organic additives such as benzyl alcohol, benzene, *n*-hexane, and *n*-hexanol.

From Figure 18, where the relative changes of the rate constants K_{mic}/K'_{mic} (the rate constants observed in micellar solution containing the probe in the presence or absence of the additive) are plotted as a function of benzyl alcohol concentration, it is obvious that the addition of benzyl alcohol causes an enhancement of the Ps reactivity toward nitrobenzene in NaLS, CTAB, CPyCl, and to a lesser degree in TGT. No effect or a slight decrease is seen in the case of NaOSO. Similar trends, although definitely less pronounced in the case of NaLS, can be recognized if benzene is the additive as shown in Figure 19.

A completely different behavior is observed for *n*-hexanol and *n*-hexane additives, as demonstrated for the CTAB system in Figure 20, where the changes of K_{mic}/K'_{mic} are displayed as a function of the nature and concentration of the various additives.

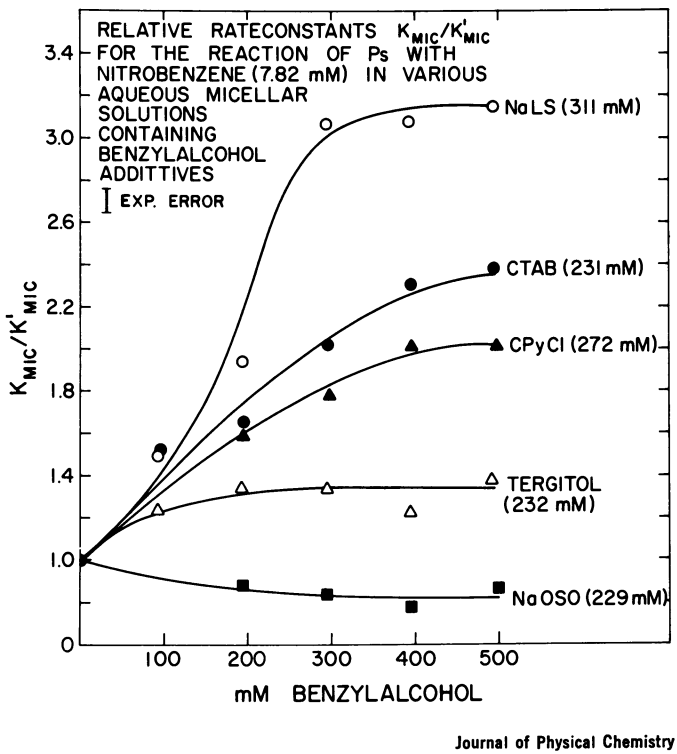

Figure 18. Relative rate constants, K_{mic}/K'_{mic}, for reactions of Ps with nitrobenzene in micellar solutions vs. concentration of benzyl alcohol additives (at room temperature) (64)

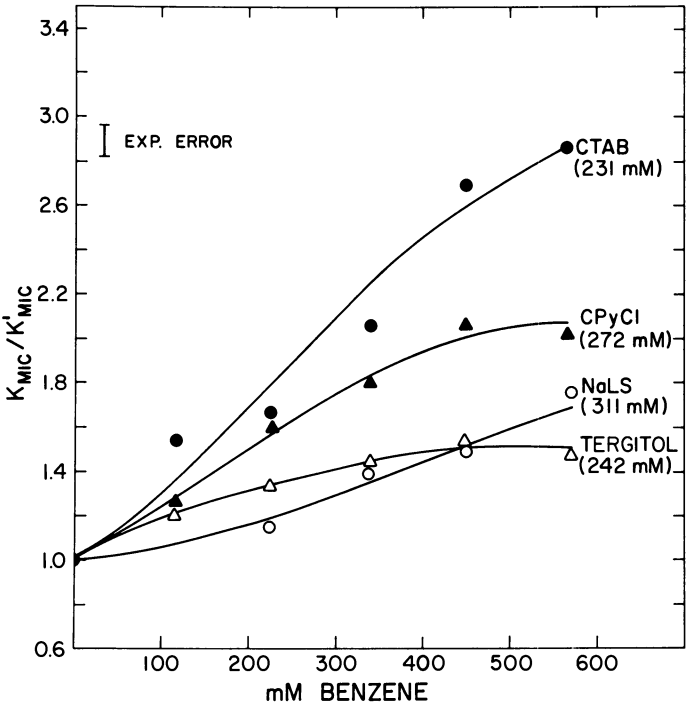

Figure 19. Relative rate constants, K_{mic}/K'_{mic}, for reactions of Ps with nitrobenzene in micellar solutions vs. concentration of benzene additives (at room temperature) (64)

Since, as discussed above (*10, 48*), the rate constants for Ps reactions with probe molecules such as nitrobenzene are sensitive to the nature of the environment in which they occur it seems logical to relate these trends to changes of the environment of the nitrobenzene probe in the micelle.

The absolute rate constants K_{obs} at various additive concentrations, e.g. in CTAB solution, can be compared with those obtained for the nitrobenzene probe molecule in pure water, benzyl alcohol, benzene, and other hydrocarbon solutions or mixtures of hydrocarbons, alcohols, and water, as schematically shown in Figure 21. From this figure it becomes rather obvious that the addition of benzene to CTAB results in absolute rate constants, K_{obs}, which are definitely greater than those observed in the aqueous phase, or in homogeneous mixtures of the corresponding hydrocarbons with the same amount of benzene present, and approach those observed in benzene solutions.

In other micellar systems such as NaLS, CPyCl, and TGT the effect of benzene additives is less pronounced.

Publication Date: June 1, 1979 | doi: 10.1021/ba-1979-0175.ch001

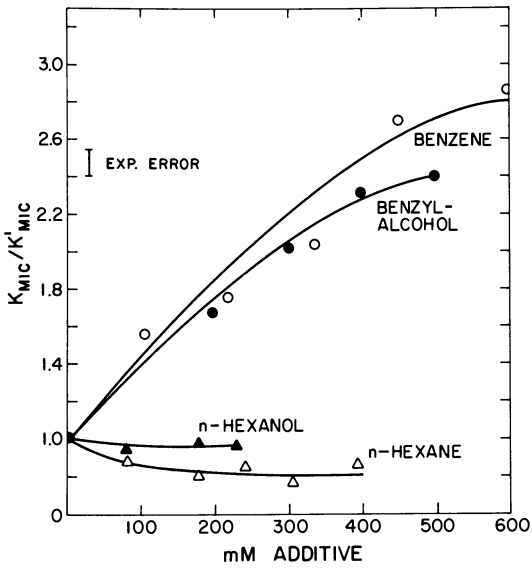

Figure 20. Relative rate constants, K_{mic}/K'_{mic}, for reactions of Ps with nitrobenzene in CTAB solutions vs. concentration of benzene, benzyl-alcohol, n-*hexane, or* n-*hexanol additives (at room temperature) (64)*

The implication of these results seems to be that the addition of benzene to the micellar systems (most obvious in the case of CTAB) provides a benzene-like environment for the nitrobenzene probe molecules. One can visualize that this is accomplished by benzene cluster or benzene gel formations within the micelle (Figure 22). Evidence for such a benzene microenvironment in which solubilized species may reside has been obtained recently from optical spectra and the measurement of dielectric constants in aqueous NaLS systems to which benzene was added (*63*). The authors postulate that the solubilized benzene is concentrated primarily at the micelle–water interface rather than in the hydrocarbon core.

As discussed above a very similar behavior is observed for the Ps rate constants in micelle systems containing benzyl alcohol additives (Figure 18). In this case NaLS and CTAB show the most pronounced increase, with K_{obs} values exceeding even those obtained for Ps nitrobenzene interaction in pure benzyl alcohol solutions as shown for CTAB solutions in Figure 21. On the other hand a slight decrease is observed in NaOSO solutions (Figure 18).

If the above assumption, namely that additives such as benzene or benzyl alcohol are forming clusters at the micelle–water interface in

Publication Date: June 1, 1979 | doi: 10.1021/ba-1979-0175.ch001

which the probe molecule can be located, is correct, then one would expect that the greatest effect on the Ps–nitrobenzene rate constants is seen in those cases where the nitrobenzene is initially, i.e. without additives present, near the micelle–water interface or in the Stern layer.

We have postulated that this is the case in the NaLS, CTAB, CPyCl, and TGT systems (*62*), whereas the indication was that nitrobenzene is located in the hydrocarbon-like core of the NaOSO micelles, which is consistent with the trends observed in this study.

The fact that the rate constants, K_{obs}, in the presence of benzyl alcohol exceed those observed in pure benzyl alcohol solution requires some additional discussion. The K_{obs} approaches values found typically in

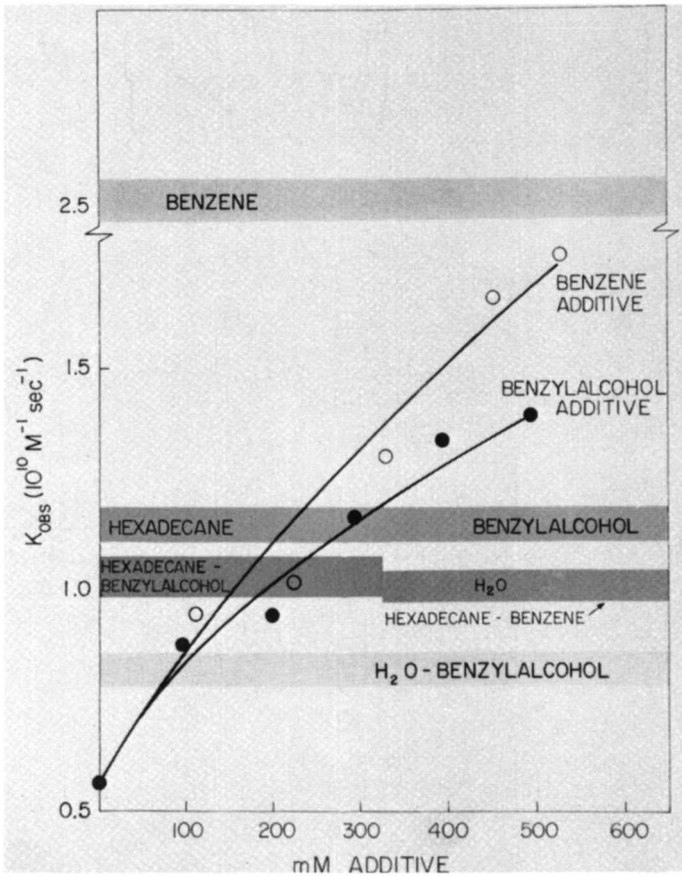

Figure 21. Absolute rate constants, K_{obs}, for Ps-nitrobenzene reactions in micellar solutions of CTAB (at room temperature) in the presence of benzene or benzyl alcohol additives (CTAB, 243 mM; nitrobenzene, 7.82 mM). (Shaded zones represent rate constants for Ps-nitrobenzene interactions in various solvents or mixtures of solvents.)

Publication Date: June 1, 1979 | doi: 10.1021/ba-1979-0175.ch001

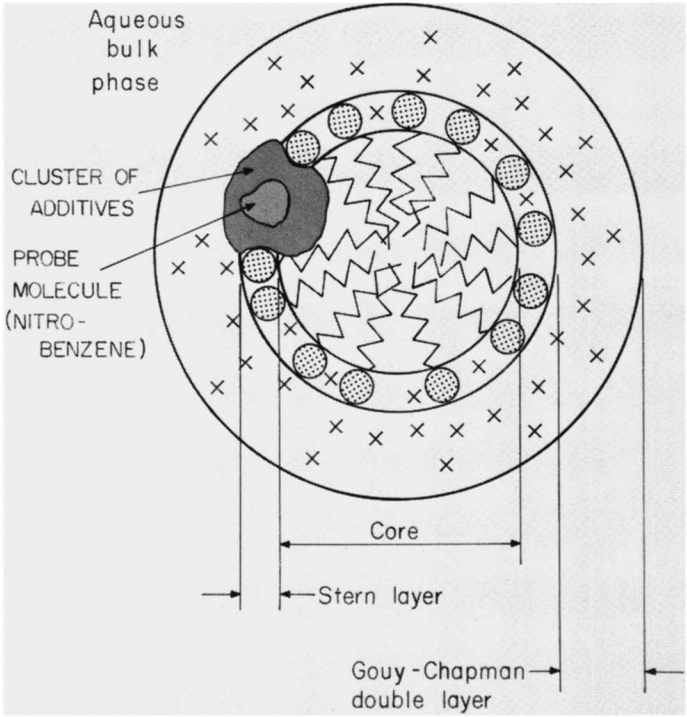

Figure 22. Schematic of probe molecule in additive cluster in micelle

aromatic solvents, which might suggest that the benzyl alcohol molecules form aggregates in the micelles showing a particular arrangement, e.g. with the aromatic ring directed to the center of the cluster and the —OH group pointing outward. In such a case one could rationalize the similarity of the rate constants observed in micellar systems with benzyl alcohol additives and in (pure) benzene solutions.

Further substance to the postulate that these additives form clusters in or at the micelle surface is added by the fact that *n*-hexanol and *n*-hexane additive in the CTAB system decrease slightly the Ps rate constants. This is consistent with the hypothesis that in this case nitrobenzene is located in a *n*-hexanol or *n*-hexane microenvironment, where the rate constants for Ps–nitrobenzene interactions, as shown schematically in Figure 23 are considerably lower.

An indication of how the surface of the micelles is changed in the presence of additives such as benzyl alcohol or benzene can be obtained by comparing the rate constants for Ps interactions in micellar solution containing Cu^{++} -ions with or without the presence of these additives.

Publication Date: June 1, 1979 | doi: 10.1021/ba-1979-0175.ch001

As discussed above, Cu^{++} ions are adsorbed on the surface of ionic micelles because of an electrostatic attraction between surface charge and Cu^{++} ions or counter ion charge and Cu^{++} ions. As a result of this adsorption process the rate constants between Cu^{++} ions and Ps dropped considerably below the values observed in aqueous solutions of Cu^{++}. The reason for the reduced reactivity of Ps toward adsorbed Cu^{++} may be seen in the fact that the Cu^{++} when adsorbed on the surface loses the character of the hydrated Cu^{++} by partial bond formation, complexation, etc. with the surface molecules, and thus reacts at a different rate with Ps.

Addition of benzene and benzyl alcohol significantly increases the Ps reaction rates in micellar systems such as CPyCl and CTAB where previous results have shown a drastic drop in the Cu^{++}–Ps reaction rates when micelles are formed. This effect is not observed in the case of TGT, which as a neutral micelle has shown no attraction for Cu^{++} -ions.

Publication Date: June 1, 1979 | doi: 10.1021/ba-1979-0175.ch001

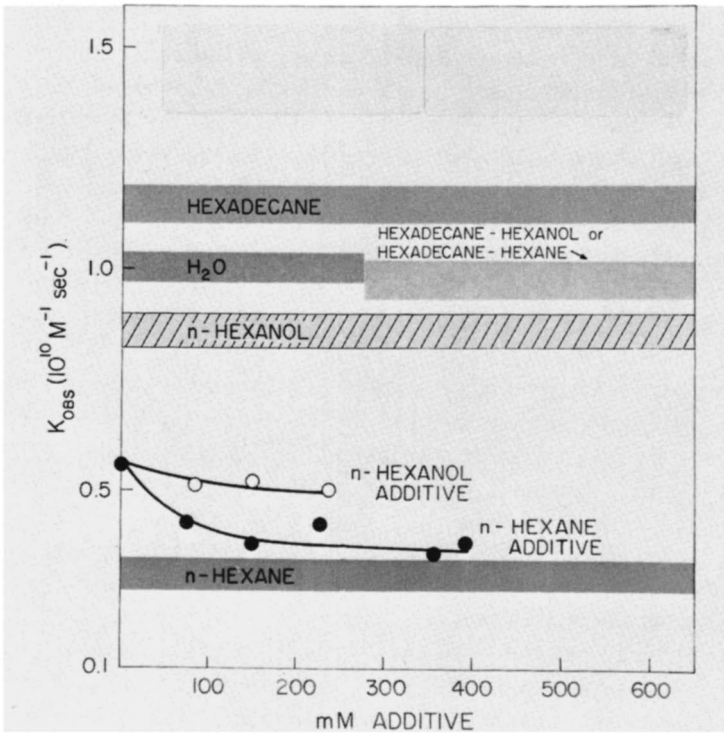

Figure 23. Absolute rate constants, K_{obs}, for Ps-nitrobenzene reactions in micellar solutions of CTAB (at room temperature) in the presence of n-*hexane or* n-*hexanol additives (CTAB, 276 mM; nitrobenzene, 9.33 mM). (Shaded zones represent rate constants for Ps-nitrobenzene interactions in various solvents or mixtures of solvents)*

It seems that these results suggest that the addition of benzene or benzyl alcohol to the CPyCl or CTAB leads to drastic changes of the micelle structure in or close to the micellar water interface. This is caused by the formation of benzene clusters, etc. (*see* above) and results in a release of Cu^{++} otherwise adsorbed on the micellar surface.

Another advantage of applying the Ps technique to the study of micellar systems may be seen in its potential to probe the position of ions and other nonfluorescent materials, where fluorescence probes clearly are not applicable and especially in biological membranes where probes may interfere with the cell functions.

Other Applications of Positronium Reactions

Further biological applications may encompass the study of the structure of enzyme systems, as recently reported by Graf and Handel (*65*), and the study of membrane systems as reported by McGrath et al. (*66*) and also by our laboratory (*67*).

Initial attempts to apply Ps interactions to the study of compounds active in photosynthesis have been done by Dworakowski et al. (*68*).

This discussion of the interaction of Ps with substrate molecules via molecule complex formation would not be complete without mentioning the work by Brandt and his co-workers (*69, 70*) who investigated the interactions of *o*-Ps with phosphorescent impurities in solids and gases. For example, by illuminating trace amounts of SO_2 or benzaldehyde in rare gases with UV light they were able to produce via intersystem crossing these species in their excited triplet states and measure their *o*-Ps quenching rates, which turned out to be extremely large.

Besides the interesting theoretical implications of this phenomenon as a neutral quantum mechanical probe, the extremely high sensitivity of Ps toward excited triplet states can be used for investigations on gas pollution, and in particular on H_2SO_4 formation, via the photodynamic oxidation of SO_2 and SO_3 in air.

Although Brandt (*69, 70*) originally suggested an interaction between Ps and triplet substrate, Ps–molecule complex formation similar to eximer formation, remains a real possibility.

In summary one may want to conclude that the potential of the Ps as a chemical probe on biological and environment work just begins to show and that undoubtedly more important applications can be found.

General Features of the Positronium Formation Process

So far I have discussed only applications of Ps atom reactions in chemistry. As I stated at the beginning of this review, the second source of information about the structure of the chemical and physical environ-

Publication Date: June 1, 1979 | doi: 10.1021/ba-1979-0175.ch001

ment is the Ps formation process itself. At the present time two different models and a combination of both are being used to explain this process.

Positrons are most commonly emitted as a result of the radioactive decay of a neutron-deficient nuclide. They lose their high kinetic energy in collisions with the surrounding matter until they reach thermal or near-thermal energies at which point the cross section for mass annihilation with an electron assumes a maximum value. However a certain fraction of these positrons may enter the bound state of the Ps.

The most widely accepted model for Ps formation is the Ore model (*1–7*) which assumes that the positrons slowing down from higher energies pass through an energy gap in which Ps formation is possible. The lower boundary of this Ore gap is defined by the expression $V-I_{Ps}$, where V is the ionization potential of the surrounding molecules and I_{Ps} the ionization potential of Ps, 6.8 eV. If the kinetic energy of the positrons exceeds V it is assumed that ionization of the surrounding molecules ($e^+ + M \rightarrow M^+ + e^- + e^+$) becomes more probable than Ps formation ($e^+ + M \rightarrow M^+ + Ps$), so that V constitutes the upper boundary of the Ore gap (Figure 24). Ps atoms can be formed in the Ore gap with kinetic energies of up to 6.8 eV and react as a kinetically excited species or after reaching thermal equilibrium.

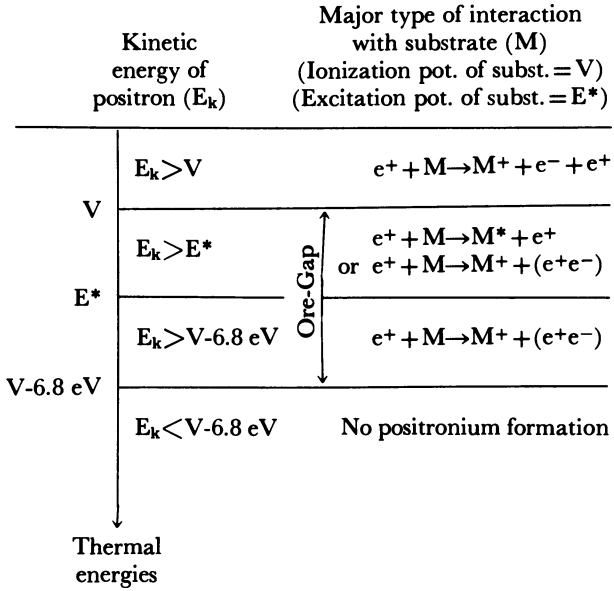

Figure 24. Schematic of Ore gap model (energetics of Ps formation)

Publication Date: June 1, 1979 | doi: 10.1021/ba-1979-0175.ch001

The experimental results, however, suggest that not all positrons form Ps and several factors have been discussed which could interfere with and inhibit this process.

The Ore model is based on the simplified assumption that all positrons whose kinetic energy lies in the Ore gap produce Ps. In practice, however, the Ps formation process in the Ore gap has to compete with all other processes that can cause moderation of the positron to energies below the lower Ore limit. The most important of these elastic and inelastic collisions with substrate molecules, the energy transferred in the second case possibly stimulating molecular vibrations and rotations. This category also includes processes that lead to the positron capture by addition of positrons to the substrate molecule AB.

$$e^+ + AB \rightarrow e^+ AB \text{ or } A + e^+ B$$

If the compound formation occurs above or within the Ore gap, the captured positrons are no longer available for the formation of Ps; therefore the yield decreased.

A second model for Ps formation which has been suggested recently by Mogensen is the spur reaction model (*71*). He assumes that Ps is formed as a result of a spur reaction between the positron and a secondary electron in the positron spur. In this model a correlation should exist between the Ps formation probability and the availability of the electrons in the spur. The Ps formation must compete with electron-ion recombination and with electron and positron scavenging by the surrounding molecules as well as with other processes.

A model which combines certain features of both models is Tao's modified spur model (*72*). In this model Tao considers both the possibility of combination of a positron with an electron created in the spur as well as the direct formation of a Ps, similar to the mechanism discussed in the Ore model, if the total kinetic energy of the resulting electron–positron pair is less than the potential energy between them.

The processes mentioned here, such as elastic scattering, stimulation of molecular vibrations and rotations in the electron volt range, and the addition of low-energy electrons (or positrons) to molecules or generation of electrons in the spur and their subsequent reactions with scavengers, etc., are of the greatest importance to the understanding of elementary processes in radiation chemistry. Thus several investigations have been carried out by Mogensen et al. (*73, 74, 75*), Tao (*72*), Byakov et al. (*76, 77*), Molin et al. (*78, 79*), Maddock et al. (*80, 81*), and our laboratory (*82, 83*) to demonstrate the interrelationship between the Ps formation process and radiation-chemical phenomena.

In the past we have interpreted our experimental results in solutions of inorganic ions in terms of the (modified) Ore gap model (*21, 22, 33*).

Publication Date: June 1, 1979 | doi: 10.1021/ba-1979-0175.ch001

It was assumed that the energetic *o*-Ps, which is formed in the Ore gap with kinetic energies varying between 6.8 eV and thermal energies, has, as any other hot atom, two alternatives. It may undergo chemical reactions while still hot, followed by a rapid annihilation of the positron in the resulting reaction products, or it can lose its excess kinetic energy in moderating collisions, becoming a thermalized Ps-atom and reacting as such.

On the other hand, hot reactions between solute and Ps-atoms have to take place shortly after the birth of the Ps before it becomes thermalized. Thus, the lifetime of the positrons incorporated in Ps atoms taking part in hot reactions will become indistinguishable from that of the free positrons or *p*-Ps.

By using this approach the experimental results obtained in aqueous solutions of inorganic ions were interpreted by assuming that only a certain fraction of all Ps-atoms formed have sufficient energy (i.e., hot Ps-atoms) to overcome the reaction barrier to react with the inorganic ions ($A_{aq}^{n+} + e^- \rightarrow A^{(n-1)+}$). In this way the redox potential of the Ps-atom could be approximated (*32, 33*).

If one wants to interpret the experimental results in terms of the simple spur reaction model (*71*) one would have to consider the competition between positron and electron combination and the reaction of the electron with the scavenger (inorganic ions).

Thus in analogy with the approach used by Hamill and several other authors (*84, 85*) for a simple competition for dry or solvated electrons in a solution one could derive the following correlation between the *o*-Ps formation probability P at a given solute concentration [M], if the *o*-Ps formation probability in the pure solvent is P°;

$$P = P^\circ/(1 + K[M])$$

where K is the rate constant for inhibition of *o*-Ps formation.

The K values assessed from this kinetic analysis are summarized in Table VIII (*83*) and plotted in Figure 25 on a logarithmic scale as a function of $-\Delta G^\circ$ for the one-electron transfer process.

A reasonable correlation exists between the free energy changes and the inhibition constants K as seen from Figure 25.

No apparent correlation, however, seems to exist between the inhibition constants K and the reported rate constants for the reactions of hydrated electrons (Table VIII) with these compounds, which makes an interpretation of the observed inhibition in terms of a competition for solvated electrons between positron and scavenger, i.e. the inorganic ions, rather unlikely.

Another possibility would involve the combination of dry electrons and positrons, in which case scavenger and positron compete for the dry

Publication Date: June 1, 1979 | doi: 10.1021/ba-1979-0175.ch001

Table VIII. Correlation Between the Free Energy Changes and the Inhibition Constants K (83)

Ion	*K* (M^{-1})	*K* (e^-aq) M^{-1} s^{-1}
Pb^{++}	2.5	3.9×10^{10}
Sn^{++}	1.2	3.4×10^{9}
Cd^{++}	0.37	5.2×10^{10}
Ag^{+}	0.35	3.2×10^{10}
H^{+}	0.22	2.4×10^{10}
Tl^{+}	0.10	3.7×10^{10}
Zn^{++}	0.10	1.3×10^{9}
Na^{+}	< 0.05	$< 10^{5}$
NO_3^-	3.5	1.1×10^{10}

Journal of Physical Chemistry

electrons (*71, 83*). Unfortunately very little is known about the rate constants or dry electron reactions so that no satisfactory comparison can be made. However, if it can be shown that the positron reacts with dry electrons to form Ps, these Ps inhibition studies should reveal valuable information about dry electrons with chemical compounds.

The correlation between the inhibition constants K and free energy for the one-electron transfer process (Figure 25) is interesting. It could be interpreted by assuming that the maximum of the cross section curve for electron attachment to the scavenger ions is closely related to the free energy change involved in this process.

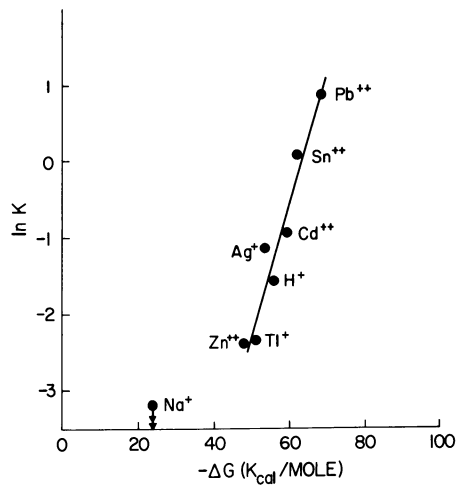

Journal of Physical Chemistry

Figure 25. The ln k vs. $-\Delta G$ for $A_{aq}^{n+} + e^- \rightarrow A_{aq}^{(n-1)+}$ for various ions in aqueous solutions (83)

$$A^{+}_{aq} + e^{-}_{dry} \rightarrow A_{aq}^{(n-1)+}$$

It could be explained also by invoking the modified Ore model. In this case one could argue that the cross section curve for attachment of Ps to these inorganic ions, resulting in Ps complex formation or electron transfer, shows certain maxima which coincide with the $-\Delta G$ values for the one-electron transfer.

Positronium Formation as a Probe in Biological and Micellar Systems

Although as outlined above the mechanism of the Ps formation process is not yet understood completely, its sensitivity toward changes in the microstructure of the environment has been amply demonstrated in the pioneering work of Graf and Handel (*65*) in enzyme proteins where the various phase changes of the surrounding water structure associated with the denaturation process were recognized clearly by the positron annihilation method. Furthermore, experiments with liquid

Publication Date: June 1, 1979 | doi: 10.1021/ba-1979-0175.ch001

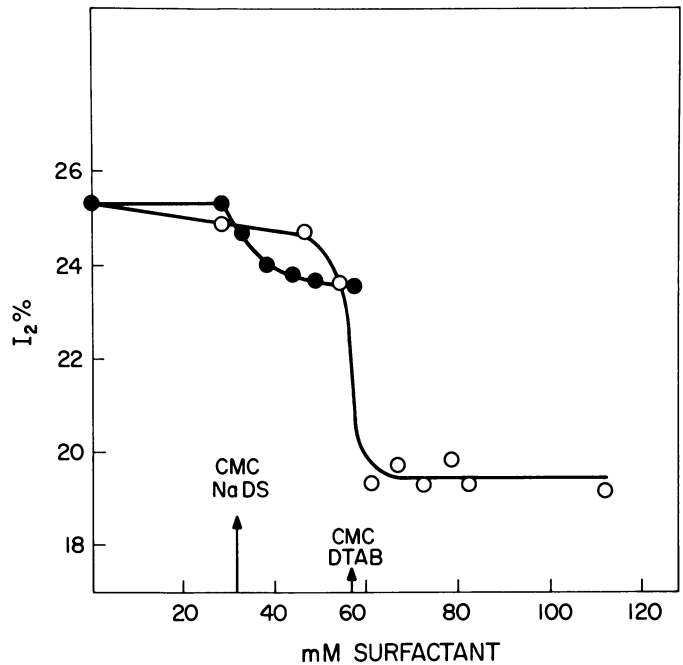

Figure 26. I_2 vs. surfactant concentration in various micellar solutions of NaDS (sodium decylsulfate) and DTAB (decyltrimethylammoniumbromide) (90). NaDS, ●; DTAB, ○; experimental error, I.

crystals by W. W. Walker et al. (*86, 87, 88*) and in our own laboratory (*89*) have shown that variations in the mesomorphic phases of the liquid crystals (a process which may also resemble expected changes in the layered membrane structures) are sensitively reflected in the positron lifetime characteristics. The most recent results from our laboratory have demonstrated that variations in shape and size of micelles also are presented in the annihilation data (*62*).

The application of the positron annihilation technique to the determination of the so-called critical micelle concentration (CMC) is of special interest. CMC is defined as the narrow range of surfactant concentration at which the micelles first become detectable, usually by some change in the physical properties, such as interfacial tension, electric conductivity, electromotive force (emf), pH-specific heat, viscosity, and the optical and spectroscopic properties of the solution. These methods gen-

Publication Date: June 1, 1979 | doi: 10.1021/ba-1979-0175.ch001

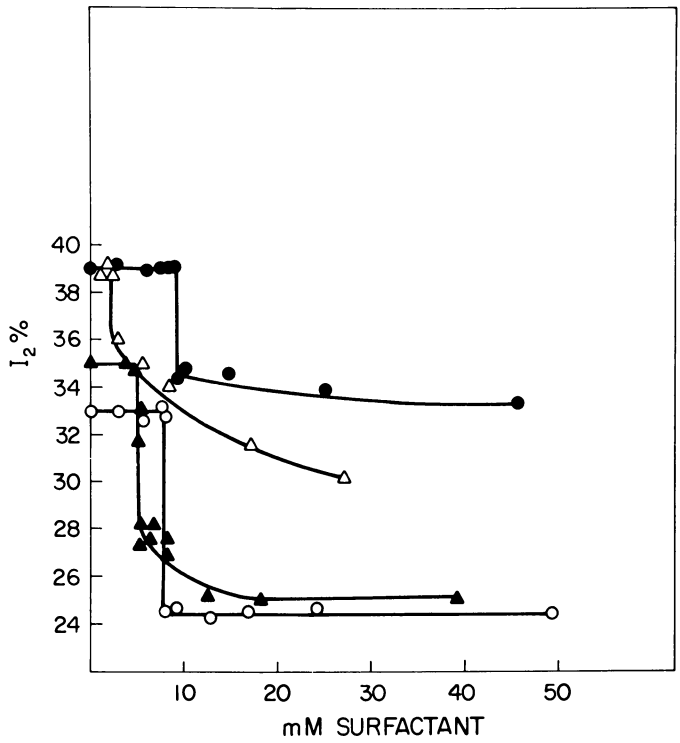

Journal of the American Chemical Society

Figure 27. I_2 vs. surfactant concentration in various micellar solutions of DAP (dodecylammoniumpropionate) and AOT (sodium di-(2'-ethylhexyl)sulfosuccinate) (90). DAP-benzene, ●; DAP-cyclohexane, ○; DAP-n-hexane, ▲; AOT-benzene, △; I, experimental error.

erally provide clear evidence for the formation of micelles; however, since the observed variation of the above physical properties at the CMC is not abrupt but occurs more or less gradually, extrapolations are required which in turn introduce an uncertainty in the determination of the CMC.

As shown in Figure 26 and 27, the Ps formation probability as indicated by the I_2 values (the intensities of the longlived component in the positron lifetime spectra) drops drastically at the CMC and provides a very convenient tool for the determination of the CMC not only in aqueous micellar systems but also for reversed micelle formation (*90*).

In a similar fashion the glass transition temperature in polymers is indicated by abrupt changes in the positron annihilation characteristics as reported recently by Tao et al. (*91, 92*).

Publication Date: June 1, 1979 | doi: 10.1021/ba-1979-0175.ch001

The Positronium Formation Process as a Test of Models Proposed in Quantum Electron Dynamics

Another interesting example of the usefulness of the Ps formation process to the solution chemical problems is its application to test certain hypothetical models in quantum electron dynamics (qed).

One of the most intriguing problems in chemical evolution is the origin of optical asymmetry in biomolecules. It is a well established fact that amino acids occurring in natural proteins belong overwhelmingly to the L series whereas natural sugars are made up almost exclusively of D optical isomers. However, very little is known about the origin of this asymmetry.

Several theories which do not consider the predominance of the L-amino acids in natural proteins as a matter of chance have been suggested. One non-chance explanation is based on the unequal decomposition of optical isomers and the subsequent generation of optical activity in light-mediated reactions.

In 1959 Ulbricht (*93*) discussed a possible connection between the asymmetry at the level of elementary particles and at the molecular level. He proposed a novel mechanism which would relate the phenomenon of asymmetry found in biological systems with parity nonconversation in weak interaction. This mechanism is based essentially on the discovery by Lee and Yang (*94*) who showed that electrons emitted in β-decays are polarized.

Ulbricht and Vester (*95*) suggested several possible mechanisms by which polarized β-decay electrons are interacting in matter to generate circularly polarized bremsstrahlung which in turn may undergo reaction with organic matter leading to asymmetric syntheses or degradation. Attempts by Ulbricht and Vester (*96*) to induce optical activity with polarized β-radiation, however, failed to confirm this hypothesis and most

of the subsequent experiments carried out by several authors (*97, 98, 99*) to generate optical activity by irradiating racemic mixtures with polarized β-radiation proved to be inconclusive.

A few years ago Garay and Hrasko et al. (*100, 101, 102*), postulated that electrons in optical active compounds possess helicity, i.e., the electron spins are aligned predominantly parallel to the motion of the electron in one and anti-parallel in the other enantiomer (helical electron gas model). A schematic presentation of this model is shown in Figure 28. The authors further postulate that positron possesses helicity when it undergoes Ps formation with these electrons. They also assume that the probability of Ps formation depends on the relative velocity of electron and positron. Thus, the probability for *o*- to *p*-Ps formation will switch when one replaces one optical isomer by the other as indicated in Figure 29. In other words, positrons which have a parallel orientation of spin and direction of motion, as emitted in the radioactive decay of certain nuclides, may interact differently with the D and L isomers of a chiral compound. This results in slight variances in the Ps formation probability and also in a change of the ratio or *o*- to *p*-Ps formation which may lead ultimately to the preferential decomposition of one optical form. Initial experiments carried out by these authors (*103*) with optically active isomers of amino acids in the solid state seemed to confirm this assumption.

In order to avoid the difficulties involved with the determination of the Ps formation probability in the solid state (where crystal defects and differences in the crystalline structure could obscure the results), we carried out precision measurements on the *o*--*p*-Ps formation probabilities with seven optical compounds in the liquid phase at various temperatures in our laboratory (*104*). In each case no significant differences between the D and L form could be found (Table IX).

Publication Date: June 1, 1979 | doi: 10.1021/ba-1979-0175.ch001

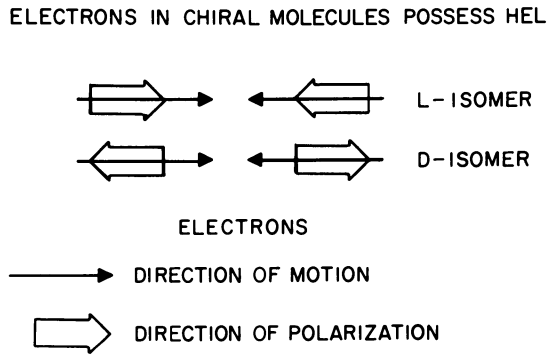

Figure 28. Helicon electron gas model (after Hrasko et al., 100, 101)

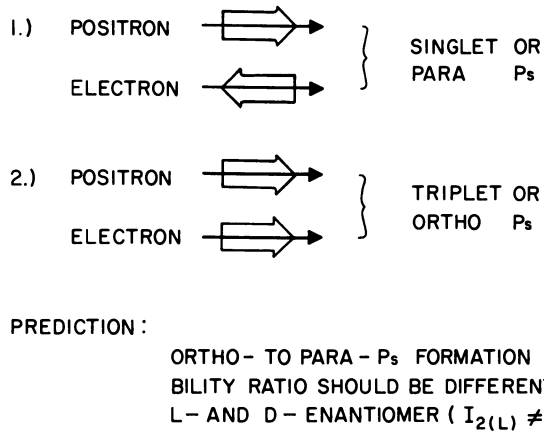

Figure 29. Hypothesis for interaction between positron and electrons in optical active molecules (after Hrasko et al., 100, 101)

Therefore, it seems important to consider the possible reasons for this discrepancy between Garay and Hrasko's hypothesis and our experimental results—apart from the possibility that the effect may be too small to be observed.

Basic to the model of interaction between positron and electrons in helical molecules is that the orbital electrons in the two optical isomers are spin-polarized (helical electron gas model) differently, for which there is no independent evidence. Another possibility is that the positron has lost its helicity when it forms Ps (*105*) or that if the spur model (*71*) applies, that the electrons are ejected from their respective orbitals. An open question remains whether these electrons retain their helicity which they might have otherwise possessed when residing in the chiral molecules as postulated by the helical electron gas model.

Table IX. Ratio of I_2 Values for Various Optical Isomers at Room Temperature (*104*)

Compound	D-*Form* (%)	L-*Form* (%)
Octanol-2	21.91 ± .40	21.28 ± .32
Diethyltartrate	17.81 ± .08	17.61 ± .35
Carvone	17.59 ± .52	17.35 ± .30
2-Aminobutanol	23.4 ± .20	23.15 ± .33
2-Methylbutanol	22.18 ± .33	22.65 ± .33 (D,L)

Publication Date: June 1, 1979 | doi: 10.1021/ba-1979-0175.ch001

It is certainly tempting to repeat these experiments with slow positrons which have helicity. As reported by Berko et al. (*106, 107*) and Roelling et al. (*107, 108, 109*), at this meeting slow positrons now have become available and could be utilized to settle this question.

Summary and Acknowledgment

In summary, I would like to point out that this review cannot possibly do justice to the accomplishments of the various groups involved today in Ps chemistry nor was it intended to give a comprehensive survey of ongoing research in this area. Thus, the literature quoted certainly is not complete.

The sole purpose of this paper was to present a short discussion of the present status of Ps chemistry and to indicate some of the future trends which I, in my personal opinion, feel might turn out to be especially fruitful.

Other topics and other research trends will be discussed by the various authors who contributed to this volume.

Acknowledgment for financial support is made to the Division of Basic Energy Science, the U. S. Department of Energy, and to the Donors of the Petroleum Research Fund administered by the American Chemical Society.

Literature Cited

1. Green, J. H., Lee, J., "Positronium Chemistry," Academic, New York, 1964.
2. Goldanskii, V. I., *At. Energy Rev.* (1968) **6**, 3.
3. McGervey, J. D., "Positron Annihilation," A. T. Stewart and L. O. Roellig, Eds., p. 143, Academic, New York, 1967.
4. Merrigan, J. A., Tao, S. J., Green, J. H., "Physical Methods of Chemistry," Vol. I, Part III, D. A. Weissberger and B. W. Rossiter, Eds., Wiley, New York, 1972.
5. Ache, H. J., *Angew. Chem., Int. Ed. Engl.* (1972) **11**, 179.
6. Green, J. H., *MTP Int. Rev. Sci.* (1972) **8**, 251.
7. Goldanskii, V. I., Virsov, V. G., *Annu. Rev. Phys. Chem.* (1971) **22**, 209.
8. *Proc. Int. Conf. Positron Annihilation, 4th, Helsingor, Denmark, 1976.*
9. Deutsch, M., *Phys. Rev.* (1951) **82**, 455.
10. Madia, W. J., Nichols, A. L., Ache, H. J., *J. Am. Chem. Soc.* (1975) **97**, 5041.
11. Kirkegaard, P., Eldrup, M., *Comput. Phys. Commun.* (1972) **3**, 240.
12. Ibid. (1974) **7**, 401.
13. Nichols, A. L., PAL-program, unpublished. (This program is a modified version of the CLSQ, Ref. *14*).
14. Cumming, J. B., BNL Report **6470**, CLSQ Nuclear Decay Analysis Program.
15. Tao, S. J., *IEEE Trans. Nucl. Sci.* (1968) **175**.
16. Kirkegaard, P., Mogensen, O., Risφ-M-1615 (PAACFIT program) 1973.
17. Gray, P. R., Cook, C. F., Tturm, G. P., *J. Chem. Phys.* (1968) **48**, 1145.

18. Gray, P. R., Sturm, G. P., Cook, C. F., *J. Chem. Phys.* (1967) **46,** 3847.
19. Bisi, A., Gambarini, G., Zappa, L., *Nuovo Cimento B* (1970) **67,** 75.
20. Shantarovich, V. P., Goldanskii, V. I., Shantarovich, P. S., Koldaeva, O. V., *Dokl. Akad. Nauk SSSR* (1971) **197,** 1122.
21. Bartal, L. J., Nicholas, J. B., Ache, H. J., *J. Phys. Chem.* (1972) **76,** 1124.
22. Bartal, L. J., Ache, H. J., *Radiochim. Acta* (1972) **17,** 205.
23. Madia, W. J., Nicholas, A. L., Ache, H. J., *J. Chem. Phys.* (1974) **60,** 335.
24. Madia, W. J., Nichols, A. L., Ache, H. J., *Ber. Bunsenges. Phys. Chem.* (1974) **78,** 179.
25. Madia, W. J., Nichols, A. L., Ache, H. J., *Appl. Phys.* (1974) **3,** 189.
26. Tao, S. J., *J. Chem. Phys.* (1974) **3,** 1.
27. Ibid., (1970) **52,** 752.
28. Bartal, L. J., Ache, H. J., *J. Phys. Chem.* (1973) **77,** 2060.
29. Nicholas, J. B., Wild, R. E., Bartal, L. J., Ache, H. J., *J. Phys. Chem.* (1973) **77,** 178.
30. Bartal, L. J., Ache, H. J., *J. Inorg. Nucl. Chem.* (1974) **36,** 267.
31. Nichols, A. L., Bartal, L. J., Wild, R. E., Ache, H. J., *Appl. Phys.* (1974) **4,** 47.
32. Bartal, L. J., Ache, H. J., *J. Inorg. Nucl. Chem.* (1974) **36,** 922.
33. Bartal, L. J., Ache, H. J., *Radiochim. Acta* (1973) **19,** 49.
34. Tao, S. J., Green, J. H., *J. Chem. Soc. A* (1968) 408.
35. Madia, W. J., Nichols, A. L., Ache, H. J., *J. Phys. Chem.* (1974) **78,** 1881.
36. Goldanskii, V. I., Shantarovich, V. P., *Appl. Phys.* (1974) **3,** 335.
37. Eldrup, M., Shantarovich, V. P., Mogensen, O. E., *Chem. Phys.* (1975) **11,** 129.
38. Briegleb, G., "Elektronen-Donator–Acceptor Komplexe," Springer–Verlag, Berlin, 1961.
39. Rose, J., "Molecular Complexes," Pergamon, Oxford, 1967.
40. "Molecular Complexes," R. Foster, Ed., *Elek Science*, London, 1973.
41. Mullikin, R. S., Person, W. R., "Molecular Complexes," Wiley, New York, 1969.
42. Schrader, D. M., ADV. CHEM. SER. (1978) **0,** 000.
43. Schrader, D. M., Wang, C. M., *J. Phys. Chem.* (1976) **80,** 2507.
44. Navin, P., Schrader, D. M., Lebeda, C. F., *Appl. Phys.* (1974) **3,** 159.
45. Cade, P. E., Farazdel, A., *J. Chem. Phys.* (1977) **66,** 2598.
46. Farazdel, A., Cade, P. F., *J. Chem. Phys.* (1977) **66,** 2612.
47. Madia, W. J., Schug, J. C., Nichols, A. L., Ache, H. J., *J. Phys. Chem.* (1974) **78,** 2682.
48. Hall, E. S., Madia, W. J., Ache, H. J., *Radiochem. Radioanal. Lett.* (1975) **23,** 283.
49. Madia, W. J., Ache, H. J., *J. Phys. Chem.* (1976) **80,** 451.
50. Jean, Y. C., Ache, H. J., *J. Phys. Chem.* (1976) **80,** 451.
51. Jean, Y. C., Ache, H. J., *J. Am. Chem. Soc.* (1977) **99,** 1623.
52. Jansen, P., Mogensen, O. E., *Chem. Phys.* (1975) **10,** 303.
53. Levay, B., Hautojarvi, P., *J. Phys. Chem.* (1972) **76,** 1951.
54. Jean, Y. C., Ache, H. J., *J. Phys. Chem.* (1977) **81,** 2093.
55. Cramer, F., Saenger, W., Spatz, H. C., *J. Am. Chem. Soc.* (1967) **89,** 14.
56. Thomas, J. K., *Acc. Chem. Res.* (1977) **10,** 133.
57. Fendler, J. H., Fndler, E. J., "Catalysis in Micellar and Macromolecular Systems," Academic, New York, 1975.
58. Fendler, E. J., Fendler, J. H., *Adv. Phys. Org. Chem.* (1970) **6,** 1472.
59. Elworthy, P. H., Florence, A. T., MacFarlane, C. B., "Solubilization by Surface Active Agents," Chapman and Hall, London, 1968.
60. Tanford, C., "The Hydrophobic Effect," Wiley–Interscience, New York, 1973.
61. Mittal, K. L., "Micellization, Solubilization, and Microemulsions," Vols. 1 and 2, Plenum, New York, 1977.

In Positronium Chemistry; Jean, Y. C., Ed.; ACS Symposium Series; American Chemical Society: Washington, DC, 1979.
Advances in Chemistry; American Chemical Society: Washington, DC, 1979.

62. Jean, Y. C., Ache, H. J., *J. Am. Chem. Soc.* (1977) **99,** 7506.
63. Mukerjee, P., Cardinal, J. R., Desai, N. R., "Micellization, Solubilization and Microemulsions," K. L. Mittal, Ed., Vol. 1, pp. 241–261, Plenum, 1977.
64. Jean, Y. C., Ache, H. J., *J. Phys. Chem.* (1978) **82,** 811.
65. Handel, E. D., Graf, G., *J. Am. Chem. Soc.* (1976) **98,** 2360.
66. McGrath, A. E., Morgan, C. G., Rada, G. K., *Biochim. Biophys. Acta* (1977) **466,** 367.
67. Jean, Y. C., Ache, H. J., unpublished results.
68. Dworakowski, J., Hendrich, W., Wesolowski, J., *Photosynthetica* (1974) **8,** 344.
69. Brandt, W., Kliauga, P., *Phys. Rev. B* (1976) **14,** 884.
70. Brandt, W., Spektor, D., *Phys. Rev. Lett.* (1977) **38,** 595.
71. Mogensen, O. E., *J. Chem. Phys.* (1974) **60,** 998.
72. Tao, S. J., *Appl. Phys.* (1976) **10,** 67.
73. Jansen, P., Eldrup, M., Mogensen, O. E., Pagsberg, P., *Chem. Phys.* (1974) **6,** 265.
74. Eldrup, M., Shantarovich, V. P., Mogensen, O. E., *Chem. Phys.* (1975) **11,** 129.
75. Mogensen, O. E., *Appl. Phys.* (1975) **6,** 315.
76. Byakov, V. M., *Int. J. Radiat. Chem.* (1976) **8,** 283.
77. Byakov, V. M., Grafutin, V. I., Koldaeva, O. V., Minaicher, E. V., Nichiporov, F. G., Obukhov, Yu. V., Stepanova, O. P., *Chem. Phys.* (1977) **24,** 91.
78. Anisimov, O. A., Molin, Yu. N., *Khim. Vys. Energ.* (1975) **9,** 539.
79. Anisimov, O. A., Raitsimring, A. M., Molin, Yu. N., *JETP Lett. (Engl. Transl.)* (1976) **33,** 91.
80. Maddock, A. G., Abbe, J. C., Haessler, A., *Chem. Phys.* (1976) **17,** 343.
81. Ibid., (1977) **47,** 314.
82. Wild, R. E., Ache, H. J., *J. Chem. Phys.* (1976) **65,** 247.
83. Ache, H. J., Wild, R. E., Bartal, L. J., *J. Phys. Chem.* (1977) **81,** 941.
84. Hamill, W. H., *J. Phys. Chem.* (1969) **73,** 1341.
85. Sawai, T., Hamill, W. H., *J. Phys. Chem.* (1970) **74,** 3914.
86. Cole, G. D., Walker, W. W., *J. Chem. Phys.* (1963) **39,** 850.
87. Ibid., (1965) **42,** 1692.
88. Cole, G. D., Merritt, W. G., Walker, W. W., *J. Chem. Phys.* (1968) **49,** 1989.
89. Nicholas, J. B., Ache, H. J., *J. Chem. Phys.* (1967) **57,** 1599.
90. Jean, Y. C., Ache, H. J., *J. Am. Chem. Soc.* (1978) **100,** 984.
91. Chuang, S. Y., Tao, S. J., Wang, T. T., *Macromolecules* (1977) **10,** 713.
92. Chuang, S. Y., Tao, S. J., Wilkenfeld, J. M., *J. Appl. Phys.* (1972) **43,** 737.
93. Ulbricht, T. L. V., *Q. Rev. Chem. Soc.* (1959) **13,** 48.
94. Lee, T. D., Yang, C. N., *Phys. Rev.* (1956) **104,** 254.
95. Vester, F., Ulbricht, T. L. V., Krauch, H., *Naturwissenschaften* (1959) **46,** 68.
96. Ulbricht, T. L., Vester, F., *Tetrahedron* (1962) **18,** 629.
97. Garay, A. S., *Nature (London)* (1968) **219,** 338.
98. Bonner, W. A., *J. Mol. Evol.* (1974) **4,** 23.
99. Bonner, W. A., Van Dorf, M. A., Yearian, M. R., *Nature (London)* (1975) **258,** 419.
100. Hrasko, P., KFKI–73–40, Report, Central Research Institute, Hungarian Academy of Sciences, Budapest.
101. Hrasko, P., Garay, A., Keszthelyi, L., *ATOMKI Közl.,* suppl. (1974) **1612,** 195–198.
102. Garay, A. S., Hrasko, P., *J. Mol. Evol.* (1974) **6,** 77.
103. Garay, A. S., Keszthelyi, L., Demeter, I., Hrasko, P., *Chem. Phys. Lett.* (1973) **23,** 549.

Publication Date: June 1, 1979 | doi: 10.1021/ba-1979-0175.ch001

104. Jean, Y. C., Ache, H. J., *J. Phys. Chem.* (1977) **81**, 1157.
105. Rich, A., *Nature (London)* (1976) **264**, 482.
106. Berko, S., Canter, K. F., "Abstracts of Papers," 2nd Joint Conference, Chemical Institute of Canada and ACS, May 1977, PHYS 74.
107. Canter, K. F., Mills, A. P., Jr., Berko, S., *Phys. Rev. Lett.* (1975) **34**, 177.
108. Stein, T. S., Kaappila, W. E., Roellig, L. O., *Phys. Lett.* (1975) **51A**, 327.
109. Roellig, L. O., ADV. CHEM. SER. (1978) **0**, 000.

RECEIVED December 2, 1977.

2

Studies of the Physical Properties of Organic Compounds Using Positronium as a Probe

WILLIAM W. WALKER

Department of Physics and Astronomy, University of Alabama, University, AL 35486

Publication Date: June 1, 1979 | doi: 10.1021/ba-1979-0175.ch002

Numerous experiments have shown that positronium formation and annihilation characteristics can be quite sensitive to the physical structure of the medium surrounding the positron. A brief survey of positron lifetime experiments dealing with phase changes and polymorphism in organic compounds is given. The results of three illustrative examples of this type of measurement are compared with results obtained by the more established techniques. These examples are tripalmitin, the binary system of n-*eicosane and* n-*docosane, and* N-(p-*propoxybenzylidene)*-p-*pentylaniline. These results show that this technique is an effective means of detecting solid–solid transitions, of observing polymorphic forms exhibited by some organics, and of measuring solid–solid transformation rates in some cases.*

It has been suggested many times in the past twenty-five years that experiments using positrons may some day be applied as a tool in the study of the solid and liquid state. However, as noted in 1953 by Bell and Graham (*1*), this is not possible until the interpretation of the observed effects is placed on firm ground. With this goal in mind a number of researchers have investigated the possible application of the positron and particularly its bound state positronium (Ps) to probe physical and chemical properties of condensed matter. Although all types of condensed materials have been examined, the discussion that follows will consider only those investigations involving changes in physical properties of organic compounds.

0-8412-0417-9/79/33-175-051$05.00/1

In Positronium and Muonium Chemistry; Ache, H.;
Advances in Chemistry; American Chemical Society: Washington, DC, 1979.

There are two major reasons why organic compounds provide an interesting setting in which to explore the question of whether or not Ps can probe the physical structure of solids and liquids. First, Ps is readily formed in reasonable quantity in most organics, and second, organics provide an abundance of multiple-phase behavior. This second reason is quite important since one of the major problems limiting the use of Ps as a probe is the fact that the observed behavior of Ps may be the result of a combination of effects which cannot be distinguished from one another by this type of measurement alone. Both polymorphic behavior and phase transitions provide physical structural changes with a minimum of other changes which would further complicate the interpretation of the results.

Publication Date: June 1, 1979 | doi: 10.1021/ba-1979-0175.ch002

The lifetime spectra of positrons annihilating in organic materials usually consist of two or three components. The longest of these components is interpreted as the lifetime of the positrons which had initially formed triplet Ps but were unable to live out their free space lifetime because of the presence of electrons in their environment. The name given to the process by which the triplet Ps has its lifetime shortened in condensed matter is pick-off. In this process the positron in triplet Ps is not annihilated with its electron partner but with an electron (of appropriate spin for singlet annihilation) from the surrounding medium. Because the electron density in the vicinity of the Ps atom is expected to change as the structure of the material changes (i.e., at phase transitions), one expects a corresponding change in the pick-off rate. Similar arguments can be offered to explain the change in the intensity of the long-lived component which is representative of the amount of Ps formed.

One of the early studies dealing with the effect of a phase transition of an organic compound on positron lifetime parameters was the experiment on the melting of naphthalene by Landes et al. (*2*). Both the lifetime and the intensity of the long-lived component were observed to increase by more than a factor of two at the solid–liquid transition, indicating that considerably more Ps was formed in the liquid and the triplet Ps was picked off at a much slower rate. In a similar experiment Cottini et al. (*3*) found no Ps formation in solid anthracene, yet Ps was formed readily in the liquid. They attributed the change to thermally induced disorder.

Subsequently numerous investigations of phase transitions of organic compounds by this technique have been carried out. For example, Brandt et al. (*4, 5*) compared the behavior of crystalline, glassy, and liquid glycerol. The observed results were explained in terms of a free volume effect in the sense that the overlap between the Ps and lattice wave functions is of primary importance in determining the pick-off rate.

Kluth et al. (*6*) have examined solid–liquid phase transitions in a number of organic crystals. They observed a correlation between changes in τ_2 (the lifetime of the long-lived component) and changes in the specific volume of the samples.

Cole et al. (*7, 8, 9*) have used the positron technique to study transitions between solid forms, liquid–crystalline forms, and the isotropic liquid phase in a number of esters of cholesterol. Solid–solid transitions were observed to provide large changes in τ_2 in cholesteryl acetate and cholesteryl propionate. These changes were attributed to changes in the free volume of the molecular lattice. It also was observed that the solution-crystallized and melt-recrystallized solid forms of the formate, butyrate, benzoate, and cinnamate esters were characterized by different positron lifetime values (*10*). In *p*-azoxyanisole and in the various esters of cholesterol examined, no positron annihilation characteristics changed at nematic-isotropic liquid or cholesteric-isotropic liquid transitions. However, the solid–mesophase or solid–isotropic liquid transitions exhibited large effects while the smectic–cholesteric transition showed a much smaller effect. These observations were interpreted as being the results of changes in the intermolecular interactions. Later studies of liquid–crystalline compounds by McNutt et al. (*11*) on *p*-azoxyanisole and by Nicholas and Ache (*12*) on four compounds showed similar results and were attributed to the same cause. Nicholas and Ache did find small changes in τ_2 and I_2 for nematic-isotropic liquid and cholesteric-isotropic liquid transitions. A correlation was found between these changes in τ_2 and the corresponding transition entropies, supporting the contention that the positron annihilation process is affected by variations in the structural regularities of the environment.

Additional solid–solid transitions have been investigated in such compounds as cyclohexane (*13*), cyclooctanone (*14*), methanol (normal and deuterated) (*15*), choline chloride (*16*), and tristearin (*17*). Other phase transition experiments with organic compounds have been performed on methyl mercaptan (*18*), *n*-tetradecane (*18*), *n*-hexadecane (*18*), *n*-octodecane (*18*), 4-butyloxybenzal-4′-ethylaniline (*19*), 4-4-bis-(pentyloxy)azoxybenzene (*20*), and octanol-2 (*21*). In addition, much work has been done on phase changes in organic polymers, but these will not be discussed here.

Several of the papers mentioned above have concluded with an expression of optimism concerning the future of the positron technique. For example, Cooper et al. (*13*) have commented that this technique provides a rapid method of surveying materials for certain solid–solid phase transitions while Chuang and Tao (*18*) have remarked that this technique could have great utility in the study of phase changes, par-

Publication Date: June 1, 1979 | doi: 10.1021/ba-1979-0175.ch002

ticularly in detecting minor changes, perhaps microscopic, before the macroscopic change takes place.

In order to demonstrate what information the Ps technique can reveal about the physical structure of organic compounds, some illustrative recent examples will be described. The examples chosen are tripalmitin (*22*), the binary system of *n*-eicosane and *n*-docosane (*23, 24*), and *N*-(*p*-propoxybenzylidene)-*p*-pentylaniline (PBPA). Comparison of results obtained by the Ps probe with those found by other techniques will be given in each case and correlations with physical structural data will be discussed.

Tripalmitin

Publication Date: June 1, 1979 | doi: 10.1021/ba-1979-0175.ch002

Positron studies of tripalmitin were chosen for inclusion in this chapter because its polymorphism has been the subject of many investigations by different techniques, including x-ray diffraction (*25*), DTA (*26*), DSC (*27*), IR spectroscopy (*28*), dielectric measurements (*29*), and nuclear magnetic resonance (NMR) (*30*). Thus the results of positron measurements can be compared with those found by more established methods.

Based on all types of previous measurements, it has been determined that tripalmitin exhibits three solid forms whose existence depends on sample preparation. These forms are labeled as α, β, and β'. β is the stable phase while α and β' are both metastable phases. The α form is produced easily by quick-cooling a sample from the melt, but β' is much more difficult to produce, requiring moderately slow cooling (~ 0.6 °C/min) from the melt of a thinly spread sample. The stable β phase may be obtained by crystallization from a solvent or by heating either of the metastable phases above their respective transition temperatures. For the purpose of comparison with the positron data, Figure 1 shows DSC thermograms obtained for the three polymorphs of tripalmitin. Observe that the α form converts into β form at 45°C, the β' form converts into the β form at 56°C, and the β form melts at 67°C.

The positron lifetime data were analyzed into two components, with τ_1 and τ_2 representing the mean lives of the shorter and the longer components, respectively. I_2 is the intensity of the τ_2 component. Figure 2 shows the positron data for a sample initially in the β form. At the solid–liquid transition (67°C) both τ_2 and I_2 show rather large increases.

Figure 3 gives the positron results for a sample initially in the α polymorph. The unexpected feature of these data is the changes in slope of τ_2 and I_2 vs. temperature near 32°C, a temperature which does not correspond to a transition according to the DSC thermograms. The fact that the change in τ_2 is gradual rather than abrupt would indicate some-

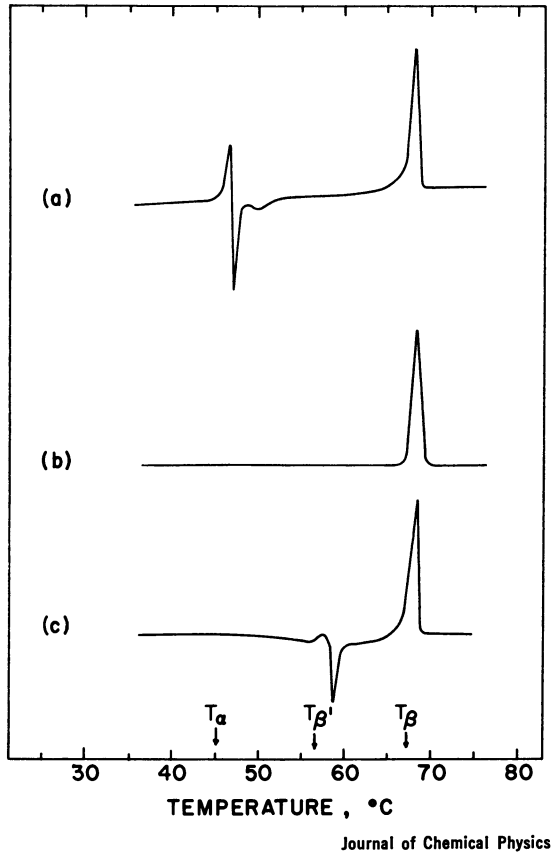

Figure 1. DSC thermograms obtained for the three polymorphs of tripalmitin: (a) α, (b) β, and (c) β′. Melting points are indicated by arrows along the baseline. (22)

Publication Date: June 1, 1979 | doi: 10.1021/ba-1979-0175.ch002

thing other than a simple phase transition. The explanation for this behavior was discovered when it was demonstrated by DSC measurements that prolonged heating (which is necessary for the positron measurements) of the α form at temperatures well below the $\alpha \rightarrow \beta$ transition temperature causes a significant decrease in the relative size of the endotherm corresponding to the $\alpha \rightarrow \beta$ transition. Thus the gradual changes in τ_2 and I_2 over the range from about 32° to 47°C have been interpreted as evidence for the gradual conversion of the pure α sample to β form.

Positron measurements on the pure β' form were obtained only at room temperature owing to the difficulty encountered in producing (and maintaining in pure β' form) samples in a quantity sufficiently large to permit measurements as a function of temperature.

Table I. Positron Lifetime Parameters for the Phases of Tripalmitin (22)

Phase	τ_2 *(nsec)*	I_2*(%)*
α	2.30 ± 0.04	19.1 ± 0.8
β'	2.23 ± 0.04	19.2 ± 0.8
β	$(1.44 - 1.60) \pm 0.04$	29.0 ± 1.2
Liquid	2.71 ± 0.03	36.9 ± 0.8

Journal of Chemical Physics

Table I summarizes the positron lifetime results for tripalmitin. The fact that the lifetime parameters for metastable forms α and β' are close in value implies that these forms have enough structural similarity to provide almost identical electronic environments as far as Ps formation and pick-off annihilation of Ps are concerned. X-ray data agree with this conclusion since it has been found (25) that the strongest short-spacing lines in the powder diffraction patterns of α and β' are almost identical (4.15 and 4.2 Å, respectively), while β has a significantly different intense short-spacing line (4.6 Å).

Although a detailed crystallographic study of tripalmitin has not been published yet, the results are expected to be similar to those re-

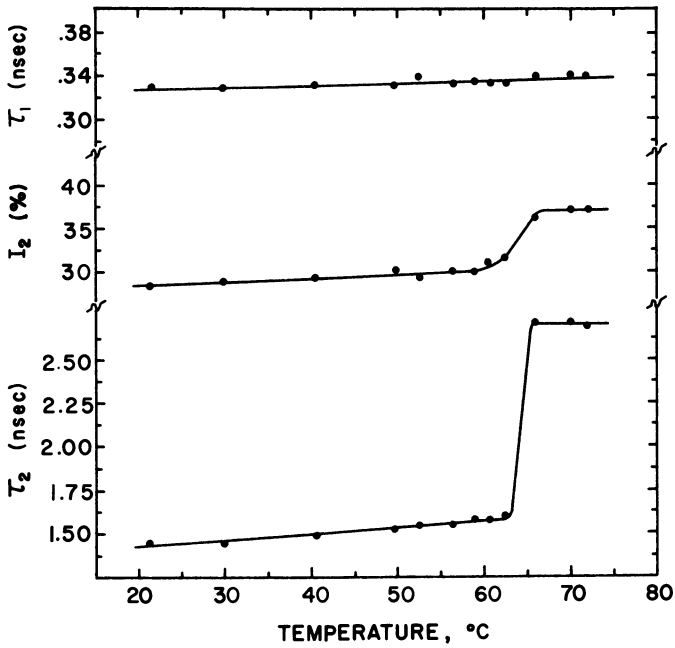

Journal of Chemical Physics

Figure 2. Positron lifetime parameters as a function of temperature in tripalmitin initially in the β polymorph (22)

Publication Date: June 1, 1979 | doi: 10.1021/ba-1979-0175.ch002

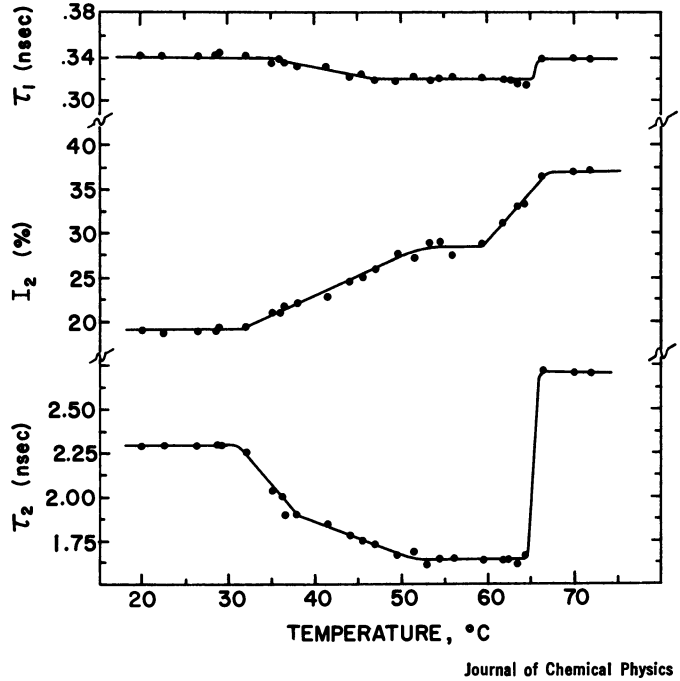

Figure 3. Positron lifetime parameters as a function of temperature in tripalmitin initially in the α polymorph (22)

ported for a similar triglyceride, trilaurin (*31, 32*). The β and β' forms of trilaurin have been found to be triclinic and orthorhombic structures, respectively. It is further known that the area of the *ab* plane in the β' form is approximately twice that of the *ab* plane in the β form while the interlayer spacing (based on the *c* dimension) differs very little. From Table I it is seen that τ_2 in the β' form is about 50% greater than τ_2 in the β form. Thus the more open structure (β') has the smaller pick-off rate (longer lifetime) as would be expected.

Binary System of n-*Eicosane and* n-*Docosane*

The binary system of *n*-eicosane ($C_{20}H_{42}$) and *n*-docosane ($C_{24}H_{46}$) provides an interesting case for application of the positron technique, since it exhibits at least six distinct solid phases whose structures have been reported previously by Lüth et al. (*33*). Their calorimetric and x-ray crystallographic studies have shown that the two terminal solids (γ_1 and γ_2) representing the pure components are triclinic. Samples of intermediate composition may include the high-temperature orthorhombic phase β_0 as well as the low-temperature orthorhombic phases β, β_1, and β_2. These phases may occur separately or in various combinations,

depending on the eicosane–docosane weight ratio and the temperature. We have attempted to examine not only the correlation of positron lifetime parameters with the phase diagram of Lüth et al. but also the relationship between changes in the lifetime of the long-lived component τ_2 and changes in the crystallographic parameters at phase transitions in these binary samples.

Figure 4 gives the positron lifetime results obtained at 21°C for 28 samples, as a function of the weight percent *n*-docosane. Shown along the baseline are the various phases expected according to the results of Lüth et al. The positron lifetime parameters for certain mixtures did not remain constant in time, decreasing gradually over a period of days or weeks. The arrows connect the initial and final values. This behavior will be discussed in more detail later.

The τ_2 has the same value in the pure *n*-eicosane and the pure *n*-docosane while mixtures of the two have a larger τ_2 value in every case. This is not surprising since the pure samples are both in triclinic phases (γ_1 and γ_2) while the mixtures are either in pure orthorhombic phases or a combination of orthorhombic and triclinic phases.

Figure 5 gives the results obtained at 10°C for all samples. At this temperature τ_2 has its largest value in the low-temperature orthorhombic phase β, decreases somewhat for the orthorhombic phases β_1 and β_2, and

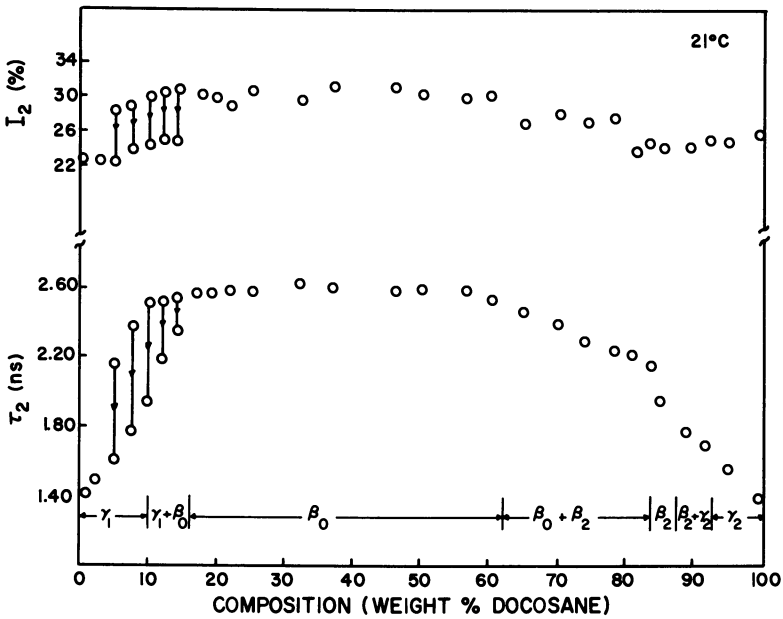

Molecular Crystals and Liquid Crystals

Figure 4. Dependence of τ_2 and I_2 on sample composition for the n-*eicosane*:n-*docosane system at 21°C* (24)

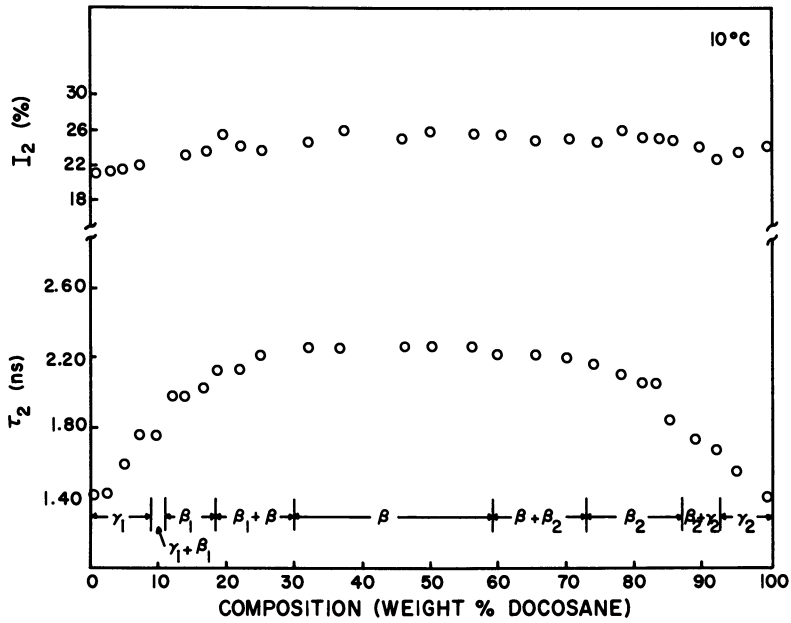

Molecular Crystals and Liquid Crystals

Figure 5. Dependence of τ_2 and I_2 on sample composition for the n-*eicosane*:n-*docosane system at 10°C* (24)

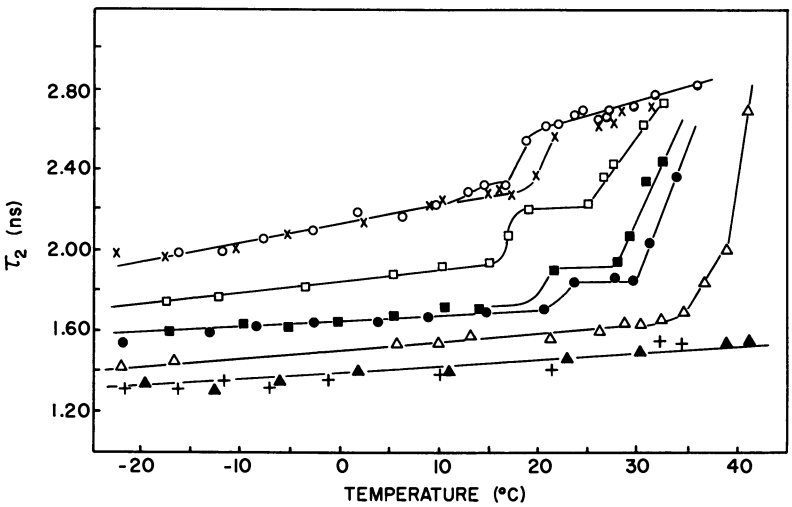

Figure 6. Dependence of τ_2 on temperature for eight samples of the n-*eicosane*:n-*docosane system. Percentage docosane:* + = *0%;* ● = *5%;* ■ = *10%;* □ = *14%;* ○ = *25%;* × = *46%;* △ = *95%;* ▲ = *100%.*

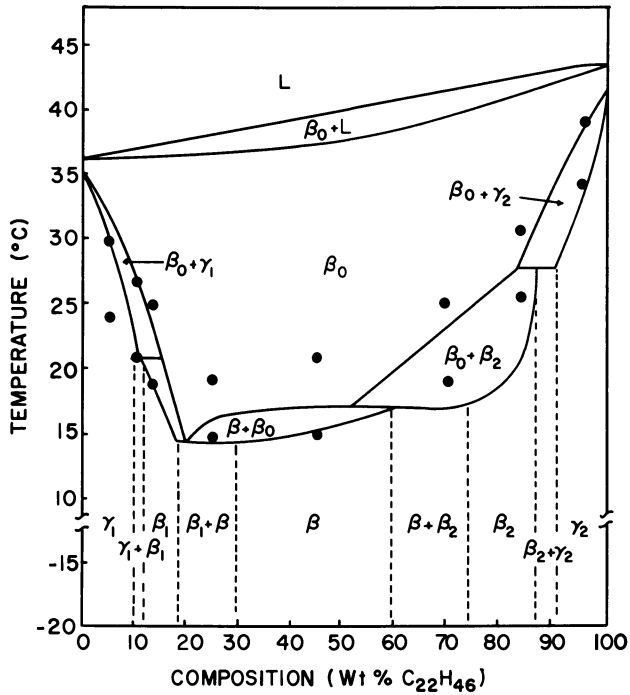

Figure 7. Phase transition temperatures as determined from positron data are shown as solid circles drawn on the phase diagram of Lüth et al. (33)

decreases still further for the triclinic phases γ_1 and γ_2. Observe that τ_2 is the same in the β_1 and β_2 phases, a fact which is not surprising since β, β_1, and β_2 forms are indistinguishable by x-ray powder diffraction.

Figure 6 gives the τ_2 variation with temperature for eight solid samples. From the points where a change of slope occurred in these data the corresponding phase transition temperatures were determined. These transition temperatures obtained from the positron measurements are shown in Figure 7 as solid circles drawn on the phase diagram of Lüth et al. (33). The general agreement is fair with the positron-determined values differing on the average by about 2 degrees from those in the phase diagram. Possible causes for these differences include the quite different heating rates used, the large differences in sample sizes, the differences in the purity of the samples, and the fact that the transition temperatures were determined by quite different techniques in the two cases.

Upon comparison with the published crystallographic data (33) for this binary system, it appears that τ_2 variations in the *n*-eicosane:*n*-docosane system depend more strongly on the lattice dimensions *a* and *b* than on dimension *c*. This conclusion is supported by the following:

Publication Date: June 1, 1979 | doi: 10.1021/ba-1979-0175.ch002

Positron Lifetime Result

1. The τ_2 values in pure *n*-eicosane and pure *n*-docosane are the same.

2. For all compositions of the β_0 phase, τ_2 is approximately constant.

3. At the transition: γ_1(triclinic) $\rightarrow$ β_0(orthorhombic) τ_2 increases about 5%.

4. At the transition: $\beta \rightarrow \beta_0$, $\beta_1 \rightarrow \beta_0$, $\beta_2 \rightarrow \beta_0$, τ_2 increases about 10%.

Structural Comment

1. The *n*-eicosane and *n*-docosane have triclinic structures with the same *a* and *b* dimensions; *c* differs by 2.5 Å.

2. For all compositions of β_0, the area of the *ab* plane is approximately the same; *c* increases monotonically as the percent of *n*-docosane increases.

3. At this transition, the area of the *ab* plane increases about 85%; interlayer periodicity (based on *c* dimension) increases $\sim$ 10%.

4. At these transitions, the area of the *ab* plane increases $\sim$ 3%; *c* dimension is virtually unchanged.

Thus, changes in τ_2 are at least qualitatively related to changes in the area of the *ab* plane of the crystalline lattice. Since τ_2 is the reciprocal of the rate at which triplet Ps is picked off by electrons of the lattice, this result agrees with the expectation that longer lifetimes will occur when the local electron density is decreased owing to lattice expansion.

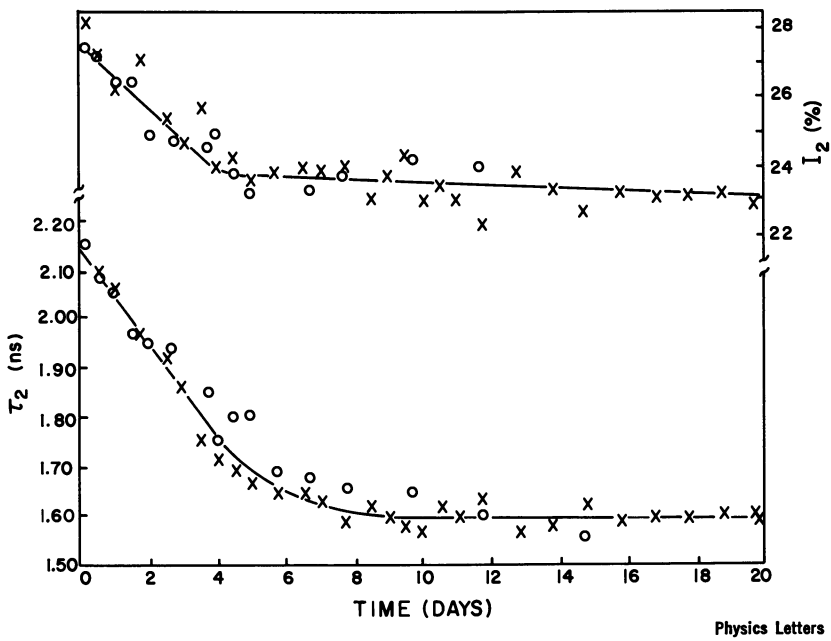

Figure 8. Time dependence of τ_2 and I_2 for sample containing 5.0% n-docosane and 95.0% n-eicosane: O = *Run 1;* × = *Run 2.* (23)

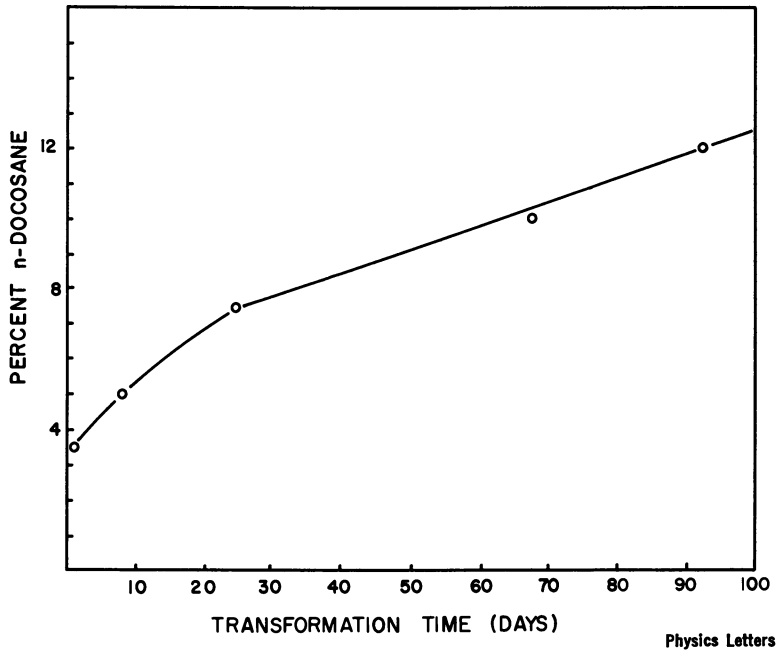

Figure 9. Time required for sample to reach equilibrium values of both τ_2 and I_2 as a function of sample composition for the n-*eicosane:*n-*docosane system* (23)

As mentioned previously, samples having compositions ranging from 3.5% to 14% *n*-docosane exhibit a time dependence in both τ_2 and I_2. These changes are reversible upon remelting the sample, thus ruling out oxidation or other chemical reactions as a cause. Lüth et al. (33) have reported a similar behavior for certain mixtures of this binary system when examined by x-ray powder diffraction. Measurements were made as a function of the time elapsed since the sample solidified from the melt, i.e., the annealing time. Shown in Figure 8 are the data obtained for one of these samples. Figure 9 gives the annealing time required to reach equilibrium values of both τ_2 and I_2 for the five samples studied. From this figure it is seen that samples having higher percentages of *n*-docosane have slower rates of transformation. The interpretation of these positron data is that these samples initially solidify in the β_0 phase and gradually transform into various combinations of the γ, β_0, and β_1 phases. β_0 is the most open structure of the three, possessing larger lattice parameters. Thus the decrease of τ_2 and I_2 during the annealing time can be attributed to the gradual transformation of the sample to a more compact structure in which there is a reduced probability of Ps formation and an increased rate of pick-off of the triplet Ps which is

Publication Date: June 1, 1979 | doi: 10.1021/ba-1979-0175.ch002

formed. These results illustrate another possible use of the Ps probe—that of measuring phase transformation rates for certain solid-state transformations that occur rather slowly.

N-(p-Propoxybenzylidene)-p-Pentylaniline

As a final example of the positron technique as a probe in the study of physical properties of organics, a compound for which no previous solid-phase studies are known to have been published will be discussed. The compound, *N*-(*p*-propoxybenzylidene)-*p*-pentylaniline (referred to hereafter as PBPA), is a liquid–crystal-forming material exhibiting the nematic phase between 34°C and 69°C. A number of studies of the solid forms of other benzylideneanilines has revealed the existence of a multiplicity of low-temperature states, some of which are metastable crystalline forms while others are referred to as glassy (*34, 35, 36, 37, 38*). Most of these studies have utilized the techniques of thermal analysis, IR absorption, Raman spectroscopy, or x-ray diffraction.

Solid samples of PBPA were prepared either by slow cooling (about .3°/min) or fast cooling (sudden immersion in liquid nitrogen) from the nematic phase. During these measurements the sample holder was contained in a heat-sealed plastic bag to prevent contamination by oxygen or moisture. Figure 10 shows the results of the positron measurements on PBPA samples. The values of τ_2 and I_2 are identical for the slow-

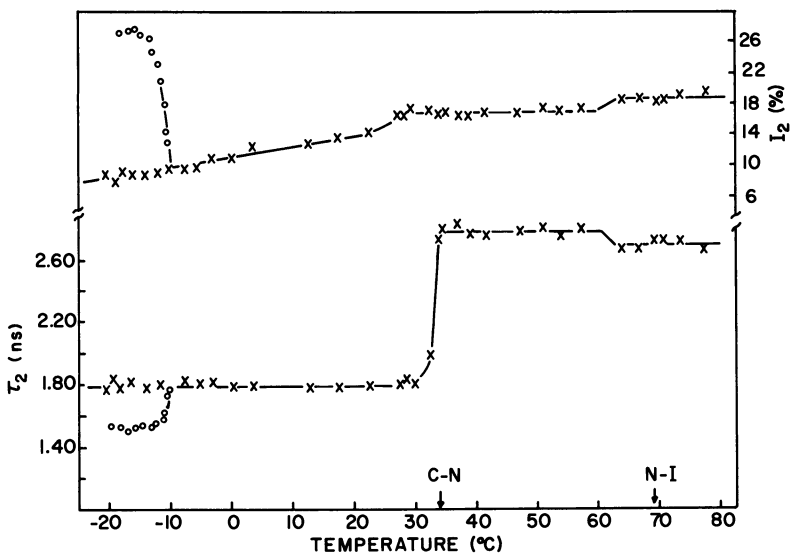

Figure 10. The τ_2 and I_2 as a function of temperature and sample treatment for PBPA: (×), slow-cooled sample; (○), fast-cooled sample.

Publication Date: June 1, 1979 | doi: 10.1021/ba-1979-0175.ch002

cooled and the fast-cooled samples except for temperatures below about −10°C. This difference indicates that PBPA can form two different solid phases at low temperatures, depending on the rate at which the sample was cooled from the nematic phase.

To corroborate this finding, DSC studies were made on similarly prepared PBPA samples. Figure 11 shows a DSC thermogram obtained for a fast-cooled sample. For a slow-cooled sample the results are the same except that the broad exotherm is absent. This type of exotherm is interpreted usually as a slow spontaneous recrystallization into a more ordered structure. Thus both the positron and the DSC measurements agree that PBPA has at least two solid forms: (a) a low-temperature metastable solid which can be obtained by quick-cooling a sample from the nematic phase and (b) a stable form which can be obtained either by slow cooling from the nematic or by heating the metastable form. The fact that different temperatures were obtained for the metastable to stable transition by the DSC and the positron techniques can be explained as being a consequence of the heating rates used. For example, in the DSC measurements the starting temperature of this transition varied over a twenty-degree interval (from approximately −25°C to about −5°C) as the sample heating rate was changed.

It is further seen that when the stable solid form transforms into the nematic phase, the intensity I_2 is affected at a temperature several de-

Publication Date: June 1, 1979 | doi: 10.1021/ba-1979-0175.ch002

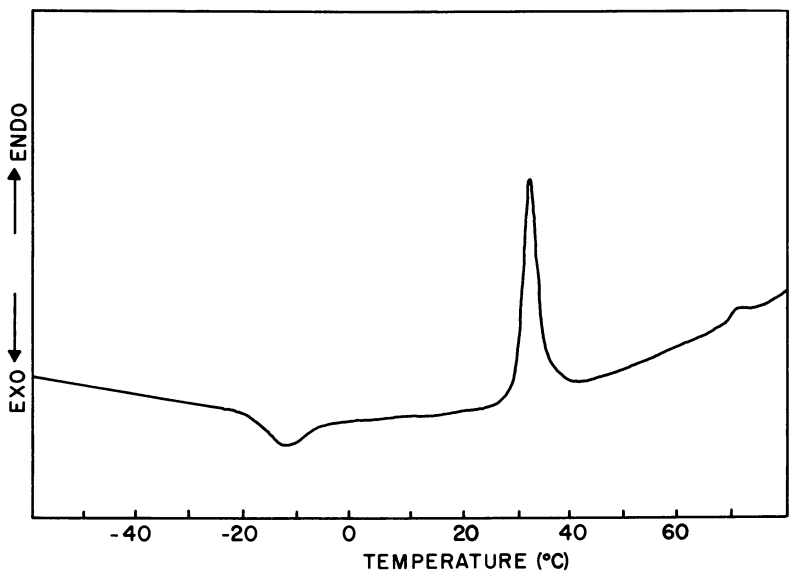

Figure 11. DSC thermogram for a quick-cooled sample of PBPA: heating rate = 10°C/min.

grees below the temperature at which the τ_2 lifetime changes abruptly. This type of behavior, which probably indicates the presence of pretransitional processes, is observed frequently when using this technique.

The transition from nematic to isotropic liquid is marked by a small increase in I_2 and a small decrease in τ_2. The size of the effects here reflects the smallness of the structural changes taking place.

Conclusions

From the experiments which have been described (as well as from other similar studies), it is clear that the technique of positron lifetime measurements has already become a useful tool with which to observe certain physical structural changes in organic solids. For example, it is a particularly effective means of detecting solid–solid phase transitions and of observing the different polymorphic forms obtained by various sample treatments. In some of these cases a qualitative correlation between changes in crystalline lattice parameters and τ_2 lifetime changes has been demonstrated. This technique is also following the progress of certain extremely slow solid–solid transformations, allowing measurement of transformation rates in some cases. However, before more quantitative use of this technique can be realized, further work is required.

Publication Date: June 1, 1979 | doi: 10.1021/ba-1979-0175.ch002

Literature Cited

1. Bell, R. E., Graham, R. L., *Phys. Rev.* (1953) **90,** 644.
2. Landes, H. S., Berko, S., Zuchelli, A. J., *Phys. Rev.* (1956) **103,** 828.
3. Cottini, C., Fabri, G., Gatti, E., Germagnoli, E., *J. Phys. Chem. Solids* (1960) **17,** 65.
4. Brandt, W., Berko, S., Walker, W. W., *Phys. Rev.* (1960) **120,** 1289.
5. Brandt, W., Spirn, I., *Phys. Rev.* (1966) **142,** 231.
6. Kluth, E. L. E., Clarke, H., Hogg, B. G., *J. Chem. Phys.* (1964) **40,** 3180.
7. Cole, G. D., Walker, W. W., *J. Chem. Phys.* (1963) **39,** 850.
8. Cole, G. D., Walker, W. W., *J. Chem. Phys.* (1965) **42,** 1692.
9. Cole, G. D., Merritt, W. G., Walker, W. W., *J. Chem. Phys.* (1968) **49,** 1980.
10. Merritt, W. G., Cole, G. D., Walker, W. W., *Mol. Cryst. Liq. Cryst.* (1971) **15,** 105.
11. McNutt, J. D., Kinnison, W. W., Searcey, M. D., *Phys. Rev.* (1972) **5B,** 826.
12. Nicholas, J. B., Ache, H. J., *J. Chem. Phys.* (1972) **57,** 1597.
13. Cooper, A. M., DeBlonde, G., Hogg, B. G., *Phys. Lett.* (1969) **29A,** 275.
14. Walker, W. W., Merritt, W. G., Cole, G. D., *J. Chem. Phys.* (1972) **56,** 3729.
15. Chuang, S. Y., Tao, S. J., *Phys. Lett.* (1970) **33A,** 56.
16. Wang, C. M., Ache, H. J., *J. Chem. Phys.* (1970) **52,** 5492.
17. Walker, W. W., Merritt, W. G., Cole, G. D., *Phys. Lett.* (1972) **40A,** 157.
18. Chuang, S. Y., Tao, S. J., "Phase Transitions," L. E. Cross, Ed., p. 363, Pergamon, New York, 1973.
19. Walker, W. W., Mueller, E. L., *Appl. Phys.* (1974) **3,** 155.

In Positronium and Muonium Chemistry; Ache, H.;
Advances in Chemistry; American Chemical Society: Washington, DC, 1979.

20. Nash, J. K., McKenney, S., Boatman, P. J., McNutt, J. D., International Conference on Positron Annihilation, 4th, Helsingør, 1976, paper G19.
21. Jean, Y., Ache, H. J., *J. Phys. Chem.* (1977) **81,** 1157.
22. Walker, W. W., Kline, D. C., *J. Chem. Phys.* (1974) **60,** 4990.
23. Walker, W. W., *Phys. Lett.* (1976) **59A,** 319.
24. Walker, W. W., *Mol. Cryst. Liq. Cryst.* (1977) **43,** 45.
25. Hoerr, C. W., Paulicka, F. R., *J. Am. Oil Chem. Soc.* (1968) **45,** 793.
26. Lutton, E. S., Fehl, A. J., *Lipids* (1970) **5,** 90.
27. Hagemann, J. W., Tallent, W. H., *J. Am. Oil Chem. Soc.* (1972) **49,** 118.
28. Chapman, D., *Nature* (1955) **176,** 216.
29. Crowe, R. W., Smyth, C. P., *J. Am. Chem. Soc.* (1950) **72,** 5281.
30. Chapman, D., Richards, R. E., Yorke, R. W., *J. Chem. Soc.* (1960) 436.
31. Vand, V., Bell, I. P., *Acta Crystallogr.* (1951) **4,** 465.
32. Larsson, K., *Ark. Kemi* (1964) **23,** 5.
33. Lüth, H., Nyburg, S. C., Robinson, P. M., Scott, H. G., *Mol. Cryst. Liq. Cryst.* (1974) **27,** 337.
34. Shinoda, T., Maeda, Y., Enokido, H., *J. Chem. Thermodyn.* (1974) **6,** 921.
35. Sciesinska, E., Sciesinski, J., Twardowski, J., Janik, J. A., *Mol. Cryst. Liq. Cryst.* (1974) **27,** 125.
36. Sorai, M., Nakamura, T., Seki, S., *Pramana* (1975) Suppl. 1, 503.
37. Janik, J. A., Janik, J. M., Mayer, J., Sciesinska, E., Sciesinski, J., Twardowski, J., Waluga, T., Witko, W., *J. de Phys.* (1975) Colloq. 1, 159.
38. Lydon, J. E., Kessler, J. O., *J. de Phys.* (1975) Colloq. 1, 153.

RECEIVED December 5, 1977.

Biochemical Applications of the Positron Annihilation Techniques

GEORGE GRAF, EDWARD D. HANDEL,[1] and PHILIP L. McMAHON

Department of Biochemistry, North Dakota State University, Fargo ND 58105

JAMES C. GLASS

Department of Physics, North Dakota State University, Fargo, ND 58105

Publication Date: June 1, 1979 | doi: 10.1021/ba-1979-0175.ch003

The potential of the positron annihilation methods for investigating biological systems has been recognized only recently. This review summarizes the work reported from various laboratories. The positron is sensitive to the electron density of matter and probes many properties of chemical systems. By this novel approach useful information has been gained concerning protein conformation and macromolecular dynamics, phase transitions in model membranes, the behavior of micellar systems, and the formation of molecular complexes. The origin of biomolecular chirality, the photosynthetic apparatus, and the structure of cell water in muscle also have been studied by these techniques. The sensitivity of the method opens new avenues to explore the nature of biological systems with minimum perturbation. Future prospects of this approach to biological systems are discussed.

The existence of the positron was first predicted theoretically by Dirac in 1930 (*1*) and observed experimentally by Anderson in 1933 (*2*). When the positron, the antiparticle of the electron, enters a chemical system, it interacts and annihilates with an electron and their combined masses are converted into gamma photons. Prior to 1951, positron research was directed primarily toward a further understanding of its fundamental

[1] Present address: Department of Chemistry, Virginia Polytechnic Institute and State University, Blacksburg, VA 24061.

0-8412-0417-9/79/33-175-067$05.25/1

In Positronium and Muonium Chemistry; Ache, H.;
Advances in Chemistry; American Chemical Society: Washington, DC, 1979.

properties. In that year, Deutsch observed the existence of a bound state of the positron and electron called positronium (Ps) (*3, 4, 5*). The unique nature of Ps and its specific interaction with matter provides information which otherwise would not be available by more conventional techniques. The versatile character of Ps reactions (oxidation–reduction, spin conversion, and pick-off annihilation) allows for the study of a wide variety of gaseous-, liquid-, and solid-state systems. These studies have been reviewed in numerous publications (For general reviews, *see* Refs. *6, 7, 8, 9, 10*).

There is also a growing number of reports dealing with the application of the positron annihilation techniques to systems of direct biochemical interest. In the early 1970's such complex phenomena as the interaction of cell water with muscle and the photosynthetic process were investigated with the angular correlation technique. These experiments showed that this method is applicable to in vivo systems and is capable of yielding new information. Other work focused on the potential of the lifetime technique in such diverse fields as amino acids and proteins, structure–function relationships in biological macromolecules, protein dynamics, model membranes, micellar systems, and macromolecular complexes of biological importance. The origin of chirality in biological systems was explored also with the positron annihilation lifetime technique. These reports show an emerging trend toward key areas such as the dynamic behavior of macromolecules, their interactions with the cellular environment, and the nature of regulatory phenomena; furthermore, the use of the positron annihilation methods to study micellar systems and model membranes bears the promise of eventual applications in pharmaceutical and clinical research.

Publication Date: June 1, 1979 | doi: 10.1021/ba-1979-0175.ch003

Theory of Positron Annihilation

The positron, the antiparticle of the electron, may be considered as a positive electron. It has the mass and spin characteristics of the electron but carries a unit positive charge. The mode of annihilation of a positron and an electron into gamma photons is dependent on the properties of the medium in which the annihilation occurs. In most studies positrons are obtained by the radioactive decay of certain naturally occurring nuclei (e.g., Na-22 and Cu-64). When high-energy positrons of several hundred KeV enter the sample they rapidly slow down to thermal energies of a few eV through ionizations and collisions. Positrons approaching thermal energies may annihilate either in a free state or in a bound state. Positrons may annihilate freely in a direct encounter with an electron. If the particles interact with their spins in antiparallel orientation (singlet state, $^1S_0$) two photons are emitted in opposite directions. When the positron

and the electron have parallel spins (triplet state, $^3S_1$) three photons are emitted with energies dependent on the angles between them. The free annihilation lifetime in condensed media is generally 0.1–0.5 nsec. The ratio of the two-photon to three-photon annihilation, 372/1, is determined by the relative probabilities of singlet- and triplet-state interactions (*9*). Experimentally observed discrepancies from this ratio indicate that the free annihilation of the positron is not the only annihilation process involved. The other mode of annihilation involves the formation of an electron-positron bound state called Ps. Ps can be regarded as the lightest isotope of hydrogen in which the proton is replaced by a positron. Ps exists in two ground states, triplet state (ortho-positronium, *o*-Ps) in which the particles have parallel spins and singlet state para-positronium, *p*-Ps) with antiparallel spins. Triplet and singlet Ps are formed in the ratio of 3/1. The intrinsic mean lifetime of *p*-Ps is 0.125 nsec while the *o*-Ps has a much longer intrinsic mean lifetime of 140 nsec.

The probability of Ps formation and the details of its subsequent annihilation are dependent on the properties of the sample. A useful model of Ps formation in gases was proposed by Ore in 1949 (*11*). The energy range in which the Ps formation is most probable (Ore gap) depends on the ionization potential (I) and the first excitation level (E) of the substrate molecule. The threshold energy for Ps formation (I − 6.8 eV) is the energy necessary to ionize the substrate molecule minus the binding energy regained upon Ps formation (6.8 eV). Positrons with energies greater than the ionization energy ionize the substrate and do not form Ps; thus the ionization energy establishes the upper limit for Ps formation. If the substrate molecule has excitation levels in the Ore gap and the positron has energies above these levels, a significant number of collisions between the positron and the gas molecules results in the excitation of the substrate; consequently most of the Ps formation occurs between E and I − 6.8 eV. The Ore model has been extended to condensed systems by taking into consideration factors such as dissociation energies and intermolecular interactions (*12, 13*).

Recently, Mogensen proposed an alternative model for Ps formation (*14*). According to this model Ps is formed in the positron spur by a reaction between the positron and an electron. Ps formation competes with the recombination of electrons and ions and the reactions of the electrons and positrons with solvent and scavenger molecules. These reactions are influenced by electron and positron solvation. Mogensen correlates Ps formation probabilities with the electron properties in the spur as determined by techniques of radiation chemistry. This model seems to be in good agreement with experimental results in liquids and solids and is a useful guide for the design of new experiments. In Mogensen's view, the spur reaction model does not exclude the validity of the

Publication Date: June 1, 1979 | doi: 10.1021/ba-1979-0175.ch003

Ore model; the positron in the spur may form Ps with a bound electron if its energy is above I − 6.8 eV. Tao combines certain features of the two models in a modified spur theory and suggests that only the fraction of *o*-Ps which is able to escape the spur has a long lifetime (*15*).

The experimentally useful aspects of positron and Ps interactions with matter are the inhibition and quenching processes. Inhibition of Ps formation is the result of interactions between positrons and substrate molecules which lower the positron energies below the threshold for Ps formation. These interactions include compound formation, i.e. attachment of a positron to a molecule, and collisions resulting in rotational and vibrational excited states of the substrate. Quenching of the Ps lifetime is the result of interactions of the Ps with the substrate molecules. Owing to the inherent short lifetime of the *p*-Ps these processes are largely limited to the *o*-Ps. In a quenching process the *o*-Ps is converted to *p*-Ps or the positron is removed from the *o*-Ps and undergoes free annihilation. These interactions lead to two-photon emission and to a considerably shortened *o*-Ps lifetime. The three major quenching mechanisms are ortho–para conversion, chemical reactions, and pick-off annihilation.

In the presence of magnetic fields or paramagnetic species the *o*-Ps can undergo ortho–para conversion. The reversal of the positron spin relative to the electron spin may result from two processes, spin-flip or electron exchange. Either of these mechanisms yields *p*-Ps which annihilates rapidly with two-photon emission.

The *o*-Ps also may enter into chemical reactions with the substrate molecules. These reactions include oxidation by electron transfer, oxidation by compound formation, oxidation by double decomposition, and reduction (*9*). The oxidation process, for example, yields free positrons with an average lifetime shorter than that of the *o*-Ps in the same medium. The formation of positron or Ps compounds with substrate molecules results in the quenching of *o*-Ps lifetimes and leads to two-photon annihilation.

Another route leading to quenched *o*-Ps lifetimes is pick-off annihilation. In this case, the positron in the *o*-Ps interacts with an electron of the substrate which has opposite spins and subsequently annihilates by two-photon emission. The quenched lifetime in many substances is inversely proportional to the electron density of the material. This relationship has been interpreted in terms of an *o*-Ps residing in low-electron density regions or cavities in the sample (*16, 17*). The free-volume model (*18, 19, 20*) relates lifetimes reduced by pick-off annihilation to structural defects or to free-volume regions. The bubble model (*21, 22, 23, 24*) postulates that the *o*-Ps resides in cavities or bubbles formed by the strong repulsive forces between the Ps and the substrate molecules. In systems of simple molecular liquids and binary mixtures, the pick-off

Publication Date: June 1, 1979 | doi: 10.1021/ba-1979-0175.ch003

lifetime can be related to bulk properties of the liquid such as surface tension and parachor (*25, 26*).

Most positrons in condensed media annihilate with the emission of two photons as the result of inhibition and quenching processes. The angular distribution between the two gamma photons depends on the kinetic energy of the positron–electron system at the instant of annihilation. If the system is at absolute rest, the two photons are emitted in exactly opposite directions. In practice, however, the system usually still has a small amount of kinetic energy which leads to deviations of a few milliradians from the ideal angular distribution of 180°. This type of measurement yields information concerning the electronic environment of the positron since the angular distribution of annihilation photons reflects the distribution of electron momenta. Free positrons usually have some kinetic energy when they annihilate, therefore the angle between the two photons deviates from 180° and leads to a broad component in the angular distribution profile. The heavier *p*-Ps loses most of its kinetic energy after formation and it is responsible for a narrow component in the distribution profile. Increased ortho–para conversion produces more positrons which annihilated as *p*-Ps and leads to the relative increase in the narrow component. Oxidation and pick-off of *o*-Ps, on the other hand, causes increased two-quantum annihilation with a relatively broad angular distribution. The shape of such an angular distribution profile yields information concerning the various annihilation mechanisms.

Publication Date: June 1, 1979 | doi: 10.1021/ba-1979-0175.ch003

Experimental Techniques

The two major experimental approaches in positron annihilation experiments are the positron lifetime technique and the angular correlation technique. In both the nature of interactions between the sample and the positron or Ps is investigated by detecting gamma–gamma coincidences (for general reviews, *see* Refs. *6, 7, 8, 9, 10*).

Positron lifetimes are measured by observing the time elapsed between the emission of a positron into the sample and its subsequent annihilation. The most commonly used source of positrons is Na-22 which has several convenient features. Among these are a half-life of 2.6 years and decay characteristics which produce a 1.28 MeV γ-ray in less than 10^{-11} sec after emission of the positron. This high-energy gamma photon is emitted simultaneously with the positron. The positron lifetime is determined as the time difference between the detection of the 1.28-MeV photon and one of the 0.51-MeV annihilation photons using a fast–slow delayed coincidence system (Figure 1). The fast circuit measures the time between detection of two photons. The detection of a photon on the start side triggers the time-to-pulse height converter (TPHC) to begin building a pulse until a stop signal is received. The amplitude of the TPHC output is proportional to the time difference between the two signals. This pulse is stored temporarily while energy discrimination is being performed in

In Positronium and Muonium Chemistry; Ache, H.;
Advances in Chemistry; American Chemical Society: Washington, DC, 1979.

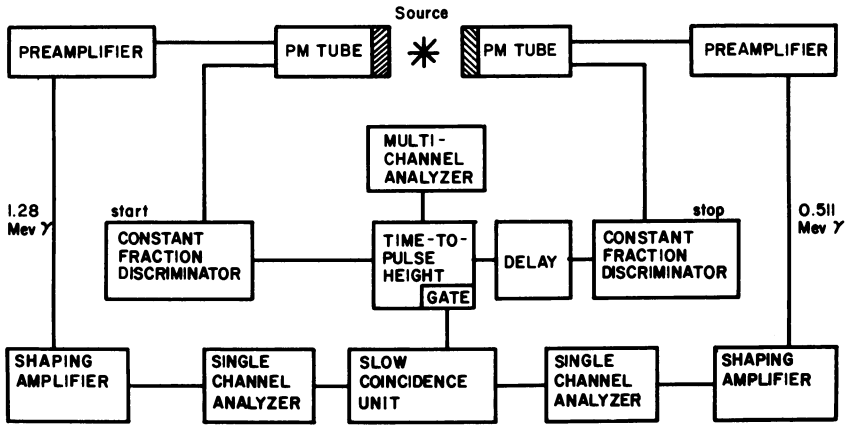

Figure 1. Experimental arrangement for determining positron lifetimes

the slow circuit. The start-side single-channel analyzer (SCA) is set to emit a signal when it receives a 1.28 MeV photon and the stop-side SCA emits a signal upon receiving a 0.51 MeV photon. If these energy requirements are met, the time signal from the TPHC is routed to the multichannel analyzer (MCA) where it is stored in a channel corresponding to its amplitude. A typical lifetime spectrum is composed of about 10^6 events. The number of events observed (number of coincidences between the corresponding gamma photons) is plotted logarithmically as a function of time, i.e., channel number, where each channel represents a time elapsed between a start and a stop signal (Figure 2).

Each one of the annihilation processes contributes a decaying exponential with a decay constant, λ_i, to the spectrum. The lifetime spectrum is analyzed as a sum of exponentials

$$N(t) = \sum_{i=1}^{n} A_i \exp(-\lambda_i t)$$

where n corresponds to the number of components, λ_i is the annihilation rate constant of each component (reciprocal mean lifetime), and A_i is a constant. Associated with each component there is an intensity (I_i), i.e., the percent of positrons annihilating in each process, which is obtained by determining the contribution of that component to the total area. Lifetime spectra are resolved normally into two or three components. In three-component analysis, the shortest lifetime (τ_i) is ascribed to *p*-Ps annihilation, the intermediate lifetime (τ_2) is attributed to free annihilation, and the longest lifetime (τ_3) is assigned to *o*-Ps annihilation process. In the case of two-component analysis τ_1 and τ_2 are combined into the first lifetime and the longer component is assigned to quenched *o*-Ps processes.

Publication Date: June 1, 1979 | doi: 10.1021/ba-1979-0175.ch003

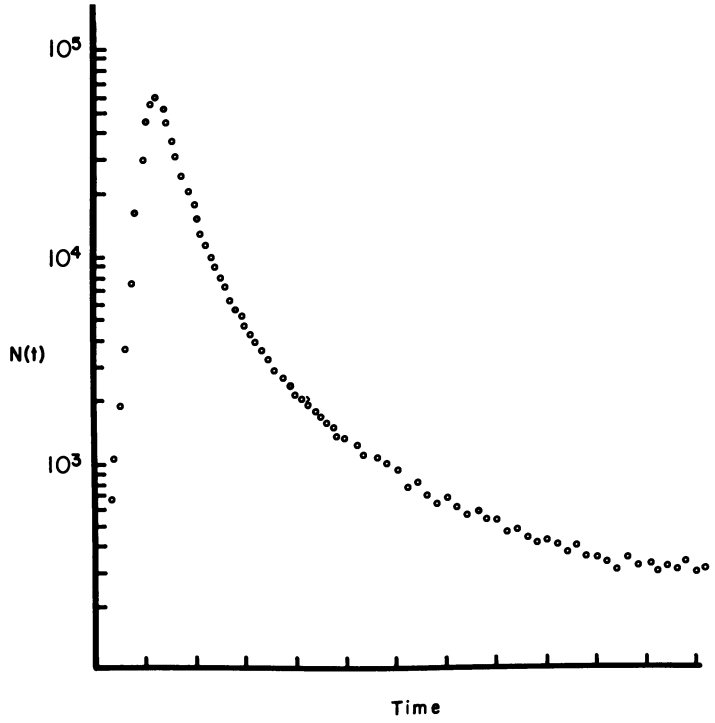

Figure 2. Typical lifetime spectrum. The number of coincidences, N(t), is plotted against time. N(t) values are stored in a MCA in which each channel represents a discrete time interval.

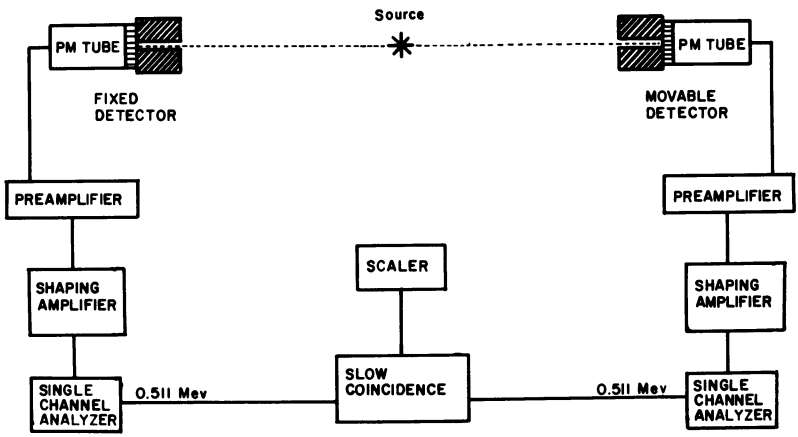

Figure 3. Experiment arrangement for determining the angular correlation of positron annihilation quanta

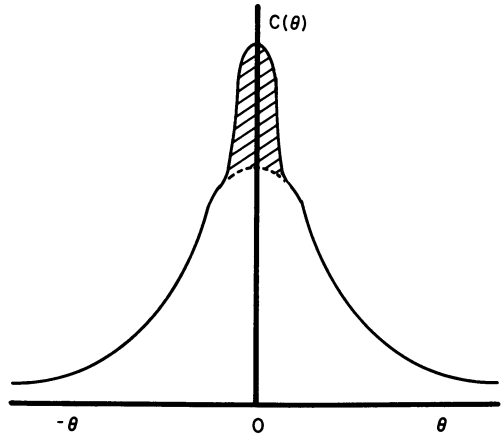

Figure 4. Typical angular correlation spectrum. The number of coincidences, C(θ), is plotted against the angle of deviation, θ, in milliradians from 180°. The shaded area represents the "narrow" component.

In angular correlation experiments only the 0.51-MeV annihilation photons are observed. These measurements are performed using a collimated two-detector, slow-coincidence system in which one detector remains fixed while the other is movable through small angles of the order of a few milliradians (Figure 3). The detection of a photon results in a detector output signal, the magnitude being proportional to the energy of the detected photon. This pulse is routed to a SCA where energy discrimination is performed. Only signals arising from 0.51-MeV photons produce an output signal from the SCA. An event is recorded when a slow-coincidence unit detects simultaneous output signals from both the fixed and movable detectors. An angular correlation spectrum is recorded by measuring coincidences for preset times at several angles and recording the number of coincidences at each angle (Figure 4).

Applications of the Technique

Ps chemistry may be useful to the biochemist in several ways. The interaction of Ps with matter reveals a number of physical and chemical properties which are important parameters in biological systems. Studies on metal defects (*27*) as well as polymer systems (*28;* for potential applications in organic coatings, *see* Ref. *29*) and polymers in which defects have been incorporated (*16*) demonstrated the sensitivity of Ps to structural irregularities. This suggests that Ps may serve as a useful probe of natural voids or free-volume regions in biological macromolecules and supramolecular structures. Studies on proteins, membranes, and the biologically relevant micelles and liposomes already have yielded interesting results.

Publication Date: June 1, 1979 | doi: 10.1021/ba-1979-0175.ch003

The Ps atom also may react with molecules in oxidation reactions and complex formation. Electron donor–acceptor relationships between biomolecules play a major role in biological processes. Information concerning these relationships may be obtained by studying reactions between these molecules and Ps. In another approach, molecules exhibiting strong interaction with Ps can be incorporated into the biological systems. In such studies the Ps annihilation characteristics reflect certain features of the local environment of the secondary probe.

These and other biochemical applications of the positron annihilation techniques will be discussed in the following sections. The major areas covered in this review include complex formation, micelles, and inclusion complexes; amino acids and proteins; synthetic phospholipid vesicles and membranes; and in vivo studies of muscle cell water and photosynthetic processes.

Publication Date: June 1, 1979 | doi: 10.1021/ba-1979-0175.ch003

Complexes, Inclusion Complexes, and Micelles

The positron lifetime spectrum represents the disappearance of positrons in the system. Since the electronic time measurement begins when a positron is formed, the spectrum can be interpreted in terms of a large number of positrons being initially present in the sample and disappearing through annihilation by the various processes. Each mode of annihilation is characterized by an annihilation constant, λ, which is the reciprocal mean lifetime, τ, of the positron.

Ps–molecule complex formation can be evaluated in a quantitative way by setting up appropriate kinetic equations accounting for the reactions of Ps (*30*). A simple reaction scheme for *o*-Ps reacting with a single species (M) in solution is given by:

$$2\gamma \xleftarrow{\lambda_p} o\text{-Ps} + \mathrm{M} \underset{k_2}{\overset{k_1}{\rightleftharpoons}} \mathrm{PsM} \xrightarrow{\lambda_c} 2\gamma$$

where λ_p is the decay rate for *o*-Ps annihilation with the solvent, k_1 and k_2 are the formation and dissociation rate constants for the Ps–molecule complex, and λ_c is the decay rate for annihilation in the complex. The annihilation rate of the long-lived component can be related to the complex formation constant by solving the appropriate rate equations for the system (*30*). Substances having high electron affinities such as nitroaromatics (*30, 31*), quinones (*32*), carbonium ions (*33*), and halogens (*34*) show a strong reactivity with Ps.

The reactivity of these compounds toward Ps is reduced when they form molecular complexes (*35, 36*). Jean and Ache (*37*) used this approach to determine complex formation constants for a number of biological substances. The complex formation constants for vitamin K_1

and α-tocopherolquinone with several electron donor molecules including indole and Vitamin D_3 were determined by their different reactivities towards Ps in their free and complexed form. They found that α-tocopherolquinone, which is believed to be one of the major products in the oxidation of Vitamin E, displays strong reactivity toward Ps. On the other hand, the nonoxidized Vitamin E shows hardly any reactivity. The difference in the behavior in the oxidation product and Vitamin E itself can be utilized for further study of metabolically important biological reactions. This work is important since it demonstrated the capability of the positron annihilation method to study complex formations which cannot be explored by conventional spectroscopic techniques.

The method is not necessarily restricted to donor–acceptor molecular complexes and Jean and Ache applied it for the study of inclusion complexes (*38*). Cyclic oligosaccharides have a toroidal shape with a central void of a few angstroms in diameter. The molecules have an internal hydrophobic surface and an external hydrophilic face. They are known for their ability to complex a variety of molecules in the cavity. Inclusion complexes are capable of catalyzing or inhibiting many chemical and biochemical reactions. The authors found that complexed molecules show drastically reduced reactivity toward Ps; thus by observing the difference in the reactivities of these compounds in their complexed and uncomplexed state it was possible to determine the molecular association constants of the systems. They observed opposite trends in reactivity between the inclusion complex and the Ps–molecule complex in solution. These results can be interpreted in terms of either geometric steric requirements or the nature of the binding forces. If these forces are hydrophobic, future studies of inclusion complexes with the positron annihilation technique offer an opportunity to characterize the nature of this interaction.

The chemical reactivity of Ps toward strong electron acceptor molecules has been exploited recently to investigate micellar systems (*39*). Micellar systems are useful simple models of membranes and are used to study the behavior of aggregates of hydrophobic moieties. The structure of a micelle is fairly well understood in terms of a spherical entity with a hydrophobic core and a polar exterior; still, more information is needed about the solubilizates that can be incorporated into the micelle as well as about the dynamics of the solubilization process (*40*). Micellar systems have been used successfully as catalysts (*41*) for many reactions and extensive studies have been performed to evaluate their influence on the course of a reaction. Jean and Ache (*39*) recently have reported the investigation of various micellar systems in which they incorporated secondary probes (nitrobenzene and copper(II) ion) which exhibit a strong reactivity toward Ps. Previous studies (*31, 42*) of Ps–molecule

Publication Date: June 1, 1979 | doi: 10.1021/ba-1979-0175.ch003

complex formation reactions show that solvent composition is important in stabilizing these complexes.

In most cases the reactivity of Ps toward nitrobenzene was reduced significantly compared with aqueous solutions. However, the rate constants obtained were not the same as those for nitrobenzene in the corresponding alkane. These results suggest that the probe molecule is located near the Stern layer where it forms molecular complexes with the various head groups. In micellar solutions containing copper(II) ion, little or no effect was observed in micelles formed from neutral or cationic surfactants whereas in the presence of anionic micelles the rate constants dropped drastically. Since copper(II) ion is much more soluble in the aqueous phase than the organic phase a reduction of its reactivity would be expected only if it interacted with the polar head groups. This explanation agrees with their experimental findings since, in anionic micelles, the copper(II) ion would be attracted to the Stern layer where it can function as a counter ion.

Publication Date: June 1, 1979 | doi: 10.1021/ba-1979-0175.ch003

Amino Acids and Proteins

The first application of the positron annihilation lifetime technique to amino acids and proteins was reported by Chuang and Tao in 1974 (*43*). They measured the annihilation parameters in solid samples of amino acids and several proteins. Their previous study on simple polymer systems (*44*) indicated a linear relationship between the molecular weight of the polymer and the lifetime of the long-lived component. Their study of amino acids revealed an empirical additivity relationship between the annihilation rate of the long-lived component and the number of strong polar groups in the amino acid molecule. However, they could not find an additivity relationship in the annihilation parameters of the protein based on the amino acid composition. The calculated values of τ_2 were always lower and did not follow the same trend as the measured values.

While recognizing the pioneering nature of their work, it is not surprising that a simple additivity relationship was not found. Biologically functional proteins exist in an aqueous cellular environment and conclusions drawn from the solid state cannot be readily extended to biological systems. Moreover, the amino acid composition and sequence of a protein molecule determines structural domains of preferred orientation and interactions. These secondary structural domains fold and interact to yield a unique tertiary structure of the macromolecule. The polypeptide chain folded in a specific three-dimensional conformation is in intimate contact with the solvent and the interaction with the environment generates structural features which are not commonly encountered in polymer and organic chemistry (*45*).

Jain et al. investigated a series of hemoglobins from different mammalian sources(*46, 47*). Hemoglobin is a quaternary protein composed of four globular subunits. Each subunit contains a nonprotein heme moiety. The positron annihilation characteristics were similar in the lyophilized samples of the hemoglobins. In contrast to the consistency of the annihilation values found in the hemoglobins, the annihilation parameters in Cytochrome c, hemin, and red blood cells were significantly different. The authors interpreted their data in terms of pick-off annihilation and attributed the low Ps formation probability in hemoglobins, as compared with other proteins, to inhibition processes which result from differences in the exposure of the hemes. Their data suggested that Ps formation is not very sensitive to variations in the amino acid composition of the proteins. Chuang and Tao's data (*43*) also support this conclusion. The merit of the work of Jain et al. is that the research was directed toward conformation, and they included in their interpretation the assumption that the *o*-Ps quenching process in proteins is primarily pick-off annihilation. The significance of this assumption becomes clear by a closer scrutiny of the dynamic nature of native protein conformation.

The native protein molecule is a dynamic structure in constant interaction with its environment. Recent developments in molecular biology generated convincing evidence that conformational transitions in macromolecular systems are essential for their function (*48, 49, 50, 51*). The modern understanding of control, energy transduction, and information transfer in biological systems is based on the emerging concepts of the dynamic properties of macromolecules. The unique three-dimensional structure of a protein molecule is determined by its one-dimensional sequence of amino acids in a given environment. Under physiological conditions the folded polypeptide chain is not static but shows some degree of fluctuation passing through sequences of conformational microstates which together constitute an experimentally observable macrostate. The continuously changing cellular demands are acting as constraints on the molecular level by selecting subsets of microstates which respond to the requirements optimally. Transitions between these subsets owing to temperature, pH, and other perturbations caused by binding of effector molecules may be monitored routinely by activity measurements. The nature of these transitions is less accessible to experimental observation. Many sophisticated techniques have been directed toward this goal, but there is no direct approach yet which can provide information about the relationships between these transitions and the overall macromolecular conformation. A plausible choice is the measurement of an observable parameter which is subject to fluctuations and is related directly to overall macromolecular conformations, such as the conformational volume of the molecule. The volume of a specific protein in solution exceeds the overall sum of specific volumes of amino acid residues slightly. The additional

Publication Date: June 1, 1979 | doi: 10.1021/ba-1979-0175.ch003

volume, named conformational volume, may reach as much as 3% of the total volume and its fluctuations may have far reaching effects on biological activity. The emerging picture is that of a protein molecule which responds as a whole to perturbations via rapid conformational transitions and concomitant variations of the conformational volume.

A direct approach to evaluate the empty spaces constituting the conformational volume or, perhaps more accurately, the extensibility of hydrophobic centers of proteins, is the positron annihilation lifetime technique. In 1976, Handel et al. (*52*) measured the temperature dependence of the lifetime and intensity parameters of the globular protein carbonic anhydrase in highly concentrated aqueous solutions over a temperature range of − 20° to 50°C. In all cases the lifetime of the short-lived component remained constant within experimental uncertainties. The lifetime of the long-lived component (τ_2) increased moderately between 20° and 40°C from 1.7–1.9 nsec and then rose further to 2.0 nsec at 50°C (Figure 5). The intensity (I_2) decreased slightly from 27% to 23% over the whole temperature range. The product $I_2\tau_2$ was constant over the temperature range − 20° to 30°C. Above this temperature $I_2\tau_2$ increased rapidly. Simultaneous measurements of the enzymatic activity of carbonic anhydrase showed a steady increase over the same temperature range. Qualitative evaluation of these data in terms of the free-volume model allowed for the following interpretation. The average lifetime of the long-lived component (*o*-Ps) is reduced by various interactions with the substrate. In the pick-off annihilation process the positron is removed from the *o*-Ps under the influence of the electron cloud of the surroundings and undergoes free annihilation. In the free-volume model τ_2 is related to the size of the cavities in which the *o*-Ps atoms are confined and I_2 represents the number of *o*-Ps atoms which are formed and subsequently quenched at these sites. The decrease in the number of free-volume sites at higher temperatures was interpreted as the redistribution and coalescence of free volumes into a system compatible with the new conformation and enhanced enzymatic activity at the elevated temperature. Increasing τ_2 values correspond to an increase of the average size of the free-volume sites which is a further indication of the merging of free volumes. These findings, when correlated with activity measurements, showed that the increase in activity involved conformational changes in which free-volume regions rearrange or combine. In addition, thermal denaturation was associated with the overall expansion of the molecule, since prolonged incubation at 40°C and at higher temperatures produced inactivation and in the irreversibly denatured protein τ_2 and $I_2\tau_2$ remained high even after returning to lower temperatures.

Still another aspect of protein dynamics is the role that the water plays in limiting the number and nature of conformational macrostates of protein molecules. The water at the protein surface is a restraining force

Publication Date: June 1, 1979 | doi: 10.1021/ba-1979-0175.ch003

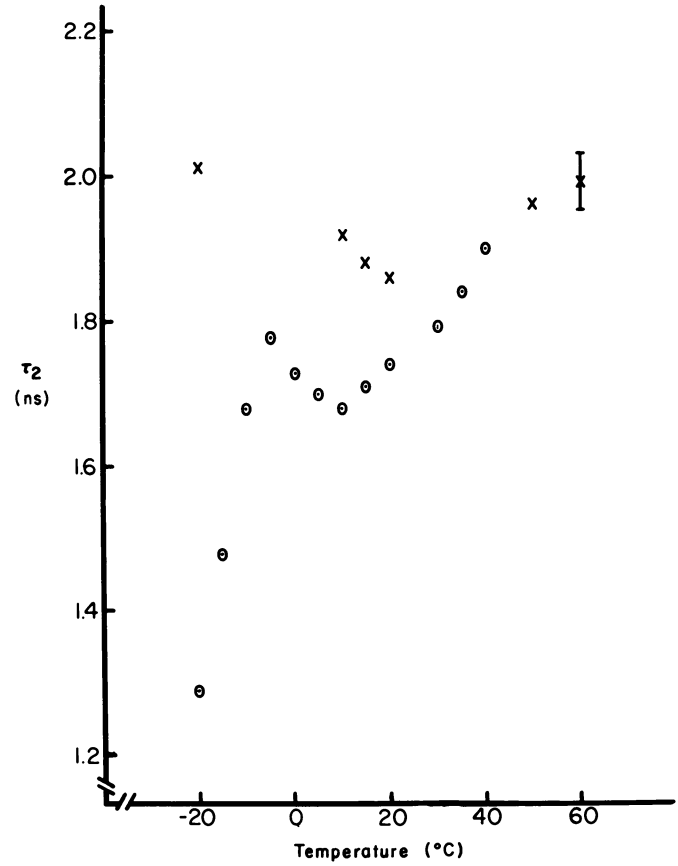

Figure 5. Temperature perturbation of the lifetime of the long-lived component, τ_2, in a 500-mg bovine carbonic anhydrase sample suspended in 1000 mg of water (46): (○), τ_2 values in enzymatically active protein; (×), τ_2 values in heat-denatured protein. Statistical error, indicated by the error bar, is ±0.04 nsec.

that lowers the local entropy and maintains the protein within a range of ordered metastable conformations. Thus the molecule is protected from denaturation while it remains capable of assuming a variety of conformations in response to the cellular demands. Although the nature of water–protein interactions is not well understood, it is clear that the water forms shells close to the protein surface—the A- and B-shells in Gurney's model (*53*)—and appears to be highly ordered (*54*). It is postulated that the adjacent A-shell imposes constraints on protein fluctuation. The more distant B-shell mediates the flow of thermal energy from the bulk water to the protein and dissipates the stresses resulting from the expansions and contractions of the molecule. These stresses, on the other hand, may induce large changes in the free volume of water.

Publication Date: June 1, 1979 | doi: 10.1021/ba-1979-0175.ch003

Handel's approach to protein–water interactions with the positron annihilation technique revealed several features of these systems (*55*). The effect of the bulk water and the protein on the positron annihilation parameters became clearly distinguishable above a critical concentration of the aqueous protein samples. When the temperature dependence of the positron annihilation characteristics were compared with those with protein–water systems the effect of the protein-bound water could be seen clearly by the shifting of the ice-water phase transition to lower temperatures. In mixtures where no bulk water was present and all of the water was tied up in the A-shell and the B-shell of the hydration sphere, these freezing-point lowering effects reached a maximum, down to − 20°C. Water of hydration is likely to be bound in such geometrical configurations that it is incapable of ice formation without extensive rearrangements. At lower temperatures the bound water joins in the ice state, as indicated by a steep decrease of τ_2. The decrease of conformational volume ($I_2\tau_2$) observed upon freezing also could be attributed to the disruption of the bound water in the A-shell. This phenomenon appears to be similar to predenaturation transitions observed by several independent techniques (such as calorimetry) during thermal denaturations of many proteins (*54*).

The pH profile of carbonic anhydrase shows that the enzymatic activity is lowest at extremes of pH and reaches a maximum at pH 6.7 (*56*). It appears from positron annihilation studies (*55*) that the activity dependence on pH is not related to any significant conformational changes in the protein. In light of this, the strong pH dependence of carbonic anhydrase activity can be interpreted as being predominantly caused by the ionization of an activity-linked group in agreement with most of the mechanistic models proposed for this enzyme.

Before leaving the section of amino acids and proteins, the area of the origin of chirality should be discussed. When considering the amino acids as building blocks of proteins one must remember that they occur naturally and overwhelmingly as L-enantiomers. Similarly, natural sugars belong almost exclusively to the D-enantiomorphic series. The origin of the optical asymmetry of biomolecules is one of the most intriguing problems in chemical evolution. Several theories based on chance and non-chance explanations have been suggested. One non-chance explanation is the unequal decomposition of optical isomers through light-mediated reactions and the subsequent generation of optical activity from racemic mixtures (*57*). Following this suggestion a series of experiments was initiated which also included the positron annihilation method. In 1959 Ulbricht postulated a possible connection between the asymmetry at the level of elementary particles and the molecular level (*58*). He proposed a novel mechanism which would relate the phenomenon of asymmetry in biological systems with the universal phenomenon of parity nonconservation in weak interactions. This proposal was based on the Nobel

Publication Date: June 1, 1979 | doi: 10.1021/ba-1979-0175.ch003

Prize winning discovery of Lee and Yang in 1956 who showed that electrons emitted in beta decay are polarized (*59*). However, the attempts to verify unequivocally Ulbricht's suggestion with positron annihilation experiments failed and in 1976 the question still was unresolved (*60, 61, 62, 63, 64*). An interesting approach was taken by Lemmon et al. (*65*) who studied the interaction of epithermal muonium (Mu) with enantiomers but were unable to detect in the residual muon polarization which would indicate selective reactivity. In 1977 Jean and Ache reported similar negative results in their attempt to detect interactions of positrons with several optically active organic liquids (*66*). At the present, at least on the evidence of positron annihilation and Mu experiments, one should seriously question the otherwise quite attractive hypothesis that the two unique chiralities found in the universe are linked causally and the molecular chirality in the biosphere is rooted in a universal law rather than in a chance occurrence.

Publication Date: June 1, 1979 | doi: 10.1021/ba-1979-0175.ch003

Vesicles and Model Membranes

Positron annihilation lifetime measurements has been applied successfully to monitor phase transitions in liquid crystals (*67, 68, 69*). These systems undergo changes in their degree of order at characteristic temperatures. The changes of the positron annihilation parameters during mesomorphic phase transitions can be correlated with the calorimetrically determined transition enthalpies and entropies. This evidence supports the assertion that the positron annihilation process is affected by variations in the structural regularities of the chemical environment. The capability of the technique to correlate structural changes and phase transitions in proteins and liquid crystals has been expanded recently to include model membrane systems. Phospholipid vesicles prepared by dispersion or sonication in an aqueous environment presently are used widely as models to study biological transport processes and other membrane properties. These vesicles undergo reversible fluid-order-phase transitions at characteristic temperatures. From the analogy between vesicle and biological membrane properties, it is safe to conclude that phase transitions are involved in the functioning of cell membranes. Macroscopically observable properties such as sugar transport in some biological systems have been studied as a function of temperature and the results show that cell membranes are liquid crystalline structures (*70*). A more thorough understanding of the dynamics of these transitions recently prompted McGrath et al. (*71*) and McMahon et al. (*72*) to probe vesicle-phase transitions by the positron annihilation lifetime technique. McGrath et al. found a pick-off lifetime of 3.3 nsec in vesicles which are fluid at 18°C (e.g., dioleoyl phosphatidylcholine) and a lifetime of 2.8 nsec in a dipalmitoyl phosphatidylcholine system which is in the gel

In Positronium and Muonium Chemistry; Ache, H.;
Advances in Chemistry; American Chemical Society: Washington, DC, 1979.

phase at the same temperature. Above the transition temperature, dipalmitoyl phosphatidylcholine gave a pick-off lifetime of 3.3 nsec. In another study performed at 18°C, a 1:1 molar ratio of dipalmitoyl phosphatidylcholine and dioleoyl phosphatidylcholine exhibited a lifetime of 3.05 nsec. From these results the authors suggest that the positron may serve as a useful probe for the extent of phase separation in biological membranes. McMahon et al., using the lifetime technique, investigated the phase transition itself over the range from 10°C below to 10°C above the transition temperature in phosphatidylcholine vesicles. They found that the method of vesicle preparation affected the results and that cholesterol incorporated into the phospholipid vesicle broadened the transition temperature.

Publication Date: June 1, 1979 | doi: 10.1021/ba-1979-0175.ch003

In Vivo Studies

Since the nature of the interaction of positrons with matter is determined through the analysis of gamma photons it can be used in the investigation of in vivo systems. Gustafson (*73*) studied Ps formation in muscle tissue using the angular correlation technique to investigate structure in cell water. The Ps formation rate is sensitive to phase transitions and it is considerably greater in ice than in liquid water (*74, 75, 76*). Gustafson's data for muscle and water at 4°C showed no enhancement in the Ps formation rate; therefore he ruled out the possibility that cell water was ordered in a hexagonal ice-like structure. The data for muscle at − 4°C show enhancement of the Ps formation rate between the values observed for water and ice. This indicates that most of the cell water undergoes normal phase transition. However, the possibility exists that cell water is in an ordered form different from ordinary ice.

Dworakowski et al. (*77, 78*) studied the photosynthetic process by the angular correlation technique. They observed an enhancement of the narrow component in irradiated solutions that contained chlorophyll and either phenylhydrazine or ascorbic acid as reductant. However, no enhancement was observed in irradiated solutions which contained only chlorophyll. This was interpreted in terms of the formation of ion radicals and radical intermediates during the photo-induced reduction of chlorophyll, since an unpaired electron in these species will increase the rate of ortho–para conversion and produce an enhanced narrow component. In their experiments with green leaves they found a slight decrease in the narrow component upon illumination with white light. White light activates the two photosystems. When the leaves were irradiated with filtered light which activates only Photosystem I, no effect on the angular correlation spectra was observed. Irradiation with filtered light which activated Photosystem II (and possibly, indirectly, Photosystem I) diminuated the narrow component. They interpreted these results in terms of

a model in which Photosystems I and II are located on the opposite sides of the thylakoid membrane. In this model, excitation of the two photosystems by irradiation leads to the formation of a positive–negative (p–n) type junction inside the thyalkoid membrane accompanied by the generation of an electric field which inhibits Ps formation.

Brandt and Kliauga (*79, 80*), using the lifetime technique, investigated the interaction of Ps with photomagnetic molecules, including photosynthetic materials in vivo such as marine algae and rhododendron leaves. The excited triplet states induced Ps spin conversion. They concluded that the photomagnetic spin conversion was primarily spin flip. In experiments with marine algae they observed no effect when they used a green filter which transmits light between the two absorption peaks of chlorophyll. In experiments using yellow and blue filtered light, centered on the chlorophyll absorption peaks, Ps quenching was observed and the results showed the correct positron action spectrum of chlorophyll.

Publication Date: June 1, 1979 | doi: 10.1021/ba-1979-0175.ch003

Future Perspectives

The positron annihilation method is a new addition to the impressive arsenal of complementary techniques available for biological research. At the same time it provides new insights into biological problems which cannot be obtained through other approaches. Current research efforts are already yielding significant information in the areas of molecule complex formation, micellar systems, macromolecular dynamics, and membrane behavior.

It is clear that the growing recognition of the importance of dynamic conformational fluctuations in macromolecular systems and the key role of the electron donor–acceptor relationship in regulatory and energy transfer processes will require new approaches and methodology in their future investigation. The positron techniques appear to be well suited to study some of these emerging concepts.

Respiration and photosynthesis both require highly organized electron transport chains for the absorption and transfer of energy. It has been suggested (*81*) that the efficiency of these chains may depend on charge-transfer complex formation. These complexes are often difficult to detect by conventional spectroscopic techniques and may be investigated by the positron method.

The charge transfer complexes also are thought to be important in cellular regulation and have even been implicated in cancer (*82*). The investigation of these biological processes also may be approached with the positron annihilation methods.

The logical extension of these studies to membranes is apparent. Positron annihilation studies may provide information concerning membrane-bound molecules and structures. The action of many drugs and

natural bioregulatory molecules such as hormone, quinone, and steroid compounds are thought to be mediated through membrane interactions or by interactions with membrane-bound structures.

The future development of Ps biochemistry is linked intimately to the overall trend of modern biology toward an integrated view of biological processes and to a deeper understanding of the quantum mechanical aspects of biological events.

Acknowledgment

This work was supported by the North Dakota Agricultural Experiment Station (Journal Article No. 828). The authors wish to thank K. McMahon and A. Huseby for the preparation of the manuscript.

Literature Cited

1. Dirac, P. A. M., *Proc. Cambridge Philos. Soc.* (1930) **26,** 361.
2. Anderson, C. D., *Phys. Rev.* (1933) **43,** 491.
3. Deutsch, M., *Phys. Rev.* (1951) **82,** 455.
4. Deutsch, M., *Phys. Rev.* (1951) **83,** 207.
5. Deutsch, M., *Phys. Rev.* (1951) **83,** 866.
6. Gol'danskii, V. I., *Atomic Energy Reviews* (1968) **6,** 3.
7. Green, J., Lee, J., "Positronium Chemistry," Academic, New York, 1964.
8. Stewart, A. T., Roellig, L. O., Eds., "Positron Annihilation," Academic, New York, 1967.
9. Merrigan, J. A., Green, J. H., Tao, S. J., "Physical Methods of Chemistry," A. Weissberger, B. W. Rossiter, Eds., Part IIID, Vol. 1, p. 501, Wiley-Interscience, New York, 1972.
10. Ache, H. J., *Angew. Chem., Int. Ed. Engl.* (1972) **11,** 179.
11. Ore, A., *Univ. Bergen, Arbok, Naturvitensk. Rekke* (1949) **9.**
12. Ferrel, R. A., *Rev. Mod. Phys.* (1956) **28,** 308.
13. Tao, S. J., Green, J. H., *J. Chem. Soc., A* (1968) **2,** 408.
14. Mogensen, O. E., *J. Chem. Phys.* (1974) **60,** 998.
15. Tao, S. J., *Appl. Phys.* (1976) **10,** 67.
16. Ogata, A., Tao, S. J., *J. Appl. Phys.* (1970) **41,** 4261.
17. Tao, S. J., *J. Chem. Phys.* (1972) **56,** 5499.
18. Brandt, W., Berko, S., Walker, W. W., *Phys. Rev.* (1960) **120,** 1289.
19. Thosar, B. V., Kulkarni, V. G., Lagu, R. G., Chandra, G., *Phys. Lett.* (1969) **28A,** 760.
20. Thosar, B. V., Lagu, R. G., Kulkarni, V. G., Chandra, G., *Phys. Status Solidi B* (1973) **58,** 415.
21. Ferrel, R. A., *Phys. Rev.* (1957) **108,** 167.
22. Roellig, L. O., "Positron Annihilation," A. T. Stewart, L. O. Roellig, Eds., p. 127, Academic, New York, 1967.
23. Buchikhin, A. P., Gol'danskii, V. I., Shantarovich, V. P., *Pis'ma Zh. Eksp. Teor. Fiz.* (1971) **13,** 624; *JETP Lett. (Engl. Transl.)* (1971) **13,** 444.
24. Buchikhin, A. P., Gol'danskii, V. I., Tatur, A. O., Shantarovich, V. P., *Zh. Eksp. Teor. Fiz.* (1971) **60,** 1136; *Sov. Phys.—JETP (Engl. Transl.)* (1971) **33,** 615.
25. Lévay, B., Vértes, A., Hautojärvi, P., *J. Phys. Chem.* (1973) **77,** 2229.
26. Lévay, B., Vértes, A., *Kém. Közl.* (1976) **46,** 540.
27. Seeger, A., *J. Phys. F* (1973) **3,** 248.

28. Hamielec, A. E., Eldrup, N., Mogensen, O., Jansen, P., *J. Macromol. Sci., Rev. Macromol. Chem.* (1973) **C9,** 305.
29. Jilek, J. H., *Prog. Org. Coat.* (1977) **5,** 97.
30. Madia, W. J., Nichols, A. L., Ache, H. J., *J. Am. Chem. Soc.* (1975) **97,** 5041.
31. Gol'danskii, V. I., Mogensen, O. E., Shantarovich, V. P., *Phys. Lett.* (1970) **32A,** 98.
32. Tao, S. J., *Appl. Phys.* (1974) **3,** 1.
33. Bartal, L. J., Ache, H. J., *J. Phys. Chem.* (1973) **77,** 2060.
34. Tao, S. J., *J. Chem. Phys.* (1970) **52,** 752.
35. Lévay, B., Hautojärvi, P., *J. Phys. Chem.* (1972) **76,** 1951.
36. Jansen, P., Eldrup, M., Jensen, B. S., Mogensen, O. E., *Chem. Phys.* (1975) **10,** 303.
37. Jean, Y.-C., Ache, H. J., *J. Am. Chem. Soc.* (1977) **99,** 1623.
38. Jean, Y.-C., Ache, H. J., *J. Phys. Chem.* (1977) **81,** 2093.
39. Jean, Y.-C., Ache, H. J., *J. Am. Chem. Soc.* (1977) **99,** 7504.
40. Mittal, K. L., "Micellization, Solubilization and Microemulsions," Vols. 1 and 2, Plenum, New York, 1977.
41. Fendler, J. H., Fendler, E. J., "Catalysis in Micellar and Macromolecular Systems," Academic, New York, 1975.
42. Hall, E., Madia, W. J., Ache, H. J., *Radiochem. Radioanal. Lett.* (1975) **23,** 283.
43. Chuang, S. Y., Tao, S. J., *J. Phys. Chem.* (1974) **78,** 1261.
44. Chuang, S. Y., Tao, S. J., *J. Appl. Phys.* (1973) **44,** 5771.
45. Némethy, G., Scheraga, H. A., *Q. Rev. Biophys.* (1977) **10,** 240.
46. Jain, P. C., Pancholi, S. C., Gupta, M. M., *Indian J. Biochem. Biophys.* (1973) **10,** 85.
47. Jain, P. C., Jain, R. R., Joshi, P., Gupta, M. M., *Indian J. Biochem. Biophys.* (1974) **11,** 340.
48. Simon, Z., "Quantum Biochemistry and Specific Interactions," Abacus, Tunbridge Wells, Kent, England, 1976.
49. Masson, R., Wistrich, A., *FEBS Lett.* (1973) **31,** 114.
50. Karplus, H., Snyder, A. G., Sykes, B., *Biochemistry* (1973) **12,** 1323.
51. Careri, G., Fasella, P., Gratton, E., *CRC Crit. Rev. Biochem.* (1975) **3,** 141.
52. Handel, E. D., Graf, G., Glass, J. C., *J. Am. Chem. Soc.* (1976) **98,** 2360.
53. Gurney, R., "Ionic Processes in Solutions," Dover Publications, New York, 1962.
54. Lumry, R., Rosenberg, A., "Proceedings of the Conference on Water at Roscoff, France," A. Alfsen, A. Berteand, Eds., French National Research Center, Paris, 1975.
55. Handel, E. D., Ph.D. Thesis, North Dakota State University, Fargo (1977).
56. Tallman, D. E., Graf, G., McNeese, T. J., Wilson, M. M., *J. Am. Chem. Soc.* (1975) **97,** 173.
57. Bonner, W. A., "Exobiology," C. Ponnanperuma, Ed., p. 209, North Holland, Amsterdam, 1972.
58. Ulbricht, T. L. V., *Q. Rev. Chem. Soc.* (1959) **13,** 48.
59. Lee, T. D., Yang, C. N., *Phys. Rev.* (1956) **104,** 254.
60. Garay, A. S., *Nature (London)* (1968) **219,** 338.
61. Garay, A. S., Keszthelyi, L., Demeter, I., Hrasko, P., *Chem. Phys. Lett.* (1973) **23,** 549.
62. Dézsi, I., Horváth, D., Kajcsos, Zs., *Chem. Phys. Lett.* (1974) **24,** 514.
63. Brandt, W., Chiba, T., *Phys. Lett.* (1976) **57A,** 395.
64. Rich, A., *Nature (London)* (1976) **264,** 482.
65. Lemmon, R. M., Crowe, K. M., Gygax, F. N., Johnson, R. F., Patterson, B. D., Brewer, J. H., Fleming, D. G., *Nature (London)* (1974) **252,** 692.
66. Jean, Y.-C., Ache, H. J., *J. Phys. Chem.* (1977) **81,** 1157.
67. Cole, G. D., Walker, W. W., *J. Chem. Phys.* (1965) **42,** 1692.

Publication Date: June 1, 1979 | doi: 10.1021/ba-1979-0175.ch003

68. Wang, C., Ache, H. J., *J. Chem. Phys.* (1970) **52,** 5492.
69. Nicholas, J. B., Ache, H. J., *J. Chem. Phys.* (1972) **57,** 1597.
70. Overath, P., Thilo, L., Träuble, H., *Trends Biochem. Sci.* (1976) **1,** 186.
71. McGrath, A. E., Morgan, C. G., Radda, G. K., *Biochim. Biophys. Acta* (1977) **466,** 367.
72. McMahon, P. L., Graf, G., Glass, J. C., "Abstracts of Papers," 174th National Meeting, ACS, Chicago, Sept. 1977, BIOL 174.
73. Gustafson, D. R., *Biophys.* (1970) **10,** 316.
74. Colombino, P., DeBenedetti, S., Degregori, I., Trossi, L., *Nuovo Cimento* (1958) **8,** 508.
75. Fabri, G., Germagnoli, E., Quercia, I. F., Turrisi, E., *Nuovo Cimento* (1963) **30,** 21.
76. Smedskjaer, L. C., Ph.D. Thesis, Technical University of Denmark, Lyngby (1973).
77. Dworakowski, J., Hejnowicz, Z., Kolodziej, H. B., Wesolowski, J., *Photosynthetica* (1970) **4,** 309.
78. Dworakowski, J., Hendrich, W., Wesolowski, J., *Photosynthetica* (1974) **8,** 344.
79. Brandt, W., Kliauga, P., *Phys. Rev. Lett.* (1973) **30,** 354.
80. Brandt, W., Kliauga, P., *Phys. Rev. B* (1974) **14,** 884.
81. Calvin, M., *J. Theor. Biol.* (1961) **1,** 258.
82. Szent-Györgyi, A., "Electronic Biology and Cancer," Marcel Dekker, New York, 1976.

RECEIVED January 23, 1978.

Publication Date: June 1, 1979 | doi: 10.1021/ba-1979-0175.ch003

Photomagnetic Positron Annihilation Effects

WERNER BRANDT

Department of Physics, New York University, New York, NY 10003

Publication Date: June 1, 1979 | doi: 10.1021/ba-1979-0175.ch004

The annihilation characteristics of positrons in phosphorescent substances can be altered by illumination with UV light. This phenomenon and its quantitative aspects agree with the idea that some positrons capture an electron to form ortho- or para-positronium, and that the interaction with the excited triplet states of the illuminated phosphor molecules quenches positronium through spin conversion. Photomagnetic positronium spin conversion cross sections are very large, approximately $10^4\pi a^2_0$. *They correspond to interaction ranges of about 30 Å and are symptomatic of the wave mechanical behavior of positronium in matter. Analysis suggests that the photomagnetic effect proceeds by a process labeled spin flip in which ortho- and para-positronium interconvert under the simultaneous quenching of the excited triplet state to the singlet molecular ground state.*

It is remarkable that UV light can alter the characteristics of positron–electron annihilation into high-energy gamma quanta in matter (*1*, *2*, *3*). The effect is caused by light-induced changes of the electronic states from which annihilation can occur. In particular, light can populate excited triplet states of molecules with singlet ground states. Interaction of positrons with triplets can affect the spin states of the positron–electron pairs and, thus, the mode of annihilation in accordance with quantum electrodynamic selection rules. The phenomenon can serve to detect traces of photo-excited triplet states in matter.

Photomagnetism

Phosphorescence is the slow emission of light in symmetry-forbidden electronic transitions. They occur from paramagnetic excited triplet states, with spin quantum number $S = 1$, to the diamagnetic singlet

0-8412-0417-9/79/33-175-089$05.00/1

In Positronium and Muonium Chemistry; Ache, H.;
Advances in Chemistry; American Chemical Society: Washington, DC, 1979.

ground state, with $S = 0$, as shown schematically in Figure 1. Triplet states are populated indirectly. Light is absorbed in allowed transitions from the ground state to excited singlet states. They can convert into excited triplet states through intersystem-level crossings, followed by rapid transitions to the lowest excited triplet state, T_1. The lifetime of T_1 is determined by the branching ratio for radiationless and phosphorescent light-emitting transitions to the singlet ground state. The triplet lifetime of large phosphor molecules can be prolonged by as much as a factor of 10^3 if they are imbedded in a rigid medium. It impedes intramolecular motion and thus suppresses radiationless transitions induced by vibronic coupling to the electronic ground state. This method commensurably enhances the steady-state triplet concentration under equal illumination conditions.

Publication Date: June 1, 1979 | doi: 10.1021/ba-1979-0175.ch004

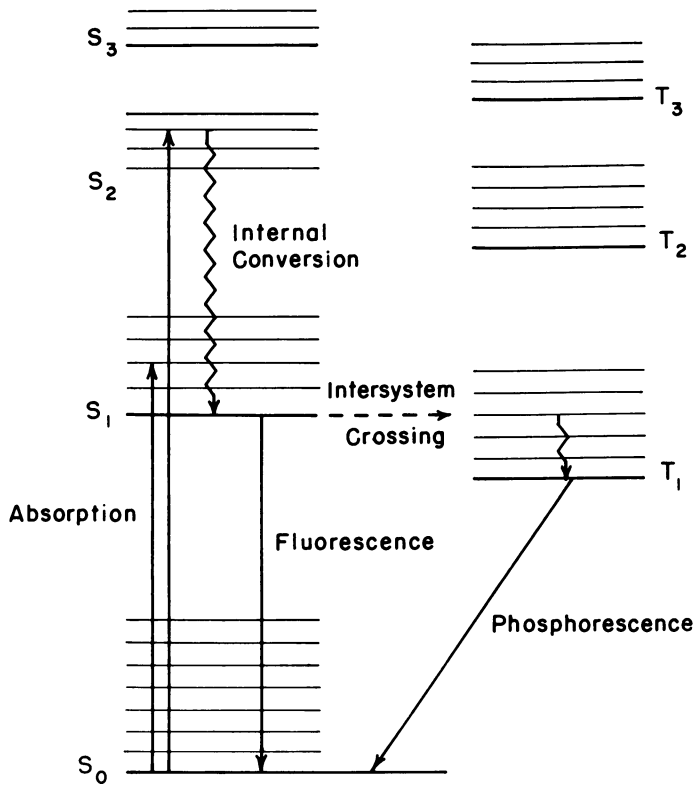

Figure 1. Schematic energy level diagram for a typical phosphor molecule (Jablonski diagram). Singlet states are labeled as S_0, S_1, . . . ; triplet states as T_1, T_2, ... The lowest excited triplet state, T_1, is denoted as T in the text.

Photomagnetism first was demonstrated macroscopically through a change of the weight of phosphorescent samples in inhomogenous magnetic fields under illumination (*4*), and microscopically through paramagnetic resonances of the photo-excited triplet states (*5*).

Positronium

When energetic positrons from a radioactive source penetrate a medium, they are slowed down by ionizing collisions. In many molecular substances a fraction can capture electrons into the stable atomic state of a positron–electron pair referred to as positronium (Ps). In a diamagnetic milieu, three-fourths of Ps forms as triplet or ortho-positronium (*o*-Ps) with $S = 1$, where one-fourth populates each of the three almost degenerate substrates of magnetic quantum numbers $m = -1$, 0, and $+1$. The remaining one-fourth of Ps forms as singlet or para-positronium (*p*-Ps) with $S = 0$ and $m = 0$.

Ps is unstable with regard to positron–electron annihilation into gamma quanta. Quantum electrodynamic selection rules permit rapid annihilation of *p*-Ps into two gamma quanta, each of energy $mc^2 = 0.511$ MeV, with the rate 8.0×10^8 sec^{-1}. They permit *o*-Ps to annihilate only into three gamma quanta, with the slow rate 7.05×10^6 sec^{-1}.

If the slowing-down conditions are shifted, for example, through additives with lower ionization potentials than that of the matrix molecules, the total Ps yield can increase or decrease depending on the details of the Ps formation process. Once formed, a Ps state can be quenched, i.e., its lifetime shortened, by interactions with the medium. They may be discussed as follows.

(1) Electron pick-off from the medium by positrons bound in the long-lived *o*-Ps state, leading to rapid paradecay into two gamma rays.

(2) Oxidation or dissociation to unbound positron states and subsequent paradecay with an electron bound in the medium.

(3) Compound formation with molecules leading to paradecay.

(4) Spin conversion in external magnetic fields or on paramagnetic molecules through the mixing of the magnetic sublevel $m = 0$ of the *o*-Ps triplet state and the *p*-Ps singlet state which are separated by a gap of only about 10^{-3} eV.

This suggests that photomagnetism can affect positron annihilation.

Commonly Studied Annihilation Characteristics

Lifetimes. Positrons are implanted in a sample from a radioactive source, usually ^{22}Na. It emits simultaneously with each positron a 1.28-MeV gamma ray which is detected. The time delay until coincidence with one of the 0.511-MeV annihilation gamma rays from the paradecay

Publication Date: June 1, 1979 | doi: 10.1021/ba-1979-0175.ch004

of the positron in the medium is recorded. The distribution of some 10^5 time delays constitutes the positron lifetime spectrum in this sample. The spectrum is decomposed into i components with intensities, I_i. They represent the probabilities with which positrons populate states with distinct disappearance rates Γ_i. Spectra for molceular substances are analyzed often in terms of two ($i = 1, 2$) or three ($i = 0, 1, 2$) components. The longest-lived component, $i = 2$, usually can be attributed in a consistent manner to the decay of *o*-Ps through electron pick-off or other Ps-quenching reactions.

Angular Correlation. The two 0.511-MeV gamma rays from paradecay emerge in opposite directions from the annihilation site to conserve momentum. Deviations from π rad, of the order of milliradians, are detected in coincidence experiments. They measure the momentum distribution of the annihilating pair in the laboratory frame. The *p*-Ps formed with probability $(1/4)\beta_{Ps}$ decays by rapid self-annihilation. The gamma rays carry away the momenta of the thermal Ps, resulting in a narrow component in the angular correlation of relative intensity $F_N = (1/4)\beta_{Ps}$. Positrons bound in *o*-Ps annihilate mostly in paradecay via pick-off of electrons bound to molecules in high momentum states. This gives rise to a broad component in the angular correlation of intensity (3/4:1/4) relative to the narrow component. Inhibition of Ps formation or Ps quenching by chemical reactions reduce the narrow component and thus lower the coincidence count rate, P, at π rad.

Doppler Shift. The energy distribution of the electrons annihilating with positrons can be measured by the Doppler shifts relative to the 0.511-MeV gamma ray energies as emitted in the positron–electron rest frame. They convey equivalent information to the momentum distribution extracted from angular correlation measurements.

Criteria for Positronium Conversion

Table I summarizes the expected changes in Γ_2, I_2, and P induced by various causes. Spin conversion of *o*-Ps enhances Γ_2 and feeds the *p*-Ps population which increases P. Only a small fraction of the much shorter-lived *p*-Ps population survives to convert to *o*-Ps. It is not enough to offset the increase in P owing to the conversion of *o*-Ps to *p*-Ps, but it enhances the *o*-Ps population I_2. Other Ps-quenching processes give different patterns of change.

The rate of *o*-Ps annihilation into three gamma quanta is proportional to I_2/Γ_2. Since both I_2 and Γ_2 are expected to increase under illumination, changes in the three-gamma rate are not specific for spin conversion. Magnetic fields quench triplet states. The efficiency is proportional to the energy separation between the triplet and the singlet

Publication Date: June 1, 1979 | doi: 10.1021/ba-1979-0175.ch004

Table I. Changes in Positron Annihilation Characteristics Caused by Positronium Quenching Through Different Processes[a]

		Ps		
Characteristic	*Change*	*Oxidation or Compound*	*Inhibition*	*Ps Spin Conversion*
o-Ps disappearance rate	$\Delta\Gamma_2$	+	0	+
o-Ps lifetime intensity	ΔI_2	0	−	+
π rad angular correlation	ΔP	−	−	+

[a] The symbols −, 0, + denote decrease, no change, and increase of the characteristic, respectively.

states. As mentioned, it is 10^{-3} eV between the ground states of *o*-Ps and *p*-Ps. In phosphor molecules, the separation between excited states is about 0.1 eV. Therefore, application of a magnetic field can demonstrate only the well-known magnetic quenching of *o*-Ps, but not the reduction of photomagnetic Ps spin conversion through the quenching of excited triplet states.

The specificity of the conversion process is demonstrated through the action spectrum, that is, light affects positron annihilation only to the extent that it is absorbed by the phosphor molecules.

Prolegomena

In designing experiments to demonstrate photomagnetic positron annihilation effects, we consider light of frequency ω and intensity $L_0(\omega)$ entering, at $x = 0$, a sample of thickness D. It consists of inert diamagnetic molecules of density n and of phosphor molecules at small concentration, c, and density $cn << n$. At depth $x < D$, the light produces a steady-state concentration, c_T, of randomly distributed phosphor molecules in the excited triplet state, T. Assuming that the Lambert–Beer law is valid, one has

$$c_T(x,\omega) = c\,\frac{\phi_T\tau_T\epsilon(\omega)L_0(\omega)\exp[-\epsilon(\omega)cnx]}{1+\phi_T\tau_T\epsilon(\omega)L_0(\omega)\exp[-\epsilon(\omega)cnx]}, \qquad (1)$$

where ϕ_T is the triplet-state formation efficiency, τ_T the triplet lifetime, and $\epsilon(\omega)$ the photoabsorption cross section which is proportional to the usual extinction coefficient. Normally conditions are far from saturation such that $c_T << c$, implying that the denominator can be set equal to 1.

Positrons from a ^{22}Na source enter the sample through the opposite surface at $x = D$. (The experiment also can be performed with both light and positrons entering at $x = 0$, with equal results.) Positrons are stopped in the sample between x and $x + dx$ with probability $\alpha_+ \times \exp$

Publication Date: June 1, 1979 | doi: 10.1021/ba-1979-0175.ch004

$[-\alpha_+(D-x)]dx$, where α_+ is the positron absorption coefficient, with the value $\alpha_+(^{22}\mathrm{Na}) = 42\ d\ \mathrm{cm}^{-1}$, d being the mass density of the sample in grams per cubic centimeter. They form Ps with the probability

$$dp_{\mathrm{Ps}}(x) = \alpha_+\beta_{\mathrm{Ps}}e^{-\alpha_+(D-x)}dx, \tag{2}$$

where β_{sP} is the Ps yield. The positron fraction $f_{\mathrm{S}} = 1 - f_{\mathrm{W}} = 1 - \exp(-\alpha_+D)$ annihilates in the sample, while the fraction f_{W} passes through the light entrance surface and annihilates in the sample wall.

As Ps and T interact, p-Ps is quenched at the rate $\kappa_p(x,\omega)$ and o-Ps at the rate $\kappa_o(x,\omega)$. Assuming that spin conversion changes p-Ps to o-Ps and o-Ps to p-Ps with efficiencies α_p and α_o, respectively, one can set

$$\kappa_p(x,\omega) = \alpha_p\nu_{\mathrm{T}}nc_{\mathrm{T}}(x,\omega); \quad \kappa_o(x) = \alpha_o\nu_{\mathrm{T}}nc(x,\omega). \tag{3}$$

The volume rate, $\nu_{\mathrm{T}} = v_{\mathrm{Ps}}\sigma_{\mathrm{T}}$, depends on the thermal Ps velocity, v_{Ps}, and the spin interaction cross section σ_{T}. Given the annihilation rates in the dark of p-Ps, $\Gamma_1^{\mathrm{off}} = \gamma_p = 8.0 \times 10^9\ \mathrm{sec}^{-1}$, and of o-Ps, $\Gamma_2^{\mathrm{off}} = \gamma_o$, the rates under illumination become

$$\Gamma_1(x,\omega) = \gamma_p + \kappa_p(x,\omega); \quad \Gamma_2(x,\omega) = \gamma_o + \kappa_o(x,\omega). \tag{4}$$

The Ps lifetime spectrum at x is

$$dn_{\mathrm{Ps}}(x,\omega;\ t) = dp_{\mathrm{Ps}}(x)\,[i_1(x,\omega)\,e^{-\Gamma_1(x,\omega)t} + i_2(x,\omega)\,e^{-\Gamma_2(x,\omega)t}], \tag{5}$$

where the intensities

$$i_2(x,\omega) = 1 - i_1(x,\omega) = \frac{\Gamma_1(x,\omega) - \gamma}{\Gamma_1(x,\omega) - \Gamma_2(x,\omega)}, \tag{6}$$

are linked to the rates through the spin-averaged rate constant $\gamma = (1/4) \times \gamma_p + (3/4)\gamma_o$.

Inasmuch as the 0.511-MeV gamma ray detector averages over sample, the recorded time-delay distribution becomes

$$n(t) = f_{\mathrm{W}}e^{-\Gamma_{\mathrm{W}}t} + f_{\mathrm{S}}(1 - \beta_{\mathrm{Ps}})\,e^{-\Gamma_{\mathrm{S}}t} + \int_0^D \frac{dn_{\mathrm{Ps}}(x,\omega;\ t)}{dx}\,dx. \tag{7}$$

The annihilation rate in the wall material is denoted by Γ_{W}, and the mean disappearance rate of unbound positrons in the sample by Γ_{S}. It is convenient to arrange the sample assembly such that either $f_{\mathrm{W}} << f_{\mathrm{S}}$ or $\Gamma_{\mathrm{W}} \gtrsim \Gamma_{\mathrm{S}}$.

Publication Date: June 1, 1979 | doi: 10.1021/ba-1979-0175.ch004

In Positronium and Muonium Chemistry; Ache, H.;
Advances in Chemistry; American Chemical Society: Washington, DC, 1979.

Analysis of data presents $n(t)$ in the form

$$n(t) = I_1 e^{-\overline{\Gamma}_1 t} + I_2 e^{-\Gamma_2 t}. \tag{8}$$

The component I_1 with mean rate $\overline{\Gamma}_1 > \Gamma_2$ subsumes the unresolved short-lived components f_W, $f_S(1 - \beta_{Ps})$, and i_1. The intensity of the long-lived component, I_2, can be approximated in terms of Equation 7 as

$$I_2 = 1 - I_1 = f_S \beta_{Ps} \frac{\Gamma_1 - \gamma}{\Gamma_1 - \Gamma_2} \tag{9}$$

with

$$\Gamma_1 = \gamma_p + \overline{\kappa}_p; \quad \Gamma_2 = \gamma_o + \overline{\kappa}_o. \tag{10}$$

The sample-averaged spin conversion rates

$$\kappa_{p,o} = \alpha_{p,o} \nu_T \phi_{T^1T^1} c n \int f(\epsilon(\omega), \alpha_+; D) \epsilon(\omega) I_0(\omega) d\omega \tag{11}$$

depend through the function

$$f(\epsilon, \alpha_+; D) \simeq \alpha_+ D e^{-\alpha_+ D} \frac{1 - \exp[-(\epsilon c n - \alpha_+) D]}{(\epsilon c n - \alpha_+) D} \tag{12}$$

on the overlap between the T profile and the positron implantation profile in the sample when illuminated with a light source of intensity $dL_0(\omega) = I_0(\omega) d\omega$ in the frequency range between ω and $\omega + d\omega$. The overlap function has the following properties.

(1) The light extinction is weak over the distance D and so small compared with the positron attenuation that $\epsilon c n << \alpha_+$; then

$$f \simeq 1 - e^{-\alpha_+ D} = f_S(D) \tag{13}$$

is equal to the fraction of positrons stopped in the sample, independent of $\epsilon(\omega)$, and

$$\kappa_{p,o} = \alpha_{p,o} \nu_T \phi_{T^1T^1} c n f_S \int \epsilon(\omega) I_0(\omega) d\omega \tag{14}$$

is proportional to the light absorption rate $A = \int \epsilon(\omega) I_0(\omega) d\omega$.

(2) The extinction in the phosphor absorption band is comparable with the positron attenuation, $\epsilon c n \sim \alpha_+$; then

$$f \simeq \alpha_+ D e^{-\alpha_+ D} \tag{15}$$

with maximum overlap when $\alpha_+ D \simeq 1$.

Publication Date: June 1, 1979 | doi: 10.1021/ba-1979-0175.ch004

(3) The extinction in the absorption band is so strong that $\epsilon cn >> \alpha_+$; then

$$f \simeq \frac{\alpha_+}{\epsilon(\omega)\, cn}\, e^{-\alpha_+ D}, \tag{16}$$

and Equation 11 depends only on the total incident light intensity in the frequency range of the absorption band where $\epsilon(\omega)$ is large, $L_0 = \int l_0(\omega) d\omega$,

$$\kappa_{p,o} = \alpha_{p,o} \nu_T \phi_T \tau_T \alpha_+ e^{-\alpha_+ D} L_0. \tag{17}$$

It is independent of the details of the spectral distribution, l_0, of the lamp and of the absorption spectrum, $\epsilon(\omega)$, of the phosphor, its concentration, c, and the sample density (n).

Most processes subsumed in (I_1,Γ_1) are independent of $\bar{\kappa}_{p,o}$. Differences in (I_2,Γ_2) between light-on and light-off can be measured to yield

$$\frac{\Delta\Gamma_2}{\Gamma_2} = \frac{\bar{\kappa}_o}{\gamma_o} \tag{18}$$

and

$$\frac{I_2}{\Delta I_2} \simeq \frac{\Delta\Gamma_1}{\Gamma_1 - \gamma} \simeq \frac{4}{3} \frac{\bar{\kappa}_p}{\gamma_p - \gamma_o}. \tag{19}$$

The intensity of the narrow component in the two-gamma angular correlation distribution, F_N, increases similarly as

$$\frac{\Delta F_N}{F_N} \simeq \frac{3\bar{\kappa}_o}{\gamma_o} \simeq \frac{3\Delta\Gamma_2}{\Gamma_2}, \tag{20}$$

which is proportional to $\Delta P/P$.

Phosphorescence lifetimes of organic molecules, τ_T, are typically of the order of 10^{-3} sec. When frozen into solid matrices, vibrational and rotational degrees of freedom are restricted, and the lifetimes can be extended to seconds or longer. Therefore, the first experimental evidence for photomagnetic Ps quenching was sought in dilute solutions of phosphor molecules in solid matrices. Still, the effects on $\Delta\Gamma_2/\Gamma_2$ and $\Delta I_2/I_2$ are small and precariously close in magnitude to the inherent uncertainties of the decomposition of lifetime spectra of condensed samples, where $\Gamma_2 \sim 1$ nsec^{-1} is not significantly smaller than $\Gamma_1 \sim 3$ nsec^{-1}.

In gas samples, where $\Gamma_2 \sim 10^{-2}\bar{\Gamma}_1$, one can experimentally integrate Equation 8 over times $t \geq t_c$ chosen such that $1 << \Gamma_2 t_c << \bar{\Gamma}_1 t_c$, to register the counts

$$N(t_c) = I_1 e^{-\bar{\Gamma}_1 t_c} + I_2 e^{-\Gamma_2 t_c} \simeq I_2 e^{-\Gamma_2 t_c}. \tag{21}$$

Publication Date: June 1, 1979 | doi: 10.1021/ba-1979-0175.ch004

The choice of t_c implies, by Equations 18 and 19, that $\Delta I_2/I_2 << \Delta\Gamma_2 t_c$ and bars experimental access to $\bar{\kappa}_p$. But the photomagnetic effects on Γ_2,

$$\Delta\Gamma_2 = \bar{\kappa}_o = \frac{1}{t_c} \log \frac{N^{off}(t_c)}{N^{on}(t_c)}, \tag{22}$$

can be measured directly without analysis, and with high statistical accuracy.

Experiments with Condensed Samples

Dilute solutions (cn is approximately 10^{-2} mol/L) of phosphor molecules were prepared in the solvents cyclohexane, glycerol, and boric acid. A solution was pipetted into a cell consisting of thin quartz walls pressed against a Teflon spacer. The spacers had thicknesses, D, in the range 1–2 mm. A ^{22}Na positron source backed by a metal strip was affixed inside to one wall at $x = D$. The assembly was submerged in liquid nitrogen inside a quartz Dewar vessel.

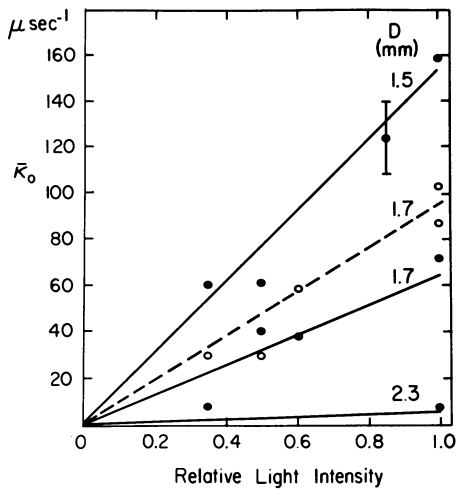

Figure 2. Measured changes of annihilation rate, $\Delta\Gamma_2$, in solids are interpreted as mean o-Ps spin conversion rates. κ_o (Equation 18). (Benzene: ●, ——; rhodamine B: ○, – – –.) They change linearly as a function of the light intensity, L_0; the relative slopes vary with sample thickness, D, *as predicted by Equation 17. With the constants listed in Table II, the slope determines the* o-Ps *spin conversion volume rate, $\alpha_o v_T$, with uncertainties of ca. ± 50%.*

Table II. Photomagnetic Quenching of Positronium

Solute	*Solvent*	$\phi_T \tau_T$ *(sec)*	D *(mm)*	$\alpha_+ D e^{-\alpha_+ D}$ $(\times 10^{-2})$	L_0 *(10^{15} photons cm^{-2} sec^{-1})*
Benzene	—	2.4	1.5	2.2	3.9
Quinone	cyclohexane	0.5	2.3	0.4	3.9
1,2 Benzanthracene	cyclohexane	0.8	2.3	0.4	3.9
trans-Stilbene	cyclohexane	0.5	2.3	3.7	3.9
Bopq [b]	cyclohexane	3×10^{-3}	1.5	3.6	621
Chlorophyll	cyclohexane	1×10^{-3}	1.5	3.6	320
Chlorophyll	ice	1×10^{-3}	1.2	3.3	320
Marine algae	water	1×10^{-3}	0.8	3.3	100
Rhodamine B	glycerol	0.6	0.8	6.2	210
Fluorescein	glycerol	2	0.8	6.2	190
Fluorescein	boric acid	2	0.8	1.3	190

[a] Characterized by the constants necessary to evaluate Equation 17. Experiments performed at 77 K, except algae in water at room temperature. Superscript "off" denotes experiments in the dark. Statistical uncertainties are quoted in parentheses.

Publication Date: June 1, 1979 | doi: 10.1021/ba-1979-0175.ch004

The light source was a high-pressure mercury lamp. It illuminated the sample through a quartz wall opposite to the positron source at $x = 0$. Two 8-cm thick water filters cooled the light by IR absorption. Gray and interference filters could be interposed between the water filters and the Dewar to change $l_0(\omega)$ uniformly, or to select frequency ranges for the study of action spectra. The conditions were those of Equations 16 and 17. The absolute light intensity, L_0, was measured with a double-beam spectrophotometer calibrated against a National Bureau of Standards light source. During the experiments, the intensity was monitored with a radiometer to correct for aging of the lamp, and to measure the reduction in intensity by gray filters. The light-on and light-off lifetime spectra were stored concurrently in the halves of a 400-channel analyzer. The duration of the light–dark cycle was about 60 sec, which was long compared with τ_T, which is about equal to 2 sec, but short enough to avoid significant temperature fluctuations in the sample.

The $\bar{\kappa}_0$ data displayed in Figure 2 are the measured changes of $\Delta\Gamma_2$, according to Equation 18. They depend on the experimental conditions as expected from Equation 17, in that they rise linearly with $L_0 = \int l_0(\omega) d\omega$, irrespective of whether $l_0(\omega)$ was reduced uniformly with gray filters, or in spectral ranges with colored filters. The solid lines indicate that the slopes depend on the sample thickness D as $\exp(-\alpha_+ D)$. Data on other samples agree also with Equation 17; some are listed in Table II.

Experiments with Gas Samples

A cylinder chamber of dimension $D = 25$-cm and 10-cm diameters was covered at the light entrance surface, $x = 0$, with a quartz window and at $x = D$ with a copper plate which held the positron source of 5-μCi ^{22}Na in an Al envelope. The light source was the same as that in the

Lifetime Data Under Various Experimental Conditions[a]

Γ_2^{off} (μsec^{-1})	$\Delta\Gamma_2$ (μsec^{-1})	I_2^{off} (%)	ΔI_2 (%)	$\alpha_o \nu_T$ (10^{-6} cm^3 sec^{-1})	$\frac{\alpha_p}{\alpha_o}$
916 (30)	158 (43)	10.1 (0.7)	3.6 (1.1)	1×10^0	12
615 (22)	131 (31)	6.7 (0.5)	0.9 (0.7)	4×10^1	6
767 (15)	55 (22)	9.0 (0.4)	0.8 (0.6)	5×10^2	9
627 (21)	29 (30)	8.1 (0.5)	0.4 (0.7)	2×10^2	9
577 (21)	144 (32)	7.5 (0.5)	1.6 (0.7)	3×10^1	8
723 (30)	138 (42)	11.0 (0.6)	1.0 (0.9)	2×10^1	4
595 (21)	156 (30)	6.3 (0.5)	1.5 (0.8)	2×10^1	9
554 (15)	37 (21)	21.5 (0.6)	1.7 (1.0)	3×10^0	12
855 (31)	103 (47)	8.7 (0.7)	1.3 (1.0)	1×10^{-2}	8
988 (36)	103 (53)	12.4 (1.1)	2.3 (1.5)	3×10^{-3}	10
553 (9)	22 (13)	11.5 (0.4)	0.5 (0.5)	3×10^{-3}	11

[b] Bis-butyloctyloxy-*p*-quaterphenyl.

Publication Date: June 1, 1979 | doi: 10.1021/ba-1979-0175.ch004

solid sample experiments, with gray and interference-color filters. The conditions were such that Equation 13 applied, and $\Delta\Gamma_2$ was related to the illumination as given by Equation 14. The rate of light absorption

$$A = \int I_0(\omega)\epsilon(\omega)\,d\omega \tag{23}$$

was calculated from the known absorption spectra, $\epsilon(\omega)$, of the phosphors and the measured absolute lamp intensity distribution $I_0(\omega)$.

A pumping and gas-mixing station permitted the filling of the chamber with a carrier gas containing a concentration of phosphor molecules. A heating mantle kept the cylinder and the gas sample at constant temperatures between 300–400 K.

The 1.28-MeV gamma-ray detector of the lifetime delayed-coincidence apparatus was placed behind the positron source, and the 0.511-MeV detector was kept next to the cylinder wall. Coincidences for times longer than t_c, which is about equal to 30 nsec, were summed and stored separately for light-on and -off in cycles of about 60-sec duration, until more than 10^4 counts were accumulated. Variations of t_c between 20 and 100 nsec changed the necessary data collection time, but did not alter the effect of illumination in the sense of Equation 22.

The chamber was charged successively at 295 K with 760 torr of Ar, N_2, and air at 48% relative humidity. The admixtures were SO_2 or benzaldehyde—C_6H_5–CHO, abbreviated as ΦCHO. The data displayed in Figure 3 demonstrate the linear increase of $-\ln(N^{on}/N^{off}) \simeq (N^{off} - N^{on})/N^{off}$ with light absorption A. It was changed relative to its maximum value, A_0, with gray filters (full symbols) or by altering $I_0(\omega)$ with filters that transmitted frequencies either lower than the phosphor absorption edge (right open symbols) or higher than the absorption edge (left open symbols).

In Positronium and Muonium Chemistry; Ache, H.;
Advances in Chemistry; American Chemical Society: Washington, DC, 1979.

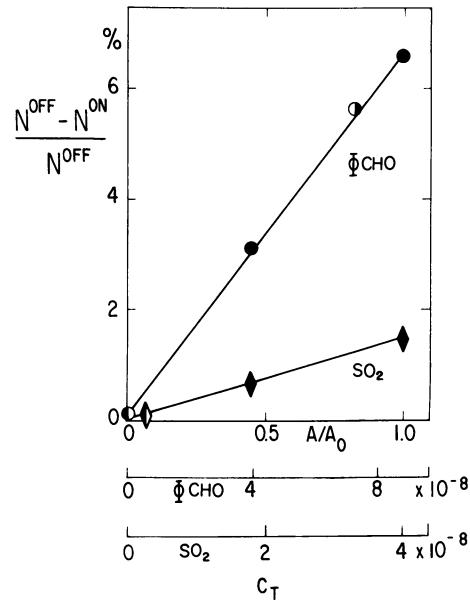

Physical Review Letters

Figure 3. Light-induced changes of counting rates in gases are proportional to κ_0, by Equation 22. They change with the light absorption A (Equation 23) as predicted by Equation 14. The maximum absorption is $A_0 = 4 \times 10^{-2}$ photons sec^{-1} per benzaldehyde and $A_0 = 7 \times 10^{-3}$ photons sec^{-1} per SO_2. Full symbols denote data taken with the full lamp spectrum and intensities varied with gray filters. The specificity of the action spectrum is demonstrated through data taken with filters passing light at lower frequency than the phosphor absorption edge (right-hand open symbols) and at higher frequencies (left-hand open symbols). The nomographic abscissae give the relations between A and c_T in Ar at 1 atm and T = 300 K. Experimental uncertainties are less than the size of the symbols (3).

Measurements under other conditions are summarized in Table III. They agree with those shown in Figure 3. The effects depend only on the triplet density $n_T = c_T n$, but are independent of the carrier gas. The gas functions merely to slow down positrons to form significant amounts of Ps in the chamber.

The nomographs in Figure 3 plot the respective triplet concentrations. The method can detect a few triplet-excited molecules in 10^8 gas molecules.

Publication Date: June 1, 1979 | doi: 10.1021/ba-1979-0175.ch004

Results

Measurements of the rate increment under illumination, $\Delta\bar{\Gamma}_2 = \kappa_o$, via Equation 14 give information about $\alpha_o\nu_T$, the product of the volume rate, ν_T, of Ps–T interaction, and the effectiveness, α_o, of the conversion *o*-Ps to *p*-Ps. High accuracy during reasonable counting times can be achieved with gases. Changes in the two-gamma angular correlation according to Equation 20 yield similar information. When the corresponding increments under illumination of the intensity, ΔI_2, of this positron lifetime component can be measured, Equations 18 and 19 may be combined to give the ratio of the para-to-ortho Ps photomagnetic conversion efficiency, α_p, to the ortho-to-para Ps conversion efficiency, α_o, as

$$\frac{\alpha_p}{\alpha_o} \simeq \frac{3}{4}\left(\frac{\gamma_p}{\gamma_o} - 1\right)\left(\frac{\Gamma_2^{off}}{\Delta\Gamma_2}\right)\left(\frac{\Delta I_2}{I_2^{off}}\right), \tag{24}$$

unencumbered by uncertainties in ν_T. While the propagation of experimental uncertainties in $\Delta\Gamma_2$ and ΔI_2 is apparently linear in Equation 24, spurious correlations between changes in I_2 and Γ_2 may be introduced in the data analysis through the decomposition of lifetime spectra into different components. The changes of positron annihilation characteristics observed under UV illumination comply with the criteria for spin conversion listed in Table I.

Table II lists $\alpha_o\nu_T$ values culled from the lifetime data of the nearly 30 condensed systems investigated. Figure 4 displays $\alpha_o\nu_T$ measured on two species of excited molecular triplet states in gases as a function of temperature under the conditions summarized in Table III. They are clearly insensitive to the nature of the carrier gas, and appear to rise with temperature, T, as $T^{1/2}$.

The last column of Table II indicates that $\alpha_p/\alpha_o = 9$ on the average, so that $\alpha_o \lesssim 0.1$. The volume rates, then, in polycrystalline nonpolar matrices and in gases are $\nu_T \gtrsim (10^{-6} - 10^{-5})\text{cm}^3/\text{sec}$. The combined evidence supports estimates based on elastic Ps–Ar scattering cross sections, namely, that the mean free path for Ps scattering in such matrices is large compared with the range of spin conversion interaction between Ps and T, and one sets $\nu_T = v_{Ps}\sigma_T$. Under the conditions of the gas experiments, the group velocity of the thermal Ps wave packet,

$$v_{Ps} = (3k_B T/m^*_{Ps})^{1/2} = 8.1 \times 10^6[T(\text{K})/300\ \text{K}]^{1/2}\ \text{cm/sec}, \tag{25}$$

with effective Ps mass $m_{Ps}^* = 2m_o$, accounts for the dominant temperature dependence of ν_T.

Table III. Summary of Experimental Conditions for

Phosphor	$\phi_T\tau_T$ *(10⁻³ sec)*	*Carrier Gas*[b]	*Parameters Varied*
Benzaldehyde (ϕCHO)	2	Ar	T,A,n_G,t_c
		N_2	T,A
		air	T
SO_2	0.03	Ar	T,A

[a] Constants pertain to the evaluation of Equation 14.
[b] At density $n_G = 2.45 \times 10^{19}$ molecules/cm³ corresponding to 760 torr at 295 K. Measurements at 0.5 n_G and 2 n_G showed no change in $\alpha_o\nu_T$.

The cross sections for Ps spin conversion by excited triplet states,

$$\sigma_T = \nu_T/v_{Ps} \simeq (10^3 - 10^4)\pi a_o^2, \tag{26}$$

given in units $\pi a_o^2 = 0.88 \times 10^{-16}$ cm², are insensitive to v_{Ps}. They signify interaction ranges, R_T, between 20 and 50 Å, which are considerably larger than the sum of the Ps deBroglie wavelength, $\lambda_{Ps} = \hbar/m_{Ps}v_{Ps} \simeq 5$ Å, and

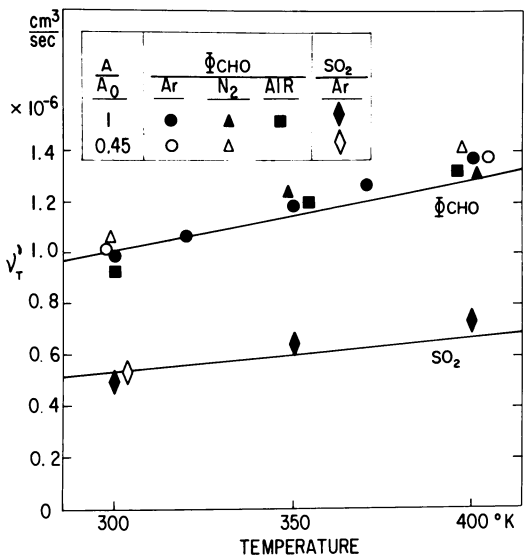

Physical Review Letters

Figure 4. Volume rates, $\nu_T' = \alpha_o\nu_T$, for spin conversion of o-*Ps with thermal velocity $v_{Ps}(T)$ (Equation 25) as deduced according to Equation 14 from data as those displayed in Figure 3 with the constants listed in Table II. The solid lines are based on a heuristic model and give roughly the T½ dependence of $v_{Ps}(T)$ (3).*

Publication Date: June 1, 1979 | doi: 10.1021/ba-1979-0175.ch004

Photomagnetic Positronium Quenching in Gases[a]

c_T[c] (ppm)	$\alpha_0\nu_T$[d] (10^{-6} cm^3 sec^{-1})	σ_T (μm^2)
0.05–20	1.2 ± 0.3	1.5 ± 0.4
0.05–0.1		
0.1		
0.02–0.04	0.6 ± 0.2	0.9 ± 0.3

[c] Triplet concentration is given by $c_T = \Phi\tau_{TT}cA$.
[d] Mean value in range 300–400 K, cf, Figure 3.

the approximate extension of an excited molecule, approximately 5 Å. Importantly, σ_T is insensitive to the proximity of inert molecules, whether they are so close in condensed systems as to hold the phosphor molecule in place, or as distant in gases as the Ps–T interaction range.

The low ν_T values in glassy solids suggest that the mean free path for Ps diffusion is small compared with R_T. In a diffusion-limited regime the Smoluchowski relation

$$\nu_T = 4\pi R_T D_{Ps} \tag{27}$$

applies. The data for molecular glasses are consistent with Ps diffusion constants, D_{Ps}, in the range $D_{Ps} = (0.01 - 0.1)cm^2/sec$.

To gain perspective one may compare $\alpha_0\sigma_T$ with cross sections for other *o*-Ps quenching processes. Examples for gases are given in Table IV. The first two entries pertain to electron pick-off on diamagnetic ($S = 0$) molecules. The third and fourth are spin conversion by electron exchange with molecules in triplet ($S = 1$) and doublet ($S = ½$) ground states. By comparison, photomagnetic Ps spin conversion has giant cross sections.

Table IV. Comparison of *o*-Ps Quenching Cross Sections in Gases of Ground-State Molecules[a]

Molecules	*S*	*Dominant Process*	*Cross Section (units $\pi a_0^2 = 0.88 \times 10^{-16}$ cm^2)*	*Reference*
N_2	0	electron pick-off	1.3×10^{-5}	*6*
Ar	0	electron pick-off	1.6×10^{-5}	*7*
O_2	1	electron exchange	1.1×10^{-3}	*8*
NO	½	electron exchange	8.4×10^{-3}	*9*
NO_2	½	electron exchange	2.8×10^{1}	*9*
SO_2*	1*	spin flip	6.8×10^{2}	*3*
ϕCHO*	1*	spin flip	1.1×10^{3}	*3*

[a] With $\alpha_0\sigma_T$ of molecules in photo-excited triplet states (*).

Publication Date: June 1, 1979 | doi: 10.1021/ba-1979-0175.ch004

Quantum Spin Statistics

Suppose the *o*-Ps wave function, $\Psi_S^m(S = 1; m = -1, 0, 1)$, and the molecular triplet state, T, $\Phi_S^m(S = 1, m = -1, 0, 1)$, interact in the initial magnetic substates Ψ_1^1 of *o*-Ps with magnetic quantum number $m = 1$ and Φ_1^0 of T with $m = 0$. The result is direct, simple scattering with wave function amplitude D, or an electron-exchange interaction with amplitude E. Considering all possible exchanges between the molecular electrons and the Ps electron yields

$$\Phi_1^0\Psi_1^1 = (D - E)\Phi_1^0\Psi_1^1 + E\Phi_1^1\Psi_1^0 - E\Phi_1^1\Psi_0^0. \quad (28)$$

The minus sign of the electron exchange amplitude E accounts for exchanges between electrons of identical spin orientation as required by the Pauli principle. This example implies the following.

(1) Simple scattering leaves *o*-Ps and T unchanged, $\Phi_1^0\Psi_1^1 \rightarrow \Phi_1^0\Psi_1^1$, and proceeds by a direct process with amplitude D, and an electron exchange process with amplitude E. The coherent amplitude $D - E$ gives a scattering cross section $(D - E)^2$.

(2) Exchange interaction scatters both *o*-Ps and T into a different magnetic sublevel, $\Phi_1^0\Psi_1^1 \rightarrow \Phi_1^1\Psi_1^0$, with amplitude E and cross section E^2.

(3) Electron exchange also converts *o*-Ps into *p*-Ps, $\Phi_1^0\Psi_1^1 \rightarrow \Phi_1^1\Psi_0^0$, with amplitude $-E$ and cross section E^2; T has been scattered into a different sublevel, $m = 1$, without changing multiplicity. This can be termed catalyzed Ps spin conversion.

Analysis of scattering from each of the $(2S + 1)^2 = 9$ possible initial *o*-Ps–T wave function combinations leads to the result that exchange

Table V. Positronium Spin-Conversion Processes[a]

Reactants	*Mechanism*	*Products*	*Conversion Cross Section*
$^3Ps + {}^3M^*$	exchange	$^1Ps + {}^3M^*$	$\frac{1}{3}E^2$
	spin flip	$^1Ps + {}^1M$	$\frac{1}{9}F^2$
$^1Ps + {}^3M^*$	exchange	$^3Ps + {}^3M^*$	E^2
	spin flip	$^3Ps + {}^1M$	F^2

$\sigma_o \equiv \sigma(^3Ps \rightarrow {}^1Ps) = \frac{1}{3}(E^2 + \frac{1}{3}F^2)$
$\sigma_p \equiv \sigma(^1Ps \rightarrow {}^3Ps) = E^2 + F^2$

Thus,			
F^2/E^2	0	1	∞
$\sigma_p/\sigma_o = \alpha_p/\alpha_o$	3	9/2	9

[a] Between *o*-Ps (^3Ps) and *p*-Ps(^1Ps) and excited phosphor molecules in the triplet state ($^3M^*$) and the singlet state (^1M) via catalytic electron exchange (E) (the excited molecular triplet $^3M^*$ retains its multiplicity) and via spin flip (F) ($^3M^*$ converts to the singlet ground state ^1M).

In Positronium and Muonium Chemistry; Ache, H.;
Advances in Chemistry; American Chemical Society: Washington, DC, 1979.

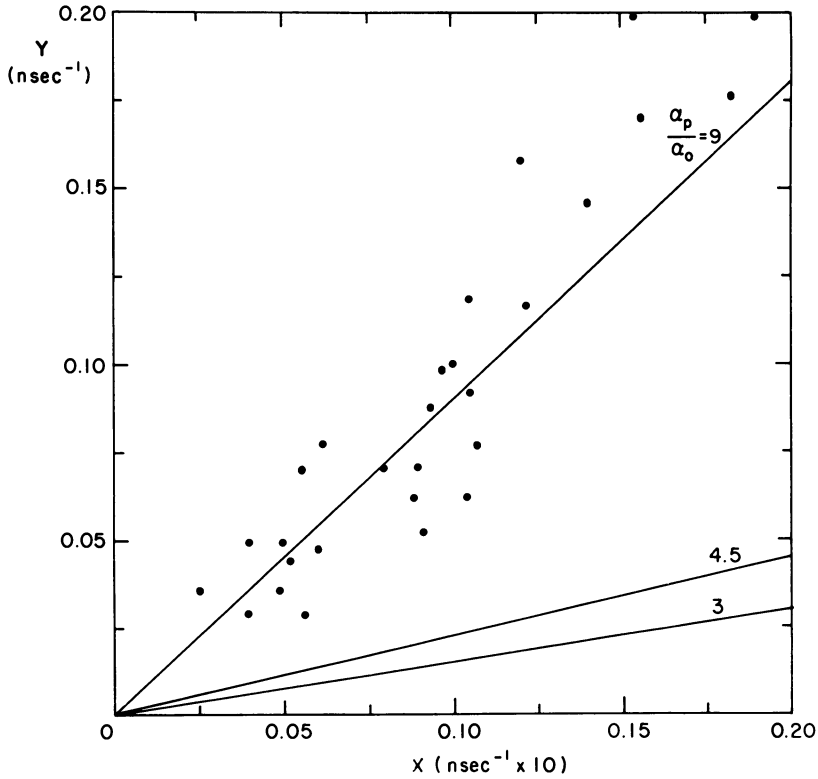

Figure 5. A plot of all light-on and light-off experimental positron lifetime data on solid samples in the form $Y = 3(\gamma_p - \Gamma_2^{off})\Delta I_2$ *vs.* $X = 4I_2^{off}\Delta\Gamma_2$, *with* $\gamma_p = 8.0$ *nsec*$^{-1}$. *The slope, by Equation 24, measures* α_p/α_o, *and the lines drawn for the values 9, 4.5, and 3 represent the three limiting cases of quantum spin statistical conversion modes discussed in the text and summarized in Table IV (2).*

scattering never changes the multiplicity of the molecular triplet wave function. In short, Ps spin conversion by electron exchange proceeds only via spin catalysis.

Excited triplets, in contrast to ground-state triplets, can change multiplicity during Ps spin conversion by exothermic transitions to the singlet ground state. We refer to this as spin flip. It amounts to phosphorescence quenching through Ps spin conversion, e.g., $\Phi_1{}^0\Psi_1{}^1 \rightarrow \Phi_0{}^0\Psi_0{}^0$, with a scattering amplitude F and cross section F^2. One can compile the contributions from Processes 1 to 3 and from spin flip under the assumption that the total spin angular momentum is conserved in the scattering event. The resulting cross sections, σ, can be deduced in terms of sums of squares of the partial scattering amplitudes as quoted in Table V.

Publication Date: June 1, 1979 | doi: 10.1021/ba-1979-0175.ch004

The ratio α_p/α_o depends on the relative magnitudes of F^2 and E^2. If $F^2 = 0$, one has the well-known value $\alpha_p/\alpha_o = 3$ for Ps quenching on paramagnetic ground-state scatterers. For excited triplet scatterers, α_p/α_o can range from 3 to 9 depending on the relative probabilities for catalytic spin exchange, E^2, and spin flip, F^2. The last column in Table II suggests that $F^2 >> E^2$. If, following Equation 24, one plots $Y = 3(\gamma_p - \Gamma_2{}^{off})\Delta I_2$ vs. $X = 4I_2{}^{off}\Delta\Gamma_2$, with $\gamma_p = 8.0$ nsec^{-1}, the available data points shown in Figure 5 scatter symmetrically about the straight line representing the slope $\alpha_p/\alpha_o = 9$. The data for photosynthesizing phosphors fall also in this range, and not near 3, as it would be if the O_2 produced in photosynthesis were the dominant Ps quencher. This suggests that spinflip dominates light-induced Ps spin conversion.

Publication Date: June 1, 1979 | doi: 10.1021/ba-1979-0175.ch004

Summary

UV light can change the annihilation characteristics of positrons in phosphorescent media. Experimental evidence on gases and solids suggests that such changes are caused by Ps spin conversion in interaction with excited triplet states. The cross sections for this process are very large, about $10^4\pi a_0^2$. The effect is specific in that only light absorbed by the phosphor molecules causes Ps quenching. Although still burdened with large experimental uncertainties, the trends in the changes of positron lifetime spectra for solids point to a new process labeled spin flip. Through Ps–T attachment or Ps scattering on T, Ps spin conversion proceeds with high efficiency, possibly through a transition from the excited molecular triplet state to the molecular singlet ground state.

Photo-induced Ps quenching appears to be a general phenomenon that occurs in gases and solids. It could help elucidate the role of excited triplet states in photosynthesis and in the energy transport of other biologically interesting processes. The sensitivity in gases over a wide range of exeprimental conditions opens the possibility of applications in pollution research related to photochemical reactions in air. The giant cross sections for Ps–T spin interaction and the ratio of about 9 of para-to-ortho Ps spin conversion probabilities in such encounters pose intriguing new quantum–theoretic questions about the scattering of leptonic atoms on excited electronic states of matter which merit study.

Acknowledgment

The possibility of affecting positron annihilation characteristics in photomagnetic substances through illumination occurred to me during a search for light stabilizers of polymers at the DuPont Radiation Physics Laboratory. The program to demonstrate and explore this effect was

pursued in collaboration with P. Kliauga, now at the Department of Radiology, Columbia University College of Physicians and Surgeons, and with D. Spektor, now at the Department of Environmental Medicine, New York University School of Medicine. The National Science Foundation and the Energy Research and Development Administration supported this research.

Literature Cited

1. Brandt, W., Kliauga, P., *Phys. Rev. Lett.* (1973) **30,** 354.
2. Brandt, W., Kliauga, P., *Phys. Rev. B* (1976) **14,** 884.
3. Brandt, W., Spektor, D., *Phys. Rev. Lett.* (1977) **38,** 595.
4. Lewis, G. N., Calvin, M., Kasha, M., *J. Chem. Phys.* (1949) **17,** 804.
5. Hutchison, C. A., Jr., Mangum, B. W., *J. Chem. Phys.* (1961) **34,** 908.
6. Coleman, P. G., Griffith, T. C., *J. Phys. B* (1973) **6,** 2155.
7. Coleman, P. G., Griffith, T. C., Heyland, G. R., Killen, T. L., *J. Phys. B* (1975) **8,** 1734.
8. Celitans, G .J., Tao, S. J., Green, J. H., *Proc. Phys. Soc.* (1964) **83,** 833.
9. Tao, S. L., Chuang, S. Y., Wilkenfeld, J., *Phys. Rev. A* (1972) **6,** 1967.

RECEIVED January 23, 1978.

Solid-State Polymerization as Studied by Positron Annihilation

YASUO ITO

Research Center for Nuclear Science and Technology, University of Tokyo, Tokyo, Japan

YONEHO TABATA

Nuclear Engineering Research Laboratory, Faculty of Engineering, University of Tokyo, Tokyo, Japan

Publication Date: June 1, 1979 | doi: 10.1021/ba-1979-0175.ch005

Position lifetimes have been measured in polymerizing media of several solid vinyl monomers, such as dimethyl-itaconate, acrylamide, methylmethacrylate, and N-*vinyl-carbazole. Both the annihilation rate and the intensity of the long-lived component changed during the polymeriza-tion. It has been shown that the annihilation rate is deter-mined by two major factors; the size of free volume and the reaction rate of ortho-positronium with active species produced by the irradiation. The intensity is determined by the amount of free volume available for ortho-positro-nium. The mean separation among such free volumes is also an important factor for determining the value of the intensity. Furthermore, the active species seems to inhibit positronium formation. Some discussion has been made on positronium migration in amorphous substances.*

When solid monomers are irradiated with ionizing radiation such as γ-rays, active species such as ions or free radicals are produced in them and it is then possible to convert the monomers to polymers even at low temperatures (*1, 2*). This particular topic of chemistry has been studied extensively since the latter half of the 1950's owing to the fact that strong radiation sources such as x-rays and γ-rays became available. Chemists were interested in the possibility of obtaining a new kind of polymer which might not be produced by ordinary catalytic methods.

0-8412-0417-9/79/33-175-109$05.00/1

In Positronium and Muonium Chemistry; Ache, H.;
Advances in Chemistry; American Chemical Society: Washington, DC, 1979.

On the other hand, the study of the solid-state polymerization also raised some fundamental problems in the field of the physical chemistry of solids: the mechanism of the solid-state reaction, the effect of solid structures on polymerization, etc.

Various research techniques have been used for the study of solid-state polymerization. In order to observe and identify the active species, ESR and various spectroscopic methods have been used successfully. Calorimetric methods have been a powerful tool for studying the thermochemical aspects of the polymerization. For the study of the solid structures of the monomers and polymers, x-ray diffraction, electron microscopy, and NMR have been used.

Some other methods also have been used in our laboratory; that is, the study of the effect of high pressure on polymerization, measurement of radiation-induced thermoluminescence of irradiated solid monomers, etc. It also seemed promising to apply the position annihilation method to the study of solid-state polymerization. Among various features of positron annihilation, the so-called free volume effect and the effect of phase transitions on positron annihilation parameters are thought to be important in conjunction with solid-state polymerization. Since free volumes change during polymerization, the pick-off annihilation rate of ortho-positronium is expected eventually to change. Solid-state polymerization is accompanied also by the accumulation of active species, which may also affect the annihilation rate of *o*-Ps or the formation probability of positronium (Ps), about which we have little knowledge at the present.

Publication Date: June 1, 1979 | doi: 10.1021/ba-1979-0175.ch005

It has been our interest to know how all these factors can affect e^+ annihilation mechanism in some practical cases. Although we presently can interpret the experimental results only qualitatively, they are full of suggestions for both the future possible direction of the application of measurements of positron annihilation and limitations upon it. This article is a review of our earlier works which have been published separately (*4, 7, 9, 10*).

Experimental

Several monomers have been chosen as the sample: *N*-vinylcarbazole (N-VCz), dimethylitaconate (DMI), acrylamide (AAm), and methymethacrylate (MMA). N-VCz and DMI were purified by recrystallization from solvents, MMA was purified by distillation and AAm was purified by sublimation. N-VCz, DMI, and AAm, which are solid at room temperature, were pressed in the form of pellets. A drop of an aqueous solution of $^{22}NaCl$ was deposited on one side of the pellets. After drying, they were faced together on the deposited side and placed in a glass ampoule which then was evacuated and sealed off. The monomer crystals

were used as obtained by crystallization or, when the crystals were too large, they were ground only slightly. This was done so that if the crystals were ground to very fine powder, the amount of *o*-Ps annihilating on the surface of the crystallites might become substantial. We do not, of course, need surface Ps for the present study.

MMA, which is liquid at room temperature, was introduced into a glass ampoule in which a positron source (^{22}NaCl sealed in 3-μ thick nickel foil) was placed in advance. This was evacuated by a freeze–thaw method and was sealed off.

The time resolution of the lifetime measurements was 0.6–0.9 nsec (typically 0.7 nsec) at full width at the half of maximum (FWHM) depending on the different set-ups of the experimental system. Since the time resolution was not good, only the lifetime, τ_2, and the intensity, I_2, of the longer-lived component were extracted from the experimental data. I_2 was defined as the ratio of the area under the exponential function to the total counts. Therefore, care must be taken since I_2 can be overestimated when τ_2 is decreased because of chemical interaction of *o*-Ps (*3*). The lifetime measurements were performed at relatively low temperatures (0°C for N-VCz, DMI, and AAm and −78°C for MMA) in order to prevent post-polymerization during the measurements. AAm also was measured and irradiated at −78°C for comparison. Polymerization does not take place at this temperature. This will be discussed later.

Publication Date: June 1, 1979 | doi: 10.1021/ba-1979-0175.ch005

Results and Discussion

Dimethylitaconate. The first example is DMI (*4*). The intensity of the long-lived component in the pure monomer solid is small (2–3%). This may be caused by a small amount of *o*-Ps annihilating on the surface of crystallites. Excepting this small component, there is no long-lived component in DMI monomer solid. This is to be expected since the density of the crystalline DMI is large. It may be that there is no free volume available for *o*-Ps in DMI monomer solid.

Polymerization takes place when the monomer solid is irradiated with γ-rays. As with most other vinyl monomers, the state of the polymer thus obtained is amorphous. The conversion ratio is not proportional to the dose of irradiation as is usually the case with solid-state polymerization (Figure 1). The lifetime spectrum changes with the irradiation dose as shown in Figure 2. Clearly the intensity of the long-lived component increases with irradiation dose, but the lifetime is unchanged. The volume change in the solid DMI was measured also as a function of the irradiation dose by dilatometry (Figure 1). The bulk volume of the monomer solid increases as polymerization proceeds, indicating that the free volume is larger in the amorphous polymer phase than in the cyrstalline monomer phase. Thus the intensity of the *o*-Ps component seems to be determined by the amount of free volume available for *o*-Ps. In a free volume in the polymer phase or in the disordered region of the polymerizing medium,

In Positronium and Muonium Chemistry; Ache, H.;
Advances in Chemistry; American Chemical Society: Washington, DC, 1979.

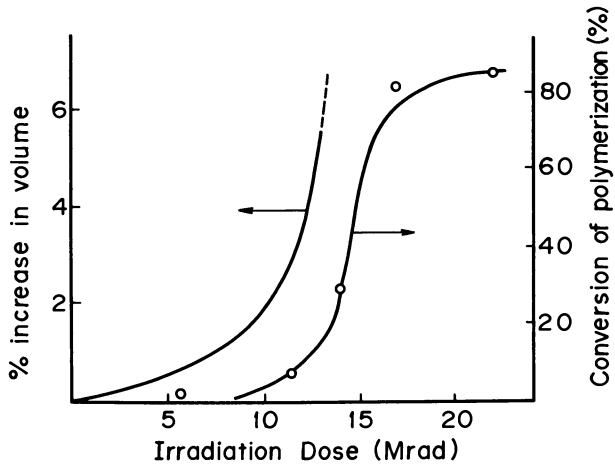

Figure 1. The conversion of polymerization and the volume change during the solid-state polymerization of DMI. Irradiation temperature, 30°C; dose rate, 2.5 × 10^5 R/hr.

o-Ps decays with a slow pick-off rate. However, in crystalline regions where the size of the free volume is not large enough, *o*-Ps may decay rapidly or it may not be formed at all.

I_2 is plotted against the yield of polymers in Figure 3. I_2 is not proportional to the polymer contents; rather the increase in I_2 is conspicuous in the earlier stage of the polymerization where the yield is small.

In another experiment, poly-DMI, obtained by the solid-state polymerization, was dissolved in DMI monomer at 50°C (mp of the DMI monomer is 35°C), and the solution quickly was solidified at − 196°C. The result of the lifetime measurement for the mixtures thus prepared also is presented in Figure 3. I_2 also is increased by the presence of dissolved polymer chains. From the result for 10% poly-DMI mixture, I_2 is much larger than is expected from the result for γ-irradiated DMI. However, when this mixture was annealed at room temperature for ten days (∇ in Figure 3), I_2 decreased appreciably.

The above results indicate that the value of I_2 is strongly dependent on the degree of disorder in the solid. To understand these phenomena it seems important to consider Ps dynamics in solids. We assume, following a theory by Brandt and Paulin (*5*), that *o*-Ps is formed even in the closely packed crystalline regions and migrates by random walks in the substance until it is annihilated or escapes into the disordered regions. The pick-off annihilation rate of *o*-Ps in the crystalline DMI is comparable with the free annihilation rate of e^+, but *o*-Ps in the large free

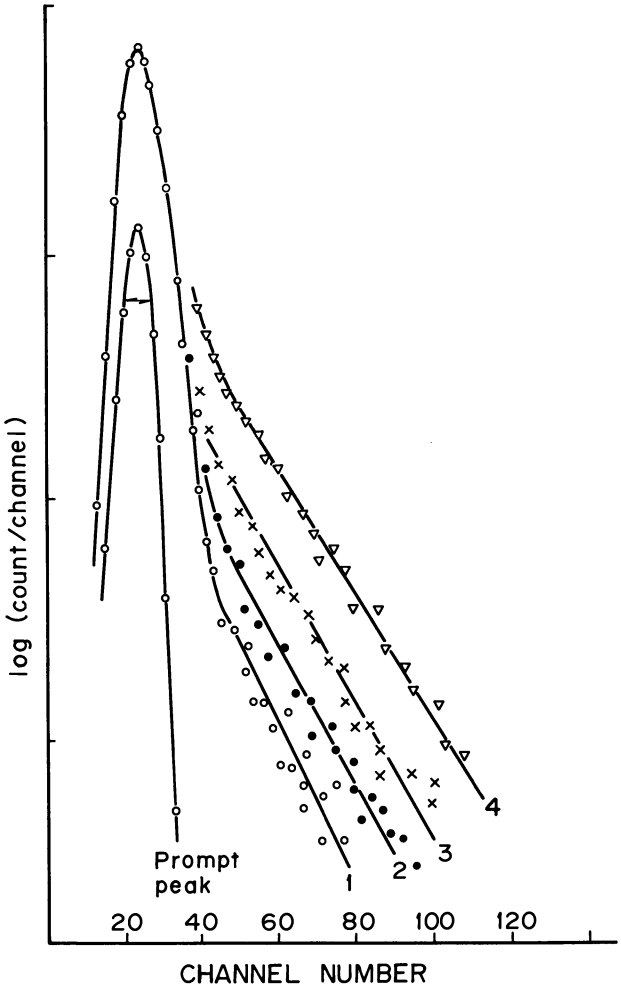

Figure 2. The change of the positron lifetime spectrum during the solid-state polymerization of DMI. (1) Before irradiation; (2) 4.5 Mrad irradiated; (3) 11.7 Mrad irradiated; (4) 17.0 Mrad irradiated.

volume regions (disordered regions) decays at a slower pick-off rate. I_2 is thus a function of both the diffusion constant of *o*-Ps and the mean separation of the disordered regions. Furthermore, when the fraction of the disordered region is large, we cannot disregard *o*-Ps which is formed intrinsically in the disordered regions. Therefore, I_2 is also a function of the amount of disordered regions. I_2 will be described then by the following equation:

$$I_2 = \Phi(1 - f)\, I_2^c + f\, I_2^d \qquad (1)$$

where f is the fraction of the disordered region with large free volumes and I_2^c and I_2^d are the assumed formation probabilities of o-Ps in the crystalline and disordered regions, respectively. The Φ is the probability of o-Ps in the crystalline regions escaping into the disordered regions. Clearly when there is no disorder in the system, $I_2 = 0$, because $f = 0$ and $\Phi = O$. The exact expression for Φ was given for the case in which the region with small free volumes can be treated as spherical particles (5):

$$\Phi = \frac{3}{2}\beta\left[(1-\beta^2) + (1+\beta^2)e^{\frac{-2}{\beta}}\right] \qquad (2)$$

where $\beta = \sqrt{D\tau}/R$; D and τ are the diffusion constant and the lifetime of o-Ps in the small free volume regions, and R is the radius of the particle. This expression cannot be applied strictly to the present case where the polymer content is small. However, an important result obtained from this expression is that Φ is an increasing function of β, and the increase in Φ is rapid when R becomes comparable with or smaller than the mean migration distance $\sqrt{2D\tau}$. We can extend this concept to our system, i.e. when the mean separation between the disordered regions becomes comparable with $\sqrt{2D\tau}$, Φ increases rapidly. The rapid increase in I_2 when the polymer content is small (Figure 3) may be explained as the result of formation of many disordered regions, the mean separation being of the same order as $\sqrt{2D\tau}$. There is little knowledge of the diffusion constant of o-Ps in organic substances. However, by using the value

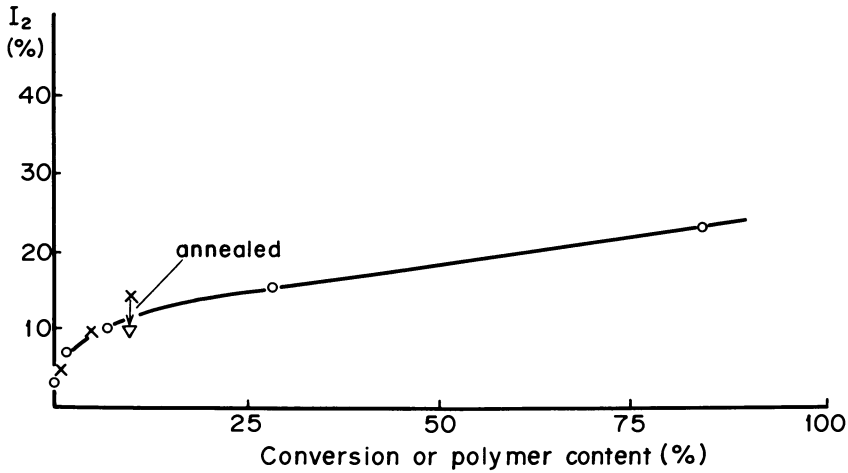

Figure 3. The intensity, I_2, of long-lived component against the conversion of polymerization or polymer content in the mixtures of mono- and poly-DMI: (○), polymerization in solid state; (×), mixture of mono- and poly-DMI.

Publication Date: June 1, 1979 | doi: 10.1021/ba-1979-0175.ch005

$D \gtrsim 4.5 \times 10^{-4}$ cm^2 sec^{-1} estimated for polypropylene (PP) (*6*) and by taking $\tau = 1.1$ nsec, we obtain $R \gtrsim 100$Å.

Equation 1 may provide a good model when the amount of polymer content is large. Because the crystallites are small in this case, Φ can be taken as equal to unity, i.e., practically all *o*-Ps produced in the crystalline regions migrates into the disordered regions. In this case we have

$$I_2 = I_2^c + f(I_2^d - I_3^c). \quad (3)$$

Fitting this equation to the linear part of Figure 3 ($f > 25\%$), we have $I_2^c = 0.13$ and $I_2^d = 0.36$. Thus the formation probability of *o*-Ps is about three times larger in the disordered region than in the crystalline region of DMI. As shown in the next section, it is the opposite for the case of AAm; the formation probability is larger in the crystalline region than in the disordered region.

Acrylamide. The second example is the polymerization of acrylamide (AAm) (*7*). Contrary to DMI, the density of AAm monomer crystal is smaller than that of polymers. This is shown by the result of a dilatometric study of the γ-irradiated AAm in Figure 4. It is known from the x-ray diffraction studies (*8*) that molecules of AAm form layers via hydrogen bondings of the type N–H—O among the amide groups, and there is a free volume of substantial size between the layers. The shape of such free volume is of plane geometry with the vinyl groups constitut-

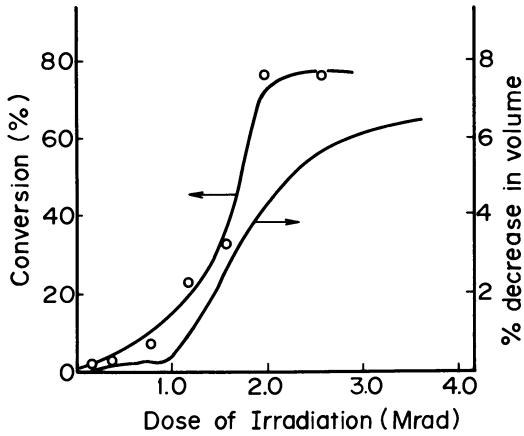

Figure 4. The conversion of polymerization and the volume change during the solid-state polymerization of AAm. Irradiation temperature, 30°C; dose rate, 2.0 × 10^5 R/hr. Note that the scale for the volume change is % decrease while the scale in Figure 1 is % increase.

Publication Date: June 1, 1979 | doi: 10.1021/ba-1979-0175.ch005

ing the surface of the walls. It may be because of this existence of sufficient free volume that the intensity of the *o*-Ps component in the monomer crystals is substantially large.

When AAm crystals are irradiated with γ-rays at 30°C, both λ_2 and I_2 decrease (Figure 5). Propionamide (PAm) also was studied for comparison. PAm is a saturated compound of AAm and, therefore, neither polymerization nor phase change takes place with irradiation, but only the free radicals similar to those observed for AAm are accumulated. The results of the lifetime measurements are shown in Figure 6 by the closed circles. I_2 decreases in irradiated PAm, but λ_2 does not decrease. We

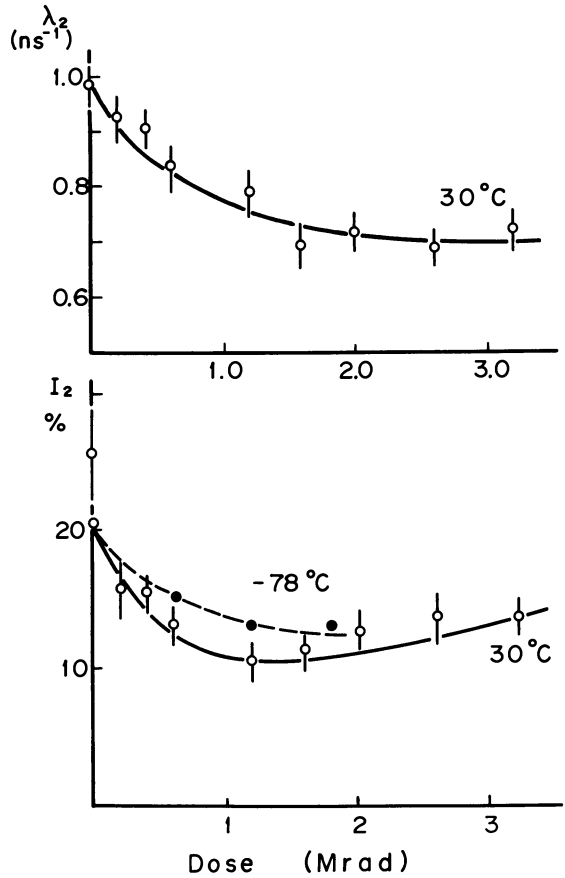

Figure 5. The annihilation rate, λ_2, and the intensity, I_2, of the long-lived component in irradiated solid AAm as a function of irradiation dose. Irradiation temperature was 30°C (○) and −78°C (●) with a dose rate of 2.0 × 10⁵ R/hr.

Publication Date: June 1, 1979 | doi: 10.1021/ba-1979-0175.ch005

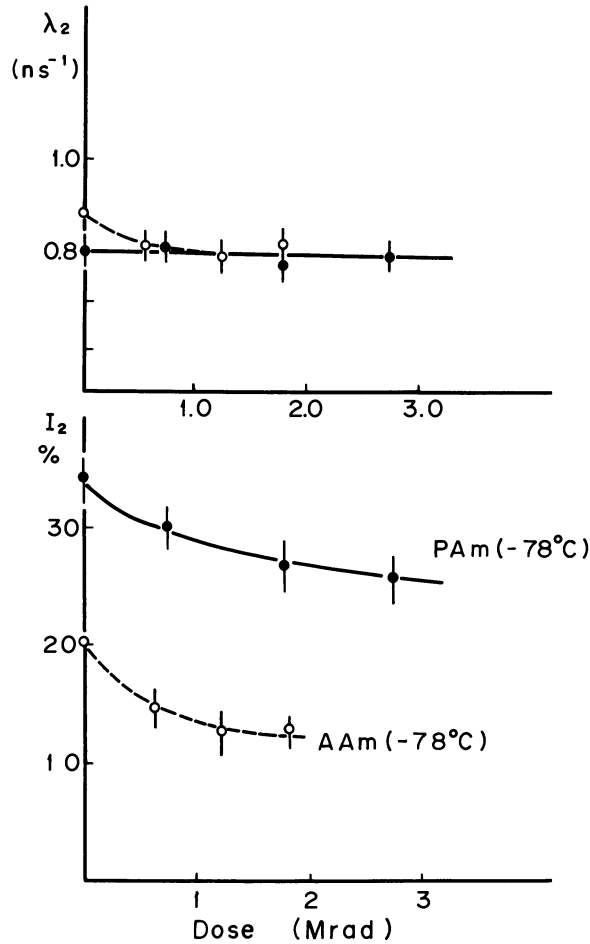

Figure 6. λ_2 and I_2 in irradiated AAm (○) and PAm (●) as a function of irradiation dose. Irradiation temperature was −78°C with a dose rate of 2.0×10^5 R/hr.

therefore conclude that the causes for the decrease in λ_2 and the decrease in I_2 are of different origin. Free radicals may be responsible for the decrease in I_2 and the decrease in λ_2 may be related to formation of enlarged free volumes in irradiated AAm.

It is interesting to note that λ_2 in AAm irradiated at − 78°C (Figure 6) decreases. At such a low temperature, the molecular motion of monomers is hindered to some extent and the polymerization does not proceed beyond a few units of monomers, i.e., only the oligomers are produced. It is further known from ESR studies that in this case the

Publication Date: June 1, 1979 | doi: 10.1021/ba-1979-0175.ch005

oligomerization takes place among the monomer molecules in the same layer in which the vinyl groups come in close contact with each other. Then a free volume of substantial size will be formed around the oligomer, and this will be added to the pre-existing, plane-shaped free volume. Such free volume will look like an open space formed by connecting through a hole of the molecular layer between the neighboring two plane free spaces or an open space swelled out into the wall of the layer. The *o*-Ps possibly can be accommodated in the larger space of the newly formed free volume, and is annihilated with a slower pick-off rate.

Here a question arises as to whether or not *o*-Ps reacts with the free radical which should be present on the end of the oligomer chain. Although we have little knowledge of the reactivity between *o*-Ps and free radicals, we cannot a priori assume that *o*-Ps does not react with free radicals. The following fact seems to indicate that the reaction between *o*-Ps and free radicals is really taking place. Solid AAm monomers, γ-irradiated at 30°C, were dissolved in water and the polymers were precipitated with excess methanol. Poly-AAm thus obtained was dried and pressed into pellets, and the e^+ lifetime measurement in it was carried out. The result was λ_2 (poly-AAm) $= 0.61 \pm 0.03$ nsec^{-1} and $I_2 = 6.4 \pm 1.0\%$ (*13*). This value of λ_2 is smaller than λ_2 in γ-irradiated AAm at high conversion (Figure 6): λ_2(γ-irradiated AAm) $= 0.72$ nsec^{-1}. Therefore, the following explanation is suggested. The effect of the free volume exceeds the effect of reaction with radicals, and the overall effect leads to a smaller λ_2.

$$\lambda_2 = \lambda_p^f + \lambda_r < \lambda_p^c$$

where λ^f_p and λ^c_p are the pick-off rates in the newly formed and crystalline free volumes, respectively. The λ_r is the rate of the reaction. On the assumption that the effect of free volume is not very different for γ-irradiated AAm and poly-AAm, the difference of λ_2: $\Delta\lambda_2 = \lambda_2$($\gamma$-irradiated AAm) $- \lambda_2$(poly-AAm) $= 0.11$ nsec^{-1} will be ascribed to λ_r.

Methylmethacrylate. The third example is MMA (*9*). I_2 in solid MMA is small ($\sim 5\%$), a result similar to that found for DMI. But when poly-MMA (PMMA) is dissolved in the liquid monomer before solidification, or when a polymer is produced by γ-irradiation of solid monomers, I_2 increases as shown in Figure 7.

Under the condition of this experiment at -78°C, the rate of solid-state polymerization is small. A large dose of irradiation is required to produce polymers. Therefore a substantial concentration of free radicals is accumulated before polymerization takes place.

The variation of τ_2 as a function of irradiation dose is shown in Figure 8. The τ_2 decreases at first and then increases again. The initial decrease in τ_2 is thought to be caused by the reaction between *o*-Ps and

Publication Date: June 1, 1979 | doi: 10.1021/ba-1979-0175.ch005

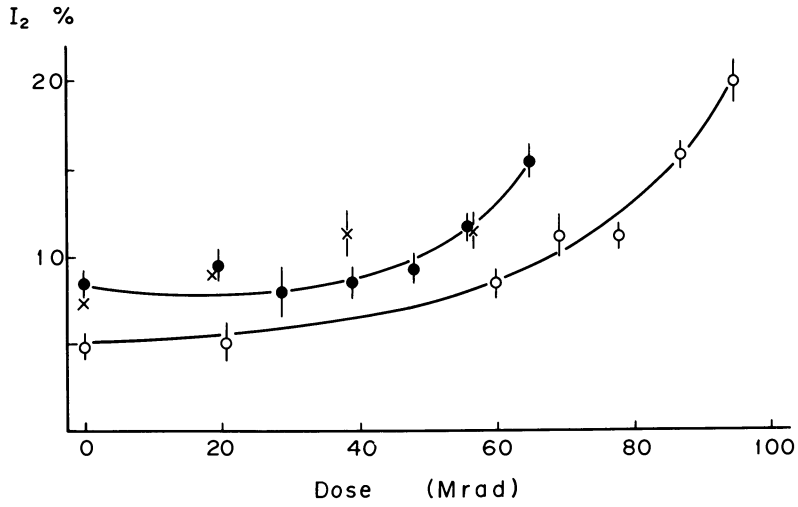

Figure 7. The intensity of the long-lived component in solid MMA (○) or in 1% PMMA–MMA (●) and 5% PMMA–MMA mixtures (×) as a function of the irradiation dose at −78°C

the free radicals formed; the later increase is ascribed to enlarged free volumes in polymers formed by irradiation. The variation in τ_2 becomes more conspicuous when the degree of disorder is increased by introducing a small amount of PMMA before irradiation. In such systems, polymer

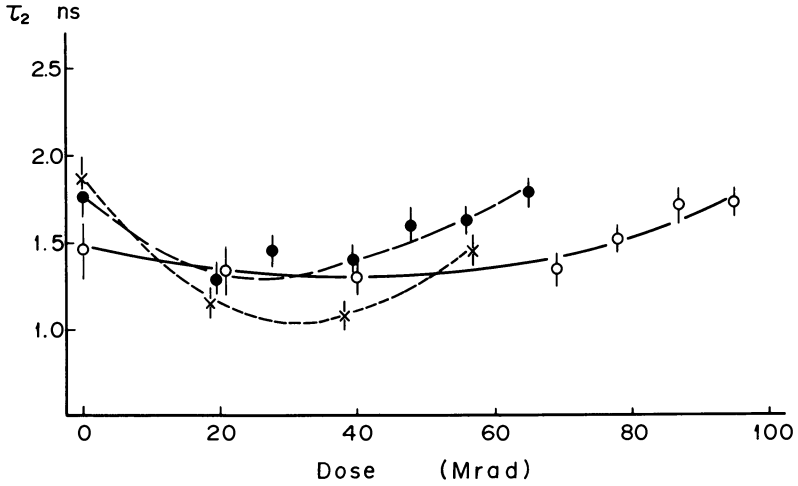

Figure 8. The lifetime, τ_2, of the long-lived component in solid MMA (○) or in 1% PMMA–MMA (●) and 5% PMMA–MMA (×) mixtures as a function of the irradiation dose at −78°C

Publication Date: June 1, 1979 | doi: 10.1021/ba-1979-0175.ch005

chains are suspended in the monomer matrix and the structure around the formed polymers is sparse. It may be that the mobility of *o*-Ps in such a sparse structure is somewhat larger than that in normal crystalline regions.

Thus two major factors, the pick-off rate of *o*-Ps in free volumes and the reaction rate of *o*-Ps with trapped radicals, again seem to be the dominant factors in determining the lifetime in the polymerized organic solids.

***N*-Vinylcarbazole.** In the following section we show an example in which an attempt was made to determine the contributions from the pick-off term, λ_p, and the reaction term, λ_r, separately for the case of *N*-vinylcarbazole (N-VCz) (*10*). The variation of λ_2 in N-VCz monomer solids as a function of irradiation dose is shown in Figure 9. The λ_2 begins to decrease at $\sim$ 5 Mrad, and with the irradiation of more than 13 Mrad, λ_2 increases again. These different dose ranges correspond to the induction period (0–5 Mrad), the propagation period (5–12 Mrad), and the termination period (more than 12 Mrad for N-VCz) of solid-state

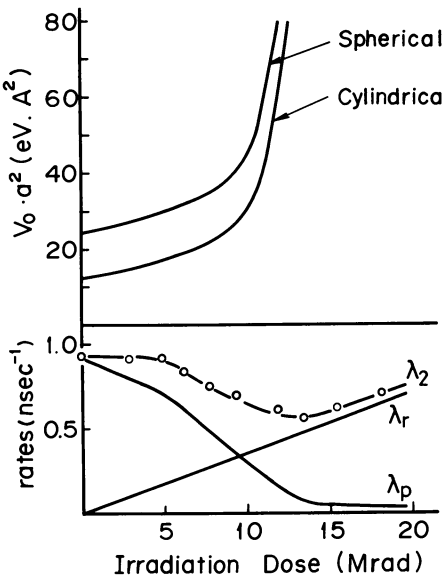

Figure 9. Change of the annihilation rate, λ_2, in solid N-VCz as a function of the irradiation dose. The pick-off rate, λ_p, and the reaction rate, λ_r, are assumed to be the components of λ_2. From the variation of λ_p, the change of the parameter V_0a^2 has been estimated for spherical and cylindrical free volumes.

Publication Date: June 1, 1979 | doi: 10.1021/ba-1979-0175.ch005

polymerization, respectively. In the propagation period in which a substantial amount of polymer is formed, free volumes of increased size are produced resulting in a decrease in the pick-off rate, λ_p. In the termination period in which polymer formation ceases and only free radicals are accumulated on the polymerizing medium, the chemical interaction term λ_r becomes significant.

We assume that the interaction term λ_r can be interpolated linearly to zero dose, and by subtracting λ_r from λ_2, we get the variation of λ_p. λ_p is shown to decrease even in the induction period suggesting that free volumes with increased size are being produced. We presume that such free volumes are closely related to the formation of nuclei of polymers, i.e. oligomers. We already have mentioned the relation between the decrease in λ_p and the formation of free volume around oligomers in the case of AAm. The structure of crystalline N-VCz is different from that of AAm, but in either case the role of the oligomers is the same in the sense that additional free volume of substantial size is formed around them.

In order to roughly estimate the mobility of *o*-Ps, we measured the spin concentration, [R], in irradiated N-VCz by the ESR method. The [R] increased linearly with irradiation dose up to 20 Mrad. Assuming that the reaction term λ_r in Figure 9 is proportional to the spin concentration, i.e., $\lambda_r = k[R]$, we have for the rate constant $k = 4.9 \times 10^{-10}$ cm^3 sec^{-1} spin^{-1}. If the Smolkovskii formula is to be applied for the reaction rate,

$$k = \omega \cdot 4\pi (r_{p_s} + r_R) (D_{p_s} + D_R) \tag{4}$$

where r is the radius, D is the diffusion constant, and ω is the probability factor for the reaction. For a rough estimation we assumed $r_{p_s} = 1$ Å, $r_R = 2$ Å, $\omega = 1$, and $D_R \ll D_{p_s}$, and we have

$$D_{p_s} = 1.3 \times 10^{-3} \text{ cm}^2 \text{ sec}^{-1}. \tag{5}$$

A similar treatment was made by us for *o*-Ps in irradiated *n*-eicosane and polyethylene (PE) (*11*), and the diffusion constant was estimated to be $0.6\text{–}1.8 \times 10^{-5}$ cm^2 sec^{-1} which is much smaller than the D_{p_s} in N-VCz. Diffusion constants also were evaluated in a similar way by Gol'danskii et al. for *o*-Ps reacting with O_2 in solid cyclohexane and solid benzene at -196°C, and the result was $D_{p_s} = 0.7\text{–}1.2 \times 10^{-3}$ cm^2 sec^{-1} (*12*). This value is close to our results in the N-VCz system (*10*).

Thus the reported values of the diffusion constants of *o*-Ps range from $10^{-3} - 10^{-5}$ cm^2 sec^{-1}. It also must be pointed out that the reaction between thermalized *o*-Ps and free radicals in DMI was not observed. These facts may suggest that the method using Formula 4 for the evaluation of reactivity of *o*-Ps with trapped radicals is not appropriate for *o*-Ps.

Publication Date: June 1, 1979 | doi: 10.1021/ba-1979-0175.ch005

In applying the Smolkovskii equation it is assumed that the free radicals are distributed homogeneously and *o*-Ps undergoes many random walks over all possible sites. However, *o*-Ps may not be migrating through every free volume equally. Generally speaking, the larger the size of the well, the lower the ground state energy is of a particle confined in a potential well. The *o*-Ps may not be an exception to this general rule, and it will be better stabilized in larger free volumes. It is quite probable, therefore, that *o*-Ps is migrating from one large free volume to another. It will be worthwhile in this connection to recall the experimental fact that λ_2 in poly-AAm ($\lambda_2 = 0.61$ nsec^{-1}) is smaller than λ_2 in AAm monomer crystals ($\lambda_2 = 0.85$ nsec^{-1}), although the specific volume of poly-AAm is smaller than the monomer crystal (*13*). In the amorphous phase of poly-AAm there may be a broad distribution in the size of free volumes. If we assume that *o*-Ps migrates through only the large free volumes, it is easy to understand why λ_2 is smaller in poly-AAm than in mono-AAm which has less overall density. It will be of great importance, therefore, to consider the disposition of active species with respect to the migration path of *o*-Ps.

The variation in λ_p in Figure 9 is interpreted to be a measure of the change of free volume in the irradiated N-VCz. However, if *o*-Ps prefers to stay in large free volumes as has been mentioned previously, λ_p is an averaged value with larger weights on larger free volumes. Thus λ_p in Figure 9 has a complicated meaning. In spite of this complexity, it is worthwhile to estimate the average value of the size of such large free volumes. One way to do so will be to use a simplified model of free volume (*14*). In this model *o*-Ps is treated as a particle confined in a potential well of appropriate geometry. We approximate the free volume either with a spherical or cylindrical potential well of radius a and potential height V_0. According to Reference 14, the calculation of λ_p is reduced to a calculation of the probability, P, of finding *o*-Ps in the excluded volume

$$\lambda_p = \lambda_0 \cdot P \tag{6}$$

where λ_0 is the annihilation rate of *o*-Ps in the excluded volume. The probability P is calculated as a function of the parameter V_0a^2. For a temporary estimation we have chosen $\lambda_0 = 3$ nsec^{-1} as was done in Reference 14. The change of the parameter V_0a^2 is shown in Figure 9 for each model of potential well. The increase in V_0a^2 is very large at the later stage of polymerization. For a definite estimation of the radius a, we must know V_0. The value of V_0 so far reported is 0.7–0.9 eV for Ps in spherical bubbles of various organic liquids (*15*) and 0.05–0.5 eV for large cavities in PP (*6*). In Reference 10 we reported a value of $V_0 =$ 3.1 eV for *o*-Ps in N-VCz, but since it was based on several assumptions,

Publication Date: June 1, 1979 | doi: 10.1021/ba-1979-0175.ch005

no great significance should be placed on the absolute value. At present there is a significant uncertainty in the evaluation of V_0. After more data are accumulated and further improvement of the free volume model is made, it may become possible to know the size of the average free volume by this method.

Concluding Remarks

The lifetime of *o*-Ps in the solid substances studied seems to be affected by two major factors. One is the pick-off annihilation rate in the free volumes available for *o*-Ps and the other is the reaction rate of *o*-Ps with active species. In the positronium chemistry of liquids it generally is accepted that the annihilation rate of *o*-Ps can be separated into two terms, the pick-off rate and the reaction rate. Our results show that the same also holds basically for *o*-Ps in solid substances, but much is left to be studied about positronium dynamics, the migration scheme, reaction rates, free volume model, etc.

The intensity of the long-lived component also seems to be strongly dependent on free volume or the degree of disorder. For some substances I_2 is larger, because the degree of disorder is larger, but for other substances (mostly polar substances) I_2 becomes smaller when the degree of disorder is increased (*13*).

Finally we would like to mention an important problem which seems to be raised by the present results—the mechanism of the decrease in I_2 in irradiated AAm, PAm, and MMA. It also has been shown by several authors that the intensity of the *o*-Ps component is decreased by free radicals in polymers (*11*) or hydrocarbons (*16*) for which no decisive explanation has yet been given. Although it is important to accumulate experimental data, it seems a general phenomenon that I_2 is decreased in irradiated organic substances. Probably either of the following concepts may explain the results, i.e. reaction of hot-Ps with the free radicals, capture of spur electrons by the free radicals, or direct annihilation of positrons with the unpaired electron in free radicals.

Literature Cited

1. Morawetz, H., "Physics and Chemistry of the Organic Solid State," p. 287, Wiley–Interscience, New York, 1963.
2. Oshima, K., Tabata, Y., *Adv. Nucl. Sci. Technol.* (1966) **3**, 267.
3. Tao, S. J., Green, J. H., *J. Chem. Soc.* (1968) 408.
4. Ito, Y., Tabata, Y., *J. Polym. Sci., Polym. Phys. Ed.* (1971) **9**, 1525.
5. Brandt, W., Paulin, R., *Phys. Rev. B* (1972) **5**, 2430.
6. Ogata, A., Tao, S. J., *J. Appl. Phys.* (1970) **41**, 4261.
7. Ito, Y., Okuda, K., Tabata, Y., *Bull. Chem. Soc. Jpn.* (1971) **44**, 1764.
8. Nitta, I., Taguchi, T., Chatani, Y., *Sen'i ken nenpo* (1959) **12**, 89.
9. Ito, Y., Arita, T., Tabata, Y., *Kobunshi Kagaku* (1971) **28**, 311.

10. Tabata, Y., Ito, Y., Oshima, K., *Org. Solid State Chem. Symp., 1968* (1969) 417.
11. Ito, Y., Tabata, Y., *Bull. Chem. Soc. Jpn.* (1975) **48**, 808.
12. Gol'danskii, V. I., Mogensen, O. V., Shantarovich, V. R., *Khim. Vys. Energ.* (1974) **8**, 124.
13. Ito, Y., Tabata, Y., *Chem. Phys. Lett.* (1972) **15**, 584.
14. Brandt, W., Berko, S., Walker, W. W., *Phys. Rev.* (1960) **120**, 1289.
15. Buchihin, A. P., Gol'danskii, V. I., Tatur, A. O., Shantarovich, V. P., *Zh. Eksp. Teor. Fiz.* (1971) **60**, 1136.
16. Buchihin, A. P., Chirkov, V. N., Shantarovich, V. P., *Khim. Vys. Energ.* (1973) **7**, 195.

RECEIVED December 5, 1977.

Positron Annihilation in Irradiated Polystyrene and Polyethylene

F. H. HSU and J. H. HADLEY, JR.

Department of Physics, Georgia State University, Atlanta, GA 30303

Publication Date: June 1, 1979 | doi: 10.1021/ba-1979-0175.ch006

Ionizing radiation is shown to produce significant changes in the positron annihilation lifetime spectra of polystyrene and polyethylene. Lifetime measurements were carried out at room temperature for samples irradiated and observed both in vacuum and in air. In each case the spectra were fit to three lifetime components. Thermal annealing was used at various stages of the experiment to check reversibility and aid in correlating the changes in lifetime spectra with the free radicals present. Primary free radicals produced in vacuum and stable products evolving from peroxy intermediates both reduce the intensity of the longest-lived component, without reducing the lifetime itself, indicating the inhibition of positronium formation. The experiment indicates the formation of a positron–carbonyl bound state in polyethylene.

Positron annihilation has proven useful as a nondestructive probe for the study of solids and defects in solids. The longer-lived positron lifetime components are sensitive to the nature of the annihilation site in solids. Very low concentrations of radiation-induced defects can have a profound effect upon the formation of positronium (Ps) in solids.

The present study attempts to gain some knowledge of radiation damage in polystyrene (PS) and polyethylene (PE) from positron annihilation lifetime measurements. While the effects of ionizing radiation upon positron decay are often quite large, they are not understood well at this stage in the development of positron annihilation as a useful tool in the study of polymers. For this reason it is of primary importance to

0-8412-0417-9/79/33-175-125$05.00/1

In Positronium and Muonium Chemistry; Ache, H.;
Advances in Chemistry; American Chemical Society: Washington, DC, 1979.

relate the results of positron annihilation studies to information obtained from more frequently used techniques such as electron spin resonance (ESR), IR spectroscopy, and linear energy transfer measurements. One can hope to gain a better understanding of the various positron decay mechanisms in polymers, and thereby make positron annihilation an even more valuable method.

Several authors have reported on positron annihilation studies in solid polymers. An article by Hamielec et al. (*1*) gives a reasonably complete list of contributors. Since then several other papers have been published (*2–7*). Recently it has been established that the positron annihilation lifetime spectra for some polymers such as Teflon and PE possess at least three components (*2–5, 8–13*). Several attempts have been made to identify the various positron decay mechanisms responsible for each of the lifetime components. It generally is agreed that the longest-lived component of the lifetime spectrum is associated with the pick-off decay of ortho-positronium (*o*-Ps). However, considerable disagreement remains with respect to the assignment of the remaining lifetime components (*2–5, 6–11*). A paper by Kerr (*5*) discusses some of the arguments associated with the intermediate-lifetime component.

Considerable work remains to be done to help understand the effects of radiation damage upon positron annihilation in polymers under various experimental conditions. There is disagreement as to the role of free radicals in determining the positron decay modes in polymers. The present work attempts to clarify that role.

Cross-linking is the most important result of ionizing radiation in PS and PE, and free radicals are the major intermediates in the radiation process. If oxygen is admitted to an irradiated polymer, the radicals (produced in vacuum) are converted to peroxy radicals. The peroxy radicals are unstable and lead to the formation of carbonyl and hydroxyl groups.

Polystyrene. Polymer chemists generally consider cross-linking to be the most important radiation process in polystyrene (PS), and there is evidence that free radicals are intermediates in the process (*14, 15*). Two free radicals (observed by ESR) are produced in PS which are stable at room temperature in vacuum (*16*). These are di-substituted benzyl radicals (denoted as Type A) formed by hydrogen extraction from an α-position carbon of the chain,

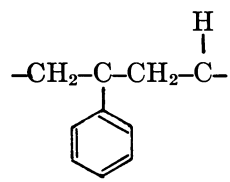

Publication Date: June 1, 1979 | doi: 10.1021/ba-1979-0175.ch006

and a cyclohexadienyl-type radical (denoted as Type B) formed by hydrogen addition to the ring,

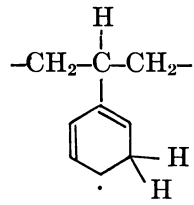

The radical yield for Type A is about ten times that for Type B for gamma doses up to 8×10^6 rad. When irradiated PS is exposed to air, oxygen destroys the primary free radicals, and peroxy intermediates are formed. The peroxy radicals decay with the generation of stable C=O and OH groups (*17*).

The physical properties of PS are relatively insensitive to moderate amounts of ionizing radiation (*18*). A slight decrease in crystallinity has been observed for very heavy doses (larger than those used in this work) of ionizing radiation (*19*).

Earlier positron annihilation studies of PS (*20, 21*) have used two-component lifetime fits, while three-component fits were used on some polymers such as Teflon (*11, 12*). The longest-lived component is attributed to the pick-off decay of *o*-Ps (*9, 21*). The intermediate component in Teflon is probably caused by a bound state other than Ps (*9, 10*).

Thosar et al. (*22*) have reported on positron studies of neutron-irradiated PS. They used a two-component lifetime fit and reported a decrease in the intensity of the long-lived component. This was attributed to the destruction of benzene ring sites for PS. They observed no effects owing to γ-irradiation and assumed that the free radicals produced did not affect the PS since they were outside the ring. The present work disagrees with the findings of Thosar et al. for γ-irradiated PS.

Polyethylene. For moderate radiation doses, two free radicals are produced in polyethylene (PE) with significant yields (*23, 24*). One is an alkyl-type radical (denoted as Radical B):

$$-CH_2-\dot{C}H-CH_2-$$

and the other is an allyl-type radical (denoted as Radical R):

$$-CH_2-\dot{C}H-CH=CH-CH_2-$$

Publication Date: June 1, 1979 | doi: 10.1021/ba-1979-0175.ch006

Radical B is produced more readily than Radical R but decays very quickly at room temperature (both are stable in vacuum at 77 K). In vacuum, two B radicals can combine giving rise to a cross-linked product. In air, both B and R radicals form peroxy radicals. The peroxy radicals then proceed to form OH or C=O groups (*25*). When oxygen is present during irradiation, one would expect to have the oxidized products of both Radicals B and R formed. On the other hand when oxygen is not admitted until after vacuum irradiation, only an appreciable number of R radicals would remain to be oxidized. PE, therefore, is a good subject for the study of the effects of various radiation products upon positron annihilation lifetime spectra.

Several studies of the effects of ionizing radiation upon positron annihilation in PE have been reported (*7, 26, 27, 28*). However, in most cases the spectra were resolved into only two components, yielding no information concerning the intermediate lifetime component (*7, 26, 28*). Another experiment (*27*) was performed in air.

Publication Date: June 1, 1979 | doi: 10.1021/ba-1979-0175.ch006

Experimental Procedure

Annihilation lifetime spectra were obtained at room temperature using conventional fast–slow coincidence circuitry with naton scintillators (*29*). The time resolution of the apparatus under actual experimental conditions was 0.35 nsec at full-width at half-maximum (FWHM). A ^{22}Na positron source of about 30 μCi was sandwiched between two disc-shaped pieces of polymer. The samples and source were mounted in a chamber that could be evacuated and remained in the chamber during irradiation and lifetime measurements.

PS samples used were obtained by aging the monomer in the presence of light; they were annealed in vacuum at 70°C for 24 hr to insure uniform polymerization. The high-density samples obtained were ordinary amorphous PS of low crystallinity. Commercially available high-density PE was used. Samples were irradiated at room temperature with ^{137}Cs gammas at a dose rate of 10^5 rad/hr. All thermal annealings were for 24 hr at 70°C (for PS) or 80°C (for PE), which were below the glass-transition temperatures.

Three sets of runs were made on each sample: (1) irradiated and observed in air, then annealed in air; (2) irradiated and observed in vacuum, then exposed to air, then annealed; and (3) irradiated and observed in vacuum, annealed in vacuum, then exposed to air. In each case the spectra can be well-resolved into three lifetime components using a six-parameter, least-square fitting program.

In Positronium and Muonium Chemistry; Ache, H.;
Advances in Chemistry; American Chemical Society: Washington, DC, 1979.

Results and Discussion

Polystyrene. Figure 1 compares the lifetime spectra for PS before and after γ-irradiation in vacuum. The computer-fitted lifetime parameters are given in Table I-a. Irradiation in vacuum reduces the intensity, I_3, of the largest-lived component. This indicates an inhibition of Ps formation and probably is caused by the presence of stable free radicals. This inhibition by free radicals has been observed in other molecular solids (*30, 31, 32*) and polymers (*13*). The vacuum irradiation produced no significant changes in the other lifetime parameters. The fact that I_2 was not affected by the irradiation is evidence that the intermediate-lifetime component is not caused by PS, but rather to another bound state (*11, 12*).

The evacuated sample then was annealed. This should have caused essentially all of the Type B radicals and most of the Type A radicals to decay. As expected I_3 returned approximately to the pre-irradiation value. This sample then was opened to air, producing another decrease in I_3. It is assumed that oxygen reacted with the remaining (mostly Type A) radicals, producing an oxygen-stabilized system that also inhibits the formation of Ps.

Another sample, first irradiated and observed in vacuum, was then opened to air and its spectrum observed before annealing. In this case (*see* Table I-b) I_3 returned only partially to its original value. The remaining inhibition probably is caused by peroxy radicals and residual primary radicals in the interior of the sample. Finally, annealing destroys

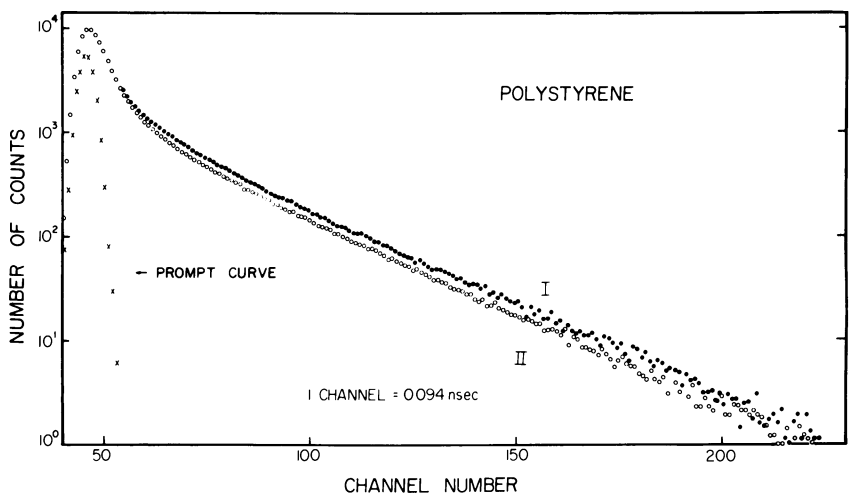

Figure 1. Lifetime spectra for PS before (I) and after (II) γ-irradiation in vacuum

Table I. Annihilation Lifetimes and Intensities for Positrons

Treatment	τ_1 *(nsec)*	τ_2 *(nsec)*
a. In vacuum		
No irradiation	0.27 ± .01	0.87 ± .02
8×10^6 rad	0.28 ± .01	0.84 ± .02
70°C anneal	0.26 ± .01	0.86 ± .02
Open to air	0.26 ± .01	0.87 ± .02
b. In vacuum		
No irradiation	0.26 ± .01	0.88 ± .02
8×10^6 rad	0.27 ± .01	0.84 ± .02
Open to air	0.26 ± .01	0.84 ± .02
70°C anneal	0.26 ± .01	0.84 ± .02
c. In air		
No irradiation	0.26 ± .01	0.82 ± .02
8×10^6 rad	0.27 ± .01	0.80 ± .02
70°C anneal	0.27 ± .01	0.79 ± .02

most of the remaining radicals, both primary and peroxy, and I_3 returns to the pre-irradiation value.

A third PS sample was irradiated in air. Lifetime spectra before and after irradiation are shown in Figure 2, and the parameters for this run are given in Table I-c. As was the case for the samples described above, radiation reduces the intensity of the longest-lived component, indicating inhibition of Ps formation. A small reduction in the lifetime itself (τ_3)

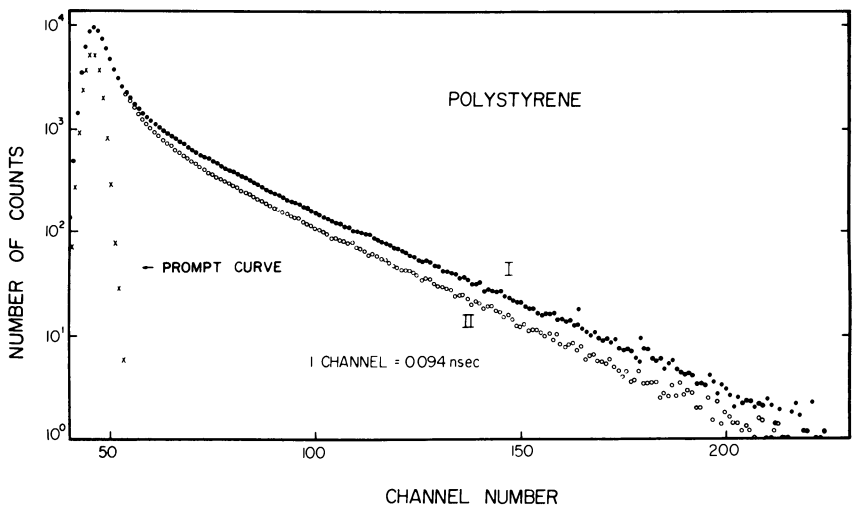

Figure 2. Lifetime spectra for PS before (I) and after (II) γ-irradiation in air

in Polystyrene γ-Irradiated in Vacuum and in Air

τ_3 (nsec)	I_2 (%)	I_3 (%)
2.36 ± .02	21.5 ± 1.1	33.8 ± .7
2.32 ± .02	20.1 ± 1.0	29.3 ± .5
2.27 ± .02	20.3 ± 1.0	33.5 ± .6
2.28 ± .02	21.6 ± 1.0	30.4 ± .5
2.36 ± .02	20.4 ± 1.0	33.2 ± .6
2.31 ± .02	20.5 ± 1.0	28.2 ± .5
2.30 ± .02	21.1 ± 1.0	31.1 ± .5
2.27 ± .02	20.9 ± 1.0	32.8 ± .5
2.33 ± .02	20.9 ± 1.0	34.1 ± .6
2.27 ± .02	21.3 ± 1.0	29.0 ± .5
2.23 ± .02	21.7 ± 1.0	34.0 ± .5

was observed also. Such a reduction would be expected if the free volume associated with the Ps site was to be diminished (*33, 34*). Increased cross-linking and attached carbonyl and hydroxyl groups, produced as final products upon the decay of the primary and oxygen-stabilized radicals, could be responsible for the reduction in free volume. Annealing kills the remaining radicals and restores the original value of I_3, but it

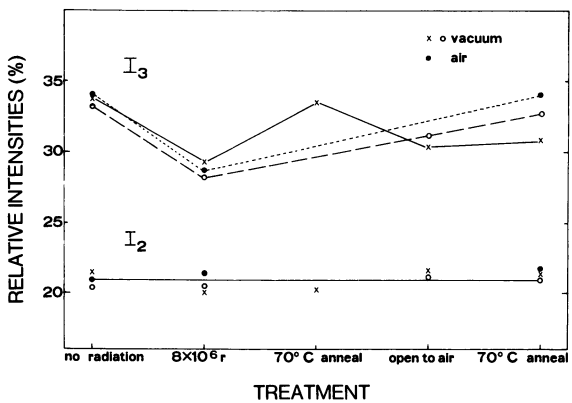

Figure 3. Measured values of I_2 and I_3 for PS samples following various experimental steps: irradiated in vacuum and annealed before exposing to air (×); irradiated in vacuum and exposed to air before annealing (○); and irradiated in air and annealed (●).

Publication Date: June 1, 1979 | doi: 10.1021/ba-1979-0175.ch006

does not affect the final stable products, leaving τ_3 at its reduced value. The step-by-step values of I_2 and I_3 for each of the three PS samples following each stage of the experiment are plotted in Figure 3. For all three samples I_2 is unaffected.

Polyethylene. The experimental procedures for PS (*see* Table II) were similar to those used for PS. When PE was irradiated in vacuum I_3 was reduced by about 10% (for a radiation dose of 5×10^6 rad). This inhibition of Ps formation is caused by the presence of free radicals. In this case the only radicals left at room temperature are the R-type ones; the B radicals having decayed—primarily by combining to create cross-linkages. The other lifetime parameters were not affected by the vacuum irradiation. Annealing the still-evacuated sample destroys most of the remaining R radicals, and I_3 returns nearly to the pre-irradiation value (Table II-a). As expected, no further change in I_3 was produced by exposing the sample to air after the radicals had been annealed out. When the sample was opened to air prior to annealing (Table IIb), I_3 also remained unchanged. Evidently the oxygen-stabilized R radicals have an inhibiting effect comparable to the primary R radicals themselves.

An equivalent radiation dose in air (Table IIc) reduced I_3 by about 30%. For irradiation in air both the B and R radicals form peroxy radicals. Evidently the final products of the peroxy intermediates associated with the B radicals reduce I_3 significantly. Annealing has little effect upon these stable products, and I_3 remains substantially reduced.

Table II. Annihilation Lifetimes and Intensities for Positrons

Treatment	τ_1 *(nsec)*	τ_2 *(nsec)*
a. In vacuum		
No irradiation	0.29 ± .01	0.78 ± .02
5×10^6 rad	0.30 ± .01	0.77 ± .03
80°C anneal	0.29 ± .01	0.76 ± .03
Open to air	0.30 ± .01	0.78 ± .03
b. In vacuum		
No irradiation	0.29 ± .01	0.79 ± .03
5×10^6 rad	0.30 ± .01	0.78 ± .03
Open to air	0.29 ± .01	0.72 ± .03
80°C anneal	0.30 ± .01	0.73 ± .02
c. In air		
No irradiation	0.28 ± .01	0.79 ± .03
5×10^6 rad	0.30 ± .01	0.72 ± .02
80°C anneal	0.30 ± .01	0.74 ± .02

Publication Date: June 1, 1979 | doi: 10.1021/ba-1979-0175.ch006

A reduction in τ_2 was observed for PE samples irradiated in or exposed to air following irradiation in vacuum without annealing. The τ_2 was not reduced for the sample irradiated and annealed in vacuum prior to exposure to air. This reduction in τ_2 is a newly observed effect, and it is clearly caused by the oxygen-stabilized final products. It can be explained by a new bound state, with a lifetime shorter than that of the intermediate component in the pre-irradiated sample generated by the oxygen-stabilized system. One of the final results of the peroxy intermediates is a carbonyl group attached to the polymer chain. Because of the large electronegativity of the oxygen atom, the carbonyl would be a favorable site for a positron–molecule-type bound state. The lifetime of this new bound state could be shorter than that of the other bound state responsible for the τ_2 component in the pre-irradiated PE. The observed lifetime then is an average value of these two lifetimes.

Summary

The experiment has shown that moderate doses of ionizing radiation make appreciable changes in the positron annihilation lifetime spectra of PS and PE. Changes in the physical properties of these polymers produced by the radiation were insignificant and were probably not responsible for the observed changes in the positron decay. The intensity of the longest-lived component, I_3, was reduced for both PS and PE. This

in Polyethylene γ-Irradiated in Vacuum and in Air

τ_3 (nsec)	I_2 (%)	I_3 (%)
2.61 ± .02	18.8 ± 1.4	18.7 ± .3
2.61 ± .02	19.0 ± 1.3	16.5 ± .3
2.58 ± .02	20.0 ± 1.3	17.9 ± .3
2.61 ± .02	19.0 ± 1.3	17.4 ± .3
2.61 ± .02	18.4 ± 1.4	19.0 ± .4
2.59 ± .02	18.8 ± 1.3	17.2 ± .3
2.58 ± .02	19.9 ± 1.4	17.0 ± .3
2.58 ± .02	19.2 ± 1.3	17.8 ± .3
2.62 ± .02	18.9 ± 1.4	19.1 ± .4
2.59 ± .02	19.2 ± 1.3	13.5 ± .4
2.62 ± .02	18.3 ± 1.4	15.2 ± .4

In Positronium and Muonium Chemistry; Ache, H.;
Advances in Chemistry; American Chemical Society: Washington, DC, 1979.

reduction, indicating inhibition of Ps formation, can be associated with both primary free radicals produced in vacuum and oxygen-stabilized radicals.

When PS was irradiated in the presence of oxygen, there was a small reduction in τ_3. This probably was caused by a reduction in free volume associated with final products produced in the decay of peroxy intermediates. The fact that I_2 is not affected by the radiation is further evidence that it is caused by the decay of a positron-bound state other than Ps. The reduction in τ_2 observed for PE irradiated in air may be caused by an additional bound state involving the positron and a carbonyl group.

Acknowledgments

The authors with to thank H. K. Tseng and G. C. Su for assistance in the collection and reduction of the experimental data.

Literature Cited

1. Hamielec, A. E., Eldrup, M., Mogensen, O., Jansen, P., *J. Macromol. Sci.* (1973) **C9**, 305.
2. Stevens, J. R., Rowe, R. M., *J. Appl. Phys.* (1973) **44**, 4328.
3. Chuang, S. Y., Tao, S. J., *J. Appl. Phys.* (1973) **44**, 5171.
4. Bertolaccini, M., Bisi, A., Gambarini, G., Zappa, L., *J. Phys.* (1974) **C7**, 3827.
5. Kerr, D. P., *Can. J. Phys.* (1974) **52**, 935.
6. West, D. H. D., McBrierty, V. J., Delaney, C. F. G., *Appl. Phys.* (1975) **7**, 171.
7. Ito, Y., Tabata, Y., *Bull. Chem. Soc.* (1975) **48**, 808.
8. Tao, S. J., Green, J. H., *Proc. Phys. Soc.* (1965) **85**, 463.
9. Brandt, W., Spirn, I., *Phys. Rev.* (1966) **142**, 231.
10. Mackenzie, I. K., McKee, B. T. A., *Can. J. Phys.* (1966) **44**, 435.
11. McGervey, J. D., Walters, V. F., *Phys. Rev.* (1970) **B2**, 2421.
12. Hsu, F. H., Hadley, J. H., Jr., *Phys. Lett.* (1971) **34A**, 317.
13. Stevens, J. R., Lichtenberger, P. C., *Phys. Rev. Lett.* (1973) **29**, 166.
14. Parkinson, W., Keyser, R., "The Radiation Chemistry of Macromolecules," M. Dole, Ed., Vol. II, Chap. 5, Academic, New York, 1973.
15. Wall, L., Brown, D., *J. Phys. Chem.* (1957) **61**, 129.
16. Harrah, L., "Organic Solid State Chemistry," G. Adler, Ed., pp. 197–210, Gordon Breach, New York, 1969.
17. Sears, W., Parkinson, W., *J. Polym. Sci.* (1956) **21**, 325.
18. Parker, M. S., Krasnansky, V. J., Achhammer, B. G., *J. Appl. Polym. Sci.* (1964) **8**, 1825.
19. Slovokhotova, N. A., Il'cheva, Z. F., Kargin, V. A., *Vysokomol. Soedin.* (1961) **3**, 191.
20. Groseclose, B., Loper, G., *Phys. Rev.* (1965) **137**, A939.
21. Jain, P. C., Bhatnager, S., Gupta, A., *J. Phys. C.* (1972) **5**, 2156.
22. Thosar, B. V., Kulkarni, V. G., Lagu, R. G., Chandra, G., *Phys. Lett.* (1966) **21**, 647.
23. Libby, D., Ormerod, M., Charlesby, A., *Polymer* (1960) **1**, 212.
24. Charlesby, A., Libby, D., Ormerod, M., *Proc. R. Soc. (London)* (1961 **A262**, 207.

25. Ohnishi, S., Sugimoto, S., Nitta, I., *J. Polym. Sci.* (1963) **A1**, 605.
26. Chandra, G., Kulkarni, V. G., Lagu, R. G., Thosar, B. V., *Phys. Lett.* (1965) **19**, 201.
27. Green, J. H., Tao, S. J., *Br. J. Appl. Phys.* (1965) **16**, 981.
28. Khan, M. N. G. A., Proc. Int. Conf. Positron Annihilation, 2nd, Kingston, Ontario, 1971, 3.24–3.42 (unpublished).
29. Hsu, F. H., Wu, C. S., *Phys. Rev. Lett.* (1967) **18**, 889.
30. Hadley, J. H., Jr., Hsu, F. H., *Chem. Phys. Lett.* (1970) **7**, 465.
31. Hadley, J. H., Jr., Hsu, F. H., *Chem. Phys. Lett.* (1971) **12**, 291.
32. Eldrup, M., Lund-Thomsen, E., Mogensen, O., *J. Chem. Phys.* (1972) **56**, 4902.
33. Brandt, W., "Positron Annihilation," A. T. Stewart, O. O. Roellig, Eds., p. 155, Academic, New York, 1967.
34. Thosar, B. V., Kulkarni, V. G., Lagu, R. G., Chandra, G., *Phys. Lett.* (1969) **28A**, 760.

RECEIVED December 2, 1977.

Positron Annihilation Processes in Diatomic and Polyatomic Gases

J. D. McNUTT and S. C. SHARMA

Center for Positron Studies, University of Texas, Arlington, TX 76019

Publication Date: June 1, 1979 | doi: 10.1021/ba-1979-0175.ch007

This chapter reviews some recent advances in our understanding of the annihilation behavior of positrons and positronium atoms in several diatomic and simple polyatomic gases. The major experimental findings for positrons are: (1) the observed annihilation rates are higher than those expected for direct annihilation, (2) these rates can be sensitive functions of temperature and density, (3) the "shoulder width" in the positron lifetime spectrum for N_2 is density dependent, (4) the addition of Ne to H_2 gas at 77 K can affect the positron–H_2 annihilation process. These results are discussed in terms of positron–molecule collision complexes and positron–molecule cluster states. Measurements of positronium formation fractions and ortho-positronium annihilation rates are also reported and are discussed in terms of chemical and conversion quenching, density fluctuations, and positronium-induced cavity formation.

As the scattering and annihilation of low energy positrons in noble gases have become better understood, increased experimental and theoretical attention has been devoted to positron interactions in molecular gases and in monatomic–molecular gas mixtures. Several of the most interesting annihilation features reported for the noble gases also have been encountered with molecular gases but are often modified by the existence of excited molecular states and by positron–molecule resonance processes. Aspects of the annihilation process that are unique to molecular gases have been observed also.

This chapter reviews some recent advances in our understanding of the annihilation behavior of positrons and positronium (Ps) atoms in

0-8412-0417-9/79/33-175-137$06.75/1

In Positronium and Muonium Chemistry; Ache, H.;
Advances in Chemistry; American Chemical Society: Washington, DC, 1979.

several diatomic and simple polyatomic gases (*1, 2, 3*). Although reference sometimes is made to the results of two-photon angular correlation and positron–molecule total scattering cross section measurements as well as to calculations of positron cross sections, positron–molecule interactions are discussed primarily in terms of their influence on positron lifetime spectra.

In addition to a constant background contribution, the lifetime spectra for positrons annihilating in gases can be resolved into three exponential components. The longest lived component, with annihilation rate λ_2, results from the annihilation of positrons bound in ortho-positronium (*o*-Ps) atoms whereas the shortest lived component results from the annihilation of para-positronium (*p*-Ps) and of positrons in the metal walls of the experimental chamber. The intermediate lifetime component, with annihilation rate λ_1, is attributed to annihilations in the gas of positrons that do not form Ps. In the noble gases and in some molecular gases, the latter component is preceded by a nonexponential region, usually called the shoulder region, which corresponds to the slowing process for positrons in the gas and the variation of the annihilation cross section with positron velocity.

Publication Date: June 1, 1979 | doi: 10.1021/ba-1979-0175.ch007

Thermalized Positrons in Pure Molecular Gases

The annihilation behavior of slow positrons in many gases can be attributed to annihilations during positron–molecule (or positron–atom) collisions. This process, often referred to as the "direct annihilation" of free positrons, is characterized by an annihilation rate, $\lambda(E)$, which is directly proportional to the density of the gas and which depends also on the kinetic energy, E, of the annihilating positron. This rate can be expressed as

$$\lambda(E) = \pi r_o^2 \, c n \, Z_{eff}(E) \tag{1}$$

where r_o is the classical radius of the electron, c is the speed of light, and n is the molecular number density of the gas. The unit "amagat" is the number of gas molecules per unit volume at a temperature of 273.2 K and a pressure of 101.3 kPa (atmospheric); 1 amagat $\approx 2.7 \times 10^{25}$ m^{-3}. $Z_{eff}(E)$ is an empirical constant, which for direct annihilations is independent of gas density and can in that case be interpreted as the effective number of electrons per molecule available for singlet annihilation during collisions with slow positrons. The measured rate, λ_1, corresponds to the average annihilation rate of positrons in thermal equilibrium with the gas. Because of polarization attractions, Z_{eff} is generally observed to be slightly larger than Z, the actual number of electrons per molecule, and to increase with decreasing positron energy.

In Positronium and Muonium Chemistry; Ache, H.;
Advances in Chemistry; American Chemical Society: Washington, DC, 1979.

Of greater interest, however, are those measurements that indicate the presence of more complex annihilation processes. More than a decade ago, Paul and Saint Pierre (*4*) and Osmon (*5*) observed that the Z_{eff} for thermalized positrons in some molecular gases were several orders of magnitude greater than Z. More recently, strong temperature and density dependencies have been observed for Z_{eff} in several molecular gases. These effects for Z_{eff} measured in NH_3 gas at different temperatures (*6*) can be seen in Figure 1. At the peak, Z_{eff} is more than 1800 times Z.

Qualitatively similar behavior has been observed with gaseous CH_4 and H_2. The ratio of λ_1 to density, which is proportional to Z_{eff}, is shown in Figure 2 for CH_4 (*7*) whereas the annihilation rate, λ_1, measured in H_2 (*8, 9*) is plotted in Figure 3. At low densities of these gases and at sufficiently high temperatures λ_1 varies linearly with the gas density (*7, 9, 10, 11*), thus corresponding to density-independent values of Z_{eff} and indicating the interaction of positrons with single molecules. However, the low density Z_{eff} values for CH_4 and H_2, being about fifteen (*7, 10*) and eight (*9, 11*) times Z, respectively, are greater than those expected for direct annihilations. For example, a recent theoretical study by Baille et al. (*12*) of the interaction of low energy positrons with H_2 molecules, which incorporates a sufficiently strong empirical polarization potential to produce total elastic cross sections in reasonable agreement with experiment (*13*), predicts a Z_{eff} at thermal energies that is an order of magnitude less than the measured values.

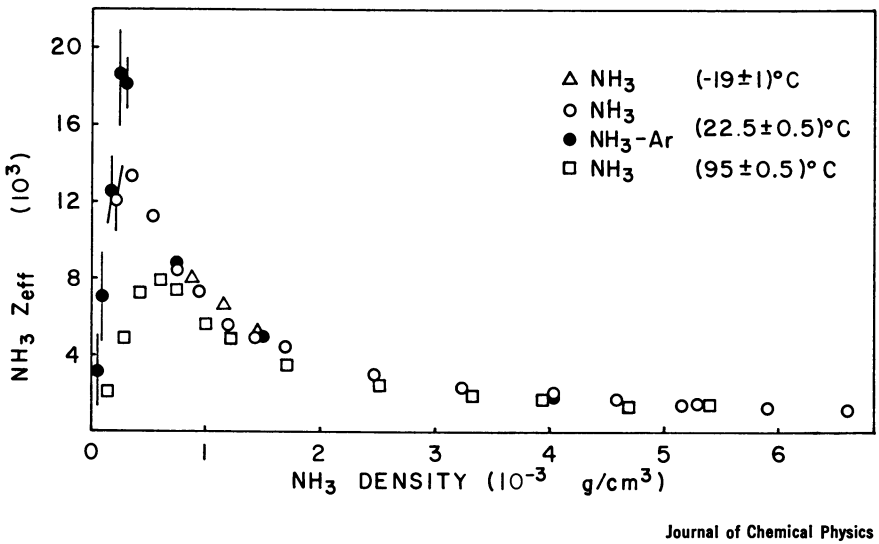

Figure 1. Z_{eff} for slow positrons annihilating with NH_3 molecules vs. NH_3 gas (partial) density at −19°, 22.5°, and 95°C. The statistical standard deviations fall within the symbols unless otherwise indicated (6).

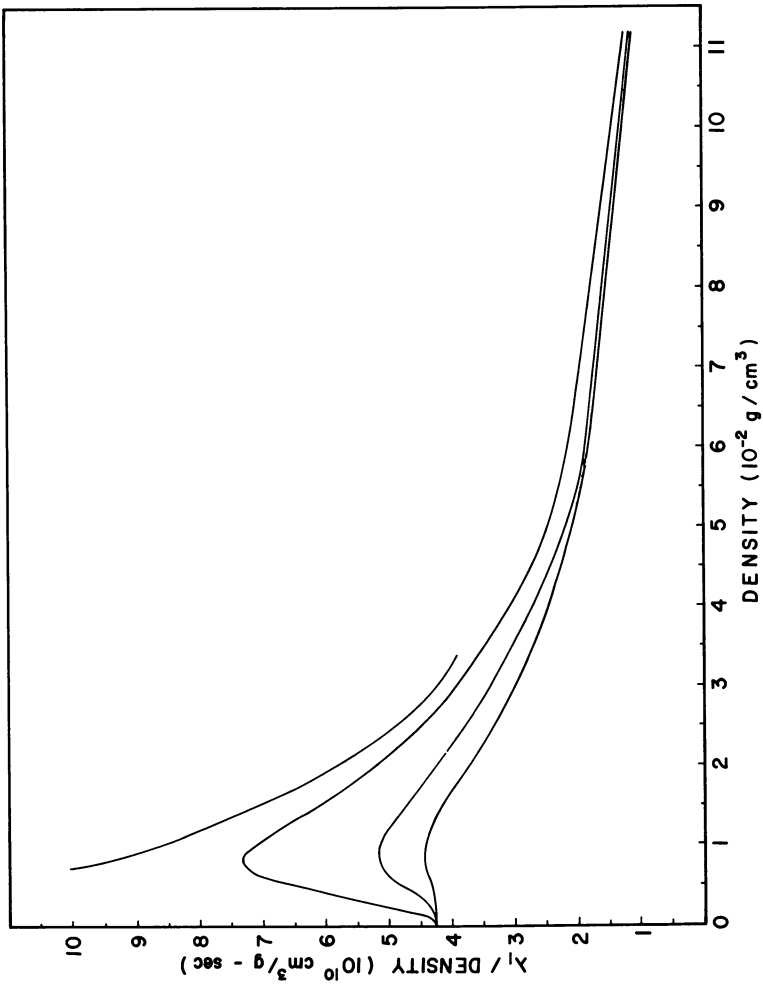

Journal of Chemical Physics

Figure 2. Hand-smoothed fits to the slow positron annihilation rate to methane gas density ratios vs. methane gas density data at 22°C (lowest curve), 4.5°C (next higher curve), −28°C (second curve from the top), and −50°C (top curve) (7).

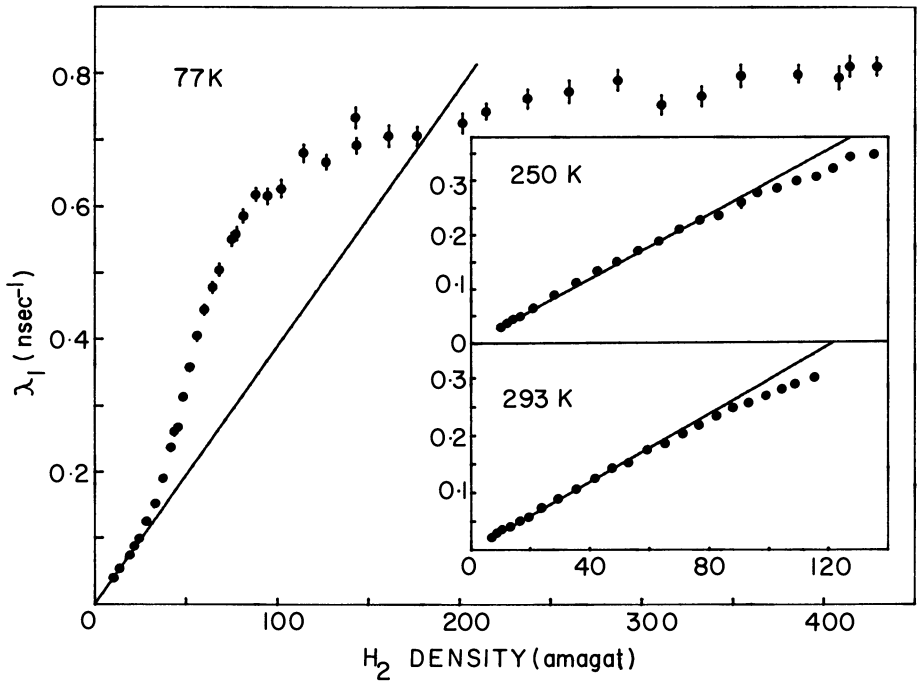

Figure 3. Annihilation rate of slow positrons vs. H_2 gas density at 77 K (9). The line represents a weighted least-squares fit to data (not all shown) below 19 amagat that is constrained to pass through the origin. The insert shows the annihilation rate of slow positrons vs. H_2 gas density at 250 and 293 K. The lines represent a weighted least-squares fit to the combined data below 21 amagat at 250 K and 47 amagat at 293 K that is constrained to pass through the origin. The statistical standard deviations fall within the symbols unless otherwise indicated.

Smith and Paul (*10*) showed that annihilation during resonance scattering of positrons on unbound levels could produce the high annihilation rates observed for CH_4 at room temperature. They proposed that a positron during a collision with a CH_4 molecule could form a virtual, vibrationally excited positron–CH_4 compound. Assuming a narrow, isolated S-wave resonance and a Maxwell-Boltzman positron energy distribution, they used the Breit–Wigner single-level formula to calculate the slow positron annihilation rate. The resonance energy for formation of such a compound should be less than the vibrational excitation threshold (0.162 eV) for CH_4 by an amount equal to the binding energy of the positron in the positron–CH_4 virtual state. However, it was later demonstrated that the Z_{eff} for CH_4 remained essentially unchanged from the room temperature value (153.7 $\pm$0.9) to temperatures as low as $-28°C$ (*7*), and that under the influence of an applied electric field, ϵ, the room-temperature Z_{eff} decreased linearly with the ϵ/density ratio (*7, 14*). It is possible that the Z_{eff} for CH_4 molecules increases rapidly enough with decreasing positron energy to compensate reduced contributions from the

Publication Date: June 1, 1979 | doi: 10.1021/ba-1979-0175.ch007

resonance at the lower thermal energies. However, the electric-field results offer strong evidence that the single-level resonance picture, at least near vibrational threshold energies, does not apply for positrons in CH_4.

The lowest excitation threshold for H_2 is that for molecular rotation at 0.044 eV. This threshold energy is not far above the thermal energy distribution at 300 K, but it is more than six times higher than the most probable positron energy at 77 K. However, (*see* Figure 3) the Z_{eff} measured for H_2 at 77 K (19.3 $\pm$0.3) is about 30% greater than that measured at both 250 and 293 K (14.8 $\pm$0.4) (*8, 9*). Here it seems very unlikely that the energy dependence of Z_{eff} in H_2 (*12*) could be strong enough to produce the observed net increase in Z_{eff} at 77 K if there were a large accompanying reduction in the contribution to Z_{eff} from resonances near the rotational threshold. Therefore if excited positron–H_2 complexes are responsible for the high Z_{eff} values measured at low H_2 densities, the positrons must enter into these complexes during thermalization. This possibility is discussed further below. The enhancement in Z_{eff} at 77 K might result from more stable complexes or more probably from those positrons that have remained free experiencing a higher Z_{eff} at the lower thermal energies.

Z_{eff} values measured for thermalized positrons in gaseous N_2 at 77 and 300 K are plotted in Figure 4 (*15*). At the lowest densities at 77 K, Z_{eff} is measured to be approximately constant as 40 $\pm$1, which is higher than the value of about 30 observed at room temperature (*16, 17, 18*). This temperature dependence of the low density Z_{eff} values is similar to that observed for H_2 gas. However, in N_2, the Z_{eff} values exceed Z by Z_{eff} is measured to be approximately constant at 40 $\pm$1, which is higher factors of only about 2 at room temperature and approximately 3 at 77 K. Considering that the spherical and anisotropic polarizabilities and the quadrupole moment of N_2 are more than twice as large as the corresponding values for H_2 and that the effects of the quadrupole and polarization interactions reinforce each other for N_2 whereas they cancel for H_2 (*19*), it might be expected that the observed annihilation rates could result entirely from direct annihilations on polarized N_2 molecules. The calculations of Darewych and Baille (*20*) offer some support for this idea. These authors investigated the interaction of low energy positrons with N_2 in the adiabatic (fixed nuclei) approximation, using one-center formalism that is similar in all respects to the positron–H_2 calculations (*12*) discussed above. Including the effect of the distortion of the electronic cloud by the incoming positron through the use of empirical, velocity-independent polarization potentials, they calculated Z_{eff} values of approximately 29 and 23 at thermal energies at 77 and 300 K, respectively. These values are less than the experimental values by only about 25%, and the calculated

Publication Date: June 1, 1979 | doi: 10.1021/ba-1979-0175.ch007

Publication Date: June 1, 1979 | doi: 10.1021/ba-1979-0175.ch007

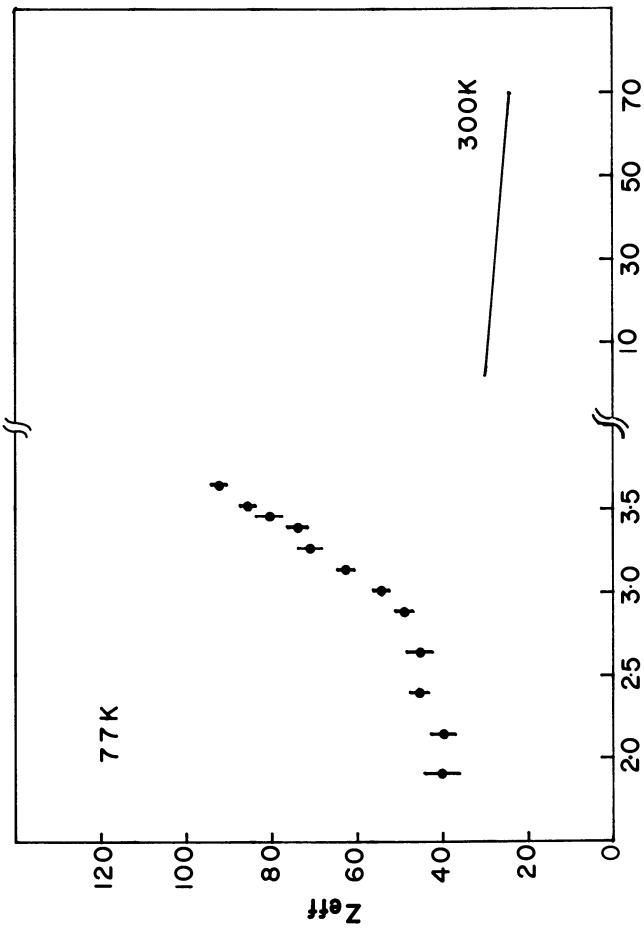

Figure 4. Z_{eff} for thermalized positrons vs. N_2 gas density at 77 K (15). The line represents the results at room temperature (16).

dependence of Z_{eff} on positron energy is in good qualitative agreement with experiment.

However, the calculations of Darewych and Baille yield total scattering cross sections that appear to have the wrong shape in the energy range 3–10 eV. Gillespie and Thompson (*21*) further investigated the positron–N_2 scattering problem, and they attribute the failure of Darewych and Baille to predict the correct energy dependence of the cross sections to the use of a very strong attractive potential. Using a weaker potential, they calculated positron–N_2 cross sections that are in fair agreement with experiment. Although they reported no Z_{eff} values, comparison with positron–atom scattering calculations leads them to suppose that their potential will be too weak to yield the large thermal energy values of Z_{eff}.

Thus, it is not possible at this stage in positron–molecule scattering theory to decide whether or not the large thermal energy values of Z_{eff}, measured at N_2 densities where λ_1 is directly proportional to density, can be attributed totally to the polarization distortion of the molecular electrons. The above discussion indicates, however, that should positron–N_2 scattering involve the formation of collision complexes, then either the formation process cannot be highly probable or the resulting states must be short lived relative to the lifetime of the bound positron.

At gas densities above specific temperature-dependent values, the annihilation rates of thermalized positrons in CH_4, H_2, and N_2 deviate from the linear dependence on density observed at lower densities. For example, for N_2 gas at 77 K, at densities greater than about 2.3 amagat, Z_{eff} is seen (Figure 4) to increase rapidly with density, indicating the interaction of positrons with two or more N_2 molecules. The same behavior is shown for CH_4 as a function of temperature in Figure 2. Calculations for N_2 have shown that at the pressures and temperatures involved, N_2 dimer formation would contribute negligibly to the annihilation rates (*15*).

It has been demonstrated recently, both experimentally (*22*) and theoretically (*23, 24, 25*), that in He gas near the gas–liquid critical point, attractive electrostatic forces cause the clustering of He atoms about low energy positrons, leading to a gas–liquid-like phase transition at temperatures both below and above the critical temperature of ordinary He liquid. The minimum gas densities at which this self-trapping of positrons in high density clusters begins increase with temperature. The onset of clustering is seen as an increase in λ_1 from the linear density dependence observed at constant temperature at lower densities to values corresponding to liquid He densities (*22, 26*). The positron localized within the droplet samples an effective density, which is obtained by weighting the density profile of the droplet with the square of the positron wave function.

Publication Date: June 1, 1979 | doi: 10.1021/ba-1979-0175.ch007

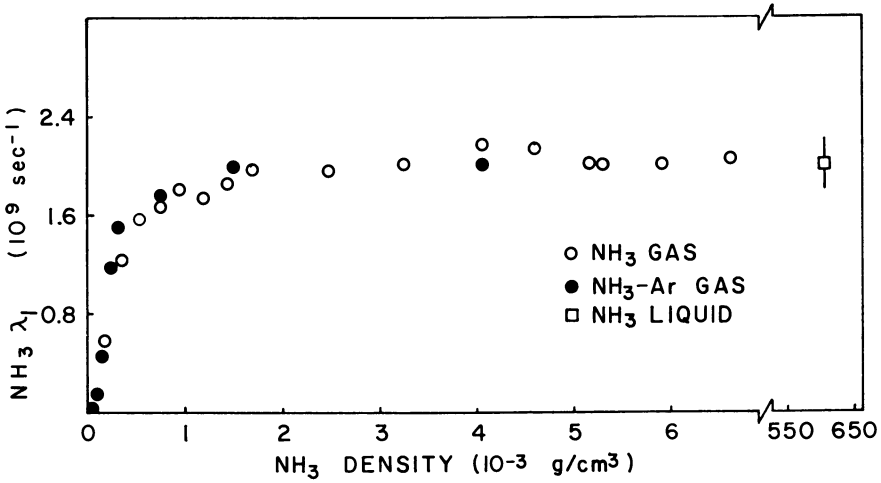

Figure 5. Annihilation rate of slow positrons with NH_3 molecules vs. NH_3 density at 22.5°C (6). The statistical standard deviations fall within the symbols unless otherwise indicated.

The similar breaking down of the linear density dependence of the annihilation rate for positrons in CH_4, H_2, and N_2 indicates the possible beginning of molecular clustering about positrons in these gases. The annihilation rate of slow positrons in NH_3 at 22.5°C is shown in Figure 5 (*6*). Molecular clustering in this case is even more pronounced in that the annihilation rate in low density NH_3 gas is approximately the same as that measured in the liquid state at several hundred times greater density. Thus, positrons in this gas density region must be annihilating in a time-averaged environment of liquid NH_3 electron density.

The concept of molecular clustering about positrons was first tested quantitatively for CH_4 molecules using the Atkins (*27*) snowball model, although it was known that this macroscopic model fails to produce a self-trapped state for positrons in He (*26*). If the gas is treated as a continuum that is electrorestricted about a positron, then the density $n(r)$ at distance r from the cluster center can be calculated approximately as

$$n(r) = N_o/v' \tag{2}$$

where

$$\int_p^{p'} v'dp = \tfrac{1}{2}N_o\alpha e^2\,\epsilon(r). \tag{3}$$

Publication Date: June 1, 1979 | doi: 10.1021/ba-1979-0175.ch007

Here N_0 is Avogadro's number, v' is the molar volume at distance r with ambient gas pressure p, $\epsilon(r)$ is the positron's electric field, and α is the molecular polarizability of the gas. From the viewpoint of cluster states, changes in λ_1 are now interpreted as being caused by changes in cluster density whereas Z_{eff} is taken to be a constant at a given temperature:

$$\lambda_1(r) = \pi r_0^2 \, c \, n(r) \, Z_{eff}. \tag{4}$$

Using a nonlinear least-squares method, this simplistic cluster model was fit to the λ_1 vs. density data for CH_4 at 22°, 4.5°, and −28°C in density regions where clustering was thought to dominate the annihilation process. The best fit, which agreed well with the data, was obtained for an "average" $r = 3.9 \pm 0.1$ Å and $Z_{eff} = 14.7 \pm 0.4$ (*7*). This Z_{eff} is in good agreement with the value of 14.5 ± 0.6 predicted for the direct annihilation of positrons in liquid CH_4 by the empirical method developed by Cova and Zappa (*28*). The subsequent extrapolation of the model, with the above parameter values, to −50°C was also in good agreement with experiment. For CH_4 the temperature and density dependence of the cluster model thus appears to be substantially correct.

Publication Date: June 1, 1979 | doi: 10.1021/ba-1979-0175.ch007

Thermalized Positrons in Monatomic–Molecular Gas Mixtures

It has been reported that for Ar concentrations up to about 0.90, the presence of neither of the gases in CH_4–Ar (*7*) or NH_3–Ar (*6*) mixtures seems to affect the annihilation process occurring with the other. The annihilation rate measured in the mixture, minus that calculated from Equation 1 for the appropriate partial density of Ar, was equal to the annihilation rate measured in the pure parent gas at the same density. This feature was exploited to measure annihilation rates with CH_4 and NH_3 at densities so low that without the additional positron stopping power of the added Ar, statistically useful lifetime spectra could not be obtained. CO concentrations ranging up to 0.12 in Ar are also known not to influence the annihilation process with either of the gases (*11*).

A similar situation was observed when Ne was added to N_2 gas at 77 K. Canter and Roellig (*29*) showed that Ne gas at 77 K is very well behaved in that the annihilation rate remains linear in density up to near liquid Ne densities and $Z_{eff} \lesssim Z$, indicating that only a direct annihilation process is operating. If, as discussed above, the appropriate annihilation rate with Ne is subtracted from that measured for the N_2–Ne mixture, the results shown in Figure 6 are obtained (*15*). The line in Figure 6 is a smoothed fit to the Z_{eff} vs. density data for pure N_2 (Figure 4) whereas the points were measured in mixtures containing 1.8 amagat of Ne. The

Publication Date: June 1, 1979 | doi: 10.1021/ba-1979-0175.ch007

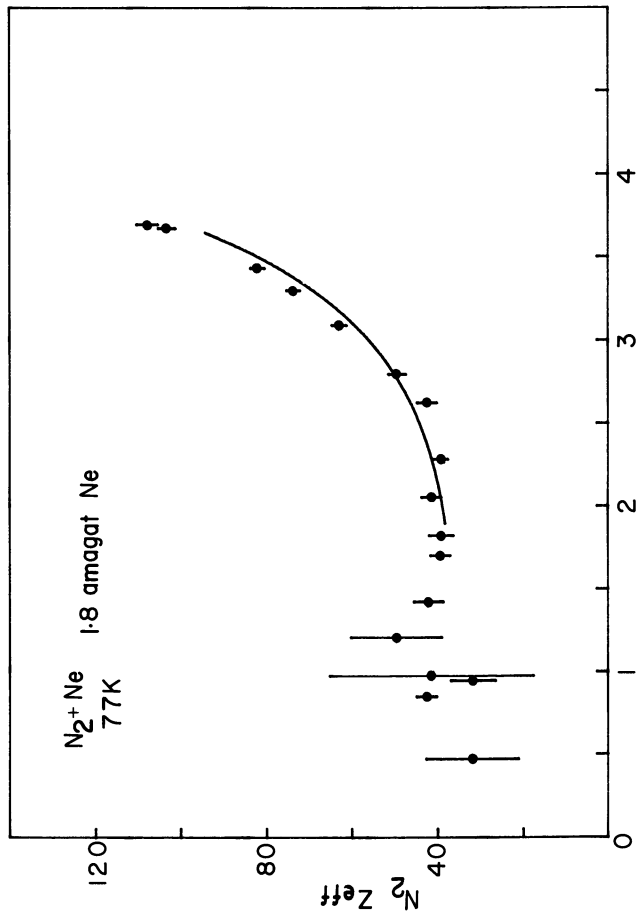

Figure 6. Z_{eff} for thermalized positrons annihilating with N_2 molecules in N_2–Ne mixtures containing 1.8 amagat Ne at 77 K vs. the partial density of N_2 gas (15). The statistical standard deviations fall within the symbols unless otherwise indicated. The line represents a smoothed fit to the Z_{eff} vs. density for pure N_2 at 77 K.

Ne concentration ranged from 0.34 to 0.66. Thus, the annihilation process for thermalized positrons in 77 K N_2, both in the low density region where Z_{eff} is constant (λ_1 linear in density) and at the higher densities where Z_{eff} is a strong function of density, is unaffected by the presence of even large concentrations of Ne.

The results were very different when Ne was added to H_2 gas at 77 K. This experiment is shown in Figure 7, where the line is a smoothed fit to the Z_{eff} vs. density data measured with pure H_2, and the points represent

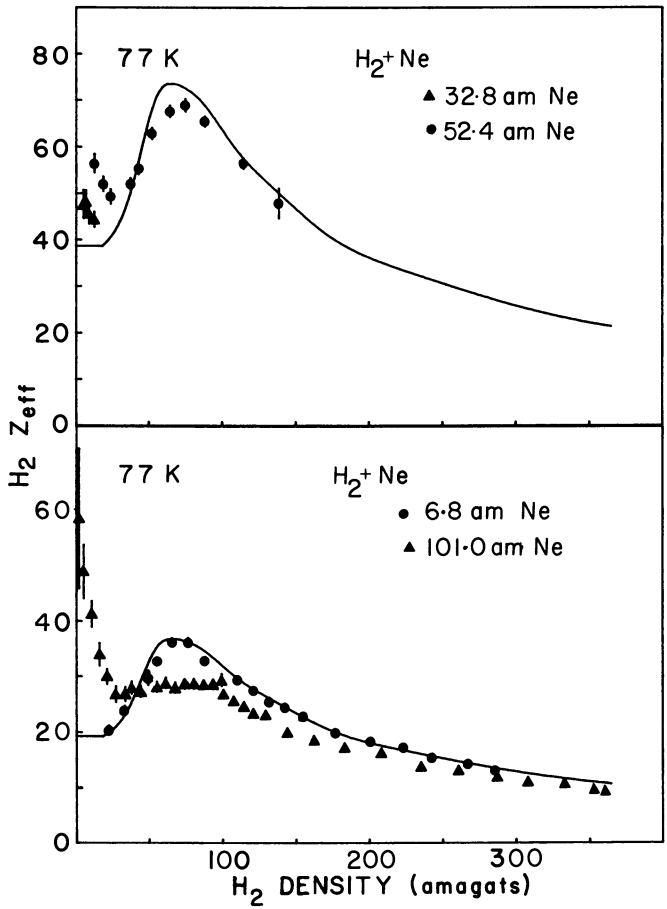

Physical Review

Figure 7. Z_{eff} for thermalized positrons annihilating with H_2 molecules in H_2–Ne mixtures containing 6.8, 32.8, 52.4, and 101.0 amagat Ne at 77 K vs. H_2 gas partial density (9). The statistical standard deviations fall within the symbols unless otherwise indicted. The lines represent a smoothed fit to the Z_{eff} vs. density data for pure H_2 at 77 K.

Publication Date: June 1, 1979 | doi: 10.1021/ba-1979-0175.ch007

the Z_{eff} values measured in the H_2–Ne mixtures (*9*). It is seen, particularly at the low H_2 densities, that the presence of various partial densities of Ne can affect the positron–H_2 annihilation processes dramatically.

A positron undergoing an elastic collision with a Ne atom suffers a fractional energy loss that is very small compared with those suffered during rotational excitation of H_2 molecules. Therefore, it is tempting to hypothesize that Ne is primarily effective in moderating more positrons into narrow resonance energy regions associated with the formation of positron–H_2 resonance states, thereby enhancing Z_{eff} at low H_2 densities and reducing the number of positrons available for cluster formation at the higher densities. These effects are now under further study.

Nonthermalized Positrons

The intermediate components (annihilation rate λ_1) of the lifetime spectra of positrons annihilating in low density H_2 (*30*) and N_2 (*15, 16, 18, 31*) gases are preceded by nonexponential shoulder regions. Several such spectra for N_2 are shown in Ref. *18*. As mentioned above, the shoulder region results from the annihilation of nonthermalized positrons and the variation of Z_{eff} with positron energy. The details of the shoulder region can be observed better by investigating the instantaneous annihilation rate $\lambda_1(t)$ or, equivalently, the instantaneous $Z_{eff}(t)$, defined by

$$\lambda_1(t) = \pi r_o^2 \, cn \, Z_{eff}(t) = [-dN(t)/dt] \Big/ \int_t^\infty [-dN(t')/dt']dt'. \quad (5)$$

The term $[-dN(t)/dt]dt$ is the rate of annihilation of positrons between times t and $t + dt$ and is found by subtracting the *o*-Ps component and background from the measured lifetime spectrum. The results so obtained for $Z_{eff}(t)$ with N_2 gas at 77 K are plotted against time-density in Figure 8 for two gas densities (*15*). The horizontal lines represent the equilibrium Z_{eff} values given by Equation 1 for the annihilation of thermalized positrons with N_2.

The nonexponential regions of positron lifetime spectra are generally characterized by the "shoulder widths" (SW), which are estimated from the $Z_{eff}(t)$ data as the time required for $Z_{eff}(t)$ to reach $[0.9(Z_{eff})_{equilibrium} + 0.1(Z_{eff})_{min}]$, which is the criterion of Paul and Leung (*32*). The shoulder width represents the time required for positrons from ^{22}Na to slow to near-thermal energies in the gas. The shoulder widths (in time-density units) and the reciprocal shoulder widths (in inverse time units) are plotted vs. N_2 density in Figures 9a and 9b, respectively (*15*). Also

In Positronium and Muonium Chemistry; Ache, H.;
Advances in Chemistry; American Chemical Society: Washington, DC, 1979.

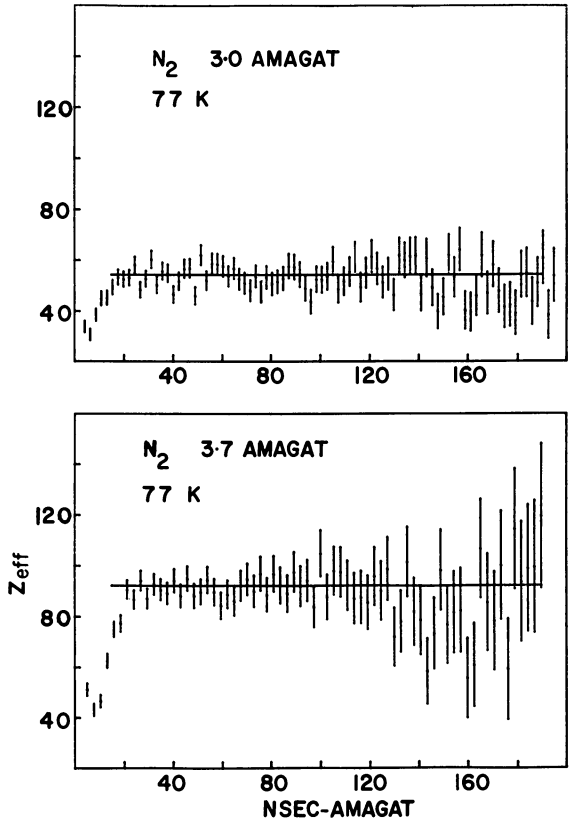

Figure 8. $Z_{eff}(t)$ vs. nsec-amagat for N_2 gas densities of 3.0 and 3.7 amagat at 77 K (15). The lines represent the equilibrium Z_{eff} results for the annihilation of thermalized positrons with the N_2 gas.

Publication Date: June 1, 1979 | doi: 10.1021/ba-1979-0175.ch007

shown are shoulder-width results measured with N_2–Ne mixtures and calculated from an appropriate modification of Equation 5. Within errors, the shoulder widths measured for pure N_2 agree with those measured for N_2–Ne mixtures containing the same partial densities of N_2 and having Ne concentrations in the range 0.34–0.61.

Shoulder widths have now been measured accurately for positrons in all the noble gases through Xe (*33*). When expressed in time-density dimensions, they are found to be independent of the gas density, with values ranging from 200 nsec-amagat for Xe to >2300 nsec-amagat for Ne (*33*). [The shoulder width in Ar has been observed recently to have a density dependence (*34*).] Density-independent shoulder widths have also been measured for low density room temperature H_2 (*30*) and N_2 (*16, 18, 31*), with values of about 2 and 14 nsec-amagat, respectively.

The solid and dashed lines in Figure 9 represent appropriately constrained least-squares fits to the data. As shown, the shoulder widths in time-density units for N_2 gas at 77 K are also independent of density for N_2 densities ≲2 amagat, with a value of about 14 nsec-amagat. This

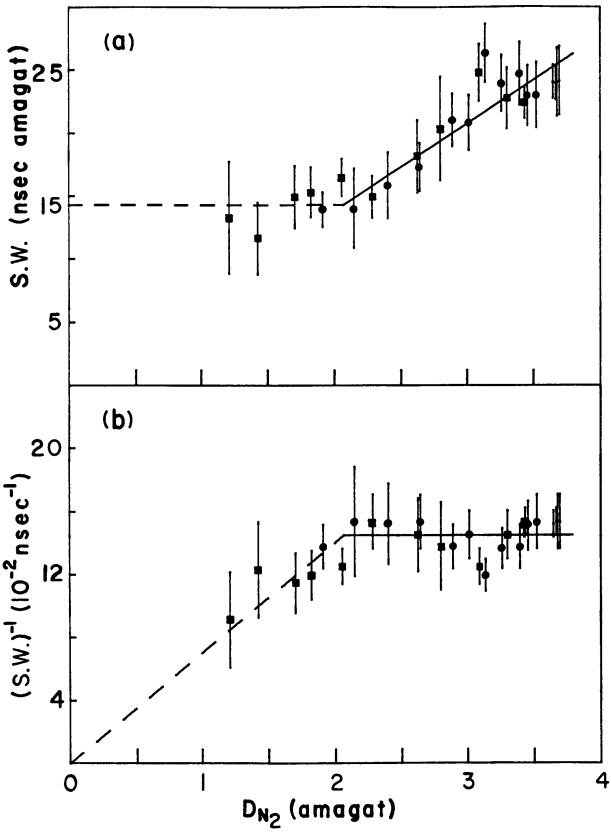

Physical Review

Figure 9. (a) Shoulder width vs. (partial) density of N_2 gas in pure N_2 (circles) and in N_2–Ne mixtures (squares) at 77 K (15). Bars indicate estimated errors. For clarity, symbols have not been used for the four highest density point. The three highest of these are derived from N_2–Ne mixtures: (– – –), obtained from a weighted least-squares fit to the reciprocal shoulder width data of Figure 9b for N_2 (partial) densities below 2 amagat that is constrained to pass through the origin; (——), represents a weighted average of the reciprocal shoulder width data of Figure 9b for N_2 densities above 2 amagat. (b) Reciprocal shoulder width vs. (partial) density of N_2 in pure N_2 and N_2–Ne mixtures at 77 K. Symbols and lines are as described for Figure 9a.

Publication Date: June 1, 1979 | doi: 10.1021/ba-1979-0175.ch007

value agrees with the room temperature result for N_2. For N_2 densities $\gtrsim 2$ amagat at 77 K, the measured shoulder widths in nsec-amagat units are no longer constant but now increase approximately linearly with N_2 density. [A similar effect has been observed recently in N_2 gas at room temperature (*35*).] As shown in Figure 9b, the shoulder width at the higher densities is now approximately constant in time units at approximately 7 nsec. Assuming that the occurrence of changes in the density behavior of both the annihilation rate (Figure 4) and the shoulder width at about 2 amagat of N_2 is more than coincidental, it is possible that the onset of self-trapping of low energy positrons within clusters is responsible for both effects (*15*).

Ortho-Positronium in Pure Molecular Gases

The rate, λ_2, at which positrons that form *o*-Ps annihilate in many gases is described at low densities by

$$\lambda_2 = \lambda_o + qn \tag{6}$$

where λ_o is the annihilation rate of *o*-Ps in vacuum and q is the quenching rate per unit density, which is a measure of the increase in λ_2 that results from *o*-Ps–molecule collisions. Of the several types of quenching processes that are known to occur with gases, the most common is called "pick-off" quenching. It occurs during an *o*-Ps–molecule collision when the positron bound in the *o*-Ps atom annihilates with a molecular electron of the opposite spin and thereby reduces its lifetime. For some gases, q from pick-off quenching remains constant up to high densities. In NH_3 gas (*6*) at 95° and 22.5°C, for example, λ_2 has been observed to be linear with density up to liquid density, with $q = 4.8 \times 10^{-4}$ (nsec-amagat)$^{-1}$.

The existence of other *o-Ps* quenching mechanisms is sometimes evidenced by quenching rates that are considerably higher than would be expected for the pick-off process. For O_2 (*36, 37*) and NO (*37, 38*), quenching rates of approximately 4.7×10^{-2} (*36*) and about 15.0×10^{-2} (*38*) (nsec-amagat)$^{-1}$, respectively, have been observed. These high rates are accompanied by an intensification of the narrow, low momentum component of the two-photon angular correlation curves (*37*) and are attributed to the conversion quenching (*39*) of *o*-Ps to *p*-Ps, wherein the electron of the *o*-Ps atom is exchanged during collision with the unpaired electron of the paramagnetic molecule.

Quenching rates that are two to three orders of magnitude greater than those typical for conversion quenching have been reported for several molecules. For example, the quenching rates for I_2 (*40*) and N_2O_4 (*38*) are about 10 and 460 (nsec-amagat)$^{-1}$, respectively. In these cases quenching is accompanied by an increase in the broad, high momentum

Publication Date: June 1, 1979 | doi: 10.1021/ba-1979-0175.ch007

component of the angular correlation curves (*41*). This suggests strongly that quenching is predominantly a chemical process resulting from the formation of Ps compounds.

In contrast to those processes that enhance the quenching rates considerably over those typical of pick-off annihilations, there exist mechanisms by which *o*-Ps atoms can reside for appreciable times in regions of less-than-average molecular density, thereby reducing the total annihilation rate. At densities less than certain "critical values," ρ^*, which decrease with temperature, λ_2 in CH_4 shows a temperature-independent linear dependence on gas density (7), with $q = 3.5 \times 10^{-4}$ (nsec-amagat)$^{-1}$. At densities greater than ρ^*, however, the λ_2 vs. density data deviate from linearity and decrease nearly exponentially with gas temperature. It has been shown recently (*42*) that this annihilation behavior in CH_4 results from nonuniformities in the spatial distribution of molecules associated with density fluctuations that are characteristic of an imperfect gas. Figure 10 is a plot of the deviations, $\Delta\lambda_2 = \lambda_2' - \lambda_2$, of the measured *o*-Ps annihilation rates from those rates, λ_2', calculated at the same density by extrapolation of the linear density dependence found at low densities vs. the fractional deviation, $\Delta\rho = (\rho - \rho_I)/\rho_I$, of the measured gas density ρ from the ideal gas density, ρ_I, calculated at the same pressure and temperature (*42*). The deviations of the actual densities from the corresponding ideal gas values serve as a measure of local density fluctuations in the gas, resulting in the production of numerous small regions of condensation and rarefaction. If these regions of density inhomogeneity have a large enough correlation length and are of sufficiently long duration, *o*-Ps atoms can reside in regions of less than average electron density, with an accompanying reduction in the annihilation rate. This is evidenced by the temperature-independent linear increase of $\Delta\lambda$ with $\Delta\rho$ seen in Figure 10 for values of $\Delta\rho$ greater than the single value (0.13) corresponding to the different values of ρ^* at the three temperatures. For relative density fluctuations smaller than that occurring at ρ^*, the local regions of density dilatation are apparently too small and short lived to influence the *o*-Ps annihilation process significantly. The importance of density inhomogeneities to the annihilation of *o*-Ps was further confirmed by correlating $\Delta\lambda$ directly with the density fluctuation distribution within the gas as computed from the isothermal compressibility of the gas at the equilibrium pressure. If this effect proves amenable to a more complete theoretical treatment, the positron annihilation technique might prove effective for further studies of local density inhomogeneities in imperfect gases.

The annihilation rate of positrons that form *o*-Ps in H_2 gas at 77 K (*9*), shown in Figure 11, has a linear dependence on density up to about 40 amagat, with $q = 1.6 \times 10^{-4}$ (nsec-amagat)$^{-1}$. This quenching rate

Publication Date: June 1, 1979 | doi: 10.1021/ba-1979-0175.ch007

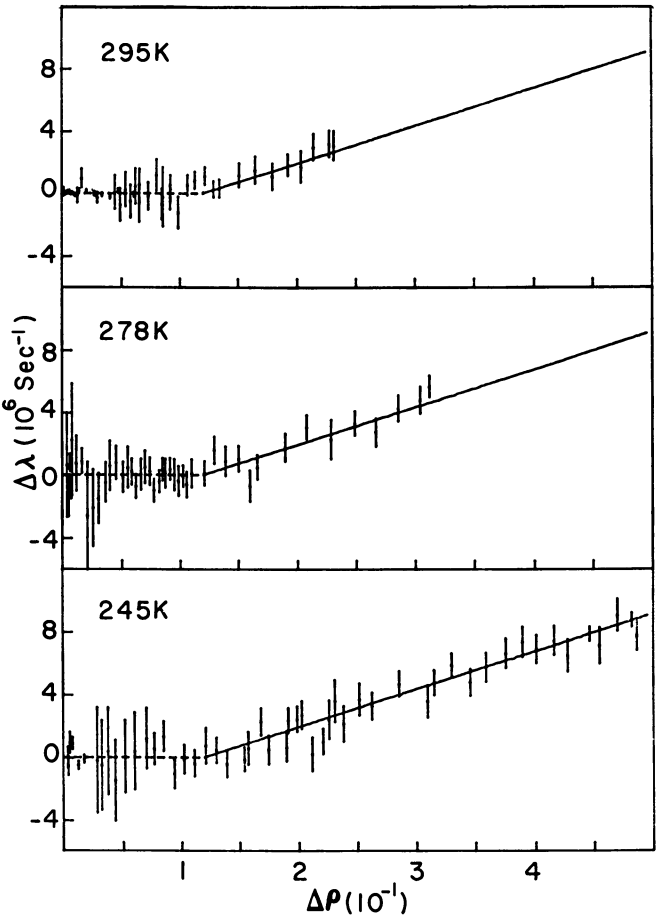

Figure 10. Deviations $\Delta\lambda = \lambda_2' - \lambda_2$ of the measured o-Ps annihilation rate, λ_2, in CH_4 gas at 295, 278, and 245 K from the annihilation rate λ_2' calculated for the same density by extrapolation of the linear density dependence observed at low densities vs. the fractional deviation $\Delta\rho = (\rho - \rho_I)/\rho_I$ of the measured CH_4 gas density, ρ, from the ideal gas density, ρ_I, calculated at the same pressure and temperature (42). (——), Represent a weighted least-squares fit to the combined data for $\Delta\rho \geq 0.13$.

agrees with those found for H_2 at 250 and 293 K for densities up to about 120 amagat (8). At densities greater than about 45 amagat, λ_2 in 77 K H_2 deviates from linearity with density in a manner that appears very similar to that observed for CH_4. However, over the range of H_2 pressures that were investigated at 77 K, the maximum fractional deviation of the meas-

Publication Date: June 1, 1979 | doi: 10.1021/ba-1979-0175.ch007

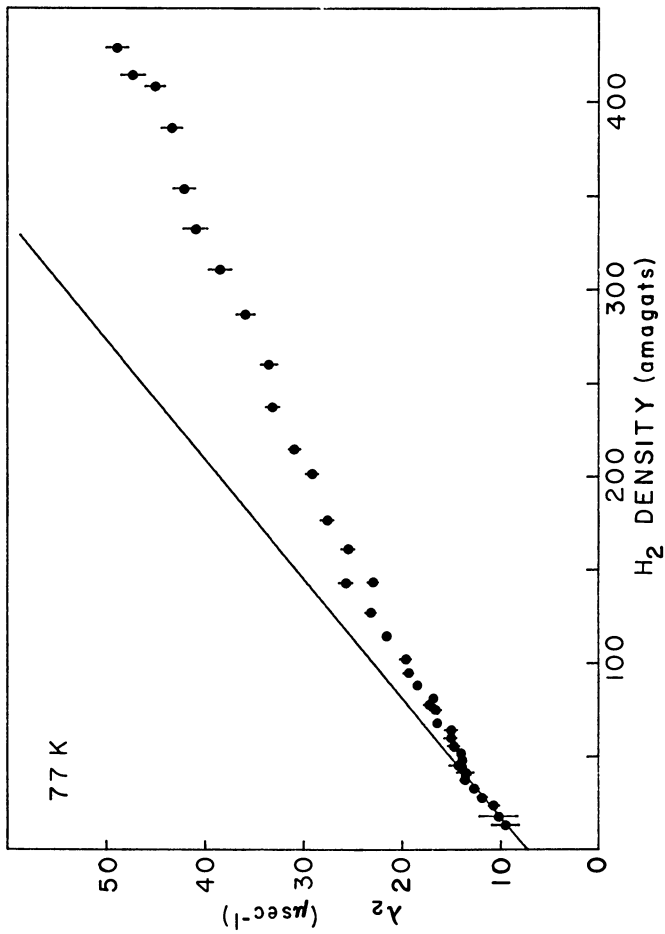

Figure 11. The o-Ps annihilation rate vs. H_2 gas density at 77 K (9). The statistical standard deviations fall within the symbols unless otherwise indicated. The line represents a weighted least-squares fit to data below 44 amagat that is constrained to pass through λ_0.

ured density from the corresponding ideal gas density is <0.07. Therefore, the nonlinear behavior of λ_2 does not result primarily from density fluctuations.

The formation of a cavity about an excess electron, either free or bound to a positron, can occur in nonpolar fluids at suitable temperatures and pressures when the short range Pauli repulsions dominate the long range polarization and quadrupole interactions. This condition is known to exist for H_2 (*43, 44*) but not for the more polarizable CH_4 molecule (*45*). If the cavity is assumed to be totally devoid of molecules, the annihilation rate λ_2 of *o*-Ps atoms in cavities can be expressed as

$$\lambda_2 = P_o(\lambda_o + qn) + (1 - P_o)\,\lambda_o = \lambda_o + P_o\,qn \qquad (7)$$

where P_o is the fraction of the *o*-Ps probability density that extends beyond the cavity into the gas. P_o, computed from Equation 7, can thus be treated as the measured quantity that is to be accounted for by any proposed cavity model.

In the simplest and most frequently investigated approach to *o*-Ps-induced cavity formation, the potential barrier presented to the *o*-Ps atom by the gas molecules outside a cavity of radius R is represented by a spherical square well of radius R and depth V (*26*). Minimization of the total energy of the system, together with the values of P_o measured at each gas temperature and density can then provide corresponding values for R and V. For example, R = 13.2 Å and V = 0.06 eV for 5.4 K He at 0.023 g/cm^3 (*26*). The V derived for several densities of He gas at ~5 K (*26*) are in reasonable agreement with theory (*46*), but the V found for higher He temperatures (*26*) and the dependence of V on density found for Ne at 45 K (*29*) and H_2 at 77 K (*9, 47, 48*) are clearly incorrect. It is also known that the energies calculated with this model are incorrect for *o*-Ps atoms trapped in cavities (*49*). Therefore, it seems that more sophisticated approaches will be required to describe quantitatively *o*-Ps-induced cavity formation in gases. In fact, the claim that *o*-Ps cavities exist in gases is quantitatively supported only by the results of H_2–Ne mixture experiments discussed below.

Ortho-Positronium in Monatomic–Molecular Gas Mixtures

For some gas mixtures, the contributions to the total quenching rate from the different gases are additive, so that

$$\lambda_2 = \lambda_o + q_1n_1 + q_2n_2 + \cdots \qquad (8)$$

where n_i are the partial densities of the gases, and q_i are the quenching rates per unit density measured for the pure gases. The presence of very

Publication Date: June 1, 1979 | doi: 10.1021/ba-1979-0175.ch007

small concentrations of a strong *o*-Ps quenching agent in a gas of relatively low quenching power, for example a slight O_2 contamination of a noble gas (*50*), can significantly increase λ_2.

Within experimental error, Equation 8 applies when Ar concentrations of 0.50–0.95 are added to room temperature CH_4 at a low density where λ_2 measured in pure CH_4 varies linearly with density (*7*). Equation 8 also describes λ_2 measured in H_2–Ne gas mixtures at 77 K at low H_2 densities. The λ_2 values found for the H_2–Ne mixtures are plotted in Figure 12 vs. the partial density of H_2 for four Ne partial densities (*9*). The Ne concentrations ranged from 0.02 to 0.98. The wide-dashed line is a smoothed fit to the λ_2 data measured for pure H_2 (Figure 11). The narrow-dashed lines are the annihilation rates calculated from Equation 8. As mentioned, these calculations agree well with the measurements at low H_2 densities. At densities greater than that at which cavity formation begins in H_2, however, the predictions of Equation 8 at the highest Ne partial density are much too high.

Although no evidence of cavity formation has been observed for pure Ne at 77 K up to densities over twice the maximum Ne density used here (*29*), it is unrealistic to assume, as was done in writing Equation 8, that the Ne in the H_2–Ne mixture is not also excluded from the cavity. Assuming this to be the case and further assuming that the average cavity radius in the mixture is essentially unchanged from that in pure H_2 the solid lines in Figure 11 are computed from

$$\lambda_2 = P_o\,(\lambda_o + q_{H_2} n_{H_2} + q_{Ne} n_{Ne}) + (1 - P_o)\,\lambda_o = [\lambda_2]_{H_2} + P_o q_{Ne} n_{Ne} \qquad (9)$$

where the subscripts H_2 and Ne refer to hydrogen and neon quantities, respectively. $[\lambda_2]_{H_2}$ is the annihilation rate measured for *o*-Ps in pure 77 K H_2 at density n_{H_2}, and P_o is obtained from Equation 7 for pure 77 K H_2 at density n_{H_2}. It is felt that the good agreement of Equation 9 with the experimental H_2–Ne data constitutes an important verification of *o*-Ps-induced cavity formation in gases.

Positronium Formation Fractions in Molecular Gases

Using a method developed by Coleman et al. (*51*), which corrects for the differences between the detection efficiencies of the two-photon and three-photon annihilation processes, accurate values for the fraction of positrons that form Ps can be deduced from measured positron lifetime spectra. The Ps formation fraction, f, measured for room temperature N_2 gas increases linearly with density from 0.19 near zero density to approximately 0.43 at 72.5 amagat (*16*). It has been suggested (*16*) that this large variation of f with N_2 density might result from the formation of N_4^+,

Publication Date: June 1, 1979 | doi: 10.1021/ba-1979-0175.ch007

Publication Date: June 1, 1979 | doi: 10.1021/ba-1979-0175.ch007

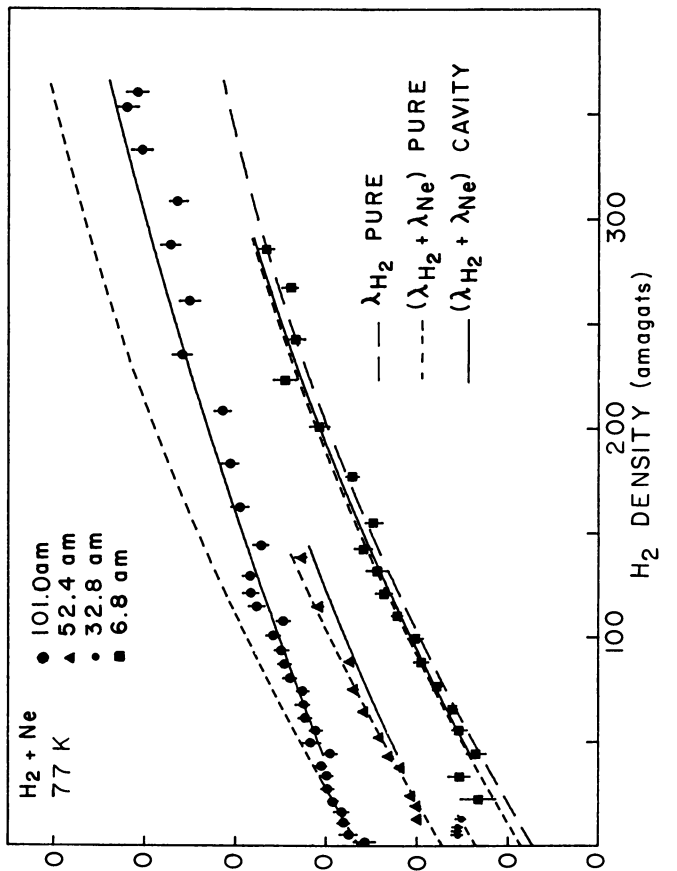

Figure 12. The o-Ps annihilation rate in H_2–Ne gas mixtures at 77 K containing 6.8, 32.8, 52.4, and 101.0 amagat Ne vs. the partial density of H_2 (9). The statistical standard deviations fall within the symbols unless otherwise indicated. The lines are described in the text.

which is known to form readily in electron collisions with N_2. If the N_4^+ were to be bound by 0.3 eV, the Ps formation threshold energy would be lowered sufficiently to allow f to rise to the maximum values observed. The maximum value of f predicted for N_2 by the Ore gap model (52) for Ps formation is 0.44.

As shown in Figure 13a, f for H_2 gas at 250 and 293 K increases from approximately 0.35 at low H_2 densities to about 0.49 near 80 amagat. The low density value is in reasonable agreement with previously measured

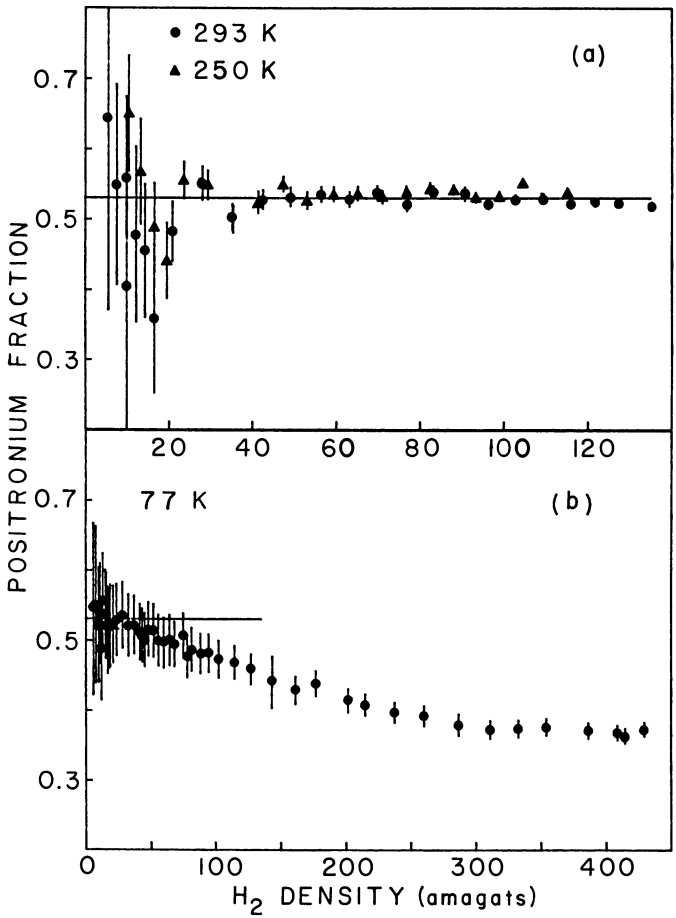

Physical Review

Figure 13. (a) Ps formation fraction vs. H_2 gas density at 293 K and 250 K (9). The statistical standard deviations fall within the symbols unless otherwise indicated: (——), represents a weighted least-squares fit to the combined data above 80 amagat; (b) Ps formation fraction vs. H_2 gas density at 77 K.

room temperature values (*53, 54*). Above 80 amagat, f remains constant at an average value of 0.49 up to the highest density of 135 amagat investigated at 250 K. This f is in agreement with the value of about 0.48 derived from two-photon angular correlation measurements on liquid H_2 (*55*). The maximum f predicted for H_2 by the Ore model is 0.44. The higher-than-expected yield of Ps might result from: (1) resonant positron–H_2 collisions occurring at energies above the Ore gap, resulting either in free positrons being preferentially scattered into the Ore gap or in the

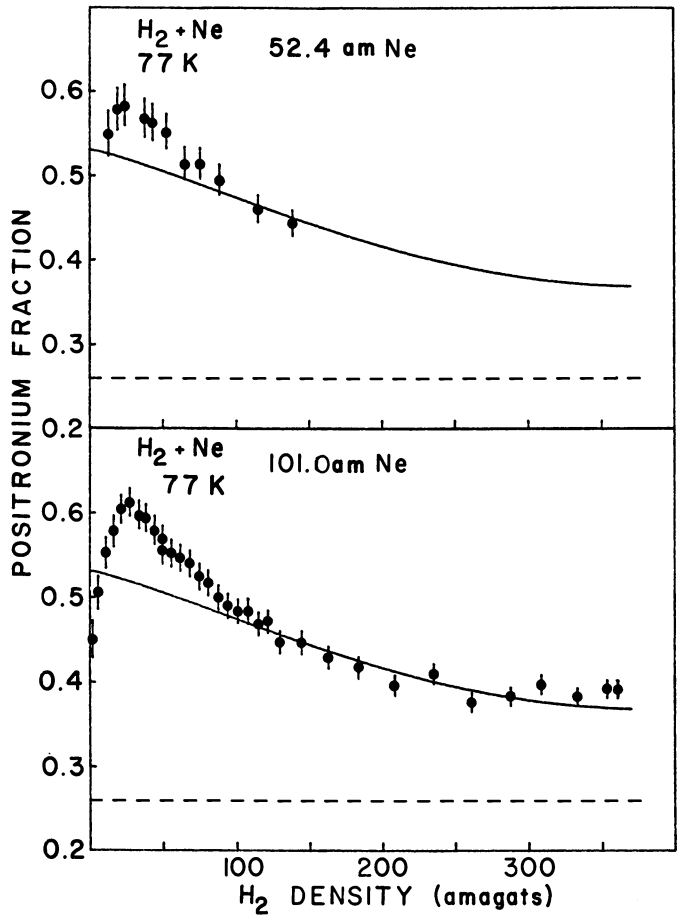

Figure 14. Ps formation fractions in H_2–Ne mixtures containing 52.4 and 101.0 amagat Ne vs. the partial H_2 gas density at 77 K (9): (——), a smoothed fit to the Ps fraction data for pure H_2 at 77 K; (– – –), Ps formation fraction for pure Ne at room temperature (51).

Publication Date: June 1, 1979 | doi: 10.1021/ba-1979-0175.ch007

direct production of Ps with low kinetic energy or from (2) an enhanced probability at high densities for collisional stabilization of Ps atoms formed by positrons having energies above the Ore gap.

The Ps fraction results for gaseous H_2 at 77 K, as shown in Figure 13b, display a completely different density dependence than that found at 250 and 293 K and constitute the first observation of a temperature dependence for f. At low H_2 densities the Ps fraction seems to be roughly constant at about 0.55, but it then falls with increasing density to approximately 0.37 at densities near 400 amagat. This decrease in f with density might be associated with the Ps–H_2 repulsive potential responsible for cavity formation. This potential would, in effect, raise the Ps formation threshold and thereby reduce f. However, neither this model nor certain e^+–H_2 interactions, which can be hypothesized as qualitatively affecting the formation of Ps in the observed manner, now appear to be without quantitative difficulties. Therefore, the complex temperature and density dependence of f in gaseous H_2 is not understood. Although the spur reaction model for Ps formation (*56*) has not been applied quantitatively to the gaseous state, it is not expected to be operative at very low gas densities (*57*). Its application, however, might be essential to an understanding of Ps yields at higher densities.

Figure 14 shows the effect on the total Ps formation fraction of the addition of Ne to H_2 at 77 K for two partial densities of Ne (*9*). The solid line is a smoothed fit to the Ps fraction data measured for pure 77 K H_2 (Figure 13b), and the dashed line represents the Ps fraction found for pure Ne at room temperature (*51*). Although the variation of f with Ne and H_2 partial densities can be interpreted qualitatively on the basis of the spur model, a semiquantitative explanation in terms of the Ore model is possible. An approximate calculation, which assumes that f for pure Ne at 77 K has a density-independent value of 0.26 and that at most two e^+–Ne or e^+–H_2 collisions in their respective Ore gaps result either in the production of Ps or the scattering of the positron out of the Ore gap, yields Ps formation fractions for the H_2–(101 amagat) Ne mixtures in reasonable agreement with experiment. In terms of the Ore model, both Ne and H_2 molecules in the mixture contribute to the total fraction at low H_2 densities whereas at high H_2 densities the Ne Ore gap is essentially closed to Ps formation because of competitive inelastic e^+–H_2 collisions.

Final Remarks

It is apparent from this review that a variety of interesting annihilation processes are available to positrons in diatomic and simple polyatomic gases and that several of these processes are, at best, understood only qualitatively. A quantitative understanding awaits much additional

Publication Date: June 1, 1979 | doi: 10.1021/ba-1979-0175.ch007

investigation of the physics and physical chemistry involved. In particular, further investigations of positron annihilation processes in gas mixtures and in pure gases in the presence of applied electric fields show promise of providing significant new information. It is clear that positron research in gases is still a wide open field with many unexplored areas and with strong potential for new and exciting discoveries.

Acknowledgment

Much of the research reported here for CH_4, NH_3, N_2, and H_2 gases was conducted by members of the Positron Group at the University of Texas, Arlington, and was supported in part by the Robert A. Welch Foundation, Houston, TX 77002 and by the National Science Foundation (Grants SMI 76-03024 and SMI 76-83578).

Literature Cited

1. Fraser, P. A., *Adv. At. Mol. Phys.* (1968) **4**, 63.
2. Goldanskii, V. I., *At. Energy Rev.* (1968) **6**, 3.
3. Massey, H., *Phys. Today* (1976) **29**, 42.
4. Paul, D. A. L., Saint Pierre, L., *Phys. Rev. Lett.* (1963) **11**, 493.
5. Osmon, P. E., *Phys. Rev.* (1965) **140**, A8.
6. McNutt, J. D., Kinnison, W. W., Ray, A. D., *J. Chem. Phys.* (1974) **60**, 4730.
7. McNutt, J. D., Summerour, V. B., Ray, A. D., Huang, P. H., *J. Chem. Phys.* (1975) **62**, 1777.
8. Brisbon, R. D., McNutt, J. D., *Int. Conf. Positron Annihilation, 4th, Helsingør, Denmark, 1976*, paper A10.
9. McNutt, J. D., Sharma, S. C., Brisbon, R. D., Franklin, M. H., Woodall, M. P., *Phys. Rev. A* (1979), in press.
10. Smith, P. M., Paul, D. A. L., *Can. J. Phys.* (1970) **48**, 2984.
11. Coleman, P. G., Griffith, T. C., Heyland, G. R., Killeen, T. L., *Appl. Phys.* (1974) **3**, 271.
12. Baille, P., Darewych, J. W., Lodge, J. G., *Can. J. Phys.* (1974) **52**, 667.
13. Coleman, P. G., Griffith, T. C., Heyland, G. R., *Appl. Phys.* (1974) **4**, 89.
14. Mao, A. C., Paul, D. A. L., *Can. J. Phys.* (1977) **55**, 235
15. Sharma, S. C., McNutt, J. D., *Phys. Rev. A* (1978) **18**, 1426.
16. Coleman, P. G., Griffith, T. C., Heyland, G. R., Killeen, T. L., *Int. Conf. Positron Annihilation, 4th, Helsingør, Denmark, 1976*, paper A13.
17. Coleman, P. G., Griffith, T. C., *J. Phys. B* (1973) **6**, 2155.
18. Tao, S. J., *Phys. Rev. A* (1970) **2**, 1669.
19. Hara, S., *J. Phys. B* (1972) **5**, 589.
20. Darewych, J. W., Baille, P., *J. Phys. B* (1974) **7**, L1.
21. Gillespie, E. S., Thompson, D. G., *J. Phys. B* (1975) **8**, 2858.
22. Hautojarvi, P., Rytsola, K., Tuovinen, P., Vehanen, A., Jauho, P., *Phys. Rev. Lett.* (1977) **38**, 842.
23. Khrapak, A. G., Yakubov, I. T., Pis'ma *Zh. Eksp. Teor. Fiz.* (1976) **23**, 466 [*Sov. Phys.—JETP (Engl. Transl.)* (1976) **23**, 422].
24. Stott, M. J., Zaremba, E., *Phys. Rev. Lett.* (1977) **38**, 1493.
25. Nieminen, R. M., *J. Phys. B* (1977) **10**, L409.
26. Canter, K. F., McNutt, J. D., Roellig, L. O., *Phys. Rev. A* (1975) **12**, 375.
27. Atkins, K. R., *Phys. Rev.* (1959) **116**, 1339.

28. Cova, S., Zappa, L., *J. Phys. B* (1968) **1**, 795.
29. Canter, K. F., Roellig, L. O., *Phys. Rev. A* (1975) **12**, 386.
30. Coleman, P. G., private communication.
31. Coleman, P. G., Griffith, T. C., Heyland, G. R., Killeen, T. L., "Atomic Physics 4," G. zu Putlitz, E. W. Weber, A. Winnacker, Eds., p. 355, Plenum Press, New York, 1974.
32. Paul, D. A. L., Leung, C. Y., *Can. J. Phys.* (1968) **46**, 2779.
33. Coleman, P. G., Griffith, T. C., Heyland, G. R., Killeen, T. L., *J. Phys. B* (1975) **8**, 1734.
34. Heyland, G. R., private communication.
35. Coleman, P. G., Heyland, G. R., private communication.
36. Chuang, S. Y., Tao, S. J., *Int. Conf. Positron Annihilation, 3rd, Helsinki, 1973.*
37. Mokrushin, A. D., Goldanskii, V. I., *Zh. Eksp. Teor. Fiz.* (1967) **53**, 478 [*Sov. Phys.—JETP (Engl. Transl.)* (1968) **26**, 314].
38. Tao, S. J., Chuang, S. Y., Wilkenfeld, J., *Phys. Rev. A* (1972) **6**, 1967.
39. Ferrell, R. A., *Phys. Rev.* (1958) **110**, 1355.
40. Chuang, S. Y., Tao, S. J., *J. Chem. Phys.* (1970) **52**, 749.
41. Chuang, S. Y., Tao, S. J., *Phys. Rev. A* (1974) **9**, 989.
42. McNutt, J. D., Sharma, S. C., *J. Chem. Phys.* (1978) **68**, 130.
43. Hernandez, J. P., *Phys. Rev. B* (1975) **11**, 1289.
44. Hernandez, J. P., *Phys. Rev. A* (1973) **7**, 1755.
45. Bruche, E., *Ann. Phys.* (1930) **4**, 387.
46. Drachman, R. J., Houston, S. K., *J. Phys. B* (1970) **3**, 1657.
47. Canter, K. F., McNutt, J. D., Roellig, L. O., unpublished data.
48. Massey, H. S. W., Burhop, E. H. S., Gilbody, H. B., "Electronic and Ionic Impact Phenomena," p. 3220, Oxford University Press, London, 1974.
49. Hernandez, J. P., *Phys. Rev. A* (1976) **14**, 1579.
50. Celitans, G. J., Tao, S. J., Green, J. H., *Proc. Phys. Soc.* (1964) **83**, 833.
51. Coleman, P. G., Griffith, T. C., Heyland, G. R., Killeen, T. L., *J. Phys. B* (1975) **8**, L185.
52. Ore, A., Universitetet i Bergen Arbok, Naturvitenskapelig rekke (1949) No. **9**.
53. Pond, T. A., *Phys. Rev.* (1952) **85**, 489.
54. de Benedetti, S., Siegel, R., *Phys. Rev.* (1954) **94**, 955.
55. Briscoe, C. V., Choi, S.-I., Stewart, A. T., *Phys. Rev. Lett.* (1968) **20**, 493.
56. Mogensen, O. E., *J. Chem. Phys.* (1974) **60**, 998.
57. Mogensen, O. E., *Int. Conf. Positron Annihilation, 4th, Helsingør, Denmark, 1976*, paper R10.

RECEIVED December 2, 1977.

8

Positronium and Positron Reactions in Positron Radiation Spur

S. J. TAO

The New England Institute, Ridgefield, CT 06877

Publication Date: June 1, 1979 | doi: 10.1021/ba-1979-0175.ch008

The study of positronium and positron reactions provides an alternative means to investigate hot radical reactions in the radiation spur. Positron and positronium react with radicals or others in the radiation spur created by the energetic positron itself. The positron may compete with other electron acceptors for electrons to form positronium. The positron also may be captured by a positron acceptor. The positronium formed may react with a radical or others to form a positronium compound. These reactions can be investigated by using the methods of positron annihilation, e.g. lifetime, angular correlation, and Doppler broadening measurements.

The experimental results by Shearer and Deutsch, who observed the lifetime of positrons from ^{22}Na in various gases, first suggested an appreciable amount of positronium (Ps) formation in these gases (*1*). Then Ore followed the suggestions by Fermi and made a thorough theoretical study on annihilation of positrons in gases (*2*). During this study, Ore described the possible formation of Ps in gases on the basis of the law of conservation of energy and the general aspects of collision theory. This is the well-known Ore Gap model. The statistical weights of triplet and singlet states indicate that three-fourths of these Ps atoms formed will be in triplet ortho state with lifetimes of 140 nsec decaying into three coplanar gamma quanta and one-fourth of them in singlet para state with lifetimes of 0.125 nsec decaying into two colinear gamma quanta (*3*).

The conversion of a Ps atom from ortho to para and para to ortho during a collision with a gas molecule and by radiation has been dis-

0-8412-0417-9/79/33-175-165$05.00/1

In Positronium and Muonium Chemistry; Ache, H.;
Advances in Chemistry; American Chemical Society: Washington, DC, 1979.

cussed by Ore (*4*). The probability of conversion per collision with a paramagnetic molecule is only of the order 10^{-7}. Obviously, if ortho-positronium (*o*-Ps) is converted to para-positronium (*p*-Ps) because of the shorter lifetime of *p*-Ps, the lifetime of *o*-Ps is reduced, or *o*-Ps is quenched, and two-quantum instead of three-quantum annihilation takes place. This kind of reaction was observed by Deutsch in his studies on three-quantum decay of positrons in oxygen (*5*).

Meanwhile, in order to explain the anomalous dependence of the lifetime of positrons on gas pressure in CCl_2F_2 at pressures below 0.4 atm, Deutsch has made the hypothesis of positron attachment to CCl_2F_2 (*5*). Ore studied the stability of the positron compound, indicated e^+Cl^- may be stable (*6*), and established a dynamical stability of a lower limit of 0.07 eV to the dissociation of e^+H^- (*7, 8*). Positronium chloride (PsCl) was claimed to be stable in the calculation by Simons (*9*). If a Ps compound is formed the *o*-Ps lifetime will be reduced considerably because of the availability of electrons of both spin state to positron in the positronium compound.

When an *o*-Ps atom collides with a molecule, the positron in the *o-Ps* atom may sense electrons in the molecule in addition to its own electrons; therefore, more annihilation may occur through the two-quantum process. The possibility of this kind of pick-off quenching to *o*-Ps was mentioned by Garwin (*10*) and Dresden (*11*), and discussed thoroughly by Ferrell (*12*). Pick-off quenching reduces *o*-Ps lifetime in liquid media to several nanoseconds or less.

Positron and Ps reactions can be studied by using the common methods used in positron annihilation studies, annihilation lifetime measurement, angular correlation, or Doppler broadening of the colinear two-gamma quanta. The quenching rate and fraction of *o*-Ps formed can be measured from the lifetime change and fraction intensity of the *o*-Ps component (in general, the longest lifetime component) in lifetime spectrum. The fraction of *p*-Ps formed and certain information regarding the quenching rate of *p*-Ps can be estimated from the intensity and the shape of the *p*-Ps component (in general, the narrow component) in either angular correlation or Doppler broadening spectrum. The reaction-rate kinetic equation of conversion was considered some years ago by Dixon and Trainor (*13*). It has been studied by many workers. For a thorough discussion of the kinetic equations, including the chemical and other probable reactions, the reader is referred to the review by Goldanskii (*14*).

The earlier works regarding Ps chemistry and positron annihilation were collected in a monograph (*15*) and the proceedings of the first International Conference on Positron Annihilation (*16*). Many review articles have appeared during the last ten years and a partial list is

Publication Date: June 1, 1979 | doi: 10.1021/ba-1979-0175.ch008

referred to here (*14–21*). This article will briefly review recent studies on Ps formation and Ps reactions in the radiation spur created by the energetic positron.

Positronium Formation

Ore Gap Model. Using argon as an example, energetic positrons lose energy quickly by collisions with argon molecules (atoms) to several tens of electron volts (22). Then a positron may lose energy by ionization either by inelastic and elastic collisions with argon, or it may pick up an electron from argon,

$$e^+ + Ar \rightarrow Ps\ (e^+e^-) + Ar^+ \quad (1)$$

Since positron and Ps are both very light, during Reaction 1 the energies possessed by Ar and Ar^+ can be neglected. From the law of conservation of energy we have

$$E(e^+) + I(Ps) = E(Ps) + I(Ar) \quad (2)$$

where E is the kinetic energy and I is the ionization potential. Since all the energies mentioned here can be only positive, we obtain the threshold energy for e^+ at which it is able to carry out the above reaction, as

$$E(e^+)_{th} = I(Ar) - I(Ps). \quad (3)$$

Because the ionization potential of most of the gases is higher than the ionization potential of Ps (6.8 eV) in most of the media an energy threshold ($E(e^+)_{th}$) exists at which positron is able to form Ps through Reaction 1.

From Reaction 2 we have

$$E(Ps) = E(e^+) + I(Ps) - I(Ar). \quad (4)$$

If the energy possessed by the formed Ps (E(Ps)) is greater than the ionization potential of Ps (I(Ps)), the Ps atom formed is not stable and is easily dissociated upon consequent collisions. Therefore, only when $I(Ar) > E(e^+) > (I(Ar) - I(Ps))$, is there a chance for a positron being able to form Ps through Reaction 1.

Positrons possessing energies higher than the lowest excitation level of argon lose energy quickly through inelastic collisions and Ps formation is not favorable. Therefore, only positrons with energies less than the

Publication Date: June 1, 1979 | doi: 10.1021/ba-1979-0175.ch008

lowest excitation level of the medium atoms, Ex(Ar), and higher than the threshold energy, I(Ar) − I(Ps), stand a good chance of forming Ps. This was the argument given by Ore (*2*). The energy range was named

$$\mathrm{Ex(Ar)} > \mathrm{E(e^+)} > [\mathrm{I(Ar)} - \mathrm{I(Ps)}] \tag{5}$$

Ore Gap by Ferrell (*12*). From the above considerations, the fraction of Ps formed (I_2) is roughly within the following limits:

$$\mathrm{I(Ps)/I(Ar)} > I_2 > [\mathrm{Ex(Ar)} - \mathrm{I(Ar)} + \mathrm{I(Ps)}]/\mathrm{I(Ar)} \tag{6}$$

Publication Date: June 1, 1979 | doi: 10.1021/ba-1979-0175.ch008

As summarized by Green and Lee (*15*) the above model provided a qualitative estimate of the fraction of positrons forming Ps in some simple gases. The above theory was not expected to hold in compound gases, dense gases, or liquids. Because of a lack of a satisfactory theory, it was modified in order to provide a certain theoretical explanation for the formation of Ps in media other than dilute simple gases.

Goldanskii considered the two competing slowing down and Ps formation processes and incorporated some parameters which assessed the effect of the slowing down process in the Ore Gap model (*14*). Tao and Green described the effect of hot Ps reactions on the final yield of Ps (*22*).

As more experimental data are gathered, it becomes obvious that the formation of Ps in condensed media is somewhat related to the positron or Ps reactions with the hot radicals in the radiation spur produced by the positron itself. Ache and his colleagues pointed out that the change of free energy of electron-capturing reactions of many cations is related to the saturation intensity of the long lifetime component (*o*-Ps component) in aqueous solutions of the cations (*23*). They explained this in terms of the Estrup–Wolfgang theory (*24, 25*) used for hot radical reactions and obtained

$$-[\ln(I_2/I_2^\circ)]^{-1} = \frac{\alpha_{\mathrm{react}}}{I} + \frac{\alpha_{\mathrm{mod}} \cdot \mathrm{const}}{I \cdot S_{\mathrm{react}} \cdot X_{\mathrm{react}}} \tag{7}$$

where α_{react} = average logarithmic energy decrement per collision between Ps and solute species, α_{mod} = average logarithmic energy decrement per collision between Ps and solvent (H_2O), I = the reactivity integral, S = the collision cross section of solute with Ps, X_{react} = the mole fraction of the solute, I_2 = the intensity of the long lifetime component, and I_2° = the intensity at C = 0.

Spur Model. Later, Mogensen suggested that Ps is formed when a thermalized positron is under the coulombic attraction of an electron in the radiation spur created by the positron so that they move together (*26*),

$$e^+ + e^- \rightarrow Ps. \tag{8}$$

Based upon the Onsager equation the fraction of Ps formed is

$$P = 1 - \exp(-r_c/r_t)$$

and

$$r_c = e^2/\epsilon kT \tag{9}$$

where r_t is the distance between a thermalized positron and a thermalized electron in a medium with a dielectric constant of ϵ, r_c is the critical distance at which the potential energy of the pair is equal to the thermal energy kT, and e is the electron charge. This is the spur model. This model could explain the fact that the fractions of Ps formation in simple liquid hydrocarbons are much higher than the simple Ore Gap theory predicted. However, its usefulness is still somewhat qualitative. In a medium with low dielectric constant such as nonpolar compounds, the value of r_c changes very little with density, while the value of r_t reduces with the increase of density. Therefore, this theory predicts an increase of Ps formation with density in a dense, gaseous medium.

A modified spur model was proposed in order to bridge the gap between the Ore Gap and spur models (*27*). It is proposed that in condensed liquid media both Reactions 1 and 8 occur. Reaction 8 is competing with the positive ions and electron scavengers, if present, in the spur for the electrons

$$e^- + M^+ \rightarrow M^* \tag{10}$$

$$e^- + Sg \rightarrow Sg^- \tag{11}$$

where M^+ is a positive ion produced by the ionization effect of the positron or other secondary electrons and Sg is an electron scavenger particle in the spur. Therefore, Reaction 1 is not affected directly by the concentration of an electron scavenger in the medium. In addition, because of the presence of positive ions the maximum fraction of Ps may be formed through Reaction 6 in only approximately $\alpha/(\alpha + 1)$, where α is the average number of ion pairs produced in the positron spur. From the above

Publication Date: June 1, 1979 | doi: 10.1021/ba-1979-0175.ch008

model a theory based upon a linear kinetic equation was developed. This theory explained the Ps formation fractions in several homologues of simple organic compounds better than the simple theory (*27*).

Other Recent Developments. Byakov has found that the relationship between the intensity of the long lifetime component and solute concentration is similar to that between $G(H_2)$ and solution concentration (*28*). He and his colleagues also studied the role of dry electrons in Ps formation in polar liquids (*29, 30*). One of their views, which is shared by Tao (*27*) and many others, is that most of the electrons are still dry when they combine with positron to form Ps.

Anisimov and Molin also studied the inhibition of Ps formation by many electron acceptors (*31, 32, 33*).

Reaction kinetics show that equations governing the Ps formation processes including Reactions 8, 10, and 11 are not linear. Based upon this, Tao derived a nonlinear theory to describe the reactions in the spur regarding Ps formation (*34*). From the shape of the calculated intensity of the long lifetime component against the concentration of an electron scavenger (acceptor) in a solvent, it can be deduced that there are at least three kinds of electron scavengers existing in the spur competing with the positron for electrons. One kind includes ionized and highly excited particles which can be produced only from the primary reactions by the energetic positron in the spur. The number of these particles is limited and they cannot be replenished after being depleted. Therefore, the intensity of the long lifetime component decreases with the concentration of the electron scavenger very slowly at low concentrations and decreases more rapidly at higher concentrations.

The second kind includes lowly excited particles which can be produced in the spur via secondary reactions. The number of these particles in a spur can be larger. The third kind includes nonexcited particles. They are always there in the spur. If one of them is removed, another may move into the spur by diffusion. Only for the third kind of electron acceptors could there be strict correlation between the Ps yield and rate constants of reactions with a solvated electron.

Certainly there are other views. In addition to the ones mentioned before, Duplatre suggested that there are two kinds of electrons which may react with positron to form Ps; one is dry electrons and another, damp electrons (*35*).

Recent work on positron annihilation in dense Xe gas indicated that at low Xe density the intensity of the long lifetime component (*o-Ps*) is 6% (*36*) and it increases with density to ca. 23% at 242 amagat (*37*). This clearly indicates that 6% of *o*-Ps forms via Reaction 1 and the rest of *o*-Ps forms via Reaction 8. This kind of increase in the intensity of the long lifetime component also has been observed when nitrogen is added

Publication Date: June 1, 1979 | doi: 10.1021/ba-1979-0175.ch008

to pure NO of low density (*38, 39*). More work on Ps formation in dense gases and gas liquid transition will shed much light on the processes of Ps formation in radiation spur.

Positronium Compounds

Owing to the short annihilation lifetime of positrons in a Ps compound, it is difficult to identify a Ps compound by normal methods of chemistry, even though the Ps compound may be stable in a chemical sense. Ps compound formation usually is detected by the anomalous characteristics in the annihilation processes. In gaseous media, because of the long but separable lifetimes of *o*-Ps and free positrons, their characteristics are much easier to detect than those in condensed media. The annihilation rate of the free positrons, $\lambda(e^+)$, its equivalent effective electron charge, Z_{eff}, and the *o*-Ps quenching rate, λ_q(*o*-Ps) of some simple gases are summarized in Table I.

The free positron annihilation rate in a gaseous medium should be roughly the value calculated from the average density of electrons in the medium provided other interactions are neglected. From Table I, the values of Z_{eff} obtained for some gases, such as Ar, N_2, and O_2 are very close to the number of electrons in their molecules. However, as mentioned before, the values of Z_{eff} for CCl_2F_2 and particularly some chemically active gases, such as NO_2 and Cl_2, are much higher than their number of electrons per molecule. This can be explained only by a

Table I. Annihilation Rates of Some Simple Gases[a]

Gas	*Z*	$\lambda(e^+)$ $ns^{-1}\ amagat^{-1}$	Z_{eff}	λ_q(*o-Ps*) $ns^{-1}\ amagat^{-1}$
Ar[b]	18	0.0053	26	0.000255
N_2[c]	14	0.0058	29	0.00022
O_2[d]	16	0.0046	23	0.023
CO_2[e]	22	—	24	0.00025
NO[f]	15	0.0069	34	0.029–0.15
NO_2[f]	23	—	720–1090	460
Cl_2[g]	34	—	1920	~ 100[i]
Br_2[d]	70	—	~ 24000	~ 400
CCl_2F_2[h]	58	0.18	860	0.0068

[a] Many earlier values can also be found in a review by P. A. Fraser (*40*).
[b] Ref. *41*.
[c] Ref. *42*.
[d] Ref. *43*.
[e] Ref. *44*.
[f] Ref. *38*.
[g] Refs. *43* and *45*.
[h] Refs. *5* and *46*.
[i] Shoulder and short tail part, the long tail part is only about 0.34 ns^{-1} $amagat^{-1}$.

Publication Date: June 1, 1979 | doi: 10.1021/ba-1979-0175.ch008

certain positron attachment (5) or positron compound forming during the collisions, such as $CCl_2F_2e^+$ and NO_2e^+. This kind of positron compound may be just a collision complex or in meta-stable state. However, once positron is attached to this compound its annihilation rate increases considerably to approximately 3×10^9 sec^{-1} because of high electron density there. As soon as the chemical lifetime of the positron complex or compound is longer than the collision time its effect will be detected.

The highest known ratio of the Z_{eff}/Z is only ca. 300. In terms of collision cross section, it is of the order of about 10^{-18} cm^2. The variation among the quenching rates, λ_q, of different gases to *o*-Ps is much greater. The ratio of the highest to the lowest λ_q reaches 10^6. The collision cross section calculated from the quenching rate reaches 10^{-15} cm^2, or the dimension of the molecules. The high value of the collision cross section indicates that nearly every collision is effective. During the collisions there are two possibilities; using NO_2 as an example, one is the removal of electron from the *o*-Ps,

$$Ps + NO_2 \rightarrow NO_2^- + e^+ \quad (12)$$

and another, a compound formation,

$$Ps + NO_2 \rightarrow NO_2e^+ + e^- \quad (13)$$

or

$$Ps + NO_2 \rightarrow NO_2Ps. \quad (14)$$

If the electron removal (Reaction 12) is the case, the free positrons produced by the reaction should annihilate at the lifetime of free positrons. Consequently, the intensity of the free positron component in a gas with high density of NO_2 should be nearly the total intensity of the positrons annihilating there, or the intensity of the free positron component plus the intensity of the *o*-Ps component which appears at lower densities of NO_2 in a gas or gas mixture of the same total density. Experimental results have shown that the intensity of the free positron component remains nearly unchanged before and after the emergence of the *o*-Ps component when the density of NO_2 is varied in an NO_2 and N_2 mixture of the same total density (*38, 39, 43*). Therefore, this is not the case.

If Reaction 13, the formation of a positron compound NO_2e^+ is assumed, a situation similar to the last one will result owing to the fact that NO_2e^+ is not expected to be a highly chemically stable compound since the free positron annihilation rate in NO_2 is much lower than the *o*-Ps quenching rate in NO_2.

Publication Date: June 1, 1979 | doi: 10.1021/ba-1979-0175.ch008

Therefore, it leaves the formation of a Ps compound, NO_2Ps, the most likely process. The annihilation lifetime of a Ps compound is expected to be roughly 3×10^{-10} sec. The *o*-Ps component separates from the prompt peak when the concentration of NO_2 is reduced to a point such that the lifetime of the *o*-Ps component is long enough and separable from the prompt peak.

For Cl_2, the *o*-Ps component consists of two parts at high Cl_2 concentrations (*42, 43*). One part appears at a higher Cl_2 concentration as a small shoulder and a short tail attached to the prompt peak, and another part appears as a long tail at lower concentrtion. The quenching rate at the shoulder and short tail part is about 300 times higher than that at the long tail part. The high quenching rate at the shoulder must be caused by some Ps reactions which take place only when Ps is hot. It can be attributed to the reaction of

$$PS + Cl_2 \rightarrow PsCl + Cl. \quad (15)$$

If the dissociation energy of PsCl is lower than that of Cl_2 (2.5 eV), Reaction 15 is endothermic and only Ps atoms with energy greater than the difference between the dissociation energy of Cl_2 and that of PsCl can undergo this reaction. Once a Ps atom is slowed down below this threshold energy, it is not effective. Since the threshold energy is estimated as not very high, about 0.5–1.0 eV, the dissociation energy of PsCl is estimated to be ca. 1.5–2.0 eV. The possible bound state of positron halides has been studied by Mogensen and his colleagues (*47, 48*).

On the theoretical side, recently the binding energies of some organic positron and Ps complexes have been calculated by Ache and his colleagues using approximate molecular orbital theory (*49*). A similar study has been made by Goldanskii and his colleagues (*50*). A more thorough study for positron affinity, Ps affinity of many organic as well as inorganic compounds and binding energy of some Ps compounds have been carried out by Schrader and Wang (*51*). Calculations for Ps halides also have been carried out by Cade and Farazdel (*52*).

Positronium Reactions

There are two kinds of Ps reactions which are important in the positron radiation spur. First, there are the very fast Ps or positron reactions. Secondly, there are the hot radical reactions, and the hot radicals can be positron, Ps, or the radicals created inside the spur.

The very fast Ps reactions such as the reaction between Ps and NO_2 can happen both inside and outside the positron spur. If the concentration of the reactant NO_2 is high enough, most of the reaction happens

Publication Date: June 1, 1979 | doi: 10.1021/ba-1979-0175.ch008

inside the spur and no *o*-Ps can escape the spur before being reacted. However, this kind of reaction can be detected easily by its fast reaction rate in very dilute concentrations of the reactant, such as NO_2, and in an inert solvent, such as N_2.

The hot radical Ps reactions mainly happen inside the spur. Using Cl_2 as an example, some of the possible reactions are shown below

$$Ps\ (hot) + Cl_2 \rightarrow PsCl + Cl \tag{15}$$

$$Ps + Cl \rightarrow PsCl\ (e^+Cl^-) \tag{16}$$

$$Ps + Cl \rightarrow e^+ + Cl^- \tag{17}$$

$$e^+ + Cl \rightarrow e^+Cl \tag{18}$$

$$e^+ + Cl^- \rightarrow e^+Cl^- \tag{19}$$

$$Ps\ (hot) + Cl_2 \rightarrow e^+ + Cl_2\ . \tag{20}$$

Reaction 15 has been discussed in the last section. The chlorine radical Cl in Reactions 16, 17, and 18 is the product of the dissociation of chlorine molecules by the energy inside the spur and the chlorine ion Cl^- is the product of the chlorine radical accepting an electron in the spur. Except for Reaction 15, the other reactions are not likely to happen in dilute or moderately dense gaseous media because of the large size of the radiation spur and the fast diffusion of all the species produced inside the spur. However, in dense gaseous or condensed media the situation should be different.

Reaction 16 is expected to happen readily in dense media. Whether the product is a Ps compound PsCl or e^+Cl^- or a highly dissociated e^+ and Cl^- (Reaction 17) will depend on the total energy possessed by the PsCl collision complex.

If the energy is low, PsCl is expected to be stable. If the energy is high, a highly dissociated state of e^+ and Cl^- may exist under their mutual coulombic attraction. During the de-excitation or slowing down of e^+ and Cl^-, if they move toward each other, a PsCl will form; if they move apart because of collision with other particles, e^+ may be separated from Cl^- with very little interaction between them. Reaction 18 is possible providing Cl is a positron aceptor. At present, there has been no indication that Cl is a positron acceptor. However, other species of radical positron acceptors may exist. Reaction 19 may occur if both e^+ and Cl^- are nearly thermalized and under the attractive influence of each other. However, this is the consequence of an electron-scavenging reaction of this type of reaction (*11*).

Publication Date: June 1, 1979 | doi: 10.1021/ba-1979-0175.ch008

If the electron attachment energy is smaller than the ionization energy of Ps, a hot Ps is required to react through the reaction (*20*). This is a type of hot Ps reaction used by Ache and his colleagues to describe the reduction of the intensity of the *o*-Ps long lifetime component in many oxidizing agents in aqueous solutions (*23, 53*). Part of this has been mentioned in Section II-B. They considered the reaction of the following type

$$\begin{array}{r} \mathrm{Ps\ (hot)} \rightarrow \mathrm{e^+ + e^-} \\ \mathrm{A^+ + e^- \rightarrow A} \\ \hline \mathrm{A^+ + Ps\ (hot) \rightarrow e^+ + A} \end{array} . \qquad (21)$$

Using a similar concept, the change of the free energy in the redox process is related to the intensity of the long lifetime component for many redox pairs in aqueous solutions, and the redox potential of Ps is evaluated (*23*).

Any hot radical Ps reactions which take place inside the spur will change the intensity rather than the lifetime of the *o*-Ps component, particularly in condensed media, where *o*-Ps lifetime is short. Therefore it is difficult to distinguish this effect from the effect of electron scavenging by radicals which reduces the fraction of *o*-Ps formed. In addition, many radicals or species which are good electron acceptors, are naturally good Ps acceptors from an energy point of view. If Reaction 11, using Cl as an example,

$$\mathrm{e^- + Cl \rightarrow Cl^-}$$

is exothermic, Reaction 16

$$\mathrm{Ps + Cl \rightarrow PsCl}$$

also should be exothermic because Reaction 19

$$\mathrm{e^+ + Cl^- \rightarrow (e^+Cl^-)}$$

must be exothermic. There is a possibility that Reactions 11, 16, and 19 all occur in the spur if a strong electron acceptor is present.

However, it has been shown that strong electron acceptors are not necessarily either strong Ps formation inhibitors or strong Ps lifetime quenching agents (*27, 54*). One reason could be that only reaction of reactions type 10 and 11 are involved for the electron scavenging (or accepting) process, but many more reactions are involved for the reduction of Ps formation. Besides, Ps formation inhibition reactions only happen inside the spur before solvation takes place. Although this situa-

Publication Date: June 1, 1979 | doi: 10.1021/ba-1979-0175.ch008

tion may make the Ps formation and fast Ps reaction processes quite complicated, these processes possibly can be sorted out clearly as shown by the case in NO_2 (*38, 39*). If so, much information about hot radical processes in the radiation spur can be obtained.

Outlook

The development of the Ore Gap model, spur theory, and their subsequent studies and modifications have brought Ps chemistry directly into the realm of hot radical chemistry happening in radiation spur. The information gathered from positron and Ps annihilation studies are different from those obtained from purely electron reaction studies. However, these two distinct paths of knowledge are complementary.

From the study of reactions of Ps and positrons, it is expected that some properties of fast hot radical reactions happening in the radiation spur in the first 10 psec or so, including the dry electron or damp electron reactions, can be investigated.

In order to separate the various processes more clearly, the work should be performed in dense gaseous media and gas–liquid transitions as well as in dilute gases and condensed media. It also is hoped that more theoretical calculations on positron and Ps compounds or complexes can be performed to determine the exact positron wave function in these compounds as well as the stabilities of them.

Publication Date: June 1, 1979 | doi: 10.1021/ba-1979-0175.ch008

Literature Cited

1. Shearer, J. N., Deutsch, M., *Bull. Am. Phys. Soc.* (1949) **24**(5), 16.
2. Ore, Aadne, *Univ. Bergen, Arbok, Naturvitensk. Rekke* (1949) **9.**
3. Ore, Aadne, Powell, J. L., *Phys. Rev.* (1949) **75,** 1696.
4. Ore, Aadne, *Univ. Bergen, Arbok, Naturvitensk. Rekke* (1949) **12.**
5. Deutsch, M., *Phys. Rev.* (1951) **83,** 866.
6. Ore, Aadne, *Phys. Rev.* (1948) **73,** 1313.
7. Ore, Aadne, *Phys. Rev.* (1951) **83,** 665.
8. Ore, Aadne, *Univ. Bergen, Arbok, Naturvitensk. Rekke* (1952) **5.**
9. Simons, L., *Phys. Rev.* (1953) **90,** 165.
10. Garwin, R. L., *Phys. Rev.* (1953) **91,** 157 (L).
11. Dresden, M., *Phys. Rev.* (1954) **93,** 1413 (L).
12. Ferrell, R. A., *Rev. Mod. Phys.* (1956) **28,** 308.
13. Dixon, W., Trainor, L., *Phys. Rev.* (1955) **97,** 733.
14. Goldanskii, V. I., *At. Energy Rev.* (1968) **6,** 3.
15. Green, J. H., Lee, J., "Positronium Chemistry," Academic, New York, 1964.
16. Positron Annihilation (Proc. First International Conference on Positron Annihilation, Detroit, U.S.A., July, 1965), A. T. Steward and L. Roellig, Eds., Academic, New York, 1967.
17. Ito, Y., Tabuta, Y., *Radioisotopes* (1972) **31,** 312.
18. Merrigan, J. A., Green, J. H., Tao, S. J., "Physical Methods of Chemistry," A. Weissberger and B. W. Rossiter, Eds., Vol. 1, Pt. IID, Wiley, New York, 1972.
19. Ache, H. J., *Angew. Chem.* (1972) **85,** 234.

20. Levay, B., *Kem. Kozl.* (1972) **27**, 221.
21. Goldanskii, V. I., Shantarobich, V. P., "Modern Physical Chemistry," E. Fluck and V. I. Goldanskii, Eds., Vol. 1, p. 269, Academic, London, 1976.
22. Tao, S. J., Green, J. H., *J. Chem. Soc.* (1968) 408.
23. Bartel, L. J., Ache, H. J., *Radiochim. Acta* (1973) **19**, 49.
24. Estrup, P. J., Wolfgang, R. J., *J. Am. Chem. Soc.* (1960) **82**, 2665.
25. Wolfgang, R. J., *J. Chem. Phys.* (1963) **39**, 2983.
26. Mogensen, O. E., *J. Chem. Phys.* (1974) **60**, 998.
27. Tao, S. J., *Appl. Phys.* (1976) **10**, 67.
28. Byakov, V. M., *Int. J. Radiat. Phys. Chem.* (1976) **8**, 283.
29. Byakov, V. M., Grafutin, V. I., Koldaeva, O. V., *ITEP, USSR, Acad. Sci. Report* (1976) **36**.
30. Bugaenko, V. I., Byakov, V. M., Grafutin, V. I., Koldaeva, O. V., Minaickev, E. V., *ITEP, USSR, Acad. Sci. Report* (1976) **154**.
31. Anisimov, O. A., Raitsimring, A. M., Molin, Yu. N., *JETP Lett.* (1975) **22**, 91.
32. Anisimov, O. A., Molin, Yu. N., Proc. International Conference on Positron Annihilation, 4th, Helsingor, Denmark, August 1976, paper G31.
33. Anisimov, O. A., Molin, Yu. N., *High Energy Chem. (Engl. Transl.)* (1975) **9**, 541.
34. Tao, S. J., Proc. International Conference on Positron Annihilation, 4th, Helsingor, Denmark, August, 1976, paper G4.
35. Duplatre, G., private communication.
36. Coleman, P. G., Griffith, T. C., Heyland, G. R., Killeen, T. L., *J. Phys. B* (1975) **8**, 1734.
37. Tseng, P. K., Chen, S. H., Chuang, S. Y., Tao, S. J., to be published.
38. Tao, S. J., Chuang, S. Y., Wilkenfeld, J., *Phys. Rev. A* (1972) **6**, 1967.
39. Chuang, S. Y., Tao, S. J., *Phys. Rev. A* (1974) **9**, 989.
40. Fraser, P. A., *Adv. At. Mol. Phys.* (1968) **4**, 63.
41. Tao, S. J., *Phys. Rev. A* (1970) **1**, 1257.
42. Tao, S. J., *Phys. Rev. A* (1970) **2**, 1669.
43. Tao, S. J., unpublished data.
44. Osmon, P. E., *Phys. Rev.* (1965) **140**, A8.
45. Tao, S. J., *Phys. Rev. Lett.* (1965) **14**, 935.
46. Green, J. H., Tao, S. J., *J. Chem. Phys.* (1963) **39**, 3160.
47. Mogensen, O. E., Shantarovich, V. P., *Chem. Phys.* (1974) **6**, 100.
48. Mogensen, O. E., Jansen, P., Proc. International Conference on Positron Annihilation, 4th, Helsingor, Denmark, August 1976, paper G15.
49. Madia, W. J., Schug, J. C., Nicholas, A. L., Ache, H. J., *J. Phys. Chem.* (1974) **78**, 2682.
50. Goldanskii, V. I., Kevdina, I. B., Shantarovich, V. P., Petersen, K., *Dokl. Akad. Nauk. SSSR* (1972) **203**, 870.
51. Schrader, D. M., Wang, C. M., *J. Phys. Chem.* (1976) **80**, 2507.
52. Cade, P., Farazdel, A., *J. Chem. Phys.* (1977) **66**, 2512, 2598.
53. Bartal, L. J., Nicholas, J. B., Ache, H. J., *J. Phys. Chem.* (1972) **76**, 1124.
54. Maddock, A. G., Abbe, J. C., Haessler, A., *Chem. Phys. Lett.* (1977) **47**, 314.

RECEIVED December 5, 1977.

9

Verification of the Spur Model of Positronium Formation and Fast Reactions of Spur Electrons as Studied by the Positron Annihilation Technique

YU. N. MOLIN and O. A. ANISIMOV

Institute of Chemical Kinetics and Combustion, Novosibirsk 630090, USSR

Publication Date: June 1, 1979 | doi: 10.1021/ba-1979-0175.ch009

The following experimental facts that support the spur model of positronium formation were verified: (1) the inhibition effect of transition metal cations; (2) the inhibition effect of electron acceptors in liquids and its absence in gases; (3) a higher intensity in polycrystalline alcohols than in liquids or glasses; and (4) a decrease of the intensity in some liquids under an electric field. Weak electron acceptors either remove or reduce the inhibition effect of strong electron acceptors. The anti-inhibition effect should be used to study fast spur electron reactions.

For many years much attention in the application of the positron annihilation technique has been given to studies of the reactions of positronium (Ps) atoms (*see,* e.g., Refs. *1* and *2* and the other chapters in this volume). These are the simplest analog of the hydrogen atom. The problem of Ps formation has attracted much less attention since the mechanism of Ps formation seemed to have no analogs among the usual chemical processes. Lately the situation has changed sharply. Mogensen (*3*) and, independently of him, Byakov et al. (*4, 5*) assumed that in the condensed phase Ps is formed as a result of a spur reaction between the positron and a secondary electron in the positron spur but not by the Ore model (*6*), which is realized in the gas phase. This new model, known as the spur reaction model, opened a wide field for application of the Ps method—studies of fast spur reactions—which holds great interest for specialists in radiation chemistry.

0-8412-0417-9/79/33-175-179$05.75/1

In Positronium and Muonium Chemistry; Ache, H.;
Advances in Chemistry; American Chemical Society: Washington, DC, 1979.

We discuss briefly the features of the two models mentioned above and the interpretation of basic experimental facts within the spur model. Discussion of experimental data in terms of the Ore model is in Refs. *1* and *2*.

In the Ore model Ps is formed during the slowing of the positron when an electron is "picked off" of a neutral molecule of the medium. Ps formation is endothermal by $V - 6.8$ eV, where V is the ionization potential of the molecules, and 6.8 eV is that of Ps. Hence, the positrons only that have an energy not less than $E_{min} = V - 6.8$ eV can form Ps. On the other hand, at a high kinetic energy of the positron its slowing, caused by ionization and excitation, prevails over Ps formation. Therefore, it is assumed that the maximum energy of Ps (E_{max}), at which Ps formation is still possible, equals either the ionization potential, V, or the first excitation potential, E^*. If the kinetic energy distribution of the positrons is random after the final excitation act (ionization), we have the following expression for the probability of Ps formation:

$$P_{Ps} = \frac{E_{max} - E_{min}}{E_{max}} = \frac{\Delta}{E_{max}} \tag{1}$$

where Δ is the width of the so-called Ore gap. At $E_{max} = E^*$, $\Delta = E^* - (V - 6.8\text{ eV})$. If the electron excitation is neglected and account is taken of only ionization, then $E_{max} = V$ and $\Delta = 6.8$ eV. Hence, in the Ore model the Ps formation probability, P_{Ps}, lies in the interval

$$\frac{6.8}{V} > P_{Ps} > \frac{E^* - (V - 6.8)}{E^*}. \tag{2}$$

Equation 2 usually predicts a correct value of P_{Ps}. In a number of cases, however, a lower value is observed experimentally. For example, P_{Ps} decreases when small amounts of some substances are added. In the Ore model a decrease in P_{Ps} (inhibition of Ps formation) is associated with many factors. For example, it is assumed that not all positrons that enter the Ore gap as they slow, form Ps. Positron capture by the molecules, annihilation upon encounters with the electrons, and the slowing that removes the positrons from the Ore gap must compete with this Ps formation. In the condensed phase the probability of Ps formation must decrease because of the absence of free volume that can be occupied by the Ps atoms formed. Formally, this situation can be described by Equation 2 with account taken of the energy of positron and Ps affinity of a given medium (i.e., the energy required to take a positron (Ps) out of this state and remove it from the medium). Finally, according to the Ore model, the Ps atoms formed can have excess kinetic energy. These "hot" atoms may enter chemical reactions so fast that experimentally the results

Publication Date: June 1, 1979 | doi: 10.1021/ba-1979-0175.ch009

are observed as inhibition of Ps formation. Taking into account the above considerations, the Ore model describes satisfactorily the results of various experiments. However, the parameters used (e.g., cross section of the capture of positrons and hot Ps atoms, the positron and Ps affinity of condensed media) are generally unknown. Therefore, interpretations are often speculative.

In the spur model it is assumed that Ps is formed as a result of a spur reaction between the positron and a secondary electron in the positron spur. The positron, losing the last 100–200 eV of its kinetic energy, creates several secondary electrons and the corresponding positive ions. After thermalization of the electrons and the positron, one of the electrons can interact with the positron, owing to coulombic forces, and form Ps. This process competes with recombination of the electrons and the positive ions and also with diffusion of the electrons out of the spur. Reactions of the electrons or the positron with the solvent molecules or with scavengers in the spur as well as solvation of the electrons and the positron or their "trapping" in the solid matrices also will decrease the probability of Ps formation. In general, this probability depends on any process that influences the conditions of charge recombination in the spur. Some of these processes are:

$$e^+ + e^- \rightarrow Ps;$$

$$M^+ + e^- \rightarrow M;$$

$$Ac + e^- \rightarrow Ac^-;$$

$$S + e^- \rightarrow e_s^-.$$

The spur model of Ps formation allows us to give a new interpretation to most experimental data on the probability of Ps formation in condensed media. Mogensen (*3, 7*) pointed out that most of the inhibitors of Ps formation are good electron acceptors, and the inhibition efficiency usually correlates with the reaction rate constants of the solvated electrons with these inhibitors. Byakov and others (*4, 8*) showed that the inhibition efficiency correlates even better with the rate constants of the corresponding reactions of the "dry" electron, which were obtained by picosecond radiolysis. These facts can be interpreted naturally by the spur model.

The well known decreased Ps yield in polar liquids vs. nonpolar liquids was accounted for (*3*) by solvation of the electrons (probably of the positrons too). This correlates well with a decreased probability of the initial recombination of the electrons and the parent ions in radiation chemical processes. A considerable difference in the Ps yield in the liquid and crystalline phases of water and methanol also is associated

with solvation effects (*3*). The anomalously small values of P_{Ps} in liquid inert gases were ascribed to larger sizes of the spur (*3*). Finally, a decrease in P_{Ps} under an external electric field in polymers (*9, 10*) and paraffins (*10*) finds its natural interpretation within the spur model in Ref. *11*.

Later, new data that fit the spur model were published. The correlation of the inhibition effect of some electron acceptors with the excess electron work function, V_0, in nonpolar solvents was found and discussed in terms of the spur model (*12, 13*). An increase in the probability of Ps formation when proton scavengers (dioxane and triethylamine) were added was observed (*14*). Jansen (*13*) proposed that the proton scavengers react with the positive parent ions and form products that cannot capture electrons. This increases the probability of electron reaction with the positron.

Although there are now many facts that favor the spur model, there are some that contradict it. Some exceptions to the correlation between the inhibition efficiency and the rate of the electron capture by the molecules were observed. For example, the inhibition effect is anomalously small or absent for such effective scavengers as CS_2, naphthalene, acetone, cysteine, sodium salicylate, and others (*3, 15, 16*). At the same time, a weak electron acceptor such as SeO_4^{2-} is a strong inhibitor of Ps formation (*16*).

As shown in Ref. *17*, it is difficult to explain in terms of the spur model the specific form of the concentration curves of the Ps yield in C_2H_5I and C_2H_5Br solutions. For these inhibitors, as well as for many other halogen-substituted hydrocarbons in nonpolar solvents, the Ps yield stops decreasing when a certain concentration is reached. These facts, also observed for many metal cations in water solutions (*18*), were interpreted successfully (*17, 19*) by the Ore model and the concept of the "hot" Ps atom.

Most of experimental data on the probability of Ps formation in condensed media can be accounted for in terms of both models, as has been done in some recent papers (*19, 20*). At the same time, Tao assumed (*15*) that the mechanism of Ps formation must combine the Ore and the spur models; the reactions of the positrons and electrons with the free radicals in the spur were an important complicating factor.

Therefore, it is important to find methodical criteria and to carry out special experiments so that a choice can be made between these two models. This procedure will allow one to outline the range of problems that can be solved by the Ps annihilation technique. The aim of this chapter is to contribute to verification of the spur model and to propose some applications of the Ps technique to studies of the fast reactions of spur electrons.

Publication Date: June 1, 1979 | doi: 10.1021/ba-1979-0175.ch009

Experimental

In our experiments, information on the value of the probability of Ps formation was obtained by an analysis of the positron lifetime spectra. Positron annihilation follows several mechanisms; therefore, the lifetime spectrum represents a superposition of several exponents, each characterized by its own lifetime τ_i. Since the component of the spectrum that corresponds to the positron annihilation via ortho-positronium (*o-Ps*) formation is characterized by the longest lifetime, this time (τ_2) can be calculated readily from the "tail" of the time distribution curve, which is described by an exponent with a lifetime τ_2. The experimental spectrum is given by a set of points that are somewhat spread; hence, to calculate a correct τ_2, one needs an averaging procedure. The most accurate τ_2 estimated from the exponential curve can be obtained if one divides the first moment of the curve by the area under the curve (the sum of decays on the tail). This method was used in our measurements (*21*). Knowing τ_2 and the sum of decays on the tail, by extrapolating the exponential curve to zero time distribution, we obtained the intensity of the long lifetime component of the spectrum, I_2. A correction was introduced, which took into account the prompt coincidence resolution curve. Since the statistical weight of *p*- and *o*-Ps are 1/4 and 3/4, respectively, $I_2 = 3/4\ P_{Ps}$ if *o*-Ps is not involved in chemical reactions before annihilation. Otherwise, the relationship between I_2 and P_{Ps} is more complicated (*7*).

The Ps lifetime spectra in condensed matter were recorded by a setup made by the standard scheme of fast–slow coincidences using a Nokia LP 4840 analyzer. As a source of positrons we used ^{22}Na, with an activity of about 5 μCi, as the NaCl salt, sealed into a thin Mylar film. Plastic scintillators, 4 cm thick and 6 cm in diameter, and FEU-30 photomultiplier tubes (USSR) were used. The first moment of the curve was calculated using a specially designed block. The first moment and the sum of decays on the tail were calculated separately for the studied and the background (CCl_4 spectrum with $I_2 = 0$) curves. After processing the data as described above, the reproduction of the measured values (with the decays on the tail being 5000–10,000 pulses) was $\Delta\tau_2 \pm 0.05$ nsec and $\Delta I_2 \pm 1\%$ (absolute %, i.e., in the units shown in Figures 2–8). The time necessary to gather these statistics for most of the liquids under study was about 10 min. The time resolution of the equipment was about 1 nsec (FWHM). The stability of the equipment allowed shorter times, 0.4–0.5 nsec, to be measured after the background curve was subtracted. The positron source and the samples were placed between the scintillators in ampules whose diameter was 1–2 cm. The solutions were not degassed. At low temperatures all measurements were done in a Dewar flask (1 cm id, 2 cm od). The reagents were CP grade.

Results

Inhibition Effect of Transition Metal Ions in Solutions. Among the experimental data used to verify the spur model, those on the influence of scavengers on the long lifetime component intensity (I_2) appear the most often. As noted, these data are consistent in most cases with the

spur model. However, for transition metal cations there are discrepancies that demand additional investigation.

The inhibition effect of some cations in water solutions was observed (*18, 22, 23, 24*) before the spur model was developed and was attributed to the reactions of nonthermalized Ps atoms with the cations. Later, Mogensen (*3*) and Byakov (*4*) interpreted these facts in terms of the spur model by spur electron capture. Refs. *4, 5, 7,* and *8* give arguments in favor of the fact that the electron does not have enough time to be solvated and reacts as a "dry" electron. From the analysis of data on inorganic ions, which are strong quenchers of Ps (in particular, transition metal cations), Tao concluded that these cations have no inhibition effects (*15*). He believed that this result contradicts the spur model since the cations in question effectively accept the electrons. On the other hand, Mogensen and others contend that a thorough analysis will reveal the quenching and the inhibition effects in similar systems (*7*).

The above contradiction is probably associated with difficulties of I_2 measurements in solutions of strong quenchers. The introduction of a quencher decreases the time, τ_2, and as τ_2 approaches the free positron lifetime, the accuracy of I_2 measurements falls sharply. Therefore, for strong quenchers the range of pronounced changes in I_2 may lie beyond the limits of available measurements.

To overcome this difficulty, it is necessary to diminish the quenching effect of the cations—i.e., to diminish their reaction rate with the thermal Ps atoms. For this purpose we used two methods. One was to increase the solvent viscosity. Since the quenching effects of transition metal cations is probably limited by diffusion, the rate constant of the thermal Ps atom must decrease with increasing viscosity. The other method was to use water–higher alcohol mixtures as solvents. Shantarovich et al. (*25*) showed that in water–propanol mixtures the rate constants of thermal Ps atom quenching by cations are 0.1–0.02 times those in water solutions.

Therefore, water–2-methyl-2-propanol mixtures (12 mol % alcohol) and glycerol were used as solvents. Co^{2+}, VO^{2+}, Mn^{2+}, Ni^{2+}, Fe^{3+}, and Cu^{2+} salts served as typical quenchers. In the range of concentrations studied the time, τ_2, for all the salts in glycerol and for $CoCl_2$, $NiCl_2$, and $VOCl_2$ salts in water–2-methyl-2-propanol was practically the same as in pure solvents ($\tau_2 = 2.2$ nsec in glycerol and $\tau_2 = 3.2$ nsec in 12 mol % 2-methyl-2-propanol–88 mol % H_2O). For stronger quenchers, $FeCl_3$ and $Cu(ClO_4)_2$, in water–alcohol mixtures we observed a small decrease in τ_2; however, in all cases τ_2 was not less than 1.5 nsec.

The results of I_2 measurements in water–2-methyl-2-propanol are presented in Figure 1a. In Figure 1b all the curves are transformed to one curve by changing the scale along the concentration axis; the transformation coefficient, β is the measure of the relative influence of various cations

Publication Date: June 1, 1979 | doi: 10.1021/ba-1979-0175.ch009

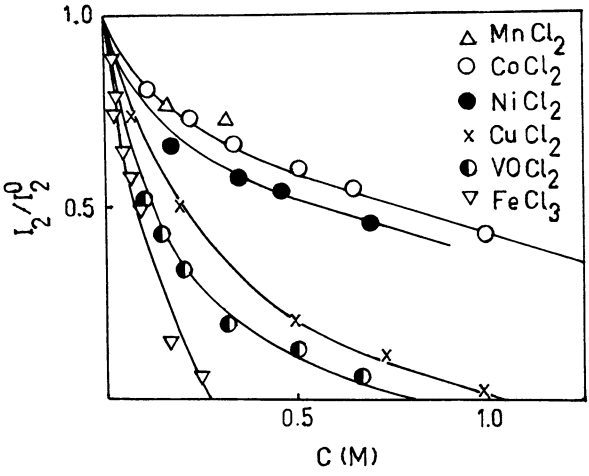

Khimiya Vysokih Energii

Figure 1a. Cation inhibition effects in water–2-methyl-2-propanol and in glycerol. Plots of I_2/I_2° vs. concentration of cations (C) in 12 mol % 2-methyl-2-propanol-88 mol % water (26).

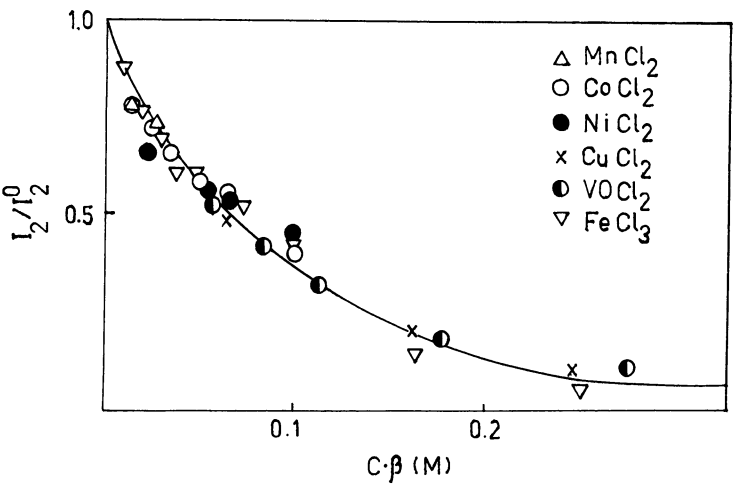

Khimiya Vysokih Energii

Figure 1b. Cation inhibition effects in water–2-methyl-2-propanol and in glycerol. Plots of I_2/I_2° vs. the reduced concentration (βC) where β is the coefficient of changing the scale along the concentration axis (26).

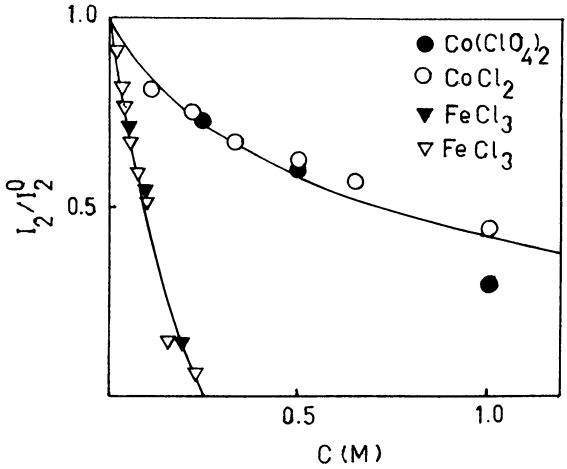

Khimiya Vysokih Energii

Figure 1c. Cation inhibition effects in water–2-methyl-2-propanol and in glycerol. Plots of I_2/I_2° *vs. C for glycerol with 4% water, (▼) (26). (Some curves for 2-methyl-2-propanol–water mixture are given for comparison, (▽).)*

on I_2. Figure 1c gives experimental data for $Co(ClO_4)_2$ and $FeCl_3$ in glycerol. The water content in glycerol was 4%; this gave a viscosity of approximately 700 cp at 21°C.

The results (*26*) show that all Ps quenchers studied are simultaneously strong inhibitors of Ps formation. Thus, these results fit the data of Ref. 7 and contradict those of *15*. Since the cations studied are effective solvated electron scavengers, our results agree with the spur model. In Table I the inhibition efficiency, β, is compared with the rate constants, K_e^-, of the solvated electrons with the corresponding cations. According

Table I. Relative Efficiency of the Inhibition Effect β and the Rate Constants of Solvated Electron K_e- in Water Solutions (*26*)

Cation	β	K_e- 10^{-10}, M *sec*$^{-1}$ *(27)*
1	*2*	*3*
Fe^{3+}	1	—
VO^{2+}	0.56	—
Cu^{2+}	0.33	3.3
Ni^{2+}	0.14	2.3
Co^{2+}	0.10	1.3
Mn^{2+}	0.08	0.008

Khimiya Vysokih Energii

Publication Date: June 1, 1979 | doi: 10.1021/ba-1979-0175.ch009

to the spur model, large values of K_{e^-} correspond to higher inhibition effects. At the same time, there is no direct proportionality between β and K_{e^-}. This is perhaps because in Ps formation, as assumed in Refs. *4* and *7*, dry, not solvated, electrons participate. Also, in comparing β and K_{e^-}, one must take into account the possible influence of the anions on the probability of Ps formation (*28, 29*).

The inhibition effect of transition metal cations can be interpreted also in the Ore model on the basis of nonthermalized Ps atom reactions (*23, 24*). Thus, our results agree with the spur model but do not exclude the Ore mechanism.

Phase Transition Effects. The spur and the Ore models lead to different conclusions concerning the influence of the phase transition on the probability of Ps formation. This discrepancy can be used for additional experimental verification of the spur model.

GAS–LIQUID. At present there is probably no doubt that the Ore mechanism is the only possible one for Ps formation in gases. The spur mechanism cannot be important here since the spur electrons leave the range of effective coulombic interaction with the positron because of the low density of the medium. However, according to the spur model, recombination of the electron and the positron in liquids is the main channel for Ps formation. Thus, if the inhibition effect of scavengers in the liquid phase is associated with spur electron capture, it must vanish in the gas phase.

To verify this prediction, we studied typical electron scavengers, Freon 12 (CF_2Cl_2) and SF_6, in the liquid phase. In the gas phase Ps formation for these substances was studied in detail earlier. CF_2Cl_2 and SF_6 gases show no inhibition effect, and their values of I_2 are 36 and 32%, respectively (*30, 31*). These values are close to those estimated in the Ore model. The results of I_2 measurements for solutions of CF_2Cl_2 in 1-decane and SF_6 in 1-hexane are given in Figure 2. Both compounds show the inhibition effect. The value of τ_2 does not change with inhibitor concentration. The value of I_2 measured in liquid Freon 12 at −29°C is 4%.

The results agree with the assumption that in the liquid phase the Ore mechanism is replaced by the spur mechanism. Indeed, CF_2Cl_2 and SF_6 capture the electrons in a dissociative manner and form Cl^- (*32*) and F^- (*33*). In the spur mechanism this capture results in the inhibition of Ps formation.

On the other hand, in the Ore model the mechanism of inhibition of Ps formation by scavengers (positron capture, reactions of epithermal Ps atoms, and so forth) might remain effective in both phases. The assumption that Ps formation is hampered in liquids by the decreasing free volume might be an alternative interpretation within the Ore model.

Publication Date: June 1, 1979 | doi: 10.1021/ba-1979-0175.ch009

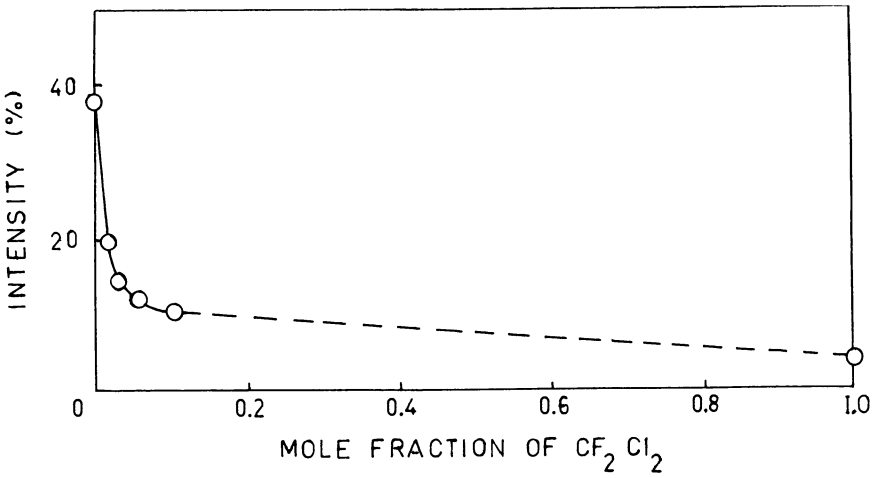

Figure 2a. CF_2Cl_2 and SF_6 inhibition effects. Plots of I_2 vs. the mole fraction of CF_2Cl_2 in decane; the point for pure CF_2Cl_2 was obtained at −29°C.

Publication Date: June 1, 1979 | doi: 10.1021/ba-1979-0175.ch009

However, in many liquids of different densities, the Ps yields are high (I_2 = 40–50%); Ps yields are approximately the same in the gas and liquid phases of ethane and propane and are about 40% (7). From this viewpoint it is difficult to explain the inhibition when small amounts of Freon 12 and SF_6 are added to the liquid (Figure 2). Thus, the experiments provide evidence for the spur mechanism of Ps formation in liquids.

The saturation of the curve of I_2 vs. SF_6 concentration can be explained readily in terms of the spur model. It is known from gas experiments (33) that a SF_6 molecule captures an electron in both a dissociative and a nondissociative way. As shown below, the latter mechanism may not lead to inhibition of Ps formation.

Liquid, Glass, and Polycrystalline Phases. According to the spur model, the probability of Ps formation must depend on the phase of the condensed substance because the phase influences the charge recombination in the spur. The spur electron (positron) capture or solvation results in a considerable slowing of the recombination of the electrons captured (10^{-8} sec) as compared with the fast initial recombination (10^{-12} sec). Since the free positron lifetime in a condensed medium is 10^{-10} sec, the electron (positron) solvation or capture must prevent Ps formation. Thus, it follows from radiation chemical data that the number of spur electrons that are avoiding the initial recombination is determined by the yield, G_{e^-}, of the electrons solvated or captured by traps. For polar substances, such as water and alcohols, this value is G_{e^-} = 1–3 electrons/100 eV for the liquid and glassy phases. In the crystalline state $G_{e^-} \approx 0$ for some

Publication Date: June 1, 1979 | doi: 10.1021/ba-1979-0175.ch009

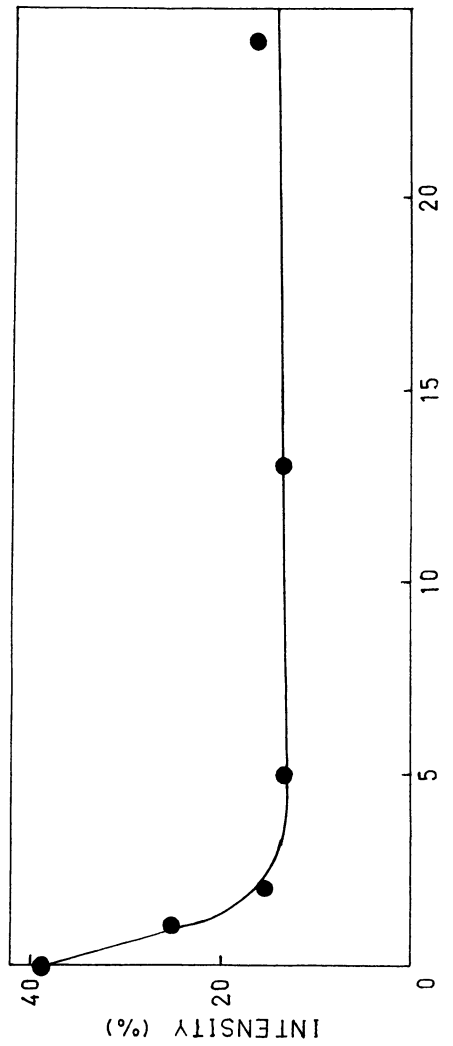

Figure 2b. CF_2Cl_2 and SF_6 inhibition effects. Plots of I_2 vs. SF_6 pressure over the saturated solution in hexane.

substances since the concentration of defects that can trap the electrons is small. Thus, the spur model predicts a considerable increase in Ps yield in the crystalline phase as compared with that in the liquid phase. At the same time, no such difference is observed between the liquid and glassy states.

Table II shows the intensity and the lifetime of the long-lived component of Ps annihilation in the liquid, glassy, and crystalline phases for some alcohols and water at various temperatures (*34*). This table also presents the values of G_{e^-} taken from Ref. *27*. The samples represent sealed, thin-walled ampules with the substance and a positron source. These were frozen in a Dewar flask that was filled with liquid nitrogen or cooled acetone. Glassy methanol at 77 K was obtained by adding 4% water. The results of repeated experiments were reproduced well in all cases except for frozen 1-heptanol. This discrepancy was associated perhaps with incomplete identity of crystallization conditions in different experiments.

Table II shows that the long lifetime component intensity, I_2, in the crystalline state is larger than in the liquid or glassy states. At the same

Table II. I_2 Measured and G_{e^-} in Liquid, Polycrystalline, and Glassy Alcohols (*34*)

System	*Structure*	*T (K)*	G_{e^-} *electron / 100 eV*	I_2 *(%)*	τ_2 *(nsec)*
Water	liquid	293	2.6	26	1.8
	polycrystal	255	0	50	0.8
Methanol	liquid	293	1.1	17	3.0
	polycrystal	77	0	34	0.8
	glass	77	2.2	15	1.7
tert-Butanol	liquid	300	—	20	3.2
	polycrystal	188	0	38	1.2
		77	0	44	0.8
n-Heptanol	liquid	293	—	21	3.1
	polycrystal	77	0	34	1.0
		77	0	31	1.1
		77	0	36	0.9
Ethanol	liquid	293	1.0	22	3.0
	glass	77	2.3	22	1.3
n-Propanol	liquid	293	1.0	21	3.0
	glass	77	—	24	1.3
iso-Propanol	liquid	293	1.0	22	3.2
	glass	77	1.1	24	1.3
n-Butanol	liquid	293	—	21	3.0
	glass	77	—	23	1.3

Publication Date: June 1, 1979 | doi: 10.1021/ba-1979-0175.ch009

time, on freezing (particularly in the crystalline state) τ_2 decreases. In discussing these results one should remember that the nature of the long lifetime component in crystalline organic substances is still questionable. Some authors (*15, 35*) believe that a short time, τ_2, and the absence of the narrow component in the spectrum of the angular correlation of annihilated gamma quanta indicate that in organic crystals no Ps is formed. On the other hand, it has been found (*36*) that the long lifetime component in ice results from Ps formation. Brandt and Wilkenfeld have theorized that a decrease in τ_2 and a broadening of the annihilation long lifetime component on freezing are associated with a decreasing volume available for localization of Ps, and they do not remark on its absence (*10*).

If we assume that in all the substances studied the long lifetime component corresponds to *o*-Ps, the results obtained agree perfectly well with the spur model. Indeed, in polycrystals, where $G_{e^-} \approx 0$, no spur electron capture occurs, and the probability of Ps formation is maximum. Note that the probability of Ps formation in liquids at room temperature and in glasses at liquid nitrogen temperatures is approximately the same. An important conclusion for radiation chemistry can be drawn from this fact in regard to the spur model. Obviously, during the times of electron and positron initial recombination (about 10^{-12} sec), liquids and glasses behave identically. Thus, the molecules of the liquid do not have enough time for reorientation so that the initial electron (positron) capture occurs in liquid alcohols as in glasses—i.e., by the traps that already exist. This conclusion agrees with results obtained by Byakov et al. (*8*), who showed that I_2 in liquid alcohols is temperature independent.

An increase in the long lifetime component intensity, I_2, has been observed recently (*37*) in the crystallization of various amides. This observation agrees with the spur model. On the other hand, in nonpolar substances—e.g., in hydrocarbons—freezing either does not influence I_2 or it decreases it (*35, 38*). In nonpolar substances, as known, the spur electron capture is hardly probable ($G_{e^-} \approx 0$) independently of the phase state. A decrease in I_2 in these substances is most likely associated with a decrease in the free volume.

Influence of an Electric Field. Comparatively sparse available data on the influence of an electric field on the probability of Ps formation in the condensed phase have been analyzed in detail by Mogensen (*11*) on the basis of the spur model. He showed that a decrease in the Ps yield in an electric field observed experimentally is in good agreement with the spur model and cannot be explained in terms of the Ore model.

The spur model interprets these results as follows. The field removes the positron and the electron from the positron spur and prevents their recombination—i.e., Ps formation. Similar effects were observed in radiation chemical experiments, which showed that an electric field decreases

Publication Date: June 1, 1979 | doi: 10.1021/ba-1979-0175.ch009

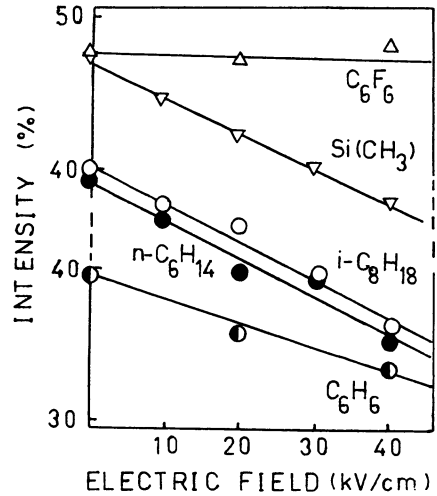

Soviet Physics—JETP

Figure 3. I_2 *vs. electric field strength* (*39*)

the probability for initial recombination of the electron and the parent ion in the electron spur. Our results (*39*), which are considered below, verify this assumption.

We studied the influence of an electric field on the probability of Ps formation in liquids—tetramethylsilane, isooctane, 1-hexane, benzene, and hexafluorobenzene. The field strength, E, varied from 0 to 40 kV/cm. The liquid and the positron source were placed between the capacitor plates, which were 0.5 cm apart. The results of I_2 measurements are given in Figure 3. In all the liquids (except hexafluorobenzene) I_2 falls with increasing E, which conforms to the spur model. The scale of the effect corresponds approximately to the results obtained by Brandt and Wilkenfeld for 1-hexane and other linear liquid hydrocarbons (*10*). The absence of the effect in hexafluorobenzene must be attributed to the fact that its molecules capture the electrons and form anion radicals $C_6F_6^-$. This capture, as shown below, does not prevent Ps formation. However, it may accelerate the slowing of the spur electron and thus decrease the initial distance between the electron and the positron in the spur, which leads to a decreasing influence of the electric field.

To interpert the results qualitatively, let us assume that, as in radiation chemical processes, in a low electric field the probability of recombination of the positron and the electron decreases by the factor (*40*)

$$P = \exp(-r_c/r_o)\ (er_c/2\,kT)\,E \qquad (3)$$

where r_o is the initial distance between the charges in the pair, $r_c = e^2/\epsilon kT$ is the critical distance corresponding to the equality of the energy of the coulombic charge interaction and the thermal energy, and ϵ is the high-

Publication Date: June 1, 1979 | doi: 10.1021/ba-1979-0175.ch009

frequency dielectric constant of the medium. If Ps is formed, the situation becomes more complicated since the electron interacts with at least two particles, the positron and the parent ion. If, as a first, rough approximation one takes into account only the electron–positron interaction, the influence of an electric field on I_2, according to Equation 3, must be described by:

$$I_2(E)/I_2(0) = 1 - \exp(-r_c/r_o)\,(er_c/2\,kT)\,E. \qquad (4)$$

With this formula and the data of Figure 3 one can calculate r_o, the initial distance between the electron and the positron after their thermalization. In all cases (except hexafluorobenzene) calculations give approximately the same value of $r_o \approx 100$ Å, which is close to the intercharge distance in the electron spur of nonpolar organic liquids known from radiation chemical experiments. Thus, the results are in accordance with the spur model. Note, however, that the distance, r_o, does not increase with electron mobility in the systems studied, as predicted (*11*) on the basis of the spur model.

Anti-inhibition Effect. The spur model predicts that in a general case, electron (positron) acceptors must decrease I_2 since they capture the spur electrons and compete with Ps formation. Indeed, as noted earlier, most electron acceptors are inhibitors of Ps formation, and the inhibition efficiency indicates the reaction rate between the electron and the acceptor. However, there are some exceptions (*see* e.g., Refs. *3* and *15*). We have shown (*42*) that active electron acceptors such as CO_2 and C_6F_6 have no inhibition effect. However, these facts must not be considered arguments against the spur model. Additional experiments with such compounds provide one of the most convincing evidences for the spur model.

We have found that the compounds mentioned either remove or reduce the inhibition effect under certain conditions. We call this phenomenon an anti-inhibition effect. Some results are listed in Table III. As shown, those molecules that have an electron affinity possess anti-inhibition properties—i.e., fluorobenzenes, perfluoropyridine, naphthalene and its substituents, CS_2, and CO_2. The anti-inhibition effect increases with the concentration of these substances. Molecules that possess no electron affinity (dioxane, 2-methyl-2-propanol, and argon) do not influence the inhibition effect.

The anti-inhibition effect cannot be understood within the Ore model, but the spur model gives a natural interpretation. Indeed, the reactions of CS_2, CO_2, C_6F_6, and naphthalene with the electrons result in molecular anion radicals with comparatively small electron-binding energies [electron affinity of molecules usually does not exceed 1.5 eV (*42*)]. However,

Publication Date: June 1, 1979 | doi: 10.1021/ba-1979-0175.ch009

Table III. I_2 in the Presence of Inhibitors

Solvent	*Inhibitor*	*Inhibitor Concentration (M)*	*Addition*
1	*2*	*3*	*4*
Benzene	C_6H_5I	0.06	C_6F_6
		0.06	
		0.06	
		0.06	
		0.06	
		0.45	
		0.45	
Hexane		0.06	
Benzene	$C_6H_5NO_2$	0.007	
	$SnCl_4$	0.012	
		0.012	
	C_6H_5I	0.06	C_5F_5N
		0.06	$CF_3C_6H_4CF_3$
		0.06	C_6F_5H
		0.06	m-$C_6F_2H_4$
		0.06	
		0.03	CS_2
		0.03	$C_{10}H_8$
		0.03	α-naphthylamine

the cross section of the interaction with the electron may have the same value as that for inhibitors. Therefore, such acceptors, which bind the electrons weakly (anti-inhibitors), must compete with inhibitors for electron capture. On an encounter with the positron, an anti-inhibitor molecule returns an electron to the positron.

On the other hand, typical inhibitors of Ps formation have much higher electron affinities. Thus, alkyl and phenyl halides capture electrons according to the mechanism of dissociative capture:

$$RX + e^- \rightarrow R + X^-.$$

As a result, the electron is bound to the halogen atom so firmly (EA $\gtrsim$ 3 eV) (*42*) that the positron fails to pick it off.

We think that the anti-inhibition effect can be used to solve many problems associated with the Ps formation mechanism. For example, is Ps formed in the condensed phase only by the spur mechanism or to some extent by the Ore mechanism? According to the above hypothesis, weak electron acceptors do not influence that fraction of Ps that could be

Publication Date: June 1, 1979 | doi: 10.1021/ba-1979-0175.ch009

and Anti-inhibitors in Solutions

Addition Concentration (M)	I_2%		
	Solvent	*Solvent + Inhibitor*	*Solvent + Inhibitor + Addition*
5	*6*	*7*	*8*
0.11	38	18	26
0.21	38	18	31
0.31	38	18	32
0.41	38	18	34
0.6	38	18	34
0.4	38	3	21
0.8	38	3	26
0.4	39	20	38
0.4	38	30	37
0.5	38	23	32
1.0	38	23	34
0.4	38	18	33
0.4	38	18	33
0.4	38	18	32
0.4	38	18	29
0.8	38	17	28
0.4	38	22	36
0.7	38	21	33
0.8	38	21	33

formed by the Ore mechanism. Therefore, in studying the concentration dependencies of the anti-inhibition effect, one can distinguish between the contributions of the two mechanisms to Ps formation.

Figure 4 shows the I_2 recovery when anti-inhibitor C_6F_6 is added to C_5H_5I–benzene solution. It is seen that I_2, at sufficiently high concentrations of C_6F_6, tends to its initial value in the pure solvent. This experiment probably shows that at least in benzene the spur mechanism gives the main contribution to Ps formation. Note that in experiments similar to that above, one should use anti-inhibitors such as C_6F_6 with a high efficiency of electron capture in the region of thermal energies (*43*). If the maximum cross section corresponds to higher energies, the anti-inhibition effect must be much weaker (shown below).

Another problem for experimental study is whether positron capture influences inhibition or anti-inhibition during the positron's slowing or after its thermalization. To answer this question, it is useful to experiment with those molecules whose positron affinity is predicted theoretically (*44*).

Publication Date: June 1, 1979 | doi: 10.1021/ba-1979-0175.ch009

Publication Date: June 1, 1979 | doi: 10.1021/ba-1979-0175.ch009

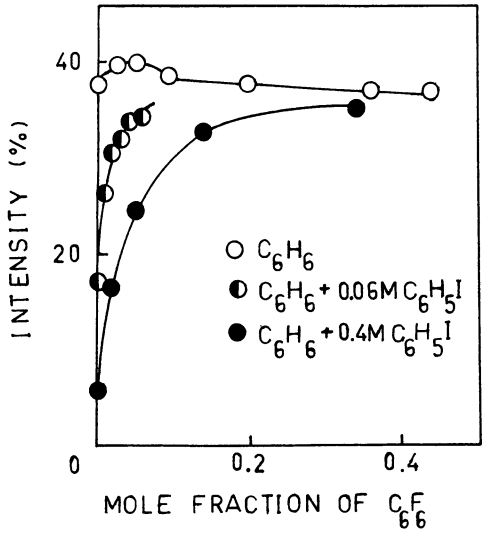

Figure 4. I_2 vs. the concentration of anti-inhibitor C_6F_6 in benzene and in benzene with 0.06M and 0.4M C_6H_5I

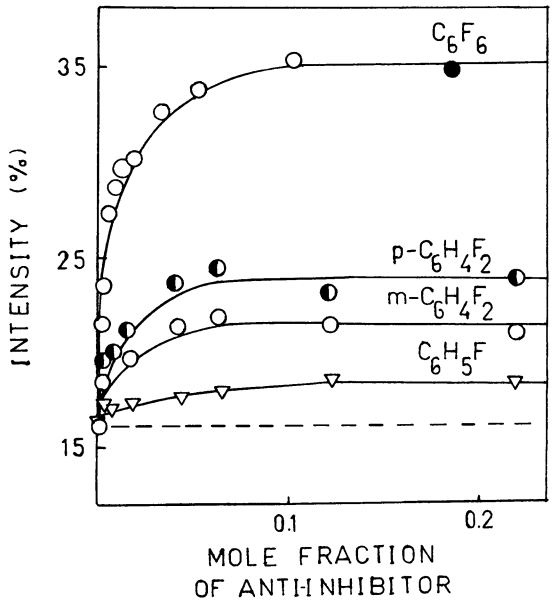

Figure 5. I_2 vs. the concentration of anti-inhibitors in benzene containing 0.1M CCl_4

Investigation of Fast Spur Reactions. Here we discuss some possibilities of the anti-inhibition effect as it is applied to studies of fast spur electron reactions. We restrict ourselves to the treatment of experimental facts in terms of the spur model only.

From experiments for the gas phase it is known that the electron capture by many molecules is resonant, with the cross section reaching its maximum at a certain energy. At thermal energies the capture may, in fact, be absent. This is the case, for example, for fluorobenzenes (*45*). Investigation of the anti-inhibition effect shows whether or not this phenomenon is preserved in the solution. Spur electrons have a wide energy spectrum. However, electrons with energy $> E^*$ (where E^* is the first excitation potential of the solvent) are rapidly slowed. Thus, the energy spectrum of the secondary electrons is within 0–E^*. If the resonant level of the electron-acceptor capture, ϵ_i, is above the thermal energies but below E^*, only some fraction of electrons can be captured during their slowing. Electrons whose initial energy is $> \epsilon_i$ can get to the region of resonant capture during their gradual slowing. Those with energy $< \epsilon_i$ are not captured at all. Thus, the higher the energy of the resonant electron capture, the less is the anti-inhibition effect.

Figure 5 represents results of our experiments on the concentration dependencies of the anti-inhibition effect of various fluorobenzenes. It is seen that I_2 reaches a constant value, which for C_6F_6 corresponds approximately to I_2 in the pure solvent; for the other compounds it is lower. Thus, mono- and dihalobenzenes capture only a portion of the spur electrons. Consequently, as in the gas phase, the molecules capture the electrons in a resonant manner. A considerable portion of the initial electrons whose energies are not sufficiently high are not captured in the region of inhibitor concentrations under study. The plateau levels in Figure 5 correspond to the sequence of the resonant energies of electron capture by the corresponding molecules in the gas [C_6F_6, 0 eV; *m*-$C_6H_4F_2$, 0.8 eV; C_6F_5H, 1.4 eV (*45*)]. This correspondence can be considered as additional evidence for the validity of the interpretation proposed by the spur model.

Note that the results obtained do not obviate the possibility of thermal electron capture by the acceptors studied. As shown by Allen et al. (*46*) in liquids, because of polarization effects, thermal electron capture by acceptors with negative electron affinity is possible. The low anti-inhibition efficiency of mono- and difluorobenzenes can be explained here by electron transfer from these molecules to the inhibitor molecules (CCl_4). This reaction must be favored energetically because the electron affinities of C_6F_5H and $C_6F_4H_2$ are lower than that of CCl_4.

The existence of two regions of inhibition effects is shown in the C_6H_5Cl–C_6F_6 system, where the concentration dependence of I_2 is S

shaped (Figure 6). We can assume that at low concentrations the anti-inhibitor competes successfully for the electrons, with the cross section of their capture by C_6H_5Cl molecules being small. At high C_6F_6 concentration other mechanisms probably become important.

Figure 7a gives experimental data that show how sensitive the electron-capture mechanism is to a slight change in molecular structure. *m*-Fluorochlorobenzene, similar to chlorobenzene, shows the inhibition effect. In accordance with the gas-phase data (*47*), this result can be treated as a dissociative electron capture, followed by formation of Cl^-. Unlike the meta derivative, *p*-fluorochlorobenzene shows no inhibition effect. On the contrary, in systems that contain an inhibitor the anti-inhibition properties of this compound are revealed (Figure 7b). Thus, either the electron capture here is not followed by dissociation, or the dissociation time gets much longer than the time of Ps formation (10^{-10} sec). Chemically, it is not surprising that the substituent in the para position influences the properties of the C–Cl bond more than the substituent in the meta position. Direct evidence for the interpretation proposed might be obtained from experiments on electron capture by *p*-fluorochlorobenzene in the gas phase.

Figure 8 demonstrates an interesting fact that the same compound, *p*-$C_6H_4Cl_2$, can show either inhibition or anti-inhibition properties under

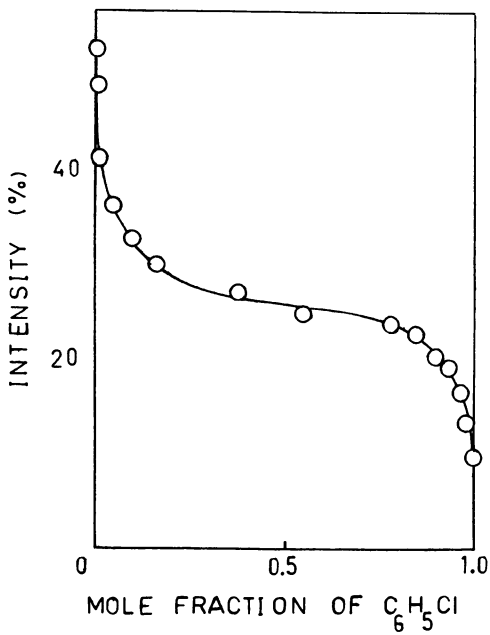

Figure 6. I_2 *vs. the composition of* C_6F_6–C_6H_5Cl

Publication Date: June 1, 1979 | doi: 10.1021/ba-1979-0175.ch009

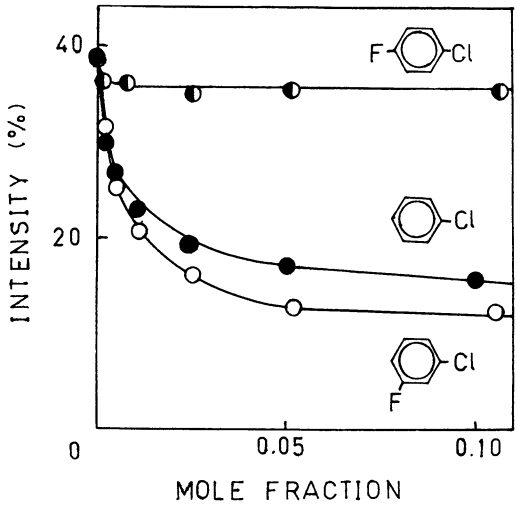

Figure 7a. Plots of I_2 vs. the concentration of halobenzenes in benzene

different experimental conditions. In benzene, as the concentration of p-$C_6H_4Cl_2$ increases, I_2 decreases from 38 to 15%. When p-$C_6H_4Cl_2$ is added to the benzene solution of C_6H_5I, the intensity of I_2, however, increases. It is possible that p-$C_6H_4Cl_2$ molecules capture some portion of electrons by the dissociative mechanism and the other portion by formation of molecular ions.

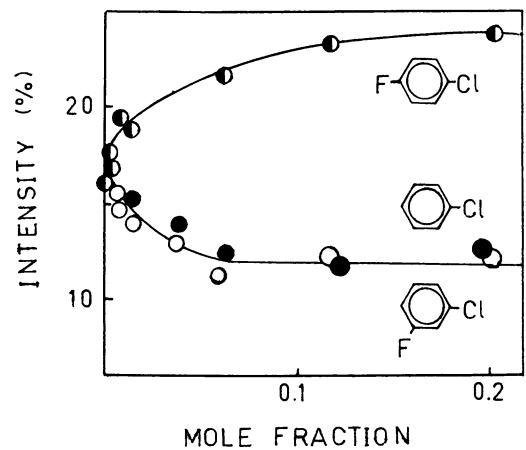

Figure 7b. Plots of I_2 vs. the concentration of halobenzenes in benzene with 0.1M CCl_4

Publication Date: June 1, 1979 | doi: 10.1021/ba-1979-0175.ch009

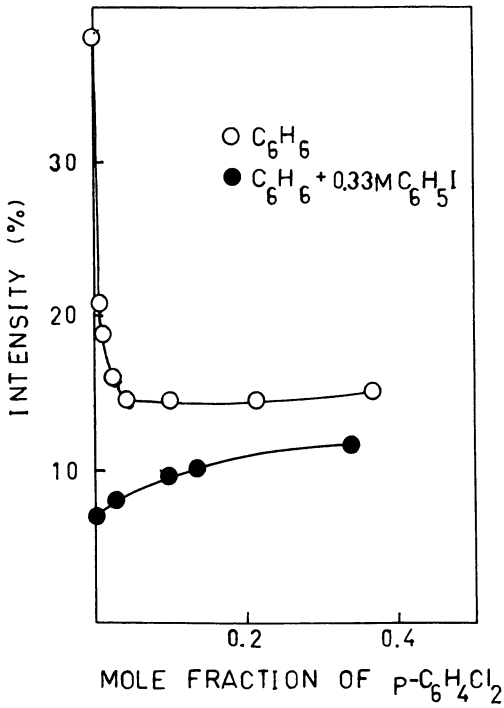

Figure 8. I_2 *vs. the mole fraction of* p-$C_6H_4Cl_2$ *in benzene (○) and in benzene with 0.33M* C_6H_5I *(●)*

Publication Date: June 1, 1979 | doi: 10.1021/ba-1979-0175.ch009

Conclusion

The experimental data given here agree well with the spur model. We obtained the following facts, which verify the spur model:

(1) inhibition effects are observed for transition metal ions, which are typical electron acceptors;

(2) electron acceptors CCl_2F_2 and SF_6 show the inhibition effect in the liquid phase and not in the gas phase;

(3) the intensity of the long lifetime component, I_2, in alcohols increases in crystalline phase as compared with the liquid or glassy phase;

(4) the probability of Ps formation decreases in nonpolar liquids under the influence of an electric field; and

(5) the anti-inhibition effect is observed for molecules that possess a weak electron affinity ($EA \lesssim 1.5$ eV).

Together with the literature data, these results are strong arguments in favor of the spur model for Ps formation in condensed media.

The spur model shows the relationship between Ps formation and radiation chemical experiments. This opens interesting possibilities for application of the Ps method to studies of the elementary radiation chemi-

cal reactions in the spur. One of the principal advantages of this method is the possibility for studying superfast spur reactions with relatively simple experimental equipment. The lifetime of a free positron in condensed media is approximately 10^{-10} sec; the recombination time of spur electrons and positrons is perhaps $< 10^{-11}$ sec. Thus, the Ps method fixes processes at times of the order of 10^{-11}–10^{-12} sec, i.e., when solvation processes are not over. The present paper shows that the Ps technique makes it possible to study superfast spur reactions, including probably epithermal electron reactions in the condensed phase.

Some problems of the Ps formation mechanism within the spur model are not clear. For example, it is not clear whether or not it is necessary to take into account positron capture together with spur electron capture. In the analysis of experimental data here it was not necessary to use the supposition on the spur positron capture. Practically all the results were in good agreement with the well-known information on the electron reactions. However, the positron reactions might create difficulties when experimental data are analyzed in terms of the spur model.

One more problem concerns the possibility of the Ore mechanism in the condensed phase. The available data do not allow us to ascertain unambiguously whether or not the Ore mechanism contributes to Ps formation in the condensed phase or at much lower densities. It is not quite clear why the Ore mechanism is so ineffective in the condensed phase. Perhaps the spur model will propose a different approach to the problems of free volume, hot Ps atoms, their energy spectra, and so forth. Solutions to these problems will be an important contribution to the application of the Ps method to fast reaction chemistry.

Publication Date: June 1, 1979 | doi: 10.1021/ba-1979-0175.ch009

Acknowledgments

The authors thank H. Ache and A. M. Raitsimring for useful discussions and also S. V. Vosel and S. V. Kiyanov for carrying out some experiments.

Literature Cited

1. Goldanskii, V. I., *At. Energy Rev.* (1968) **6**, 3.
2. Ache, H. J., *Angew. Chem.* (1972) **11**, 179.
3. Mogensen, O. E., *J. Chem. Phys.* (1974) **60**, 998.
4. Byakov, V. M., *Int. J. Radiat. Phys. Chem.* (1976) **8**, 283.
5. Byakov, V. M., Goldanskii, V. I., Shantarovich, V. P., *Dokl. Akad. Nauk SSSR* (1974) **219**, 633.
6. Ore, A., Universitetet i Bergen Arbok, Naturvitenskabelig rekke (1949) No. **9**, 1–16.
7. Eldrup, M., Shantarovich, V. P., Mogensen, O. E., *J. Chem. Phys.* (1975) **11**, 129.
8. Byakov, V. M., Grafutin, V. I., Koldaeva, O. V., Minaichev, E. V., Nichiporov, F. G., Obukhov, Yu. V., Stepanova, O. P., *Prepr. ITEPh, Moscow* (1976), No. **62**.

9. Bisi, A., Fasana, A., Zappa, L., *Phys. Rev.* (1961) **124,** 1487.
10. Brandt, W., Wilkenfeld, J., *Phys. Rev. B* (1975) **12,** 2579.
11. Mogensen, O. E., *Appl. Phys.* (1975) **6,** 315.
12. Levay, B., Mogensen, O. E., *J. Phys. Chem.* (1977) **81,** 373.
13. Jansen, P., Ph.D. thesis, Research Establishment, Risø, 1976.
14. Jansen, P., Eldrup, M., Mogensen, O. E., Pagsberg, P., *Chem. Phys.* (1974) **6,** 265.
15. Tao, S. J., *Appl. Phys.* (1976) **10,** 67.
16. Maddock, A. G., Abee, J. Ch., Haessler, A., *Chem. Phys. Lett.* (1977) **47,** 314.
17. Ito, Y., Tabata, Y., *Int. Conf. Positron Annihilation, 4th, Helsingør, Denmark, 1976,* paper G6.
18. Bartal, L. J., Nicholas, J. B., Ache, H. J., *J. Phys. Chem.* (1972) **76,** 1124.
19. Wild, R. E., Ache, H. J., *J. Chem. Phys.* (1976) **65,** 247
20. Maddock, A. G., Abbe, J. Ch., Haessler, A., *Chem. Phys.* (1976) **17,** 343.
21. Anisimov, O. A., Ph.D. thesis, Novosibirsk, 1976.
22. Rohrlich, F., Carlson, B. C., *Phys. Rev.* (1954) **93,** 38.
23. Nicholas, J. B., Wild, R. E., Bartal, L. J., Ache, H. J., *J. Phys. Chem.* (1973) **77,** 178.
24. Bartal, L. J., Ache, H. J., *Radiochim. Acta* (1972) **17,** 205.
25. Shantarovich, V. P., Goldanskii, V. I., Molin, Yu. N., Permilov, V. P., Skubnevskaya, G. I., *Izv. Akad. Nauk SSSR, Ser. Khim.* (1967) **10,** 2188.
26. Anisimov, O. A., Molin, Yu, N., *Khim. Vys. Energ.* (1975) **9,** 541.
27. Pikaev, A. K., "Solvated Electron in Radiation Chemistry," Nauka, Moscow, 1969.
28. Handeli, D., Lambrecht, R. M., *Chem. Phys. Lett.* (1976) **37,** 187.
29. Mogensen, O. E., Shantarovich, V. P., *Chem. Phys.* (1974) **6,** 100.
30. Green, J. H., Tao, S. J., *J. Chem. Phys.* (1963) **39,** 3160.
31. de Benedetti, S., Siegel, R., *Phys. Rev.* (1954) **94,** 955.
32. Chen, C. L., Chantry, P. J., *Bull. Am. Phys. Soc.* (1972) **17,** 1133.
33. Christophorou, L. C., McCorkle, D. L., Carter, J. C., *J. Chem. Phys.* (1971) **54,** 253.
34. Anisimov, O. A., Molin, Yu. N., *Khim. Vys. Energ.* (1975) **9,** 376. [*High Energy Chem. (Engl. Transl.)* (1976) **9,** 331].
35. de Blonde, G., Chuang, S. Y., Hogg, B. G., Kerr, D. P., Miller, D. M., *Can. J. Phys.* (1972) **50,** 1619.
36. Smedskjar, L., Trumpy, G., *Appl. Phys.* (1974) **5,** 49.
37. Ito, Y., Tabata, Y., *Chem. Phys. Lett.* (1972) **15,** 584.
38. Thosar, B. V., Lagu, R. G., Kulkarni, V. G., Chandra, G., *Phys. Stat. Sol. B* (1973) **55,** 415.
39. Anisimove, O. A., Raitsimring, A. M., Molin, Yu. N., *Sov. Phys. JETP Lett. (Engl. Transl.)* (1975) **22,** 91.
40. Hummel, A., Schmidt, W. F., *Radiat. Res. Rev.* (1974) **5,** 199.
41. Anisimov, O. A., Molin, Yu. N., *Khim. Vys. Energ.* (1975) **9,** 539.
42. "Energy of Chemical Bonds: Ionization Potentials and Electron Affinities," V. N. Kondratyev, Ed., Nauka, Moscow, 1974.
43. Gant, K. S., Christophorou, L. G., *J. Chem. Phys.* (1976) **65,** 2977.
44. Schrader, D. M., Wang, C. M., *Int. Conf. Positron Annihilation, 4th, Helsingør, Denmark, 1976,* paper G2.
45. Naff, W. T., Cooper, C. D., Compton, R. N., *J. Chem. Phys.* (1968) **49,** 2784.
46. Allen, A. O., Gangwer, T. E., Holroyd, R. A., *J. Phys. Chem.* (1975) **79,** 25.
47. Naff, W. T., Compton, R. V., Cooper, C. D., *J. Chem. Phys.* (1971) **54,** 212.

RECEIVED December 5, 1977.

10

Theory of the Structures of Intermediates in Positronium Chemistry

D. M. SCHRADER

Chemistry Department, Marquette University, Milwaukee, WI 53233

Publication Date: June 1, 1979 | doi: 10.1021/ba-1979-0175.ch010

Different mechanisms for positron annihilation in a chemical medium are distinguished by different intermediates. All measured annihilation properties (lifetime, angular correlation, etc.) are in fact properties of that intermediate which exists just prior to annihilation. The structures of these intermediates have been studied quantum mechanically as an adjunct to laboratory measurement of annihilation properties. The quantum mechanical studies involve calculating approximate wave functions for one-positron, many-electron systems. Some scattering states have been studied in this way for atoms, but all molecular studies so far focus on bound positrons or positronium atoms The questions of whether such bound states exist for particular molecules, and of the properties of those bound states which do exist, have been addressed in several studies. The most successful of these (1) permits one to examine positron/positronium–molecule interactions at a more fundamental level than was hitherto possible.

Positron/positronium (Ps) chemistry takes place somewhere between the beginning of the initial positron/Ps–reactant molecule encounter and annihilation. What happens in the intermediate region of the reaction coordinate is of great interest to the chemist. If we can understand this region at the level of positron/Ps interactions with individual molecules, we can map out the whole of positron/Ps chemistry.

Our knowledge of this intermediate region is presently very hazy. The experimental literature contains many speculations about structures of intermediates. Frequently these speculations are quite sensible and are widely and uncritically accepted by the community, but are incorrect. A

0-8412-0417-9/79/33-175-203$10.00/1

In Positronium and Muonium Chemistry; Ache, H.;
Advances in Chemistry; American Chemical Society: Washington, DC, 1979.

number of examples are given later in this chapter, but two may be profitably presented here: (1) positrons bound to conjugated molecules are widely assumed to occupy π molecular orbitals. This notion is very sensible, for in that way the positive positron can avoid the repulsive nuclei and be close to the polarizable π electrons. However, our calculations suggest that the positrons find a way to avoid the nuclei and reside in the sigma system at the same time. (2) It is widely assumed that if a positron binds to a polar molecule, the positron is localized at the negative end of the molecule. This is also very sensible, and probably correct for ionic molecules. However, for polar covalent molecules our calculations suggest that the positron finds another part of the molecule more hospitable for reasons of differential polarizability which are discussed below.

The key to understanding the structures of intermediates is, we believe, afforded by quantum mechanical calculations in interaction with certain kinds of experimental work such as angular correlation measurements and studies of substituent influences (e.g., *2*). In this chapter we describe our own efforts to develop a useful quantum mechanical method for understanding the interactions of positron/Ps atoms with complex (i.e., simple organic) molecules.

In order to be useful, a quantum mechanical method (or any chemical method, whether experimental or theoretical) must be reasonably inexpensive, generally applicable, and reliable. Our method is quite inexpensive but is only acceptable in the other two areas, and much work remains to be done in its development. However, judging from our success in agreeing with experiments in those few cases where comparison is possible, we believe our present approach accounts at least qualitatively for the leading quantum mechanical features determining positron/Ps–molecule interactions. In short, our method seems to be a useful qualitative tool at present, but is not yet a quantitative tool.

In the following sections we review previous work on positron/Ps–molecule interactions in order to place our method in historical perspective. We discuss the structural features of interest to us and describe tactics to get at these features. We describe our method; we discuss our results with emphasis on comparisons between our work and experimentation. Finally, we discuss possible extensions and new applications of our approach.

Previous Work

Some significant theoretical work on positron/Ps–atom interactions has been done; here we restrict our attention to positron/Ps interactions with molecules and discuss atomic calculations only if they bear directly on the molecular problem. A considerable amount of early work on

Publication Date: June 1, 1979 | doi: 10.1021/ba-1979-0175.ch010

molecular crystals takes the positron "wave function" or orbital to be a constant (*3,4*). This work is not of interest to us because the focus of our work is the detailed intramolecular character of the positronic orbital. Columbino, Fiscella, and Trossi (*5*) made an approximate ad hoc correction for the intramolecular structure of the positronic orbital in graphite; but the approach used by these authors contains large uncertainties and is difficult to justify from first principles.

The earliest work known to us in which the interatomic structure of the positronic molecular orbital is considered is that of Chuang, Holt, and Hogg (*6*). These authors, in a calculation on methane, integrate a Schrodinger-type equation for the positronic orbital ψ_+ inside spherical cells centered at each nucleus with radii equal to the quantum mechanical average electronic radius for each isolated atom. By imposing the boundary conditions $\psi_+ = 1$ and $\psi_+' = 0$ at the cell boundaries: they match an assumed $\psi_+ \equiv 1$ outside the cells. In this way the positron density is reduced inside each atom in accordance with the static potential of that atom.

The Fourier transform of the products of appropriate hybrids of electronic atomic orbitals and these positronic functions are calculated and then squared, added together, and integrated over angles to yield the spherically averaged momentum distributions which are compared with the results of angular correlation measurements. The reduction of ψ_+ inside the atoms calculated by these authors improves the agreement with experiment very markedly in the high-momentum region. The same technique is applied to ammonia (*7*), hexane, and decane (*8*) with similarly encouraging results.

The principal defect in this approach is that the procedure for combining the contributions to the momentum distributions suggests that the authors are not properly taking into account the overall molecular symmetry. This symmetry plays a very important role in determining the momentum distribution of oriented molecules (*9*), although it is possible that spherical averaging reduces its importance.

One should recognize that, despite this defect, Hogg's group at Winnipeg pioneered in providing the first method for calculating positron/Ps–molecule interactions, which was widely applicable to a variety of molecular systems, based upon sensible quantum mechanical arguments, and gave results in good agreement with experiments.

More recently, the complete neglect of differential overlap (CNDO) method (*10*) was parameterized for positron/Ps–molecule-bound states (*11*). This is in very much the same spirit as our own work, described in this chapter. By calculating positronic molecular orbitals (PMOs), Madia et al. endowed the positronic charge density with a symmetry corresponding correctly to the molecular symmetry, thus avoiding the

Publication Date: June 1, 1979 | doi: 10.1021/ba-1979-0175.ch010

deficiency in the Winnipeg calculations noted above. The work of Madia et al. differs from ours mainly in the parameterization for the positron: they used no experimental positron/Ps–atom input, but instead resorted to an argument involving the virial theorem to relate the positron–core interaction integrals to the electron–core interaction integrals. This produced unphysical positron and Ps affinities (PsA's) for some molecules, and it was generally difficult to relate their calculated results to experiments.

Structural Features of Interest and Theoretical Tactics

The intra-atomic behavior of the positron was successfully incorporated into the wave function by Hogg and co-workers, and Madia et al. showed how the interatomic features were to be treated. The principle outstanding problem has to do with the details of the motion of the positron in a milieu of electrons.

Although each electron is strongly attracted to the positron, the electrons avoid each other because of the exclusion principle and their mutual repulsion. These effects are accounted for reasonably well by applying the conventional Hartree–Fock Theory to the electrons. However, using this method for the positron introduces an unacceptably large error in the wave function.

The electron–positron attraction corresponds to a local maximum in the exact (and unknown) wave function when the positron is close to an electron. This maximum is missed completely by the Hartree–Fock method because it is an independent-particle method, whereas the attraction is a two-particle effect. The resulting errors in calculated positron and PsA's and annihilation rates are quite large: affinities often have the wrong sign, and the rates are often too small by an order of magnitude. Reference to Ps hydride (PsH) (a proton, two electrons, and a positron) illustrates the problem. In Table I we have arranged several PsH wave functions in the order of increasing quality as indicated by the total energy. The Hartree–Fock calculation gives a binding energy of the wrong sign and an annihilation rate that is too small by a factor of eight.

One also see a monotonic relationship between the calculated annihilation rate and the binding energy. This is not surprising since both quantities depend strongly on building up the local maximum in the wave function mentioned above. In spite of the inability of the Hartree–Fock method to provide this maximum, Cade and Farazdel (*21*) have calculated some Hartree–Fock wave functions for Ps fluoride (PsF), Ps chloride (PsCl), Ps bromide (PsBr), and Ps iodide (PsI). The best estimate of the Ps binding energy, or PsA, is given by

$$\mathrm{PsA} = \mathrm{PA}^{-} + \mathrm{EA} - 6.8\ \mathrm{eV} \qquad (1)$$

Publication Date: June 1, 1979 | doi: 10.1021/ba-1979-0175.ch010

where PA^- is the theoretical estimate of the positron affinity of X^- from Koopmans' theorem, EA is the experimental electron affinity, and 6.8 eV is the binding energy of Ps. The Hartree–Fock values of PA^- are definitely too low because of the deficiencies of that method noted above, so the use of Equation 1 will provide a lower bound for PsA. To this Cade and Farazdel apply a small correction for differences in electron correlation between PsX and X^-, and report lower bounds of PsA's of 1.66, 0.80, 0.19, and −0.45 eV for PsF, PsCl, PsBr, and PsI, respectively. Thus, PsH seems to be an unfavorable system for an application of the Hartree–Fock method, and PsF, PsCl, and PsBr are almost certainly bound.

While these results are very useful, it is preferable to calculate directly the local maximum in the wave function and thus avoid the error in the calculated value of PA^-. A theory for this has been presented (*22*), but the method is so difficult to execute that no application has yet appeared in the literature. However, a perturbative approach has been applied in some positron–atom elastic-scattering calculations (*23*).

Publication Date: June 1, 1979 | doi: 10.1021/ba-1979-0175.ch010

Table I. PsH Binding Energies and Annihilation Rates for Several Approximate Wave Functions

	Total Energy (au)	*Binding Energy (eV)*	*Annihilation Rate ($nsec^{-1}$)*
Hartree–Fock[a]	−0.6675	−2.24[b]	0.3[c]
Modest configuration-interaction[d]	−0.750128	+0.00348	0.82[e]
Valence bond-like[f]	−0.7584	+0.228	2.02[g,h]
Modest Hylleraas-type[h]	−0.7742	+0.658	2.10
Ambitious configuration interaction[i]	−0.7842	+0.931	2.20
AmbitiousHylleraas-type[j]	−0.78679	+1.001	2.33
Exact calculation	?	?	?
Experiment	?	?	?

[a] Ref. *12*.
[b] An alternative value, −0.849 eV, is obtained from Equation (1).
[c] Ref. *13*.
[d] Ref. *14*.
[e] Ref. *15*.
[f] Ref. *16*.
[g] Ref. *17*.
[h] Ref. *18*.
[i] Ref. *19*.
[j] Ref. *20*.

In contrast to calculated annihilation rates, calculated momentum distributions are frequently given very well by Hartree–Fock wave functions. This apparent anomaly has an explanation: the measured and calculated momentum distribution is that for the center of mass of the annihilating particles. They are certainly strongly accelerated about each other (which produces the maximum in the exact wave function and hence determines the rate of the annihilation process) but the momentum associated with this acceleration is only relative between the two particles, and has no component in the center of mass frame. Two men who are arm wrestling on a floating raft to not affect the motion of the raft. Thus the very motion which the Hartree–Fock method ignores is not transmitted to the annihilation photons (except as an infinitesimal energy shift), and as a consequence simple wave functions are often adequate for calculating momentum distributions. Using their Hartree–Fock wave functions for Ps halides, Farazdel and Cade (*24*) have calculated annihilation rates and momentum distributions. While the former are too small by factors of 7–40 (*24*), the calculated momentum distributions are in better agreement with experimentation, especially for observations on aqueous chloride ions (*25*).

The point of this section is to emphasize the importance of somehow getting the local maximum into the wave function for calculations of positron/Ps affinities or annihilation rates. In our approximate method for structure calculations of positron/Ps–molecule complexes, we put this maximum into the wave function indirectly, by parameterizing our theory to experimentation. Our method is based on an approximation to the Hartree–Fock method, so the logical inconsistency is obvious: the very form of our assumed wave function limits the accuracy of the result, but we are parameterizing the method to experimentation. Although this approach is obviously and quite frankly inconsistent, its spirit has a long and wide history in applications of quantum mechanics in chemistry. The most successful recent example is Dewar's modification of intermediate neglect of differential overlap (INDO) (*26, 27*). Pople's original CNDO parameterization was more logical; he tried to fit ab initio calculations (*10*) which corresponded to the form of the CNDO wave function.

We feel justified in accepting these inconsistencies because of the paucity in our present knowledge of the structures of positron/Ps–molecule bound systems. Since almost nothing is known, a theory which provides only low-quality information is still useful. Our approach is the advantage of being very inexpensive; only about 1/1000 as much computer time is required for one of our calculations compared with an ab initio Hartree–Fock calculation. Therefore, we can treat large numbers of molecules and study trends in positron/Ps interactions as functions of substituent changes, small changes in structures, etc.

Publication Date: June 1, 1979 | doi: 10.1021/ba-1979-0175.ch010

In Positronium and Muonium Chemistry; Ache, H.;
Advances in Chemistry; American Chemical Society: Washington, DC, 1979.

PMO/1: An Approximate Method for Studying Positron/Positronium–Molecule Interactions

Full details of the parameterization scheme have been given already (*1*), so we will simply outline the high points here. The basis for the purely electronic part of the theory is unchanged from that originally given by Pople and Segal (*10*). Our task, then, is to append a positron to the existing theoretical framework, using a set of approximations and parameterization schemes resembling Pople's original as closely as possible. Our reasons for not originating a new method at this time is simply because the systems we are dealing with are so novel and poorly understood that we want a method which is understood completely as possible; otherwise we will have one equation with two unknowns, so to speak. CNDO/2 is an attractive method for a number of reasons, among which is that it is a "valence only" theory: core electrons are not treated explicitly. A binding positron certainly will not be found in the core, so we can focus our efforts on the important interactions—the positron with valence electrons.

To keep things as simple as possible, we treat only first-row atoms (i.e., hydrogen plus lithium through fluorine), we consider only closed electronic shells, and we use notation as close as possible to that of Pople and Beveridge (*28*).

The wave function for the positron/Ps–molecular complex we take to be

$$\Psi = \psi_p(p)\alpha(p) \times [\text{Slater determinant of EMOs}]. \tag{2}$$

The ψ_p is the positronic molecular orbital (PMO) and α indicates spin up for the positron. The bracketted term is a familiar Slater determinant of doubly occupied electronic molecular orbitals (EMOs), ψ_i. Each type of MO is expanded in a linear configuration of atomic orbitals (LCAO) basis set:

$$\begin{aligned} \psi_i &= \Sigma_\mu C_{\mu i}\phi_\mu \\ \psi_p &= \Sigma_\mu C_{\mu p}\phi_\mu. \end{aligned} \tag{3}$$

The ϕ_μ is a Slater-type atomic orbital and the positronic basis function ϕ_μ is described below. The coefficients are arranged in columns,

$$\mathbb{C}_i = \begin{bmatrix} C_{1i} \\ C_{2i} \\ \vdots \end{bmatrix} \qquad \mathbb{C}_p = \begin{bmatrix} C_{1p} \\ C_{2p} \\ \vdots \end{bmatrix} \tag{4}$$

called column vectors. These are determined as eigenvectors of the Roothaan–Hartree–Fock Equations (*29, 30*),

$$\begin{aligned}(\mathbb{F} - \epsilon \cdot \mathbb{1})\,\mathbb{C}_i &= \mathbb{O} \\ (\mathbb{F}_p - \epsilon_p \mathbb{1})\,\mathbb{C}_p &= \mathbb{O}\end{aligned} \quad , \tag{5}$$

one for each MO. The matrices in Equation 5 are described next, but first we note that each effective Hamiltonian above, $\mathbb{F}$ and $\mathbb{F}_p$, depends implicitly upon the whole set of MOs $\mathbb{C}_i$ and $\mathbb{C}_p$. Thus we must solve Equation 5 self consistently, and in so doing we account for the distortion of the EMOs owing to the presence of the positron.

The Hamiltonians $\mathbb{F}$ and $\mathbb{F}_p$ are greatly simplified from their full-fledged Hartree–Fock form by introducing the approximation that the product of two different orbitals, $\phi_\mu \phi_\nu$, is identically zero everywhere in space. This is a much stronger statement than orbital orthogonality, and this zero differential overlap (ZDO) approximation gives CNDO its distinguishing characteristics.

This approximation is applied everywhere except in one place: The off-diagonal elements of $\mathbb{F}$ and $\mathbb{F}_p$ are taken to be, for ϕ_μ and $\phi_{\bar{\mu}}$ on atom A, and ϕ_ν and $\phi_{\bar{\nu}}$ on atom $B \neq A$,

$$\begin{aligned}F_{\mu\nu} &= \frac{1}{2} S_{\mu\nu} (\beta_A^\circ + \beta_B^\circ) - \frac{1}{2} P_{\mu\nu} \gamma_{AB} \\ F_{\bar{\mu}\bar{\nu}} &= \frac{1}{2} S_{\bar{\mu}\bar{\nu}} K (\beta_A^\circ + \beta_B^\circ)\end{aligned} \tag{6}$$

where $S_{\mu\nu}$ and $S_{\bar{\mu}\bar{\nu}}$ are calculated overlap matrix elements (i.e., ZDO is not used in Equation 6). Note these overlap matrix elements do not appear in Equation 5 because when ZDO is applied to $\mathbb{S}$, the unit matrix $\mathbb{1}$ results. The β_A° are atomic-bonding parameters (*10*) and K is a constant to be determined from experimentation.

The diagonal elements of $\mathbb{F}$ and $\mathbb{F}_p$ are

$$\begin{aligned}F_{\mu\mu} &= -\frac{1}{2}(I_\mu + A_\mu) - \sum_B Q_B \gamma_{AB} - \frac{1}{2}(P_{\mu\mu}{}^{-1})\gamma_{AA} - \sum_B P_{\bar{B}\bar{B}} \gamma_{\bar{B}A} \\ F_{\bar{\mu}\bar{\mu}} &= -PA_{\bar{\mu}} + \sum_B Q_B \gamma_{\bar{A}B} + \gamma_{\bar{A}A}.\end{aligned} \tag{7}$$

These matrix elements represent the interaction of an electron (positron) with atom **A**. Similarities in the two equations are evident. The dominant part of $F_{\mu\mu}$ is the (negative of the) average of the ionization potential and electron affinity for an electron in orbital ϕ_μ, $-1/2(I_\mu + A_\mu)$; the corresponding part of $F_{\bar{\mu}\bar{\mu}}$ is the (negative of the) positron affinity of the ion A^- for a positron in orbital $\phi_{\bar{\mu}}$, $-PA_{\bar{\mu}}$. These quantities are taken from experiments. The second term of each matrix element represents the attraction (repulsion) of the electron (positron) with other atoms in

Publication Date: June 1, 1979 | doi: 10.1021/ba-1979-0175.ch010

the molecule. Q_B is the net charge of atom **B**, being the difference between the core charge Z_B and the valence electron population P_{BB}. Pople and Segal parameterized this interaction in terms of the electronic repulsion integral,

$$\gamma_{AB} = \left\langle \phi_\mu(1)\phi_\nu(2) \left| \frac{1}{r_{12}} \right| \phi_\mu(1)\phi_\nu(2) \right\rangle \tag{8}$$

where ϕ_μ is on atom A and ϕ_ν on atom B, and ϕ_μ and ϕ_ν are both taken to be *s*-type Slater-type orbitals (STOs) for the purpose of calculating this integral. Similarly, we parameterize the positron–core interaction in terms of the electron–positron interaction integral,

$$\gamma_{A\bar{B}} = \left\langle \phi_\mu(1)\phi_{\bar{\nu}}(p) \left| \frac{1}{r_{1p}} \right| \phi_\mu(1)\phi_{\bar{\nu}}(p) \right\rangle. \tag{9}$$

The third terms of $F_{\mu\mu}$ and $F_{\bar{\mu}\bar{\mu}}$ are a correction to the first terms, and (for the electron) a correction for exchange. $P_{\mu\mu}$ is the electron population attributable to the STO ϕ_μ. The fourth term of $F_{\mu\mu}$, which is contained in the second term of $F_{\bar{\mu}\bar{\mu}}$, is the electron–positron interaction, $P_{\bar{B}\bar{B}}$ being the positron population on atom B.

Equations 6 and 7 are developed with full supporting arguments by Schrader and Wang (*1*). The important thing to note here is that $\mathbb{F}_p$ contains some of the same parameters as $\mathbb{F}$, and is derived in a spirit identical to that of Pople and Segal. The parameters which remains as a vehicle for calibrating our theory with experiment are K, the proportionality constant in Equation 6 and the positron affinity of A^-, $PA_{\bar{\mu}}$ in Equation 7. Before proceeding to a determination of these parameters, we need to specify a basis set for the PMOs, $\{\phi_{\bar{\mu}}\}$.

Fortunately, a basis set which is extremely convenient computationally is also very sensible. They are the STOs—identical to those for the electron except for the exponential parameters. STOs are convenient because we can use the existing computer code with new exponential parameters to calculate the matrices $S_{\bar{\mu}\bar{\nu}}$ and $\gamma_{\bar{A}B}$. STOs are sensible because the 2*s* and 2*p* STOs, being zero at the nucleus, keep the positron away from the repulsive core. For the hydrogen atom, we use a 2*s*-type STO instead of a 1*s*-type for this reason. However, we emphasize that these 2*s*- and 2*p*-type functions are meant to describe the lowest positronic orbital.

The argument for determining the exponential parameters $\zeta_{\bar{A}}$ is as follows: in the atom PsA, the positron is probably orbiting at a radius equal to that of the extra electron in A^-. Therefore, we fix $\zeta_{\bar{A}}$ so that the positronic orbital $\phi_{\bar{\mu}}$ is stretched out to overlap maximally with the extra

Publication Date: June 1, 1979 | doi: 10.1021/ba-1979-0175.ch010

electron in A^-. The desired value of $\zeta_{\bar{A}}$ is simply the electronic value times r_{A^-}/r_A, the ratio of the radii of A^- and A. The radius of the fluorine ion is known, and the others can be estimated (*1*), giving values for all the $\zeta_{\bar{A}}$ except $\zeta_{\bar{H}}$ for which a superior determination is possible (*see* below).

This argument is perfectly sensible but it is another example of the surprises in store for those who try to understand what the positron is doing in atoms and molecules, for the Hartree–Fock calculation of Cade and Farazdel (*21*) show that the positron in PsF is actually more than twice as extended as our argument suggests. The limitations and strengths of the Hartree–Fock method are fairly well understood, and it seems most unlikely that the shape and approximate size of the positronic charge density is very much in error, despite the lack of electron–positron correlation (unless long-range dipolar polarization of the fluoride ion core by the positron plays a surprisingly important role). Thus, PMO/1 should be regarded as provisional until an improved positronic basis set is contrived to agree more with the Hartree–Fock orbitals. The great strength of semiempirical methods is that inadequacies in one area such as this are compensated for when the parameterization to experiment is performed. Thus, correcting this defect in our basis set will change values of other parameters in the theory but probably not the final results, at least not by very much. The calculations of Cade and Farazdel were not available to us when we were formulating PMO/1.

Using $\zeta_{\bar{A}}$ obtained from our argument, one calculates $S_{\bar{\mu}\bar{\nu}}$ and $\gamma_{\bar{A}B}$ for Equation 7. The effect of using basis functions $\{\phi_{\bar{\mu}}\}$ which are too large around the nuclei should not vitiate our conclusions for the following reason: our calculated $\gamma_{\bar{A}\bar{A}}$ are higher than they would have been using the more extended Hartree–Fock orbitals for the positron; but since the latter orbitals include no electron–positron correlation, their use to calculate $\gamma_{\bar{A}\bar{A}}$ would give values which are too low. Correlation enhances the interaction integral, so our calculated values might not be too bad. The $S_{\bar{\mu}\bar{\nu}}$ values which we calculate are automatically correct for one-atom integrals, and the effect of using more extended positronic orbitals will push some of the two-atom $S_{\bar{\mu}\bar{\nu}}$ integrals up and reduce others as comparisons with the work of Madia, Schug, Nichols, and Ache (*11*) have shown. Therefore, the effect of not using more extensive orbitals for the calculating of $\mathfrak{P}$ is unclear.

Now we proceed to input values of $PA_{\bar{\mu}}$ from experiment. These can be related PsA's, with Equation 1. The experimental information on PsA's of our eight atoms (hydrogen plus lithium through fluorine) is very sparse indeed. There are only two highly uncertain experimental PsA's, one rather good theoretical PsA, and one negative bit of information. The hydrogen atom will not bind a positron (*31*). The totality of knowledge of positron and Ps affinities of our eight atoms is given in Table II. A

Publication Date: June 1, 1979 | doi: 10.1021/ba-1979-0175.ch010

glance at this table would convince even the most optimistic researcher that he doesn't have enough data. Careful interpolation procedures are required, and the farther we get from the known values in Table II the more uncertain our results. Table II reveals the greatest weakness of PMO/1, and suggests a magical brew of art and science will be needed to fill in the unknown quantities. Thus our parameterization problem is quite different from that of Pople and Segal (*10*) in parameterizing CNDO/2. These workers had every atomic energy level needed as well as a great many diatomic data.

An important quantity which is buried in the theory is $U_{\bar{s}\bar{s}}$, the repulsion between a positron and an atomic core. The positron affinity of A^- ($PA_{\bar{\mu}}$) can be related to $U_{\bar{s}\bar{s}}$ by (*1*)

$$U_{\bar{s}\bar{s}} = -PA_{\bar{\mu}} + (Z_A + 1)\gamma_{\bar{A}A} \tag{10}$$

where Z_A is the core charge of atom A. $PA_{\bar{\mu}}$ can be related to PsA by Equation 1. Substituting values gives, for oxygen and fluorine

$$\begin{aligned} U_{\bar{s}\bar{s}}(O) &= 7\,\gamma_{\bar{O}O} - 6.63 \text{ eV} \\ U_{\bar{s}\bar{s}}(F) &= 8\,\gamma_{\bar{F}F} - 6.20 \text{ eV}. \end{aligned} \tag{11}$$

Since $\gamma_{\bar{A}\bar{A}}$ are already in hand, $U_{\bar{s}\bar{s}}$ for O and F are obtained from experiments in this way. Inadequacies in the basic set described above reflected in values of $\gamma_{\bar{A}\bar{A}}$ are at least partly cancelled at this point in the calibration of our theory.

Table II. Available Binding Data for Our Eight Atoms

Atom	*Positron Affinity*	*Positronium Affinity*
H	$\leqslant 0$[a]	1.01 eV[b]
Li	?[c]	?
Be	?	?
B	?	?
C	?	?
N	?	?
O	?	2.2 ± 0.5 eV[d]
F	?	2.9 ± 0.5 eV[d,e]

[a] Ref. *31*.
[b] Ref. *20*.
[c] A recent calculation by Clary (*19*) on positronic lithium, e^+Li, yields 0.854 eV as the positron affinity of Li. This result, which should be easily improvable since it lies 0.558 eV above the Ps + Li^+ threshold, appeared after the formulation of PMO/1, and so is not part of its parameterization.
[d] Ref. *32*.
[e] Cade and Farazdel's (*21*) calculated lower bound is 1.75 eV, consistent with the older experimental value.

Publication Date: June 1, 1979 | doi: 10.1021/ba-1979-0175.ch010

$U_{\bar{s}\bar{s}}$ can be calculated also:

$$U_{\bar{s}\bar{s}}^{calc} = \left\langle \phi_{\bar{2s}} \left| -\frac{1}{2}\nabla^2 + \frac{Z}{r} - 2J_{1s} \right| \phi_{\bar{2s}} \right\rangle \quad (12)$$

(Z is the nuclear charge and J_{1s} is the potential of a core 1*s* electron). The values obtained from Equation 12 are only 8.2% higher than those from Equation 11. This kind of comparison provides one of the few available tests of the quality and internal consistency of a semiempirical method, and the concordance here is very encouraging. Similar comparisons of the corresponding electronic quantities, U_{ss} and U_{ss}^{calc}, can be made for all eight atoms, thus providing a means of extrapolating from fluorine and oxygen through lithium (*1*).

Positron and PsA's can be calculated now for these atoms using Equations 1 and 10. Our results, which amount to predictions for these quantities, are very rough indeed, and yet might be of some interest as higher quality information becomes available. They are given in Table III. The positron affinities given there are noted to be linearly related to the electron affinities of 2*s* holes as averaged over states by Pople and Segal. Extrapolating to hydrogen gives − 1.20 eV as its positron affinity, consistent with the findings of Aronson, Kleinman, and Spruch (*31*). We can relate this value to $U_{\bar{s}\bar{s}}(H)$ and $\gamma_{\bar{H}\bar{H}}$ using the proper variants of Equations 1 and 10:

$$U_{\bar{s}\bar{s}}(H) - \gamma_{\bar{H}\bar{H}} = 1.20 \text{ eV} \quad (13)$$

Similarly, from the PsA, 1.01 eV (*20*), we can write

$$U_{\bar{s}\bar{s}}(H) - 2\,\gamma_{\bar{H}\bar{H}} = -7.07 \text{ eV} \quad (14)$$

A simultaneous solution of these two equations gives $U_{\bar{s}\bar{s}}(H)$ and $\gamma_{\bar{H}\bar{H}}$, and from the latter quantity one can infer $\zeta_{\bar{H}}$, thus completing the atomic parameterization, except for the problem of finding values of $U_{\bar{p}\bar{p}}$.

This quantity is not very crucial because the 2*p* positronic orbital is considerably higher in energy than the lowest *s* orbital, so PMOs contain little 2*p* character. Nevertheless it must be determined and the procedure, which is somewhat similar to that for choosing values of $U_{\bar{s}\bar{s}}$, is given elsewhere (*1*).

The last undetermined parameter in our theory is K, the proportionality constant between the atomic bonding parameters β_A° for electrons and their positronic counterparts. This is the sole bonding parameter for the whole group of atoms because we have just one diatomic datum from experiments: the PsA of the OH radical, which is said to be less than 1.5 eV (*32*).

Publication Date: June 1, 1979 | doi: 10.1021/ba-1979-0175.ch010

In principle the procedure for determining K is simple: do a series of calculations on PsOH with various values of K until the desired PsA (which we somewhat arbitrarily take to be 1.0 eV) is produced. From Equation 1 we see that the PsA is the sum of the positron affinity of OH^- and the electron affinity of OH (less a constant). The latter is 1.825 ± 0.002 eV (*34, 35*), and the former is gotten by applying Koopmanns' theorem in a PMO/1 calculation: PA^- is the (negative of the) eigenvalue of the occupied PMO in PsOH. A simple calculation gives -5.97 eV as the desired value of ϵ_p in Equation 5. Unfortunately, we find that no choice of K yields this value! As an expedient, we use Koopmanns' estimation of the electron affinity in place of the experimental value. This estimation is $-\epsilon_i$ (Equation 5) for the highest occupied EMO in OH^-. Madia, Nichols, and Ache (*2*) resorted to the same expediency. This procedure will be followed consistently in applications of PMO/1 to other molecules, so perhaps some of the uncertainties in using the approximate theoretical value will cancel out.

For PsOH, the expediency admits not one, but two, values of K, namely ± 0.136. The choice of sign is immaterial for the energy of PsOH (but not for the PMO) because of the quantum mechanical simplicity of CNDO and OH, but the choice is very important for most other molecules. Had we chosen the positive value, we would have calculated unphysically large positron affinities for most molecules with the positron being concentrated in the interatomic regions. We know the positron will avoid these regions for the same reason electrons are attracted there. One way nature has to reduce charge density in an unfavorable region of a molecule is to put a wave function node there. $K = -0.136$ does this, and that is our choice.

This completes the parameterization of PMO/1, so we turn now to a discussion of our application of this technique.

Results of PMO/1

We have calculated wave functions for about 65 different molecules M, for each of M^-, e^+M, and PsM (In most cases we have taken our geometrics from Bowen et al. (*36*) and Sutton et al. (*37*)). Thus we have calculated electron affinities and positron affinities for Equation 1, and PsA's from Equation 1. Some overall features of our results can be pointed out now.

Table III shows a markedly increasing repulsion for e^+ in going from hydrogen to fluorine. Presumably this is a reflection of the decreasing polarizability and relatively decreasing nuclear shielding. Thus the most electronegative element in this group of eight is the least attractive for positrons. In a compound containing fluorine, we therefore will see

Publication Date: June 1, 1979 | doi: 10.1021/ba-1979-0175.ch010

Table III. Estimates of Missing Affinities from Table II

Atom	*Positron Affinity (eV)*	*Positronium Affinity (eV)*
H	−1.20[a, b]	Table II
Li	−1.51[c]	−2.11
Be	−1.83	−2.65
B	−3.22	−1.35
C	−4.54	+0.07
N	−6.46[b]	+1.16
O	−8.48[b]	Table II
F	−11.05	Table II

[a] Equation 13 and preceeding text.
[b] These estimates are consistent with the results of Golden and Epstein (*33*).
[c] Recently Clary (*19*) calculated 0.854 eV for the positron affinity of lithium. Our value is thus much too low. Clary's value does not imply the stability of e^+Li, because his energy is 0.558 eV above the rearrangement threshold for $Ps + Li^+$. Thus, even 0.854 eV is apparently too low.

Publication Date: June 1, 1979 | doi: 10.1021/ba-1979-0175.ch010

opposing effects influencing positron binding: the fluorine atom will attract electrons to itself and thus become more attractive to the positron; but according to data in Table III, it has a large deficit to overcome. The obvious question is: how much extra charge must an atom acquire to bind a positron? The answer will not provide a quantitative guide to positronic bonding in molecules owing to the influence of neighboring atoms, but it will help us to understand qualitatively the nature of positron–molecule interactions.

The interaction between a positron and an atom with q excess electrons is, within the framework of PMO/1,

$$U_{\bar{s}\bar{s}} - (Z_A + q)\gamma_{\bar{A}A} . \tag{15}$$

We have used this expression before: for example, Equation 13 has $q = 0$ and Equation 14 has $q = 1$. The critical number of electrons for bonding, q_0, is gotten by equating Expression 15 to zero:

$$q_0 = \frac{U_{\bar{s}\bar{s}}}{\gamma_{\bar{A}A}} - Z_A \tag{16}$$

All the quantities on the right side are available, and Table IV gives the results. There we see that fluorine has to acquire a very large charge indeed in order to present a bonding site to a positron. This magnitude of charge shift does not occur in covalent compounds. Even hydrogen, the most hospitable element to a positron, rarely acquires enough extra electrons in covalent compounds to bind a positron directly. Clearly, if any neutral molecule is going to bind a positron, the source of the

In Positronium and Muonium Chemistry; Ache, H.;
Advances in Chemistry; American Chemical Society: Washington, DC, 1979.

binding will either be a large polarization of the electronic charge by the positron, or some more subtle effect. In any case, one does not expect any covalent molecule to have a large positron affinity.

Although this concept of critical charge for binding a positron is instructive, it is at the same time somewhat artificial because it is well known from quantum mechanics that even an arbitrarily small attractive charge will support an infinite number of bound states of an interacting particle (*33*). Therefore the quantity q_0 in Table IV should rigorously be regarded not as an actual charge, but rather simply as a parameter indicating the relative importance of core repulsion ($U_{\bar{s}\bar{s}}$) and valence electron attraction ($\gamma_{\bar{A}A}$) for a positron.

Question: Why Do Positrons Bind to Some Molecules and Not to Others? ANSWER #1. Long-range dipolar binding plays an important role. Theoretically, a point dipole will bind an electron (and hence, alternatively, a positron) if its dipole moment is larger than a certain critical value, namely 1.625 D (*39, 40, 41, 42, 43*). The same is true of an extended structureless dipole (*44*), and of a point dipole surrounded by any charge distribution which is spherically symmetrical and overall neutral (*42*). Crawford (*45*) and Crawford and Garrett (*46*) discuss electron affinities of more realistic molecular models, and it seems clear that their conclusions should be qualitatively the same for positron affinities: nonsphericity of charge distributions, vibrations, and rotations should be expected usually to make only small changes in the critical dipole moment for binding.

Thus NH_3, H_2O, and HF are on the borderline (1.47, 1.85, and 1.82 D, respectively), but LiH, LiF, and BeO (6.33, 6.19, and $\sim$ 6 D, respectively) are unambiquous positron binders. Our calculations give only very modest success with this latter group: the calculated positron affinities are + 0.45, − 0.81, and − 1.09 eV, respectively; i.e., LiF and BeO are calculated not to bind a positron. This is certainly incorrect, and further modifications of PMO/1 are necessary. One can actually make a reasonable estimate of the positron binding energy of simple dipolar

Table IV. Critical Atomic Electron Population for Binding a Positron

Atom	q_0 *(Equation 16)*
H	0.145
Li	0.280
Be	0.269
B	0.359
C	0.415
N	0.494
O	0.561
F	0.640

Publication Date: June 1, 1979 | doi: 10.1021/ba-1979-0175.ch010

Table V. Comparison Charge Distributions and Bonding in LiH and e^+LiH

	LiH	*e^+LiH*
Electron population		
Li	.73	.62
H	1.27	1.38
Positron population		
Li	—	.25
H	—	.75
Dipole moment (debye) [a]	6.19 [b]	6.40 [c]
Covalent bond orders [d]		
electronic	1.23	1.18
positronic	—	.79
total	1.23	1.97

[a] Calculated values.
[b] Experimental value is 5.88 D (*49*).
[c] Ignoring the positron.
[d] Equations 17 and 18.

molecules from data given by Wallis, Herman, and Milnes (*47*) and by Turner, Anderson, and Fox (*48*). Our next parameterization of this problem, PMO/2, will incorporate this important dipolar binding mechanism; until then, one should apply PMO/1 to ionic system with considerable caution.

Notwithstanding, it is interesting to compare the charge distribution and bonding in LiH and e^+LiH. The relevant numbers are given in Table V. The highly dipolar electronic charge in LiH is polarized even more by adding a positron, which itself resides 75% on the hydrogen. Some will take this number to be too low. A widespread assumption, especially in the older literature, is that the positron resides completely on the anion in ionic crystals (*12, 50, 51, 52, 53*).

The electronic bond orders given in Table V are calculated, following Mullikan (*54*) and convention, from

$$p_{AB} = 2 \sum_{\mu(A)} \sum_{\nu(B)} P_{\mu\nu} S_{\mu\nu}. \tag{17}$$

That is, the electron population attributable to the overlap charge distribution involving atomic orbitals ϕ_μ and ϕ_ν is multiplied by the calculated overlap integral and summed over all ϕ_μ-ϕ_ν pairs for μ on atom A and ν on B. We define the positronic bond order as:

$$p_{AB} = -2 \sum_{\mu(A)} \sum_{\nu(B)} P_{\mu\nu} S_{\mu\nu}. \tag{18}$$

The negative sign is crucial because we know that if a positron contributes to bonding, it will do so by avoiding the repulsive internuclear region and by squeezing the molecule together from the outside, which is the opposite from electrons. Therefore, positive bonding contributions are given by PMOs having an internuclear node, hence the negative sign above. It is not clear that the numbers obtained from Equations 17 and 18 can be compared as though they are in the same units, but we do so here until a more rigorous interpretation is formulated. One should definitely not compare our calculated bond orders with our calculated atomic electronic/positronic populations. The latter quantities are calculated in the ZDO approximation and add up to the number of electrons/positrons present.

The numbers in Table V suggest the positron contributes a surprising 40% of the total Li–H bond strength in e^+LiH. One also notes a slight reduction in the electronic bond order in e^+LiH compared with LiH, owing in this case to an increase in the polarity of the EMO. Still the total bond order in e^+LiH is 60% larger than in LiH. If the positron had been entirely on the hydrogen, there would have been a zero-calculated contribution to the bond order.

Equations 17 and 18 do not include ionic contributions, which are surely very important for this molecule. The electronic contribution to the ionic bond strength in e^+LiH is 1.98 times larger than in LiH, shown by comparing the products of net core plus electron charges. However, in e^+LiH, both atoms have positive net charges when the positron is counted, so the ionic contribution to the total bond strength in e^+LiH is negative. It is 3.20 times larger in magnitude than the ionic contribution to binding in LiH.

Thus by adding a positron to LiH one greatly strengthens the covalent contribution to the bond and weakens the ionic contribution. Clearly an ab initio calculation on this simple system would be very useful in sorting out these large, opposing effects.

Trends within a group of related molecules should be revealed by PMO/1 despite its weakness as a predictor of absolute properties. Therefore our calculations on the fluoroethylenes would seem to be useful if interpreted properly. We calculated positron affinities for ethylene and all possible fluoro derivatives. The results (Table VI) indicate that none of them bind, and that there is no discernable relationship between dipole moment and (lack of) binding. The only trend visible is a strong correlation between the number of fluorine atoms and the strength of the positron–molecule repulsion—another manifestation of the critical charge concept (Table IV).

ANSWER #2. Positrons can substitute for missing hydrogens in radicals if the radicals are big enough and/or contain no atoms with a

Publication Date: June 1, 1979 | doi: 10.1021/ba-1979-0175.ch010

Table VI. Calculated Positron Affinities of Ethylene and Its Fluoro Derivatives (*1*)

Molecule	*Positron Affinity (eV)*	*Dipole Moment (D)*[a]
C_2H_4	− 0.01	0
C_2H_3F	− 0.07	1.43
$C_2H_2F_2$(trans)	− 0.64	0
$C_2H_2F_2$(cis)	− 0.62	2.42
$C_2H_2F_2$(1,1)	− 0.30	1.38
C_2HF_3	− 0.72	1.40
C_2F_4	− 2.89	0

[a] Ref. *49*.

q_o (Table IV) larger than that of carbon. The radicals $C_2H_5 \cdot$ and $C_6H_5 \cdot$ bind a positron, phenyl more strongly than ethyl. These radicals are large enough to permit enough electron relaxation to generate a binding potential for a positron. Methyl and $C_2H_3 \cdot$ are too small, and the radicals NH_3, OH, and HO_2 do not bind a positron because either they are too small or they contain an atom so repulsive (*see* Table IV) that the positron cannot find a binding site. The data is in Table VII. The geometry used for these calculations is that of the parent molecule, with one hydrogen atom simply erased; i.e., geometries appropriate to the structure of the radical were not used. Table VII also gives a comparison with observed proton affinities of these radicals. There is no correlation between our calculated positron affinities and these proton affinities, which is puzzling in view of the correlations found for weak acids (*see* below). Perhaps the lack of correlation here is caused by our choice of geometries.

For the two bound species in Table VII the bound positron is highly localized on hydrogen atoms, but there is a major difference: for $C_2H_3 \cdot$ the positron binds near the missing hydrogen, but in $C_6H_5 \cdot$ the positron

Table VII. Calculated Positron Affinities of Some Simple Radicals[a] (*1*)

Radical	*Positron Affinity (eV)*	*Proton Affinity (eV)*[b]
CH_3	− 0.16	5.39 ± 0.01
C_2H_3	− 0.01	7.33 ± 0.05
C_2H_5	+ 0.09	6.44
C_6H_5	+ 0.27	9.33 ± 0.11
NH_2	− 0.14	8.0 ± 0.1
OH	− 0.78	6.37 ± 0.12
HO_2	− 0.66	6.35 ± 0.06

[a] Geometries are those of the parent compound with one hydrogen atom simply erased.
[b] Calculated by Schrader and Wang (*1*) from data listed by Franklin (*55*).

binds across the ring. Figure 1 gives the electron(positron) charges of R · and e^+R ·. In the case of C_6H_5 ·, the carbon from which the hydrogen atom is missing has acquired a substantial negative charge, − 0.05, and the positron polarizes the radical so strongly that the electronic contribution to the total dipole moment is more than reversed in e^+R · compared with R ·. This result illustrates the dangers in trying to deduce where a positron will go in a molecule by looking only at the molecule itself (a procedure used by Goldanskii and Shantarovich (*56*); and it shows the importance of allowing for the polarization of the electronic charge cloud

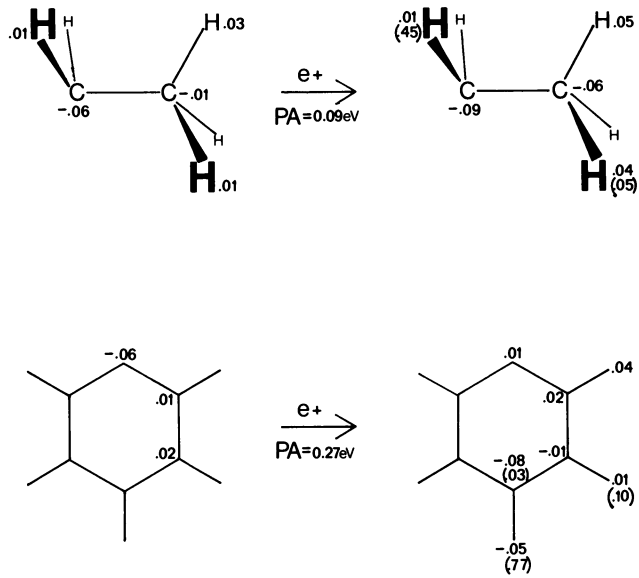

Figure 1. Electron (positron) charges in the radicals C_2H_5·, C_6H_5·, $e^+C_2H_5$·, and $e^+C_6H_5$·. Values not shown are evident from symmetry or are insignificant.

by solving Equation 5 with full electron–positron self-consistency. This polarization is evidently the difference between binding and not binding a positron.

Our calculations show that the PMO in $e^+C_6H_5$ · is in the sigma system, and that the atomic charges in C_6H_5 · are dominated by the sigma system, not pi. By adopting a sigma-type PMO, the positron is able to avoid the repulsive interior of C_6H_5 · and avail itself of the less repulsive (Table IV) hydrogens.

It is interesting that, even though the positron is in a sigma MO, it is polarization of the pi electrons which accounts for binding (Figure 2).

Publication Date: June 1, 1979 | doi: 10.1021/ba-1979-0175.ch010

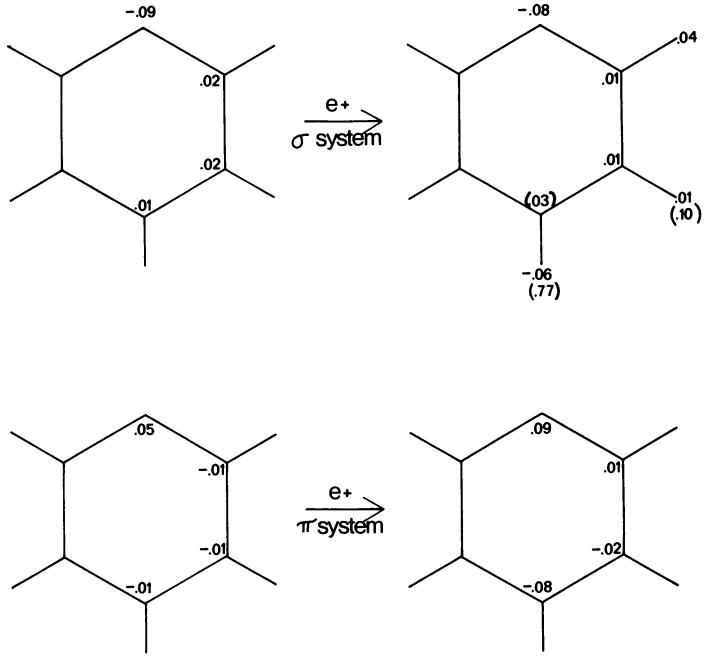

Figure 2. Electron (positron) charges in the sigma and pi systems in $C_6H_5\cdot$ and $e^+C_6H_5\cdot$. The positron adopts a sigma MO, but it is the polarization of the pi electrons which provides an attractive potential for the positron.

ANSWER #3. A positron will bind to any anion, in particular to anions of acids. We studied 12 weak acids and found an average positron affinity of 6.82 ± 0.68 eV, suspiciously close to that of the electron (6.80 eV), but much less than that of a fixed-point negative charge (13.60 eV).

The 12 acids appear to fall into two sets, each of which shows a strong correlation between pK_a values and positron affinities (Figure 3). One expects a weaker acid, which binds a proton more strongly, to also bind a positron more strongly. But we do not know why this expected correlation is manifested in two separate sets of acids. For the acids in the larger set, the acidic proton is bound to a fairly electronegative group (e.g., all the acids with COOH groups are in the larger set), whereas in the smaller set the oxygen which releases the proton is itself bound to a group which is not very electronegative.

We don't know quite what to make of these observations. Perhaps we should interpret these correlations with caution since the positron affinity is a gas phase quantity, where pK_a involves the solvent, and hence contains entropic contributions.

Publication Date: June 1, 1979 | doi: 10.1021/ba-1979-0175.ch010

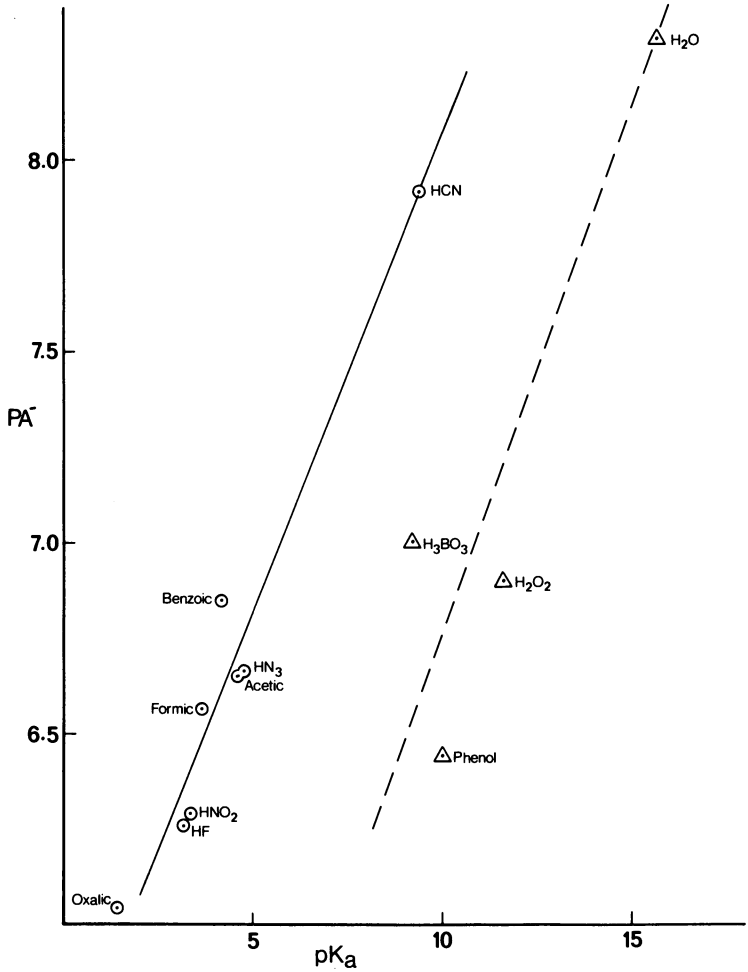

Figure 3. Correlation between positron affinities of weak acid anions and pK_a

ANSWER #4. Although the positron does not appear to be a typical electrophile in reactions with aromatic systems, it seems to bind readily to monosubstituted benzenes. Studies on eight such molecules show that the positron binds to seven. For these the positron is highly localized on the ortho hydrogen syn to an acyl oxygen; or, if there is no acyl oxygen, the positron binds to the para hydrogen. This is shown in Figure 4, where the eight molecules are arranged according to the effect of the substituents on aromatic substitution, the strong activators coming first. Some of the charge distributions shown in Figure 4 are sensitive to small

Publication Date: June 1, 1979 | doi: 10.1021/ba-1979-0175.ch010

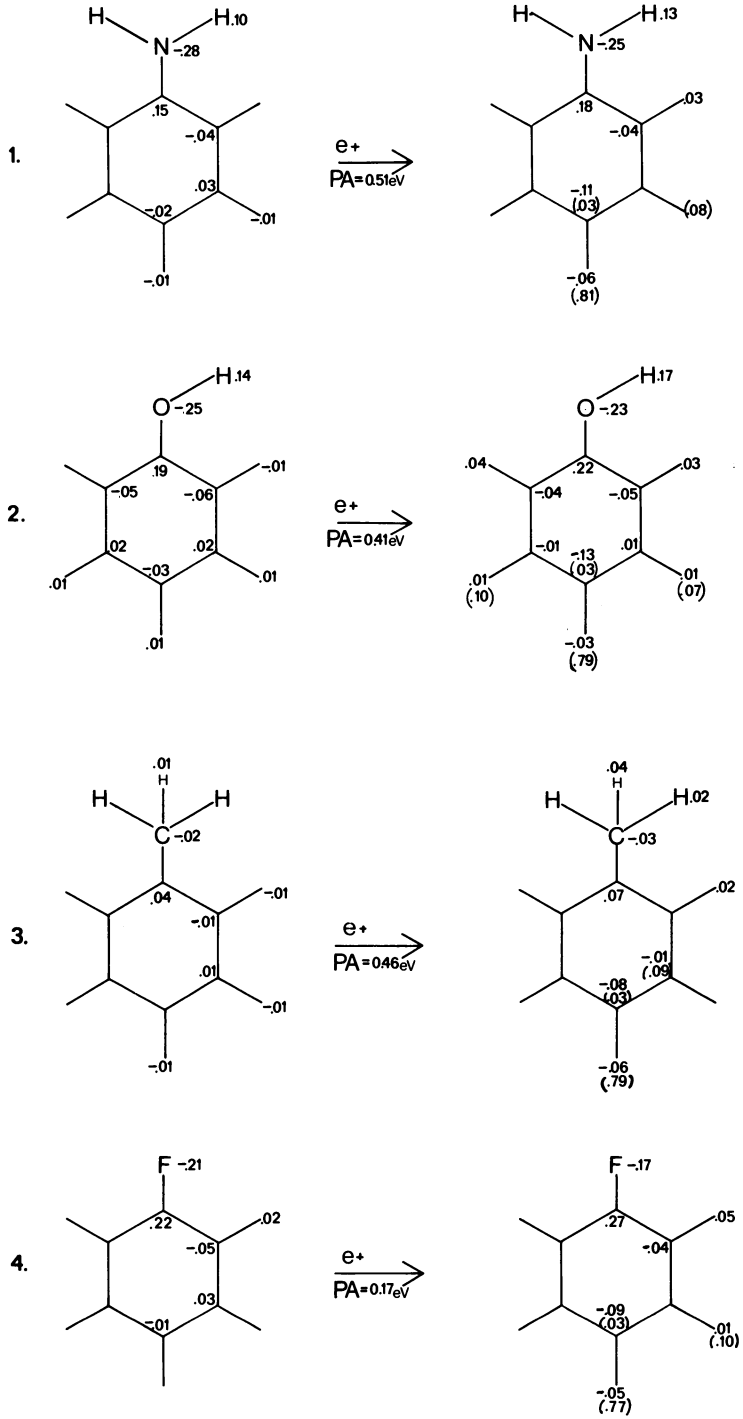

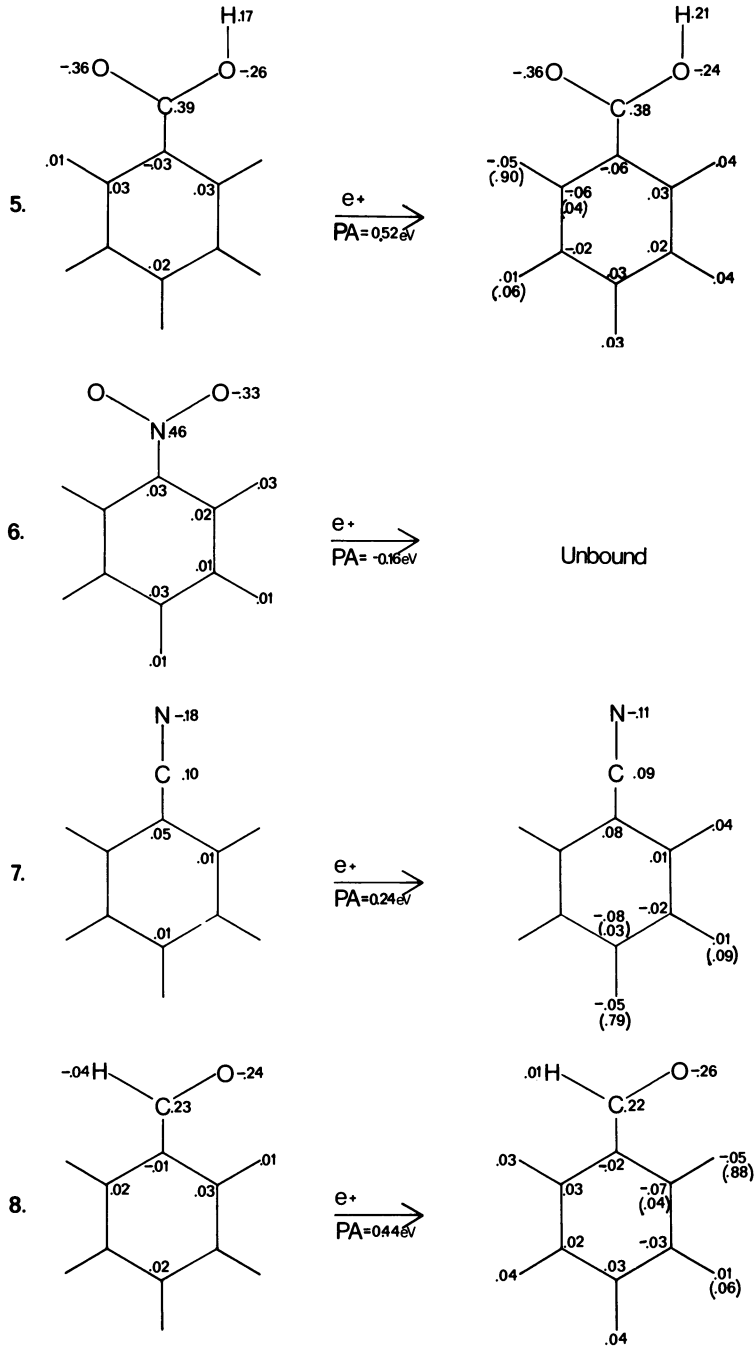

Figure 4. Electron (positron) charges in C_6H_5X and $e^+C_6H_5X$. Values not shown are evident from symmetry (or are significant).

geometry changes. Since we did not fully investigate this effect, the details of the distributions shown there should be regarded as provisional.

Polarization of the electronic distribution by the positron seems to dominate the metal director characteristics of the last four molecules in Figure 4, except for nitrobenzene. There is a correlation between the calculated positron affinities and the strength of the ring activators for these six molecules without an acyl oxygen, and another similar correlation for the two with oxygen. The correlation is not a strong one, but the ring activators without an acyl oxygen (1, 2, and 3) have an average positron affinity of 0.46 ± .04 eV, while the deactivators without acyl oxygens (4 and 7) have an average positron affinity of only 0.20 ± 0.04 eV. Single acyl oxygens (5 and 8) seem to stabilize the positron strongly (PA = 0.48 ± 0.04 eV) but nitrobenzene will not bind a positron at all despite its large dipole moment. This large dipole attracts the positron electrostatically to a region of the molecule which the positron finds relatively unpolarizable (high q_o values, Table IV), so the positron sees opposing forces. Apparently there are too many of these high q_o atoms near the ortho hydrogens in nitrobenzene, whereas in benzoic acid and benzaldehyde there are fewer, and they tend to have higher electron populations. The positron can sit on a friendly hydrogen and still participate in the large negative charge accumulated at the nearby oxygen.

The small positron affinity of fluorobenzene (0.17 eV) and the large Ps affinity of F (2.9 ± 0.5 eV) beg the question: is $e^+C_6H_5F$ stable enough to dissociate to $C_6H_5\cdot$ and PsF? Estimates of the C–F bond strength (5.1 eV (*57*)) and the ionization potential of $C_6H_5\cdot$ (8.76 eV (*55*)) can be combined with the calculated affinities and the binding energy of Ps (6.8 eV) to yield a value of about 4 for eV for ΔE for the reaction

$$e^+C_6H_5F \rightarrow C_6H_5^+ + PsF. \qquad (19)$$

Thus the reaction is very unfavorable.

It is interesting to study the molecular orbitals in $e^+C_6H_5F$ as a prototype. The molecule has C_{2v} symmetry and 33 MOs with the following symmetry: A_1 (15), A_2 (2), B_1 (5), and B_2 (11). The pi MOs are A_2 and B_1. Widespread assumption puts the positron in a pi orbital as noted above, but our calculations show the bound PMO to be A_1, a sigma orbital, and that there are twelve σ PMOs lower than the lowest pi. The positronic $1a_1$ MO is shown roughly in Figure 5, lower right corner. It has a large number of nodes between bonded atoms, in particular on the para C–H bond. This contributes positively to the covalent bond order (Equation 18), the positronic contribution to this bond order being 0.25 (compared with the electronic part, 1.36). The $1a_1$ PMO is similar in appearance to the $15a_1$ (upper left corner of Figure 5). Also, the $15a_1$

Publication Date: June 1, 1979 | doi: 10.1021/ba-1979-0175.ch010

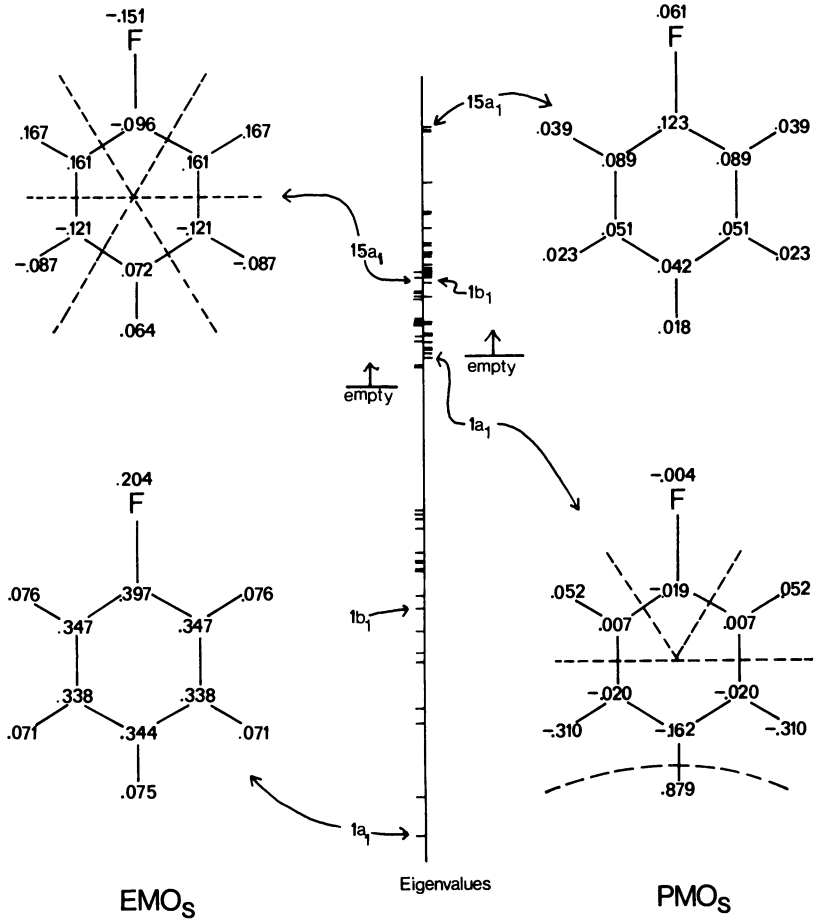

Figure 5. EMOs (left side) and PMOs (right side) of $e^+C_6H_5F$. Shown are all eigenvalues together with coefficients of s-type MOs in the lowest and highest of each, with nodes (– – –).

PMO, the highest of the 33 PMOs, is nodeless, and appears much like the lowest EMO, $1a_1$. At first it is slightly disorienting to try to associate highly noded MOs with strong binding and nodeless MOs with strong antibonding, but that's the way the positron is.

Benzene itself will not bind a positron, nor will parabenzoquinone or borazine. Perhaps these molecules are too symmetrical, not providing a unique site for the positron, which it seems to need for binding.

SUMMARY OF POSITRON BINDING ENERGETICS. These results show that dipolar binding is one of several effects involved, and the others may be dominant for some molecules. The explanation of positron binding is not simple, and calculations (perhaps with an improved parameterization)

Publication Date: June 1, 1979 | doi: 10.1021/ba-1979-0175.ch010

on more molecules with and without solvent sheaths, geometry optimization, etc., are called for. Our most dissappointing failure is in not getting more reasonable binding for highly dipolar molecules, for which theory appear to provide an unambiquous answer (*45, 46*). This was not apparent to us when we constructed the parameterization for PMO/1. Polarizability plays an important role, including differences in polarizabilities of parts of molecules. In this regard the concept of the critical charge for binding (Table IV) is useful.

Several features which have come out of our calculations seem real despite the very approximate nature of the theory. One of these is that if a positron binds to an aromatic system, it goes into a sigma orbital. Its orbital in any bound molecule is highly exteriorized and usually localized on a single hydrogen. Strangely, even though a bound positron is strongly localized, it nevertheless seems to require a large molecule for binding: of twelve neutral diatomics studied, only one, LiH, binds a positron in our approximation; of six neutral triatomics, none binds a positron; aside from LiH, the smallest neutral positron binder is C_2H_5, the ethyl radical; but out of eleven aromatics studied, seven will bind a positron in our approximation. Of 46 neutral molecules for which positron binding was studied, ten were found to bind. Seven of these are monosubstituted aromatics, two are radicals, and one is LiH.

Being localized on a large molecule implies the molecule can't be very symmetrical. Apparently benzene, parabenzoquinone, and borazine are too symmetrical to provide a unique site for localization of a bound positron.

It is very clear that a positron does not behave as a kind of light proton: It is so much lighter that it has a quite different behavior (*see* Figure 1, e.g.). Many other aspects of positron–molecule energetics and structure are much less straightforward. In this connection, Cade's project of calculating SCF wave functions for positronic molecular systems (*58*) should provide valuable insight into positronic charge distributions.

Question: Why Do Ps Atoms Bind to Some Molecules and Not to Others? A molecule which binds a Ps atom is doing two things, at least in the sense of a Born–Haber cycle: it is acquiring an extra electron, and then the anion is acquiring a positron. The electron affinity is much smaller than the positron affinity of the anion (6.8 ± .7 eV, *see* above discussion on weak acids); in fact, the statistical spread (0.7 eV) of the latter quantity is larger than many molecular electron affinities. This variation in positron affinity from one anion to another depends upon several factors, all of them poorly understood. Polarizability, dipole moments, and other structural features are sure to be involved. At any rate, it is just this deviation of PA^- (positron affinity of the anion) from 6.8 eV which, together with the electron affinity, determines the PsA of a molecule:

Publication Date: June 1, 1979 | doi: 10.1021/ba-1979-0175.ch010

$$PsA = (EA) + (PA^- - 6.8\ eV). \quad (1)$$

Each parenthetical quantity is small and uncertain, so our calculation of PsA's is less certain than that of positron affinities.

In our original work (*1*) we quoted an uncertainty in each of our determinations of PsA. This uncertainty was in connection with the use of an alternative Born–Haber cycle which yields the expression

$$PsA = EA(e^+M) + PA - 6.8\ eV \quad (20)$$

where $EA(e^+M)$ is the electron affinity of the complex e^+M. Of course, the two equations should give the same result, except when the various affinities are calculated with an approximate method, as in the case here.

We now believe that we should not have used Equation 20. We now hold this view because the determination of the bonding parameter K is based upon Equation 1, not Equation 20. Therefore, calculations on all molecules should follow Equation 1. The use of Equation 20 to determine K would have lead to a different value, and this second value should have been used in conjunction with Equation 20 to calculate PsA for molecules. In future work, this correction will be made. Meanwhile, in this work we will quote only PsA values calculated with $K = -0.136$ and Equation 1.

For two molecules, the quoted uncertainties in our earlier work gave rise to an uncertainty of sign in PsA. These ambiguities are now removed, and our calculations of PsA for these two molecules are:

$$\begin{aligned} &\text{ozone,} && PsA = +0.65\ eV \\ &\text{benzaldehyde,} && PsA = -0.56\ eV. \end{aligned} \quad (21)$$

That is, we now predict that ozone will bind a Ps atom by 0.65 eV, and that benzaldehyde will not bind Ps. In the case of ozone, one should note the PsA of the oxygen atom ($2.2 \pm .5$ eV, Table II) and the bond strength in ozone (1.04 eV) show that the complex PsO_3 is probably unstable to dissociation.

$$PsO_3 \rightarrow PsO + O_2, \qquad \Delta E = -0.5 \pm 0.5\ eV. \quad (22)$$

Similarly, the attachment of Ps to ozone is dissociative:

$$Ps + O_3 \rightarrow PsO + O_2, \qquad \Delta E = -1.1 \pm 0.5\ eV. \quad (23)$$

ANSWER #1. Ps will bind to many (most?) radicals made by removing a hydrogen atom from a closed shell molecule. We studied fourteen such molecules and found that the radical binds Ps in thirteen cases. The

Publication Date: June 1, 1979 | doi: 10.1021/ba-1979-0175.ch010

exception is NO which repels Ps very strongly indeed (PsA $\simeq -10.0$ eV). The thirteen Ps binders are radicals from a wide variety of compounds: hydrocarbons, acids, (strong and weak), bases, water (the PsA of OH is our one molecular input datum from experiment) and H_2O_2.

In the case of formic as well as acetic acids, Ps will bind whether the acidic or a covalent hydrogen is removed, but with some differences in energetics. The only strong acid in the six studied in this way has a radical with a calculated PsA typical of the whole set, so there is no correlation between acid strength and PsA among the acids studied.

The data is in Figure 6, which also shows the calculated electron and positron atomic charges. Several features can be noted, but not all of these are easily explained. First of all we see that, in positronic compounds which have overall electrical neutrality, in contrast to those reviewed above with an overall charge of + 1, the positron is not constrained to be on the periphery of the molecule, nor is it constrained to be localized on a hydrogen atom. In Figure 6 we see quite a different pattern: in a neutral positron–anion system, the positron may see one or more atoms with an accumulation of negative charge larger than that of the critical binding charge (Table IV). These molecules are numbered 2, 4, 5, 7, and 8 in Figure 6, and the atoms with an excess electron population larger than the critical value are starred. We see for those molecules that the positron is as frequently localized on an adjacent atom as on a starred atom. The expected populations are shown by 2, 4, and

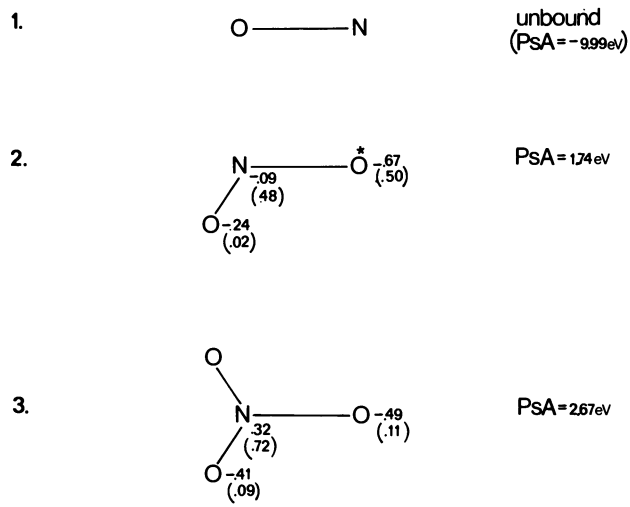

Publication Date: June 1, 1979 | doi: 10.1021/ba-1979-0175.ch010

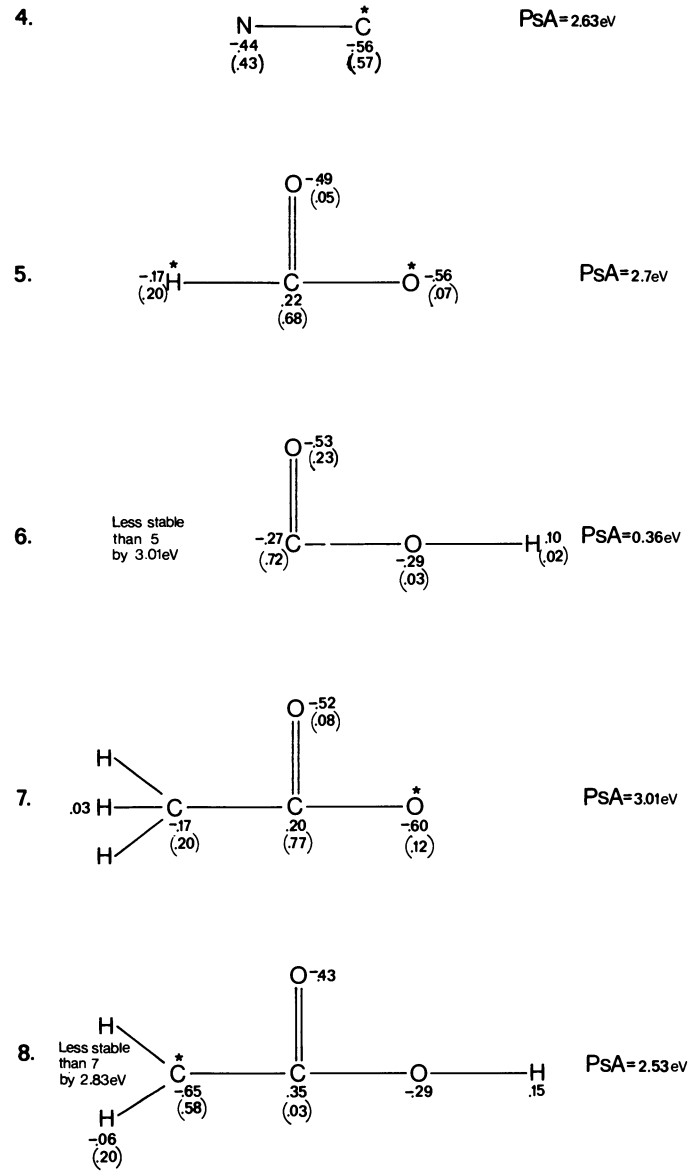

Figure 6. Calculated electron (positron) charge for compounds PsR, and PsA's for some radicals R with acidic parents HR. In the parent compound HR, the hydrogen is bonded to the right-most atom in each radical above. The geometries used in the calculation are those of gaseous HR with the H erased.

Publication Date: June 1, 1979 | doi: 10.1021/ba-1979-0175.ch010

8, and the unexpected by 5 and 7. Thus the critical charge concept is not so useful for rationalizing positron populations of neutral positronic compounds as of those with a net positive charge.

A dominant pattern seems to be: the positron sits on a central carbon or nitrogen bonded to two or more highly negative oxygens, even if the central carbon or nitrogen is far from its own critical charge (Table IV). The only clear counter example is 8; 2 is the borderline. This seems to be a strong trend, evidenced even in cases for which the central atom has a deficit of electrons (3, 5, and 7). The trend is shown also by nitrobenzene and ozone (*see* below).

Figures 7 and 8 show the data for some radicals R · from nonacidic parents HR. There are no central atoms with two or more bonded oxygens for any molecules in Figures 7 or 8. The atomic populations in Figure 7 seem reasonable on a simpler basis than that found in Figure 6.

Figure 8 has only hydrocarbons, and for them the populations are regular, simple, and expected. The positron and the extra electron, and hence the Ps atom, is highly (60–65%) localized on the carbon from which the hydrogen is erased. On the other hand, for the molecules in Figures 6 and 7, the positron is localized on the atom from which the hydrogen was erased for only half the cases (2, 4, 6, 8, and 9; counter

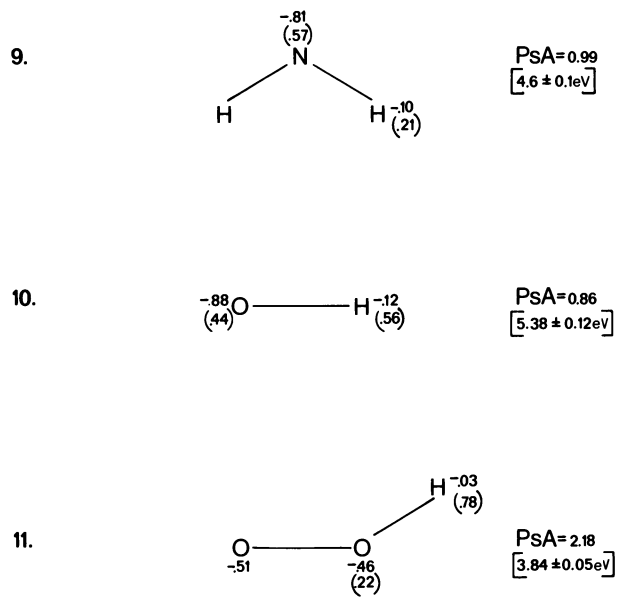

Figure 7. Calculated electron (positron) charges and PsA's for some compounds PsR, where HR is not acidic. Hydrogen atom affinities (55) are given in brackets.

Publication Date: June 1, 1979 | doi: 10.1021/ba-1979-0175.ch010

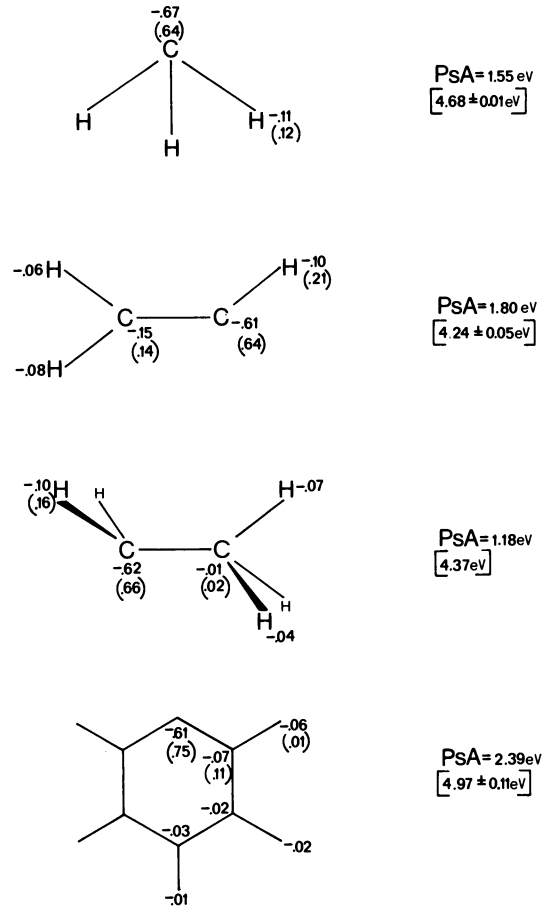

Figure 8. Calculated electron (positron) charges and PsA's for molecules PsR, where HR is a hydrocarbon.

examples are 3, 5, 7, 10, and 11), and for those examples (except 6) the extra electron is localized on the same atom as the positron and not for the counter examples (Table VIII). Thus if the Ps population can be assigned to a single atom in a molecule (2, 4, 8, 9), that atom is the one missing the hydrogen (except for 6). All the hydrocarbons (Figure 8) are examples of this. The positron population in C_6H_5Ps (Figure 8) are starkly different from those in $e^+C_6H_5$ (Figure 1).

Our results suggest that Ps will bind to almost any radical formed by removing a hydrogen atom. This property is not at all specific. Even in the cases of formic and acetic acid, Figure 6, Ps binding is indicated whether the acidic or a covalent hydrogen is removed. The Ps–R bond

Publication Date: June 1, 1979 | doi: 10.1021/ba-1979-0175.ch010

Table VIII. Concordance between Where the Positron Sits and the Identifiability of Positronium[a]

Positron Localized		*Extra Electron Localized on*	
On the Atom from Which H Has Been Erased	*Adjacent to*	*Same Atom as Positron*	*Different*
2	3	2	3
4	5	4	5
6	7	8	6
8	10	9	7
9			10

[a] The numbers refer to the molecules in Figures 5 and 6.

Publication Date: June 1, 1979 | doi: 10.1021/ba-1979-0175.ch010

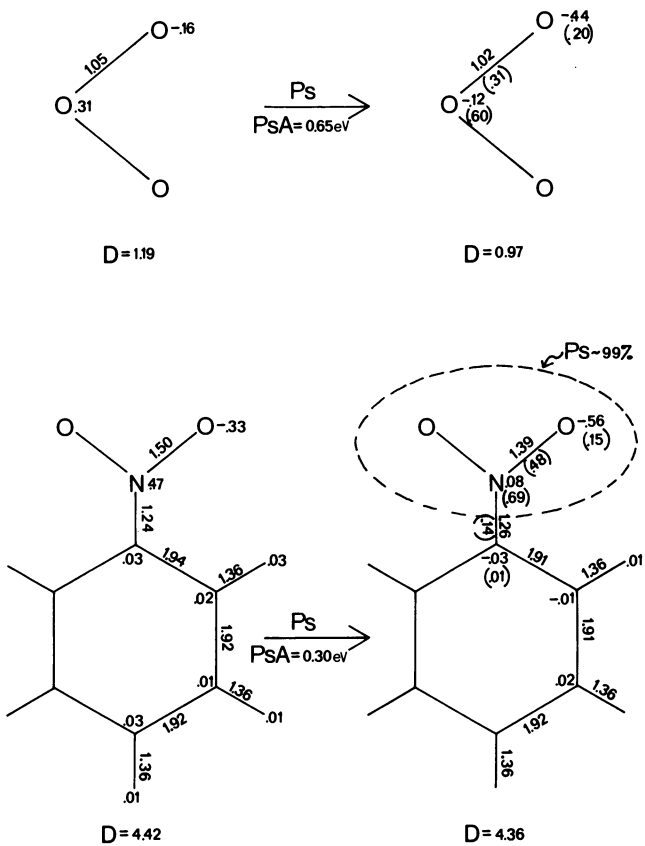

Figure 9. Calculated electron (positron) charges and Ps affinities for PsO_3 and $PsC_6H_5NO_2$. Dipole moments are also calculated. Experimental values (49) are 0.52–0.65 D for O_3 and 4.27 D for nitrobenzene.

seems to be stronger if the acidic hydrogen has been removed, and the resulting molecules (CHCOOPs and CH_3COOPs) seem to be more stable (than CPsCOOH and $CH_2PsCOOH$), although geometry optimization (which was not performed) may alter these observations.

The Ps binding energy in CH_3COOPs, 3.01 eV, is the largest PsA we have calculated to date.

ANSWER #2. Ps will sometimes bind to a molecule containing a unique atom bound to two oxygens. All the radicals with two or more oxygens in Figure 6 are examples, and besides these we have found two closed shell molecules (ozone and nitrobenzene). Benzoic acid is a counter example(PsA $=$ $-$ 1.03 eV). We do not claim to have discovered a trend for closed shell molecules on the basis of two examples and one counter example, but the populations in these two examples are interesting, and seem to follow a pattern shown in Figures 6, 7, and 8. The population and affinities are given in Figure 9.

In both cases the positron is localized on a central atom bonded to highly negative oxygens. This central atom in ozone is of course another oxygen, and it has a smaller electron population than its neighbors. In $PsC_6H_5NO_2$, the nitrogen has a positron population of 0.69 even though it has a deficit of electrons. This apparently anomalous behavior has already been noted for $PsNO_2$, CHCOOPs, and CH_3COOPs (Figure 6).

One wonders, since $PsNO_2$ is so stable (Figure 6), whether the attachment of Ps to nitrobenzene will be dissociative:

$$Ps + C_6H_5NO_2 \xrightarrow{?} C_6H_5\cdot + PsNO_2. \qquad (24)$$

A rough estimate of the C–N bond strength in nitrobenzene is obtained by averaging C–N bond strengths for some simple compounds where the carbon is hybridized sp^3 (59) and by ignoring $\Delta H - \Delta E$ differences. This number (approximately 2.5 eV) combined with the calculated PsA of NO_2 (1.7 eV) suggests that Equation 24 is unfavorable by about 0.8 eV. Apparently Ps will not split off NO_2.

We now consider the charge and bond order shifts when nitrobenzene combines with Ps. The covalent bond orders, calculated with Equations 17 and 18, are shown in Figure 9. The ionic bond order. given by $q_A q_B / R_{AB}$ can be studied also, although we do not relate numerical values for bond orders for the two types of bonds here. Figure 9 shows that the electron in Ps goes almost half (.39) to nitrogen and about half (.46) to the two oxygens, and the positron goes 69% to the nitrogen and 30% to the oxygens. The positronic charge of the NO_2 group is thus about 99. The net electron population of the NO_2 group is not .85 ($=$ .46 $+$ .39) but 1.04 owing to an accumulation of .19 in nitrobenzene itself. On this basis one might say Ps is approximately 99% localized on the nitro group in $PsC_6H_5NO_2$.

Publication Date: June 1, 1979 | doi: 10.1021/ba-1979-0175.ch010

The dipole moment of a large molecule (nitrobenzene) which binds a localized neutral group (Ps) will not change much, as shown by our calculated moments in Figure 9. Ozone shows similar behavior.

The electronic part of covalent bond orders (shown in Figure 9) is seen to suffer slightly between N and O and to remain essentially constant elsewhere in the molecule. Presumably this is because the added electron must go into a low antibonding orbital which is localized in the NO_2 group. But the positronic contribution to the N–O bond is considerable (26%), resulting in a net increase in the covalent bond order of 19%. The N–C covalent bond is likewise augmented by 13%. The only significant ionic contribution to binding in $C_6H_5NO_2$ and in $PsC_6H_5NO_2$ is in the N–O bond which doubles its ionic character when Ps is added. Thus Ps overall makes a definitely positive contribution to bonding in

Publication Date: June 1, 1979 | doi: 10.1021/ba-1979-0175.ch010

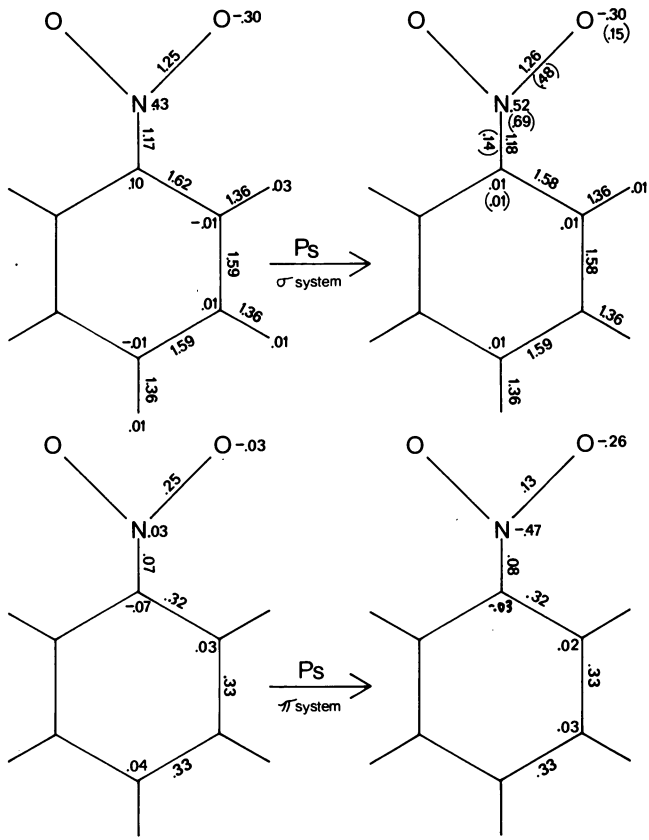

Figure 10. Sigma and pi contributions to the charges and bond orders in Figure 9

$PsC_6H_5NO_2$. The contrast to the contribution of e^+ to bonding in e^+LiH (discussed above) is marked.

The sigma and pi contributions to the charges and covalent bond orders are given in Figure 10. We have assumed that the two oxygens contribute three electrons and the nitrogen one to the pi system to arrive at the indicated net electronic charges. It is interesting and puzzling that the electron in Ps goes into the pi system of $PsC_6H_5NO_2$ and the positron into the sigma system. Nevertheless both particles go to the NO_2 group.

SUMMARY OF Ps BINDING ENERGETICS. This discussion is but a sample of the possible studies which might be made of Ps–molecule interactions. The picture emerging is fairly simple: the Ps atom can behave as an ultralight hydrogen atom in the sense of being localized near the position in the molecule where a hydrogen atom might find a stable site. A second and less general type of binding site is an atom bound to two oxygens.

Comparisons with Experiment

A compendium of experimental cross sections for quenching ortho Ps (*o*-Ps) recently has been given by Klobuchar and Karol (*60*). We have reproduced that portion of their compendium for those molecules for which we have done calculations. This is given as Table IX. Pick-off

Table IX. Comparison between Observer Quenching Ability and Calculated Positronium Affinities of Some Small Molecules

Molecule	*Quenching Cross Section* (A^2)	*Chemical vs. Spin-Flip Quenching*[a]	*Positronium Affinity*[b] (*eV*)
H_2	0.44×10^{-5}[c]		− 5.25
N_2	1.0×10^{-5}[d]		− 12.40
CO_2	1.4×10^{-5}[c]		− 11.45
CH_4	1.8×10^{-5}[d]		− 6.03
O_2	1.0×10^{-3}[e]	0%	− 9.11
NO	8.4×10^{-3}[f]	0%	− 9.99
O_3/O	1.6[e,g]		+ 1.1[h]
N_2O_4/NO_2	26[i]	25%[a]	+ 1.2[j]

[a] Ref. *61*. The value 25% is for NO_2.
[b] Ref. *1*.
[c] Ref. *62*.
[d] Ref. *63*.
[e] Ref. *60*.
[f] Ref. *64*.
[g] Value for ozone.
[h] $-\Delta E$ for the process $Ps + O_3 \rightarrow PsO + O_2$. Ps affinities of O_3 and O are 0.65 eV (this work) and 2.2 ± 0.5 eV (Table II).
[i] Value for NO_2.
[j] $-\Delta E$ for the process $Ps + N_2O_4 \rightarrow PsNO_2 + NO_2$. Ps affinities for N_2O_4 and NO_2 are −3.84 and +1.74 eV, respectively (*1*).

Table X. Comparison of Positronium Affinities for Three Substituted Benzenes

M	$-\Delta H_{eq}$ *for* $Ps + M \rightleftharpoons PsM$ [a]	*Observed Positronium Affinity* [b]	*Calculated Positronium Affinity* [c]
Toluene	~ 0.0 eV		− 2.51
Nitrobenzene	0.20 ± .01	0.16 ± .01 eV	0.30
p-Benzoquinone	0.33 ± .02		− 1.92

[a] Ref. *2*.
[b] Ref. *65*.
[c] Ref. *1*.

quenchers have cross sections of the order of $10^{-5}A^2$, and spin-flip quenchers, $10^{-3}A^2$. The two molecules with quenching cross sections on the order of their geometrical cross sections are those which evidently chemically combine with Ps. Our calculations of PsA's are in perfect accord with this picture, indicating nonbonding for the pick-off and spin-flip quenchers, and bonding for the others.

Recently Madia, Nichols, and Ache (*2*) have measured ΔH for the

$$Ps + M \rightleftharpoons PsM \tag{25}$$

equilibrium for a large variety of molecules M. Of these we have studied three: toluene, nitrobenzene, and parabenzoquinone. Goldanskii, Kevdina, Shantarovich, and Petersen (*65*) have interpreted their observations on nitrobenzene in terms of a model which permits them to estimate the PsA. These results and our own are collected in Table X, which show nearly quantitative agreement between theory and experiment for nitrobenzene, complete agreement for toluene, and disagreement for quinone. We suspect that geometry optimization is not the reason for the failure of the theory for quinone. A full treatment of this problem waits for PMO/2.

Nichols, Madia, and Ache (*66*) find it probable that Ps attack of nitrobenzene is at the NO_2 group. Our calculations, summarized in Figure 9, indicate that Ps is about 99% localized on NO_2. The agreement is complete.

The Future

One expects that our information about positron/Ps–atom and –molecule interactions will improve with time. As we find out more about the structure of bound complexes, we will be able to improve procedures for extrapolating to larger systems. One such procedure is PMO/1, and since its formulation two years ago, we have already learned enough to warrant

Publication Date: June 1, 1979 | doi: 10.1021/ba-1979-0175.ch010

a new parameterization. A good deal of this new information comes from the Hartree–Fock calculation on PsF by Cade and Farazdel (*21*). One reason why expensive calculations such as this should be performed on a few systems is precisely what we are saying here: to provide input to the much less expensive semiempirical methods. We hope that this kind of information will continue to be produced and freely exchanged in the spirit of good science.

Probably the highest quality information available on positron/Ps–atom interactions aside from the Ps hydride work (*20*) are scattering data: theoretical phase shifts for elastic $e^+ - H$ (*67, 68, 69, 70*) and $e^+ - He$ scattering (*71, 72*), and experimental elastic scattering cross sections for $e^+ - Ne$ and $e^+ - Ar$ collisions (*73, 74*). In view of the great need for positron/Ps–atom interaction parameters, this information should be incorporated into PMO/2. We are presently working on this problem.

It is very easy to criticize PMO/1 with the aid of hindsight of the two years since its formulation. Many of its defects and weaknesses have been described above. For example, better positron and PsA's of the atoms and diatoms are needed, including for those values which are negative; the positronic basis functions should be extended to be more like Cade's SCF orbitals, but augmented in some way to give the effect of electron–positron correlations; we need 2p orbitals for the positron on hydrogen; we need to get the binding energies for simple dipoles right; etc.

Despite all these problems, PMO/1 gives agreement with experiment more frequently than not. One feels that it must incorporate the essential features of positron/Ps–atom and –molecule interactions in some fairly satisfactory, if only qualitative, way. In Tables IX and X we have moderate to good agreement with experiment both for large and for small molecules.

Our interpretation of the results of our calculations in terms of detailed analyses of electron and positron populations and bond orders, and positron/PsA's has undoubtedly gone farther than the reliability of PMO/1 warrants, at least in some cases. Yet no alternative to investigating details of structure and energetics of positronic complexes exists at this writing. Therefore we must choose between somewhat speculative interpretation of results of uncertain basis and a barren insistence on rigor. The speculative choice is much more tempting and we have succumbed happily, hoping meanwhile that we do not unduly mislead the unwary. Our choice is risky in that it invites criticism and leaves one vulnerable to being corrected later. We accept the risk in order to open some questions, stimulate discussion, and (who knows?) even inspire further research.

Publication Date: June 1, 1979 | doi: 10.1021/ba-1979-0175.ch010

Acknowledgments

We are grateful to A. W. Jache for instructive comments, to D. T. Haworth for a critical reading, to H. J. Ache for encouraging us to write this overview, and to P. J. Karol for making some of his results available to us prior to publication.

Literature Cited

1. Schrader, D. M., Wang, C. M., *J. Phys. Chem.* (1976) **80,** 2507.
2. Madia, W. J., Nichols, A. L., Ache, H. J., *J. Am. Chem. Soc.* (1975) **97,** 5041.
3. Berko, S., Kelley, R. E., Plaskett, J. S., *Phys. Rev.* (1957) **106,** 824.
4. Chuang, S. Y., Hogg, B. G., *Can. J. Phys.* (1967) **45,** 3895.
5. Columbino, P., Fiscella, B., Trossi, L., *Nuovo Cimento* (1963) **27,** 589.
6. Chuang, S. Y., Holt, W. H., Hogg, B. G., *Can. J. Phys.* (1968) **46,** 2309.
7. Holt, W. H., Chuang, S. Y., Cooper, A. M., Hogg, B. G., *J. Chem. Phys.* (1968) **49,** 5147.
8. Chuang, S. Y., Hogg, B. G., *Nuovo Cimento* (1968) **B58,** 381.
9. Schrader, D. M., Kim, J. K., *Appl. Phys.* (1974) **4,** 249.
10. Pople, J. A., Segal, G. A., *J. Chem. Phys.* (1966) **44,** 3289.
11. Madia, W. J., Schug, J. C., Nichols, A. L., Ache, H., *J. Phys. Chem.* (1974) **78,** 2682.
12. Goldanskii, V. I., Ivanova, A. V., Prokopev, E. P., *Zh. Eksp. Teor. Fiz.* (1964) **47,** 659; *Sov. Phys.—JETP (Engl. Transl.)* (1965) **20,** 440.
13. Goldanskii, V. I., private communication (1969).
14. Ludwig, O. G., Parr, R. G., *Theor. Chim. Acta* (1966) **5,** 440.
15. Ludwig, O. G., private communication (1969).
16. Neamtan, S. M., Darewych, G., Oczkowski, G., *Phys. Rev.* (1962) **126,** 193.
17. Darewych, G., M.S. thesis, University of Manitoba (1961).
18. Lebeda, C. F., Schrader, D. M., *Phys. Rev.* (1969) **178,** 24.
19. Clary, D. C., *J. Phys. B* (1976) **9,** 3115.
20. Page, B. A. P., Fraser, P. A., *J. Phys. B* (1974) **7,** L389.
21. Cade, P. E., Farazdel, A., *J. Chem. Phys.* (1977) **66,** 2598.
22. Schrader, D. M., *Phys. Rev. A* (1970) **1,** 1070.
23. Jean, Y.–C., Schrader, D. M., *Phys. Rev.* (1978) **18,** 2030.
24. Farazdel, A., Cade, P. E., *J. Chem. Phys.* (1977) **66,** 2612.
25. Mogensen, O. E., Shantarovich, V. P., *Chem. Phys.* (1974) **6,** 100.
26. Bingham, R. C., Dewar, M. J. S., Lo, D. H., *J. Am. Chem. Soc.* (1975) **97,** 1285, 1294, 1302, 1307.
27. Dewar, M. J. S., Lo, D. H., Ramsden, C. A., *J. Am. Chem. Soc.* (1975) **97,** 1311.
28. Pople, J. A., Beveridge, D. L., "Approximate Molecular Orbital Theory," McGraw-Hill, New York, 1970.
29. Roothaan, C. C. J., *Rev. Mod. Phys.* (1951) **23,** 69.
30. Hall, G. G., *Proc. R. Soc. London* (1951) **A205,** 541.
31. Aronson, I., Kleinman, C. J., Spruch, L., *Phys. Rev. A* (1971) **4,** 841.
32. Tao, S. J., Green, J. H., *J. Phys. Chem.* (1969) **73,** 882.
33. Golden, S., Epstein, I. R., *Phys. Rev. A* (1974) **10,** 761.
34. Celotta, R. J., Bennett, R. A., Hall, J. L., *J. Chem. Phys.* (1974) **60,** 1740.
35. Hotop, H., Patterson, T. A., *J. Chem. Phys.* (1974) **60,** 1806.
36. Bowen, H. J. M., et al., "Tables of Interatomic Distances and Configurations in Molecules and Ions," Special Publ. No. **11,** Chemical Society, 1958.

37. Sutton, L. E., et al., "Tables of Interatomic Distances and Configurations in Molecules and Ions, Supplement 1956-1959," Special Publ. No. **18**, Chemical Society, 1965.
38. Messiah, A., "Quantum Mechanics," Vol. 1, p. 417, North Holland, 1961.
39. Levy-Leblond, J. M., *Phys. Rev.* (1967) **153**, 1.
40. Mittleman, M. H., Myerscough, V. P., *Phys. Lett.* (1966) **23**, 545.
41. Turner, J. E., Fox, K., *Phys. Lett.* (1966) **23**, 547.
42. Brown, W. B., Roberts, R. E., *J. Chem. Phys.* (1967) **46**, 2006.
43. Coulson, C. A., Walmsley, M., *Proc. Phys. Soc., London* (1967) **91**, 31.
44. Fermi, E., Teller, E., *Phys. Rev.* (1947) **72**, 399.
45. Crawford, O. H., *Mol. Phys.* (1971) **20**, 585.
46. Crawford, O. H., Garrett, W. R., *J. Chem. Phys.* (1977) **66**, 4968.
47. Wallis, R. F., Herman, R., Milnes, H. W., *J. Mol. Spectrosc.* (1960) **4**, 51.
48. Turner, J. E., Anderson, V. E., Fox, K., *Phys. Rev.* (1968) **174**, 81.
49. Weast, R. C., Ed., "Handbook of Chemistry and Physics," 51st ed., Chemical Rubber Co., 1970–1.
50. Ferrell, R. A., *Rev. Mod. Phys.* (1956) **28**, 308.
51. Millett, W. E., Castillo-Bahena, R., *Phys. Rev.* (1957) **108**, 257.
52. Wallace, P. R., *Sol. St. Phys.* (1960) **10**, 1.
53. Ivanova, A. V., Prokopev, E. P., *Zh. Eksp. Teor. Fiz.* (1965) **48**, 1155; *Sov. Phys.—JETP (Engl. Transl.)* (1965) **21**, 771.
54. Mulliken, R. S., *J. Chem. Phys.* (1955) **23**, 1833, 1841.
55. Franklin, J. L., et al., "Ionization Potentials, Appearance Potentials, and Heats for Formation of Gaseous Positive Ions," Nat. Std. Ref. Data Sys., Nat. Bur. Stand. (1969) 26.
56. Goldanskii, V. I., Shantarovich, V. P., *Appl. Phys.* (1974) **3**, 335.
57. Kerr, J. A., *Chem. Rev.* (1966) **66**, 465.
58. Cade, P. E., public remarks (June 1977).
59. Darwent, B. deB., "Bond Dissociation Energies in Simple Molecules," Nat. Std. Ref. Data Sys., Nat. Bur. Stands. (1970) 31.
60. Klobuchar, R. L., Karol, P. J., personal communication, 1977.
61. Mokrushin, A. D., Goldanskii, V. I., *Zh. Eksp. Teor. Fiz.* (1967) **53**, 478; *Sov. Phys.—JETP (Engl. Transl.)* (1968) **26**, 314.
62. Osmon, P. E., *Phys. Rev.* (1965) **140**, A8.
63. McNutt, J. D., Summerour, V. B., *Phys. Rev. B* (1972) **5**, 2019.
64. Chunang, S. Y., Tao, S. J., *Phys. Rev. A* (1974) **9**, 989.
65. Goldanskii, V. I., Kevdina, I. B., Shantarovich, V. P., Petersen, K. (1972), cited by Goldanskii and Shantarovich (*56*).
66. Nichols, A. L., Madia, W. J., Ache, H. J., *J. Phys. Chem.* (1974) **78**, 1881.
67. Schwartz, C., *Phys. Rev.* (1961) **124**, 1468.
68. Bhatia, A. K., Temkin, A., Drachman, R. J., *Phys. Rev. (Sect.) A* (1971) **3**, 1328, 1335.
69. Houston, S. K., Drachman, R. J., *Phys. Rev. A* (1971) **3**, 1335.
70. Bhatia, A. K., Temkin, A., Eiserike, H., *Phys. Rev. A* (1974) **9**, 219.
71. Humberston, J. W., *J. Phys. B* (1973) **6**, L305.
72. Campeanu, R. I., Humberston, J. W., *J. Phys. B* (1975) **8**, L244.
73. Kauppila, W. E., Stein, T. S., Pol, V., Jesion, G., *Int. Conf. Positron Annihilation, 4th, Helsingor, Denmark, 1976.*
74. Kauppila, W. E., Stein, T. S., Jesion, G., *Phys. Rev. Lett.* (1976) **36**, 580.

RECEIVED February 2, 1978.

11

Temperature-Dependent Behavior of Positron Annihilation in Metals

M. J. FLUSS, R. P. GUPTA[1], L. C. SMEDSKJAER, and R. W. SIEGEL

Materials Science Division, Argonne National Laboratory, Argonne, IL 60439

Publication Date: June 1, 1979 | doi: 10.1021/ba-1979-0175.ch011

The experimental techniques used to study defects by positron annihilation spectroscopy (PAS) are described briefly. Application of the two-state trapping model (TSTM) to the extraction of monovacancy formation enthalpies, H_{1v}^F*, in metals from PAS data is shown to have limitations. The parameters entering the TSTM are potentially temperature dependent, and a degree of uncertainty in these parameters is reflected in the determination of* H_{1v}^F*. A practical consequence of these uncertainties is a present limitation of 3–5% in the accuracy of PAS measurements of* H_{1v}^F *in metals. Lifetime experiments yield one method by which the uncertainties in the temperature-dependent parameters of the TSTM, except for the trapping rate per unit concentration of vacancies, can be taken into account naturally.*

The positron has found wide application as a probe for atomic and molecular systems. The positron itself is the antiparticle of the electron, and hence an electron–positron pair is unstable and will annihilate, emitting one or more gamma rays. The use of the positron as a probe is based on the detailed study of this emitted annihilation radiation. Since energy and momentum must be conserved in the annihilation process, the emission of just a single gamma ray is improbable, requiring the proximity of a "third" body, such as a nucleus. What is usually observed is the two-gamma ray annihilation. The three-gamma decay is

[1] Present address: Section de Recherches de Métallurgie Physique, Centre d'Etudes Nucleaires de Saclay, 91190 Gif-sur-Yvette, France.

0-8412-0417-9/79/33-175-243$07.00/1

In Positronium and Muonium Chemistry; Ache, H.;
Advances in Chemistry; American Chemical Society: Washington, DC, 1979.

also observed very seldomly and only if two-gamma decay is forbidden owing to angular-momentum conservation rules.

Application of the positron is based on two possible positron–electron states—positronium (Ps) and the "free" positron. In the Ps state the positron is bound to a single electron, a situation that is analogous to that with the hydrogen atom. This system was postulated (*1*) and named (*2*) before its eventual confirmation by Deutsch (*3*). In the free state the positron interacts with many electrons and, therefore, the description of the state has the character of a many-body problem. Both the positron and the Ps atom are light particles and thus are difficult to confine to a small region of space according to the Heisenberg uncertainty principle. They will, therefore, sample large regions of their surrounding structure and are thus versatile probes. The delocalized feature of Ps in a perfect lattice has been nicely demonstrated both for quartz (*4, 5*) and for ice(*6*). In imperfect structures the Ps atom or the free positron tends to localize in regions of low electron density away from the ion cores. This localization is reflected in the subsequent annihilation radiation and provides the basis for the application of positron annihilation to the study of defects in solids.

Publication Date: June 1, 1979 | doi: 10.1021/ba-1979-0175.ch011

At present, positrons are usually obtained from radionuclide sources, which emit the positron with sufficient energy to penetrate most materials to a few hundred microns, thereby permitting studies of their bulk properties. Recently, low energy positron sources have also been developed (e.g., *see* Ref. 7) that produce positrons that annihilate in the surface region, opening the possibility for studies of surface properties by positrons. This potential application has been reviewed recently in this SERIES by Brandt (*8*).

The development of the application of the positron to materials problems involving defects has been a consequence of the localization or trapping of the positron at atomic vacancy (or vacancy-like) sites in the bulk of metals and the formulation of a discrete-state model, commonly called the two-state trapping model (*9, 10, 11*), to treat these problems. This model has been the basis for interpreting almost all experimental positron data involving metallic systems in which vacancy-like defects are present. The application of positron annihilation spectroscopy (PAS) to the study of atomic defects in metals has developed rapidly since the discovery of positron trapping in vacancy-like defects (*12, 13*), principally because it was recognized that PAS could provide a way to measure the formation enthalpies of atomic vacancies under equilibrium conditions. However, the ultimate utility of PAS depends largely on establishing a physical understanding of the positron in metals. For an extensive review of the applications of positrons in metals *see* Refs. *14, 15, 16, 17, 18*; for reviews of the use of PAS for solids in general *see* Refs. *19* and *20* for two

more complete treatises. A recent review by Siegel (*21*) discusses PAS in comparison with other methods for studying atomic vacancies in metals.

Positron Annihilation Spectroscopy

Two types of information can be obtained from positron annihilation experiments: (1) that related to the electron density and (2) that related to the distribution of electrons in momentum space. A schematic of positron annihilation is shown in Figure 1. A lifetime experiment yields information related to the electron density (a typical lifetime apparatus is shown in Figure 2) since the decay rate of the positron is proportional to the positron–electron density overlap. Angular-correlation or Doppler-broadening experiments (shown in Figures 3 and 4), on the other hand, yield information regarding the distribution of corresponding electron momenta.

Figure 2 shows a schematic of the type of lifetime apparatus used in several laboratories. Lifetime measurements use (in the case of ^{22}Na) the 1.28-MeV gamma ray, the so-called "birth gamma," to start a time-to-pulse height converter (TPHC). The stop signal for the TPHC is derived from the detection of one of the two 511-keV annihilation gamma rays. One of the major experimental problems that arises in precise lifetime measurements is the ability to maintain the long term stability of the electronic equipment, which often operates at its design limits. Some aspects of this problem have been overcome recently by new data acquisition techniques (*22, 23*).

It is generally accepted that the positron is thermalized when it annihilates (*24, 25*). The momentum of the annihilating positron–electron pair is thus mainly that of the electron. The momentum of the positron–

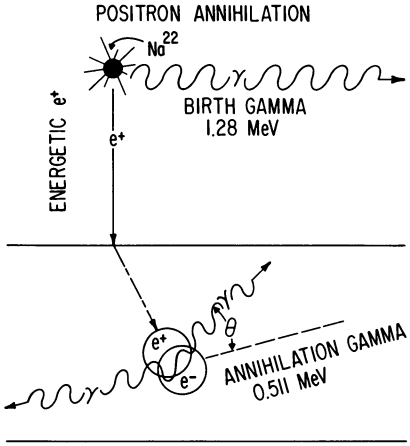

Figure 1. The positron is emitted from a ^{22}Na nucleus and penetrates several microns into the solid. Its annihilation with an electron results in the emission of two 511-keV gamma rays. The distribution of time differences between the 1.28-MeV birth gamma and 511-keV annihilation gamma is used to measure the positron lifetime. The deviation from collinearity and the Dopler shift of the two 511-keV gamma rays are related to the momentum distribution of the annihilating positron–electron pair and are used in angular-correction and Doppler-broadening experiments, respectively.

Publication Date: June 1, 1979 | doi: 10.1021/ba-1979-0175.ch011

electron pair with respect to the laboratory frame of reference causes a Doppler shift in the energy of the annihilation gamma ray. The observable manifestation of this shift is a broadening of the 511-keV line beyond that caused by the finite resolution of the gamma-ray spectrometer. Thus, the resolution of the detector is of paramount importance. Presently, the typical resolution obtained with Ge(Li) or intrinsic Ge detectors is 1–1.5 keV at 511 keV. The two annihilation gamma rays are exactly antiparallel in the center-of-mass frame. However, because the center of mass moves with respect to the laboratory frame, a small angular deviation, $\theta = p_e/mc$, between the emitted gamma rays is observed, where p_e is the momentum of the electron, m is its mass, and c is the velocity of light. A typical resolution for angular-correlation equipment is 0.2–0.5 mrad, which is adequate for most applications. As a rule of thumb, a 4-mrad geometric resolution can be thought of as being equivalent to 1 keV energy resolution. Thus, in an angular-correlation experiment one can obtain a much better resolution than with Doppler broadening. It should be kept in mind, however, that although the resolution of Ge detectors is

Publication Date: June 1, 1979 | doi: 10.1021/ba-1979-0175.ch011

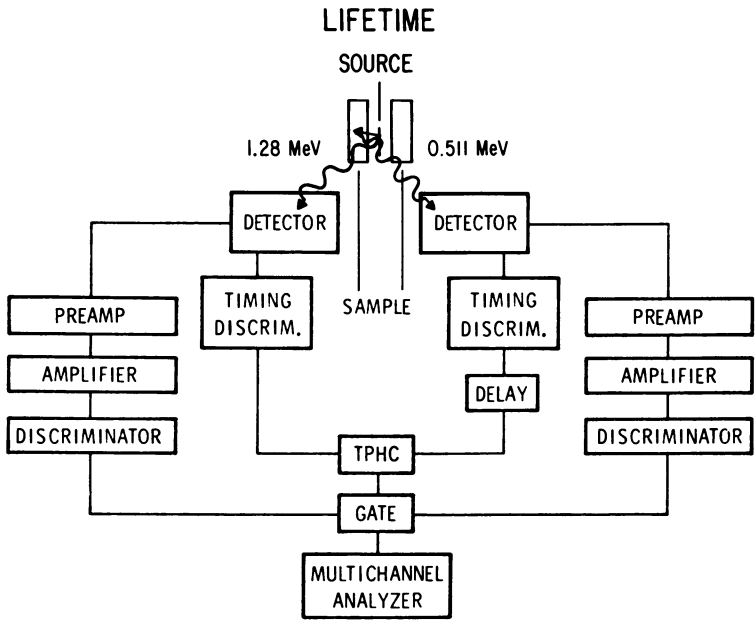

Figure 2. Schematic of a lifetime apparatus (26). Timing signals are derived from the birth and annihilation gamma rays using fast plastic scintillators coupled to suitable phototubes. These time intervals are measured with a time-to-pulse height converter (TPHC), and their distribution is stored in a multichannel analyzer. Some energy selection or gating is required to obtain suitable timing resolution. These "side-channel" discriminators are shown.

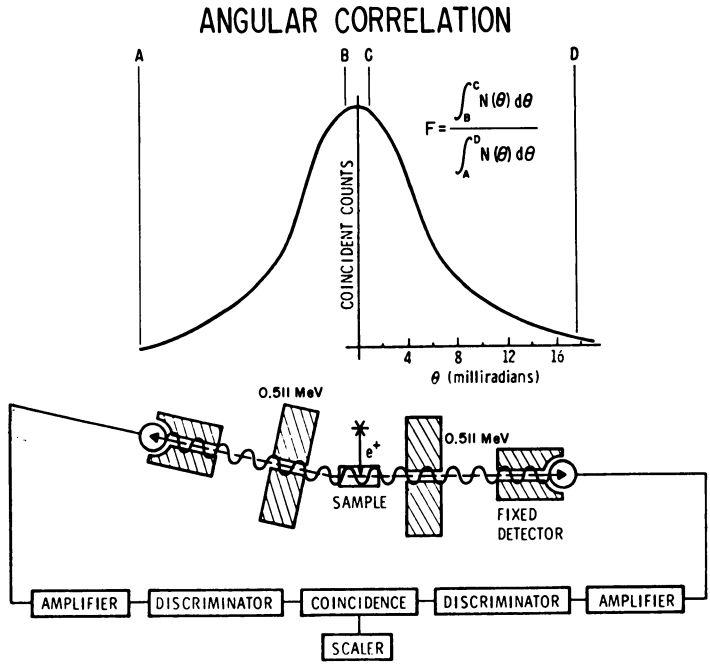

Figure 3. Schematic of angular correlation equipment (26). Lead collimators are represented as cross-hatched objects. Typical of such long parallel-slit instruments (note that the slits are perpendicular to the page) is the use of remote sources that are suitably shielded from the detectors' view. The detectors are NaI(Tl) scintillators of sufficient length to allow integration over one component of the momentum distribution. The commonly used peak-count parameter, F, is defined diagramatically in its experimental sense as the normalized peak-count rate determined by integrating a small central region under the peak.

Publication Date: June 1, 1979 | doi: 10.1021/ba-1979-0175.ch011

comparable with the effect being measured, the counting rate is very high. For angular correlation the situation is reversed to some extent. Therefore, the choice between these two methods is in no way obvious since poor resolution can often be offset by good statistics if the resolution function is known.

Defects in Metals

PAS methods have found application in equilibrium and nonequilibrium studies of defects in metals. Experiments on metals in nonequilibrium states have revealed significant qualitative information regarding complex defect systems because of the defect-specific nature of the positron toward vacancy-like sites (e.g., vacancies, vacancy clusters, voids, and dislocations). The emphasis in this area recently has been on

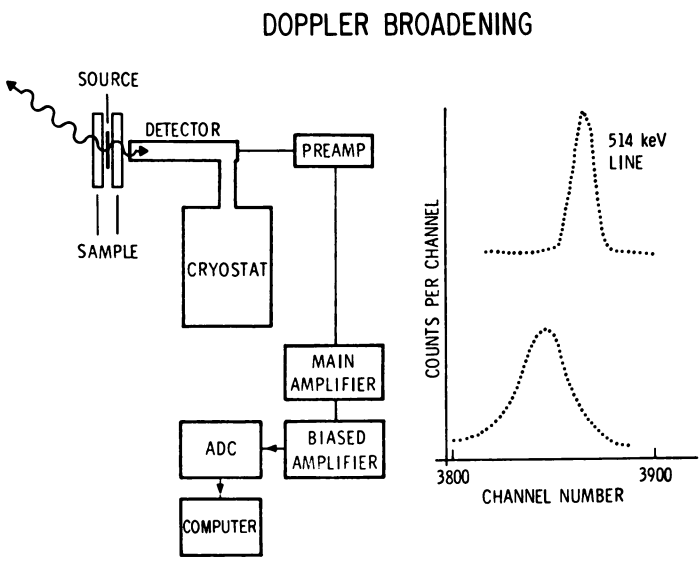

Figure 4. Schematic of a Doppler-broadening apparatus using a sandwich source (although remote sources also can be used (26)). Such equipment provides high count rates with poorer resolution than is obtained with angular-correlation instrumentation. Electronic instabilities must be monitored and removed either with online or offline techniques. Also shown is the instrumental resolution represented by the 514-keV gamma-ray line, which is compared with a 511-keV annihilation spectrum. Note that the resolution is similar in width to the Doppler-broadened data itself.

the annealing behavior of radiation damage introduced into various metals (for a bibliography and an example of such experiments *see* Ref. *26*). Particular attention has been given to the behavior of positrons in voids or aggregates of vacancies (*27–33*).

Another type of nonequilibrium experiment, which is useful in studying the propagation of the positron in metals, is the measurement of positron annihilation at a fixed ensemble of trapping centers. In this type of experiment one hopes to study the positron trapping rate per unit concentration of defect traps, μ, as a function of temperature. It is important in such experiments to demonstrate that the trapping centers remain the same in nature and concentration during the entire temperature cycle. Only a few such experiments designed to study the specific trapping rate, μ_{1v}, at monovacancies (*34, 35, 36, 37*) have been performed to date although their fundamental importance has been recognized for some time.

In the past decade considerable effort in using PAS to study defects in metals has concentrated on the quantitative determination of the

Publication Date: June 1, 1979 | doi: 10.1021/ba-1979-0175.ch011

temperature dependence of equilibrium vacancy concentrations in pure metals. The equilibrium concentration of monovacancies, in atomic fraction, as a function of temperature and pressure is given by,

$$C_{1v} = \exp[-(E_{1v}^F + PV_{1v}^F - TS_{1v}^F)/kT] \quad (1)$$

where E_{1v}^F, V_{1v}^F, and S_{1v}^F are the monovacancy formation energy, entropy, and volumes, respectively. Until recently, equilibrium experiments have focused on studies in which temperature alone was varied. For these studies the vacancy formation enthalpy, $H_{1v}^F = E_{1v}^F + PV_{1v}^F$, was measured. At atmospheric or lower pressures the term PV_{1v}^F is negligible ($<10^{-5}$ eV), and hence $H_{1v}^F \simeq E_{1v}^F$ since $H_{1v}^F \sim 1$ eV in metals. Now pressure-dependent experiments are also being carried out, and measurements of the vacancy formation volume in indium and cadmium (*38, 39*) using PAS have been reported recently.

The utility of PAS to determine the vacancy formation enthalpy depends on the fact (already mentioned) that the positron in most metals can be trapped at vacant sites with significant changes in its annihilation characteristics (*21*). At the time of thermalization the positron is expected to be found in a Bloch state, which is extended throughout the crystal. In the presence of vacancies one would expect to find the positron in an energetically favorable lower energy state, localized in a vacancy. However, this is not always the case since the relaxation time associated with this localization in a single vacancy is much greater than the positron lifetime. The transition to the localized state proceeds through the trapping process, probably governed by the golden rule (*40*), and the fraction of positrons that are trapped at vacancies depends on the concentration of vacancies. At low vacancy concentrations ($\lesssim 10^{-7}$) the positron is in an extended Bloch state while at high vacancy concentrations ($\gtrsim 10^{-4}$) it is almost always localized in the vacancy at the time of annihilation. At intermediate concentrations of vacancies the positron could be found in either the Bloch or vacancy-trapped state. It is this probability distribution and its connection to the vacancy concentration that is the basis for the application of PAS to vacancy-defect problems via the two-state trapping model.

The Trapping Model

The two-state trapping model (TSTM) is shown schematically in Figure 5 and is described by two first-order differential equations,

$$dN_b/dt = -N_b\lambda_b - N_b\kappa \quad (2a)$$

$$dN_v/dt = +N_b\kappa - N_v\lambda_v \quad (2b)$$

Publication Date: June 1, 1979 | doi: 10.1021/ba-1979-0175.ch011

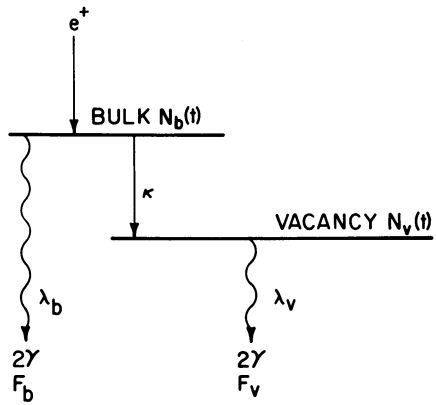

Figure 5. Positron two-state trapping model (TSTM). A positron in the bulk or Bloch state either annihilates at a rate λ_b or is trapped by vacancies at a rate κ, where it eventually annihilates at a slower rate λ_v. The corresponding peak-count parameters, F_b and F_v, for annihilations from the bulk and vacancy-trapped states are indicated.

Publication Date: June 1, 1979 | doi: 10.1021/ba-1979-0175.ch011

where N_b and N_v are the fractions of positrons in the bulk and vacancy-trapped states, respectively, and λ_b and λ_v are the two-gamma decay rates from these states. The quantity κ is the total trapping rate of the positron from the bulk to the vacancy-trapped state.

The mean lifetime of the positron can be expressed in terms of the two-gamma decay rates (*41, 42*) as,

$$\bar{\tau} = I_b \tau_b + I_v \tau_v \tag{3}$$

where $\tau_b = \lambda_b^{-1}$ and $\tau_v = \lambda_v^{-1}$ are the positron lifetimes in the bulk and vacancy-trapped states, respectively. The intensities, I_b and I_v, are the probabilities that a positron will annihilate from these respective states and are related by $I_b + I_v = 1$. Note that $I_b = \lambda_b(\lambda_b + \kappa)^{-1}$. Various shape parameters, F, are used to describe the momentum distributions observed in angular-correlation or Doppler-broadening measurements. Many of these shape parameters are expected to be a linear combination of signals from the positron annihilation in the bulk and vacancy-trapped states. This relationship is expressed by,

$$F = I_b F_b + I_v F_v \tag{4}$$

where F_b and F_v are the shape parameters that represent annihilation from the bulk and vacancy-trapped states, respectively. For example, one

such shape parameter, a peak-count parameter, F, can be defined as shown graphically in Figure 3. Clearly, Equations 3 and 4 demonstrate that mean-lifetime and line shape-parameter experiments are similar. Since both mean-lifetime and Doppler-broadening experiments describe the system by a single parameter ($\bar{\tau}$ or F), these should be distinguished from more complete lifetime experiments, in which the spectra are resolved into their components, yielding λ_b, λ_v, and κ.

The quantities F_b, F_v, λ_b, and λ_v are related to the electron–positron overlap. Clearly, these must be different for the two states if a significant change in the annihilation characteristics is to be observed experimentally as a result of positron trapping . The positron densities in the bulk or Bloch state and the vacancy-trapped state of the positron for aluminum are shown in Figures 6 and 7. The results shown were obtained from an augmented plane-wave (APW) calculation (*43, 44*). It can be seen that in the Bloch state the positron is distributed throughout the crystal, where it prefers the interstitial regions because of its repulsion from the

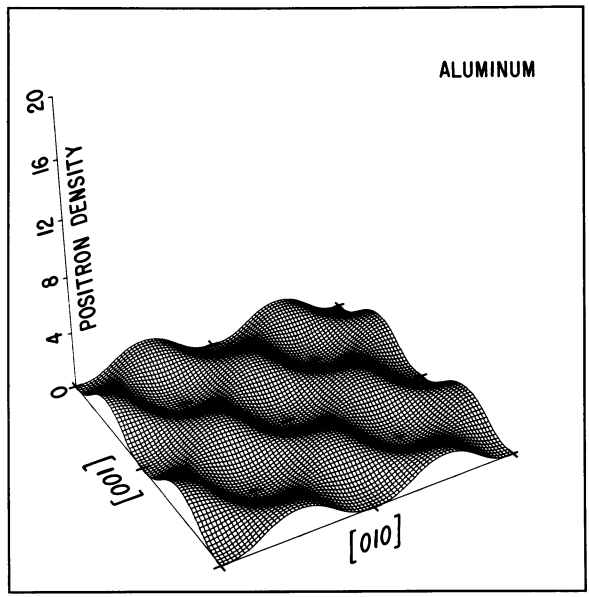

Figure 6. Spatial distribution of the positron density in the Bloch state of the positron in aluminum for the (001) plane (44). A network of only 13 atoms is represented. There are three atomic sites each along [010] and [100] axes as indicated by crosses. The repulsion of the positron by the ion cores and its accumulation in the interstitial regions is seen clearly.

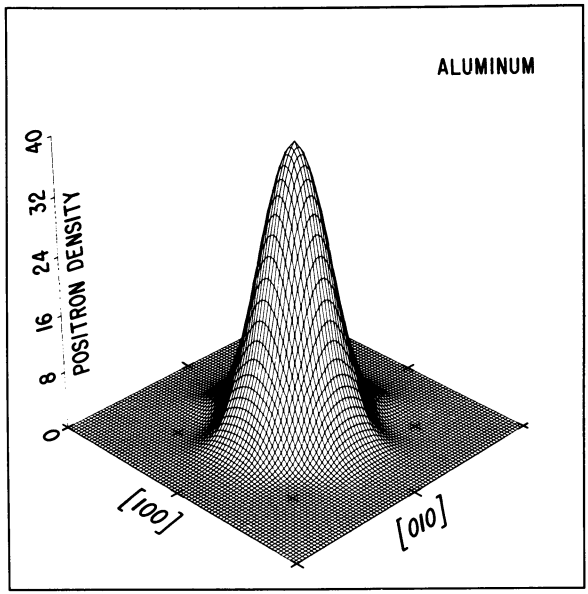

Figure 7. Spatial distribution of the positron density in the vacancy-trapped state of the positron in aluminum in the (001) plane (44). The vacancy is represented by the absence of an aluminum atom at the center of the network of atoms described in Figure 6. A large pileup or localization of the positron is evident at the vacant site. The anisotropy in the positron density arising from the presence of nearest neighbor ion cores is also visible.

Publication Date: June 1, 1979 | doi: 10.1021/ba-1979-0175.ch011

ion cores. On the other hand, the positron finds itself bound to the vacancy site, with a binding energy of about 3.3 eV and a density distribution that is highly localized. The consequences of this localization are: (1) a smaller overlap with the electrons since the electron density is relatively low in the vacancy, leading to a longer positron lifetime; and (2) an increase in the contribution to the angular-correlation or Doppler-broadening spectra from the low momentum components relative to the high momentum ones, owing to the missing ion core in the vacancy. This, in turn, gives rise to an increase in the shape parameter, F, as usually defined. Thus, both $\bar{\tau}$ and F increase with increasing positron trapping in vacancies and, hence, increasing vacancy concentration.

The quantity κ, shown in Figure 5 and entering into the rate equations (2a and 2b), is the probability per unit time that a positron will become trapped in a defect and is proportional to the defect concentration. For a sufficiently dilute concentration of monovacancies—so dilute that clusters of more than one vacancy can be neglected—one obtains

$\kappa = \mu_{1v}C_{1v}$, where μ_{1v} is the specific trapping rate per unit concentration of monovacancies and C_{1v} is the concentration of monovacancies. If μ_{1v} shows only a weak temperature dependence compared with C_{1v}, the measurement of κ as a function of temperature will, according to Equation 1, result in the determination of $H_{1v}^F(= E_{1v}^F + PV_{1v}^F)$. The accuracy to which the formation enthalpy can be determined will depend therefore not only on the experimental uncertainty in κ but also on the degree to which the temperature dependence of μ_{1v} is unknown.

The rate equations (Equations 2a and 2b) of this model are identical to the simple parent–daughter relationship found in nuclear decay, with a branching for the parent. Upon solution, these yield the familiar expression for this type of scheme, representing the fraction of positrons surviving in the system at time t,

$$N(t) = N_b(t) + N_v(t) = I_1 \exp(-\Lambda_1 t) + I_2 \exp(-\Lambda_2 t) \quad (5)$$

where $I_1 + I_2 = 1$, and the I and Λ values can be obtained from the data if the spectra are resolved into two components. Note that the measured intensities, I_1 and I_2, differ from I_b and I_v in Equations 3 and 4. Note also that resolution of a lifetime spectrum into its respective components involves deconvolution of the data. This makes the uncertainties on the I and Λ values quite large since resolution of the equipment is often of the same magnitude as the signal itself.

The physical parameters of the TSTM can be expressed directly in terms of the parameters obtained from a lifetime experiment by solving Equations 2a and 2b with the boundary conditions, $N_b(t = 0) = 1$ and $N_v(t = 0) = 0$. The relationships are

$$\lambda_b = I_1 \Lambda_1 + I_2 \Lambda_2 \quad (6a)$$

$$\lambda_v = \Lambda_2 \quad (6b)$$

$$\kappa = I_2 (\Lambda_1 - \Lambda_2). \quad (6c)$$

In contrast to Equation 6c, the determination of κ from either momentum or mean-lifetime experiments involves additional assumptions, as shown in the equations that relate κ to $\bar{\tau}$ and F, as follows:

$$\kappa\tau_b = (F - F_b)/(F_v - F) \quad (7a)$$

$$\kappa = \lambda_b(\bar{\tau} - \tau_b)/(\tau_v - \bar{\tau}). \quad (7b)$$

In the shape-parameter analysis of momentum experiments the quantity $\tau_b = \lambda_b^{-1}$ is not measured at all. The quantities F_b and F_v can be determined only at the low and high temperatures, respectively, and must be

Publication Date: June 1, 1979 | doi: 10.1021/ba-1979-0175.ch011

extrapolated to the intermediate region where a significant vacancy signal exists. A similar observation holds for the $\bar{\tau}$ analysis with regard to τ_b and τ_v; however, in this case $\tau_b = \lambda_b^{-1}$ can at least be measured at temperatures below the vacancy-sensitive region. In conclusion, since $\bar{\tau}$ or F can be measured to a very high precision, they provide a way to obtain a precise determination of κ from Equation 7b or a quantity proportional to κ from Equation 7a provided the assumptions about τ_b, F_b, and F_v are correct. Unfortunately, there is no way of knowing from these experiments themselves whether or not the assumptions are correct. On the other hand, lifetime experiments in which the spectrum is resolved into its components determine κ without any assumptions, except those of the TSTM itself, but with considerably increased uncertainty.

Publication Date: June 1, 1979 | doi: 10.1021/ba-1979-0175.ch011

Comparison of Momentum and Lifetime Experiments

An example of positron annihilation data obtained with Doppler-broadening equipment is shown in Figure 8 (45). Two cases are represented: polycrystalline copper at 435°C and at 1020°C. The first case

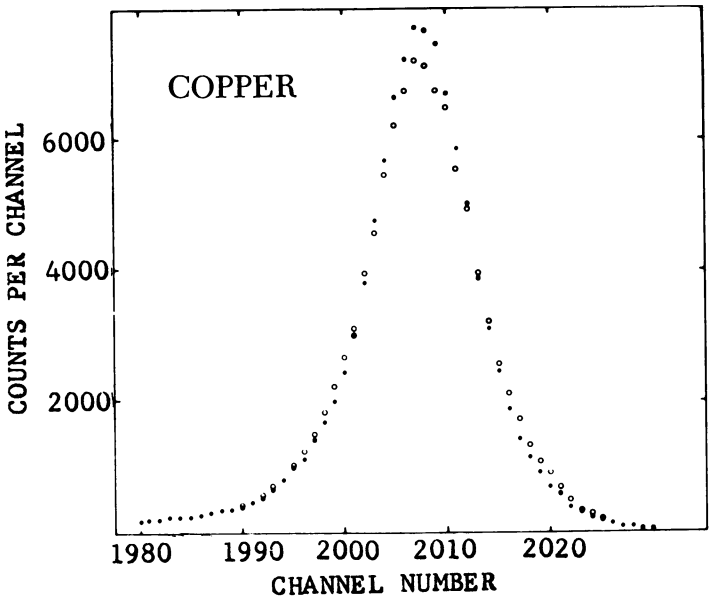

Figure 8. Positron annihilation data obtained in a Doppler-broadening experiment for copper (45). Open circles are data taken at 435°C, and closed points are data taken at 1020°C. These represent the extreme cases of no vacancy signal present and complete trapping, respectively.

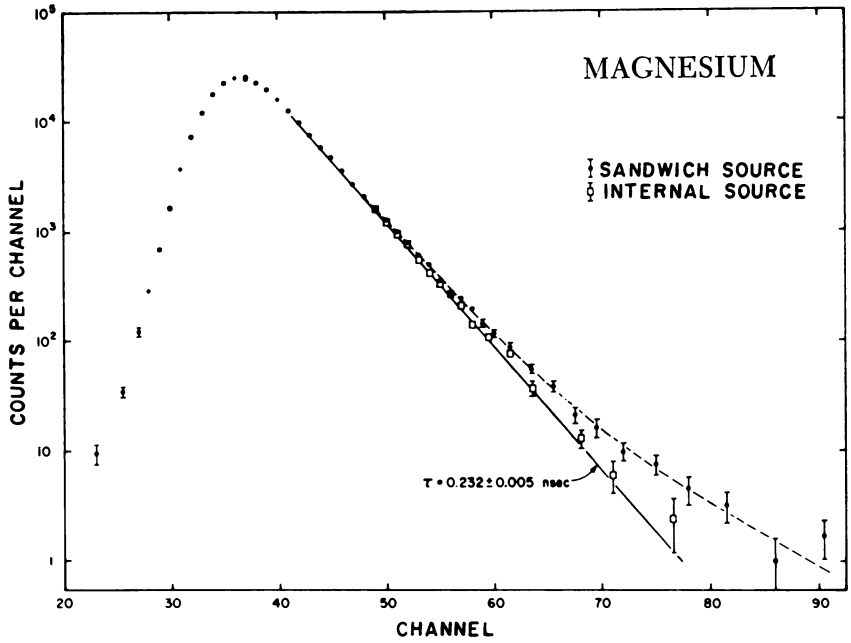

Figure 9. Lifetime spectra in magnesium with a sandwich source and an internal source produced by activation (46). The figure indicates the additional component in the spectrum attributed to the source component present with sandwich sources.

represents the type of data obtained when there are effectively too few trapping centers for which the positron can be sensitive; the second case represents the situation in which all the positrons apparently annihilate in the trapped state. Momentum measurements can be carried out with either the radioactive source of positrons in a sandwich configuration between two samples (as shown in Figures 2 and 4) or, preferably, with a remote source (as shown in Figure 3), which can avoid many questions concerning source component and sample contamination by material from the radioactive carrier.

In contrast, lifetime experiments can be carried out only with the sandwich source-sample arrangement at present since time of flight of the positron and efficiency problems prohibit the use of remote sources. Lifetime experiments are very valuable because they provide direct information about the bulk and vacancy-trapped states of the positron. Also the annihilation information from positrons in extraneous places (e.g., surfaces of the sample) can be removed from the data as long as these annihilations result in a distinctly resolvable lifetime component in the spectrum. Such a lifetime component has been identified by Weisberg and Berko

Publication Date: June 1, 1979 | doi: 10.1021/ba-1979-0175.ch011

(*46*), as shown in Figure 9. Here the lifetime spectrum obtained with an internal source produced by activation is compared with that obtained with a sandwich source. This advantage of lifetime experiments is not available to the momentum experiments, which raises a question about the effect that any possible temperature dependence of such extraneous components can have on the interpretation of momentum data.

Qualitatively, lifetime and momentum measurements do seem to respond to the change in the concentration of vacancies in strikingly similar ways. As an example of this similarity over a wide temperature range we have chosen the data of Herlach et al. (*47*) taken on gold (Figure 10). The two sets of data correspond to the Doppler-broadening wing parameter (the fractional area of selected regions in the wings of the Doppler-broadened line) and the mean lifetime, measured by observing the shift in the centroid of the lifetime spectrum (centroid-shift

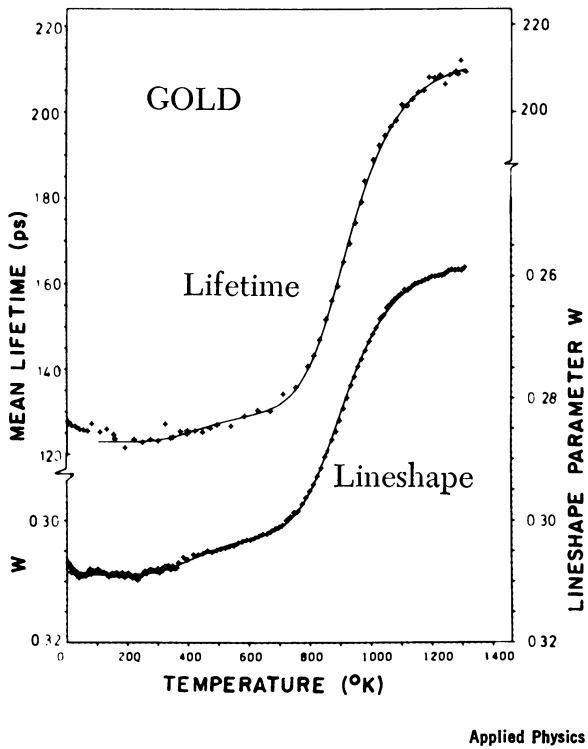

Applied Physics

Figure 10. Mean lifetime, $\bar{\tau}$, and the line shape parameter W (wing parameter) as a function of temperature for gold (47). The dominant feature of both functions is the S-shaped response to the presence of thermally generated vacancies.

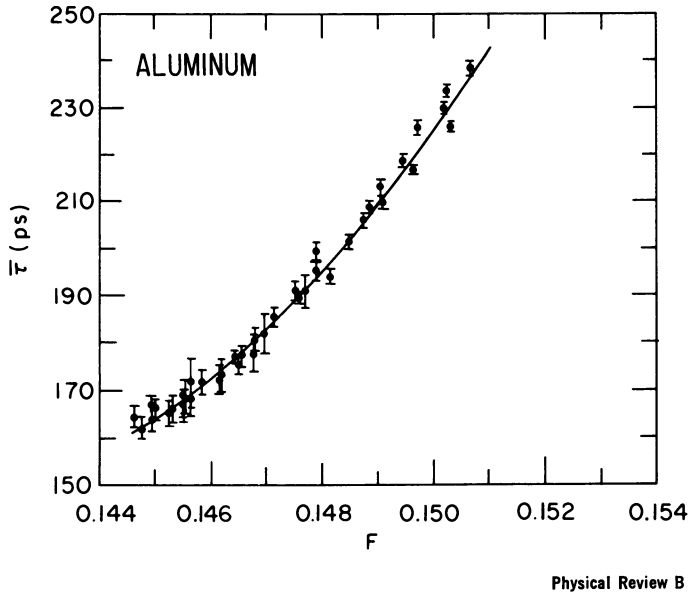

Figure 11. Mean lifetime, $\bar{\tau}$, vs. the peak-count line shape parameter, F, *from Doppler broadening for aluminum* (41). *The data shown include the temperature region in which positrons are sensitive to the presence of thermally generated vacancies.*

Publication Date: June 1, 1979 | doi: 10.1021/ba-1979-0175.ch011

method), each as a function of temperature. The vacancy-sensitive region is typified by the S-shaped behavior that dominates the higher temperature region of the curves. Even at the lower temperatures the data exhibit similar behavior. Determination of the monovacancy formation enthalpy from these data involves fitting all components of the observed curve. This means that one must have a physical understanding of the upper and lower temperature regions that surround the vacancy-sensitive region so that the vacancy response alone can be isolated from the total signal.

The two sensitivities of the positron, one to electron momenta and the other to electron density, cannot be expected a priori, to respond in the same way to the relative changes in the contributions from valence and core electrons in the bulk and vacancy-trapped states of the positron. This will result in different temperature dependences τ_b and F_b as well as τ_v and F_v. A further complexity, which also might affect a comparison between lifetime and momentum measurements, is the existence of high momentum components associated with the valence electrons themselves. This is a consequence of the delocalization of the positron and the nonuniform nature of the electron density. An experiment in which two

components of the momentum were measured for aluminum, carried out by Mader et al. (*48*), resulted in the first detailed study of these high momentum valence signals in the angular distribution.

Figure 11 shows the result of a combined study of the momentum peak-count parameter, F, and the mean lifetime, $\bar{\tau}$, calculated according to Equation 3, in aluminum (*41*). The curvature observed could be caused by the temperature dependencies of τ_b, F_b, τ_v, and F_v. However, the simple TSTM may give an inadequate description of the system investigated.

In contrast to positron lifetimes, which have a clear physical significance, various shape parameters, not always possessing such significance, have been invented to describe the changes in the momentum distribution as a function of temperature. These types of parameterizations of data have been reviewed recently in some detail by Campbell (*49*). The arguments often presented for the choice of one parameter over another are based on statistical rather than physical criteria. Statistically optimized parameters can be highly sensitive; however, comparison between different parameters (e.g., peak-count and wing parameters) can be difficult because their physical meaning is not clear.

Publication Date: June 1, 1979 | doi: 10.1021/ba-1979-0175.ch011

Prevacancy Effects

The observation with PAS of the thermally generated vacancy-trapped state is not universal for all metals (*14, 21*). For example, a metal that does not exhibit trapping is magnesium, as shown in Figure 12 (*18*). The weak temperature dependence observed here was attributed to effects from the lattice expansion with increasing temperature. However, the picture of a simple weak temperature dependence of the bulk state of the positron, depending only on thermal expansion of the lattice, was

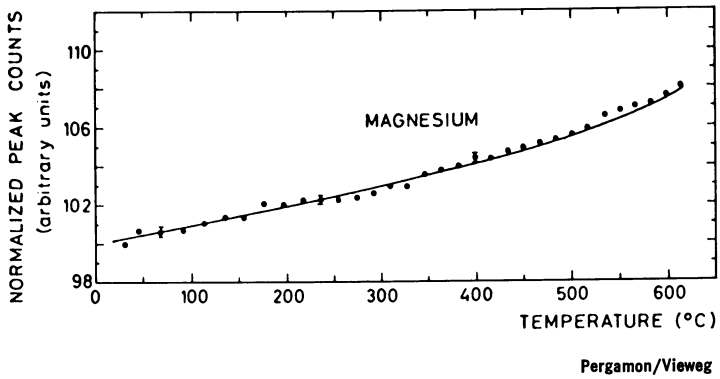

Figure 12. Normalized peak counts, F, *as a function of temperature for magnesium* (18)

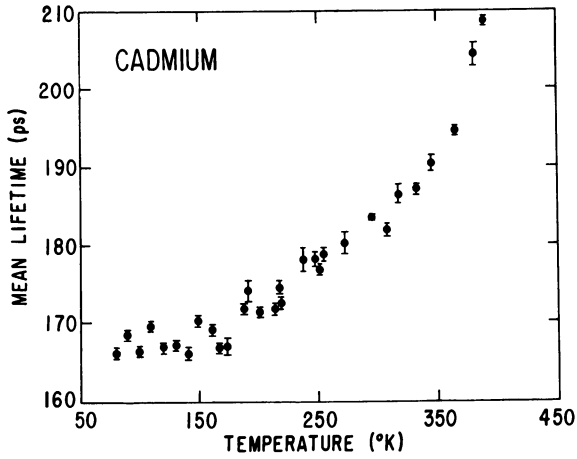

Journal of Physics F, Metal Physics

Figure 13. Positron mean lifetime, $\bar{\tau}$, as a function of temperature in cadmium (53). Note the nonlinear behavior of $\bar{\tau}$ in the prevacancy region and the start of a rapid rise of $\bar{\tau}$ in the vacancy-sensitive region above approximately 350 K.

shaken by the observation of highly nonlinear temperature dependences discovered in cadmium (*50, 51*). Confirmation of the effect reported for cadmium was obtained with both angular-correlation (*52*) and lifetime measurements (*53*) (the latter shown in Figure 13). The angular-correlation measurements on cadmium by Kim and Buyers (*52*) were interpreted as showing that the positron becomes more localized in this intermediate temperature region. The localization was established by observing the "smearing" of the momentum distribution at the Fermi edge.

The existence of a similar effect in copper, as reported by Lichtenberger (*51*), could not be confirmed in work reported by Smedskjaer et al. (*54*) and Rice-Evans et al. (*45*). In the work by Smedskjaer et al. both lifetime and Doppler-broadening experiments were reported (*see* Figure 14). The possibility of differences in the method of parameterization can be raised. However, for cadmium both the parameter used by Lichtenberger (*51*) and the peak-count parameter used by Kim and Buyers (*52*) seem to have had the same sensitivity to the prevacancy effect.

It has been reported recently (*55*) that indium exhibits a prevacancy nonlinearity even more distinct than that observed for cadmium. The results, obtained from peak-count Doppler-broadening data, show an almost plateau-like behavior. No corresponding lifetime experiments on this material have been reported in this temperature region. However, the possibility of more subtle effects regarding source components or

Publication Date: June 1, 1979 | doi: 10.1021/ba-1979-0175.ch011

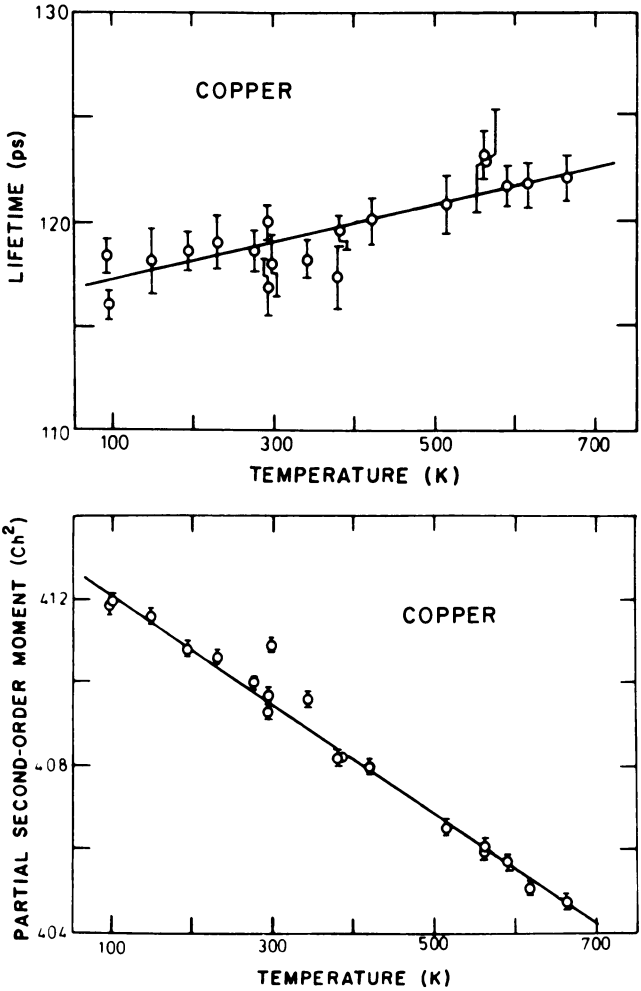

Journal of Physics F, Metal Physics

Figure 14. Top: positron lifetime in copper as a function of temperature in the prevacancy region. The data reveal a linear temperature dependence over the temperature range of the experiment. Bottom: partial second-order moment (a shape parameter) of the Doppler-broadened spectrum in copper as a function of temperature. The full curve is the linear least-squares fit that passes through the data points. Both curves are from Ref. 54.

Publication Date: June 1, 1979 | doi: 10.1021/ba-1979-0175.ch011

sample purity have now been raised by the contradictory results of Rice-Evans et al. (*56*), who observed no such nonlinearity. Recent experimental evidence indicates that in cadmium other effects that are equal to the static lattice expansion play a role in the reported anomalous behavior (*57*).

The nonlinear temperature-dependent behavior in cadmium has resulted in a search for the origin of this effect, and attempts have been made to explain it in terms of the propagation mechanism of the positron through matter. There are, of course, obvious effects expected from temperature changes. With increasing temperature the ion cores move further apart, thus reducing the overlap of the positron with the electrons of the metal. In addition, the lattice is also a dynamic structure, and the positron–electron interaction should be affected by the changing phonon spectrum of the metal with temperature. The delocalized nature of the positron thus leads to the possibility that the positron preferentially occupies the more open (dilated) regions of the lattice (*see* Refs. 58 and 59 and a number of recent papers reviewed in Ref. *60*). As an extreme example of such an effect, Seeger (*61*) has interpreted the anomalous behavior in cadmium in terms of the existence of a metastable state, in which the positron is "self-trapped" by a strong interaction with the lattice. This proposal, however, has not been universally accepted (*62, 63*).

The effect of lattice vibrations on the positron lifetime in the Bloch state, τ_b, was investigated by Tam et al. (*58, 59*), using a Debye model for the phonon spectrum, and by Stott and West (*64*), using an Einstein model. This subject has been considered most recently by Gupta et al. (*65*). In cadmium the core contribution to the total annihilation rate, $\lambda_b = \tau_b^{-1}$, is large, about 39% of λ_b (*20*). Contrast this value with a relatively small core contribution of approximately 19% of λ_b in aluminum (*20*). This large core contribution to λ_b in cadmium is expected to result in a significant change in the core contribution to λ_b from phonon interactions with both the core electrons and the positron, owing to the localized nature of the core-electron density. Larger effects from phonons for cadmium than for aluminum are indeed predicted theoretically (*58, 59, 64, 65*). Further, the phonon contributions to the positron annihilation characteristics for both lifetime and momentum measurements have been shown (*65*) to be larger than the contributions from static lattice expansion. However, when the magnitude of the contribution from phonon-coupling effects is added to that expected from lattice expansion, the resulting value still does not account fully for the magnitude of the observed temperature dependence of $\tau_b(T)$ in cadmium, although it seems to in aluminum (*65*). The effect of positron–phonon interactions on the positron lifetime in the vacancy-trapped state, on the other hand, is not

Publication Date: June 1, 1979 | doi: 10.1021/ba-1979-0175.ch011

expected to be significant, owing to the localized nature of the trapped positron and to the stabilizing influence of the positron trapped in the vacancy (*66*).

Testing the Two-State Trapping Model

Neither temperature nor pressure is an explicit variable of the trapping model. However, the parameters λ_b, λ_v, and κ that appear in the TSTM are potentially temperature and pressure dependent. Lifetime measurements in which all the component lifetimes are measured by deconvolution techniques are uniquely important because direct model-dependent information about the two states of the system is provided by such experiments. Thus, one way of partially testing the validity of the TSTM, with the assumption of single-state population at $t = 0$, is to compare the bulk lifetime obtained using Equation 6a (remembering that the I and Λ values are experimentally determined quantities) with the known or expected variations of the bulk lifetime with temperature and/or pressure.

Experiments of this type have been carried out on two metals, lead (*67*) and aluminum (*41*), under equilibrium conditions, in which significant positron trapping at vacancies was present. The results reported for lead indicated a possible temperature dependence for the bulk lifetime beyond that expected from simple linear extrapolation from low temperatures. Subsequent measurements at the same laboratory have, however, indicated that the magnitude of this observation is sensitive to some experimental uncertainties, one of which is the nature of the source component (*68*). A better established temperature dependence was determined for the bulk lifetime in aluminum (Figure 15). In this case the uncertainty limits for this effect, arising from the uncertainty in the instrumental resolution function, were determined. Even very large estimates of this uncertainty (shown in Figure 15) could not remove the anomalously large temperature dependence of the bulk lifetime. However, it is not clear whether or not the deduced bulk-lifetime temperature dependence in lead and/or aluminum is real or whether or not the TSTM, its assumptions, or the analyses based on it are just too simple. The possibility has been raised that the trapping model could be modified to include a finite slowing-down time of the positron (*69*), during which trapping in vacancies is enhanced; this might explain such an effect. Further work is needed to answer the questions raised by these experiments in lead and aluminum.

In their different analyses (*41, 67*) the two groups of workers also extracted the temperature dependence of the vacancy-trapped positron lifetime, τ_v. These results are shown in Figures 16 and 17 for lead and

Publication Date: June 1, 1979 | doi: 10.1021/ba-1979-0175.ch011

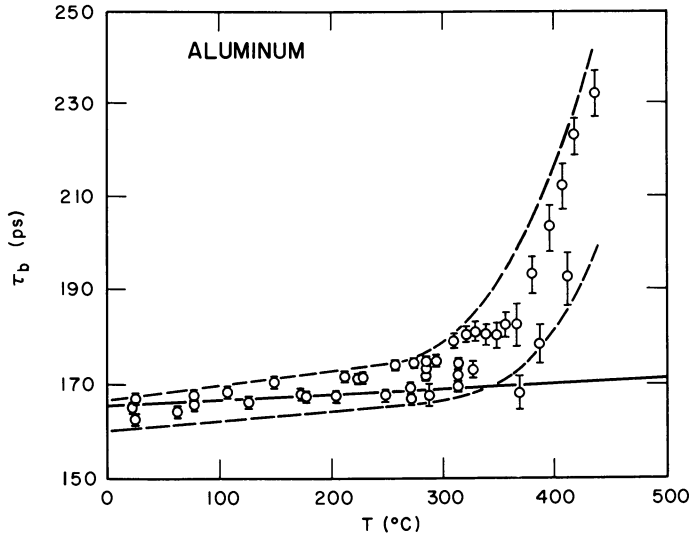

Physical Review B

Figure 15. Bulk lifetime, τ_b, vs. temperature T, *for aluminum* (41). *The points and their error bars were obtained using the most likely resolution function. (– – –), Smoothed fits to the same data using extreme estimates of the uncertainty in the resolution function. (——), The temperature dependence obtained from the APW calculations of Ref.* 43 *on the basis of lattice expansion alone.*

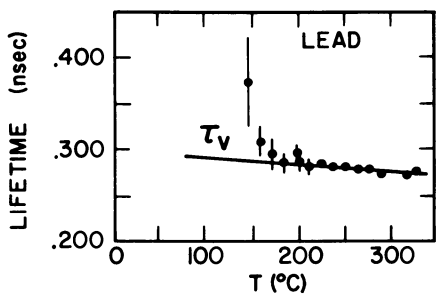

Physics Letters

Figure 16. Measured temperature dependence of the vacancy-trapped positron lifetime τ_v for lead (69): *(——), the negative temperature dependence of τ_v according to Ref.* 69.

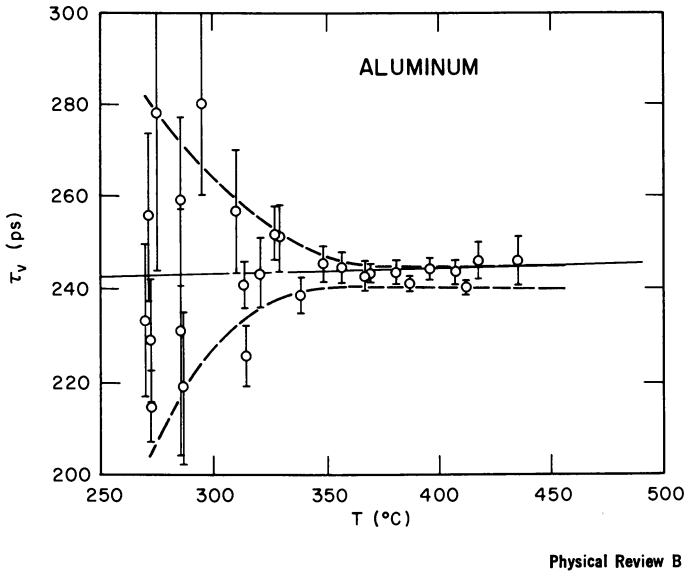

Figure 17. Positron lifetime in the vacancy-trapped state, τ_v, for aluminum vs. temperature, T (41).
Description of the points and the (– – –) are the same as for Figure 15. (——), shows the temperature dependence obtained from APW calculations of Ref. 43 on the basis of lattice expansion alone.

aluminum, respectively. For aluminum the temperature dependence of τ_v is very weak. The data for lead, however, show a significant negative temperature dependence for τ_v, possibly attributable to the greater lattice relaxation around the vacancy in lead than in aluminum, and/or to expected differences in anharmonic effects (*47*).

Gupta and Siegel (*43, 44*) investigated the change in the positron lifetime associated only with the static volume expansion of the lattice in aluminum 250°–650°C. The fractional increase in the positron lifetime, both in the Bloch state and the vacancy-trapped state, was slower than expected from the fractional volume change ($\Delta V/V$) caused by thermal expansion alone. The increase was linear and was about 75% of ($\Delta V/V$) for the Bloch state of the positron and approximately 50% of ($\Delta V/V$) for the trapped state. The results of these calculations are compared with the experimental data shown in Figures 15 and 17. The calculated variation of τ_v with temperature is seen to be consistent with the experimental measurements of the vacancy-trapped positron lifetime in aluminum. In addition, the variation in τ_b from lattice expansion when combined with the change caused by positron–phonon coupling (*66*) is in quite good agreement with the temperature dependence measured experimentally below 370°C in aluminum (*41*).

Publication Date: June 1, 1979 | doi: 10.1021/ba-1979-0175.ch011

The Trapping Rate

As mentioned above, using the assumption that $\kappa = \mu_{1v}C_{1v}$, it is possible to deduce the monovacancy formation enthalpy directly from the temperature dependence of κ. Arrhenius plots of ln (κ/λ_b) vs. T^{-1} obtained from peak-counting angular-correlation data (*70*) are shown, as an example, in Figure 18. Although these plots exhibit straight-line behavior, this result is not tacit proof (however desirable) that their slopes necessarily yield accurate values of H_{1v}^F for the metals indicated. Inherent in these and similar plots of PAS data, which are derived with assumptions regarding the temperature dependences of F_b and F_v, are often additional assumptions about the temperature independence of τ_b and μ_{1v} (*see* Equation 7a). Specific experiments designed to measure the temperature dependences of these parameters are required.

Apart from the possible temperature dependences of τ_b, τ_v, F_b, and F_v, that of μ_{1v} must also be considered. Three models have been proposed for the temperature dependence of μ_{1v}: (1) a $T^{-\frac{1}{2}}$ dependence based on a diffusing positron scattered by phonons (*71*), (2) a T^0 dependence based on the assumption that the positron behaves in a fully quantum-mechanical manner (*72*), and (3) a $T^{\frac{1}{2}}$ dependence based on the idea that the positron encounters vacancies at a rate that is related to its classical velocity (*73*). For a review of these models *see* the paper by Bergersen and Taylor (*74*). On the basis of quantum-mechanical models McMullen

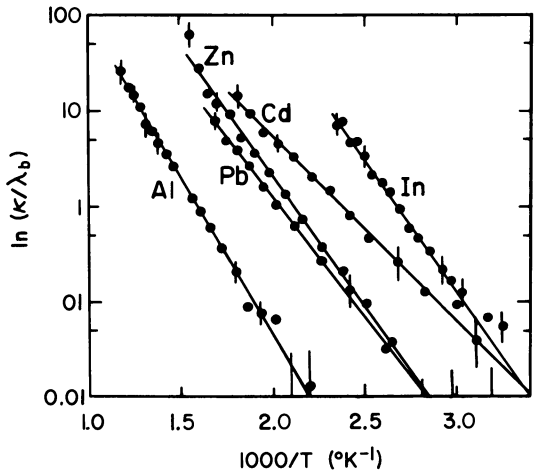

Figure 18. Arrhenius plots of (κ/λ_b) for five metals (70) deduced from peak-counting angular-correlation experiments. The slope of a line corresponds to the vacancy formation enthalpy if μ_{1v} and λ_b are temperature independent.

(*75*) has shown that μ_{1v} is temperature independent both for freely propagating (no scattering from phonons) and diffusing (scattered from phonons) positrons. This conclusion is valid for the case of monovacancies, regardless of the strength of the trap within reasonable limits (*75*).

Experiments that can differentiate between these proposed temperature dependences are difficult to perform. McKee et al. (*35*) performed an experiment on quenched gold samples and interpreted their results as supporting a T^0 dependence. Some doubt, however, has been raised about the validity of this experiment since the vacancy clusters could have dominated the positron trapping in their samples (*34*). In contrast, the work of Hall et al. (*34*), also for quenched-in vacancies in gold, suggests a positive temperature dependence for μ_{1v} at $T^{\frac{1}{2}}$–T^1. The temperature dependence of μ_{1v} seems to be an unsettled question. Fortunately, however, the theoretically suggested temperature dependences are all weak in comparison with the exponential temperature dependence of C_{1v}. Thus, as discussed below, neglect of any temperature dependence in μ_{1v} for the present is likely to have only a small effect on the determination of H_{1v}^F in metals by PAS.

Publication Date: June 1, 1979 | doi: 10.1021/ba-1979-0175.ch011

Vacancy Formation Enthalpy

The annihilation behavior of the positron in a metal is sensitive to a number of temperature effects. The problem considered here is: to what extent do the various temperature-dependent effects and uncertainties regarding them affect our ability to deduce vacancy formation enthalpies with an accuracy approaching that of the statistical precision (about 1%) of current PAS experiments. The prevacancy effects, the uncertainty in the temperature dependence of μ_{1v}, and the anomalous behavior observed in the bulk lifetimes in lead and aluminum each contribute to this problem to a greater or lesser degree. Further, the temperature-dependent effects associated with lattice expansion and phonon coupling of the positron enter this problem through the temperature-dependent behavior of the parameters τ_b, τ_v, F_b, and F_v in different ways, depending on whether one is performing lifetime or momentum (angular-correlation or Doppler-broadening) experiments.

Dramatic changes in the propagation mechanism of the positron in the same temperature region where vacancy sensitivity is observed could certainly be important to the validity of such experiments. Whether or not the observed prevacancy effects in indium and cadmium indicate that such a problem exists is still an open question. However, detailed theoretical considerations of this topic tend to indicate that although self-trapping is a possible mechanism, it is unlikely for most metals, including cadmium and indium (*62, 63*).

The effect of the temperature dependence of the positron trapping rate at monovacancies, while remaining an open question, can be investigated from the pragmatic viewpoint of establishing the sensitivity of the deduced vacancy formation enthalpy to the range of proposed temperature dependences of μ_{1v}. Hall et al. (*76*) estimated this effect for their data in aluminum and gold, measured with a lifetime technique. An uncertainty of approximately 5% in H_{1v}^F for gold could be assigned to the range of likely temperature dependences for μ_{1v}. Herlach et al. (*47*) found that their value for H_{1v}^F in gold would be increased by about 4% if a temperature dependence of $\mu_{1v} \propto T^{-\frac{1}{2}}$ were assumed instead of a constant μ_{1v}. For aluminum, the data of Fluss et al. (*41*) indicate that a variation of 3% in H_{1v}^F could be attributed to these two choices. Thus, the effects on H_{1v}^F are small.

The anomalously strong temperature dependence of the bulk lifetime of the positron observed in aluminum and lead (*41, 67*) raises serious questions concerning the TSTM and its related assumptions (discussed above). The data obtained at the highest temperatures in aluminum, where there is a dramatic change in the apparent bulk lifetime, do not contribute significantly to the determination of the vacancy formation enthalpy. This point is discussed in Ref. *41* by a comparison of H_{1v}^F values obtained by various PAS methods. Clearly, this high temperature data region can also be avoided, as it was in Ref. *41*, at least until this problem is understood. Even if, as suggested by Warburton and Shulman (*69*), a prethermalization-enhanced trapping were invoked to explain this problem, the deduced value of H_{1v}^F for the case of lead would be affected by 4% at most, assuming a thermalization of 20 psec (*69*).

The temperature dependencies of the bulk and vacancy-trapped state lifetimes are inherently taken into account by the application of Equation 6c. Lifetime experiments using Equation 6c involve the minimum number of model (TSTM) assumptions because the temperature dependences of τ_b and τ_v are implicitly included in the analysis. On the other hand, shape-parameter analyses involve curve fitting. Thus, it is not surprising that for indium significantly different results were obtained for H_{1v}^F when the prevacancy effect observed in Ref. *55* was not found by Rice-Evans et al. (*56*). In the prior case (*55*) a value of $H_{1v}^F = 0.48$ eV was reported while for the latter (*54*) $H_{1v}^F = 0.59$ eV was found, a difference of 20%. For a more representative case, Rice-Evans et al. (*45*) investigated the consequences of the various curve-fitting assumptions regarding F_b and F_v as applied to Doppler-broadening measurements in copper, in which no prevacancy effect was observed by the authors. For the range of common assumptions about temperature dependences, the deduced monovacancy formation enthalpy varied from 1.32 to 1.26 eV, a range of only 5%.

Publication Date: June 1, 1979 | doi: 10.1021/ba-1979-0175.ch011

Summary

Positron annihilation spectroscopy (PAS) has been established as a useful new technique for studying defects in metals under equilibrium and nonequilibrium conditions. Various special methods now have been developed for applying PAS momentum and lifetime measurements to such studies although lifetime measurements are somewhat more well defined with respect to the two-state trapping model. A period has apparently been reached in the development of PAS when more detailed physical understanding of the positron in metals would be helpful in making PAS as accurate as it can be precise. Improvements in experimental and data analysis methods should lead to further testing of many of the analysis assumptions. For the present, experimental uncertainties exist, but they tend to be outweighed by physical uncertainties arising from our lack of complete understanding of the various temperature-dependent effects to which the positron is sensitive. A practical consequence of these uncertainties is a present limitation of 3–5%, under favorable circumstances, on the accuracy of PAS determinations of vacancy formation enthalpies in metals.

Publication Date: June 1, 1979 | doi: 10.1021/ba-1979-0175.ch011

Literature Cited

1. Mohorovicic, S., *Astr. Nachr.* (1934) **253**, 94.
2. Ruark, A. E., *Phys. Rev.* (1945) **68**, 278.
3. Deutsch, M., *Phys. Rev.* (1951) **82**, 455.
4. Brandt, W., Coussot, G., Paulin, R., *Phys. Rev. Lett.* (1969) **23**, 522.
5. Greenberger, A., Mills, A. P., Thompson, A., Berko, S., *Phys. Lett.* (1970) **32A**, 72.
6. Mogensen, O. E., Kvajic, G., Eldrup, M., Milosevic-Kvajic, M., *Phys. Rev.* (1971) **B4**, 71.
7. Canter, K. F., Mills, A. P., Jr., Berko, S., *Phys. Rev. Lett.* (1974) **33**, 7.
8. Brandt, W., ADV. CHEM. SER. (1976) **158.**
9. Brandt, W., "Positron Annihilation," A. T. Stewart and L. O. Roellig, Eds., p. 155, Academic Press, New York, 1967.
10. Bergersen, B., Stott, M. J., *Solid State Commun.* (1969) **7**, 1203.
11. Conners, D. C., West, R. N., *Phys. Lett.* (1969) **30A**, 24.
12. MacKenzie, I. K., Khoo, T. L., McDonald, A. B., McKee, B. T. A., *Phys. Rev. Lett.* (1967) **19**, 946.
13. Berko, S., Erskine, J. C., *Phys. Rev. Lett.* (1967) **16**, 471.
14. Seeger, A., *Crystal Lattice Defects* (1973) **4**, 221.
15. Seeger, A., *J. Phys. F, Metal Phys.* (1973) **3**, 248.
16. Doyama, M., Hasiguti, R. R., *Crystal Lattice Defects* (1973) **3**, 139.
17. Seeger, A., *Appl. Phys.* (1974) **4**, 183.
18. Triftshäuser, W., "Festkörperprobleme" ("Advances in Solid State Physics"), H. J. Queisser, Ed., Vol. XV, p. 381, Pergamon/Vieweg, Braunschweig, 1975.
19. Dekhtyar, I. Ya., *Phys. Rep.* (1974) **9**, 243.
20. West, R. N., *Adv. Phys.* (1973) **22**, 263.
21. Siegel, R. W., *J. Nucl. Mater.* (1978) **69, 70**, 117.
22. Smedskjaer, L. C., Fluss, M. J., *Int. Conf. Positron Annihilation, 4th, Helsingør, Denmark, 1976*, paper H9.

23. Fluss, M. J., Smedskjaer, L. C., *Int. Conf. Positron Annihilation, 4th, Helsingør, Denmark, 1976*, paper H10.
24. Perkins, A., Carbotte, J. P., *Phys. Rev. B* (1970) **1**, 101.
25. Kubica, P., Stewart, A. T., *Phys. Rev. Lett.* (1975) **34**, 852.
26. Gauster, W. B., *J. Vac. Sci. Technol.* (1978) **15**, 688.
27. Mogensen, O., Petersen, K., Cotterill, R. M. J., Hudson, B., *Nature (London)* (1972) **239**, 98.
28. Cotterill, R. M. J., MacKenzie, I. K., Smedskjaer, L., Trumpy, G., Träff, J. H. D. L., *Nature (London)* (1972) **239**, 99.
29. Hodges, C. H., Stott, M. J., *Solid State Commun.* (1973) **12**, 1153.
30. Nieminen, R., Manninen, M., *Solid State Commun.* (1974) **15**, 403.
31. Eldrup, M., Mogensen, O. E., Evans, J. H., *J. Phys. F., Metal Phys.* (1976) **6**, 497.
32. Hautojärvi, P., Heinio, J., Manninen, M., Nieminen, R., *Phil. Mag.* (1977) **35**, 973.
33. Gauster, W. B., *J. Nucl. Mater.* (1976) **62**, 118.
34. Hall, T. M., Goland, A. N., Jain, K. C., Siegel, R. W., *Phys. Rev. B* (1975) **12**, 1613.
35. McKee, B. T. A., Jamieson, H. C., Stewart, A. T., *Phys. Rev. Lett.* (1973) **31**, 634.
36. Conners, D. C., Crisp, V. H. C., West, R. N., *Phys. Lett. A* (1971) **33**, 180.
37. Conners, D. C., Crisp, V. H. C., West, R. N., *J. Phys. F, Metal Phys.* (1971) **1**, 355.
38. Dickman, J. E., Jeffery, R. N., Gustafson, D. R., *Phys. Rev. B* (1977) **16**, 3334.
39. Dickman, J. E., Jeffery, R. N., Gustafson, D. R., *J. Nucl. Mater.* (1978) **69, 70**, 604.
40. Hodges, C. H., *Phys. Rev. Lett.* (1970) **25**, 284.
41. Fluss, M. J., Smedskjaer, L. C., Chason, M. K., Legnini, D. G., Siegel, R. W., *Phys. Rev. B* (1978) **17** ,3444.
42. Fluss, M. J., Smedskjaer, L. C., Chason, M. K., Legnini, D. G., Seigel, R. W., *J. Nucl. Mater.* (1978) **69, 70**, 586.
43. Gupta, R. P., Siegel, R. W., *Phys. Rev. Lett.* (1977) **39**, 1212.
44. Gupta, R. P., Siegel, R. W., unpublished data.
45. Rice-Evans, P., Hlaing, T. C., Rees, D. B., *J. Phys. F, Metal Phys.* (1976) **6**, 1079.
46. Weisberg, H., Berko, S., *Phys. Rev.* (1967) **154**, 249.
47. Herlach, D., Stoll, H., Trost, W., Metz, H., Jackman, T. E., Maier, K., Shaefer, H. E., Seeger, A., *Appl. Phys.* (1977) **12**, 59.
48. Mader, J. J., Berko, S., Krakauer, H., Bansil, A., *Phys. Rev. Lett.* (1976) **37**, 1232.
49. Campbell, J. L., *Appl. Phys.* (1977) **13**, 367.
50. Lichtenberger, P. C., Schulte, C. W., MacKenzie, I. K., *Appl. Phys.* (1975) **6**, 305.
51. Lichtenberger, P. C., Ph.D. thesis, University of Waterloo, Ontario, 1974.
52. Kim, S. M., Buyers, W. J. L., *J. Phys. F, Metal Phys.* (1976) **6**, L67.
53. Smedskjaer, L. C., Fluss, M. J., Chason, M. K., Legnini, D. G., Siegel, R. W., *J. Phys. F, Metal Phys.* (1977) **7**, 1261.
54. Smedskjaer, L. C., Fluss, M. J., Legnini, D. G., Chason, M. K., Siegel, R. W., *J. Phys. F, Metal Phys.* (1977) **7**, 1715.
55. Segers, D., Dorikens-Vanpraet, L., Dorikens, M., *Appl. Phys.* (1977) **13**, 51.
56. Rice-Evans, P., Hlaing, T., Chalgar, I., *Phys. Lett.* (1977) **60A**, 368.
57. McGervey, J., Sen, P., MacKenzie, I. K., McMullen, T., *J. Phys. F, Metal Phys.* (1977) **7**, 2255.

58. Tam, S. W., Sinha, S. K., Siegel, R. W., *Bull. Am. Phys. Soc.* (1977) **22,** 440.
59. Tam, S. W., Sinha, S. K., Siegel, R. W., *J. Nucl. Mater.* (1978) **69, 70,** 596.
60. Nieminen, R. M., Manninen, M., "Positrons in Solids," Chap. IV, "Topics in Current Physics," P. Hautojärvi, Ed., Springer-Verlag, Berlin, 1979.
61. Seeger, A., *Appl. Phys.* (1975) **7,** 85.
62. Leung, C. H., McMullen, T., Stott, M. J., *J. Phys. F, Metal Phys.* (1976) **6,** 1063.
63. Hodges, C. H., Trinkaus, H., *Solid State Commun.* (1976) **18,** 857.
64. Stott, M. J., West, R. N., *J. Phys. F, Metal Phys.* (1978) **8,** 635.
65. Gupta, R. P., Fluss, M. J., Siegel, R. W., unpublished data.
66. Tam, S. W., Siegel, R. W., *J. Phys. F, Metal Phys.* (1977) **7,** 877.
67. Sharma, S. C., Berko, S., Warburton, W. K., *Phys. Lett.* (1976) **58A,** 405.
68. Berko, S., private communication.
69. Warburton, W. K., Shulman, M. A., *Phys. Lett.* (1977) **60A,** 448.
70. McKee, B. T. A., Triftshäuser, W., Stewart, A. T., *Phys. Rev. Lett.* (1971) **28,** 358.
71. Seeger, A., *Phys. Lett.* (1972) **40A,** 135.
72. Hodges, C. H., *Phys. Rev. Lett.* (1970) **25,** 284.
73. Connors, D. C., West, R. N., *Phys. Lett.* (1969) **30A,** 24.
74. Bergersen, B., Taylor, D. W., *Can. J. Phys.* (1974) **52,** 1594.
75. McMullen, T., *J. Phys. F, Metal Phys.* (1977) **1,** 2041.
76. Hall, T. M., Goland, A. N., Snead, C. L., Jr., *Phys. Rev. B* (1974) **10,** 3062.

RECEIVED March 20, 1978. Work supported by the U.S. Department of Energy.

ANNPEAK: A Program for Lineshape Analysis of Doppler Broadening of Positron Annihilation Photons

JAMES J. KELLY and RICHARD M. LAMBRECHT[1]

Chemistry Department, Brookhaven National Laboratory, Upton, NY 11973

Publication Date: June 1, 1979 | doi: 10.1021/ba-1979-0175.ch012

A flexible program for the lineshape analysis of Doppler broadend spectra of positron annihilation photons was developed to calculate the lineshape parameters Q, W, L, FWHM, μ, and $\sigma_2{}^M$ from a normalized annihilation spectrum. An improved linear selection method was used to limit lineshape dependence on the background correction. This program was used to analyze the Doppler broadened annihilation spectra obtained with a spectrometer using two-point digital stabilization. Nuclear lines of ^{133}Ba and ^{207}Bi were used for energy calibration purposes. The program described has convenient options for optimization and output of data.

Positron annihilation spectroscopy (PAS) is becoming widely used in applied and fundamental studies in chemical physics, applied physics, materials science, and energy-related research (For a comprehensive bibliography of the field, *see* Ref. *1*). The Doppler broadening of positron annihilation photons with high-resolution Ge(Li) detectors is now gaining acceptance, though its use has been advocated strongly for several years (*2*). The methods of lineshape analysis are often unique to a given investigator and are generally semi-empirical (*2–11*). We have incorporated a variety of the lineshape parameters that have been used previously into an analytical routine called ANNPEAK. Our experience with this program and the instrumentation used to develop it is described.

[1] Person to whom inquiries should be addressed.

0-8412-0417-9/79/33-175-271$05.00/1

Doppler broadened lineshapes can be approximately represented as a distribution comprised of the convolution of the instrumental resolution function and the superposition of an inverted parabola and a Gaussian. The difference between positron(ium) annihilation with low momentum conduction electrons (inverted parabola) and high momentum conduction electrons are extracted by a measurement of the differences between the extremes. Figure 1 illustrates a sample normalized spectrum and depicts the arbitrary channel boundaries used for the determination of the lineshape parameters denoted by the letters *Q*, *W*, and *L*, and the full width at halfmax (FWHM). The regions of maxi-

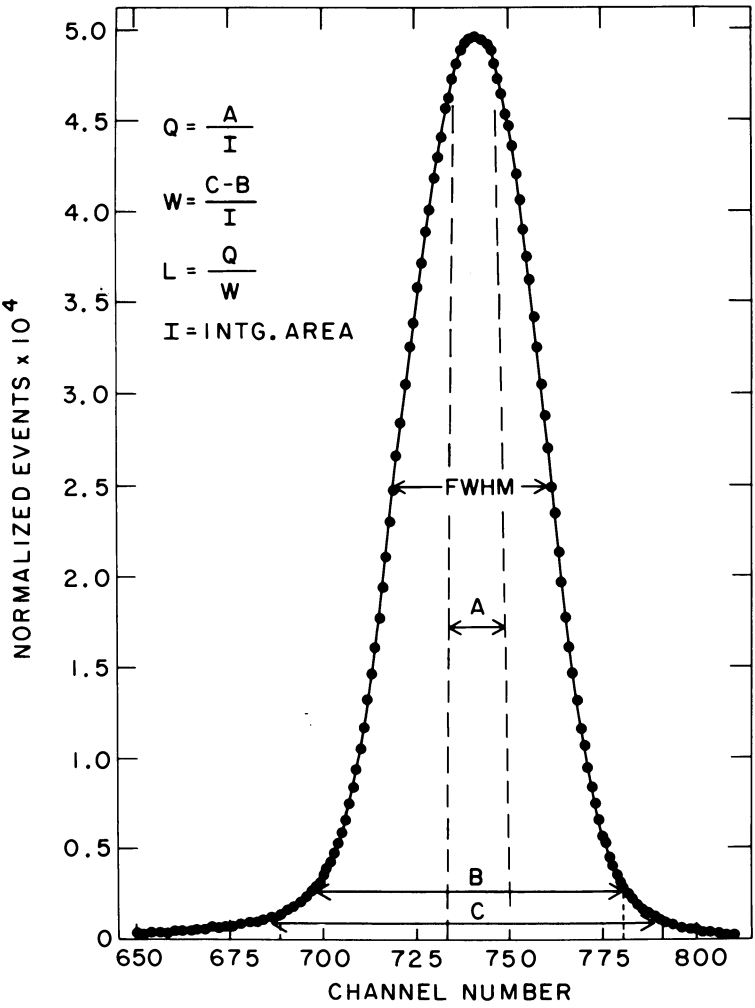

Figure 1. Definition of lineshape parameters for Doppler broadened annihilation photons

Publication Date: June 1, 1979 | doi: 10.1021/ba-1979-0175.ch012

mum change in the normalized spectra are in the area (A) of the narrow central region and in the areas of the wings associated with the broadest part of the distribution. Q is the ratio of the area (A), the sum N_i of events, in the central region of thepeak divided by the integral area (I) in the complete normalized spectrum. W is sensitive to changes in the fraction of annihilation events occurring with high momentum electrons (C–B) divided by (I) in the spectrum. C and B are chosen to be symmetrical regions of the wings of either side of the central region to the area of the spectrum. The definition of Q is identical to MacKenzie's (*2*) definition of S. However, the notation S has not been consistently used to denote a value identical to the L parameter (*11*).

The selection of the channel boundaries for A, B, and C are selected arbitrarily to enhance changes in Q, W, or L. To a rough approximation, Q is a reflection of annihilation with conduction electrons, whereas W is a reflection of annihilation with core electrons. L can be related to the ratio of conduction-to-core electrons ($L = Q/W$) provided the boundaries of A, B, and C are selected properly.

The centroid (μ) and the variance, i.e., second moment (σ_2^M) are calculated by

$$\mu = I^{-1}(\sum_i iN_i) \text{ and } \sigma_M^2 = I^{-1}(\sum_i (i - \mu)^2 N_i)$$

where I is the area of the spectrum and N_i represents the number of detected events in channel i of the annihilation spectrum. The total energy of the annihilating system can be calculated from μ; whereas σ_M^2 is an indicator of the shape of the spectrum. Campbell (*7*) has discussed the statistical properties of four lineshape parameters.

The purpose of this chapter is to make the data reduction routine available to other workers in the field and to facilitate increased uniformity in the manner in which lineshape parameters for the Doppler broadening of positron annihilation photons are reported (Singru, Lal, Tao, and Lambrecht have tabulated Doppler broadening results which have appeared in the 1949–1975 literature) (*11*).

Experimental

Spectra were collected with a PGT intrinsic Ge detector having a resolution of 1.098 keV for the 511.865 keV nuclear line of ^{106}Ru. A Canberra spectroscopy amplifier (2010) and a Northern Scientific (NS 720A) 4096 channel pulse height analyzer equipped with a two-point digital stabilizer (NS-454) were operated at a dispersion of approximately 63 eV channel^{-1}. Our approach has been to stabilize on nuclear lines rather than on a pulser, and to avoid gain stabilization on the 511-keV annihilation peak. In our experiments, zero stabilization was performed on the 356.005-keV line of ^{133}Ba and gain stabilization was performed on the 569.670-keV

Publication Date: June 1, 1979 | doi: 10.1021/ba-1979-0175.ch012

line of ^{207}Bi. The background from ^{133}Ba and ^{207}Bi in the region of annihilation photopeak is low and linear. We are cautious of using ^{97}Ru (497 keV) for gain stabilization because of its proximity to the annihilation photopeak, and the distortion it can introduce on lineshape analysis of the 511-keV photopeak.

A linear calibration of each recorded spectrum is obtained by use of the 356.005 and 383.851-keV photons of ^{133}Ba and the 569.670-keV photons of ^{207}Bi. These nuclides are useful because of their suitability for two-point stabilization and for use in establishing the energy calibration of each spectrum. ANNPEAK can handle an arbitrary number of calibration and stabilization reference peaks. The dispersion of the system has proved stable to three parts in 10^5, when the laboratory temperature was monitored at 22° ± 1°C.

We observed that for the large total count rate, the apparent lineshape of the annihilation photopeak was sensitive to count rate, but that for low total count rate it was essentially independent of count rate. This is an important consideration. The calibration was independent of the low count rate maintained in the references. The multichannel analyzer (MCA) was interfaced to an NS-708F control unit, and the data was recorded automatically by a Wang Co. Mod 7/8 magnetic tape drive. The tapes were subsequently reduced on a CDC 7600 computer by ANNPEAK, using the tape reading routines provided.

Publication Date: June 1, 1979 | doi: 10.1021/ba-1979-0175.ch012

Results and Discussion

The background substraction problem for solid-state detectors has been a subject of considerable discussion (*see* for example Refs. 3–10 and 14–18). One must avoid introducing an artificial shape dependence into the lineshape parameters. Generally a least-squares analysis is used to remove a linear background. If the regions from which the background is determined are preset, fixed intervals, then relatively more will be subtracted out of a wide peak than a narrow peak. The use of a linear background usually can be justified if care is taken to select the endpoints for the least-squares analysis such that artifacts of lineshape dependence are minimized. The method used by ANNPEAK is to supply a background optimization option with an arbitrary number of trial widths (AWIDTH) which are marked off symmetrically from the maximum count rate channel of the 511-keV photopeak. The calculation of the lineshape parameters is repeated for each AWIDTH. The optimum AWIDTH is then located by examination of the AWIDTH dependence of lineshape parameters. Figure 2 depicts the dependence of the FWHM, Q, W, L, and the centroid on the value of AWIDTH. The same type of lineshape parameter dependence on AWIDTH also was observed using a Ge(Li) detector with a resolution of 2.5 keV for the 514-keV line of ^{85}Kr. Therefore, AWIDTH is preferably chosen on the flat portion of all the plateaus as illustrated in Figure 2. The smallest least-squares linear background is then subtracted from the wings of the photopeak without

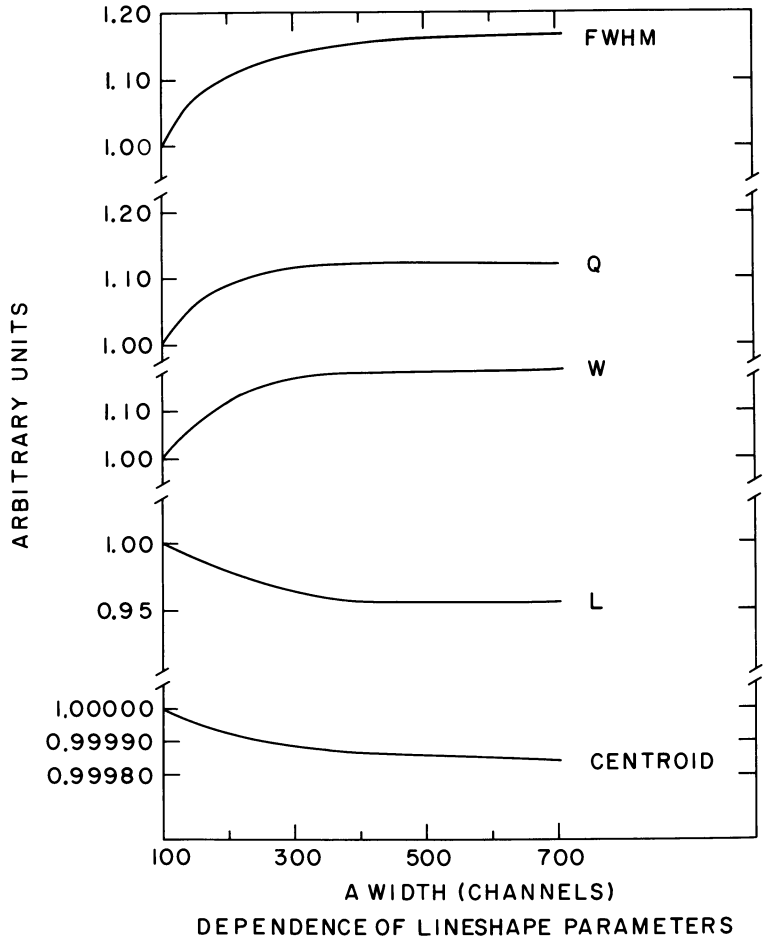

Figure 2. Dependence of lineshape parameters on AWIDTH (in channels) utilized for background subtraction (see text)

influence from the other features of the spectrum. The AWIDTH optimization procedure incorporated into ANNPEAK minimizes the shape dependence introduced into the various lineshape parameters and enables a more satisfactory comparison of spectra taken under different experimental conditions. The data in the spectra are normalized (in our case, to peak channel counts) before the lineshape parameters are extracted.

The definitions of the regions *A*, *B*, and *C* (in Figure 1) usually are selected to maximize an effect, and are arbitrary to that extent. An optimization parameter OPTIM provides for optimizing AWIDTH or for varying the integration widths (*A*, *B*, and *C*) to suit a given experimental application. Once the boundaries of the lineshape parameters have been

Publication Date: June 1, 1979 | doi: 10.1021/ba-1979-0175.ch012

selected, the boundaries for the system are retained while the influence of another variable parameter, e.g. temperature, additive concentration, etc. is studied.

Typically three or more successive runs are obtained for a given experimental condition. For each group of runs, the first may be selected for an optimization run of ANNPEAK. The program then can be used for each individual spectrum to calculate the channel location of each reference; the energy channel^{-1} calibration factor; the total and annihilation photopeak count rates; the annihilation photopeak channel; and the lineshape parameters (FWHM, centroid, second moment, Q. W, and L). If the spectra are designated identical (NID = 1), the averages and standard deviations of the annihilation peak parameters for a specified group of spectra are tabulated. The output option provides several convenient combinations for printing the main results: the raw and reduced data of the annihilation and/or reference peaks and a line printer plot of the annihilation peak. The last is useful for judging the smoothness of the central channels for visual inspection of the stability of the system.

Notes on ANNPEAK Card Structure. An initial block of comments in the main program provides the details of the input data. The following is provided as clarification. The first five cards supply the control and optimization parameters. Note that NCHAN is the total number of data points contained in the spectrum (4096 in our case). BWIDTH represents the trial width in channels chosen around the reference peaks. The BWIDTH card is omitted if NCAL = 0. The next NCAL + 1 cards contain the starting channel and number of channels in subgroups centered on each of the reference peaks and the annihilation peak (last). NCAL may be 0. The number of channels to be analyzed must be larger than 2 · BWIDTH + 2N for the references and 2 · AWIDTH + 2N for the annihilation peak. N is the number of points (about 20) used for the linear fit and it determines the endpoints of the background line. The next group of cards gives the energies in keV of the NCAL (if any) reference peaks in the same order as the preceding group. The next card (NID = 1) or group of cards (OPTIM = 1) supplies AWIDTH. The next group of cards contains the identification numbers that label each spectrum. The data are then supplied on magnetic tape, with the format described in the reading routines, or on cards in 10(I7) format. The program decks consist of 1050 cards, including comments and a subroutine for reading tapes generated on the Northern Scientific equipment. Except for the tape-reading routines, the program has been converted to FORTRAN ANSI standard. The execution time of a spectrum on the CDC 7600 is about 1 sec. Several hundred spectra have been analyzed with ANNPEAK. The program is available on request from Brookhaven National Laboratory on cards, magnetic tape, or a floppy disk compatible with a PDP 11/34 computer.

Publication Date: June 1, 1979 | doi: 10.1021/ba-1979-0175.ch012

In Positronium and Muonium Chemistry; Ache, H.;
Advances in Chemistry; American Chemical Society: Washington, DC, 1979.

Additional Comments. Figure 3 illustrates a typical Doppler broadened spectrum collected with a ^{22}Na source sandwiched between two silicon crystals. The lineshape parameters obtained for B- and P-doped (*p*- and *n*-type) Si of 100 and 111 orientations were independent of the dopant and orientation (*12*). A test case is provided with the program. Also shown in Figure 3 is our instrumental resolution as determined using ^{106}Ru. We advocate the adoption of ^{106}Ru in the description of the characteristics of spectrometers used for measurement of Doppler broadening of positron annihilation photons because of its 269-day half-life, and

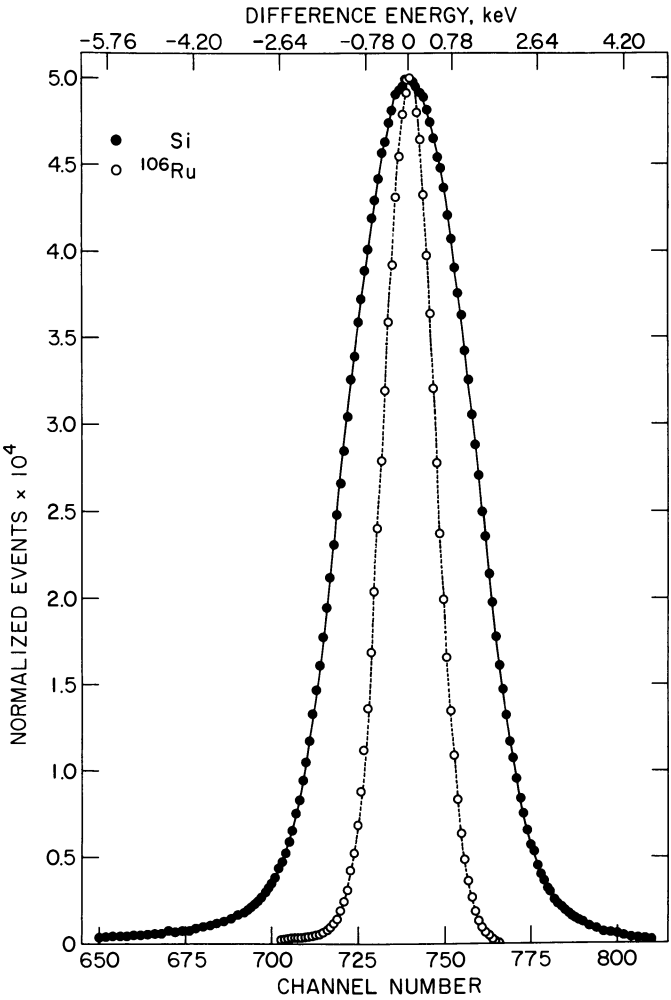

Figure 3. Normalized spectra depicting the detector resolution for ^{106}Ru (511.865 keV) and the Doppler broadened positron annihilation photopeak in Si

Publication Date: June 1, 1979 | doi: 10.1021/ba-1979-0175.ch012

its ideal principal photon at 511.865 keV. ^{106}Ru is inexpensive and readily available. An accurate description of the resolution function is required for the deconvolution of Doppler broadened spectra (*13–18*). Doppler broadening of positron annihilation photon spectroscopy has proved to be complementary to positron lifetime spectroscopy in chemical systems in which Ps is formed. Perhaps the first example of success is studies of aqueous solutions of 22 different simple anions of sodium and silver salts (*19, 20*). Detailed results will be presented elsewhere.

Literature Cited

1. Lambrecht, R. M., "Antimatter–Matter Interactions I. Positrons and Positronium, 1930–1974," Brookhaven National Laboratory Report, BNL 50510, July 1975.
2. MacKenzie, I. K., *Phys. Lett. A* (1970) **33**, 279.
3. Lichtenberger, P. C., Ph.D. Thesis, University of Waterloo, 1974.
4. Jackman, T. E., Schulte, C. W., Campbell, J. L., Lichtenberger, P. C., MacKenzie, I. K., Wormald, M. R., *J. Phys. F.* (1973) **4**, L1.
5. Leber, R. E., Lambrecht, R. M., *J. Chem. Phys.* (1972) **57**, 2273.
6. Hood, G. M., Schultz, R. J., Carpenter, G. J. C., *Phys. Rev. B* (1976) **14**, 1503.
7. Campbell, J. L., *Appl. Phys.* (1977) **13**, 365.
8. Myllyla, R., Karras, M., *Appl. Phys.* (1975) **7**, 303.
9. Grynszpan, R., "Abstracts of Papers," 173rd National Meeting, ACS, New Orleans, March 21–25, 1977, NUCL 58.
10. Dauwe, C., Dorinkens, M., Dorinkens-Vanpraet, L., Segers, D., *Appl. Phys.* (1974) **5**, 117.
11. Singru, R. M., Lal, K. B., Tao, S. J., Lambrecht, R. M., *Atomic Data and Nuclear Data Tables* (1978) **20**, 475.
12. Kelly, J. J., Lambrecht, R. M., *Phys. Lett. A* (1977) **60**, 475.
13. Shizume, K., Inouc, H., Yoshizawa, Y., *Nucl. Instrum. Methods* (1976) **173**, 599.
14. Okada, S., Ito, Y., Tabata, Y., *Bull. Chem. Soc. Jpn.* (1977) **26**(3), 139.
15. Jackman, T. E., Lichtenberger, P. C., Schulte, C. W., *Appl. Phys.* (1974) **5**, 259.
16. Hotz, H. P., Mathiesen, J. M., Hurley, J. P., *Phys. Rev.* (1968) **170**, 351.
17. Dannefaer, S., Kerr, D. P., *Nucl. Instrum. Methods* (1975) **131**, 119.
18. McNelles, L. A., Campbell, J. L., *Nucl. Instrum. Methods* (1975) **127**, 73.
19. Handeli, D., Lambrecht, R. M., *Chem. Phys. Lett.* (1976) **37**, 187.
20. Lambrecht, R. M., presented at the 9th International Symposium on Hot Atom Chemistry, Virginia Polytechnic Institute and State University, Blacksburg, Va., September 18–23, paper 64.

RECEIVED November 7, 1978. Research carried out at Brookhaven National Laboratory under contract with the U.S. Department of Energy and supported by its Division of Basic Energy Sciences.

13

Muonium Chemistry—A Review

DONALD G. FLEMING, DAVID M. GARNER, LOUIS C. VAZ[1], and DAVID C. WALKER—TRIUMF and Dept. of Chemistry, University of British Columbia, Vancouver, B.C., V6T 1W5, Canada

JESSE H. BREWER—TRIUMF and Dept. of Physics, University of British Columbia, Vancouver, B.C., V6T 1W5, Canada

KENNETH M. CROWE—Lawrence Berkeley Laboratory and Dept. of Physics, University of California, Berkeley, CA 94270

Publication Date: June 1, 1979 | doi: 10.1021/ba-1979-0175.ch013

The muonium atom can properly be regarded as an ultralight isotope of hydrogen, in which the proton nucleus is replaced by a positive muon of only one-ninth its mass. Within the Born–Oppenheimer approximation, the chemical identical up to differences in reaction dynamics; thus, muonium chemistry studies greatly extend the range of observable mass-sensitive effects in chemical kinetics. The theoretical background of muonium chemistry is presented and applied to thermal kinetic studies in both gas- and liquid-phase systems, drawing on current experimental results (primarily from TRIUMF and SIN) which reveal both normal and inverse dynamic isotope effects. Associated phenomena such as muonium hot atom reactions are also discussed.

Chemical reactions of hydrogen atoms constitute some of the most elementary processes in physical chemistry. The theory of the absolute rates of such reactions often has been clarified by measurements of isotope effects, differences in the reactions of the three naturally occurring isotopes of hydrogen: protium, deuterium, and tritium. The positronium (Ps) atom has been thought of as an ultralight isotope of hydrogen, but the analogy is poor, since chemical binding of Ps is a

[1] Present address: Fiscia Nuclear, I.F., U.F.R.J., Cidade Universitaria A-307, Rio de Janeiro, Brazil.

0-8412-0417-9/79/33-175-279$12.50/1

In Positronium and Muonium Chemistry; Ache, H.;
Advances in Chemistry; American Chemical Society: Washington, DC, 1979.

qualitatively unique process. However, there is a true light isotope of hydrogen available for study in the form of the muonium (Mu) atom. The nucleus of Mu is the positive muon (μ^+), an unstable elementary particle with a lifetime of 2.20 μsec and a mass 0.1126 times that of the proton. Mu (μ^+e^-) atoms almost always form when positive muons are stopped in matter (*1, 2, 3*), and usually react soon thereafter to form chemical bonds with molecules of the medium (*4–16*).

This chapter provides the historical and experimental background for a discussion of Mu chemistry and the μ^+ depolarization technique. A convenient theoretical structure is developed which relates the thermal chemical reactivity of Mu to several observable effects on the μ^+ polarization. This theory is applied to experimental data in extracting rate constants for thermal reactions of Mu in both liquid- and gas-phase systems. In this chapter the thermal reaction rates of Mu are compared with corresponding hydrogen (H) atom values, epithermal reactions of Mu are discussed in some detail, and the present and projected status of Mu chemistry studies is evaluated.

Publication Date: June 1, 1979 | doi: 10.1021/ba-1979-0175.ch013

Muons, Muonium, and Depolarization

The muon has enchanted particle physicists for years as the inexplicable heavy electron; except for lifetime and mass its properties are identical to those of electrons (or, in our case, positrons). Indeed, the negatively charged muon acts exactly like a heavy electron, forming muonic atoms in which the μ^- orbits tightly about the nucleus, well inside any electronic orbits (*17, 18, 19*). Muonic hydrogen, consisting of a proton and a μ^-, chemically resembles a neutron and is a poor analogue of atomic hydrogen in any conventional chemical sense. The positive muon, on the other hand, is more of a light proton than a heavy positron. Its mass is much closer to that of a proton than to that of a positron, and it does not annihilate with electrons. Furthermore, when it forms an atom, the nucleus is still some 207 times as heavy as the orbiting electron. Unlike the Ps atom (*20, 21*) which has no proper nucleus, the Mu atom has almost exactly the same size and binding energy as the H atom, and to high precision satisfies the Born–Oppenheimer picture of a nearly massless electron adiabatically screening a heavy, quasistationary nucleus. From a chemical point of view, then, muonium differs from hydrogen only in mass and in small corrections for nuclear motion or possible effects of its different nuclear magnetic moment.

The weak interaction is both the source and demise of muons. Most muons originate in pion (π) decay, along with a muonic neutrino (ν_μ) or antineutrino ($\bar{\nu}_\mu$), depending upon the charge. Here we will be concerned only with positive muons. Thus the reaction in which our μ^+ is born is

In Positronium and Muonium Chemistry; Ache, H.;
Advances in Chemistry; American Chemical Society: Washington, DC, 1979.

$$\pi^+ \rightarrow \mu^+ + \nu_\mu . \tag{1}$$

A striking feature of weak interactions is parity violation, an example of which is the fact that all neutrinos have negative helicity—that is, their spins always point in the direction opposite to their momentum. Since the pion has zero spin, the muon's spin must cancel that of the neutrino; simultaneously, the momenta of the muon and neutrino must be equal and opposite in the pion's rest frame; thus, the muon from pion decay is forced to have negative helicity as well. This is of great significance experimentally, for it insures that a muon beam coming off in a given direction from pion decay at rest will be nearly 100% polarized opposite to its momentum.

The muon later decays in the reaction

$$\mu^+ \rightarrow e^+ + \nu_e + \bar{\nu}_\mu . \tag{2}$$

Here again the unique helicity of the neutrino leads to a parity violation; in this case the (easily detected) decay positron has a tendency to come off along the spin of the muon, in a pattern of the form

$$dN_e/d\Omega \sim (1 + a \cos\theta) \tag{3}$$

where a is the decay asymmetry and θ is the angle between the μ^+ and e^+ emission direction (*3, 22, 23, 24, 25*). The decay asymmetry has an average value of one-third, giving a rather sensitive indication of the degree and direction of polarization of the muon spins. This effect was observed first in 1957 (*22, 23, 24, 25*), at which time it was noticed that the degree of residual polarization of the stopped muons depended strongly upon the stopping medium.

Several earlier theoretical papers (*26, 27, 28*) pointed the way to an understanding of the measured residual polarization as being caused by a process of fast depolarization of positive muons in condensed matter—the result of brief formation of Mu atoms in which the hyperfine coupling of the muon with the electron leads to rapid motions of the muon spin. The depolarization is incomplete only because of chemical reactions of the Mu atom which place the muon in a diamagnetic environment, a feature of the process which was early recognized (*4, 5, 6, 7*) to provide an opportunity for study of the chemistry of Mu.

Liquids were the first media in which Mu chemistry was studied extensively—initially by a group at Dubna (*4, 5, 6, 7*) and later by a group at Lawrence Berkeley Laboratory (LBL) (*3, 8, 9*).

Early gas phase experiments were carried out at high pressure as part of an effort to measure the hyperfine structure of Mu (*1, 2, 29, 30*), a highly successful program still active today (*31*). Historically, gas-phase

Publication Date: June 1, 1979 | doi: 10.1021/ba-1979-0175.ch013

studies near 1-atm pressure were extremely difficult (*32*) owing to a low stopping density of high momentum conventional μ^+ beams derived from π^+ decay in flight. More recently, a low-momentum surface μ^+ beam has been developed (*33*). Gas-phase Mu chemistry near 1-atm pressure was studied first at LBL using such a beam (*10*).

With the advent of higher-intensity meson factories such as Tri-University Meson Facility (TRIUMF) in Vancouver and Schweizerisches Institute für Nuklearforschung (SIN) near Zurich, comprehensive studies of Mu chemistry have become increasingly feasible. In addition to the continuing program of liquid-phase Mu chemistry measurements at Dubna, an impressive series of experiments in liquids has been performed at SIN by a group from the University of Zurich (*11, 12, 13, 14*). Liquids are also being studied at TRIUMF; however, the main thrust of the TRIUMF program has been in gas-phase studies, where the unique combination of high intensity and a surface μ^+ beam which stops in a few inches of gas at 1 atm has allowed very gratifying investigations of Mu chemistry in gases (this will receive special emphasis in this review).

Publication Date: June 1, 1979 | doi: 10.1021/ba-1979-0175.ch013

Experimental Method

Several approaches have been taken to study the effects of the stopping medium upon the muon's apparent initial polarization (*3*). Each relies upon the asymmetric decay and the coupling of the μ^+ spin to an external magnetic field through its magnetic moment. We will not attempt a comprehensive review here, but only describe briefly the transverse field techniques used in the measurements to be discussed.

Muon Spin Rotation (μ^+SR). In this method, a beam of polarized positive muons is stopped in a target in a uniform magnetic field perpendicular to the μ^+ spin polarization direction. If the muons stop and stabilize in a diamagnetic environment, their spins precess in the plane perpendicular to the magnetic field at the free muon Larmor frequency.

$$\omega_\mu = 2\pi\,\gamma_\mu B, \text{ where } \gamma_\mu = 0.0136\ \text{MHz/G} \tag{4a}$$

Eventually the muon decays and the decay positron is most likely to be detected by an array of scintillation counters in the plane of precession if the μ^+ spin is pointing in their direction. The e^+ detection probability thus oscillates in time as the muon polarization sweeps past the counter, with θ in Equation 3 given by $(\omega_\mu t + \emptyset_o)$, where $\emptyset_o$ is the initial phase angle of the muon spin with respect to the e^+ counters. A high-resolution clock is started by the signal in one counter array as the muon enters the target, and stopped by the signal in the positron counter, if and when the decay positron is detected. The resultant measured time intervals are binned into a time histogram which is equivalent to the detection probability as a function of time. This distribution falls off exponentially because of the decay lifetime of the muons, and has a superimposed

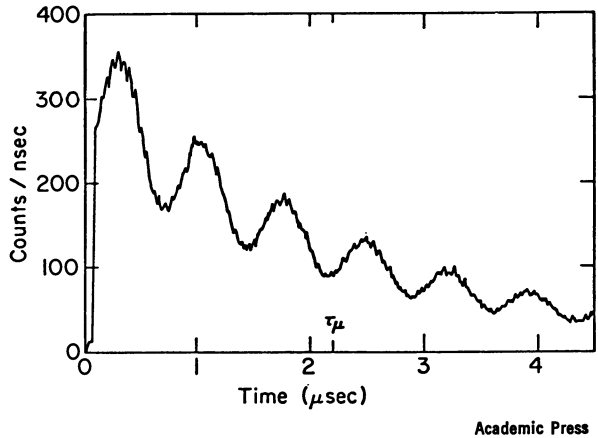

Figure 1. Typical experimental time spectrum showing μ^+ precession (μ^+SR) in 100 G external field. The target is CCl_4. The data, obtained at LBL, is grouped into 10 nsec bins for graphical clarity.(3)

Publication Date: June 1, 1979 | doi: 10.1021/ba-1979-0175.ch013

oscillation whose phase and amplitude are a measure of the direction and magnitude of the apparent initial muon polarization. Of course, real detectors have finite dimensions and there are various solid angle corrections to Equation 3. There are also corrections owing to target geometry and beam polarization. In practice, these can all be absorbed into the empirical asymmetry, A_μ, which replaces a in Equation 3. An example of an experimental time histogram is shown in Figure 1 for muons stopping in CCl_4, where virtually no depolarization occurs.

The quantity measured in this way (usually in liquid targets) is called the residual polarization (P_{res}) of the μ^+ in its final (diamagnetic) environment; P_{res} depends markedly upon the chemical characteristics of the stopping medium (as mentioned earlier) because of the reactivity of Mu, the depolarizing agent. One then must develop a theory (*9, 27, 28, 34, 35, 36*) to relate P_{res} to the concentration of reagent in solution, allow-extraction of biomolecular rate constants for thermal chemical reactions of Mu atoms.

Muonium Spin Rotation (MSR). In oxygen-free liquids (*11, 12, 13, 14, 37*), some solids (*3*), and in many gas targets (*1, 2, 10, 15, 16, 30*), stopping muons capture electrons from the medium forming long-lived Mu atoms. In contrast to the free μ^+ precession described above (μ^+SR) one now is able to observe directly the precession of Mu atoms themselves. In the Mu atom, the spins of the μ^+ and the e^- are coupled together by the hyperfine interaction which may be thought of as the effect of the field ($B_0 = 1585$ G) owing to the μ^+ magnetic moment on the magnetic moment of the e^-. In weak fields ($B << B_0$), this interaction locks the muon and electron spins together to form a net spin of $F = 0$ (singlet) or 1 (triplet). In the triplet state, the net spin is twice that of the free muon, while the net magnetic moment is approximately that of the electron, which is ca. 207 times larger than the muon's. The notable result is that the Mu atom triplet state precesses ca. 103 times faster than

In Positronium and Muonium Chemistry; Ache, H.;
Advances in Chemistry; American Chemical Society: Washington, DC, 1979.

the free muon in the same magnetic field, as long as the field is too weak to compete with the hyperfine field, B_0. That is,

$$\omega_{Mu} = 2\pi\gamma_{Mu}B, \text{ where } \gamma_{Mu} = 1.39 \text{ MHz/G}. \quad (4b)$$

This fast precession is reflected in the positron distribution from muons in Mu—defining the MSR technique. A sample MSR time spectrum is shown in Figure 2 for muons stopping in argon gas in a field of 2 G. It is qualitatively similar to that for the free μ^+ precession shown in Figure 1 at a field of 100 G, except that the amplitude is decreased by a factor of two owing to the half of the Mu ensemble which forms in the $m_F = 0$ state, which does not precess.

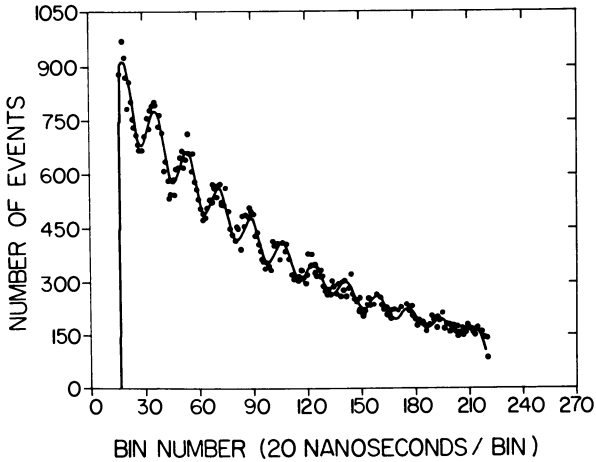

Figure 2. Typical experimental time spectrum showing Mu precession (MSR) in a field of 2.2 G. The target is Ar gas at 1 atm pressure. The data, obtained at LBL, fit to an expression of the form of Equation 5.

General Transverse Field Method. In general some muons will be in diamagnetic environments while others are in Mu atoms. In finite transverse field the time dependence of the μ^+ spin polarization in Mu becomes complicated, as discussed below. Furthermore, a complete description has to take into account the evolution of the μ^+ polarization through several stages of environment, such as $\mu^+ \rightarrow$ Mu $\rightarrow$ diamagnetic molecule, which begin and end at times which are distributed statistically. This leads to a rather elaborate expression for the time dependence $P_\mu(t)$ of the μ^+ ensemble spin polarization component in a fixed direction, which will be derived in the next section. In any case the experimental distribution of positron detection times will be of the form

$$\frac{dN_e(t)}{d\Omega} = \{N_o[BG + e^{-t/\tau_\mu}(1 + A_o P_\mu(t))]\} \quad (5)$$

Publication Date: June 1, 1979 | doi: 10.1021/ba-1979-0175.ch013

where N_0 = a normalization factor, BG = time-independent background from accidental counts, etc., $\tau_\mu = \mu^+$ lifetime (2.2 μsec), and A_0 is an empirical maximum asymmetry parameter (typically about 0.3).

Time Dependence of the Muon Polarization

Since the coupled spin system of the Mu atom plays an ubiquitous role in most μ^+SR phenomena, our first task is to describe the motions of that system in some detail.

Time Dependence of the μ^+ Spin in Muonium. The polarized muon generally captures an unpolarized electron from the medium, so that Mu is formed in two spin states with equal probability: $|A\rangle = |\vec{\uparrow}\vec{\rightarrow}\rangle$ and $|B\rangle = |\vec{\uparrow}\vec{\leftarrow}\rangle$, where $\vec{\uparrow}$ refers to the μ^+ spin and $\rightarrow$ or $\leftarrow$ refers to the e^- spin direction. We have used an unusual notation to emphasize that the original spin direction is perpendicular to the magnetic field. Shortly we will use $\hat{z}$, the field direction, as a quantization axis, defining $\hat{x}$ as the initial muon spin direction. First however, we can describe equally well any spin state in terms of its total angular momentum along the original spin direction, using the notation $|F.M\rangle_\perp$. In this basis $|A\rangle = |1, +1\rangle_\perp$, which would be a stationary state of the hyperfine Hamiltonian in zero field; but the state describing the other half of the ensemble is a superposition of two zero-field eigenstates: $|B\rangle = (|1,0\rangle_\perp + |0,0\rangle_\perp)/\sqrt{2}$. Thus, even in zero field, it would oscillate between $|\vec{\uparrow}\vec{\leftarrow}\rangle$ and $|\vec{\downarrow}\vec{\rightarrow}\rangle = (|1,0\rangle_\perp - |0,0\rangle_\perp)/\sqrt{2}$ at the hyperfine frequency $\nu_0 = 4463$ MHz, which may be thought of as the frequency of precession of the muon in the field of the electron's magnetic moment. As a result of this fast hyperfine oscillation, half of the free Mu ensemble appears to be completely depolarized within about 10^{-10} sec. and $|B\rangle$ is an eigenstate of the Zeeman Hamiltonian (*1, 2,3*), and the motion of the spins becomes more complex. In order to describe it, we first express $|A\rangle$ and $|B\rangle$ in the basis $|F,M\rangle||$ labelled according to total angular momentum along the field direction, $\hat{z}$. The basis $|F,M\rangle||$ is obtained from the basis $|F,M\rangle_\perp$ by a simple rotational transformation of $\pi/2$ about the $\hat{y}$ axis. The resultant expressions for the initial state vectors can be expressed in terms of the basic states $|m_\mu,m_e\rangle$ referred to the $\hat{z}$ quantization axis as follows:

$$|A(0)\rangle = \frac{1}{2}(|\uparrow\uparrow\rangle + |\uparrow\downarrow\rangle + |\downarrow\uparrow\rangle + |\downarrow\downarrow\rangle); \tag{6}$$

$$|B(0)\rangle = \frac{1}{2}(-|\uparrow\uparrow\rangle + |\uparrow\downarrow\rangle - |\downarrow\uparrow\rangle + |\downarrow\downarrow\rangle).$$

Publication Date: June 1, 1979 | doi: 10.1021/ba-1979-0175.ch013

Again we use a menmonic notation using arrows to denote spin direction. Then we expand our states in the Zeeman eigenstates $|i\rangle$ corresponding to energy eigenvalues $E_i = \hbar\omega_i$. These are given in terms of $|m_\mu, m_e\rangle$ by (*1, 2, 3*):

$$\begin{aligned} |1\rangle &= |\Uparrow\uparrow\rangle \\ |2\rangle &= s|\Uparrow\downarrow\rangle + c|\Downarrow\uparrow\rangle \\ |3\rangle &= |\Downarrow\downarrow\rangle \\ |4\rangle &= c|\Uparrow\downarrow\rangle - s|\Downarrow\uparrow\rangle \end{aligned} \tag{7}$$

where

$$c = \frac{1}{\sqrt{2}}\left[1 + \frac{x}{\sqrt{1+x^2}}\right]^{1/2}$$

$$s = \frac{1}{\sqrt{2}}\left[1 - \frac{x}{\sqrt{1+x^2}}\right]^{1/2} \tag{8}$$

and

$$x = (\omega_e + \omega_\mu)/\omega_o = \frac{B}{B_o}.$$

Here, $\omega_o = 2\pi\nu_o$ is the hyperfine frequency in Mu (2.8×10^{10} rad/sec); $\omega_e = (m_e/m_\mu)\omega_\mu \simeq 207\,\omega_\mu$ is the electron Larmor frequency. As mentioned previously, $B_o = 1585$ G and may be thought of as the field at the electron owing to the muon's magnetic moment. Having made this final transformation of basis, we can write down the time dependence by inspection, since each eigenstate has the simple exponential dependence exp $(-i\omega_i t)$:

$$\begin{aligned} |A(t)\rangle &= \frac{1}{2}e^{-i\omega_1 t}\,|\,1\rangle + \alpha\, e^{-i\omega_2 t}\,|\,2\rangle \\ &\quad + \frac{1}{2}e^{-i\omega_3 t}\,|\,3\rangle - \beta\, e^{-i\omega_4 t}\,|\,4\rangle \\ |B(t)\rangle &= -\frac{1}{2}e^{-i\omega_1 t}\,|\,1\rangle + \beta\, e^{-i\omega_2 t}\,|\,2\rangle \\ &\quad + \frac{1}{2}e^{-i\omega_3 t}\,|\,3\rangle + \alpha\, e^{-i\omega_4 t}\,|\,4\rangle \end{aligned} \tag{9}$$

where $\alpha = (s + c)/2$ and $\beta = (s - c)/2$, and the frequencies are given by

Publication Date: June 1, 1979 | doi: 10.1021/ba-1979-0175.ch013

$$\omega_1 = \frac{\omega_0}{4} + \omega_-$$

$$\omega_2 = \frac{-\omega_0}{4} + \sqrt{\frac{\omega_0^2}{4} + \omega_+^2}$$

$$\omega_3 = \frac{\omega_0}{4} - \omega_- \qquad (10)$$

$$\omega_4 = \frac{-\omega_0}{4} - \sqrt{\frac{\omega_0^2}{4} + \omega_+^2}.$$

Here $\omega_\pm \equiv 1/2\ (\omega_e \pm \omega_\mu)$.

In order to relate the time dependence of the state vectors to the motion of the muon polarization, we must take the expectation value of the muon's Pauli spin operator: $\vec{P}_\mu = <\vec{\sigma_\mu}>$. For this, it is most convenient to work in the basis $|m_\mu, m_e\rangle$, where the effect of the Pauli matrices is simply defined. We are interested only in the muon polarization in the $(\hat{x} - \hat{y})$ plane perpendicular to the $(\hat{z})$ field direction; it can easily be shown, in fact, that if there is no initial polarization along the field, none will develop. Thus we can pack all the interesting information into a single complex quantity, using the compact notation

$$\tilde{P}_\mu \equiv P_x{}^\mu + i\, P_y{}^\mu. \qquad (11)$$

This "complex muon polarization" (of the μ^+ in Mu) can be evaluated from the definition of the expectation value:

$$\tilde{P}_\mu = \frac{1}{2} \langle A(t) | (\sigma_x{}^\mu + i\, \sigma_y{}^\mu) | A(t) \rangle + \frac{1}{2} \langle B(t) | (\sigma_x{}^\mu + i\, \sigma_y{}^\mu) | B(t) \rangle. \qquad (12)$$

Substituting Expressions 9 for $|A(t)\rangle$ and $|B(t)\rangle$ (using the $|m_\mu m_e\rangle$ basis) Into Equation 12 yields the following result (*2, 3, 38, 39, 40*):

$$\tilde{P}_\mu(t) = \frac{1}{2} [c^2 (e^{i\omega_{12}t} + e^{-i\omega_{34}t}) + s^2 (e^{i\omega_{23}t} + e^{i\omega_{14}t})] \qquad (13)$$

where $\omega_{ij} \equiv \omega_i - \omega_j$, using the definitions in Equation 10.

Publication Date: June 1, 1979 | doi: 10.1021/ba-1979-0175.ch013

This expression can be rewritten via trigonometric identities and previous definitions as follows:

$$\tilde{P}_\mu(t) = e^{i\omega_- t} \cos\left(\frac{\omega_0}{2} t\right)\left[\cos\left(\frac{\omega_0}{2} + \Omega\right) t - i\delta \sin\left(\frac{\omega_0}{2} + \Omega\right) t\right] \quad (14)$$

where

$$\delta = c^2 - s^2 = \frac{x}{\sqrt{1 + x^2}}$$

and

$$\Omega = \frac{1}{2}(\omega_{23} - \omega_{12}) = \frac{\omega_0}{2}(\sqrt{1 + x^2} - 1).$$

The weak field ($x << 1$) limit of Equation 14 is especially interesting, both for conceptualization and because most experiments are performed in this region:

$$\tilde{P}_\mu(t) \underset{x \to 0}{\rightarrow} \frac{1}{2} e^{i\omega_- t}\{\cos \Omega t + \cos(\omega_0 + \Omega) t\}. \quad (15)$$

The motion of the muon polarization thus can be factored into two parts: an overall precession in the $x - y$ plane at the free Mu Larmor frequency ω_-, multiplied into two terms whose time dependences are pure modulations. The modulation frequency Ω is relatively slow; in low field it can be approximated by $\Omega = \omega_+^2/\omega_0$. The other modulation frequency, ω_0, is extremely high, well beyond the time resolution of the experimental apparatus.

The low-field time dependence described in Equation 15 can be examined conveniently from two points of view: in the limit of very early times (fast viewpoint), $\cos \Omega t \approx 1$, and the motion consists of a fast hyperfine oscillation modulated by slower Mu precession. Experimentally, the positron detector is fixed in the plane of precession, so that we observe only the $\hat{x}$ or $\hat{y}$ projections (i.e., the real or imaginary parts) of the muon polarization, so precession is not distinguished from modulation. Figure 3 shows the time dependence of Re $\tilde{P}_\mu(t)$ which we would expect to observe for free Mu in a 100 G applied field if our apparatus had sufficient time resolution. Practically, the hyperfine oscillations are too fast to see (period = 0.225 nsec), and we observe motion only on a longer time scale. This brings us to the slow viewpoint, in which $\cos(\omega_0 + \Omega)t$ averages to zero and the motion apparently consists of a Mu precession signal modulated by a beat frequency Ω.

Publication Date: June 1, 1979 | doi: 10.1021/ba-1979-0175.ch013

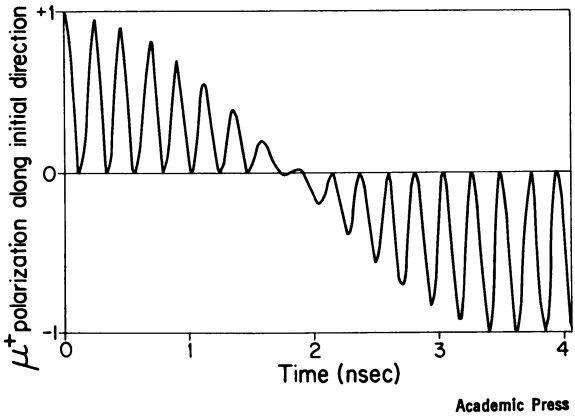

Figure 3. Time evolution of the real part of the muon polarization in free Mu in a 100-G transverse field. The fast oscillations at the hyperfine frequency, ω_0, are not directly observed experimentally.(3)

Here we will deal directly with this slow viewpoint only in the extreme low field limit (a few gauss) where the beating also can be neglected and Mu precession treated simply as a faster version of the μ^+ precession mentioned already.

The slow and fast viewpoints each relate to a separate type of application to the study of chemical reactions of Mu atoms. The fast viewpoint finds its application to Mu chemistry in studies in the liquid phase (μ^+SR) whereas the slow viewpoint provides the basis for MSR studies in both gases and liquids.

Muonium Precession and Chemistry in Gases and Liquids. Precession of Mu atoms on the slow time scale described above can be observed if free Mu is exceptionally stable (uncombined for $\gtrsim 10^{-7}$ sec) and unaffected by magnetic interactions such as spin exchange (*see* Figure 2). Mu precession has been observed only recently in liquids (*11, 37*) but it is a familiar phenomenon in some solids (*3, 38, 39, 41*) and inert gases (*10, 15, 16, 30, 32*). In such cases a relatively slow chemical reaction of Mu atoms with scavenger molecules is reflected directly in the exponential decay of the amplitude of the Mu precession signal: like the microwave power absorption in an ESR experiment on transient radicals, the amplitude of the Mu precession is proportional to the probability of the active species remaining uncombined at the time of observation. Although experiments with muons are radically different from ESR transient studies, in many ways they are formally identical. With the most convenient time scale between 10^{-7} and 10^{-6} sec, the MSR technique is ideally suited for measuring quite fast reaction rates of free Mu atoms.

Normally a time spectrum like that shown in Figure 2 is corrected for any constant background and for the exponential decay of the muons themselves, and the remaining MSR signal is ideally fitted to the form

$$P_\mu(t) = e^{-\lambda t}\,\mathrm{Re}\,\tilde{P}_\mu(t) \quad \text{(positron detectors } \| \text{ to beam direction} \quad (16)$$

or

$$P_\mu(t) = e^{-\lambda t}\,\mathrm{Im}\,\tilde{P}_\mu(t) \quad \text{(positron detectors } \perp \text{ to beam direction,}$$

where $\tilde{P}_\mu(t)$ is given by Equation 15, usually in its extreme low field limit ($\Omega = 0$), and λ is a pseudo first-order chemical rate constant. The empirical form actually used in Equation 5 in these instances includes a background free μ^+ precession term, and can be written simply as

$$A_o P(t) = A_\mu \cos(\omega_\mu t - \phi) + A_{Mu} e^{-\lambda t} \cos(\omega_{Mu} t + \phi) \qquad (17)$$

It is from the relaxation rate λ that information is obtained about the chemical reactivity of Mu atoms, by varying the concentration of scavenger molecules. Recent results in gases and liquids are discussed in the next section.

Residual Polarization Studies and Muonium Chemistry in Liquids. The main distinction between studies of Mu chemistry in gases and liquids is that in liquids the Mu precession signal itself is rarely seen, because of the rapidity of chemical reactions in the denser liquids. Only in carefully prepared inert solutions (*37*) do Mu atoms remain uncombined at observation times (typically about 50 nsec after the muon thermalizes, allowing measurement of the MSR signal (*11,12, 13, 14*). We can much more easily detect the slower precession of the μ^+ itself, which by this time is incorporated into a diamagnetic molecule and is magnetically free. The amplitude and phase of this precession, extrapolated back to $t = 0$ (the time at which Mu is formed initially), constitute all the available information in the form of the residual muon polarization, P_{res}. Thus, ironically, it is via experimental observation of μ^+ precession on the extremely long time scale of microseconds that one can infer information about the reactions of Mu atoms on the fast time scale of a few hyperfine periods (approximately 10^{-9} sec or less).

Since each Mu atoms reacts chemically at a different time, each muon emerges from the Mu environment with a different spin direction, so that the residual polarization generally is reduced and rotated with respect to the initial muon polarization. We will keep account of both the magnitude and direction of P_{res} by letting it be a complex quantity in keeping with the foregoing formulation of $P_\mu(t)$: the real part is the polarization component along $\hat{x}$ (the original spin direction) and the

Publication Date: June 1, 1979 | doi: 10.1021/ba-1979-0175.ch013

imaginary part is the component in the $\hat{y}$ direction, perpendicular to both the $\hat{x}$ and the external field. Most data of this type has been taken with positron counters in the μ^+ beam direction; we will treat only this case. Here the observable precession signal is the real part of $P(t)$, the exact (complex) time-dependent polarization of the entire muon ensemble. As mentioned earlier, in the $\mu^+SR(P_{res})$ technique, observation of this signal begins long after the rapid motions of the muon spin in Mu have settled down to the slow precession of the free muon spin in a dimagnetic environment; thus, on the time scale of the chemical interactions of the Mu atom, the observations take place at $t \rightarrow \infty$, and we can define the observable quantity as

$$P_{obs}(t) = \lim_{t \rightarrow \infty} \text{Re}\, P(t). \tag{18}$$

The experimental precession signal is fitted to the form (recall Equations 3 and 5

$$P_{obs}(t) = |P_{res}| \cos(\omega_{\mu} t + \phi), \tag{19}$$

which is equivalent to

$$P_{obs}(t) = \text{Re}\, \{P_{res}\, e^{i\omega_{\mu} t}\}$$

with the definition

$$\tan \phi = \text{Im}(P_{res})/\text{Re}(P_{res}). \tag{20}$$

Thus we can derive P_{res} from $P(t)$ by dividing out the free μ^+ precession as if it had started at $t = 0$, and taking the limit:

$$P_{res} = \lim_{t \rightarrow \infty} P(t) \exp(-i\omega_{\mu} t). \tag{21}$$

Thus the theoretical task is reduced to a calculation of $P(t)$.

AN ANALYTIC EXPRESSION FOR THE RESIDUAL POLARIZATION. The ensemble muon polarization at time t is formally given by

$$P(t) = \sum_{q} f_q\, P_q(t), \tag{22}$$

where q represents the fate of a fraction f_q of the muon ensemble, and $P_q(t)$ is the polarization at time t of that fraction. In general, the muon is expected to undergo many different kinds of reaction channels often involving radical species as intermediates (*9, 34, 35, 36*). Ultimately, the

Publication Date: June 1, 1979 | doi: 10.1021/ba-1979-0175.ch013

μ^+ must find itself in a diamagnetic environment on a time scale $\lesssim 10^{-8}$ sec in order to contribute to the observable residual polarization. For brevity we sketch here the theoretical development of the simplest reaction process—namely, one in which the μ^+ is placed in a diamagnetic environment in a single rate-determining reaction of the Mu atom (e.g., Mu + I_2 → MuI + I).

In this case, there are only two types of fates of interest: muons still in uncombined Mu atoms at time t and muons in diamagnetic products following reaction at times $t' < t$. Since the probability of reaction per unit time, λ, is constant, the probability of a Mu atom remaining free until time t is $e^{-\lambda t}$, and the probability of a reaction within dt' of time t' is $\lambda e^{-\lambda t'} dt'$. Thus the still uncombined Mu atoms give a contribution to $P(t)$ of

$$P_1(t) = e^{-\lambda t} \tilde{P}_\mu(t), \tag{23}$$

while those muons which evolve in Mu until time t' react and then precess as free muons until time t, give a contribution

$$dP_2(t',t) = \lambda e^{-\lambda t'} \tilde{P}_\mu(t') e^{i\omega_\mu (t-t')} dt'.$$

Recall that $\tilde{P}_\mu(t)$ is the complex μ^+ polarization in free Mu atoms (Equation 12). The latter class of contributions can be summed over $t' < t$ to give the net contribution from all such fates,

$$P_2(t) = \int_0^t \lambda e^{-\lambda t'} \tilde{P}_\mu(t') e^{i\omega_\mu (t-t')} dt'. \tag{24}$$

In the limit of $t \to \infty$ (i.e., for $\lambda t >> 1$), $P_1(t) \to 0$ (i.e., all the Mu atoms react eventually); meanwhile, the term $\exp(-i\omega_\mu t)$ in the definition of P_{res} (Equation 21) cancels the term $e^{i\omega_\mu t}$ under the integral in $P_2(t)$. Thus Equation 21 takes the form (dropping the prime on t')

$$P_{res} = \lambda \int_0^\infty \tilde{P}_\mu(t) \exp[-(\lambda + i\omega_\mu)t] dt. \tag{25}$$

Substituting Equation 13 into Equation 25 allows a general calculation of P_{res} but the resulting expression is somewhat unwieldy in this form (*40*). However, many residual polarization experiments are carried out in low fields, in which case the approximate form of Equation 15 can be used for $\tilde{P}_\mu(t)$ ($\cos \Omega t = 1$ in the fast viewpoint discussed earlier) resulting in

$$P_{res}(x << 1) \approx \frac{\lambda}{2}\left[\frac{1}{\lambda - i\omega_-} + \frac{\lambda}{\lambda^2 + \omega_0^2}\right]. \tag{26}$$

Publication Date: June 1, 1979 | doi: 10.1021/ba-1979-0175.ch013

By fitting both the phase (*see* Equation 20) and the magnitude of the residual μ^+ polarization, we are able to extract an experimental value for the pseudo first-order rate constant λ and hence a value for the true bimolecular rate constant k.

Certain qualitative features of the residual polarization technique are immediately apparent from the form of Equation 26. For the case of an ultrafast reaction ($\lambda >> \omega_0 >> \omega_-$), one obtains the expected result, $P_{res} \rightarrow \lambda/2(1/\lambda + \lambda/\lambda^2) = 1$. That is, if all the Mu atoms react at $t \approx 0$, the polarization has no chance to change from its initial value (*see* Figure 3). Over most of the convenient range of reagent concentrations, however, reactions are slow ($\lambda << \omega_0$) and we obtain

$$P_{res} \approx \frac{\lambda}{2}\left(\frac{1}{\lambda - i\omega_-}\right) = \frac{1}{2}\left(\frac{1}{1 + \omega_-^2\tau^2}\right)(1 + i\omega_-\tau), \qquad (27)$$

where $\tau \equiv 1/\lambda$ is the mean chemical lifetime of a thermal Mu atom. Equation 27 has two interesting limits. First, for $\omega_-\tau << 1$ (reaction faster than Mu precession),

$$P_{res} \rightarrow \frac{1}{2}(1 + i\omega_-\tau)$$

or (28)

$$|P_{res}| \rightarrow \frac{1}{2} \quad \text{and} \quad \phi \rightarrow \omega_-\tau.$$

That is, the hyperfine oscillations average the muon polarization to one-half and the muons get a chance to precess through a small average angle $\omega_-\tau$ while in Mu. This feature is readily apparent in the experimental results and will be referred to again in the discussion to follow. A second limiting situation is $\omega_-\tau >> 1$ (reaction slower than Mu precession), for which

$$P_{res} \rightarrow \frac{i}{2\omega_-\tau}$$

or (29)

$$|P_{res}| \rightarrow 0 \quad \text{and} \quad \phi \rightarrow \pi/2.$$

In this case the large angle of phase shift combines with the vanishing magnitude of the residual polarization to produce frustration on the part of the experimenter who wishes to observe the distinctive phase shift by μ^+SR.

Publication Date: June 1, 1979 | doi: 10.1021/ba-1979-0175.ch013

HOT-ATOM REACTIONS. So far we have discussed only the fates of those muons which thermalize in free Mu atoms. There is also a significant probability that newly formed Mu atoms will participate in hot-atom reactions while still epithermal (about $1 - 10$ eV). These reactions will be discussed in more detail below; their effect on P_{res} is mentioned here. Since such reactions occur at $t \approx 0$ (the slowing down time is approximately 10^{-12} sec (*3*)), there is no opportunity for these muons to be depolarized. The fraction h of muons underoging hot-atom reactions thus contributes a constant unrotated component h to the overall residual polarization, while the contribution from thermal reactions of Mu atoms must be multiplied by a factor $(1 - h)$ representing the remaining fraction of the ensemble. Thus

$$P_{res} \text{ (overall)} = h + (1 - h)\ P_{res} \text{ (Equation 25)}. \qquad (30)$$

For the typical situation of moderately dilute reagents in solution, it is assumed that hot-atom reactions (*3, 8, 9*) take place only with solvent molecules and thus contribute a constant fraction h independent of the chemical lifetime τ. In H_2O, for example, $h \approx 0.6$, which would be the value of P_{res} at zero concentration predicted by Equation 30. However, more recent results (*12, 13, 14*) suggest a possible concentration dependence of Mu hot-atom reactions. Moreover, hot atom reactions placing the μ^+ in a radical environment also may be possible. These effects will be referred to again in the following discussion.

Results and Discussion

Treatment of the reaction kinetics of Mu atoms in the ensemble of events comprising the experimental sample is simplified greatly by the fact that there is literally one Mu atom at a time in the target. Even over an entire run, only about 10^8 muons are stopped in the target, compared with typical reagent concentrations of approximately 10^{19} cm^{-3} in the liquid phase and 10^{16} cm^{-3} in the gas phase. This permits the correct use of pseudo first-order kinetics so that the reaction rate, λ, of Mu is exactly proportional to the reagent concentration, $[X]$. The constant of proportionality is just the bimolecular rate constant, k:

$$\lambda = k[X] \qquad (31)$$

This relationship holds in the following discussions of both gas- and liquid-phase results.

Studies of the Gas Phase. GAS-PHASE EXPERIMENTAL TECHNIQUES. One problem which plagued early gas-phase muon studies was the momentum spread of conventional beams, in which muons are produced from pion decay in flight; after an appropriate energy degrader, these

Publication Date: June 1, 1979 | doi: 10.1021/ba-1979-0175.ch013

muons enter the target with kinetic energies from zero to several tens of MeV. This necessitated the use of high pressures of moderator gas (Table I and Reference 42) to stop a sufficient number of muons. This inconvenience has been eliminated using surface muon beams, developed initially at Lawrence Berkeley Laboratory (LBL) (*10, 33*) and now in use at TRIUMF (*15, 16*) in which muons originate from pions which have come to rest in the production target. Such a beam provides 4.1 MeV muons which are effectively monoenergetic, nearly 100% polarized, and will stop in about 25 cm of Ar gas at 1-atm pressure. This creates an improved environment for gas-phase studies of atomic physics and muonium chemistry, since theoretical calculations are more reliable in the ideal gas regime near 1-atm pressure.

A diagram of the apparatus used at TRIUMF is shown in Figure 4. Surface muons are transported in vacuum, trigger a (thin) counter, and stop in the center of the gas target (an Al cylinder of 36-l capacity fitted with a thin mylar window). The target vessel is placed in the center of a pair of Helmholtz coils as shown in the diagram, which provide a field of $\leq$ 80 G uniform to better than 1% over the stopping region. The incident μ^+ triggers a start pulse to a high frequency time-digital converter (clock), which is interfaced through CAMAC to a PDP-11/40

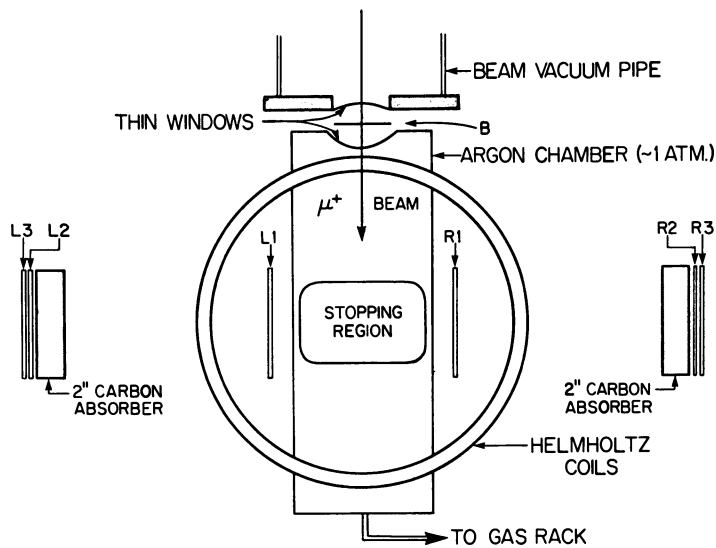

Figure 4. Diagram of the apparatus for gas-phase studies. The incident μ^+ beam is transported in vacuum and triggers a thin (0.015") start counter denoted 'B'. Later, a decay e^+ may trigger either the left (L1 · L2 · L3) or right (R1 · R2 · R3) counter telescopes. The magnetic field is out of the paper (the vertical direction).

Table I. Fraction of Free Muon and of Muonium Formed in Rare Gases[a]

Target Gas	*Pressure (atm)*	f_{μ^+} *(%)*	f_{Mu} *(%)*
He	50	99 (±5)	1 (±5)
He + .015% Xe	50	83 (±15)	—
He + .09% Xe	50	25 (±9)	75 (±9)
Ne	26	100 (±2)	0 (±2)
Ne + .15% Xe	26	19 (±3)	81 (±3)
Ar	30	35 (±5)	65 (±5)
Xe	44	10 (±5)	100[b]
N_2	1		~ 100[c]

[a] From Ref. *42*.
[b] No error estimate given.
[c] Preliminary result from TRIUMF.

computer. Decay positrons are detected by two sets of counter telescopes placed symmetrically at 90° to the incident μ^+ beam. The clock is stopped by an electron coincidence in either the right or left counters, and the resultant time interval is routed accordingly in the computer. The time distributions accumulated from about 10^6 such events form μ^+SR or MSR time spectra, a typical example of which has been shown earlier in Figure 2.

Muonium Formation and Charge Exchange. The typical gas-phase Mu experiment uses an inert moderator gas in which the μ^+ slows down and eventually (within about 10^{-9} sec) thermalizes. In most cases the μ^+ will pick up an electron from a gas atom and thermalize as neutral Mu, which then manifests itself in the low field precession signal of an MSR spectrum. However, in pure helium (He) and neon (Ne) there is no Mu signal in the MSR spectra, indicating the absence of free thermal Mu in the target (*42*). Moreover, in high-field μ^+SR spectra there is a large μ^+ precession signal, indicating that most muons thermalize as positive ions.

This observation can be understood qualitatively in light of the ionization potentials ϵ_I of Mu, He, and Ne, which are 13.5 eV, 24.5 eV, and 21.5 eV, respectively. Once the kinetic energy of the μ^+ falls below the value $\Delta \equiv \epsilon_I$ (Moderator) $-\epsilon_I$(Mu), it cannot obtain an electron from the moderator. This effect is familiar as the Ore gap phenomenon in Ps formation. However, such a qualitative explanation of Mu nonformation breaks down when we consider the formation of Mu in argon (Ar) moderator, where about 70% of the muons thermalize as Mu atoms, despite the fact that $\Delta = 2.3$ eV. To understand these results properly we must describe the atomic physics of charge-changing collisions between μ^+ or Mu and gas atoms at various energies; for this we resort to analogy with a rather impressive body of data on the collisions of hydrogen isotopes (*43, 44, 45*).

In a collision between a hydrogen isotope and a heavier gas atom or molecule, the charge-changing cross section generally is assumed to depend only on the velocity of the impinging light species, not on its mass (*43, 44, 45*). Thus we can expect a μ^+ or Mu atom with kinetic energy T_μ to experience the same charge-changing cross sections as a proton or H atom with the same velocity—i.e., with a kinetic energy $T_p = (M_p/M_\mu)T_\mu = 8.85\ T_\mu$. The cross sections for electron capture (σ_{10}) and electron loss (σ_{01}), characterizing the reactions

$$\mu^+ + Z \xrightarrow{\sigma_{10}} Mu + Z^+$$

and (32)

$$Mu + Z \xrightarrow{\sigma_{01}} \mu^+ + Z^-,$$

are plotted in Figure 5a as functions of proton or muon kinetic energy for several moderator gases Z. The curves are taken from References *43, 44,* and *45* and represent the results of proton transmission experiments down to a kinetic energy of $T_p \approx 2$ KeV.

A proton or muon slowing down in one of these gases will be more likely to end up in the neutral state at thermal energies if σ_{10} is larger than σ_{01} at low energy, and vice versa. This can be seen explicitly in Figure 5b, which shows the fraction of protons in the neutral state as a function of energy. Although these data do not extend to very low energies, the trends are clearly in the direction of the observed final charge state of the muon in the various moderators (Table I).

Some qualitative experimental information about the energy dependence of Mu formation (σ_{10}) cross sections has been obtained by adding small xenon (Xe) impurities to He and Ne gas targets and measuring the Mu and μ^+ precession amplitudes as functions of Xe concentration. This procedure was first adopted in a high-pressure gas study at Los Alamos Meson Physics Facility (LAMPF) (*42*) and is now being used at TRIUMF for measurements near one atmosphere pressure. It is assumed that the μ^+SR and MSR asymmetries A_μ and A_{Mu} obey the normalization $A_\mu + 2\,A_{Mu} = A_o$, where A_o is the empirical maximum asymmetry, so that the fraction of muons in charge state μ^+ or Mu can be expressed as $f_+ = A_\mu/A_o$ and $f_o = 2\,A_{Mu}/A_o$. Table I summarizes the experimental data in this form.

One conclusion can be drawn immediately from the results listed in Table I and from the TRIUMF data in Figure 6a: Mu forms with high probability in epithermal collisions with Xe, but comparatively rarely in thermal collisions, even though the reaction

$$\mu^+ + Xe \rightarrow Mu + Xe^+ \quad (33)$$

Publication Date: June 1, 1979 | doi: 10.1021/ba-1979-0175.ch013

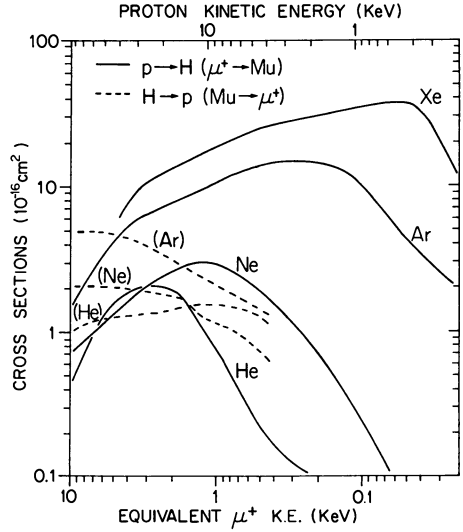

Figure 5a. Charge-exchange total cross sections for H (and Mu) in various gases. Energy decreases from left to right; proton kinetic energy is plotted at the top, with the equivalent muon energy at the bottom. Electron-capture cross sections, (——); electron-loss cross sections, (– – –) (from Refs. 43, 44, and 45).

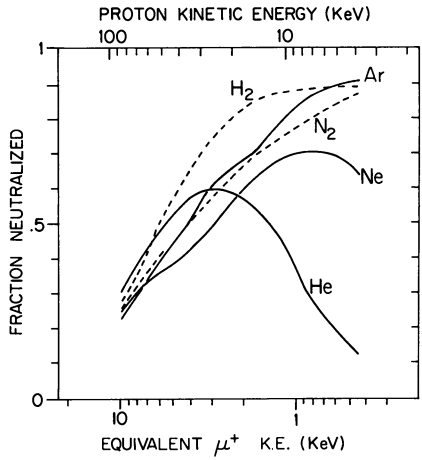

Figure 5b. Fractions of protons (or muons) as neutral H (or Mu) atoms in various gases as a function of proton (muon) kinetic energy. Proton kinetic energy is plotted at the top with the equivalent muon energy at the bottom.

Publication Date: June 1, 1979 | doi: 10.1021/ba-1979-0175.ch013

is exothermic by 1.4 eV. If this were not true, one would observe a μ^+SR signal with a fast relaxation owing to the conversion of μ^+ to faster-precessing Mu, and no MSR signal. Certainly the only way both signals can be seen in the same sample is if the μ^+ ensemble is differentiated at $t \approx 0$ (i.e., during thermalization) into μ^+ and Mu components which do not interconvert after thermalization. This is what is observed.

From elastic scattering on neon atoms with a hard sphere cross section $\sigma_{el}(Ne) \approx 10^{-15}$ cm^2, one expects the μ^+ to take only about 200 collisions to slow down from 200 eV to 0.05 eV; with about 100 ppm of Xe impurity added to the Ne, one can expect only about 0.08 ($\sigma_{10}(Xe)/\sigma_{el}(Ne)$) Mu-forming collisions with Xe in this region. Yet, as can be seen from Figure 6a (and supported by the data in Table I), the actual probability of forming Mu is more than 50% in this system. This shows that $\sigma_{10}(Xe)$ is at least 10 times $\sigma_{el}(Ne)$ over a wide range of energies. Since the electron probably is captured from the attractive tails of the Lennard–Jones potential, which extend far beyond the repulsive hard core, and since Xe is a much larger atom than Ne, this seems quite plausible. This model is also in accord with the fact that it takes relativel y more Xe to cause Mu

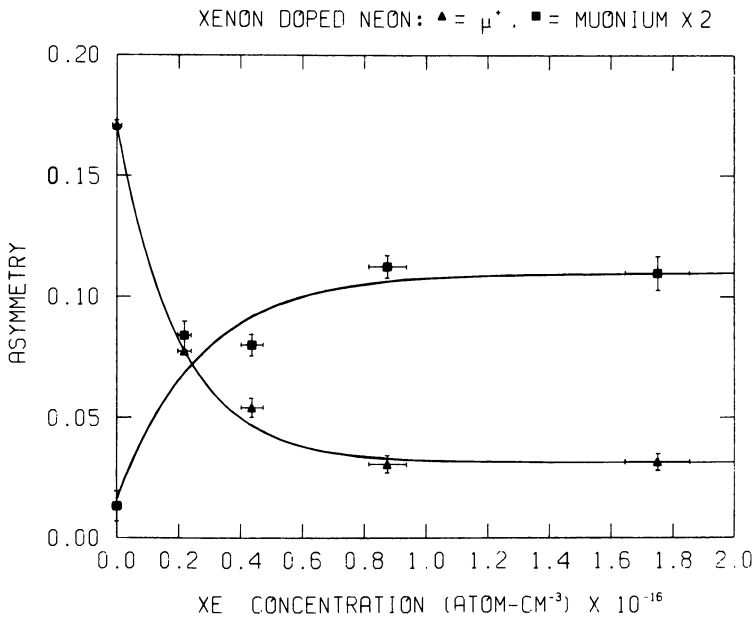

Figure 6a. Muon and Mu asymmetries in Ne doped with Xe as a function of Xe concentration. The non-zero asymptotic muon asymmetry at high Xe concentration is probably due to muons that have scattered into the walls of the aluminum gas target vessel. The curves shown are based on a very simple model of velocity-independent cross sections. Data are from TRIUMF.

formation in He than in Ne; since the μ^+ is moderated approximately 5 times faster in He than in Ne, such an effect is expected for epithermal (not thermal) reactions.

As mentioned above, it is surprising that Reaction 33 proceeds epithermally with such high efficiency but only slowly, if at all, after the μ^+ thermalizes. A proposed explanation is that the μ^+ does not thermalize as a free charge, but forms μ^+Ne molecular ions, which are expected to be bound by about 1.8 eV. The first vibrationally excited state also should be bound, by about 1 eV. Thus the reaction

$$\mu^+\text{Ne} + \text{Xe} \rightarrow \text{Ne} + \text{Mu} + \text{Xe}^+ \qquad (34)$$

is endothermic from the groundstate, but might be equally exothermic from the first excited state. Recent unpublished results from TRIUMF show a relaxation rate for the μ^+SR signal which increases linearly with Xe concentration (*see* Figure 6b), indicating a thermal process of reac-

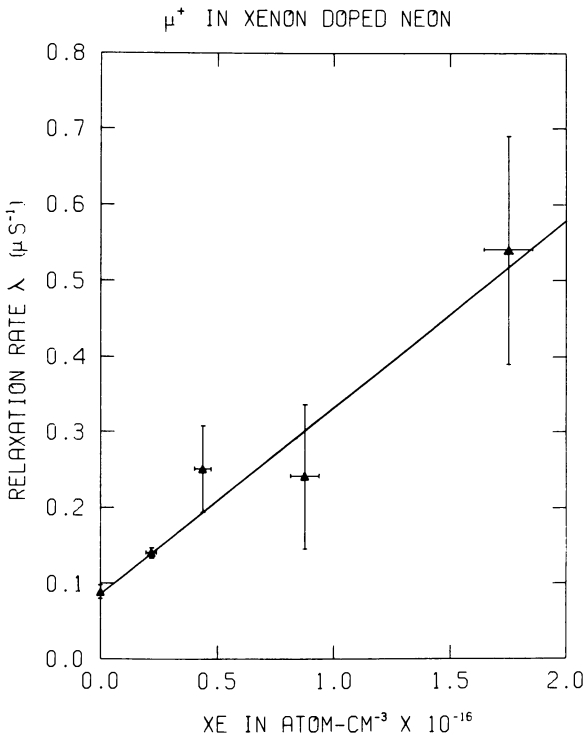

Figure 6b. The rate of free muon relaxation in Xe-doped Ne as a function of Xe concentration at 295 K. This corresponds to the thermal production of Mu with a bimolecular rate constant $k = 2.4 \pm 0.3 \times 10^{-11}$ *cm*^{3} *atom*$^{-1}$ *sec*$^{-1}$.

Publication Date: June 1, 1979 | doi: 10.1021/ba-1979-0175.ch013

tion Type 33 or 34 in addition to the (dominant) epithermal process. Temperature-dependent measurements should show if this effect is really caused by reactions of Type 34 for the first excited state of μ^+Ne—a very interesting possibility.

As a tool for probing the details of atomic physics, the μ^+ offers little competition to existing atomic beam techniques, as a glance at the literature shows. However, the μ^+SR/MSR technique is particularly sensitive to one parameter of general interest: what fraction of H isotopes will thermalize as neutral atoms? This may prove useful to atomic physicists.

For most gas-phase Mu experiments, there are only two requirements that the moderator gas must fulfill: it must provide copious amounts of Mu and it must not be chemically reactive with added reagent. In this regard we initially used Ar as a moderator but more recently we have turned to N_2 because of its larger signal amplitude.

Publication Date: June 1, 1979 | doi: 10.1021/ba-1979-0175.ch013

MUONIUM CHEMISTRY IN THE GAS PHASE. In the gas-phase chemistry experiments, a small amount of reactant (e.g., Cl_2) is added to the moderator gas by the following simple technique: a small reservoir of known volume is filled with reagent gas to a measured pressure of between about 100 and 800 torr; the reagent then is flushed with moderator gas into the previously evacuated target vessel (36-L capacity) to bring the total pressure up to just over 1 atm (a slight positive pressure is maintained to prevent possible O_2 contamination). Typical concentrations for fast reactions are approximately 10^{16} molecules cm^{-3} but in some cases of very slow reactions (e.g., HCl) pure reagent (10^{19} molecules cm^{-3}) was used.

In pure inert moderator gas, the MSR signal caused by coherent Mu precession is long-lived, as shown in Figure 2 and Figure 7 (*top*). The background relaxation rate in pure moderator, λ_0, is probably caused by field inhomogeneities. Reactive collision of a Mu atom with a reagent molecule, e.g.,

$$Mu + Cl_2 \rightarrow MuCl + Cl \qquad (35)$$

places the muon into a diamagnetic environment, breaking the muon–electron hyperfine interaction. This causes a further relaxation of the MSR signal owing to the removal of these muons from the ensemble of precessing Mu atoms, as shown in Figure 7 (*bottom*). This relaxation caused by spin dephasing is described by $\lambda = 1/T_2$ in Equation 17, in analogy with NMR and ESR. Parenthetically, the minimum observable value of T_2 is $\approx$ 100 nsec, which is much longer than the slowing down time of the μ^+ in the gas; therefore, Mu definitely is thermalized before it reacts. The overall relaxation rate is given by

$$\lambda = \lambda_o + k[X] \quad (36)$$

where k is the bimolecular rate constant for the reaction of interest. The predicted linear dependence of λ on reagent concentration [X] is shown in Figure 8 for the reaction of Mu + Cl_2 (*15, 16*) and in Figure 9 for the reaction of Mu + HBr.

At TRIUMF, we have measured room temperature (295 K) bimolecular rate constants for the reactions Mu + Br_2 (*10*), Cl_2 (*15, 16*), Mu + F_2, Mu + HI, and Mu + HBr, and have obtained an upper limit for the Mu + HCl reaction rate constant. In addition, we have measured the room temperature rate constant of Mu + O_2 (*see* Figure 10). This reaction is fundamentally different from the others cited—we believe it

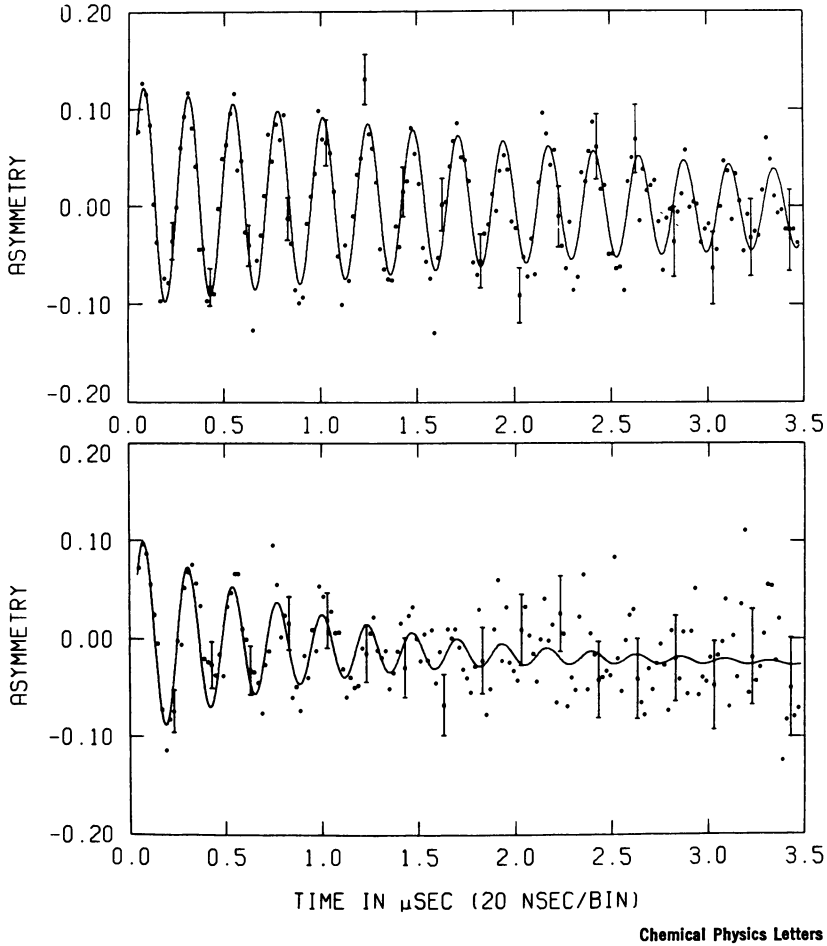

Figure 7. TRIUMF MSR signal in pure Ar (top) *and in Ar with 18.9 × 10^{-6}M Cl_2 present* (bottom). *The magnetic field is 3.0 gauss.* (16)

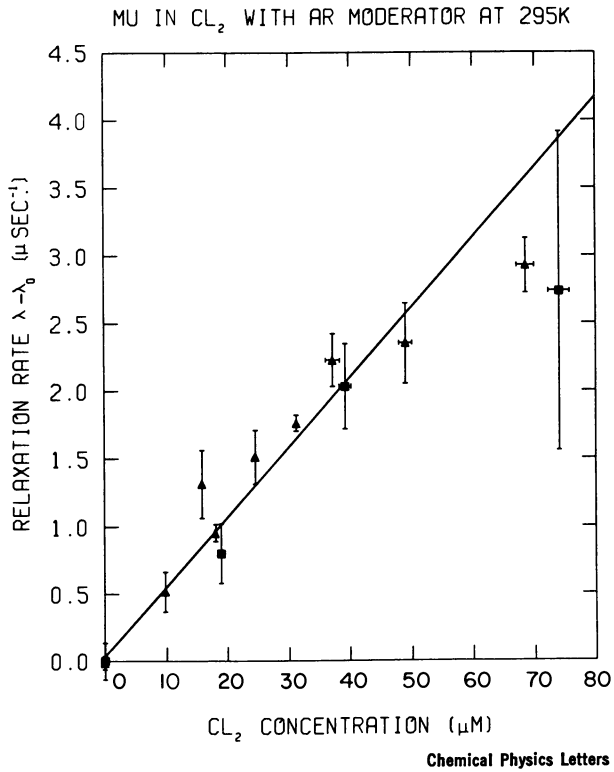

Figure 8. Chemically induced Mu relaxation rate $\lambda - \lambda_0$ *as a function of* Cl_2 *concentration: data from LBL, (△); data from TRIUMF, (□). The straight line is a* χ^2*– minimum fit to the data giving* $k = (5.2 \pm 0.4) \times 10^{10}$ *l/mol-sec.* (16)

is primarily caused by spin exchange with the paramagnetic O_2 and not to a chemical reaction.

Of primary importance to the study of chemical reactions is a measurement of the temperature dependence of the reaction rate, which is expressed usually by the familiar Arrhenius equation.

$$k = A\, e^{-E_a/RT} \tag{37}$$

Thus, raising the temperature increases the reaction rate of the bimolecular reaction, as illustrated in Figures 11 and 12 for the reaction of Mu + F_2 between 295 and 385 K. The measured activation energies (E_a) for Mu + Cl_2 and Mu + F_2 are 1.4 and 0.9 kcal/mol, respectively. The Mu + F_2 result provides good evidence for an important contribution from quantum mechanical tunneling to the reaction kinetics. This will be discussed later in the chapter.

Publication Date: June 1, 1979 | doi: 10.1021/ba-1979-0175.ch013

Publication Date: June 1, 1979 | doi: 10.1021/ba-1979-0175.ch013

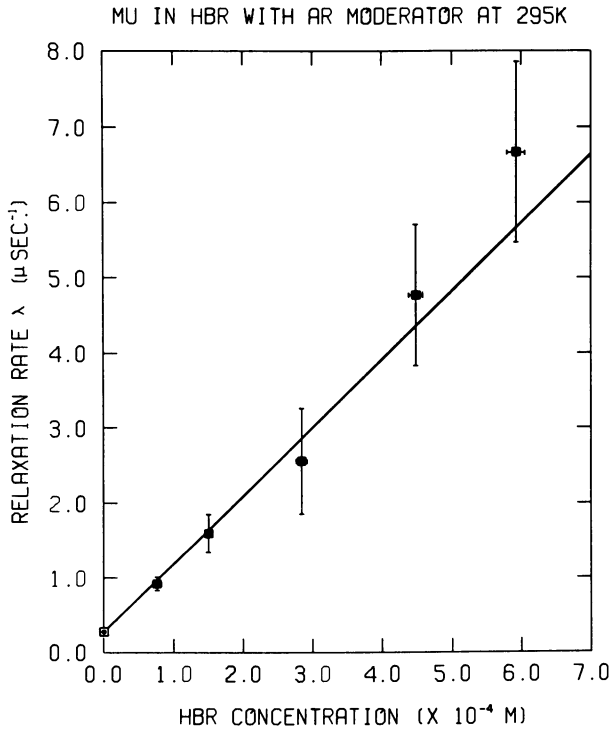

Figure 9. Mu relaxation owing to chemical reaction with HBr in Ar at room temperature corresponding to a bimolecular rate constant of (9.1 ± 1.0) × 10^9 l/mol-sec. The data were obtained at TRIUMF.

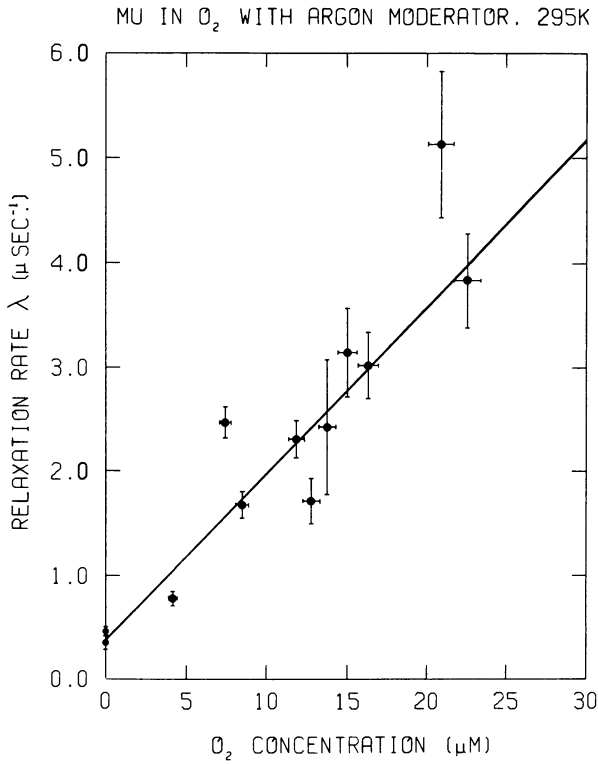

Figure 10. TRIUMF data showing Mu relaxation owing to O_2 in Ar at 295 K corresponding to a bimolecular rate constant of (1.6 ± 0.6) × 10^{11} $l/^1$ mol-sec. The relaxation is probably caused by spin exchange between the Mu and paramagnetic oxygen rather than chemical reaction.

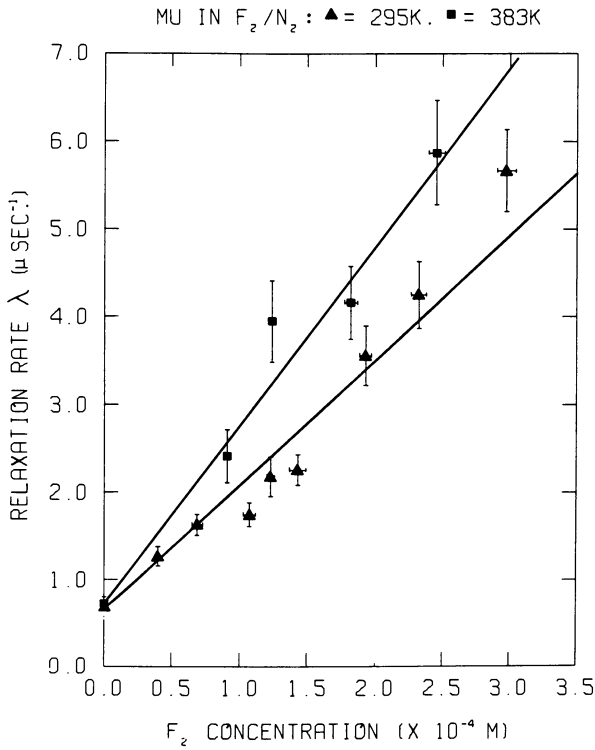

Figure 11. The effect of temperature on the rate of Mu reaction with F_2 in N_2. 295K yielding a bimolecular rate constant of (1.4 ± 0.1) × 10^{10} l/mol-sec, (△); 383K yielding a bimolecular rate constant of (2.0 ± 0.1) × 10^{10} l/mol-sec, (□). Data from TRIUMF.

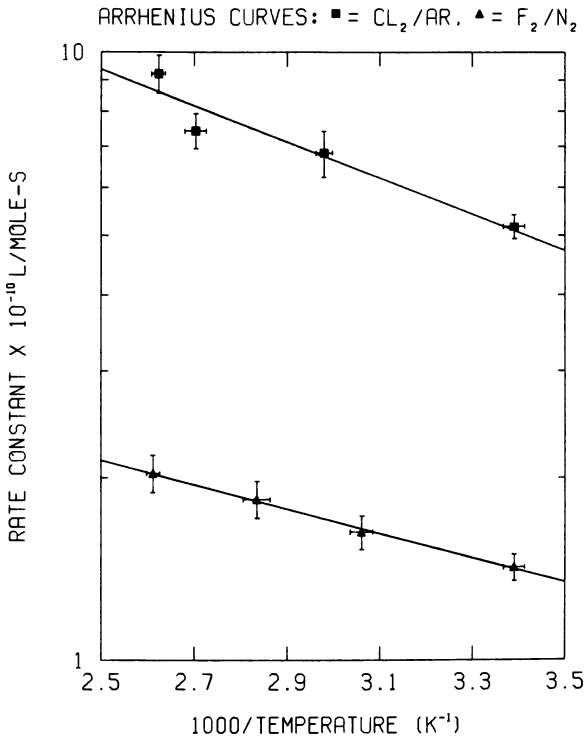

Figure 12. Arrhenius plots for the reaction of Mu with F_2 in N_2 and Cl_2 in Ar, obtained at TRIUMF. The Arrhenius expression for the F_2 reaction is $\log_{10}k = (10.83 \pm 0.20)-(200 \pm 50)/T$ and for the Cl_2 reaction is $(11.72 \pm 0.14) - (297 \pm 44)/T$.

Table II. Reaction Rate Parameters for Muonium

Reaction	$k(295°K)$[a]	E_a(kcal/mol)
F_2	1.4 ± 0.1	0.92 ± 0.23
Cl_2	5.1 ± 0.2	1.36 ± 0.21
Br_2	24 ± 3	—
		H-atom Reaction Type
HCl	≤ 0.000034[b] ± 0.000005	abstraction
		exchange
HBr	0.9 ± 0.10	abstraction
		exchange
HI	2.5 ± 0.1	abstraction
O_2	16.0 ± 0.7[c]	

[a] k(× 10^{10} l/mol sec).
[b] Upper limit only.
[c] There exists a stoichiometric ambiguity of a factor of 2 (*see* Ref. *80*).

The TRIUMF gas-phase Mu reaction rate parameters obtained to date are summarized in Table II. Rate parameters for the corresponding H atom reactions are included in the table; a comparison of these is discussed below.

Comparison of Muonium and Hydrogen Rate Constants. As stated earlier, Mu and H are isotopes of the simplest atom, chemically similar in every respect except for their masses, which differ by a factor of 8.84. One can treat both accurately in the Born–Oppenheimer approximation. A detailed comparison of chemical reaction rates for Mu and H thus provides a unique opportunity for testing models of dynamic isotope effects in chemical kinetics. Such comparisons between H and D (deuterium) already have revealed large differences in reaction rate which in some cases are considered indicative of a quantum mechanical tunneling contribution to the rate (*46, 47, 48, 49*). The much lighter Mu atom displays marked tunneling behavior, further elucidating the role of that process in chemical kinetics. Comparisons of H and tritium (T) have been made also, but since T usually starts out as a hot atom (*50, 51*), these studies are somewhat more difficult to interpret. Only the thermal reactions of the Mu and H atoms are compared here.

In gases (at normal pressure) the mean free path of a Mu atom is many molecular radii, and the concepts of collision rates and cross sections

Publication Date: June 1, 1979 | doi: 10.1021/ba-1979-0175.ch013

Muonium and Hydrogen in the Gas Phase

Hydrogen			
k(295°K)[a]	*E_a(kcal/mol)*	*k_{Mu}/k_H(295°K)*	*H Atom Ref.*
0.20 ± 0.05	2.4 ± 0.2	5.2–10	*76–78*
0.09 ± 0.01	2.2 ± 0.1	13–19	*79*
1.7 ± 0.6	1.8 ± 0.3	2.1–4.8	*76*
0.41 ± 0.04	1.4 ± 0.2	11–14	*80*
1.15 ± 0.15	1.15 ± 0.1	3.8–5.3	*81, 82*
2.2 ± 1.5	1.0 ± 0.5	5.7–38	*10*
2(0.0021[c] ± 0.0002)	3.1 ± 0.3	½(0.013–0.020)[c]	*83–85*
0.000018[d] ± 0.000018	≥ 4.0	~ 1.9	*86*
0.21 ± 0.02	2.6 ± 0.1	3.5–5.3	*87*
≤ 0.0023	5–6	350–440	*87*
0.86 ± 0.39	1.2 ± 0.4	1.9–5.7	*88, 89*

[d] Upper limit (i.e., $< 3.6 \times 10^5$ l/mol sec).
[c] Probably spin exchange, not chemical reaction.

Publication Date: June 1, 1979 | doi: 10.1021/ba-1979-0175.ch013

are well defined. Thus the rate constant for a specific relative velocity of the reagents is proportional to that velocity and the reaction cross section

$$k(v) \sim v\sigma(v) \tag{38}$$

where σ is generally a function of velocity owing to dynamic effects such as activation energies and tunneling probabilities. Of course, in a thermal process we observe the average of $k(v)$ over the thermal velocity distribution

$$k \equiv \langle k(v) \rangle_v \sim \bar{v}\sigma_{eff}, \tag{39}$$

where $\bar{v}$ is the mean thermal velocity and σ_{eff} is an effective average reactive cross section. If we temporarily neglect dynamic effects in σ, we can treat σ_{eff} as a constant geometrical cross section. Although this hard sphere collision model is inaccurate, it is conceptually useful. For example, the rate constant is proportional to the mean velocity, $\bar{v}$; this in turn is proportional to $m^{-1/2}$ where m is the mass of Mu or H, neglecting the motion of the (heavy) scavenger molecules. This produces a kinetic enhancement factor of $\sqrt{m_H/m_{Mu}} \approx 3$ in the ratio of the reaction rates, k_{Mu}/k_H, which is referred to as the kinetic isotope effect. Any additional differences in k_{Mu} and k_H are then probably caused by dynamic isotope effects related to σ_{eff}.

Table II summarizes the reaction rate data for the general reactions

$$Mu + X_2 \rightarrow MuX + X, X = F, Cl, Br \quad (40)$$

and

$$Mu + HX \rightarrow MuH + X, X = Cl, Br, I. \quad (41)$$

The rate parameters for the analogous H atom reactions are included as well as the isotope effect ratios, k_{Mu}/k_H. A number of comments on the data in Table II should be made. For the Mu + HX reactions, we cannot differentiate between abstraction (Equation 41) and exchange (Mu + HX → MuX + H), and therefore the Mu entries in the table represent the total reaction rate for both reaction channels. Separate entries for the analagous H atom reaction rates for abstraction and exchange are given where available. The very slow reaction of Mu + HCl is at the lower limit of the MSR method and only represents an upper limit to the reaction rate constant.

Large inconsistencies exist in the literature values for the H atom reaction rate parameters. In some cases, such as the H + Br_2 reaction, the reaction rates have never been measured directly but have been obtained by measurement of ratios of competitive reaction rates. Even the reaction rates that have been measured directly have widely varying reported values; for example, two recent measurements of the H + Cl_2 reaction (*52, 53*) give room temperature rate constants differing by a factor of four. The source of ambiguity in directly measured reaction rates is competitive interference reactions caused by the presence of several reactive species in relatively large concentration. Wall recombination of H or X atoms are common examples. Since MSR is a one-atom-at-a-time technique, these kinds of interferences do not exist in the Mu reaction rate measurements. The precision of the MSR results is about ± 10%, but since these measurements in gases are presently being performed only at TRIUMF, we have no independent check of their accuracy. An estimate of the reproducibility of the MSR technique was obtained in our study of the Mu + Cl_2 reaction which was performed first at LBL and, later, at TRIUMF using the same technique but a completely different experimental apparatus. The rate constants at 295° K were $k = 5.5 \pm 0.3$ and $4.7 \pm 0.6 \times 10^{10}$ L mol^{-1} sec^{-1} at LBL and TRIUMF, respectively.

In spite of the experimental uncertainties, it is clear from Table II that the reaction rates of Mu + X_2 exceed the analogous H atom reaction rates by more than the nominal kinetic isotope factor of three, indicating the presence of a dynamic isotope effect. The only detailed theoretical calculation of a Mu reaction is that owing to Connor, Jakubetz, and

Publication Date: June 1, 1979 | doi: 10.1021/ba-1979-0175.ch013

Manz (*54, 55*) who compared collinear reaction rates of Mu and H with F_2. At room temperature, they predict the ratio of k_{Mu}/k_H to be 5.9 which is in accord with the experimental value of Albright et al. (*see* Table II). Furthermore, they calculate apparent activation energies of 1.1 and 2.1 kcal/mol at 300°K for the Mu and H reactions respectively, in good agreement with experiment. These calculations show that the Mu + F_2 reaction rate is dominated by quantum mechanical tunneling at room temperature. The effect of tunneling in these calculations is demonstrated further in the curvature of the Arrhenius plot shown in Figure 13 for Mu, H, D, and T reactions with F_2. By extrapolating the tunneling contribution to the isotope effect from F_2 to Br_2, one would expect the order of isotope effect ratios k_{Mu}/k_H to be $F_2 > Cl_2 > Br_2$, the same order as H activation energies. The deviation from this order for Br_2 in the table is probably a manifestation of the uncertainty in the H atom reaction rate which has never been determined directly.

The reactions of H atoms with hydrogen halides are dominated by abstraction for the cases of HCl, HBr, and HI, and this also should be true for Mu reactions with HBr and HI. In the case of HCl, however, the H atom reaction is near a thermodynamical limit as evidenced by the fact that it is 100 times slower than the HBr reaction. For Mu, this limit is crossed since the much higher zero point energy of MuH makes the Mu + HCl reaction endothermic by about 6 kcal/mol. This accounts for

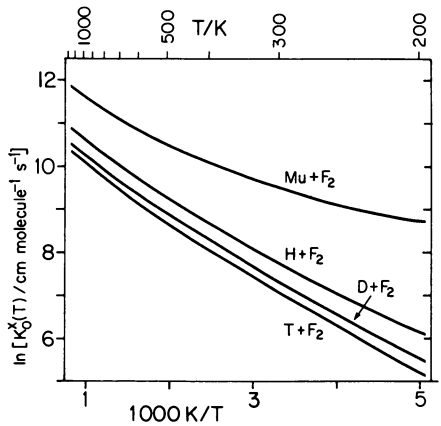

Figure 13. Theoretical Arrhenius plots for the reactions of T, D, H, and Mu with F_2. At high temperatures the ratio $k_{Mu}:k_H:k_D$ is determined by the mean of velocity; but near room temperature the Mu + F_2 reaction is enhanced owing to quantum tunneling. (From Refs. 54, 55).

Publication Date: June 1, 1979 | doi: 10.1021/ba-1979-0175.ch013

the observation that Mu reacts more slowly with HCl than H does in the abstraction reaction. Perhaps the Mu + HCl reaction is dominated by exchange rather than abstraction, in which case it is probably faster than the corresponding H atom exchange reaction.

It is not clear whether the Mu + HX reactions reveal any dynamic isotope effect or whether such an effect enhances or retards the rate. These exchange reactions suggest an inverse dynamic isotope effect. The hydrogen analogue of the Mu + HCl reaction has been cited as an example for transition state theory in which a quasi-bound intermediate molecule is formed (*56, 57, 58*). In such a reaction intermediate, the zero point motion for the Mu-activated complex would be higher than the zero point motion for the analogous H complex giving rise to a larger activation energy. This could account for such an inverse isotope effect.

Thermal Muonium Chemistry in Liquids. MSR STUDIES. Assuming the rate constant for Mu + O_2 spin exchange to be the same in the gas (Figure 10) and liquid phases, typical dissolved O_2 concentrations of 2×10^{-4} *M* at room temperature lead to Mu relaxation times of only 30 nsec, too fast to be readily observable. However, by degassing the target sample it has been possible to observe directly the MSR signal in inert solvents such as water and some alcohols (*12, 13, 14, 37*). These results also have been confirmed recently at TRIUMF. In exact analogy to the above description of MSR studies in the gas phase, one can monitor the disappearance of the Mu precession signal in the liquid phase to obtain bimolecular rate constants for the reactions of Mu in different solvents. Such studies are being actively pursued by the group at SIN (*11, 12, 13, 14*).

However, the amplitude of the MSR signal in liquids is considerably weaker than observed in gases; for runs with modest statistics (about 10^6 events) it is often only revealed through its Fourier transform. A time and frequency spectrum obtained at TRIUMF is shown in Figure 14 (*see* Reference *37* also). The weaker Mu signal amplitude is not completely compensated by the diamagnetic μ^+ fraction; SIN results indicate $P\mu^+ = 0.62$ and $P_{Mu} = 0.20$, for the polarizations of μ^+ and Mu components in H_2O, respectively, leaving a missing muon fraction of 0.18. We return briefly to this point in the ensuing discussion, noting here that it surely reflects some very early stage of Mu depolarization, possibly via the formation of short-lived muonic radicals.

Despite the weak MSR signals seen in liquids, the SIN group has managed to obtain a number of very interesting results (*11, 12, 59, 60*). A sample of their data is shown in Figure 15 for aqueous solutions of fumaric acid. As in the gas-phase studies discussed previously (Figure 7), the amplitude of the MSR signal clearly relaxes faster with increasing fumaric acid concentration; the solid curves fit to the data using essen-

Publication Date: June 1, 1979 | doi: 10.1021/ba-1979-0175.ch013

tially the same expression as in Equation 17. As in Figures 8 and 9 a plot of λ vs. concentration should be a straight line, as shown in Figure 16 for the SIN data. Since the initial Mu amplitude is 4 to 5 times lower than that obtained in the gas phase, one must acquire approximately 20 times as many events to achieve the same accuracy for individual determinations of λ. Nevertheless, least-squares fits to SIN data yield rate constants with precision comparable with TRIUMF gas-phase results ($\pm$ about 10%). Recent SIN results are presented in Table III; rate constants for Mu reactions are compared with corresponding H atom values as well as with Mu rate constants obtained earlier by the residual polarization technique (*8, 9, 34*). Later we will discuss the comparisons between Mu and H atom rate constants.

Publication Date: June 1, 1979 | doi: 10.1021/ba-1979-0175.ch013

Table III. Muonium and Hydrogen-Atom Rate Constants in Aqueous Solutions[a]

Substrate	k_{Mu} (M^{-1} sec^{-1})	k_H[b] (M^{-1} sec^{-1})	k_{Mu}/k_H
Methanol	$< 3 \times 10^4$	2.5×10^6	< 0.01
Ethanol	$< 3 \times 10^5$	2.1×10^7	< 0.015
2-Propanol[c]	$\sim 7 \times 10^5$	6.8×10^7	~ 0.01
2-Butanol[c]	1.1×10^6	1.3×10^8	0.01
Formate ion (pH > 7)	7.8×10^6	1.2×10^8	0.07
Maleic acid (pH 1)	1.1×10^{10}	8×10^9	1.4
Fumaric acid (pH 1)	1.4×10^{10}	7×10^9	2
MnO_4^-	2.5×10^{10}	2.4×10^{10}	1
Ag^+	1.6×10^{10}	$(1–3) \times 10^{10}$	~ 1
NO_3^-	1.5×10^9	9×10^6	~ 170
	(1.2×10^{11})[d]		
	(1.7×10^{10})[e]		
Acetone	8.7×10^7	2.8×10^6	30
Ascorbic acid (pH 1)	1.8×10^9	1.7×10^8	10
OH^-	1.7×10^7	1.8×10^7	1
	(1.8×10^9)[e]		
ClO_4^-	$< 10^7$	—	—
	(3.8×10^{10})[d]		
	(1.2×10^9)[e]		
H^+, Na^+, Cl^-	$< 2 \times 10^5$	$< 10^5$	—

[a] Refs. *11, 12, 13, 14.*
[b] Ref. *65.*
[c] Mu values are preliminary.
[d] Ref. *8.* From P_{res}—may involve radical reactions, etc.
[e] Ref. *7.* From P_{res}—may involve radical reactions, etc.

Publication Date: June 1, 1979 | doi: 10.1021/ba-1979-0175.ch013

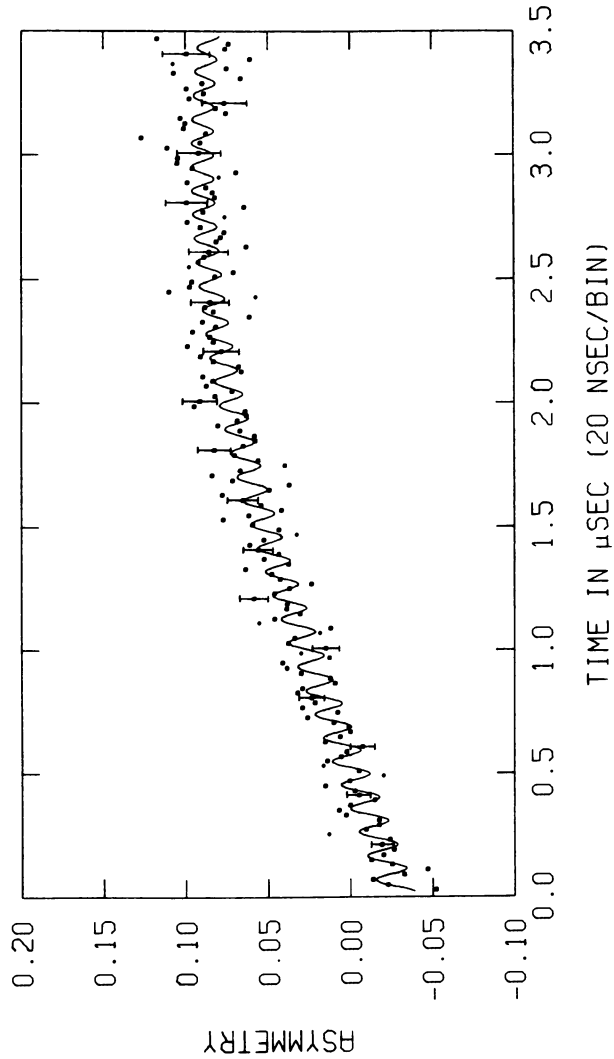

In Positronium and Muonium Chemistry; Ache, H.;
Advances in Chemistry; American Chemical Society: Washington, DC, 1979.

Publication Date: June 1, 1979 | doi: 10.1021/ba-1979-0175.ch013

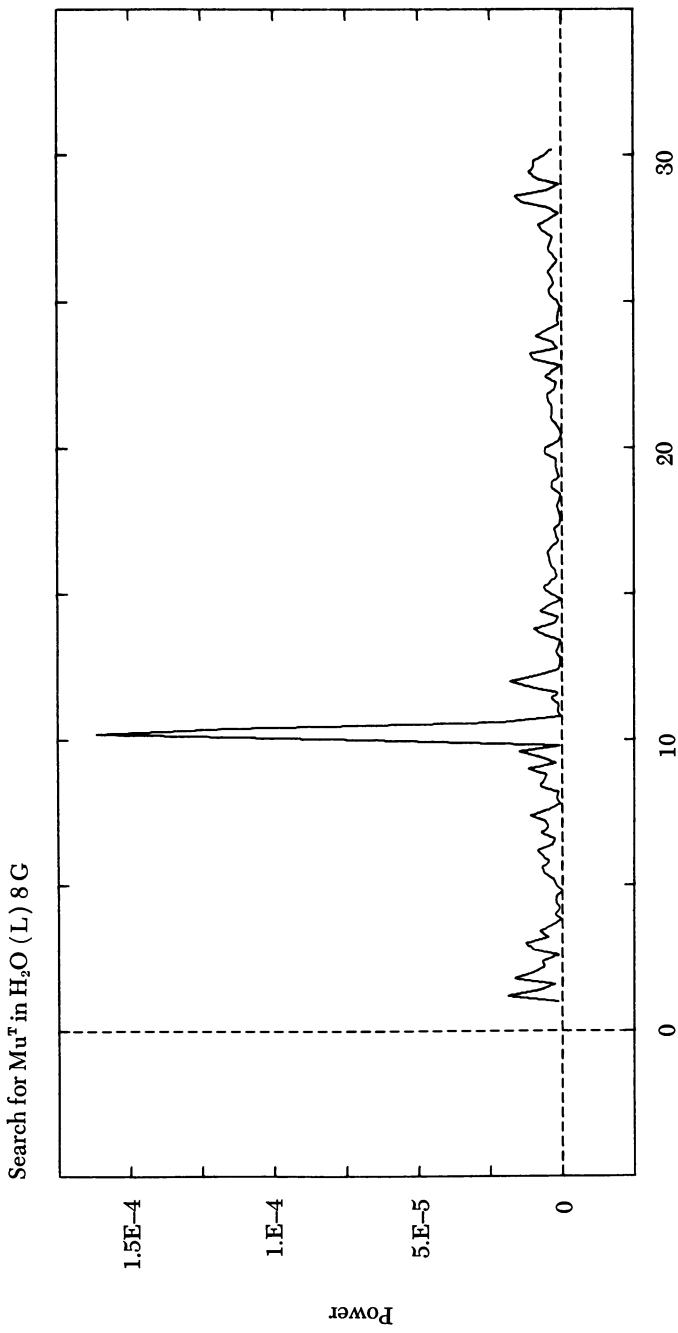

Figure 14. TRIUMF data showing Mu precession in degassed water at 6.5 G, obtained with surface muons in a Teflon cell with a mylar window

Publication Date: June 1, 1979 | doi: 10.1021/ba-1979-0175.ch013

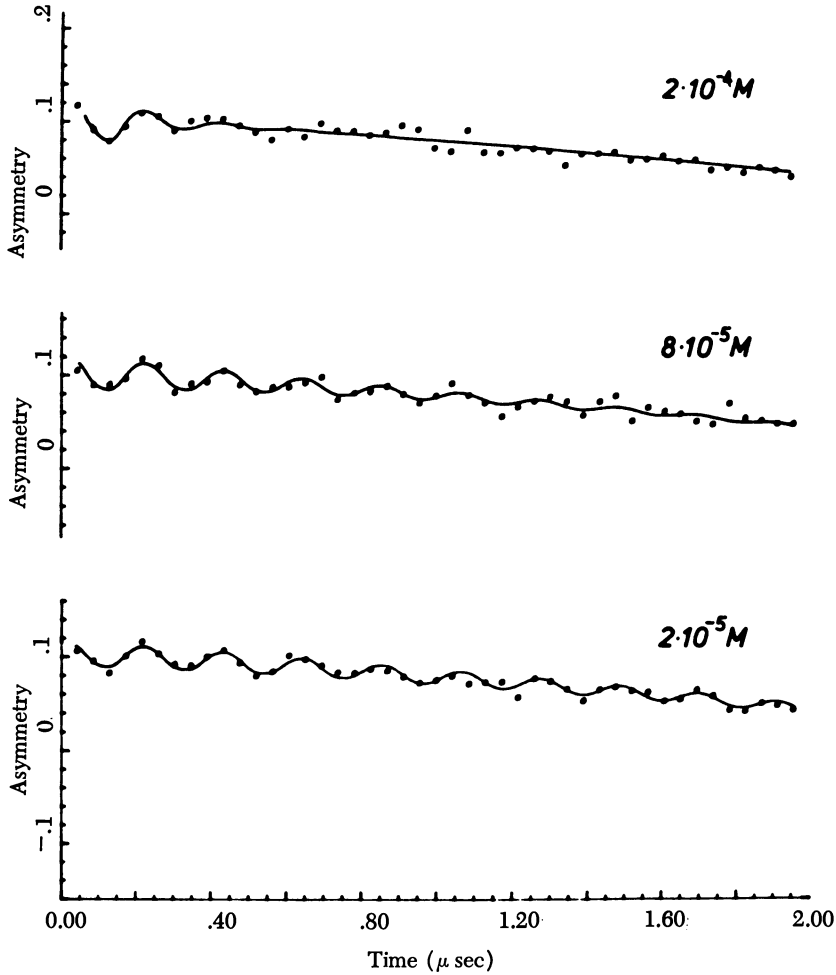

Figure 15. MSR signals for aqueous solutions of fumaric acid. The data were taken at SIN (Refs. 12, 13, 14*).*

Publication Date: June 1, 1979 | doi: 10.1021/ba-1979-0175.ch013

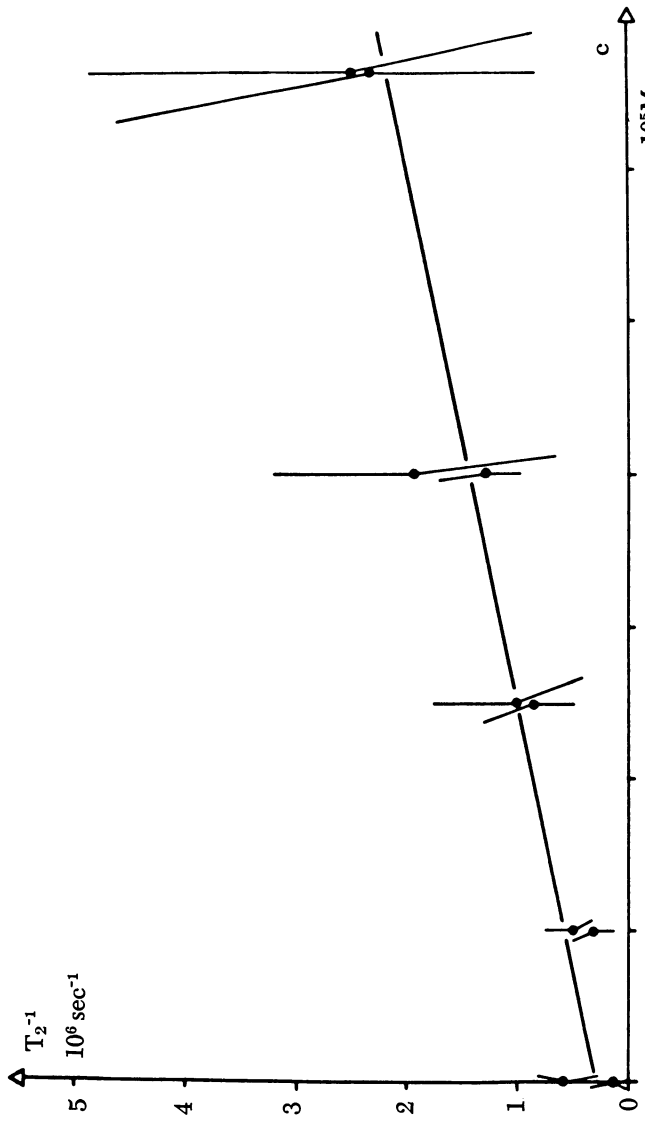

Figure 16. Mu relaxation rates owing to chemical reaction with fumaric acid in water (see *Refs.* 12, 13, 14)

P_{res} (μ^+SR) STUDIES. The residual muon polarization which results when the μ^+ is placed in a diamagnetic environment by the simplest sort of process has been treated already. To recapitulate, it is not the free Mu precession signal that is observed directly but only the result of Mu atom reactions occurring at very early times. The experimental observable then is the residual μ^+ polarization, from which we infer the nature of the chemical reactions that produced it via a suitable theoretical transform. Qualitatively, if Mu reacts very quickly then we expect a large P_{res} and a small phase angle from the brief Mu precession; conversely, if Mu reacts slowly, the μ^+ will be depolarized effectively when placed in its final chemical environment, giving a small P_{res} and a relatively large phase angle for the thermal reaction component. In practice, P_{res} approaches the hot atom fraction h (no phase rotation) for very slow reactions.

Figure 17 shows experimental data for P_{res} as a function of I_2 concentration, obtained for the reaction of Mu + I_2 at 103 G in methanol; the upper half shows the magnitude of P_{res} (Equation 21) while the lower half shows the phase (Equation 20). The solid curves are theoretical fits using Equation 30. The hot atom fraction is 0.52 ± 0.02. Both

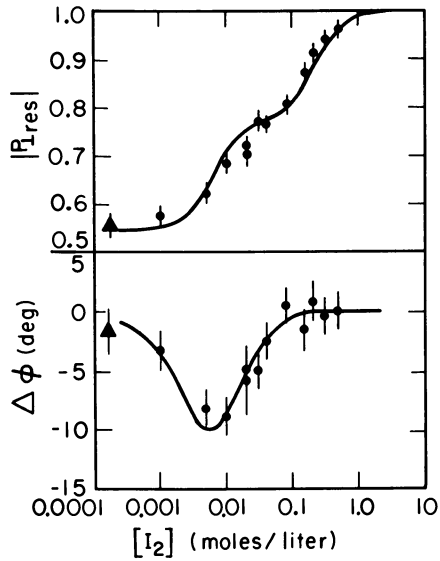

Figure 17. Experimental data from LBL and best fit for dependence of residual polarization upon concentration of I_2 in methanol at 103 G (Leftmost points are for pure methanol (P_{res} = h) and are therefore actually infinitely far off scale.) (3)

the plateau effect in P_{res} and the phase dip are ubiquitous characteristics of this simple depolarization mechanism, which historically has been called the proper Mu mechanism (*7, 9, 27, 28*). The formalism developed earlier is in good agreement with the experimental data. The extracted bimolecular rate constant at 103 G is $(13.1 \pm 1.6) \times 10^{10}$ L mol^{-1} sec^{-1}. A weighted average of fits to the data obtained at other fields at both TRIUMF and LBL, using the expression in Equation 30, gives $k = 14 \pm 2 \times 10^{10}$ (*40*) in excellent agreement with the value obtained previously by fitting essentially the same data with a much more general theory involving diagonalization of the spin density matrix (*8, 9, 34*).

The thermal reaction involved is presumably

$$Mu + I_2 \rightarrow MuI + I \tag{42}$$

by analogy with the corresponding reaction for the H atom, for which the rate constant in aqueous solution is reported (*61, 62, 63*) to be 2×10 L mol^{-1} sec^{-1}. If differences between solvents can be neglected, one concludes that Mu reacts with I_2 in solution about 7 times as fast as H does, although if there are large uncertainties in the rate measured for the H atom reaction there may well be little real difference in these numbers. Such a large rate constant is close to or at the diffusion-controlled limit and lends support to the contention that in solution Mu acts chemically just like H. It is important, however, to measure the rate constant for this reaction by the direct MSR technique. We turn now to a brief discussion of the effect of radicals on the depolarization of the μ^+.

The mechanism for μ^+ depolarization considered above is the simplest one possible, i.e., placing the μ^+ in a diamagnetic environment in a single step, as exemplified by Equation 42. In general, we may expect the overall reaction scheme to be more complicated, possibly involving intermediate μ^+ radicals as suggested for the thermal reaction scheme of Mu with Br_2 in benzene (*8, 9, 34, 64*):

$$Mu + Br_2 \xrightarrow{k_a} MuBr + Br \tag{43a}$$

$$Mu + C_6H_6 \xrightarrow{k_b} C_6H_6Mu \tag{43b}$$

$$C_6M_6Mu + Br_2 \xrightarrow{k_c} \text{diamagnetic compounds.} \tag{43c}$$

Here there is competition between these reactions; but ultimately the μ^+ must find itself in a diamagnetic environment in a short time compared with the period of Mu precession if any polarization is to remain. Indeed, attempting to reproduce the measured P_{res} on the assumption of just the

Publication Date: June 1, 1979 | doi: 10.1021/ba-1979-0175.ch013

proper Mu mechanism discussed above (i.e., Equation 43a only) fails badly, as shown by the dashed lines in Figure 18. On the other hand, assuming that the complete reaction scheme involving free radicals gives much better fits to the data, as shown by the solid curves in the same figure. Similar studies of Mu chemistry in aqueous solutions of H_2O_2, ClO_4^-, and NO_3^- revealed the presence of free radical mechanisms as a general feature of Mu chemistry in liquids (*8, 9, 34, 35, 36*).

It has been pointed out (*35*) that such general reaction schemes as that represented in Equation 43 have more parameters than can be determined both uniquely and precisely from fitting the P_{res} data usually available, and thus are more appropriate for qualitative than for quantitative analyses. There are several large discrepancies between rate constants extracted from P_{res} and MSR data; a dramatic example is the rate constant for Mu + ClO_4^- in H_2O: the value extracted by the P_{res} technique is at least 10^5 faster than that extracted from the direct MSR method. The source of these discrepancies is not yet known, but the MSR technique is clearly more precise when applicable. Thus, while the P_{res} method is both qualitatively and quantitatively useful in simple Mu mechanism studies, it is mainly valuable qualitatively in complicated

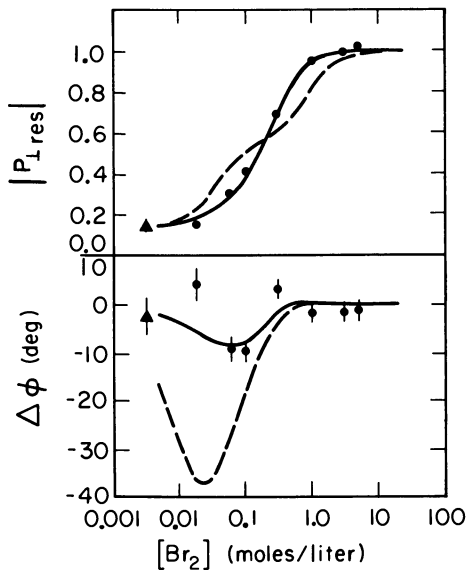

Figure 18. Residual muon polarization in benzene as a function of the concentration of dissolved bromine. Data from LBL. Best fit without radicals, (– – –); best fit with radicals, (——).(3)

Publication Date: June 1, 1979 | doi: 10.1021/ba-1979-0175.ch013

problems. In particular, there may be many situations in which short-lived radical intermediates cannot be detected by the MSR technique, but leave an unambiguous qualitative signateur in the P_{res} data from μ^+SR. The residual polarization technique therefore remains an important tool despite its limited numerical precision in complicated cases. It is particularly useful for studying the hot-atom fraction *h*.

DISCUSSION OF THERMAL MUONIUM REACTIONS IN LIQUID WATER. Table III gives the values of k for the reaction of thermalized Mu atoms with several solutes in aqueous solution obtained from the dependence of the Mu atom lifetime on solute concentration (*11–14, 59, 60*). They are compared with published data for the analogous H atom reactions. The reactants may be divided into at least three groups. In the first group (first five reagents) the H atom reaction is regarded as an abstraction reaction, in which an H attached to a C (carbon) atom is abstracted. It is clear that H is much more efficient than Mu at this process. Furthermore, it is possible that the fastest of these Mu reactions, with formate, is an addition rather than abstraction reaction. Apparently Mu does not abstract H efficiently in solution. In this respect Mu more closely resembles solvated electrons than hydrogen atoms.

Of the next four reactions, the rate constants for both Mu and H are of the order of 10^{10} L mol^{-1} sec^{-1} and consequently they are close to the expected diffusion-controlled limit. Since these reactions evidently occur on almost every collision no isotope effect would be expected in so far as the diffusion constant itself may be slightly higher for the lighter particle. Indeed the ratio k_{Mu}/k_H ranges between 1 and 2 for those diffusion-limited rate constants. It is interesting to note that the reaction with maleic and fumaric acids should be addition reactions to a C=C double bond, whereas reaction with MnO_4^- and Ag^+ (silver) should be simple reduction by electron transfer.

In fact the rate constants for the reaction of H, Mu, Ps, and solvated electrons (e_{aq}^-) with MnO_4^- (which is the only reagent for which all four rate constants are readily available) are very nearly the same. They all lie within the range $2–3 \times 10^{10}$ L mol^{-1} sec^{-1} (*11, 65*) which is regarded—for Ps and e_{aq}^- at least (*66*)—to be essentially the diffusion-controlled limit. This implies that both the diffusion coefficients and interaction radii are very nearly the same for the three uncharged species.

The reaction of Mu with nitrate, acetone, and ascorbic acid are much more efficient than are the corresponding H atom reactions. The isotope effect, however, is much too variable in these three examples to warrant comment at this stage. It might be noted also that e_{aq}^- reacts much more efficiently than Mu with NO_3^- and acetone but less so with ascorbic acid; so there is no general analogy between the types of reactions exhibited by Mu and e_{aq}^-.

Publication Date: June 1, 1979 | doi: 10.1021/ba-1979-0175.ch013

Mu and H have the same rate constant for reaction with OH^-. This is a particularly interesting reaction in that it represents the interconversion of Mu as an acid to its conjugate base, which is e^-_{aq}. Perhaps like H (*67*)

$$Mu + OH^- \rightarrow e^-_{aq} + MuOH$$

Mu has a $pK_a < 9.7$.

Hot Atom Reactions and Epithermal μ^+SR Studies. EXPERIMENTAL TREATMENTS AND RESULTS. One quantity of considerable interest that emerges from a study of the residual polarization in liquids is the hot-atom fraction, h, the low-concentration limit of P_{res} (X). This is shown in Figure 17 (for Mu + I_2 in CH_3OH) and in Figure 18 (for Mu + Br_2 in benzene) to yield $h = 0.54 \pm 0.02$ and 0.13 ± 0.01, respectively. In the analysis of References 8 and 9, based on the theoretical formulation given in Reference 34, this fraction is assumed to be entirely caused by hot-atom reactions in the solvent which place the μ^+ in a dimagnetic environment essentially at $t = 0$. Therefore h is assumed to be independent of both reagent concentration (even for very concentrated solutions, up to 10*M* in some cases) and applied magnetic field. The hot atom fraction defined in this way varies from a minimum of h approximately equal to 0.13 in benzene to a maximum of h about equal to 1.0 in CCl_4. We do not know just how hot the Mu atom is when such reactions occur, but evidence from gas-phase studies (*see* above discussion) suggests that stable Mu first forms at kinetic energies of about 200 eV. Lower energies are sampled then as the Mu atom slows down by collisions.

How does one distinguish between epithermal and thermal processes in liquids? In the direct MSR technique discussed earlier, this is, in principle, straightforward. Any differences in epithermal processes between solvents would be reflected in a change in the initial amplitude of Mu precession, as opposed to the relaxation of the signal owing to thermal processes. However, as noted above, the signal amplitudes are weak ($\lesssim 2\%$) and care must be exercised in the interpretation of these numbers.

In our P_{res} studies, we have assumed the epithermal process to be caused entirely by reactions with the solvent. These can be distinguished from a possible thermal process (with the solvent) by observing the magnetic field dependence of P_{res} and/or by measuring the phase dependence of Mu precession in the limit of zero reagent concentration. Since epithermal processes are expected to occur at very early times ($t < 10^{-9}$ sec) they will be unaffected by magnetic fields (in sufficient time for Mu precession) and, more crucially, the phase angle θ in $P_{res} = |P_{res}|e^{i\theta}$ represented by Equation 20 should return to zero in the limit of zero reagent concentration (because of the constant, unrotated hot-atom

Publication Date: June 1, 1979 | doi: 10.1021/ba-1979-0175.ch013

contribution). A good example of the latter effect can be seen in Figure 17 (*bottom*) for the reaction of Mu with I_2 in methanol. The magnetic field independence of h for this reaction has been verified (*8, 9, 40*); h is 0.54 ± 0.02 for fields varying between 103 and 4500 G.

On the other hand, there are some difficulties created with this concept. The missing muon fraction has prompted a different interpretation of h, which casts further doubt on the previously mentioned contribution of μ^+ radicals in the overall μ^+ depolarization process. For example, Percival et al. (*11, 12, 13, 14*) have presented a consistent interpretation of the reaction of Mu with NO_3^- and MnO_4^- in aqueous solution which involves no μ^+ radicals, contrary to the LBL interpretation (for NO_3^-) discussed earlier (Table III). Percival et al. claim that h depends on solute concentration, with full (re)polarization ($P_{Mu} + P_{\mu^+} = 1$) observed for NO_3^- concentrations as low as 0.1*M*. Evidently in these solutions the missing polarization fraction of 0.18 may be restored by some fast process involving NO_3^-. These effects have lead the authors to suggest that free radical reactions in the spur at the end of the μ^+ track (*68*) may obscure epithermal processes in certain solutions.

This section of the chapter concentrates on epithermal reactions in pure liquids. In some cases the epithermal reaction hypothesis has been checked directly by either field or phase variations as noted above and is reinforced by the observation of long-lived Mu, for example, in H_2O and some alcohols (*12, 13, 14, 37*) (*see* also Figure 14). Consequently, it seems reasonable to identify the measured residual polarizations in such media with the diamagnetic hot-atom fractions, h_D. It should be noted, nevertheless, that it is much more difficult experimentally to determine with accuracy the amplitude of the μ^+SR (or MSR) signal than its relaxation. Corrections for beam polarization, target thickness, counter geometry, etc., need to be correctly normalized before the values of h_D can be obtained. For instance, the target thickness can affect both the polarization of stopping muons (owing to the momentum spread in conventional muon beams) and the measured electron asymmetries (thicker targets preferentially absorb lower energy positrons, which have smaller asymmetries). The standard procedure, noted previously, is to normalize P_{res} by the asymmetry found for CCl_4 under identical experimental conditions. The use of CCl_4 as the normalizing medium in liquid chemistry is justified by the fact that it gives essentially the same asymmetry as the maximum found in simple metals such as copper (Cu) or aluminum (Al). In the case of thick targets, corrections must be made for the different stopping power for both muons and positrons.

In order to circumvent the need to apply such stopping power corrections to obtain P_{res}, at TRIUMF we have used the nearly monoenergetic (4 MeV) surface muon beam in conjunction with the thin cell (4 mm)

Publication Date: June 1, 1979 | doi: 10.1021/ba-1979-0175.ch013

depicted in Figure 19. This cell was placed at 45° to the incident muon beam with two positron telescopes at 90° (as in Figure 4). The samples were thick enough to stop all the muons but sufficiently thin so that the spectrum of emitted positrons was not influenced seriously by the density of the liquid being studied. Data obtained by the above method compares well in fact with data obtained from different laboratories using conventional muons corrected for density. A sample of the results is given in Table IV, which, along with values in Table V, forms the basis for the subsequent discussion. The data in Table V comes from several sources, including recent (corrected) results from TRIUMF using conventional muons. Data obtained at LBL in mixtures of CH_3OH with $CHCl_3$ and with benzene are given in Figures 20 and 21. We have plotted the measured asymmetry as a function of volume fraction, rather than of mole fraction as was done previously (*3, 69*). Volume fraction is a more appropriate variable for this discussion since it is approximately proportional to the fraction of time during the slowing down process that the

Publication Date: June 1, 1979 | doi: 10.1021/ba-1979-0175.ch013

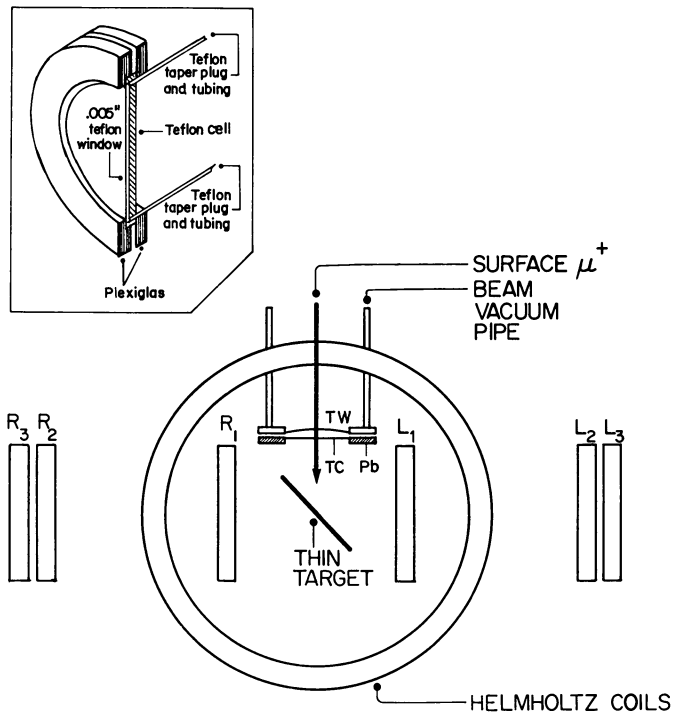

Figure 19. Sketch of the thin Teflon cell used at TRIUMF with "surface" muons and its arrangement with respect to the counters (TC is the thin counter which defined the μ^+ beam; L1, L2, and L3 are the left-hand-side counters and R1, R2, and R3 are the right-hand-side counters).

Table IV. Comparison of Data Obtained on P_{res} from TRIUMF Using Surface Muons with Data from LBL, JINR[a] (corrected P_{res} 0° mode), and SIN, Where Possible[b]

Target Liquid	*TRIUMF*	*LBL*	*JINR*	*SIN*
CCl_4	1	1	1	1
$CHCl_3$	0.86 ± .04	0.85 ± .04	0.80 ± .06	
H_2O	0.61 ± .02	0.59 ± .02[c]	0.62 ± .04	0.62 ± .01
D_2O	0.57 ± .04	0.59 ± .02		0.57 ± .03
CH_3OH	0.56 ± .04	0.54 ± .02[c]	0.58 ± .05	0.61 ± .01
$(CH_3)_2CHOH$	0.61 ± .04	0.64 ± .01		0.57 ± 0.5[d]
$C\text{–}C_6H_{12}$	0.68 ± .04	0.67 ± .02	0.68 ± .05	0.67 ± 0.5[d]
$C\text{–}C_6H_{10}$	0.47 ± .03		0.48 ± .05	
C_6H_6	0.12 ± .02	0.13 ± .01[c]	0.15 ± .03	0.21 ± 0.05[d]
CS_2	0.16 ± .03	0.11 ± .01		0.18 ± 0.05
$(CH_3)_2CO$	0.54 ± .05			0.50 ± 0.05
$Si(CH_3)_4$	0.54 ± .03			
C_5H_{12}	0.64 ± .04			
C_7H_{16}	0.65 ± .04			
$C_{10}H_{22}$	0.67 ± .05			
2,2,4-Trimethyl-pentane	0.61 ± .05			

[a] JINR is the Joint Institute for Nuclear Research, Dubna, U.S.S.R., Refs. *4, 5, 6, 7*.

[b] The errors quoted arise from the uncertainty due to the statistics of the experiment and do not take account of other possible sources of error.

[c] These data were obtained as limiting in values titration curves and therefore required no density corrections.

[d] Preliminary values.

Publication Date: June 1, 1979 | doi: 10.1021/ba-1979-0175.ch013

epithermal Mu atoms spend in contact with each ingredient. (Mole fraction takes no account of the relative sizes of the molecules involved.) Asymmetries in the mixtures can be correlated with h_D because the phase change measurements did not show the characteristic dip which would occur if thermal reactions of Mu were involved.

DISCUSSION. What chemical or physical properties of the target materials influence P_{res}? Why do epithermal Mu atoms react efficiently to form diamagnetic products with liquids such as CCl_4 or $CHCl_3$ and quite inefficiently with others such as CS_2 or benzene? Let us consider some possibilities.

Bond Energy. Could it simply be that the efficiency of reaction increases as the strength of the bond to be broken decreases? Care must be exercised in considering this question for two reasons: firstly, most molecules contain more than two types of atoms and more than one type of bond, and it is not known which bond is broken. Secondly, the epithermal Mu atom will thermalize more rapidly during collisions with lighter atoms so that as the chemical constitution is changed the number of collisions made during thermalization will change. Consequently it is

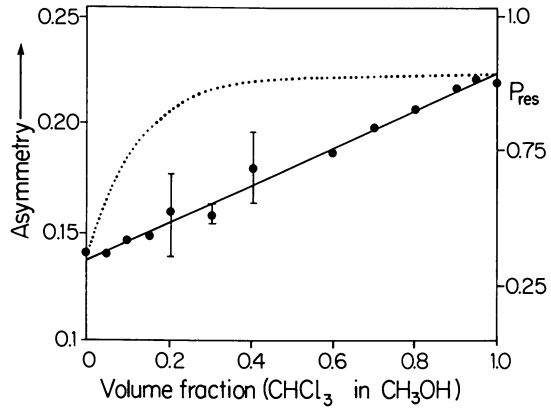

Figure 20. Data from LBL on $CH_3OH/CHCl_4$ mixtures, plotted as measured asymmetry and P_{res} against volume fraction of the mixtures. The data were taken in a transverse field of 100 G. (The dotted line indicates how the asymmetry is expected to vary if selective reaction by $CHCl_3$ were possible, or if spur scavenging by $CHCl_3$ occurred).

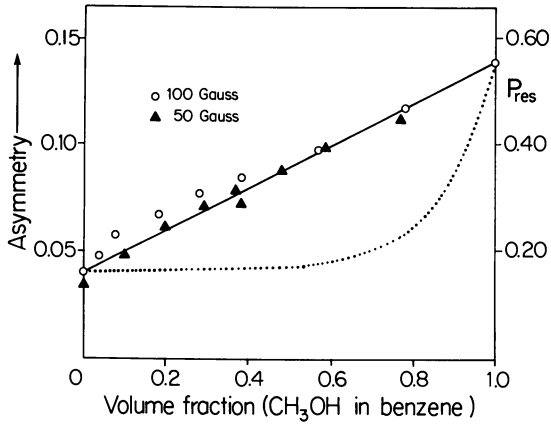

Figure 21. Data from LBL (100 G) and JINR (50 G) showing asymmetry and P_{res} as a function of volume fraction in CH_3OH/benzene mixtures. (The dotted line indicates how the asymmetry should change if benzene gave "sponge-like" protection to CH_3OH.)

Publication Date: June 1, 1979 | doi: 10.1021/ba-1979-0175.ch013

Table V. Collection of Residual Muon Polarization Data from Various Sources

Target	P_{res}	*Reference and Comments*
CCl_4	1	By definition. B. E. = 78
$SiCl_4$	0.48	TRIUMF[a] B. E. = 91
$SnCl_4$	0.99	TRIUMF B. E. = 76
$TiCl_4$	1.00	TRIUMF B. E. = 102
Cyclohexane	0.68	Table IV
Cyclohexene	0.47 (0.55)	JINR[b]
1,4-Cyclohexadiene	0.40 (0.47)	JINR
1,3-Cyclohexadiene	0.32 (0.38)	JINR
Benzene	0.15 (0.18)	JINR
Hexane	0.62	LBL
Hexene	0.50	LBL
Hexyne	0.43	LBL
2-Propanol	0.62	Table IV
Acetone	0.54	Table IV
C_6H_6	0.15 (0.18)	JINR[c]
C_6H_5Cl	0.23 (0.27)	JINR
C_6H_5Br	0.38 (0.45)	JINR
C_6H_5I	0.49 (0.59)	JINR
$C_6H_5CH_2Cl$	0.35 (0.42)	JINR
$C_6H_5CHCl_2$	0.46 (0.55)	JINR
$C_6H_5CCl_3$	0.57 (0.68)	JINR
$CHCl_3$	0.85	Table IV
CH_2Cl_2	0.70	LBL
C_6H_5OH	0.38	LBL
Glycerol	0.75	LBL

[a] Obtained using conventional muons at TRIUMF.
[b] Original values (Refs. *4, 5, 6, 7*) were measured relative to $CHBr_3$ and are given in parenthesis. The values in column two are normalized to the TRIUMF value for cyclohexene from Table IV.
[c] As in *a* but normalized to JINR value for benzene from Table IV.

Publication Date: June 1, 1979 | doi: 10.1021/ba-1979-0175.ch013

not meaningful to attempt to compare CCl_4, for instance, with C_6H_6 on the basis of bond energies because both of the above factors are involved.

However, CCl_4 can be compared with the other tetrachlorides of Group IV elements since all are believed to be bonded tetrahedrally. They differ only by virtue of the size and mass of the central atom (and hence of the whole molecule); but there is a regular progression of this down the series. Table V gives the P_{res} data for CCl_4 (1.0), $SiCl_4$ (0.48), and $SnCl_4$ (0.99) whose bond energies follow the same order—78, 91, and 76 kcal mol^{-1}, respectively. Silicon (Si), which forms considerably stronger bonds with chlorine (Cl) than do the other two, has a much lower hot fraction. But this simple correlation breaks down completely when one includes $TiCl_4$, which has equivalent tetrahedral bonding. Here the bond strength is even higher than in $SiCl_4$, being 102 kcal/mol, yet P_{res}

is 1.0. There may be additional reasons for P_{res} in $TiCl_4$ being high, or in $SiCl_4$ being low, but if both are given equal weight then there is no simple correlation between bond energy and P_{res} evident from this series.

π-Bonding. There is a very striking correlation here. First, P_{res} has a value less than 0.49 only in compounds with π-bonding; second, the greater the extent of π-bonding the smaller P_{res} is. For example, hexane has $P_{res} = 0.62$, hexene, 0.50; and hexyne, 0.43. Also 2-propanol has $P_{res} = 0.63$ compared with acetone which is 0.54. Third, P_{res} decreases with increasing π bond conjugation. Thus, for cyclohexane $P_{res} = 0.68$; for cyclohexene, 0.47; for 1,4 cyclohexadiene, 0.40; 1,3 cyclohexadiene, 0.32; and for benzene, 0.15. The presence of π-bonding evidently plays a very significant role in reducing P_{res}. Perhaps the relatively low lying electronic energy levels enhance the thermalization process thereby curtailing the lifetime of the Mu atom in an epithermal state.

Two comparisons are worth noting. Firstly, in radiation chemistry the radiation yields of H_2 in cyclohexane, cyclohexene, and benzene are 5.6, 1.3, and 0.039 mol/100 eV, respectively (*68*). Yields of other products (such as total C_{12} molecules) show a similar trend, namely that chemical decomposition and chemical change decrease sharply with increasing unsaturation and particularly conjugated unsaturation. Secondly, in tritium recoil studies (*50, 51*) addition reactions at unsaturated bonds tend to dominate the overall chemistry in alkenes and alkynes. Addition reactions may occur also with hot Mu atoms but the species formed in such reactions during the lifetime of the muon generally will not be diamagnetic.

Solvent Mixtures—Thermalization Times. The linearity of the P_{res} against volume-fraction plots for both $CH_5OH/CHCl_3$ and CH_3OH/C_6H_6 (Figures 20 and 21) strongly implies that epithermal reactions of Mu proceed quite indiscriminately—simply according to the bulk composition. If during their period of reactivity the hot Mu atoms interacted with either component in alternative (competitive) ways then the plots would have been curved in the sense indicated by the dotted lines of Figures 20 and 21: that is, benzene would have partially protected methanol in these mixtures, and Mu would have reacted preferentially (selectively) with chloroform in its mixtures with methanol.

This lack of discrimination suggests that the epithermal Mu has only a very short period of time in which to react during the thermalization process. During that time period it is essentially in contact with only one molecule, so that its probability of reacting in that one instance depends simply upon the molecule with which it happens to be in contact. In this way the observed linear fractional sum of these probabilities in the mixtures can arise. We conclude therefore that a period of the order of time taken to travel one or two molecular diameters is all that is available

Publication Date: June 1, 1979 | doi: 10.1021/ba-1979-0175.ch013

for chemical reaction to give diamagnetic species at epithermal energies. Put another way, this suggests that the energy range over which epithermal reactions occur is of the order of the energy loss per collission.

Again, a comparison with radiation chemistry may be made drawing on two examples. In mixtures of benzene and cyclohexane the yield of H_2 is a markedly nonlinear function of composition, with benzene showing sponge-like protection of cyclohexane (*70*). The yield of solvated electrons in liquid mixtures is dominated by the solvent of higher dielectric constant, owing to competitive scavenging over most of the composition range (*71, 72, 73*). These examples highlight the significance of the nonselective reactions observed for epithermal Mu atoms.

Spur Reactions. Epithermal reactions often are distinguished from thermal reactions in being unaffected by the presence of scavengers in moderate concentrations (up to approximately 2*M*). This method, however, would not distinguish epithermal reactions from spur reactions, where the latter could involve the interaction of the thermalized muon with an ion or radical present in the large spur at the end of the muon track. As noted earlier, the SIN group is actively pursuing such reactions as an explanation for the missing muon fraction, although involving very fast thermal reactions. For instance, an electron formed from one of the last ionizations of μ^+ would rapidly give Cl^- in CCl_4 so that the intraspur combination of μ^+ with Cl^- could be mistaken for an epithermal reaction of Mu with CCl_4.

However, the mixtures discussed above seem to totally exclude this as a possible explanation for the hot atom processes. Providing the mixtures are nearly ideal (intimately mixed on the molecular level), in $CH_3OH/CHCl_3$ mixtures, for instance, $CHCl_3$ will capture spur electrons quite adequately over the range 0.3–1.0 in volume fraction, with the result that P_{res} would be nearly invariant over that range. Consequently the data would have resembled the dotted lnie of Figure 20. Equally, methanol and benzene should interface with each other's spur reactions. Apparently spur reactions as the source of P_{res} can be excluded, at least for those compounds whose mixtures give linear plots like Figures 20 and 21.

Other Factors. The probability of an epithermal reaction taking place during a thermalizing collision should depend strongly upon the actual chemical composition of the medium—perhaps on the polarizability of the atoms involved, on the electron density, the molecular or bond dipoles, and possibly other factors. Certain trends are evident from the data available, some of which is in Tables IV and V. Thus P_{res} increases progressively with mono-, di-, tri-, and tetrahalo substitution; P_{res} increases in the order H, Cl, Br (bromide), I (iodine), when these are substituents in aliphatic or aromatic hydrocarbons. The OH group, whether in H_2O

Publication Date: June 1, 1979 | doi: 10.1021/ba-1979-0175.ch013

or the aliphatic alcohols, gives $P_{res} = 0.61 \pm 0.04$. This is slightly lower than the corresponding unsubstituted hydrocarbon, as if the presence of OH actually depresses P_{res}. Yet three OH groups increase P_{res} substantially (glycerol has $P_{res} = 0.75$) as does an OH on benzene (phenol has $P_{res} = 0.38$ compared with benzene, 0.13).

Conclusions. The fact that P_{res} varies from approximately 1.0 to about 0.1 for a range of common liquids has in fact been known for many years (*22, 23, 24, 25*) but there is still no overall satisfactory rationalization of these data.

Our basic conclusions are the following. Epithermal Mu atom reactions are assumed to occur and as such they have to occur over a very short time span (perhaps narrow energy range) comparable to the typical time for one or two collisions in the liquid phase. Consequently there is no preferential interaction with one component in mixtures. When the target molecules contain π bonds the probability of reaction is reduced further. There does not seem to be a direct dependence of the probability of reaction on the strength of the bond being broken; but certain empirical trends are evident, particularly with regard to number and nature of the halogen atoms present.

Moreover, no obvious correspondence exists between the efficiency of hot Mu and hot T reactions; but it should be noted that the two methods involved are concerned with the fate of Mu or T on quite different time scales—Mu incorporated (perhaps temporarily) in diamagnetic molecules during times $\lesssim 10^{-9}$ sec and T finally residing in stable molecules hours after the primary reactions.

Publication Date: June 1, 1979 | doi: 10.1021/ba-1979-0175.ch013

Concluding Remarks

The experimental results and theoretical interpretations reviewed here provide solid evidence that studies of Mu chemistry are a practical and exciting reality. In both the gas and liquid phase, reaction rate constants can be measured by the MSR technique to a precision of 10% (and better). Such measurements in the gas phase have really only become possible with the development of surface μ^+ beams (*33*) which stop in a few inches of gas at 1 atm of pressure. Also, the amplitude of the Mu precession signal in inert gases is relatively large and the method is established now for a detailed study of the chemical reaction rates of the Mu atom (*10, 15, 16*). Atomic physics studies of muon charge exchange and spin flip collision processes (e.g., Mu + O_2) also can proceed in parallel. In the liquid phase, the MSR signals are much weaker, for reasons which are not yet understood; and there appears to be a significant missing muon fraction (*11, 12, 13, 14*). Such weak signals

In Positronium and Muonium Chemistry; Ache, H.;
Advances in Chemistry; American Chemical Society: Washington, DC, 1979.

may have the disadvantage of curtailing the wide applicability of the technique in different solvents. In contrast to this, the $\mu^+SR(P_{res})$ technique (*8, 9, 34*) can be studied in most common solvents and generally yields large signal amplitudes, which can be used to study both epithermal and thermal reaction processes. The P_{res} technique still holds considerable promise for liquid-phase Mu chemistry, but present ambiguities in the theoretical interpretation of the reaction path, particularly those involving μ^+ radicals, need to be clarified before its quantitative predictions can be treated with confidence. While the results discussed herein indicate the reliability of the method, more measurements (e.g., of temperature and solvent dependence of the reaction rates) are needed to firmly cement the foundations of Mu chemistry. Such studies are being undertaken for liquids and gases at several meson-producing laboratories, notably TRIUMF and SIN.

It is possible that these techniques will find more direct applications in the field of H atom chemistry. For instance, studies of Mu chemistry in liquids can complement H atom investigations in which the H atoms commonly are produced by radiolysis of hydrogenic materials (e.g., water) and followed via their ESR signal (*74, 75*). The μ^+ depolarization technique has some distinct advantages. Mu atoms can be introduced into any medium, including proton-free liquids or highly alkaline solutions (bases convert H atoms to solvated electrons—though they probably also do so with Mu); literally one Mu atom is in the sample at a time—therefore, there is relatively little radiation damage and the various recombination problems which can complicate H-atom studies are nonexistent. There may be many interesting reactions which can only be studied by Mu methods. This technique also lends itself quite naturally to a study of hot-atom reactions, with implications for hot H and other atoms.

An important goal of investigations in Mu chemistry is a better understanding of the physical processes involved in the chemical reactions of the simplest atom, and perhaps the simplest types of reaction. Of particular interest is tunneling in these reactions. Isotopic comparisons may be limited by the availability of precise values for the absolute reaction rates of H and D atoms (which in the cases of Mu studies thus far are known with less accuracy than those of Mu). Since the muon mass is only one-ninth the size of the proton, the Born–Oppenheimer approximation should be applicable (contrary to Ps) and tunneling is bound to be relatively more important than it is in the case of the H atom. Since Mu, H, and D differ in mass by factors up to 18, this series is bound to provide the most exacting tests of theoretical models of isotope effects in chemical reaction dynamics. Indeed, present results on Mu + F_2 have already revealed the potential of the technique (*54, 55*). In this

Publication Date: June 1, 1979 | doi: 10.1021/ba-1979-0175.ch013

In Positronium and Muonium Chemistry; Ache, H.;
Advances in Chemistry; American Chemical Society: Washington, DC, 1979.

case the room-temperature reaction rate is predicted to be dominated by tunneling and the calculated ratio of k_{Mu}/k_H is in good accord with the experimental results.

Although the background of this subject lies in intermediate energy physics, the results it is producing are having a striking impact on the understanding of basic chemical reaction mechanisms and dynamics.

Acknowledgment

The authors are most grateful to R. Mikula and Y. C. Jean for providing some of the unpublished data from TRIUMF. Financial support from the National Research Council of Canada is acknowledged.

Publication Date: June 1, 1979 | doi: 10.1021/ba-1979-0175.ch013

Literature Cited

1. Hughes, V. W., *Annu. Rev. Nucl. Sci.* (1966) **16**, 445.
2. Hughes, V. W., McColm, D. W., Ziock, K., Prepost, R., *Phys. Rev.* (1970) **1A**, 595.
3. Brewer, J. H., Crowe, K. M., Gygax, F. N., Schenck, A., "Muon Physics," V. W. Hughes, C. S. Wu, Eds., Academic, New York, 1975.
4. Firsov, V. G., Byakov, V. M., *Sov. Phys.—JETP (Engl. Transl.)* (1965) **20**, 719.
5. Firsov, V. G., *Sov. Phys.—JETP (Engl. Transl.)* (1965) **21**, 786.
6. Babaev, A. I., Balats, M. Ya., Myasishcheva, G. G., Obukhov, Yu. V., Rogonov, V. S., Firsov, V. G., *Sov. Phys.—JETP (Engl. Transl.)* (1966) **23**, 583.
7. Minaichev, E. V., Myasishcheva, G. G., Obukhov, Yu. V., Rogonov, V. S., Savel'ev, G. I., Smilga, V. P., Firsov, V. G., *Sov. Phys.—JETP (Engl. Transl.)* (1974) **66**, 1926.
8. Brewer, J. H., Crowe, K. M., Gygax, F. N., Johnson, R. F., Fleming, D. G., Schenck, A., *Phys. Rev.* (1974) **A9**, 495.
9. Brewer, J. H., Ph.D. Thesis, University of California, Lawrence Berkeley Laboratory Report **LBL-950** (1972), unpublished.
10. Fleming, D. G., Brewer, J. H., Garner, D. M., Pifer, A. E., Bowen, T., DeLise, D. A., Crowe, K. M., *J. Chem. Phys.* (1976) **64**, 1281.
11. Percival, P. W., Roduner, E., Fischer, H., Camani, M., Gygax, F. N., Schenck, A., *Chem. Phys. Lett.* (1977) **47**, 11.
12. Percival, P. W., Fischer, H., Roduner, E., Camani, M., Gygax, F. N., Schenck, A., Graf, H., Int. Conf. on Positron Annihilation, 4th, Helsingor, Denmark, August 1976.
13. Roduner, E., Percival, P. W., Fischer, H., Camani, M., Gygax, F. N., Schenck, A., Symposium on Meson Chemistry and Mesomolecular Processes, Dubna, U.S.S.R., June 1977.
14. Percival, P. W., Roduner, E., Fischer, H., ADV. CHEM. SER. (1979) **175**, 335.
15. Fleming, D. G., Brewer, J. H., Garner, D. M., *Ber. Bunsenges. Phys. Chem.* (1977) **81**, 159.
16. Fleming, D. G., Garner, D. M., Brewer, J. H., Warren, J. B., Marshall, G. M., Clark, G., Pifer, A. E., Bowen, T., *Chem. Phys. Lett.* (1977) **48**, 393.
17. Weissenberg, A. O., "Muons," North-Holland, Amsterdam, 1963.
18. Feinberg, G., Lederman, L. M., *Annu. Rev. Nucl. Sci.* (1963) **13**, 431.
19. Yamazaki, T., Nagamine, K., Nagamiya, S., Hashimoto, O., Sugimoto, K., Nakai, K., Kobayashi, S., *Phys. Scr.* (1975) **11**, 133.

20. Goldanskii, V. I., Firsov, V. G., *Annu. Rev. Phys. Chem.* (1971) **22,** 209.
21. Ache, H. I., *Angew. Chem., Int. Ed. Engl.* (1972) **11,** 179.
22. Garwin, R. L., Lederman, L. M., Weinrich, M., *Phys. Rev.* (1957) **105,** 1415.
23. Friedman, J. I., Telegdi, V. L., *Phys. Rev.* (1957) **106,** 1290.
24. Sens, J. C., Swanson, R. A., Telegdi, V. L., Yovanovitch, D. D., *Phys. Rev.* (1957) **107,** 1465.
25. Swanson, R. A., *Phys. Rev.* (1958) **112,** 580.
26. Nosov, V. G., Yakovleva, I. V., *Sov. Phys.—JETP (Engl. Transl.)* (1963) **16,** 1236.
27. Ivanter, I. G., Smilga, V. P., *Sov. Phys.—JETP (Engl. Transl.)* (1968) **27,** 301.
28. Ivanter, I. G., Smilga, V. P., *Sov. Phys.—JETP (Engl. Transl.)* (1971) **33,** 1070.
29. Favart, D., McIntyre, P. M., Stowell, D. Y., Telegdi, V. L., deVoe, R., Swanson, R. A., *Phys. Rev. Lett.* (1971) **27,** 1336.
30. Mobley, R. M., Amato, J. J., Hughes, V. W., Rothberg, J. E., Thompson, P. A., *J. Chem. Phys.* (1967) **47,** 3074.
31. Casperson, D. E., Crane, T. W., Denison, A. B., Egan, P. O., Hughes, V. W., Mariam, F. G., Orth, H., Reist, H. W., Souder, P. A., Stambaugh, R. D., Thompson, P. A., zu Pulitz, G., *Phys. Rev. Lett.* (1977) **38,** 956.
32. Barnett, B. A., Chang, C. Y., Yodh, G. B., Carroll, J. B., Eckhause, M., Hsieh, C. S., Kane, J. R., Spence, C. B., *Phys. Rev.* (1975) **A11,** 39.
33. Pifer, A. E., Bowen, T., Kendall, K. R., *Nucl. Instrum. Methods* (1976) **135,** 39.
34. Brewer, J. H., Gygax, F. N., Fleming, D. G., *Phys. Rev.* (1973) **A8,** 77.
35. Percival, P. W., Fischer, H., *Chem. Phys.* (1976) **16,** 89.
36. Fischer, W. E., *Helv. Phys. Acta.* (1976) **49,** 629.
37. Percival, P. W., Fischer, H., Camani, M., Gygax, F. N., Rüegg, W., Schenck, A., Schilling, H., Graf, H., *Chem. Phys. Lett.* (1976) **39,** 333.
38. Gurevich, I. I., Ivanter, I. G., Makariyna, L. A., Meleshko, E. A., Nikol'skii, B. A., Roganov, V. S., Selivanov, V. I., Smilga, V. P., Sokolov, B. V., Shestakov, V. D., Takovleva, I. V., *Phys. Lett.* (1969) **29B,** 387.
39. Ibid., *Sov. Phys.—JETP (Engl. Transl.)* (1971) **33,** 253.
40. Fleming, D. G., Brewer, J. H., Garner, D. M., Gygax, F. N., Crowe, K. M., Johnson, R. F., Patterson, B. C., Lawrence Berkeley Laboratory, Report **LBL-4675** (1976) unpublished.
41. Brewer, J. H., Fleming, D. G., Crowe, K. M., Johnson, R. F., Patterson, B. D., Portis, A. M., Gygax, F. N., Schenck, A., *Phys. Scr.* (1975) **11,** 144.
42. Stambaugh, R. D., Casperson, D. E., Crane, T. W., Hughes, V. W., Kaspar, H. F., Souder, P., Thompson, P. A., Orth, H., zu Pulitz, G., Denison, A. B., *Phys. Rev. Lett.* (1974) **33,** 568.
43. Allison, S. K., *Rev. Mod. Phys.* (1958) **30,** 1137.
44. Massey, H. S. W., Burop, E. H. S., "Electronic and Ionic Impact Phenomena," Oxford University Press, London, 1969.
45. Tawara, H., Russek, A., *Rev. Mod. Phys.* (1973) **45,** 178.
46. Laidler, K. J., Polanyi, J. C., *Prog. React. Kinet.* (1965) **3,** 1.
47. Wolfsberg, M., *Acc. Chem. Res.* (1972) **5,** 225.
48. Wolken, G., Jr., Karplus, M., *J. Chem. Phys.* (1974) **60,** 351.
49. Truhlar, D. G., Wyatt, R. E., *Annu. Rev. Phys. Chem.* (1976) **27,** 1.
50. Wolfgang, R., *Prog. React. Kinet.* (1965) **3,** 97.
51. Root, J. W., Ph.D. Thesis, University of Kansas, Lawrence (1964).
52. Wagner, H. Gg., Welzbacher, U., Zellner, R., *Ber. Bunsenges. Phys. Chem.* (1976) **80,** 902.
53. Ambridge, P. F., Bradley, J. N., Whytock, D. A., *J. Chem. Soc., Faraday Trans. 1* (1976) **72,** 1157.

Publication Date: June 1, 1979 | doi: 10.1021/ba-1979-0175.ch013

54. Connor, J. N. L., Jakubetz, W., Manz, J., *Chem. Phys. Lett.* (1977) **45**, 265.
55. Connor, J. N. L., Manz, J., private communication.
56. Westenberg, A. A., deHaas, N., *J. Chem. Phys.* (1968) **48**, 4405.
57. Truhlar, D. G., Kupperman, A., *J. Phys. Chem.* (1969) **73**, 1772.
58. Wood, G. O., *J. Chem. Phys.* (1972) **56**, 1723.
59. Percival, P. W., Roduner, E., Fischer, H., "Abstracts of Papers," 2nd Joint Conference CIC/ACS, Montreal, June 1977, PHYS 110.
60. Percival, P. W., Roduner, E., Fischer, H., Camani, M., Gygax, F. N., Schenck, A., "Abstracts of Papers," 2nd Joint Conference CIC/ACS, Montreal, June 1977, PHYS 111.
61. Rama Ras, K. V. S., Kamala, R., Jain, K. S., *Proc. Nucl. Radiat. Chem. Symp., 1964 (1965)* 73.
62. Perner, D., Schuler, H., *J. Phys. Chem.* (1966) **70**, 2224.
63. Thomas, J. K., *J. Phys. Chem.* (1967) **71**, 1919.
64. Brewer, J. H., Crowe, K. M., Johnson, R. F., Schenck, A., Williams, R. W., *Phys. Rev. Lett.* (1971) **27**, 297.
65. Anbar, M., Farhataziz, Ross, A. B., NSRDS-NBS (1975) **50**.
66. Hart, E. J., Anbar, M., "The Hydrated Electron," Wiley–Interscience, New York, 1970.
67. Walker, D. C., *Q. Rev.* (1967) **21**, 79.
68. Spinks, J. W. T., Woods, R. J., "Radiation Chemistry," Wiley, New York, 1976.
69. Brewer, J. H., Fleming, D. G., Symposium on Practical Applications of Accelerators, Los Alamos, 1973, Report **LA-5535-C** (unpublished).
70. Manion, J. P., Burton, M., *J .Phys. Chem.* (1952) **56**, 560.
71. Kemp, T. J., Salmon, G. A., Wardman, P., *in* "Pulse Radiolysis," M. Ebert, et al., Eds., p. 256, Academic, 1965.
72. Brown, B. J., Barker, N. T., Sangster, D. F., *J. Phys. Chem.* (1971) **75**, 3639.
73. Cooper, T. K., Walker, D. C., Gillis, H. A., Klassen, N. V., *Can. J. Chem.* (1973) **51**, 2195.
74. Eiben, K., Fessenden, R. W., *J. Phys. Chem.* (1971) **75**, 1186.
75. Neta, P., Fessenden, R. W., Schuler, R. H., *J. Phys. Chem.* (1971) **75**, 1654.
76. Albright, R. G., Dodonov, A. F., Lavrovskaya, G. K., Morosov, I. I., Tal'roze, V. L., *J. Chem. Phys.* (1969) **50**, 3632.
77. Rabideau, S. W., Hecht, H. G., Lewis, W. B., *J. Magn. Reson.* (1972) **6**, 384.
78. Levy, J. B., Copeland, B. K. W., *J. Phys. Chem.* (1968) **72**, 3168.
79. Homann, K. H., Schweinfurth, H., Warnatz, J., *Ber. Bunsenges. Phys. Chem.* (1977) **81**, 724.
80. Ambidge, P. F., Bradley, J. N., Whytock, D. A., *J. Chem. Soc., Faraday Trans. 1* (1976) **72**, 1157.
81. Bemand, P. P., Clyne, M. A. A., *J. Chem. Soc., Faraday Trans. 2* (1977) **73**, 394.
82. Wagner, H. Gg., Welzbacher, U., Zellner, R., *Ber. Bunsenges. Phys. Chem.* (1976) **80**, 902.
83. Ambidge, P. F., Bradley, J. N., Whytock, D. A., *J. Chem. Soc., Faraday Trans 1* (1976) **72**, 2143.
84. Westenberg, A. A., deHaas, N., *J. Chem. Phys.* (1968) **48**, 4405.
85. Clyne, M. A. A., Stedman, D. H., *Trans. Faraday Soc.* (1966) **62**, 2164.
86. Endo, H., Glass, G. P., *Chem. Phys. Lett.* (1976) **44**, 180.
87. Endo, H., Glass, G. P., *J. Chem. Phys.* (1976) **80**, 1519.
88. Jones, W. E., MacKnight, S. D., Teng, L., *Chem. Rev.* (1973) **73**, 407.
89. Sullivan, J. H., *J. Chem. Phys.* (1962) **36**, 1925.

RECEIVED January 23, 1978.

14

Radiation Chemistry and Reaction Kinetics of Muonium in Liquids

PAUL W. PERCIVAL, EMIL RODUNER, and HANNS FISCHER

Physical Chemistry Institute, University of Zürich, 8001 Zürich, Switzerland

Publication Date: June 1, 1979 | doi: 10.1021/ba-1979-0175.ch014

The muonium chemistry research performed at the Swiss Institute for Nuclear Research is reviewed. Muonium has been detected in water and other liquids, and rate constants for reactions in aqueous solutions were determined. Comparison with hydrogen atom data reveals marked isotope effects, and these are discussed in terms of transition state theory. Relaxation of the muonium signal in ice below 160 K is consistent with slowing of the translational diffusion of muonium atoms. The distribution of muon polarization between muonium and muon-substituted diamagnetic molecules has been investigated in water, ice, and aqueous nitrate solutions. It is suggested that muonium or the free muon itself interacts with transient radicals produced in the terminal spur of the muon track.

The background and underlying principles of muonium (Mu) chemistry have been dealt with in a preceding paper (*1*), as has the experimental technique, known as μ^+SR. Therefore, except for the brief notes in the next paragraph, this chapter is confined to the description and discussion of experimental results. These stem from work carried out at the Swill Institute for Nuclear Research (SIN). The SIN muon channel supplies a continuous high-energy (10–60 MeV) beam of longitudinally spin-polarized muons. The facility is, therefore, well suited to the study of dense target materials as opposed to the "Arizona Mode" beam at TRIUMF (*1*), which is ideal for gas-phase studies. Accordingly, we have investigated the liquid-phase chemistry of Mu, with the main effort centered on water and aqueous solutions.

0-8412-0417-9/79/33-175-335$05.25/1

In Positronium and Muonium Chemistry; Ache, H.;
Advances in Chemistry; American Chemical Society: Washington, DC, 1979.

In general the spin polarization of positive muons that are stopped in an experimental sample can give rise to two precession signals, which are observable by μ^+SR. (A third type of precession signal has been detected since the Montreal symposium. It arises in certain organic liquids and is attributed to muonic free radicals (*2*).) The first, present in all but a few substances, is the simple nuclear Larmor precession of the muon (13.55 kHz/G). It arises from bare muons or muons incorporated in diamagnetic molecules, and we refer to it here as the diamagnetic signal. The second signal comes from muons that have combined with an electron to form Mu ($Mu \equiv \mu^+e^-$). Mu signals have been observed only in a limited number of substances. Their nature is described below. Diamagnetic and Mu signals are characterized by their frequencies, phases, amplitudes, and decay rates. In samples of chemical interest the frequencies are determined by the external field only and thus merely serve to identify the signals. Similarly, except in a few cases, the phases are of no interest. The amplitudes are very important, however, since they lead to determination of the fractions of initial muon polarization carried over into the different muonic species. We label the Mu and diamagnetic polarizations P_M and P_D, respectively. The rates of decay also contain valuable information since they are determined by spin relaxation and chemical reaction rates.

Publication Date: June 1, 1979 | doi: 10.1021/ba-1979-0175.ch014

Muonium in Liquids

The allowed transitions between the energy levels of a Mu atom in a field transverse to the initial muon polarization give rise to four precession frequencies. Two of these are too high to be detected under normal conditions (the typical resolution of μ^+SR assemblies is 1 nsec). At very low field ($\lesssim$ 10 G) the two observable frequencies are degenerate and take the value 1.4 MHz/G. At higher fields a splitting is evident, and this gives rise to a beat pattern in the precession signal. This is shown clearly in Figure 1, which shows the Mu precession signal for a sample of quartz in a transverse field of 101 G.

Although Mu has been identified in both gas (*3, 4, 5, 6, 7*) and solid (*8, 9, 10, 11, 12*) phases for more than a decade, it escaped detection in liquids until our first experiments at SIN in 1975 (*13*). Weak precession signals were observed in the Fourier transforms of μ^+SR histograms accumulated for a sample of water at a number of different fields. Analysis of the splitting of the observed frequencies supported assignment of the signals to Mu atoms that exhibited a muon–electron hyperfine frequency consistent with the vacuum value (4463 MHz). A more recent example of Mu precession, as evident in the Fourier transform of a μ^+SR histogram, is shown in Figure 2. Figure 3 displays a time spectrum

In Positronium and Muonium Chemistry; Ache, H.;
Advances in Chemistry; American Chemical Society: Washington, DC, 1979.

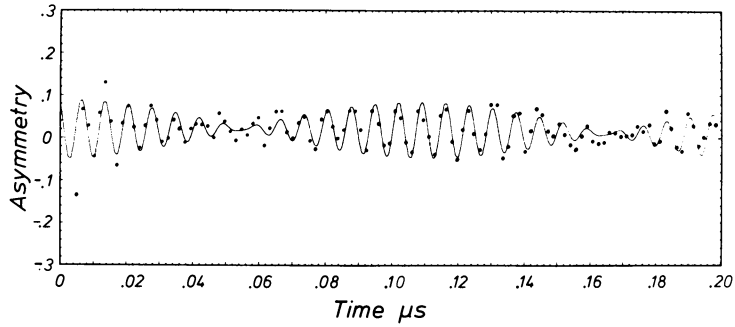

Figure 1. Mu precession in quartz at 101 G

showing the degenerate Mu precession arising in water at about 4 G applied field. The constant amplitude of the signal demonstrates lack of chemical reaction or spin relaxation on the microsecond time scale.

The Mu signal in water accounts for 20% of the initial muon polarization (only half of which is actually detectable at the observable frequencies). This is clearly one reason why its detection came so much later than for solids and gases, where up to 100% of the initial muon polarization occurs in Mu. A second pitfall is the presence of dissolved oxygen in undegassed liquid samples. Oxygen is expected to both undergo fast chemical reaction with Mu and to cause rapid spin relaxation via Heisenberg spin exchange.

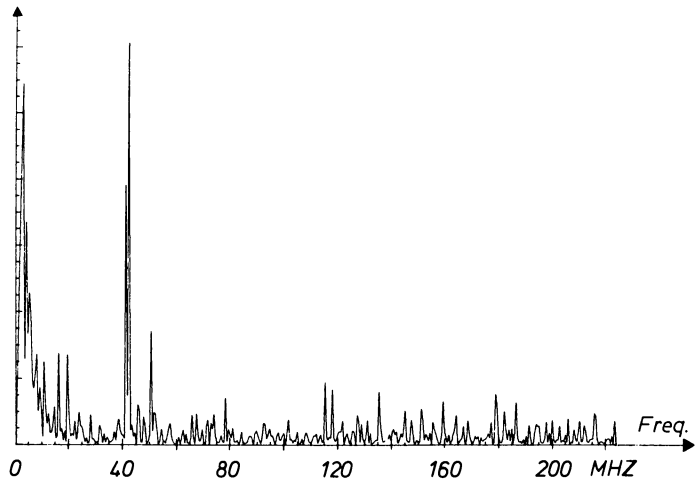

Figure 2. Fourier transform showing splitting of the Mu precession frequencies in water at 30 G

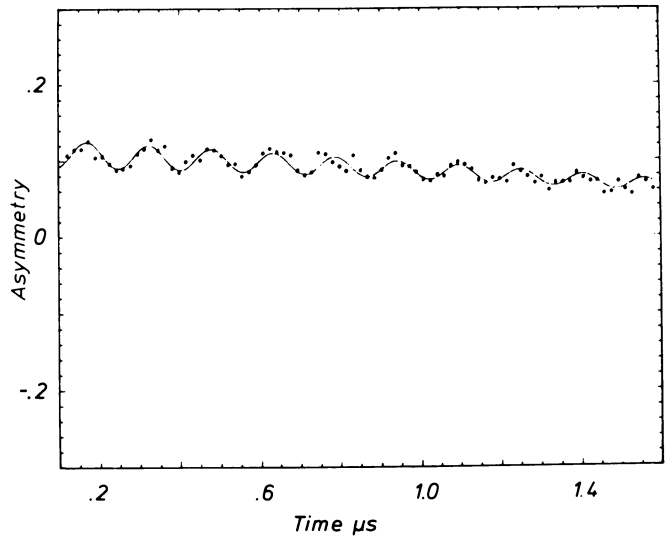

Figure 3. Mu precession in water at about 4 G

Since its detection in water, Mu has also been observed in methanol, ethanol, diethyl ether, and dioxane (*14*). Water, as all other liquids so far studied, also exhibits a diamagnetic precession signal; more than 60% of the initial muon polarization manifests itself in this way. However, the sum of diamagnetic and Mu polarizations, P_D and P_M, is significantly less than unity. This also applies for methanol and ethanol (*see* Table I). The problem of the missing fraction of polarization is discussed later.

Table I. Muon Polarizations in Pure Substances

Sample	P_D[a]	P_M[a]
H_2O, liquid	0.622 ± 0.006	0.196 ± 0.003
H_2O, ice ($T > 160$K)	0.480 ± 0.004	0.52 ± 0.02
D_2O, liquid	0.57 ± 0.03	0.18 ± 0.01
D_2O, ice ($T > 160$K)	0.393 ± 0.005	0.63 ± 0.01
CH_3OH	0.61 ± 0.01	0.19 ± 0.02
CD_3OD	0.51 ± 0.02	0.31 ± 0.05
C_2H_5OH	0.59 ± 0.03	0.20 ± 0.04
Aluminum, granular	0.990 ± 0.007	—

[a] Relative to $P_D = 1.0$ for CCl_4.

Publication Date: June 1, 1979 | doi: 10.1021/ba-1979-0175.ch014

Muonium Kinetics in Aqueous Solution

Since Mu is long lived in pure water (on the microsecond time scale dictated by the muon lifetime, 2.2 μsec), it is possible to study its rates of reaction with dissolved substrates by simply following the rates of disappearance of the precession signal (*15*). The interest in such a study lies in the comparison of Mu rate constants with those of the hydrogen atom. The magnitude and direction of the measured kinetic isotope effects provide useful tests of chemical reaction theories. Mu kinetics has thus become a major part of our research program, with about 20 rate constants determined to date.

Experimental Method and Results. The experimental method is entirely analogous to that described by Fleming et al. (*1, 16, 17*) for their gas-phase kinetic measurements. Experiments were always performed at low magnetic field, so that the μ^+SR histogram was given by (*16*)

$$S = N\{B + e^{-t/\tau}[1 + A_D e^{-t/T_{2D}} \cos(\omega_D t + \phi_D) + A_M e^{-t/T_{2M}} \cos(\omega_M t + \phi_M)]\} \quad (1)$$

where N is a normalization factor, B is the background (usually < 0.01), and τ is the muon lifetime. A_D, ω_D, and ϕ_D represent the asymmetry (i.e., the amplitude),, frequency, and phase of the diamagnetic signal and A_M, ω_M, and σ_M are the aspmmetry, frequency, and phase of Mu. In addition, the decays of the muon and Mu precession signals are characterized by effective relaxation times T_{2D} and T_{2M}. Relaxation of the diamagnetic signal is negligible in nonparamagnetic aqueous solutions (*15*). The Mu decay rate $\lambda = T_{2M}^{-1}$ is given by

$$\lambda = \lambda(o) + k[X] \quad (2)$$

where $k[X]$ is the rate of the pseudo first-order reaction with substrate X, and $\lambda(o)$ is the decay rate in pure water. During an experiment 10^8 muons at most are stopped in a few milliliters of solution, so there is a negligible change in the concentration of X.

Mu precession signals for three concentrations of fumaric acid are shown in Figure 4 together with the best fits to Equation 1. The increase in λ with solute concentration is clearly visible; extracted values are plotted in Figure 5. The straight line is the least-squares fit of the data to Equation 2, and its slope gives the rate constant, $k = 1.4 \times 10^{10} M^{-1}$ sec^{-1}. In the same way rate constants have been determined for reactions with a variety of substances in aqueous solution. The results are gathered in Table II, where they are compared with literature values for hydrogen atom reactions. We have determined further that $k < 2 \times 10^5 M^{-1}$ sec^{-1} for H^+, Na^+, and Cl^- since there was no visible Mu decay in $5M$ solutions of HCl and NaCl. Similarly $k < 1 \times 10^7 M^{-1}$ sec^{-1} for ClO_4^- was deduced from the lack of decay in $0.1M$ $HClO_4$.

In Positronium and Muonium Chemistry; Ache, H.;
Advances in Chemistry; American Chemical Society: Washington, DC, 1979.

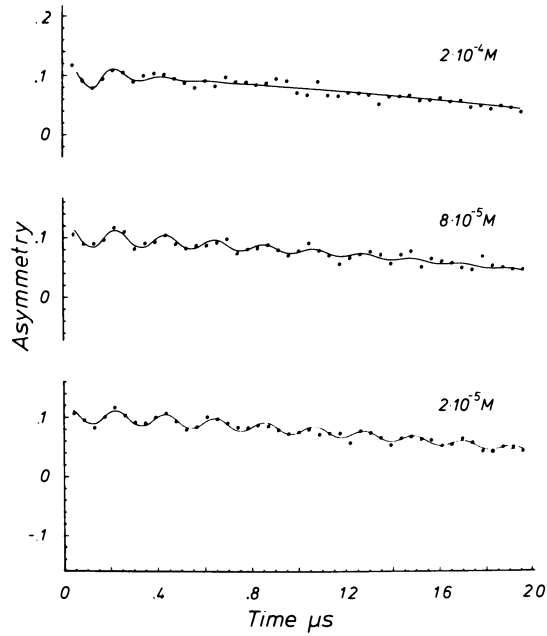

Figure 4. Mu precession signals in aqueous solutions of fumaric acid

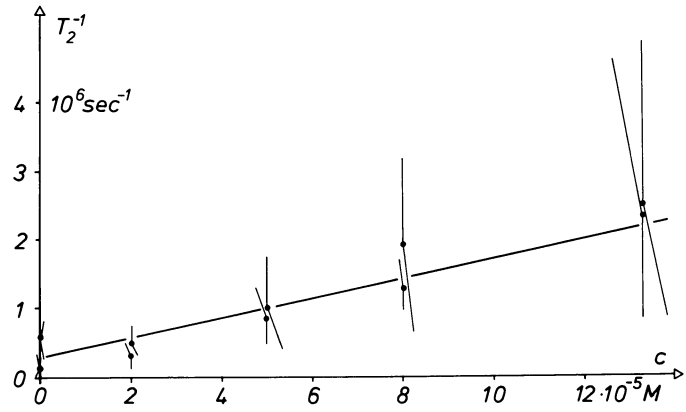

Figure 5. Mu decay rates at different concentrations of fumaric acid. The rate constant is given by the slope of the least-squares line.

Publication Date: June 1, 1979 | doi: 10.1021/ba-1979-0175.ch014

Table II. Comparison of Rate Constants for Muonium and Hydrogen Atoms in Aqueous Solution

	k_H (M^{-1} sec^{-1})	k_{Mu} (M^{-1} sec^{-1})	$\frac{k_H}{k_{Mu}}$
Hydrogen abstraction			
methanol	2.5×10^6	$< 3 \times 10^4$	> 83
ethanol	2.1×10^7	$< 3 \times 10^5$	> 70
2-propanol	6.8×10^7	$\simeq 7 \times 10^5$	100
2-butanol	1.3×10^8	1.1×10^6	118
formate ion	1.24×10^8	7.8×10^6	16
Bromine abstraction			
bromoacetic acid (pH 1)	2.6×10^8	1.5×10^9	0.17
2-bromopropionic acid (pH 1)	9.5×10^8	4.0×10^9	0.24
3-bromopropionic acid (pH 1)	1.7×10^8	$\simeq 3 \times 10^8$	0.6
Hydrogen addition to olefins			
maleic acid (pH 1)	6×10^8	1.1×10^{10}	0.06
fumaric acid (pH 1)	9×10^8	1.4×10^{10}	0.06
ascorbic acid (pH 1)	1.1×10^8	1.8×10^9	0.06
dihydroxyfumaric acid (pH 1)	9×10^7	4.5×10^7	2
Diffusion-controlled reactions			
MnO_4	2.4×10^{10}	2.5×10^{10}	1
Ag^+	1.15×10^{10}	1.6×10^{10}	0.7
Further reactions			
acetone (pH 1)	2.8×10^6	8.7×10^7	0.03
HO^-	1.5×10^7	1.7×10^7	1
NO_3^-	9×10^6	1.5×10^9	0.006

Publication Date: June 1, 1979 | doi: 10.1021/ba-1979-0175.ch014

Discussion. The substrates in Table II are grouped according to type of reaction with hydrogen (*18, 19*). The Mu reactions are assumed to be analogous and are:

hydrogen atom abstraction

$$RH + Mu \rightarrow R\cdot + MuH; \quad (3)$$

bromine abstraction

$$RBr + Mu \rightarrow R\cdot + MuBr; \quad (4)$$

addition to olefinic double bonds

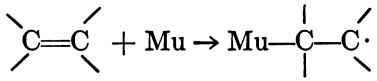

(5)

fast oxidation at or close to the diffusion-controlled limit

$$MnO_4^- + Mu \rightarrow u^+ + MnO_4^{2-} \tag{6}$$

and

$$Ag^+ + Mu \rightarrow \mu^+ + Ag^\circ; \tag{7}$$

and the miscellaneous reactions

$$(CH_3)_2CO + Mu \rightarrow (CH_3)_2\dot{C}OMu \tag{8}$$

$$OH^- + Mu \rightarrow MuOH + e_{aq}^- \tag{9}$$

$$NO_3^- + Mu \rightarrow MuO^- + NO_2. \tag{10}$$

Publication Date: June 1, 1979 | doi: 10.1021/ba-1979-0175.ch014

The (assumed) diffusion-controlled reactions show little or no kinetic isotope effect. This is in accord with the nearness of the Mu and hydrogen atomic radii, which is expected to lead to close similarity in diffusion constants and reaction radii. Almost all other reactions show marked isotope effects; hydrogen abstraction is lower for Mu while bromine abstraction and addition to an olefinic bond are faster.

Transition state theory states that the rate constant for the reaction

$$A + B \rightarrow \text{products} \tag{11}$$

is given by

$$k = \Gamma \cdot \frac{RT}{Nh} \cdot \frac{Q^{\neq}}{Q_A Q_B} \cdot \exp\left(-\frac{E}{RT}\right) \tag{12}$$

where Γ is a transmission factor (including the effect of tunneling), Q_A, Q_B, and $Q^{\neq}$ are the molecular partition coefficients of the reactants and the transition state (excluding the vibration equivalent to translation along the reaction coordinate), and E is the activation energy for the reaction—i.e., the difference between the ground state electronic and vibrational energies of transition state and reactants:

$$E = E^{\neq} - E_A - E_B. \tag{13}$$

When this theory is applied to the hydrogen atom abstraction as in Equation 3, the predicted isotope effect becomes

$$\frac{k_H}{k_M} = \frac{\Gamma_H}{\Gamma_M} \cdot \frac{Q_M}{Q_H} \cdot \frac{Q^{\neq}_{HX}}{Q^{\neq}_{MX}} \cdot \exp\left\{\frac{(E^{\neq}_{MX} - E^{\neq}_{HX})_{vib}}{RT}\right\} \cdot \exp\left\{\frac{(E_M - E_H)_{el}}{RT}\right\} \tag{14}$$

In Positronium and Muonium Chemistry; Ache, H.;
Advances in Chemistry; American Chemical Society: Washington, DC, 1979.

Table III. Comparison of Experimental Isotope Effects with BEBO Calculated Values for the Fourth Factor in Equation 14

Substrate	k_H/k_M	*BEBO*
Methanol	> 83	103
Ethanol	> 70	73
2-Propanol	$\simeq 100$	37
2-Butanol	118	37
Formate	16	8

where the difference in activation energies ($E_H - E_M$) has been factored into its vibrational and electronic parts. The first factor on the right of Equation 14 is 1 if tunneling is unimportant and otherwise favors the reaction of Mu. A ratio of translational partition functions comes next; its value is 1/27 in the gas phase and presumably is somewhere between this value and 1 for liquids. The total partition functions for the transition state should be very similar at room temperature, so that the third factor is not much different from 1. The fourth factor arises from the difference in vibrational zero-point energy in the transition states; it is the only factor that can have a value much greater than 1. Finally, the electronic activation energies are equal within the Born–Oppenheimer approximation, thus predicting a value of 1 for the last factor. In reality it should be a little less.

Since hydrogen atom abstraction is slower for Mu than for hydrogen, the fourth factor of Equation 14 must be of overriding dominance. To estimate its magnitude, bond lengths and force constants for the transition states were estimated by the bond energy–bond order method (BEBO) (*20*), assuming the usual linear structure Mu · · · H · · · R and treating R as a single heavy atom. Table III lists the predicted values of the dominant factor of Equation 14 and compares them with the experimental isotope effects. The predictions clearly account for the approximate magnitude of the isotope effects and demonstrate that tunneling in particular must play only a minor role in the hydrogen abstraction reaction at room temperature.

The remaining reactions in Table II have not been subjected to theoretical analysis, but we suspect that tunneling will be found to be important. This is thought to be the case for hydrogen addition to olefins (*21*).

H_2O and D_2O Ices

Experimental Results. The Mu precession signal in H_2O and D_2O ices is much stronger than in the corresponding liquids. This is partly the result of a smaller diamagnetic fraction in the ices (*see* Table I) but

Publication Date: June 1, 1979 | doi: 10.1021/ba-1979-0175.ch014

also because all the initial muon polarization is accounted for—i.e., there is no missing fraction, as is the case for liquid H_2O and D_2O. Examples of the diamagnetic and Mu signals in ice are in Figure 6.

The initial amplitudes of the two signals lead to values of P_D and P_M, and the results are plotted as a function of temperature in Figures 7 and 8 for H_2O and D_2O ices, respectively. The dashed lines drawn through the points are intended as guides only and are based on the more precise P_D values. The Mu polarization, plotted as $1-P_M$, is scattered about the dotted lines, confirming the absence of a missing fraction over the whole ice temperature range. P_M and P_D are essentially constant between the melting point and 160 K, but below this temperature P_M seems to grow at the expense of P_D.

Relaxation rates T_{2M}^{-1} and T_{2D}^{-1} were also determined, assuming exponential decay kinetics. Values of T_{2D} of approximately 0.12×10^6 sec^{-1} were found for H_2O above 160 K, with an increase to 0.23×10^6 sec^{-1} at 98 K. Diamagnetic relaxation in D_2O ice above 160 K was negligible ($\leq 0.05 \times 10^6$ sec^{-1}), as in liquid water, but again an increase was found at lower temperatures (0.13×10^6 sec^{-1} at 96 K). In D_2O T_{2M}^{-1} was constant at 2×10^6 sec^{-1} over the whole temperature range whereas in H_2O T_{2M}^{-1} increased from the same value above 160 K to about 5×10^6

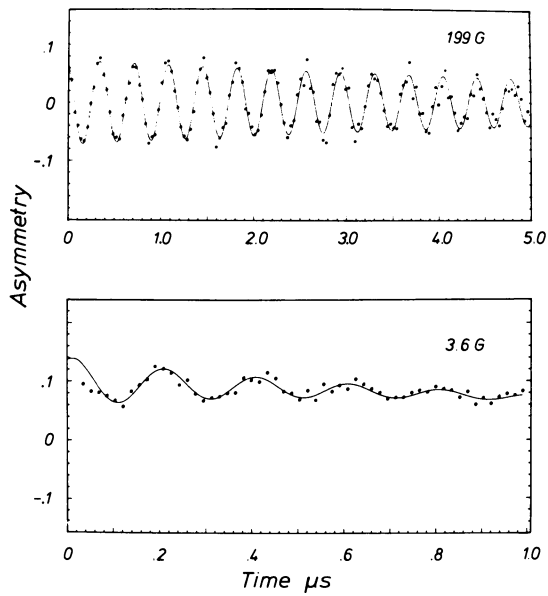

Figure 6. Muon (at 199 G) and Mu (at 3.6 G) precession in H_2O ice at 240 K

Publication Date: June 1, 1979 | doi: 10.1021/ba-1979-0175.ch014

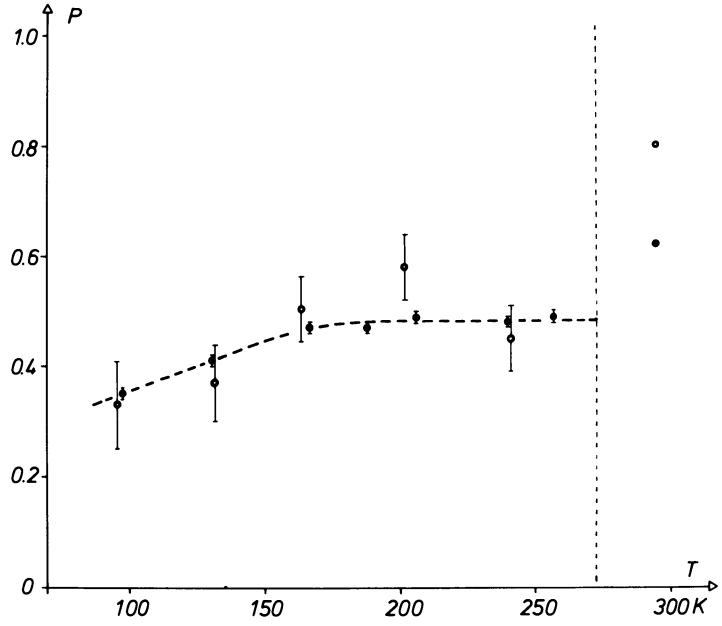

Figure 7. Temperature dependence of P_D (●) *and* $(1 - P_M)$ (○) *for* H_2O

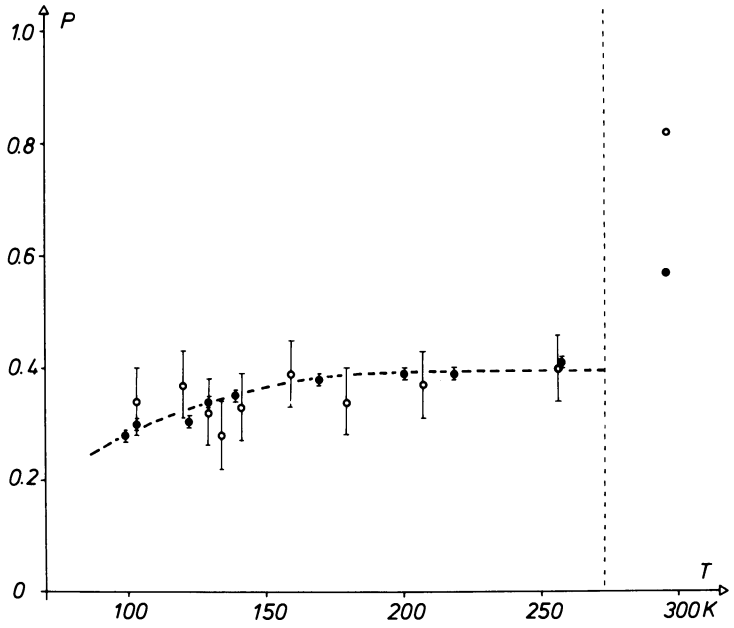

Figure 8. Temperature dependence of P_D (●) *and* $(1 - P_M)$ (○) *for* D_2O

at 132 K and 7×10^6 at 96 K. Gurevich et al. (*22*) reported values of $T_{2M}^{-1} = (2.0 \pm 0.2 \times 10^6$ sec^{-1} and $(5.7 \pm 0.9) \times 10^6$ sec^{-1} for D_2O and H_2O ice, respectively, at 77 K.

Discussion. The temperature dependence of our ice results shows intriguing similarities to the results of Shiraishi et al. (*23*)for hydrogen atoms. These authors performed ESR studies on hydrogen atoms in neutral and acidic ice over the same temperature range. They found a large increase in the ESR line width (which is proportional to the electron spin relaxation rate T_{2e}^{-1}) below 160 K; they also found dramatic changes in the magnitude of the observed chemically induced electron spin polarization (CIDEP) below and above this temperature. Both results are interpreted as being caused by the trapping of the hydrogen atoms that undergo translational diffusion at higher temperatures. Spin relaxation is caused by modulation of the dipolar coupling between the unpaired electron on the hydrogen and the protons of the surrounding water molecules.

It is instructive to assume that Mu is subject to the same dynamics as hydrogen atoms in ice and thus to estimate T_{2M}^{-1}. In very low fields the Mu relaxation is given by one-half of the electron spin-lattice rate T_{1e}^{-1}, which in the motional narrowing region ($\omega_e\tau < 1$, where τ is the motional correlation time) is equal to T_{2e}^{-1}. If a simple exponential correlation function is assumed for the fluctuating dipoles, then the T_{2e}^{-1} at low field is twice that at high field (3 kG) where the ESR measurements were made (*24*). Thus, T_{2M}^{-1}(exp) should be equal to the T_{2e}^{-1} measured by Shiraishi et al. This means that T_{2M}^{-1} is predicted to be 1×10^7 sec^{-1} at 160 K and 6×10^7 sec^{-1} at 110 K. Clearly the magnitude of the dipolar relaxation mechanism is more than enough to account for the observed values of T_{2M}^{-1}; indeed, we might propose that the correlation time for Mu translation is somewhat shorter than for hydrogen at the same temperature. A further prediction is that there should be faster relaxation in H_2O than in D_2O because of the larger proton magnetic moment. The effect is observed but is weaker than the expected factor of 16. This discrepancy and the lack of temperature dependence in D_2O are consistent with the existence of a further relaxation process that is both isotope and temperature independent. It is dominant for Mu in D_2O and in H_2O above 160 K, but its nature is unknown. Gurevich et al. (*22*) analyzed their measurements of T_{2M}^{-1} at 77 K exclusively in terms of the dipolar mechanism and concluded from the relatively small isotope effect that Mu does not diffuse in ice at 77 K.

Although trapping of diffusing Mu atoms can explain part of the observed relaxation behavior, it fails to explain the temperature dependence of the Mu and diamagnetic fractions. Since no polarization is lost in the muon distribution process (in ice), the process must be over in a

Publication Date: June 1, 1979 | doi: 10.1021/ba-1979-0175.ch014

time that is short compared with the inverse hyperfine frequency (3×10^{-11} sec). One possibility is that the diamagnetic fraction arises from the products of epithermal Mu reactions. Thus, the muon distribution reflects the competition between reaction and thermalization of energetic Mu atoms. It has been suggested that the diamagnetic fraction in ice is lower than that in water because of a greater efficiency of the hydrogen-bonded water structure in slowing Mu (*25*).

This seems unlikely. The observed temperature dependence of the muon distribution below 160 K would have to be attributed to the thermalization process—i.e., a change in the nature or magnitude of the hydrogen bonding. We know of no such change. Further, it has been reported that the fraction of recoil atoms that react epithermally (79%) is the same for water and ice (*26*). If this is also true for Mu, any (temperature independent) epithermal contribution to the diamagnetic fraction in water must be small. Other possible causes of the muon distribution in water and ice involve the radiation chemistry of the muon, and this is considered below.

Publication Date: June 1, 1979 | doi: 10.1021/ba-1979-0175.ch014

Radiation Chemistry

Scavenging Experiments. MOTIVATION AND METHOD. As mentioned, there is a missing fraction of polarization in pure water in contrast to ice. This problem clearly calls for explanation as does the whole question of the factors governing the distribution of muons and their spin polarization among the various muonic species. The fate of the muon and its polarization are decided at times that are short compared with the earliest that are directly observable by μ^+SR (10^{-7} sec). The use of large concentrations of scavengers to study fast processes in radiation chemistry is well established (*27*), and we have begun to apply this method to Mu studies. As an illustration, we describe our most thorough scavenging study to date, which utilized sodium nitrate.

Since 5*M* sodium chloride has no effect on the Mu and diamagnetic fractions found in water, we assumed from the start that the effects about to be described are caused by the nitrate rather than by the sodium ion. We wished to measure P_M and P_D as a function of nitrate concentration, but as shown earlier (Equation 10 and Table II), Mu reacts with nitrate. Therefore, it is impossible to tell directly whether or not the initial Mu fraction (designated h_M) is influenced by large NO_3^- concentrations.

In certain circumstances h_M can be determined by the residual polarization method. Residual polarization is that part of the muon polarization originally in reacting Mu that is carried into the diamagnetic products. A mathematical treatment can be found in the chapter by Fleming et al., so an example suffices here. Figure 9 shows the computed

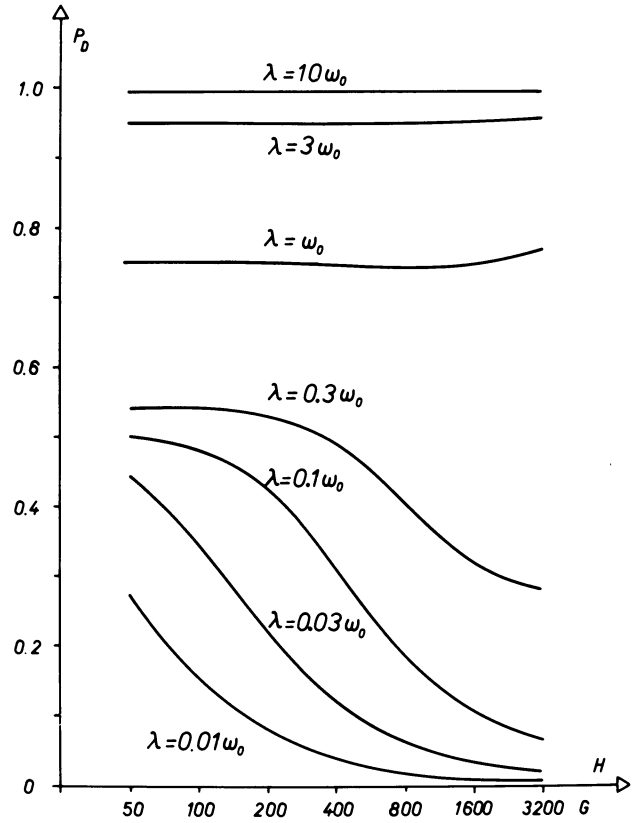

Figure 9. Computed magnetic field dependencies of the residual polarization for various rates, λ, of the reaction Mu → diamagnetic products

residual polarization for the single-step reaction, Mu → diamagnetic products, as a function of reaction rate and applied magnetic field. The initial Mu fraction, h_M, was taken as 1. Reaction rates between 0.01 ω_0 and ω_0 give rise to characteristic field dependencies; the span of the field dependence for a given λ reflects h_M. The total diamagnetic fraction as measured in an experiment, P_D, is equal to the sum of the residual polarization and any (field-independent) initial diamagnetic fraction h_D.

RESULTS. P_D was measured for pure water and nitrate concentrations between 0.1 and 5.0*M*, and for magnetic fields between 50 and 1600 G. The results are shown in Figure 10. The lines drawn through the experimental points represent best fits according to the following scheme:

$$\mathrm{Mu}^* \xrightarrow[\text{fast}]{\text{very}} h_D D_1 + (1 - h_D)\ \mathrm{Mu} \qquad (15)$$

Publication Date: June 1, 1979 | doi: 10.1021/ba-1979-0175.ch014

$$\mathrm{Mu} \xrightarrow{\lambda} D_2. \tag{16}$$

Mu* is some unknown precursor, which, in a very short time ($<\omega_0^{-1}$), gives either the diamagnetic product, D_1, or thermal Mu. (In previous publications (*13, 28*) we have assumed Mu* to be epithermal Mu.) The thermal Mu fraction reacts at rate λ to give further diamagnetic products, D_2.

The results of a computer analysis are shown in Table IV. The rate $_2$ was equal to $k_M[NO_3^-]$, where k_M is the rate constant determined by the direct method (Table II). Fits in which λ was a free parameter showed no significant improvement and led to the same mean value for k_M. Similarly, no improvement was found by allowing h_M to vary

Publication Date: June 1, 1979 | doi: 10.1021/ba-1979-0175.ch014

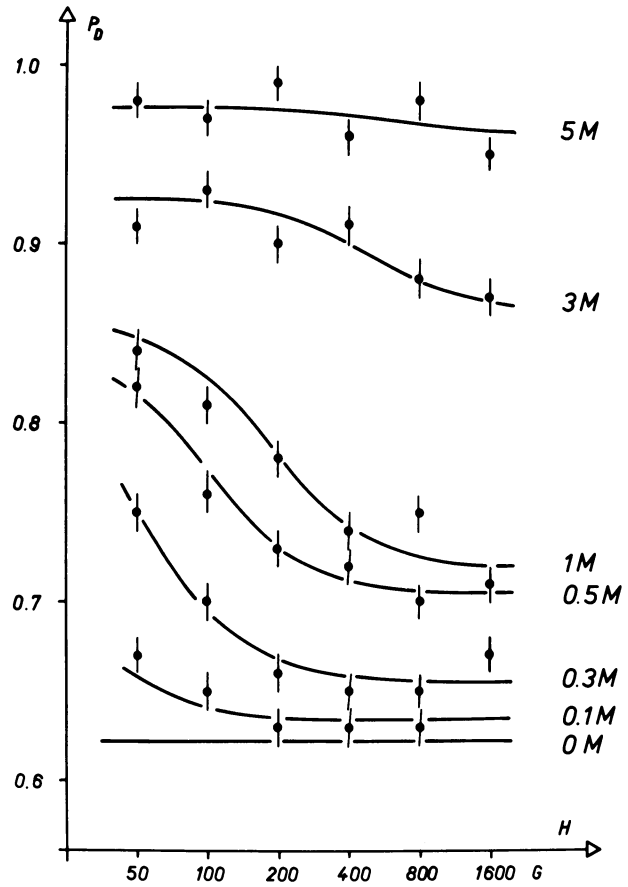

Figure 10. Muon polarization in aqueous nitrate solutions

Table IV. Best-Fit Values of h_D for Nitrate Solutions

Concentration, M	h_D
0.1	0.64
0.3	0.66
0.5	0.70
1.0	0.72
3.0	0.85
5.0	0.95

independently of h_D; best results were always obtained with $h_M + h_D = 1$. Thus, in contrast to pure water, no missing fraction was found for the nitrate solutions. Since h_D for 0.1*M* NO_3^- is only a little larger than that in pure water, the missing fraction has been replaced by an increase in h_M. This suggests that the missing fraction observed for pure water is really the result of depolarized Mu and that 0.1*M* NO_3^- suffices to quench the depolarization process. At higher NO_3^- concentrations h_D increases at the expense of h_M. Again it seems that NO_3^- interferes with the muon/Mu chemistry of water by quenching or scavenging some reactive species.

The Missing Fraction. The only reaction partners for Mu in pure water are those produced along the track of the incoming muon. Of these, the excess electron (presolvated e^- and hydrated e_{aq}^-) is the most reactive with NO_3^- (*29*):

$$e_{aq}^- (e^-) + NO_3^- \rightarrow NO_3^{2-} \qquad k_{aq} = 1 \times 10^{10} M^{-1}\,\text{sec}^{-1}. \qquad (17)$$

Here we examine whether or not interactions between the hydrated electron and Mu can give rise to the missing fraction observed in water. The role of the excess electron in determining the muon distribution is considered below.

The reaction of a hydrated electron with Mu can be assumed to be analogous to the reaction with hydrogen (*19*).

$$Mu + e_{aq}^- \rightarrow MuH + OH^- \qquad (18)$$

We propose, however, that not every encounter between Mu and e_{aq}^- will lead to reaction. In particular, it is reasonable to expect that an encounter that leads to a triplet radical pair will be unreactive (*30*). During the encounter the electronic spin functions will evolve because of the electron–electron dipolar interaction, so that the electron-spin polarization in each species will, in general, have changed after separation. A related effect is the chemically induced electron-spin polarization (CIDEP) often observed in ESR spectra taken during radical reactions (*31*). In our case the strong muon–electron hyperfine coupling leads in low field to an oscillatory transfer of the initial muon polarization to the

Publication Date: June 1, 1979 | doi: 10.1021/ba-1979-0175.ch014

Mu electron and back. The nonreactive encounter should then result in loss of part of this polarization to e_{aq}^-. Preliminary calculations show that this rudimentary model can account for part, but not all, of the missing fraction (*32*); a more sophisticated theoretical treatment is required to handle a realistic model.

According to the above hypothesis nitrate scavenging of e_{aq}^- quenches the missing fraction, 0.1*M* being sufficient. This can be tested against the predictions of the diffusion kinetic model of the radiation spur in water (*33*). Intraspur radical recombination is found to be 80% complete at 10^{-9} sec, but a scavenger concentration of 0.1*M* is sufficient to provide appreciable competition.

Possible Origins of the Muon Distribution. The observed increase in h_D occurs at higher NO_3^- concentrations than that necessary to compete with the Mu depolarization process. Thus, the reactions leading to the distribution of muons between h_D and h_M must be correspondingly faster. Further, the absence of depolarization at this stage implies reaction rates $\geq 10^{11}$ sec^{-1}. We propose, therefore, that the scavenged species is the dry electron, e^-, (*34*) rather than e_{aq}^-. A possible reaction scheme is shown below (Scheme I).

Scheme I

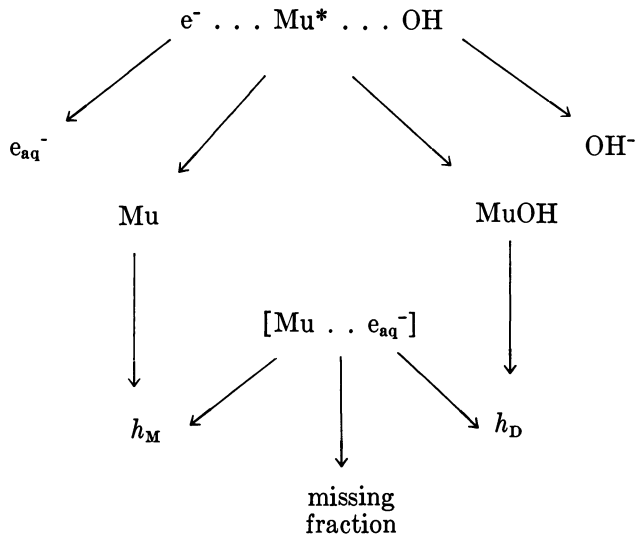

Shortly after formation, Mu* is in the neighborhood of e^- and OH which wer created in the terminal spur of the muon track. Reaction with OH leads to h_D, complete escape gives h_M, whereas encounter with the electron (in the mean time hydrated) can bring about depolarization.

Publication Date: June 1, 1979 | doi: 10.1021/ba-1979-0175.ch014

Addition of NO_3^- results in scavenging of e_{aq}^-, and at larger concentrations e^-, which otherwise serves to remove OH. The increased lifetime of the OH radical favors the Mu + OH combination, and thus h_D increases at the expense of h_M. A weak point in this scheme is that at $5M$ NO_3^- 95% of the muons contribute to h_D (see Table IV), and thus there remains only a small probability that Mu* escapes reaction with OH.

An alternative hypothesis, inspired by the spur model of positronium formation (*see* other chapters in this volume), is summarized in Scheme II.

Scheme II

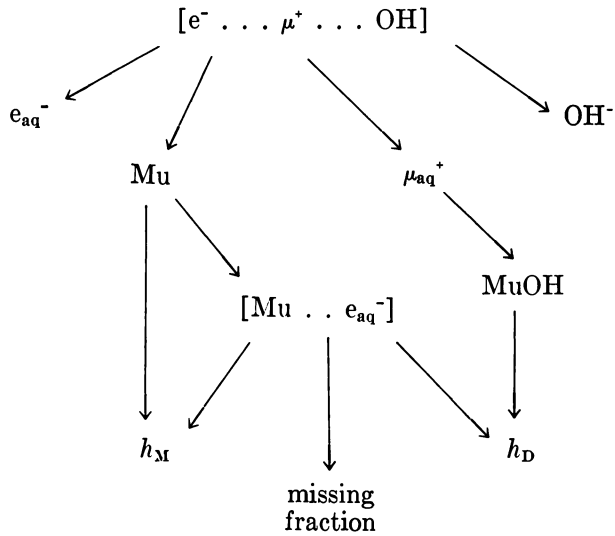

The important difference from Scheme I is that we start with μ^+ in the terminal spur itself rather than Mu*. Mu formation competes with escape and hydration of the electron and muon. Muon hydration leads, via fast proton transfer to a neighboring water molecule, to MuOH and thus contributes to h_D. It is this reaction branch that is favored by dry electron scavenging by high nitrate concentrations. In ice, hydration (more generally trapping) processes are much slower, and a higher Mu fraction (without depolarization) is predicted. Further, the reported slower trapping of electrons in D_2O– than in H_2O–ice (*35*) is consistent with the observed larger Mu fraction in the former.

Muon Thermalization in Liquids. The involvement of transient species created in radiation spurs is common to Schemes I and II proposed above. This fundamental assumption is very much open to question, however. In the past it has been assumed that Mu formation occurs at such high energies (10^4–10^2 eV) that the neutral atom escapes the

Publication Date: June 1, 1979 | doi: 10.1021/ba-1979-0175.ch014

radiation damage caused along the muon track. This idea stems from theoretical and experimental results for the gas phase, however (*see* Ref. *1*); little or no direct information is available for liquids. Although much of the above discussion is pure speculation, it seems impossible to explain the experimental observations regarding missing fraction and muon distribution without recourse to transient reaction partners for Mu or the muon itself. Should our ideas be supported by further results, Mu chemistry will provide a powerful means for studying end-of-track effects in radiation chemistry.

Conclusions

It has been shown that Mu can be detected directly in water and other liquids. Rate constants for Mu reactions were determined, and comparison of results with hydrogen atom data reveals large kinetic isotope effects. Thus, Mu kinetic studies promise to be of great value in testing chemical reaction theories for the liquid phase. The initial muon polarizations of the various fractions in water, aqueous nitrate solutions, and ice can be understood only in terms of interactions of Mu or the free muon with radicals produced in the terminal spur of the muon track.

Publication Date: June 1, 1979 | doi: 10.1021/ba-1979-0175.ch014

Acknowledgments

Parts of the work reviewed here were performed in collaboration with M. Camani, F. N. Gygax, W. Rüegg, and A. Schenck (Laboratory for High Energy Physics, ETH Zürich) and J. Hochmann (Physical Chemistry Institute, University of Zürich). We thank the staff of the Swiss Institute for Nuclear Research for technical and financial support. The project is funded by the Swiss National Foundation for Scientific Research.

This work is based on papers presented by F. N. Gygax and P. W. Percival at the symposium on Positronium and Muonium Chemistry at the CIC/ACS Meeting, Montreal, May–June 1977, and by H. Fischer at the Ninth International Symposium on Hot Atom Chemistry, Blacksburg, VA, September 1977.

Literature Cited

1. Fleming, D. G., Garner, D. M., Vaz, L. C., Walker, D. C., Brewer, J. H., Crowe, K. M., ADV. CHEM. SER. (1979) **175**, 279.
2. Roduner, E., Percival, P. W., Fleming, D. G., Hochmann, J., Fischer, H., *Chem. Phys. Lett.* (1978) **57**, 37.
3. Mobley, R. M., Bailey, J. M., Cleland, W. E., Hughes, V. W., Rothberg, J. E., *J. Chem. Phys.* (1966) **44**, 4354.
4. Hughes, V. W., McColm, D. W., Ziock, K., Prepost, R., *Phys. Rev. A* (1970) **1**, 595; **2**, 551.

5. Stambaugh, R. D., Casperson, D. E., Crane, T. W., Hughes, V. W., Kaspar, H. F., Souder, P., Thompson, P. A., Orth, H., zu Putlitz, G., Denison, A. B., *Phys. Rev. Lett.* (1974) **33,** 568.
6. Barnett, B. A., Chang, C. Y., Yodh, G. B., Caroll, J. B., Eckhause, M., Hsieh, C. S., Kane, J. R., Spence, C. B., *Phys. Rev. A* (1975) **11,** 39.
7. Fleming, D. G., Brewer, J. H., Garner, D. M., Pifer, A. E., Bowen, T., Delise, D. A., Crowe, K. M., *J. Chem. Phys.* (1976) **64,** 1281.
8. Myasishcheva, G. G., Obukhov, Yu. V., Roganov, V. S., Firsov, V. G., *Zh. Eksp. Teor. Fiz.* (1967) **53,** 451 [*Sov. Phys.—JETP (Engl. Transl.)* (1968) **26,** 298].
9. Gurevich, I. I., Ivanter, I. G., Makariyna, L. A., Mel'eshko, E. A., Nikol'skii, B. A., Roganov, V. S., Selivanov, V. I., Smilga, V. P., Sokolov, B. V., Shestakov, V. D., Takovleva, I. V., *Phys. Lett.* (1969) **29B,** 387.
10. Gurevich, I. I., Ivanter, I. G., Mel'eshko, E. A., Nikol'skii, B. A., Roganov, V. S., Selivanov, V. I., Smilga, V. P., Sokolov, B. V., Shestakov, V. D., *Zh. Eksp. Teor. Fiz.* (1971) **60,** 471 [*Sov. Phys.—JETP (Engl. Transl.)* (1971) **33,** 253].
11. Crowe, K. M., Johnson, R. F., Brewer, J. H., Gygax, F. N., Fleming, D. G., Schenck, A., *Bull. Am. Phys. Soc.* (1972) **17,** 594.
12. Brewer, J. H., Crowe, K. M., Gygax, F. N., Johnson, R. F., Patterson, B. D., Fleming, D. G., Schenck, A., *Phys. Rev. Lett.* (1973) **31,** 143.
13. Percival, P. W., Fischer, H., Camani, M., Gygax, F. N., Rüegg, W., Schenck, A., Schilling, H., Graf, H., *Chem. Phys. Lett.* (1976) **39,** 333.
14. Percival, P. W., *Faraday Discuss. Chem. Soc.* (1977) **63,** 192.
15. Percival, P. W., Rodunder, E., Fischer, H., Camani, M., Gygax, F. N., Schenck, A., *Chem. Phys. Lett.* (1977) **47,** 11.
16. Fleming, D. G., Garner, D. M., Brewer, J. H., Warren, J. B., Marshall, G. M., Clark, G., Pifer, A. E., Bowen, T., *Chem. Phys. Lett.* (1977) **48,** 393.
17. Fleming, D. G., Brewer, J. H., Garner, D. M., *Ber. Bunsenges. Phys. Chem.* (1977) **81,** 159.
18. Neta, P., *Chem. Rev.* (1972) **72,** 533.
19. Anbar, M., Ross, F., Ross, A. B., "Selective Specific Rates of Reactions of Transients from Water in Aqueous Solution. II. Hydrogen Atom," Government Printing Office, Washington, D.C., 1975.
20. Johnston, H. S., Parr, Ch., *J. Am. Chem. Soc.* (1963) **85,** 2544.
21. Kelley, R. D., Klein, R., Scheer, M. D., *J. Phys. Chem.* (1970) **74,** 4301.
22. Gurevich, I. I., Meleshko, E. A., Muratova, I. A., Nikol'skii, B. A., Roganov, V. S., Selivanov, V. I., *Zh. Eksp. Teor. Fiz., Pis'ma. Red.* (1973) **18,** 608 [*Sov. Phys.—JETP Lett. (Engl. Transl.)* (1973) **18,** 357].
23. Shiraishi, H., Kadoi, H., Katsumura, Y., Tabata, Y., Oshima, K., *J. Phys. Chem.* (1976) **80,** 2400.
24. Carrington ,A., McLachlan, A. D., "Introduction to Magnetic Resonance," Ch. 11, Harper and Row, New York, 1967.
25. Brewer, J. H., Crowe, K. M., Gygax, F. N., Schenck, A., "Muon Physics," Vol. 3: "Chemistry and Solids," V. W. Hughes and C. S. Wu, Eds., p. 3, Academic Press, New York, 1975.
26. Aratono, Y., Tachikawa, E., *J. Inorg. Nucl. Chem.* (1977) **39,** 555.
27. Mozumder, A., Magee, J. L., *Int. J. Radiat. Phys. Chem.* (1975) **7,** 83.
28. Percival, P. W., Fischer, H., *Chem. Phys.* (1976) **16,** 89.
29. Anbar, M., Bambenek, M., Ross, A. B., "Selected Specific Rates of Reactions of Transients from Water in Aqueous Solution. I. Hydrated Electron," Government Printing Office, Washington, D.C., 1973.
30. Kaptein, R., "Chemically Induced Magnetic Polarization," L. T. Muus, P. W. Atkins, K. A. McLauchlan, and J. B. Pedersen, Eds., p. 1, Reidel Publishing Co., Dordrecht, Holland, 1977.

Publication Date: June 1, 1979 | doi: 10.1021/ba-1979-0175.ch014

In Positronium and Muonium Chemistry; Ache, H.;
Advances in Chemistry; American Chemical Society: Washington, DC, 1979.

31. McLauchlan, K. A., "Chemically Induced Magnetic Polarization," L. T. Muus, P. W. Atkins, K. A. McLauchlan, and J. B. Pedersen, Eds., p. 107, Reidel Publishing Co., Dordrecht, Holland, 1977.
32. Percival, P. W., Roduner, E., Fischer, H., *Chem. Phys.* (1978) **32**, 353.
33. Draganić, I. V., Draganić, Z. D., "The Radiation Chemistry of Water," p. 171, Academic Press, New York, 1971.
34. Lam, K. Y., Hunt, J. W., *Int. J. Radiat. Phys. Chem.* (1975) **7**, 317.
35. Stradowski, Cz., Hamill, W. H., *J. Phys. Chem.* (1976) **80**, 1431.

RECEIVED February 2, 1978.

INDEX

Publication Date: June 1, 1979 | doi: 10.1021/ba-1979-0175.ix001

A

In Positronium and Muonium Chemistry; Ache, H.;
Advances in Chemistry; American Chemical Society: Washington, DC, 1979.

B

Publication Date: June 1, 1979 | doi: 10.1021/ba-1979-0175.ix001

C

Publication Date: June 1, 1979 | doi: 10.1021/ba-1979-0175.ix001

D

E

Publication Date: June 1, 1979 | doi: 10.1021/ba-1979-0175.ix001

In Positronium and Muonium Chemistry; Ache, H.;
Advances in Chemistry; American Chemical Society: Washington, DC, 1979.

F

G

Publication Date: June 1, 1979 | doi: 10.1021/ba-1979-0175.ix001

H

I

Publication Date: June 1, 1979 | doi: 10.1021/ba-1979-0175.ix001

J

K

L

Publication Date: June 1, 1979 | doi: 10.1021/ba-1979-0175.ix001

M

Publication Date: June 1, 1979 | doi: 10.1021/ba-1979-0175.ix001

N

Publication Date: June 1, 1979 | doi: 10.1021/ba-1979-0175.ix001

O

P

Publication Date: June 1, 1979 | doi: 10.1021/ba-1979-0175.ix001

Publication Date: June 1, 1979 | doi: 10.1021/ba-1979-0175.ix001

Publication Date: June 1, 1979 | doi: 10.1021/ba-1979-0175.ix001

Publication Date: June 1, 1979 | doi: 10.1021/ba-1979-0175.ix001

Publication Date: June 1, 1979 | doi: 10.1021/ba-1979-0175.ix001

Q

R

Publication Date: June 1, 1979 | doi: 10.1021/ba-1979-0175.ix001

S

Publication Date: June 1, 1979 | doi: 10.1021/ba-1979-0175.ix001

T

V

W

X

Z

Publication Date: June 1, 1979 | doi: 10.1021/ba-1979-0175.ix001

The text of this book is set in 10 point Caledonia with two points of leading. The chapted numerals are set in 30 point Garamond; the chapter titles are set in 18 point Garamond Bold.

The book is printed offset on Text White Opaque 50-pound. The cover is Joanna Book Binding blue linen.

Jacket design by Sharri Harris.
Editing and production by Candace A. Deren.

The book was composed by Service Composition Co., Baltimore, MD, printed and bound by The Maple Press Co., York, PA.